Stony Brook University

Synthesis of Novel Conjugated Materials

– Push-Pull Conjugated Diynes and 1,7-Phenanthroline Derivatives

A Dissertation Presented

by

Xiuzhu Ang

to

The Graduate School

in Partial Fulfillment of the

Requirements

for the Degree of

Doctor of Philosophy

in

Chemistry

Stony Brook University

December 2015

Stony Brook University

The Graduate School

Xiuzhu Ang

We, the dissertation committee for the above candidate for the

Doctor of Philosophy degree, hereby recommend

acceptance of this dissertation.

Dr. Nancy S. Goroff – Dissertation Advisor
Professor and Associate Provost, Department of Chemistry

Dr. Jonathan G. Rudick - Chairperson of Defense
Assistant Professor, Department of Chemistry

Dr. Joseph W. Lauher – Third Member of Defense
Professor, Department of Chemistry

Dr. Kevin Yager – Outside Member of Defense
Staff Scientist, Center for Functional Nanomaterials, Brookhaven National Laboratory

This dissertation is accepted by the Graduate School

Charles Taber
Dean of the Graduate School

Abstract of the Dissertation

Synthesis of Novel Conjugated Materials

– Push-Pull Conjugated Diynes and 1,7-Phenanthroline Derivatives

by

Xiuzhu Ang

Doctor of Philosophy

in

Chemistry

Stony Brook University

2015

This thesis is composed of two separate sections, focusing on developing novel conjugated materials.

The first section describes attempts towards synthesis of push-pull polydiacetylenes (PDAs), substituted by alternating electron-rich and electron-poor groups. These polymers are expected to have extensive conjugation and low energy band gaps, and therefore potential application in organic photovoltaic cells and nonlinear optics. We targeted push-pull PDAs by solid-state polymerization of appropriate diyne monomers. Oxalamide host molecules containing Lewis acidic or basic side groups are introduced to pre-organize the push-pull diynes in a co-crystal scaffold through Lewis acid-base interactions. Several novel diynes with iodine as electron donor

and nitrile or carboxylic acid as electron acceptor have been synthesized. One co-crystal, containing 4-(iodobuta-1,3-diyn-1-yl)benzoic acid as the monomer and bis(pyridyl) oxalamide as the host, has been prepared successfully. The co-crystal has ruby color. Its structure is determined by single-crystal XRD. However, the monomers in the co-crystal do not have appropriate geometry for solid-state polymerization.

The second section focuses on developing tunable hole-blocking layers (HBL) in new CIGS-based thin-film solar cells, in collaboration with the Eisaman group at Brookhaven National Laboratory. 1,7-Phenanthroline derivatives are targeted as novel HBL materials for their large energy band gap, tunable energy levels and morphologies. Several aryl/alkyl substituted 1,7-phenanthroline derivatives have been synthesized. 2,8-Dimethyl-1,7-phenanthroline is considered the most promising HBL material among all synthesized compounds for having both large energy band gap and powdery morphology. Both organic and CIGS photovoltaic devices containing 2,8-dimethyl-1,7-phenanthroline as HBL were fabricated in collaboration with the Kymissis group at Columbia University. According to the efficiency measured under AM1.5G illumination, including a HBL can enhance the PCE of the organic device from 0.9 to 5.0%, and the CIGS device from 3.2×10^{-4} to 0.11%.

Acknowledgement

I would like to sincerely express my gratitude to my research advisor, Dr. Nancy S. Goroff. It is her continuous guidance, support and encouragement that navigate me through my graduate research. Her mentorship helps me to grow as an organic chemist, and an independent scientist. Her optimistic and patient characteristics encourage me when facing challenges. Her cheerful personality also create a pleasing atmosphere in the group. I would also like to acknowledge the chair and third member of my dissertation committee, Dr. Jonathan G. Rudick and Dr. Joseph W. Lauher. Their insightful suggestion during my first and third meetings, and my research seminars are truly appreciated. I also thank Dr. Kevin Yager, who is kindly serving as the outside member for my dissertation committee.

I would thank all the Goroff group members, both previous and present, for their help and support all the time. I thank Dr. Racquel C. DeCicco for helping me get started in the group, Dr. Daniel Resch and Hongjian Jin for helping with the X-ray crystallography, and Dr. Allison Black for offering suggestion on coupling reactions. I thank our group members Dr. Dave Connors, Mattew Freitag, Usmanu Salisu, Bin Sun, Dandan Yang, Gizem Eren, Xianzhi Liu, and Ce Chen.

Furthermore, nothing of my project described in Chapter 4 would be accomplished without significant contributions of our collaborators. I would specially thank Dr. Matthew Eisaman for his great inspiration on developing novel thin-film solar cells. I thank Dr. Goroff for letting me undertake this project, which inspired me greatly. I thank Prof. Ioannis Kymissis at Columbia University for helping with the thermal evaporation deposition. I also thank Dr. Nanditha Dissanayake and Ahsan Ashraf in the Eisaman group, and Kostas Alexandrou in the Kymissis

group for their efforts on this project. I thank Dr. Mingzhao Liu, Dr. Dmytro Nykypanchuk and Dr. Jessica Hoy in CFN, BNL for mentoring me on cyclic volrammetry and AFM.

In addition, I appreciate everyone in SBU who has contributed to this dissertation through collaborative efforts. I thank Dr. Brian Phillips for helping with solid-state NMR spectroscopy, Dr. Christopher Yong for Raman spectroscopy, Dr. Bela Ruzsicska for MS spectroscopy. I thank Dr. Ming Yu Ngai for letting me use the GC-MS in his group, and Dr. Jonathan G. Rudick for letting me use the UV-vis spectroscopy in his group. I also thank Dr. James Marecek and Dr. Francis Picart for assisting my NMR experiments.

I would like to express my thanks to the entire Main Office staff of the Chemistry Department for their help with administrative matters. In particular, I would like to acknowledge Katherine Hughes for answering all questions for the past years. In addition, I appreciate Mike Teta for keeping our laboratory as a safe working environment and the NSF for funding.

This dissertation is dedicated to my dearest husband Qiangqiang Shi, and my parents. Their continuous support and love have been a great encouragement for me to achieve my Ph.D. in chemistry. Above all, I thank God for all His great love, mercy and righteousness.

Description for a General Audience

My research focuses on developing novel organic conjugated materials. A material can be called conjugated when the electrons can to some extent move across the entire molecule, instead of fixed on a single atom. The mobility of electrons can result in potential semi-conductivity. In addition, unlike inorganic materials, organic materials can potentially be light, transparent, and easily modified. Therefore, organic conjugated materials have great applications in light or electricity responsive devices, e.g. solar cells.

There are two main sections in my dissertation. The first section describes attempts towards making push-pull conjugated polydiacetylenes (PDAs). The PDA is essentially a conjugated rod composed of only carbon. Push-pull PDAs are carbon rods carrying alternating groups that accept electrons and give away electrons. Electrons have the tendency to move from the groups that gives them away to the groups that accept them across the conjugated rod. This moving tendency can potentially make them useful in electronics. In addition, the structures of push-pull PDAs are not symmetric, which makes them able to respond to high-energy light, e.g. laser, in an interesting way. For example, if a laser beam goes through a push-pull PDA, the output frequency may be doubled. Although push-pull conjugated PDAs have very interesting properties, they are very difficult to make.

Our approach to make such PDAs starts from making repeat units, also precursors, of PDAs, which are called push-pull diynes. If these repeat units are organized properly, upon exposure to external energy, they can react to form push-pull PDAs. Diynes can only undergo further reaction to

generate PDAs if they are organized with a specific orientation. Most diynes cannot organize so perfectly on their own, which is why making PDAs is difficult. We proposed to organize diynes through a so called "host-guest" strategy. The push-pull diynes are called the guests. The materials used to organize them are called the hosts. Crystals that contain one kind of the hosts and one kind of the guest molecules can be generated, and they are called co-crystals. In the co-crystal, hosts can align the guests appropriately. The guests can react with each other to form PDAs. Previous group members have successfully made the PDA carrying only iodine atoms employing this method.

It is the first time we tried to arrange push-pull diynes in co-crystals. Several proposed push-pull diynes have been designed and made. One co-crystal has been prepared successfully, and its structure has been determined. The push-pull diyne (guest) molecules are aligned by the host molecules in the co-crystal. However, the diyne molecules are too far away from each other, so they cannot react. The co-crystal we obtained indicates that it is possible to organize push-pull diynes in a host-guest system. We need to expand the structures of hosts, guests and conditions of forming co-crystals, in order to generate a co-crystal with diynes organized perfectly for formation of a PDA.

The second section focuses on developing tunable hole-blocking layers (HBL) in novel CIGS-based solar cells, in collaboration with the Eisaman group at Brookhaven National Laboratory. Solar cells are multi-layer electronic devices that can convert sunlight into electricity. In this project, CIGS, a mixture of four materials, works as the sunlight responsive layer. Electrons in the CIGS absorbs the energy of sunlight and want to leave the places, also called "holes", that hold

them. Once they are separated from holes, the electrons drift to one electrode, and holes drift to the other electrode. The movement of electrons and holes is what generates electricity. The power conversion efficiency (PCE) is an important parameter that determines the performance of solar cells. It can be calculated by the percentage of the sunlight shining on to the cell that is converted into electricity.

However, after electrons are separated from the holes, they can only move freely for an extremely short period of time. If an electron gets too close to a hole before it arrives at the electrode, the electron will fit into the hole and release the energy it carries. This process is called "recombination". It reduces the efficiency of the solar cell. To minimize the recombination process, a hole-blocking layer (HBL) is proposed to be placed in the cell. The HBL helps transport electrons to the electrode, and blocks holes drifting in the same direction, therefore it prevents electrons and holes from getting too close.

We designed and made several conjugated candidates that could have the desired properties. They are known materials, and have similar structures to the commercialized HBL material, indicating similar properties. However, they have never been studied as HBL materials in solar cells. After investigating the properties of our synthesized materials, one of them is targeted as the most promising HBL material. The HBL is placed in both an organic solar cell and a CIGS-based solar cell. The CIGS-based solar cell has a novel architecture developed by the Eisaman group. The cells are fabricated in collaboration with the Kymissis group at Columbia University. The best results among all measurements indicate that including a HBL can enhance the PCE of the organic solar cells from 0.9 to 5.0%, and the CIGS solar cell from 3.2×10^{-4} to 0.11%. The significant

improvements indicate the material we made can function as a HBL to reduce the recombination and enhance the efficiency. The new material expands the scope of organic materials that can be used as HBL materials in solar cells.

Table of Contents

Table of Figures

Table of Schemes

Table of Tables

Table of Abbreviations

PDA	Polydiacetylene
DA	Diacetylene
NLO	Nonlinear optics
CIGS	Copper indium gallium selenide
HBL	Hole-blocking layer
PCE	Power conversion efficiency
CV	Cyclic voltammetry
MIM	Metal-insulator-metal
VASE	Variable angle spectroscopic ellipsometry
Hex	Hexane
EA	Ethyl acetate
DMSO	Dimethyl Sulfoxide
***t*-BuOK**	Potassium *tert*-butoxide
Ar	Argon
R_f	Retention factor
THF	Tetrahydrofuran
M.p.	Melting point
CuI	Copper(I) Iodide
$Pd(PPh_3)_2Cl_2$	Palladium(II) bis(triphenylphosphine) dichloride
PPh_3	Triphenylphosphine
$(i\text{-}Pr)_2NH$	Diisopropylamine
Et_2O	Diethyl ether

TMS	Trimethylsilyl
CH_2Cl_2	Dichloromethane
TIPS	Triisopropylsilyl
SHG	Second harmonic generation
***p*TS**	*p*-Toluene sulfonate
E_g	Energy band gap
XRD	X-ray Diffraction
PV	Photovoltaic
PDA-4BCMU	PDA- bis(4 butoxy-carbonyl methyl urethane)

Chapter 1 Introduction

1.1 Introduction on Carbon-rich Materials and Polydiaceylenes (PDAs)

1.1.1 Carbon-Rich Materials

Carbon-rich materials have been employed extensively in materials science and technology over time. Their electrical and optical properties have been explored profoundly.[1] Commonly known carbon materials such as graphite and diamond have been used for thousands of years. Microscopic study of carbon nanostructures was catalyzed by the discovery of fullerene in 1985.[2] The substantial unsaturated and delicate nanostructures discovered offer great charge/energy transfer ability. As the synthetic methods and modification techniques of fullerenes develop, various derivatives have been broadly utilized in photovoltaic technologies. Following fullerene, carbon nanotubes (CNT) including single-wall nanotubes (SWNT) and multi-wall nanotubes (MWNT), and further functionalized derivatives have been developed extensively.[3] In addition to randomly arrayed CNT architectures in bulk composite materials and thin films, organized CNT architectures are discovered to considerably enhance properties of individual CNT as well as exhibit new functionalities. Figure 1.1 shows various carbon nanostructures.

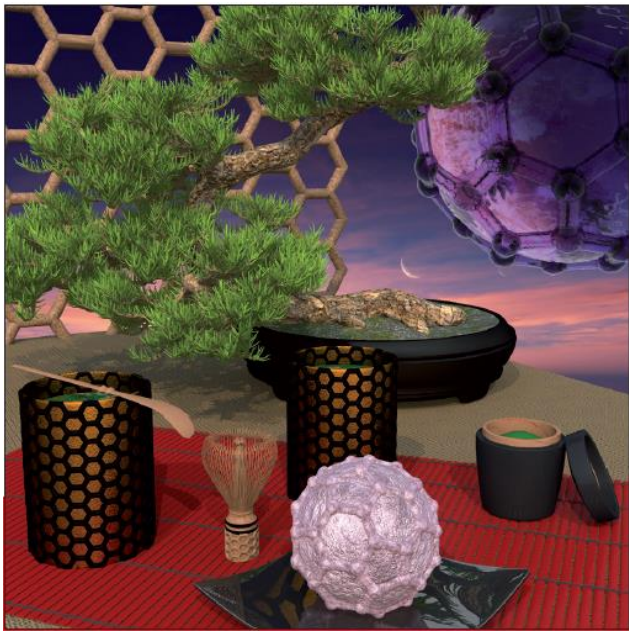

Figure 1.1 Carbon Nanostructures[4]

(Reprinted with permission from ref. 4, Copyright 2014, John Wiley & Sons, Inc.)

Furthermore, 2D graphene has been found the world's thinnest and strongest material.[5] This single-atom-thick sheet of carbon atoms arrayed in a honeycomb pattern can be a great conductor of heat and electricity. Functionalization of graphene greatly expands their potential applications in electronic devices.

1.1.2 Push-Pull Conjugated polymers

Conjugated polymers contain alternating saturated/unsaturated bonds and extensively delocalized π-electrons along their backbones. The conjugation length increases in proportional to the number of repeat units. When the number of repeat units is increased by one, it leads to hybridization of energy levels. Therefore, the HOMO and LUMO of conjugated polymers appear band-like behavior. The energy gap between valence band (highest-lying filled band) and conduction band

(lowest-lying empty band) becomes smaller than that of monomers, which leads to increasing conductivity. Associated with their intrinsic variety through synthesis as another advantage, these electro-active polymers possess great potential in various applications including nonlinear optics, photovoltaic devices, sensors, etc. Figure 1.2 shows structures of several widely used conjugated polymers.

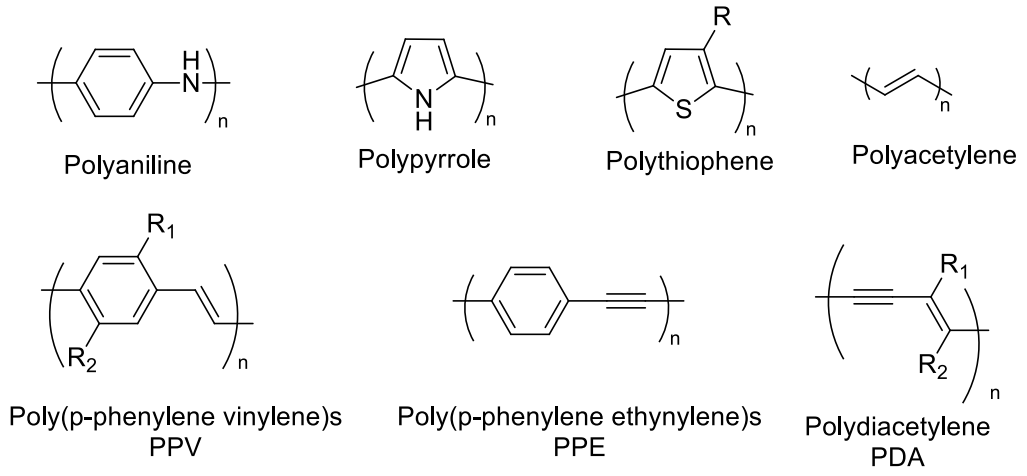

Figure 1.2 Examples of conjugated polymers

In 1963, Weiss and coworkers[6] first reported oxidized iodine-doped polypyrrole was able to reach conductivity as high as 1.0 S/cm.[6] They published a series of papers describing how doping electron donating or withdrawing moieties on polypyrrole can generate semi-conductivity with *n*- or *p*-type characteristics.[6-7] In 1977, Heeger, MacDiarmid and Shirakawa[8] reported remarkably enhanced conductivity of polyacetylenes $(CH)_x$ through halogen doping, because halogens can form charge-transfer complexes with $(CH)_x$. The Nobel Prize in chemistry in 2000 was awarded "for the discovery and development of conductive polymers".[9] More recently, conjugated polymers, such as poly(3-hexylthiophene) (P3HT) and poly(p-phenylene vinylene) (PPV), have been widely employed as the active layer in organic solar cells and organic light emitting diodes (OLED).[10]

As mentioned before, semi-conductivity of conjugated polymers is primarily based on their low energy band gap. Therefore, tuning HOMO and LUMO levels by modifying structures is essential to tune the conductivity of such polymers. One of the most effective approaches is to functionalize polymer backbones with electron-rich and electron-poor groups,[11] resulting in "push-pull conjugated polymers". According to the Frontier Molecular Orbital (MO) Theory, when establishing a push-pull system, the HOMO and LUMO of electron rich and poor functionalities interact to generate a new HOMO and a new LUMO with an energy band gap, E_g, smaller than either moiety.

A wide range of push-pull polymers have been developed and employed in organic photovoltaic cells.[12] Figure 1.3 shows one of the recently reported[13] polymer tandem solar cells utilizing conjugated polymer PDTP-DFBT containing both electron rich and poor functionalities as the electron donor phase, while fullerene derivatives $PC_{61}BM$ or $PC_{71}BM$ as the electron acceptor phase. The polymer has a bandgap of 1.38 eV, as well as a high carrier mobility and deep HOMO level. Its spectral absorption ranges from 710 to 820 nm, and spectral response reaches 900 nm. With a proper design of the blend thickness, the single junction cell (PDTP-DFBT: PC71BM) reached a PCE of as high as 7.9%, under standard reporting condition. By adding another photon-active layer composed of P3HT (E_g ~1.9 eV), the absorbing spectrum covers from 350 to 900 nm. The achieved tandem solar cell reached a PCE as high as 10.6%.

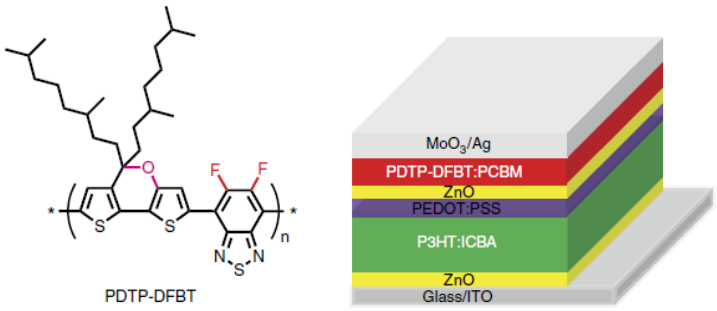

Figure 1.3 Chemical structure of the polymer (PDTP-DFBT) and the structure of achieved tandem solar cells[13]

(Reprinted with permission form Ref. 13, Copyright 2013, Nature Publishing Group)

As mentioned before, it is feasible to modify structures of push-pull polymers to achieve required E_g. In 2014 Tae In Ryu and coworkers[14] reported a series of poly(diketopyrrolopyrrole) (PDPP) based push-pull polymers containing various electron donors. Polymers were employed in ITO/PEDOT:PSS/Polymer:$PC_{71}BM$/TiO_2/Al photovoltaic devices as the photon-active layer (Figure 1.4). They investigated optical and electrochemical properties as well as morphologies of the polymers, as well as efficiencies and stabilities of fabricated devices. As a result, the PDPPDTT polymer exhibited a low E_g (1.77 eV) and appropriate morphology, and therefore led to the highest efficiency among all PDPP-based polymer inserted solar cell (6.11%).

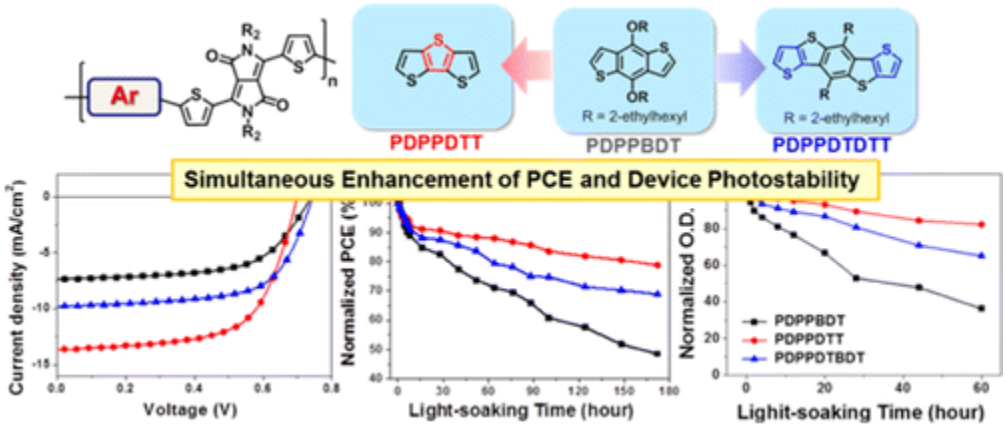

Figure 1.4 Structures and properties of PDPP-based push-pull polymers[14]

(Reprinted with permission from ref.14, Copyright 2014, American Chemical Society.)

1.1.3 Polydiacetylenes (PDAs)

Polydiacetylenes (PDAs) are a unique class of conjugated polymers, containing a linear backbone composed of alternating triple and double bonds (Figure 1.5). They can be synthesized by 1,4-polymerization of diynes. The laboratory of Wegner[15] gave the first report on PDA synthesis in the solid state in 1969, after which there has been considerable research on synthesis of PDAs with various side-chains. Properties of PDAs, such as chromic, electronic and nonlinear optical properties, have therefore been explored and developed for applications.

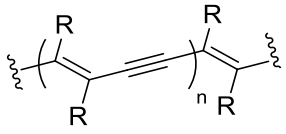

PDA

Figure 1.5 General structure of polydiacetylenes (PDAs)

Chromatic Transformation

PDAs display a color transformation between blue (around 640 nm) and red (around 500 nm) phases, when exposed to external stimuli such as heat, light, pH, electricity, etc.[16] There have been many theories on mechanism of the color change.[17] One well-known is that electron delocalization along the linear π-conjugated backbone makes PDAs deep blue. External stimuli can disrupt the conjugated network and result in shorter conjugation length, which turns PDAs from blue to red.[16] Michel Schott[18] however demonstrated that it is the geometrical constraints of side groups that make the polymer backbone highly planar or non-planar, with different colors. When the backbone is highly planar, PDAs appear blue. While externally initiated, side chains are able to rearrange to make PDA backbones non-planar, which causes chromatic transformation to red. In fact, both blue and red chains can have imperfect conjugation.[19] The color transition when PDAs bind to biological targets, such as peptides, has a different mechanism. It has been hypothesized that molecular recognition between side chains on PDAs and peptides makes bulky complexes that cause repulsion between each other.[19] To release the strain, the packing of side groups changes the arrangement of the PDA backbone and leads to chromatic transformation.

The stimuli-responsive PDAs have extensive potential applications in sensing, imaging and display technologies.[20] For instance, the Kim group[21] fabricated PDA-embedded polymer fibers by electrospinning. Such fibers displayed blue-to-red transition when exposed to gasolines. By modifying polymer matrix, gasolines of different components can be detected selectively. They also incorporated PCDA diyne monomers with Brij 78 (a commercial non-ionic surfactant) to make a colorimetrically reversible ink (Figure 1.6).[22]

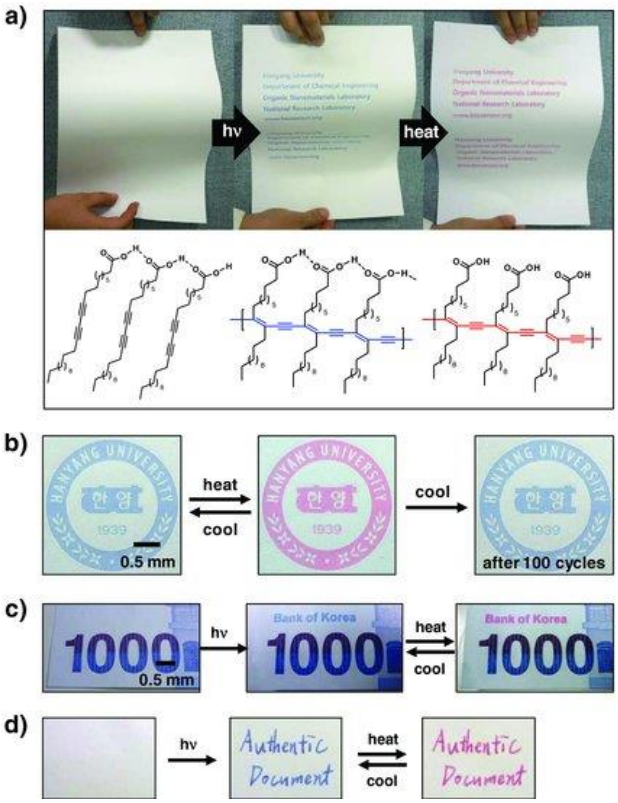

Figure 1.6 PDA incorporated colorimetrically reversible ink[22]

(Reprinted with permission from ref.22, Copyright 2011, John Wiley & Sons, Inc.)

3D PDA-based supramolecular constructions have become a highly versatile sensing platform due to highly enhanced surface areas.[23] Because red-phase PDAs are fluorescent, while blue-phase PDAs are not, a fluorescence signal can be generated when blue-to-red transition happens.[23b] The Kim group[24] also reported a fluorescent transformation of PDA vesicles induced by molecular recognition between PDA-linked antibody and peptide components of prostate specific antigen (PSA). The detection limit was 10 ng/mL. By adding a secondary response, the sensitivity of such PDA vesicles could be further enhanced by 100-fold (Figure 1.7).[24]

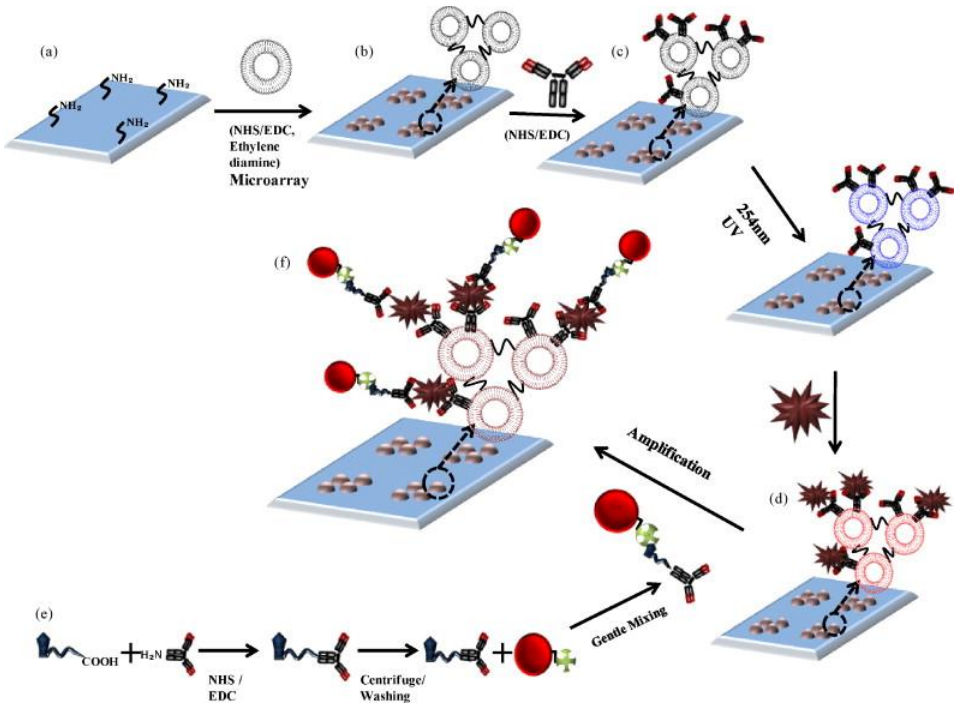

Figure 1.7 The signal amplified detection of PSA using PDA vesicles coated chips[24]

(Reprinted with permission from ref.24, Copyright 2010, John Wiley & Sons, Inc.)

Nonlinear Optics (NLO)

Nonlinear optics (NLO) describes the polarization of materials responds to applied electromagnetic fields in a nonlinear way, to generate new electromagnetic field with different physical properties. Applications of NLO include optical switching, amplification, beam steering and image processing.[25] [26] Second harmonic generation (SHG) is the first observed nonlinear-optical phenomena, discovered in a single crystal quartz by Frank and coworkers in 1961.[25] It converted the frequency of a ruby laser (694.3 nm) into the ultraviolet (347. 15 nm). Although the conversion efficiency was only 10^{-4} % in their best experiments, it was truly a breakthrough. Rentzepis and Pao first observed SHG in an organic material, benzpyrene, in 1964.[27]

Theory of optical nonlinearity was established afterwards.[25] When a material is treated with an oscillating external electric field (light), the weakly bound electrons around nuclei of atoms redistribute. The macroscopic polarization (***P***) resulted can be expressed as in eqn. 1-1. P_0 is the static dipole of the material, $\chi^{(1)}$ the linear polarizability, $\chi^{(2)}$ the second-order polarizability, and $\chi^{(3)}$ the third-order polarizability. At sufficiently intense electric filed, e.g. lasers, polarization of the material becomes nonlinear. Consequence of $\chi^{(2)}$ and $\chi^{(3)}$ is to produce light with frequencies different from the incident light (frequency doubling, tripling, mixing, etc.).

$$\boldsymbol{P = P_0 + \chi^{(1)}E + \chi^{(2)}E^2 + \chi^{(3)}E^3} \qquad \text{eqn. 1 - 1}$$

Inorganic materials, such as potassium dideuterium phosphate(KDP), lithium niobate($LiNbO_3$) and barium titanate ($BaTiO_3$), have been studies and commercialized in nonlinear optics.[26] Their optical nonlinearity is mainly due to nuclear movement in the external electric field, and partially due to movements of electrons.[28] However, organic compounds show optical nonlinearity primarily based on π-conjugation.[29] Electron density can redistribute easily due to delocalization in a conjugated system. Furthermore, organic materials have advantageous inherent diversity, since it is feasible to modify backbones and functional groups as desired. PDAs therefore become very attractive NLO materials because 1) they have highly conjugated backbones; 2) it is feasible to synthesize PDAs with various side chains, as either 1D single crystals or 2D oriented films, which offers great chances to optimize properties.

Third-Order Polarizability of PDAs. The NLO properties of *p*TS-PDA have been explored after the synthesis of *p*-toluene sulfonate polydiacetylene (*p*TS-PDA) as macroscopic single crystal with

all trans planar structure became feasible.[15] According to Sauteret et al in 1976,[30] the *p*TS-PDA and TCDU-PDA (Figure 1.8) single crystals can reach $\chi^{(3)}$ comparable to those measured in some classical inorganic NLO crystals. $\chi^{(3)}$ parallel to the polymer chain was observed to be much larger than perpendicular, which confirmed that the enhancement of $\chi^{(3)}$ is due to the π-electrons delocalization. Further research has been extended to single crystals and thin-films of PDAs with side groups other than *p*TS or TCDU.[31] [32]

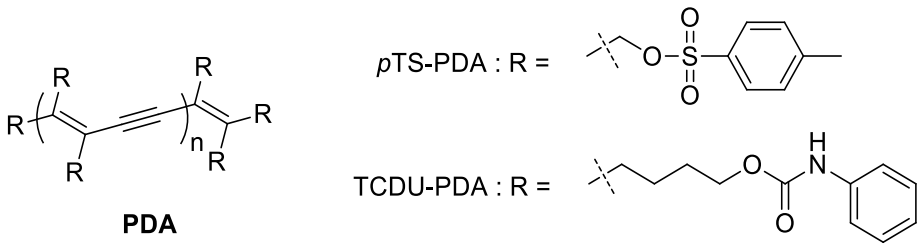

Figure 1.8 Structure of *p*TS-PDA and TCDU-PDA

The third-order polarizability, $\chi^{(3)}$, of PDAs can be improved by enhancing the π-conjugation in two ways. One is to introduce π-conjugated, such as aromatic or acetylenic, substituents on PDA backbones. Researchers have put efforts on synthesizing polymers of triynes and tetraynes,[33] as well as aryldiynes(will be discussed in **1.1.4**). The other optimization method is to increase the π-conjugated backbone density. Ladder-type PDAs have then been designed with π-conjugation between backbones (Figure 1.9).[34] Since monomers for ladder-type PDAs undergo polymerization more intricately comparing to simple capped diynes, the polymeric material resulted display imperfect structure and deteriorated crystallinity that are difficult to characterize, which makes studying their NLO properties more challenging. Therefore, optimized synthesis of laddered PDAs is required to further explore NLO properties of such PDAs.

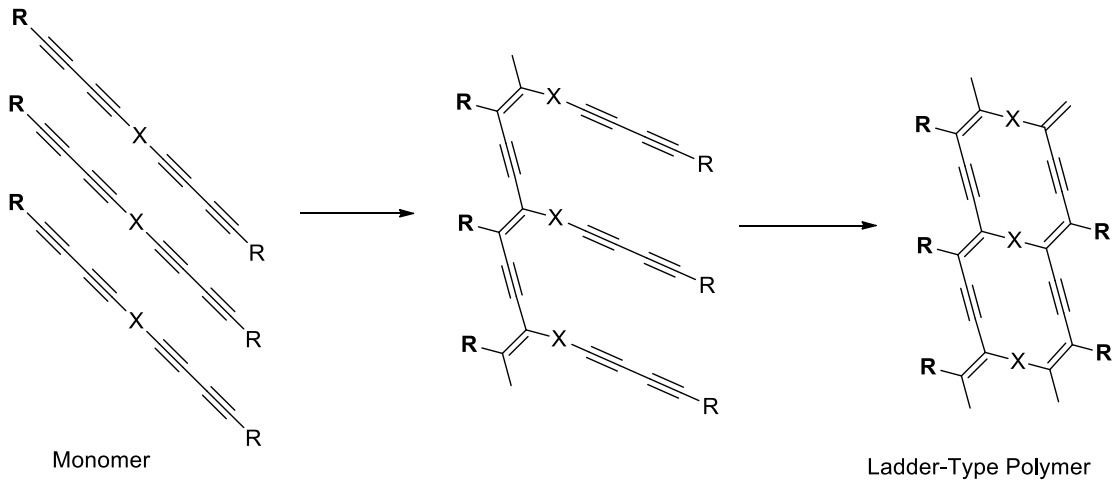

Figure 1.9 Synthesis of ladder type PDAs[34a]

Second-Order Polarizability of PDAs. Since the early study in 1970 by Davydov[35] et al, second-order polarizability has been realized only exhibiting in non-centrosymmetric molecules.[36] As mentioned before, 3,4-Benzpyrene and 1,2-benzanthracene were the first organic compounds found displaying $\chi^{(2)}$.[27] Therefore, most second-order NLO materials are based on non-centrosymmetric electron donor-(π-conjugated bridge)-electron acceptor (D-π-A) organic system where electrons delocalize along the molecules and distribute non-symmetrically. *p*-Nitroaniline molecule (Figure 1.10) is one of the simplest examples, and has been investigated both theoretically and experimentally.[37] Stronger donors and acceptors, as well as longer conjugation between donor and acceptor units, are promising to result in even higher $\chi^{(2)}$.[38]

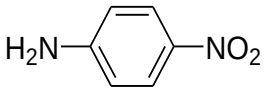

Figure 1.10 Simple D- π-A organic system

Push-Pull PDAs as NLO

As mentioned before, PDAs display large $\chi^{(3)}$ due to the one-dimensional π-conjugation. A large $\chi^{(2)}$ can be achieved by introducing donor and acceptor units upon conjugated systems. Therefore, Researchers have been investigating non-symmetric PDAs, containing alternating electron rich and poor substituents, which would be likely to carry both large $\chi^{(2)}$ and $\chi^{(3)}$.[39] In 1989, Yoshimura[39c] predicted influence of donors and acceptors on the energy levels of PDAs. In 1991, Nakano et al[39a] demonstrated that $\chi^{(3)}$ of PDAs is influenced greatly by the pattern of donors and acceptors. Later a detailed analysis was presented by Gu et al[39b] about how chain length and donor/acceptor moieties would influence hyperpolarizability of substituted PDAs. They built up four substituted PDA systems as models for calculation (Figure 1.11). It was confirmed that longer PDA chains and stronger push-pull effect can result in larger $\chi^{(2)}$. In the PDA_DA model, the push-pull effect diminishes significantly when the distance between D and A becomes longer. In the PDA_DDAA model, the applied electric filed is along the conjugated backbone, which is perpendicular to the electron transfer path from donors to acceptors across the backbone. Therefore $\chi^{(2)}$ along the main axis is small. In the PDA_DAAD model, the applied electric filed is almost on the same orientation of electron transfer path, which leads to a large $\chi^{(2)}$ value. They also indicated that the bigger the substituents, the stronger the electron-transfers, and the larger the maximum $|\chi^{(2)}|$ value can be. Although the theoretical prediction indicates great potential of push-pull PDAs as NLO material, synthesis of these PDAs bearing alternating donors and acceptors in an ordered way has been very challenging, mostly due to the difficulty in controlling arrangements of diyne monomers in the solid state. Consequently, experimental $\chi^{(2)}$ values of these PDAs are to be further investigated.

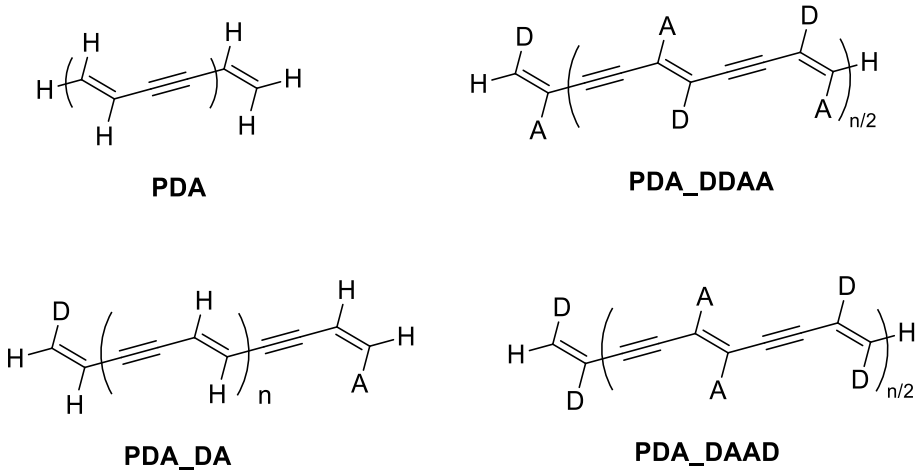

Figure 1.11 Push-pull PDA systems used to illustrate their second-order nonlinearity[39b]

Photo-Induced Charge Transfer. There have been extensive research focusing on the conductivity of PDAs because of the great linear π-conjugation. The energy band gap of PDAs, E_g, generally ranges from 2.0 to 3.0 eV,[40] depending on side functionalities. Such a band gap makes it difficult to generate high concentration of charges at room temperature, so PDAs are good insulators (dark conductivity is 10^{-15} to 10^{-9} S/cm).[41] However, charges and carriers can be created by several methods, e.g. chemical doping with strong oxidizing or reducing reagents.[42] It was reported that iodine vapor doped *p*TS-PDA single crystal can reach a maximum conductivity of 2×10^{-2} S/cm.[42a]

Photo-induced excitation of PDAs has been explored for potential photovoltaic applications. Different from inorganic materials generating free charges and carriers, organic materials generate excitons (a bound state of electrons and carriers that are attached to each other by electrostatic Coulomb force) when irradiated by photons with energies larger than E_g. The binding energy of excitons for PDAs is approximately 0.5 eV,[43] which means 0.5 eV is required to release free charges and carriers from excitons. There have been studies on charge transfer between PDAs

(electron donor) and C_{60} (electron acceptor) by mixing them together and applying external energy. The idea is to extract electrons from PDA excitons and promote them transport onto C_{60}, creating charged species on both components. The released carriers could be delocalized along the conjugated chains of PDAs to overcome rapid recombination. Given the fact that PDAs can absorb visible light, if this *p-n* junction (PDA-C_{60} junction) could generate photo-induced electricity, it would provide PDAs great potential applications in photovoltaic technology.

Heeger and co-workers[44] investigated two PDAs (PDA- bis(4 butoxy-carbonyl methyl urethane) (PDA-4BCMU), PDA-poly(bis-p-chlorocinnamate, 10, 12-docosadiyn-1,22-diol (PDA-ClCin22), Figure 1.12) in composites with C_{60}. A mixed solution of PDAs and C_{60} was drop-casted to be disordered films. Two para-phenylene vinylene (PPV)-C_{60} composites were also examined for comparison. On the contrary to the hypothesis, PDAs:C_{60} composites exhibited no detectable transient photocurrent even when C_{60} was added up to 50 wt%, while PPV experienced enhanced photo-induced electron transfer to C_{60} even upon addition of 1 wt% C_{60}. The real reason for the absence of charge transition was not fully understood yet. Heeger and co-workers proposed that it was primarily due to the binding energy (~0.5 eV) of excitons in PDAs was sufficiently large so that charges are not able to separate and transfer. They also considered that the morphology of PDA:C_{60} composites might be another issue, because the compatibility between C_{60} and PDAs was unknown and PDAs were made as disordered films rather than single crystals. The real reason for the absence of charge transition is still not fully understood yet.

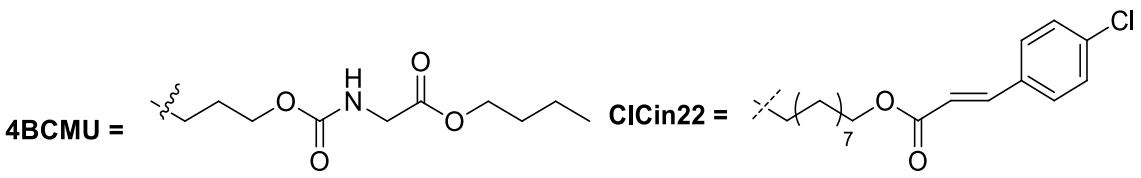

Figure 1.12 Structure of 4BCMU and ClCin22 capped groups[44]

A few years later D. Comoretto et al[45] reported that forms of PDAs, blue or red, could make a difference on their photo-physics. According to their prior work,[46] in the red form of PDA-4BCMU, only neutral triplet excited states appeared (Figure 1.13), determined by the characteristics of magnetic field dependence of the transient excited-state.[46] However, in the blue form of PDA-4BCMU, charged singlet excited states (Figure 1.13) were observed in their steady-state photo-induced absorption (PA) experiments in addition to neutral excited states, indicated by a low-frequency photo-induced absorption of infrared activated vibrational modes.[47] The charged singlet states are expected easier to dissociate and transfer charges from polymers to acceptors than neutral states, because they have smaller binding energy than neutral states (Figure 1.13). This discovery indicates that the blue or red phase of PDAs is necessary to be considered when exploring their photo-induced charge separation.

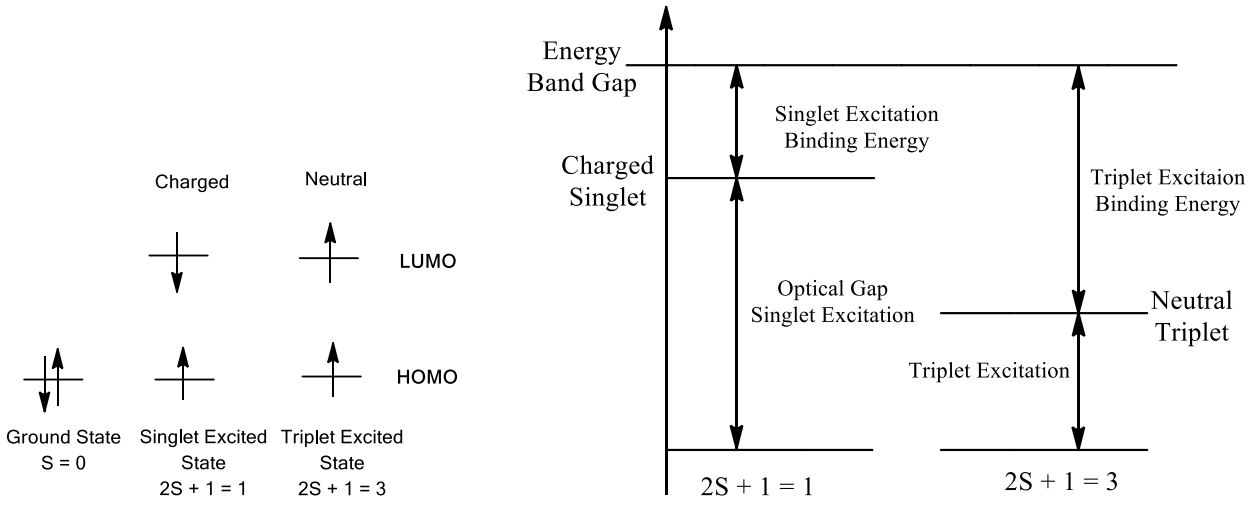

Figure 1.13 Charged singlet excited state and neutral triplet excited state

Carbazolyl substituted PDAs (PCzDAs) therefore drew interest because there were only charged states observed when exciting the blue PCzDAs substituted by carbazolyl group directly adjacent to PDA backbones (Figure 1.14).[48] When methylene groups were added between carbazolyl group and the backbone, both charged and neutral excitons were observed.[49] In red form of PCzDAs, long-lived neutral triplet excitons dominated when excited.[50] The Brabec group[49] then studied charge transfer between one blue PCzDAs (polyCPDO, Figure 1.14) and PCBM, which had higher solubility in PDAs than C_{60}. However, they still could not detect any charge transfer process. Possible explanation given included: 1) the interaction between polyCPDO and PCBM is weak, so that the interface is not a good contact for charge transport; 2) excitons are stabilized by deep traps so they cannot release charges. Therefore, photo-induced charge generation of PDAs remains an open question and great potential. There have been several groups utilizing PDA derivatives as photon active layer in photovoltaic devices, and the resulting efficiencies were all low.[51] Synthesis and investigation on novel PDAs attaching various functional groups may offer new inspiration.

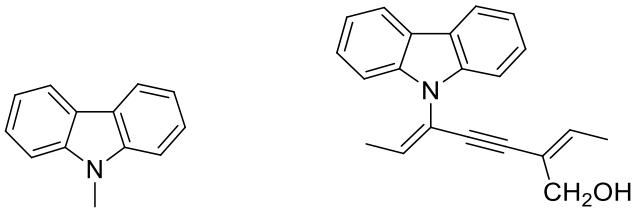

Figure 1.14 Structure of carbazoyl group and polyCPDO[49]

1.1.4 Fabrication of PDAs

Structural Requirements for Synthesizing PDAs

Solid-stated topochemical polymerization of diynes can be initiated photochemically (by UV, X-ray, γ-ray),[52] thermally,[52a, 53] or by pressure.[54] According to Baughman's study[55] published in 1974, 1,4- polymerization of diynes is preferred when the repeat distance between diyne monomers is 5 Å, and the angle between diyne rods and stacking axis is 45° (Figure 1.15). Such parameters required precise self-organization of diyne monomers.

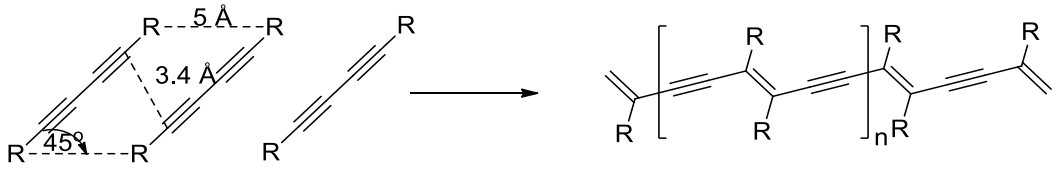

Figure 1.15 Structural parameters for 1,4-polymerization of diynes

Wegner and co-workers[53, 56] established approaches to synthesize single crystals of polymers from single crystals of pre-organized diyne monomers containing side functional groups. The earliest example is the crystallization and polymerization of bis(*p*-toluene sulphonate) of 2,4-hexadiyne-1,6-diol (Figure 1.16), abbreviated as *p*TS. The side *p*TS groups help diynes form crystals of good quality, and provide proper geometry to diynes for 1,4-polymerization. Furthermore, single-crystal

XRD analysis of both monomers and polymers helps elucidate the structural alteration through the polymerization reaction profoundly.

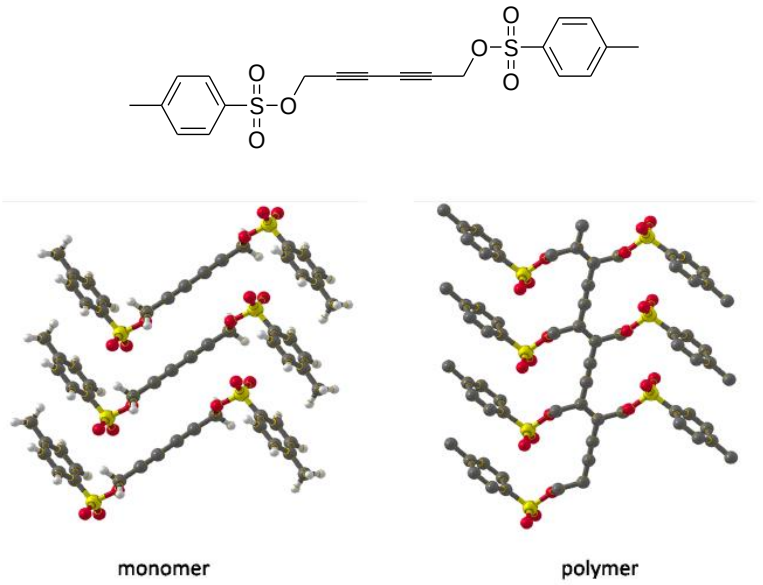

Figure 1.16 Single crystal structure of monomers and polymers of bis(*p*-toluene sulphonate) of 2,4-hexadiyne- 1.6-diol[57]

(Reproduced with permission of the International Union of Crystallography http://journals.iucr.org/)

End-capped groups of diynes can introduce intermolecular interactions, including electrostatics, hydrogen bonds, donor-acceptor or ion coordination. These interactions can have great influence on the assembly of diynes. Strong H-bonds form between urea, amide, carboxylic acid and carbamide groups, as well as π - π stacking between phenyl and carbazole et al, have been extensively utilized to help stabilizing diyne monomers and offer proper repeat distance and angle (Figure 1.17).[56] Side chains can also provide PDAs physical and chemical properties for diverse applications.

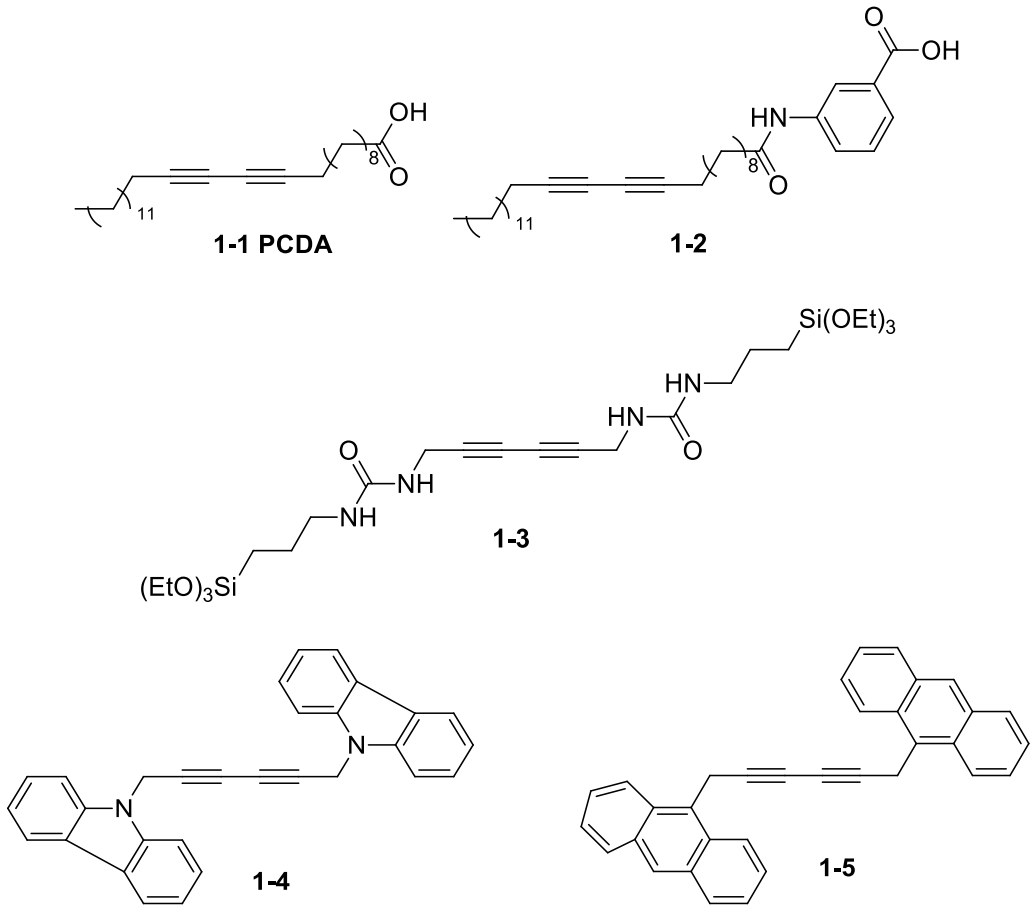

Figure 1.17 Structures of capped diynes capable to self-organize in the solid state

Polymerization of Aryldiynes and Non-Symmetric Diynes

Aryl groups can be a significant extension of the conjugation of the PDA backbone, and provide extra stability. As mentioned before, aryl groups are likely to enhance the optical and electrical properties of PDAs greatly. However, according to Curties and co-workers' work,[58] the rigidity of the directly attached aryl group makes polymerization challenging. In the monomer, sp hybridized acetylenic carbons form 180° bonds, and they need to convert from sp to sp^2 hybridization forming 120° bonds through polymerization. In the known crystal-to-crystal polymerizations, the diyne groups rotate 32-35°, and the substituents rotate another 25-28°. If the substituents are aryl groups, it is very difficult to rotate such big groups for such a big degree without breaking the crystals.

Therefore, even though π-π stacking between phenyl rings is a favorable interaction to generate order, synthesizing PDAs from diynes capped by aryl groups directly are limited. Single crystals of such PDAs have never been reported.

Very recently, Tokito et al[59] reported the synthesis and solid-state polymerization of diynes directly attached to *N*-carbazolylphenyl (*N*-CzPh) group on one side, and carbamates with various R groups on the other side (Figure 1.18). *N*-CzPh group was targeted since the planar structure can offer strong π-π stacking. H-bonds between carbamate (urethane)s on the other side also assisted solid-state self-assembly of diynes. Upon UV irradiation, for all the three monomers in Figure 1.18, there is an emerging UV absorption around 600 nm within minutes, which confirmed polymerization. Single-crystal XRD confirmed two monomer single crystal structures. They concluded that it is possible to polymerize diynes with one directly bonded aromatic side group and one flexible side group. A small deviation in molecular structure would lead to very different structural parameters in crystals, and very different polymerization reactivity.

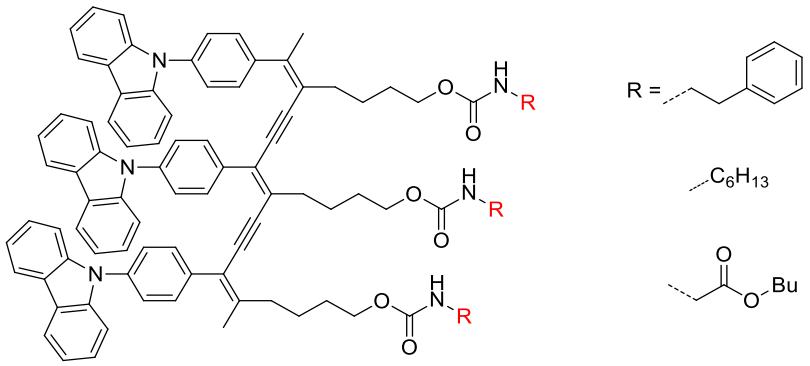

Figure 1.18 Polymerization of diynes attached by N-carbazolylphenyl groups on one side[59]

Shichao Wang and co-workers[60] reported synthesis of polymer of non-symmetric diynes substituted by *p*/*m*-nitrophenyl group on one side and ethylene hydroxide on the other side. Monomers can be aligned through the hydrogen bonds between the methylene and nitro groups (Figure 1.19). Only the *m*-nitrophenyl substituted diyne can polymerize upon UV-irradiation to form a blue PDA. UV spectroscopy, Raman spectroscopy and powder XRD confirmed the formation of polymers.

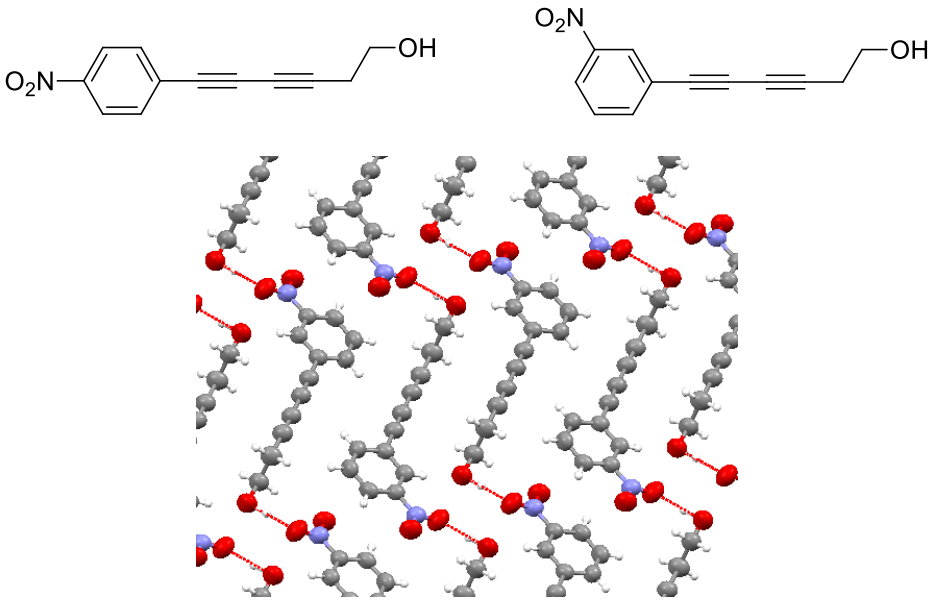

Figure 1.19 Crystal structure of *m*-nitrophenyl substituted diyne

Matsuo et al[61] reported solid-state polymerization of monomers containing two diphenylbudadiyne linked by amino groups to synthesize ladder polymers (Figure 1.20). Polymerization of the **1-12-n** series in the solid state were attempted by UV 254 nm irradiation and γ-irradiation. Monomers **1-12-2**, **1-12-3** and **1-12-4** were found polymerize. Polymerization was determined by color change into blue, UV-vis diffuse reflectance spectrum, solid-state ^{13}C NMR spectrum, and powder XRD. Solid-state ^{13}C NMR also indicated the polymer yields were approximately 45% for all three **1-12-n** monomers. Polymerization of the **1-13-n** series (Figure 1.20) was attempted by γ-

irradiation. All **1-13-n** monomers polymerized, and reached approximately 80% yields. Their results clarified that ladder polymers of two linked diynes directly bonded to aromatic groups can be synthesized experimentally. The group that links two diynes contains amide groups that can form intermolecular hydrogen bonding networks, and help organize monomers with appropriate geometry for polymerization.

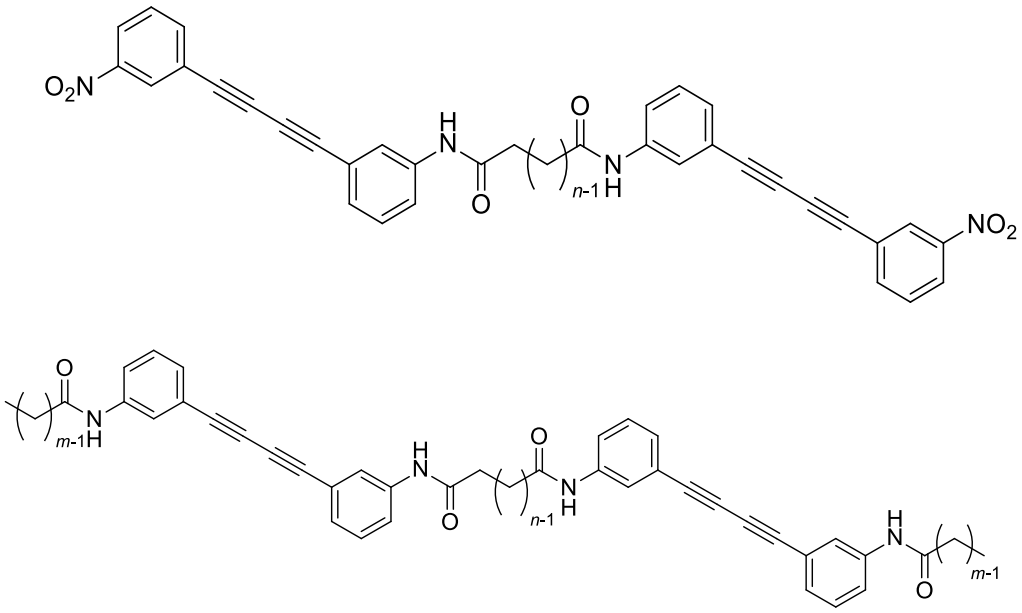

Figure 1.20 Structures of **N**-n and m**A**-n monomers[61]

The Morin group[62] reported a topochemical polymerization of a diarylbutadiyne derivative in both the gel and solid states (Figure 1.21). The phenyl attached amide helped self-assembly of diyne monomers with required structural parameters for polymerization. In gels, conformational changes during polymerization could be easier than in crystals. Therefore, they prepared diyne monomer in the gel form (10 mg/mL in toluene) and irradiated it at 254 nm for 4 h. A dark orange and then red PDA was obtained. Furthermore, they dried the monomer gel on a glass slide to be a dry film.

The film turned dark blue rapidly upon irradiation. Both UV and Raman spectroscopy confirmed the formation of PDAs. The dark blue PDA was soluble in THF, and it displayed reversible thermal induced chromatic transformation. Interestingly, if they cast a methanol solution of the monomer as a dry film, the film does not undergo polymerization upon UV irradiation.

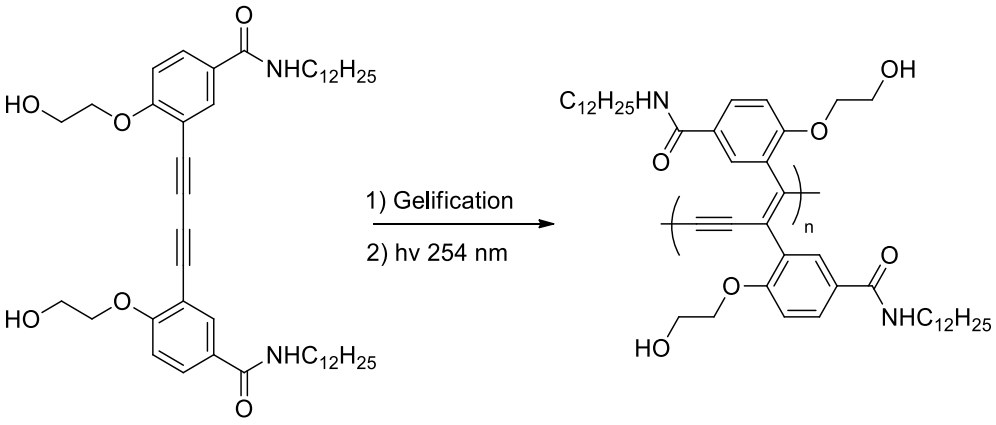

Figure 1.21 Topochemical polymerization of diarylbutadiyne derivatives[62]

Frauenrath and co-workers[63] synthesized an PDA substituted by alternating benzoate and pentafluorobenzoate groups from the co-crystal of 2,4-hexadiynylene dibenzoate and 2,4-hexadiynylene bis(pentafluorobenzoate) (Figure 1.22). The electrostatic attraction between benzoate and pentafluorobenzoate made monomers organize in an alternating way. Although the repeat distances between monomers in the co-crystal are not identical, 3.76 and 5.10 Å, as shown in Figure 1.22, UV-irradiation leads to a deep red copolymer. Single-crystal XRD confirmed that such copolymer has randomly distributed 74 % monomers and 26 % polymers, but the polymers are strictly PDAs with alternating benzoate and pentafluorobenzoate groups. Interestingly, single-crystal of 2,4-hexadiynylene dibenzoate and single-crystal of 2,4-hexadiynylene bis(pentafluorobenzoate) do not undergo topochemical polymerization.

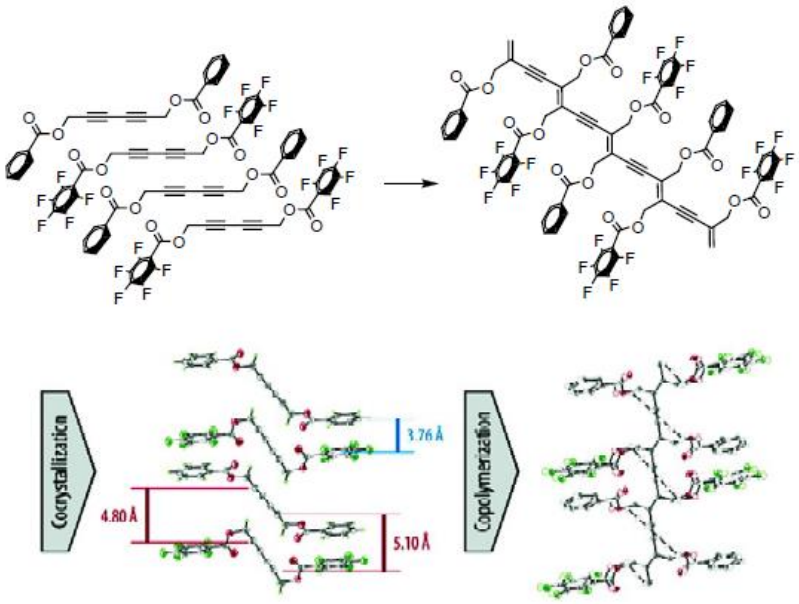

Figure 1.22 Alternating PDA co-polymers[63]

(Reprinted with permission from ref.63, Copyright 2006, American Chemical Society.)

The fluorine substituted phenyl ring can stack in a favorable way for polymerization, according to experimental results. Okada et al[64] have designed and synthesized non-symmetric diyne monomers with 2,5- and 3,5-bis(trifluoromethyl)phenyl groups as one of the capped groups, and electron donors attached phenyls as the other (Figure 1.23). Three of all the synthesized diynes (diyne **1-14**b, **1-14**c, **1-15**j) can polymerize upon γ-ray irradiation, while the others stay stable even exposed to such high energy. They propose that it is the large intermolecular polarization that makes most such non-symmetric diynes unpolymerizable. Diyne **1-15**j is found to undergo single-crystal-to-single-crystal polymerization, with a 90 % polymerization conversion. The structure of generated polymer (named poly-MADF) is determined by single-crystal XRD, where methylaminobenzne groups all align on one side of polymer backbone and bis(trifluoromethyl)benzene groups on the other. Further investigation on the third-order nonlinearity ($\chi^{(3)}$) of poly-MADF indicates that poly-

MADF has much higher $\chi^{(3)}$ than some known PDAs, e.g. *p*TS-PDA. The results confirm that PDAs with extended conjugation can reach higher $\chi^{(3)}$.[64]

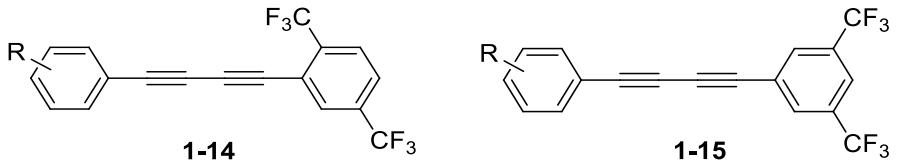

R: a= 2-CH_3O, b= 3-CH_3O, c= 4-CH_3O, d= 4-CH_3S, e= 2-NH_2, f= 3-NH_2,
g= 4-NH_2, h =$_2$-NH_2, i= 2-CH_3NH_2, j= 3-CH_3NH_2, k= 4-CH_3NH_2

Figure 1.23 Nonsymmetric diynes bearing acetylenic aromatic moieties[31]

Milburn et al[65] prepared other push-pull, and aromatic diyne derivatives for their potential as liquid crystalline and optical electronic materials.[65] Most of them showed liquid crystalline behavior upon heating (Figure 1.24) instead of solid-state polymerization.[31] Differential scanning calorimetry indicates formation of both smectic mesophase of monomers and nematic mesophase of polymers (both smectic and nematic are used to describe liquid crystals).

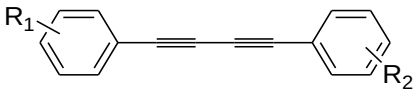

R1 = -OCH_3, OH, -$NHC_xH_{(2x+1)}$
R2 = NO_2

Figure 1.24 Nonsymmetric diynes bearing acetylenic aromatic moieties[65]

1.1.5 Host-Guest Strategy to Synthesize PDAs

Even though PDA single crystals have drawn great attention, their synthesis is limited, since most diyne monomers are not capable of organizing themselves independently into precursor structures

consistent with the prerequisites for 1,4–polymerization. Researchers have been exploring ways to arrange monomers with required geometry. Fowler and Lauher[66] proposed and developed an innovative host-guest system, where diynes are the guests. Host molecules contain urea or oxalamide functionalities (Figure 1.25) that provide a suitable spacing matching the spacing required for preparing diynes for 1,4- polymerization.

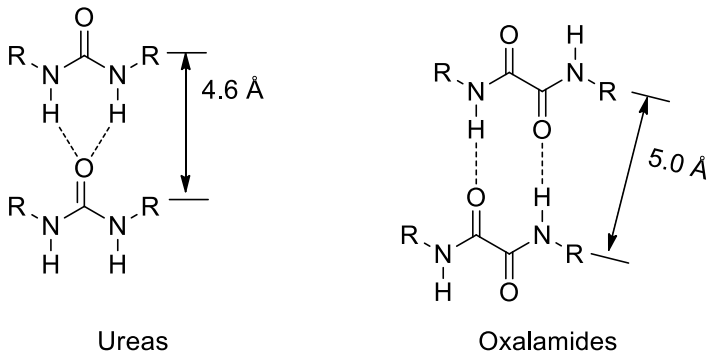

Figure 1.25 Repeat distance provided by hydrogen-bonding network[66]

Host and guest molecules are able to assemble through Lewis acid-base interaction, so that the repeat distance between hosts can be inherited by guest diynes. Early developed hosts and guests interact through relatively strong hydrogen bonds between carboxylic acid and pyridine groups (Figure 1.26),[67] and the appropriate organization of host-guest macromolecular assembly leads to PDA single crystals successfully. Single crystal XRD determines the structure and helps fundamental understanding of intermolecular interactions. Employing this host-guest strategy, various polydicatylenes and polytriacetylenes have been synthesized as promising candidates for functional materials.

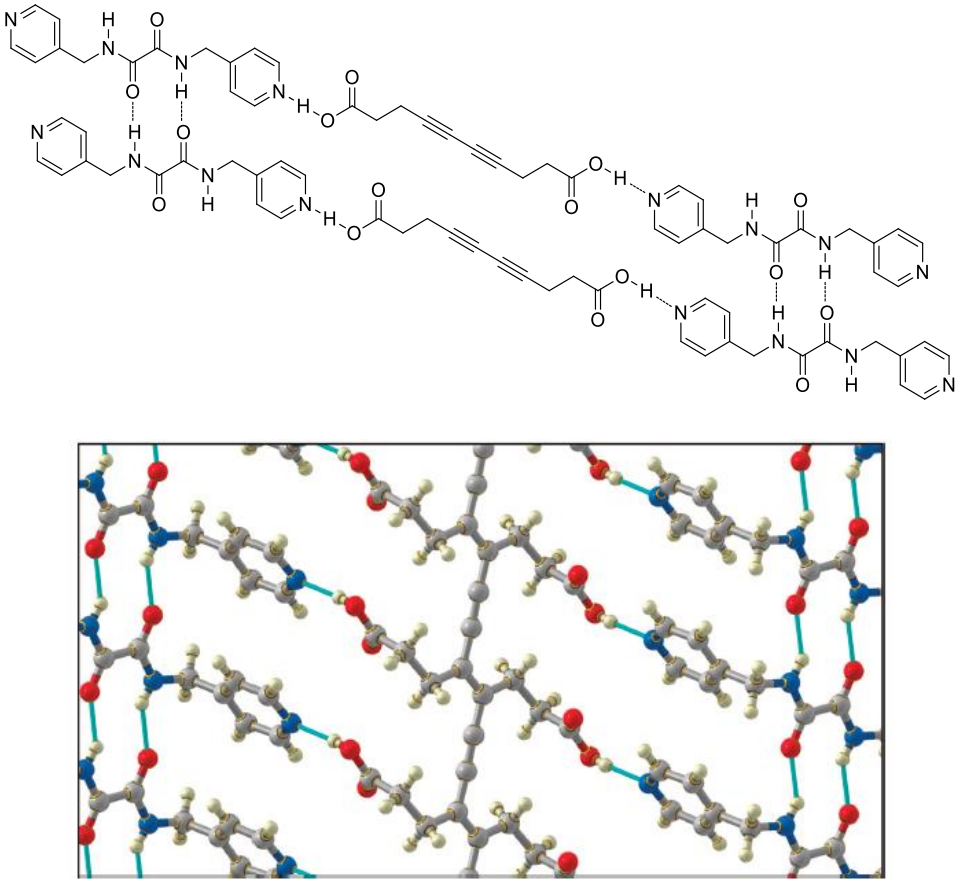

Figure 1.26 A designed single-crystal-to-single-crystal polymerization[67]

(Reprinted with permission from ref.67, Copyright 2008, American Chemical Society.)

In 2005, Curtis, Lee, Fowler, and Lauher[58] reported their work on polymerization of dipyridinyldiynes (Figure 1.27), where pyridines directly bonded to PDA backbones. Turning the acetylenic aromatic pyridine requires high energy during the polymerization, so the 4,4′-dipyridinyldiyne only polymerize under UV irradiation in the co-crystal. The synthesized polymer is soluble in acidic aqueous solution, and Raman showed instinct peaks belong to PDAs.

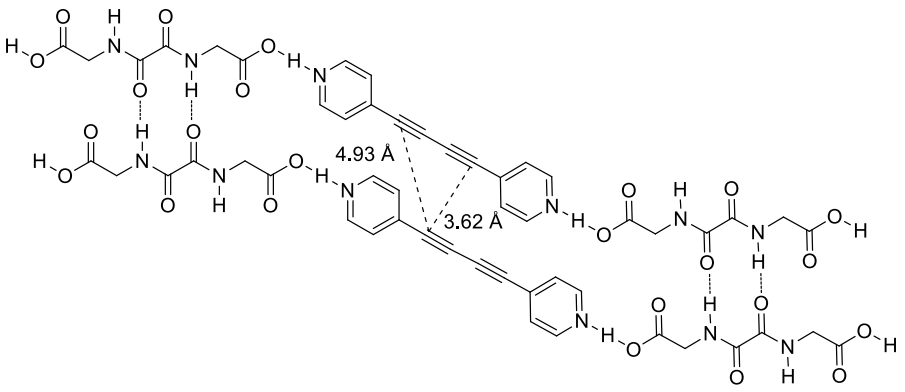

Figure 1.27 Co-crystal structure of dipyridinyldiyne and bis(carboxylic acid)oxalamide host[58]

In 2008, Li, Fowler, and Lauher[68] reported the first single-crystal structure of poly(terminal aryldiyne), successfully prepared from the single crystal of an organic salt containing a dicarboxylic acid host and a terminal aryldiyne guest (Figure 1.28). The topochemical polymerization goes to completion when heating the co-crystal at over 100 ℃ for more than two weeks. It is the first example of using an anion host to organize a cationic guest. It is also the first single crystal of poly(arylacetylene), which experimentally declares preparing single crystals of PDAs directly attached by aromatic groups can be achieved through the host-guest strategy.

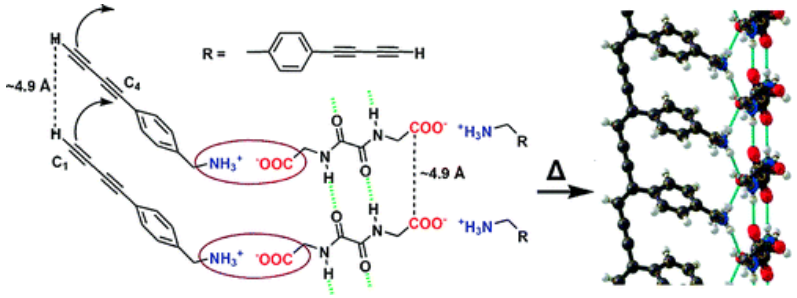

Figure 1.28 Thermially polymerized poly(aryldiacetylene) single crystal[68]

(Reprinted with permission from ref. 68, Copyright 2009, American Chemical Society.)

Our group has previously prepared poly(diiododiacetylene) (PIDA)[69] through the host-guest strategy, which is indeed a breakthrough of synthesizing PDA with only iodine-atom substituents. Figure 1.29a, b show the co-crystal composed of diiodobutadiyne **1-6** and bis(nitrile) oxalamide host **1-7** (Figure 1.30). Through the Lewis acid-base interaction between iodines and nitrile/carbonyl groups, diyne **1-6** is organized with required geometry for polymerization in blue co-crystal (Figure 1.29b). Upon natural light for two to three days, the blue monomer co-crystal turns to golden polymer co-crystal, as shown in Figure 1.29c.

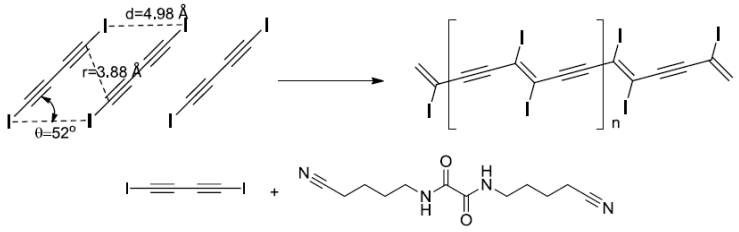

(a)

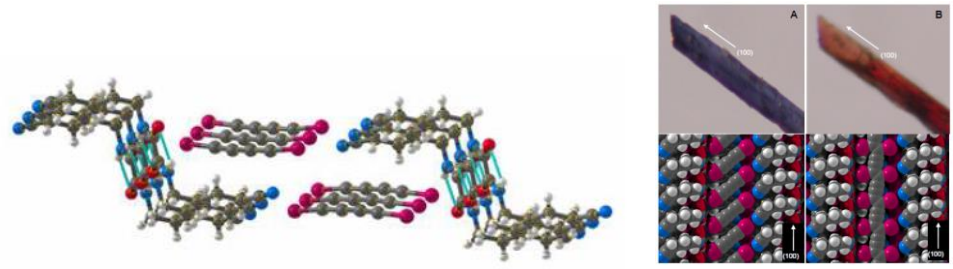

(b) (c)

Figure 1.29 Crystal structure of diiodobutadiyne co-crystal and PIDA co-crystal[69-70]

((c) Reprinted with permission from ref. 70, Copyright 2008, American Chemical Society.
(b) Reprinted with permission from ref.69, Copyright 2006, The American Association for the Advancement of Science.)

According to Heeger, McDiaramid, and Shirakawa's discovery[71] that halogen doping can enhance conductivity of PDAs significantly, the PIDA prepared in our group may have an extraordinary potential as an organic conductor. In addition, the reactive halogens on PIDA make it a practical

precursor for further functionalization. Since the capped iodine is Lewis acidic, all introduced host molecules contain Lewis basic side groups with oxalamide functionalities (Figure 1.30). Co-crystals **1-6:1-7**, **1-6:1-8**, and **1-6:1-11** exhibit spontaneous topochemical polymerization of **1-6** to afford PIDA, while the pyridine-included co-crystals (**1-6:1-9**, **1-6:1-10**) requires above 3 GPa of external pressure to overcome energy barrier for rearrangements to give desired PIDA.[54] Further functionalization of PIDA in our group is on progress for applications. Besides, synthesis of analogous polymers is also been explored.

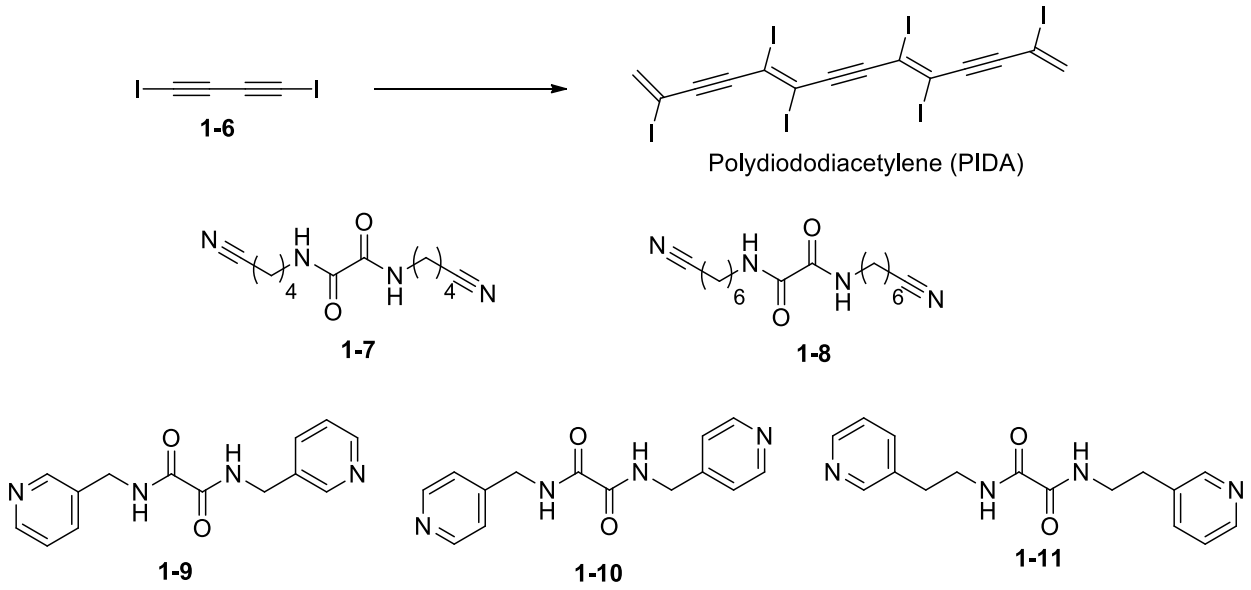

Figure 1.30 Diiodobutadiyne and host molecules[69]

1.2 Introduction to CIGS Thin-Film Solar Cells

1.2.1 History of CIGS Solar Cells

Photovoltaic (PV) technologies have experienced a significant improvement since photovoltaic effect was first observed by A.E. Becquerel in 1839.[72] The solar cell is one of the most promising approaches to convert sunlight into electricity efficiently, providing sustainable energy. The very

first silicon-based photovoltaic device was produced by Russell Ohl of Bell Laboratories in 1941.[73] Crystalline silicon heterojunction solar cells have reached 25% power conversion efficiency (PCE).[74] However, although significantly improved, the commercialization of silicon-based solar cells is still limited by their high expense. Organic polymers have therefore been explored extensively to be promising alternative candidates for their low cost, flexibility, light weight, and large-area manufacturing compatibility. The general low PCE of organic solar cells remains a main challenge. Although novel low band-gap polymers have been developed, and multiple junction architectures can widen the absorption spectrum, the highest PCE so far (10 – 11 %) is much lower than that of inorganic solar cells.

The polycrystalline $Cu(In_x, Ga_{1-x})(S_ySe_{1-y})_2$, (CIGS) based solar cells have drawn great interest as low-cost cells that can yield comparable PCEs to that of Si-based cells. The first chalcopyrite-based solar cell was reported in 1974[75] by the Bell Telephone Laboratory. It was composed of a $CuInSe_2$/CdS *p-n* heterojunction. The cell has a spectra response across a wide-band. $CuInSe_2$ has a band-gap of 1.04 eV. Adding Ga to partially replace In can increase the band gap to be 1.1 - 1.2 eV, which resulted in high-efficiency devices. Sulfur is another element that can modify the band gap.[76] Therefore, $CuInSe_2$ was developed to a polycrystalline thin film of the more general composition, $Cu(In,Ga)(S,Se)_2$. The wide tunable range of band gaps from 1.0 eV for $CuInSe_2$ to 2.4 eV for $CuGaS_2$ is a great advantage of CIGS-based photovoltaic cells.

The typical architecture of CIGS-based device was first described in 1985.[77] The combination of a *p*-type CIGS absorption layer and a wide-gap *n*-type window layer has been retained. Typically, a CIGS cell is composed of Mo back contact on glass, *p*-type CIGS absorber, CdS or other n-type

buffer layer, undoped ZnO, *n*-type transparent conductor (Doped ZnO or In_2O_3), metal grid, antireflection coating, and an additional glass layer to protect the cell (Figure 1.31). In 2011, CIGS cells deposited on a rigid glass substrate were recorded reaching 20% efficiency.[78] In 2013, small area CIGS cells on flexible polyimide film were reported reaching 20.4% PCE[79]. These milestone results demonstrated CIGS cells are remarkably competitive comparing to Si-based cells.[80]

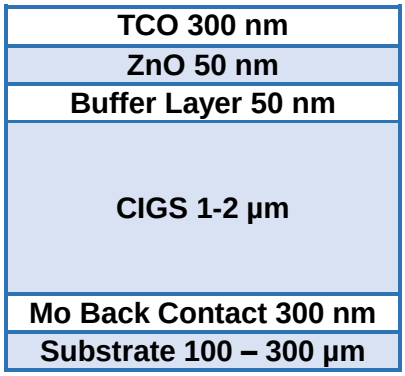

Figure 1.31 A typical architecture of CIGS-based solar cell[81]

1.2.2 Working Principles of Solar Cell

A solar cell is essentially a semi-conductive diode, including both *p*-type layer and *n*-type layer (Figure 1.32). Upon external energy (electric field, light, heat, etc.), *p*-layer can be positively charged, with electrons diffusing to the *n*-layer (Figure 1.32a). If there is an external circuit, current starts flowing (short-circuit current (I_{sc})). As the *p*-layer becomes more positive, and *n*-layer more negative, a built-in electric field (Figure 1.32b) is established and enhanced gradually near the interface. Electrons therefore have to overcome this built-in field to flow from *p*-layer to *n*-layer. When the external circuit is cut, a voltage (positive on *n*-type side, negative on *p*-type side) across the cell is caused by the flow of electrons from p-layer to n-layer. This voltage is called "open-

circuit voltage (V_{oc})". There are two key operations of solar cells, photogeneration and charge separation,[82] which will be discussed in detail.

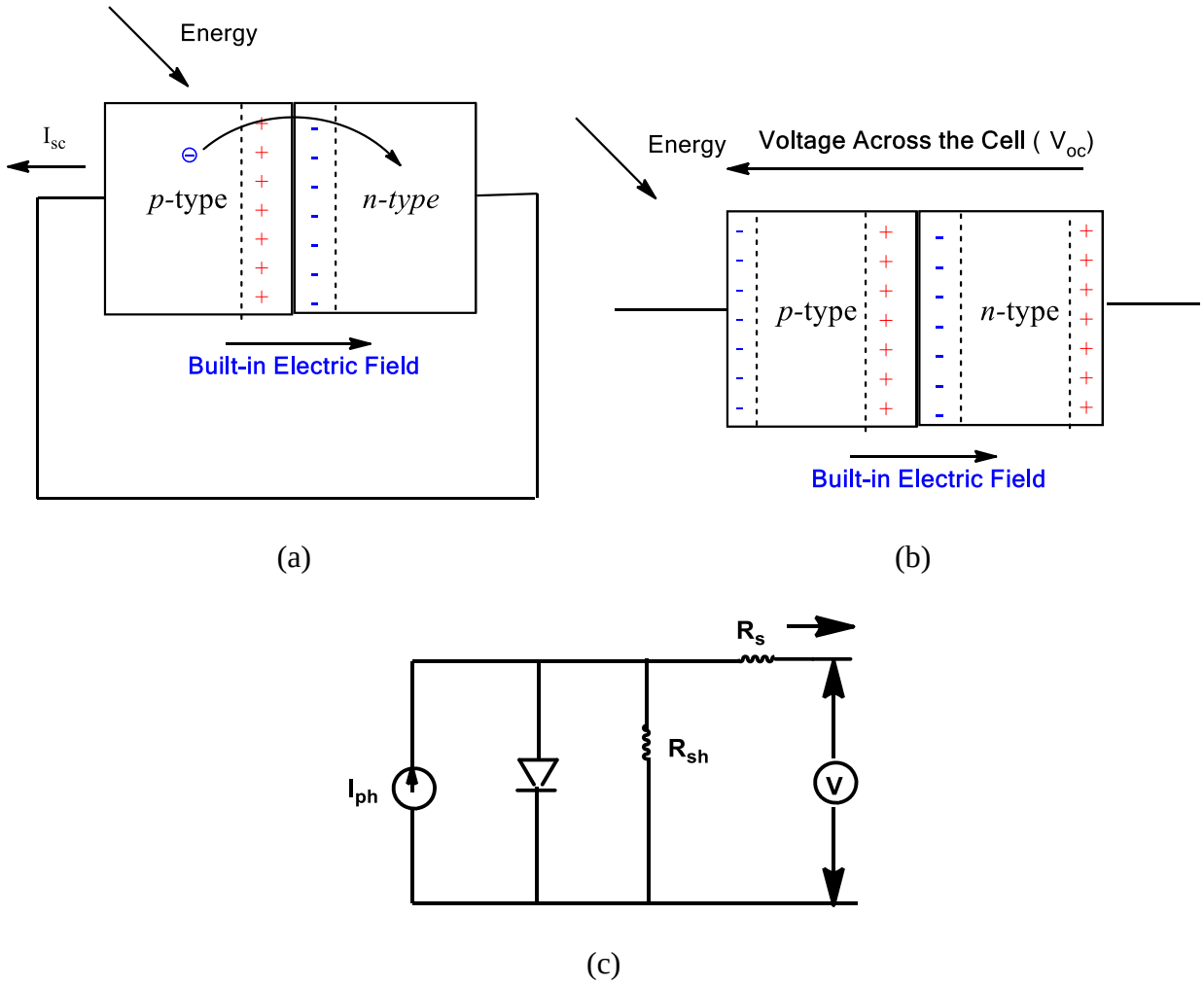

Figure 1.32 (a) short circuit current (I_{sc});[83] (b) open-circuit voltage (V_{oc});[83] (c) Simple equivalent circuit model for conventional *p*-*n* junction solar cells[84]

Photogeneration. The active layer in PV cells should be able to absorb incoming photons and convert them into electron-hole pairs (Figure 1.33). In this step, the energy band gap (E_g) of the active layer predominates. In theory, photons with energy $h\nu < E_g$ do not contribute to

photogeneration at all, while photons with energy hν > E_g will generate electron-hole pairs and thermalize the excess energy (hν - E_g). When E_g decreases, more photons with energy hν > E_g can be absorbed, resulting in increasing maximum photogenerated electric current density J_{ph}. On the other hand, When E_g increases, the net energy transferred to each electron-hole pair, which equals to E_g, increases. To reach an optimal balance, there exists a theoretical optimum E_g = 1.1 eV of sunlight absorption layer where "a maximum of energy can be transferred from the incident sunlight to the totality of photogenerated electron-hole pair".[82]

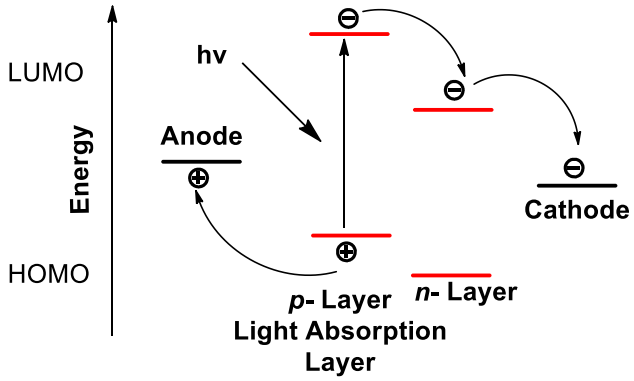

Figure 1.33 Working principle of photovoltaic cells

Charge Separation. Every photo-generated electron corresponds to one carrier generated. These electrons and carriers can only remain excited for a very short period of time. If electrons and carriers cannot separate and transport effectively, they would recombine with their electrical energy lost thermally. External circuit is able to be generated only when the photogenerated electron-hole pairs are separated effectively, with electrons and carriers drifting to respective electrodes. If there is too much recombination in the bulk or on the interface, the solar cell will not work well.

As shown in Figure 1.34, in the dark (nonilluminated, no photogenerated current, and no recombination), a PV cell has a semiconductor diode behavior, as mentioned. Upon illumination, IV curve can be superimposed by the diode IV characteristics in the dark. The short circuit (I_{sc}) is the starting point to generate power in an external load. The open-circuit voltage (V_{oc}) is the maximum voltage a PV cell can provide to the external load. I_{sc} depends critically on charge separation and transport in the photon-active layer, and V_{oc} depends on the difference between the HOMO of *p*-layer and the LUMO of *n*-layer as well as electrode work functions. Since $P = IV$, the maximum power can be calculated at the P_{max} point, where the fill factor FF = P_{max} / ($I_{sc} \times V_{oc}$). I_{sc}, V_{oc} and FF are the three key parameters to characterize solar cell performance. Calculation of the theoretical maximum efficiencies obtainable with an ideal band gap taking detailed balance into consideration was first presented by Shockley and Queisser.[85] Their calculation indicated a maximum efficiency of 30.5 %, when the light absorption material has a band gap of 1.35 eV and is illuminated by a black body radiation of 6000 K. Though the same calculation method, they generate another maximum efficiency of 33 %, when the light absorption material has a band gap of 1.35 eV and is illuminated by a sunlight simulator (AM 1.5 spectrum).[86]

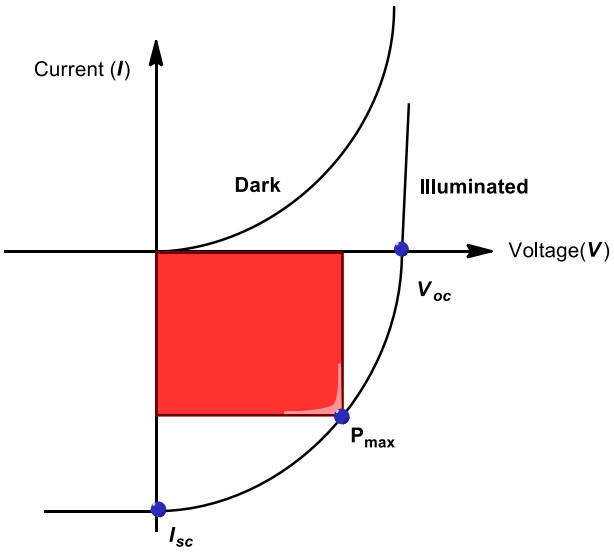

Figure 1.34 IV-characteristic of a solar cell[82]

1.2.3 Bottle Necks of CIGS Cell

CIGS-based thin-film *p*-*n* junction photovoltaic cells benefit from light absorption in the *p*-type CIGS region, and electron-hole separation assisted by *n*-type ZnO. CIGS cells with n-type ZnO directly deposited on top do not give high efficiency. A CdS layer placed in between can generate a favorable energy band alignment to CIGS and to ZnO. Therefore it facilitates efficient charge separation and collection. Furthermore, a CdS buffer layer covers the polycrystalline CIGS absorber surface, protecting it against damage or chemical reactions during the subsequent ZnO deposition process. In addition to all the advantages, CdS has several disadvantages such as reducing the spectrum absorption in the active layer in the blue region because of low E_g = 2.4 eV , as well as causing environmental contamination.[87]

The major limits of materials that prevent PCE of CIGS from reaching the SQ limit 33% include the following aspects: 1) Optical and charge-collection loss in both the transparent conductor ZnO

and CdS buffer layers costs 5%; 2) Interfacial recombination at the CdS/CIGS heterojunction and bulk recombination within the space-charge region in CIGS cost 7.4% loss in efficiency. Because inorganic sub-layer materials have inflexible properties that are difficult to optimize, novel architectures of devices composed of different sub-layer materials have become essential for a breakthrough.

1.2.4 Hole-Blocking Layer (HBL)

As mentioned, an external circuit can be generated only when photogenerated electron-hole pairs are separated effectively with electrons and carriers drifting to respective electrodes, an external circuit is able to be generated. To minimize charges recombination, a HBL is therefore proposed between the active layers and the cathode. The LUMO of the HBL has to match that of the optically active layer, which allows electrons drifting through, while the HOMO has to be at least 3.5 eV lower than the LUMO to block carriers (Figure 1.35). Furthermore, a HBL material should be transparent across visible spectrum to minimize optical loss; as well as easily deposited, thermally stable and electronically tunable.

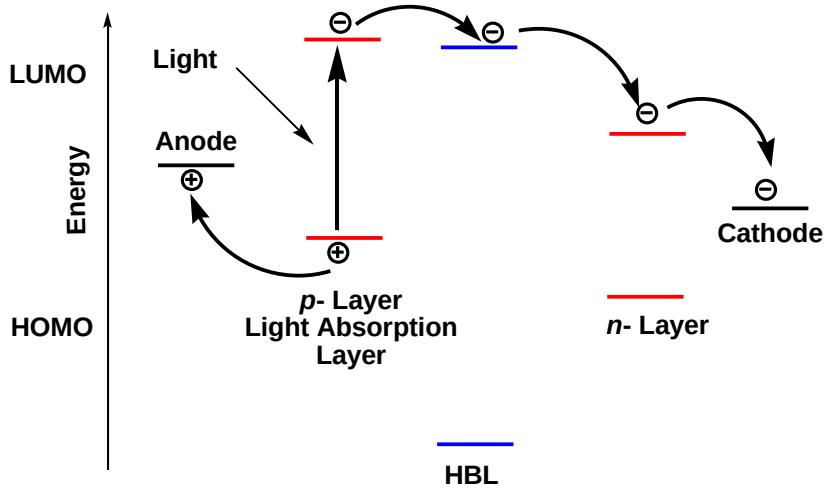

Figure 1.35 Role of hole-blocking layer in solar cells

The idea of HBL originates from electrode buffer layers, which were initially established for organic light-emitting diodes (OLEDs) and later employed in organic solar cells. Electrode buffer layers includes cathode buffer layer (CBL) and anode buffer layer (ABL). They can reduce the energy barrier between the photoactive layer and the electrode, form a good electrical contact within the device, and therefore improve the charge collections on electrodes.[88] CBL materials, including HBL, can provide an ohmic contact between anode and acceptor layer, help transport electrons, and block carriers. Zinc oxide (ZnO),[89] titanium oxide (TiOx),[90] transition metal oxides,[91] cesium carbonate(Cs_2CO_3),[92] and aluminum oxide (Al_2O_3) are frequently used inorganic buffer layer materials.

The Forrest group[93] is the first to use bathocuproine (BCP) (Figure 1.36) as organic HBL in a CuPc/ PTCBI (3,4,9,10-perylenetetracarboxylic-bis-benzimidazole) bilayer organic PV cell. The LUMO of BCP is measured −3.5 eV, matching the LUMO of CuPc to transport electrons. The HUMO of BCP is −7.0 eV, low enough to prevent carriers getting though. The 3.5 eV energy band-gap is large enough to make it transparent across the visible spectrum. The Forrest group[93]

also demonstrated that if the BCP HBL was omitted, the PV cell photocurrent response was significantly reduced, indicating that the BCP layer prevents carrier diffusion to and subsequent quenching at the cathode/organic interface.

There has been extensive research on the functions of BCP in organic PV cells. The Fostiropoulos group[94] reported studies of the function of BCP in ITO/CuPc(ZnPc)/C_{60}/BCP/Al organic photovoltaic cells. It was demonstrated that in the *p*-*n* bilayer-based cell, diffusion of Aluminum during deposition into the *n*-type C_{60} layer causes interface exciton combination. A BCP buffer layer in between can block the diffusion, as well as establish an Ohmic contact between Al and C_{60} which result in more efficient electron transport from C_{60} to Al. In addition, BCP also acts as an optical spacer, which redistributes the light intensity in the whole device. It reduces the cancellation between the incident light and the back-reflected light in the photo-active layer near the electrode, and can result in more excitons.[95] Overall, a cell with BCP displayed ~70% higher short circuit current intensity than that without BCP.

Although BCP has become a popular and commercially available HBL material, it easily crystallizes in the presence of moisture, which makes the electronic properties unstable in the long term. Therefore, new HBL materials have been investigated. In 2006, the Lee group[96] explored bathophenanthroline (BPhen)(**1-13**) (Figure 1.36) as a HBL in standard CuPc/C_{60} PV cell. The HOMO (−6.4 eV) and LUMO (−2.9 eV) of BPhen are similar to those of BCP. Significantly, the electron transporting ability of BPhen (~ 10^{-4} cm^2/Vs)[97] is two orders of magnitude higher than that of BCP. The BPhen-based devices presented a 45% increase in PCE over that of an equivalent device with a BCP HBL.

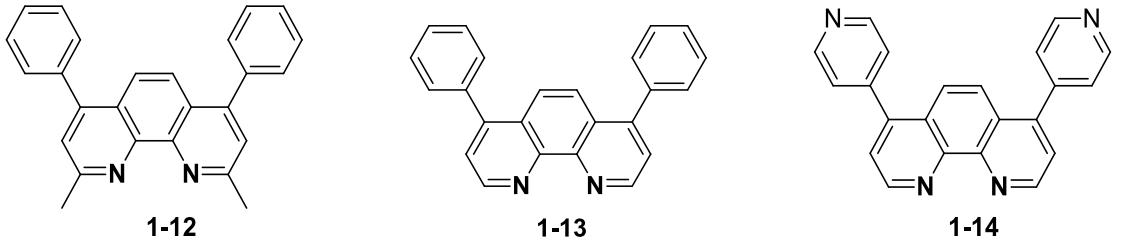

Figure 1.36 Structures of BCP (**1-12**), BPhen (**1-13**) and DMPP (**1-14**)

In 2013, the Mullen group[98] introduced a new HBL material, 2,9-dimethyl-4,7-di(pyridine-4-yl)-1,10-phenanthroline (DMPP) (**1-14**) (Figure 1.36). They demonstrated that the LUMO and HOMO levels of DMPP are both slightly lower than those of BPhen, because pyridine is an electron withdrawing group. The E_g is identical to the E_g of BCP, which is 3.5 eV, large enough to block carriers and be transparent across the visible spectrum. On the other hand, the low HOMO energy level of BPhen could better prevent carriers drifting to the cathode. The ZnPc: C_{60} solar cell has a PCE of 3.5 % including DMPP as the HBL, which is comparable to the PCE of 3.1% including BPhen as the HBL.

In addition to 1,10-phenanthroline derivatives described above, 1,3,5-tris(N-phenylbenzimidazol-2-yl)benzene (TPBi) and tris-8-hydroxy-quinolinato aluminum (Alq3) were also investigated as HBL materials (Figure 1.37).[99] Alq3 was first used by Tang and VanSlyke.[100] It has been a popular electron transport material in electroluminescent diodes. However, the LUMO of Alq3 is not as low as that of BCP, and the electron mobility of Alq3 is much lower (1×10^{-6} – 1×10^{-7} $cm^2\ V^{-1}\ s^{-1}$) than that of BCP (~10^{-4} $cm^2\ V^{-1}\ s^{-1}$).[101] Therefore, the hole-blocking capacity of Alq3 is limited. As to TPBi, it is significantly more expensive than BCP, and it forms

crystals over time, similar to BCP.[101] Therefore, BCP remains one of the most popular HBL materials.

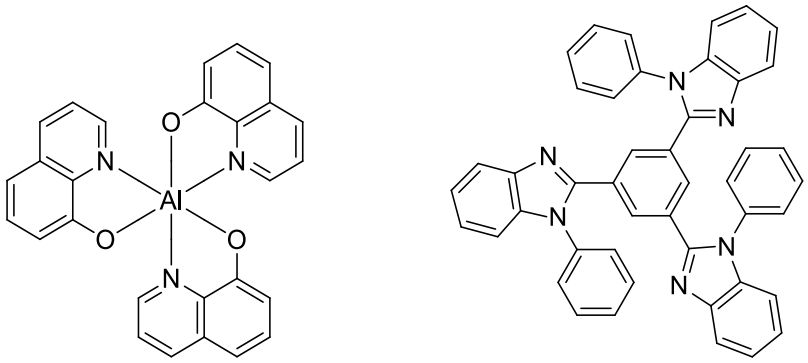

Figure 1.37 Structure of Alq3 and TPBi

1.3 Purpose and Organization of this Thesis

This dissertation particularly focuses on developing novel conjugated materials. This thesis is composed of two main projects. The second project is in Chapter 4, which describes developing small organic molecules as the HBL material to optimize a modified polycrystalline $Cu(In_x, Ga_{1-x})(S_ySe_{1-y})_2$, (CIGS), based thin-film solar cell.

In chapter 2 we describes attempts to prepare push-pull PDAs, substituted by alternating electron rich and poor groups. The push-pull PDAs are attractive for their properties in theory, but they are very difficult to make, essentially due to the poor self-organization ability of monomers. We explains the design of novel push-pull diynes as the monomers of push-pull PDAs. Synthetic details of all synthesized diynes were described. We employed a "host-guest" strategy to pre-organize synthesized diynes, where the push-pull diynes work as the guest and an oxalamide based molecules as the host. We proposed to pre-organize diynes in a co-crystal scaffold formed by host with appropriate repeat distance and angle for polymerization in an ordered way. We successfully

obtain one co-crystal. The structure has been determined by single crystal XRD. The geometry of diyne monomers in the co-crystal is analyzed in detail.

In chapter 3 we briefly present follow up characterization experiments regarding to the diiodooctatetrayne and bis(pyridyl) oxalamide co-crystal, whose preparation was mainly accomplished by Alison Black, one of our previous group members.

In chapter 4, we describe a collaboration with the Eisaman group in the Sustainable Energy Department in Brookhaven National Lab and the Kimissis group in Columbia University, focusing on developing new organic small molecules as HBL materials in CIGS-based thin-film solar cells. The design of 1,7-phenanthroline derivatives as HBL materials is explained. Synthetic details of 1,7-phenanthroline derivatives are described. Upon all characterizations described in chapter 4, 2,8-dimethyl-1,7-phenanthroline **4-1** is targeted as the most promising HBL material among all the synthesized compounds for having appropriate optical and electronic properties, and powdery morphology. According to the best results among all our measurements, including phenanthroline 4-1 as the HBL can improve the power conversion efficiency of both the organic photovoltaic device and the CIGS-based device significantly. To further expand the scope of organic small molecules that can work as HBL materials, we also discuss synthesis and properties of 2,4-diphenylquinoline derivatives. In this work, we developed the HBL application of known materials that potentially have the required properties, but were never used as the HBL materials.

References:

1. Chernick, E. T.; Tykwinski, R. R., Carbon-rich nanostructures: the conversion of acetylenes into materials. *J. Phys. Org. Chem.* **2013,** *26* (9), 742-749.
2. Kroto, H. W.; Heath, J. R.; O'Brien, S. C.; Curl, R. F.; Smalley, R. E., C_{60}: buckminsterfullerene. *Nature* **1985,** *318* (6042), 162-163.
3. De Volder, M. F. L.; Tawfick, S. H.; Baughman, R. H.; Hart, A. J., Carbon nanotubes: present and future commercial applications. *Science* **2013,** *339* (6119), 535-539.
4. Gao, P.; Li, A. R.; Tai, M. H.; Liu, Z. Y.; Sun, D. D., A Hierarchical Nanostructured Carbon Nanofiber–In2S3 Photocatalyst with High Photodegradation and Disinfection Abilities Under Visible Light. *Chem. Asian. J.* **2014,** *9* (6), 1663-1670.
5. Novoselov, K., Nobel lecture: Graphene: Materials in the flatland. *Rev. Mod. Phys.* **2011,** *83* (3), 837.
6. McNeill, R.; Siudak, R.; Wardlaw, J.; Weiss, D., Electronic conduction in polymers. I. The chemical structure of polypyrrole. *Aust. J. Chem.* **1963,** *16* (6), 1056-1075.
7. (a) Bolto, B. A.; McNeill, R.; Weiss, D., Electronic conduction in polymers. III. Electronic properties of polypyrrole. *Aust. J. Chem.* **1963,** *16* (6), 1090-1103; (b) Bolto, B. A.; Weiss, D., Electronic conduction in polymers. II. electrochemical reduction of polypyrrole at controlled potential. *Aust. J. Chem.* **1963,** *16* (6), 1076-&.
8. Shirakawa, H.; Louis, E. J.; MacDiarmid, A. G.; Chiang, C. K.; Heeger, A. J., Synthesis of electrically conducting organic polymers: halogen derivatives of polyacetylene,$(CH)_x$. *J. Chem. Soc., Chem. Commun.* **1977,** (16), 578-580.
9. Nobelprize.org. Nobel Media AB. The Nobel Prize in Chemistry 2000. http://www.nobelprize.org/nobel_prizes/chemistry/laureates/2000/ (accessed Dec. 9, 2015).
10. (a) Günes, S.; Neugebauer, H.; Sariciftci, N. S., Conjugated polymer-based organic solar cells. *Chem. Rev.* **2007,** *107* (4), 1324-1338; (b) Hauch, J. A.; Schilinsky, P.; Choulis, S. A.; Childers, R.; Biele, M.; Brabec, C. J., Flexible organic P3HT:PCBM bulk-heterojunction modules with more than 1 year outdoor lifetime. *Sol. Energ. Mat. Sol. C.* **2008,** *92* (7), 727-731.
11. Ajayaghosh, A., Donor–acceptor type low band gap polymers: polysquaraines and related systems. *Chem. Soc. Rev.* **2003,** *32* (4), 181-191.
12. (a) Chen, Z.; Cai, P.; Chen, J.; Liu, X.; Zhang, L.; Lan, L.; Peng, J.; Ma, Y.; Cao, Y., Low band-Gap conjugated polymers with strong interchain aggregation and very high hole mobility towards highly efficient thick-film polymer solar cells. *Adv. Mater.* **2014,** *26* (16), 2586-2591; (b) Steckler, T. T.; Henriksson, P.; Mollinger, S.; Lundin, A.; Salleo, A.; Andersson, M. R., Very low band gap thiadiazoloquinoxaline donor–acceptor polymers as multi-tool conjugated polymers. *J. Am. Chem. Soc.* **2014,** *136* (4), 1190-1193; (c) Lei, T.; Dou, J.-H.; Ma, Z.-J.; Yao, C.-H.; Liu, C.-J.; Wang, J.-Y.; Pei, J., Ambipolar polymer field-effect transistors based on fluorinated isoindigo: high performance and improved ambient stability. *J. Am. Chem. Soc.* **2012,** *134* (49), 20025-20028.
13. You, J.; Dou, L.; Yoshimura, K.; Kato, T.; Ohya, K.; Moriarty, T.; Emery, K.; Chen, C.-C.; Gao, J.; Li, G., A polymer tandem solar cell with 10.6% power conversion efficiency. *Nature Commun.* **2013,** *4*, 1446.

14. Ryu, T. I.; Yoon, Y.; Kim, J.-H.; Hwang, D.-H.; Ko, M. J.; Lee, D.-K.; Kim, J. Y.; Kim, H.; Park, N.-G.; Kim, B.; Son, H. J., Simultaneous enhancement of solar cell efficiency and photostability via chemical tuning of electron donating units in diketopyrrolopyrrole-based push–pull type polymers. *Macromolecules* **2014,** *47* (18), 6270-6280.
15. Wegner, G., Topochemical reactions of monomers with conjugated triple bonds. I. Polymerization of 2.4-hexadiyn-1.6-diols deivatives in crystalline state. *Z. Naturforsch. B.* **1969,** (7), 824-&.
16. Jelinek, R.; Ritenberg, M., Polydiacetylenes–recent molecular advances and applications. *RSC Adv.* **2013,** *3* (44), 21192-21201.
17. Lee, D.-C.; Sahoo, S. K.; Cholli, A. L.; Sandman, D. J., Structural aspects of the thermochromic transition in urethane-substituted polydiacetylenes. *Macromolecules* **2002,** *35* (11), 4347-4355.
18. Schott, M., The colors of polydiacetylenes: a commentary. *J. Phys. Chem. B* **2006,** *110* (32), 15864-15868.
19. Lee, J. S. Molecular design and self-assembly of polydiacetylene for biosensors and sensor arrays. The University of Michigan, 2011.
20. (a) Ngampeungpis, W.; Tumcharern, G.; Pienpinijtham, P.; Sukwattanasinitt, M., Colorimetric UV sensors with tunable sensitivity from diacetylenes. *Dyes. Pigments.* **2014,** *101* (0), 103-108; (b) Ramakers, B. E. I.; Bode, S. A.; Killaars, A. R.; Hest, J. C. M. v.; Löwik, D. W. P. M., Sensing cell adhesion using polydiacetylene-containing peptide amphiphile fibres. *J. Mater. Chem. B* **2015**; (c) Samyn, P.; Shroff, K.; Prucker, O.; Rühe, J.; Biesalski, M., Fluorescent sensibility of microarrays through functionalized adhesive polydiacetylene vesicles. *Sensor. Actuat. A: Phys.* **2014,** *214* (0), 45-57.
21. (a) Yoon, J.; Chae, S. K.; Kim, J.-M., Colorimetric sensors for volatile organic compounds (VOCs) based on conjugated polymer-embedded electrospun fibers. *J. Am. Chem. Soc.* **2007,** *129* (11), 3038-3039; (b) Yoon, J.; Jung, Y.-S.; Kim, J.-M., A combinatorial approach for colorimetric differentiation of organic solvents based on conjugated polymer-embedded electrospun fibers. *Adv. Funct. Mater.* **2009,** *19* (2), 209-214.
22. Yoon, B.; Ham, D. Y.; Yarimaga, O.; An, H.; Lee, C. W.; Kim, J. M., Inkjet printing of conjugated polymer precursors on paper substrates for colorimetric sensing and flexible electrothermochromic display. *Adv. Mater.* **2011,** *23* (46), 5492-5497.
23. (a) Kolusheva, S.; Zadmard, R.; Schrader, T.; Jelinek, R., Color fingerprinting of proteins by calixarenes embedded in lipid/polydiacetylene vesicles. *J. Am. Chem. Soc.* **2006,** *128* (41), 13592-13598; (b) Kim, J.-M.; Lee, Y. B.; Yang, D. H.; Lee, J.-S.; Lee, G. S.; Ahn, D. J., A polydiacetylene-based fluorescent sensor chip. *J. Am. Chem. Soc.* **2005,** *127* (50), 17580-17581.
24. Kwon, I. K.; Kim, J. P.; Sim, S. J., Enhancement of sensitivity using hybrid stimulus for the diagnosis of prostate cancer based on polydiacetylene (PDA) supramolecules. *Biosens. Bioelectron.* **2010,** *26* (4), 1548-1553.
25. *Nonlinear optical materials*. American Chemical Society: 1991; Vol. 455, p 128.
26. Bredas, J. L.; Adant, C.; Tackx, P.; Persoons, A.; Pierce, B. M., Third-order nonlinear optical response in organic materials: theoretical and experimental aspects. *Chem. Rev.* **1994,** *94* (1), 243-278.
27. Rentzepis, P.; Pao, Y. H., Laser-induced optical second-harmonic generation in organic crystals. *Appl. Phys. Lett.* **1964,** *5* (8), 156-158.

28. Ray, P. C., Size and shape dependent second order nonlinear optical properties of nanomaterials and their application in biological and chemical sensing. *Chem. Rev.* **2010,** *110* (9), 5332-5365.
29. (a) Hermann, J. P.; Ricard, D.; Ducuing, J., Optical nonlinearities in conjugated systems: β - carotene. *App.Phys. Lett.* **1973,** *23* (4), 178-180; (b) Bramley, R.; Le Fevre, R., 11. Molecular polarisability: phenylpolyenals and diphenylpolyene ketones. *J. Chem. Soc. (Resumed)* **1962**, 56-63.
30. Sauteret, C.; Hermann, J. P.; Frey, R.; Pradère, F.; Ducuing, J.; Baughman, R. H.; Chance, R. R., Optical nonlinearities in one-dimensional-conjugated polymer crystals. *Phys. Rev. Lett.* **1976,** *36* (16), 956-959.
31. Sarkar, A.; Okada, S.; Matsuzawa, H.; Matsuda, H.; Nakanishi, H., Novel polydiacetylenes for optical materials: beyond the conventional polydiacetylenes. *J. Mater. Chem.* **2000,** *10* (4), 819-828.
32. Kolinsky, P., New materials and their characterization for photonic device applications. *Opt. Eng.* **1992,** *31* (8), 1676-1684.
33. Okada, S.; Hayamizu, K.; Matsuda, H.; Masaki, A.; Nakanishi, H., Structures of the polymers obtained by the solid-state polymerization of diyne, triyne, and tetrayne with long-alkyl substituents. *Bull. Chem. Soc. Jpn.* **1991,** *64* (3), 857-863.
34. (a) Matsuzawa, H.; Okada, S.; Sarkar, A.; Matsuda, H.; Nakanishi, H., Synthesis of polydiacetylenes from novel monomers having two diacetylene units linked by an arylene group. *Polym. J.* **2001,** *33* (2), 182-189; (b) Inayama, S.; Tatewaki, Y.; Okada, S., Solid-state polymerization of conjugated hexayne derivatives with different end groups. *Polym. J.* **2010,** *42* (3), 201-207; (c) Okada, S.; Hayamizu, K.; Matsuda, H.; Masaki, A.; Minami, N.; Nakanishi, H., A new conjugated ladder polymer synthesized by solid-state polymerization of a hexayne compound. *Chem. Lett.* **1992,** *21* (2), 301-304.
35. Davydov, B.; Derkacheva, L.; Dunina, V.; Zhabotinskii, M.; Zolin, V.; Koreneva, L.; Samokhina, M., Connection between charge transfer and laser second harmonic generation. *ZhETF Pisma Redaktsiiu* **1970,** *12*, 24.
36. Di Bella, S., Second-order nonlinear optical properties of transition metal complexes. *Chem. Soc. Rev.* **2001,** *30* (6), 355-366.
37. (a) Karna, S. P.; Prasad, P. N.; Dupuis, M., Nonlinear optical properties of *p* - nitroaniline: An abinitio time - dependent coupled perturbed Hartree–Fock study. *J. Chem. Phys.* **1991,** *94* (2), 1171-1181; (b) Teng, C.; Garito, A., Dispersion of the nonlinear second-order optical susceptibility of an organic system: p-nitroaniline. *Phys. Rev. Lett.* **1983,** *50* (5), 350.
38. Marder, S. R.; Kippelen, B.; Jen, A. K. Y.; Peyghambarian, N., Design and synthesis of chromophores and polymers for electro-optic and photorefractive applications. *Nature* **1997,** *388* (6645), 845-851.
39. (a) Nakano, M.; Yamaguchi, K.; Fueno, T., Coupled-Hartree-Fock calculations of the third-order hyperpolarizabilities of substituted polydiacetylenes. *Chem. Phys. Lett.* **1991,** *185* (5–6), 550-554; (b) Ohnishi, S.-i.; Orimoto, Y.; Gu, F. L.; Aoki, Y., Nonlinear optical properties of polydiacetylene with donor-acceptor substitution block. *J. Chem. Phys.* **2007,** *127* (8), 084702-084702; (c) Yoshimura, T., Theoretically predicted influence of donors and acceptors on quadratic hyperpolarizabilities in conjugated long - chain molecules. *App. Phys. Lett.* **1989,** *55* (6), 534-536; (d) Chen, W.; Yu, G.-t.; Gu, F. L.; Aoki, Y., Investigation on nonlinear optical properties of ladder-structure

polydiacetylenes derivatives by using the elongation finite-field method. *Chem. Phys. Lett.* **2009,** *474* (1–3), 175-179; (e) Kim, W. H.; Bihari, B.; Moody, R.; Kodali, N. B.; Kumar, J.; Tripathy, S. K., Self-Assembled Spin-Coated and Bulk Films of a Novel Poly(diacetylene) as Second-Order Nonlinear Optical Polymers. *Macromolecules* **1995,** *28* (2), 642-647.

40. Lochner, K.; Bässler, H.; Tieke, B.; Wegner, G., Photoconduction in polydiacetylene multilayer structures and single crystals. Evidence for band-to-band excitation. *Phys. Status Solidi B* **1978,** *88* (2), 653-661.
41. Hoofman, R. J. O. M., *Charge transport in polydiacetylenes*. TU Delft, Delft University of Technology: 2000.
42. (a) Sakamoto, M.; Wasserman, B.; Dresselhaus, M. S.; Wnek, G. E.; Elman, B. S.; Sandman, D. J., Enhanced electrical conductivity of polydiacetylene crystals by chemical doping and ion implantation. *J. Appl. Phys.* **1986,** *60* (8), 2788-2796; (b) Takami, K.; Kuwahara, Y.; Ishii, T.; Akai-Kasaya, M.; Saito, A.; Aono, M., Significant increase in conductivity of polydiacetylene thin film induced by iodine doping. *Surf. Sci.* **2005,** *591* (1), L273-L279; (c) Koichi, B.; Hitoshi, K.; Yoshikazu, S.; Shuji, O.; Hidetoshi, O.; Hiro, M.; Hachiro, N., Chemical doping into nanocrystals of poly(diacetylene). *Jpn. J. Appl. Phys.* **2008,** *47* (5R), 3769.
43. Yaron, D.; Moore, E. E.; Shuai, Z.; Brédas, J. L., Comparison of density matrix renormalization group calculations with electron-hole models of exciton binding in conjugated polymers. *J. Chem. Phys.* **1998,** *108* (17), 7451-7458.
44. Sariciftci, N.; Kraabel, B.; Lee, C.; Pakbaz, K.; Heeger, A.; Sandman, D., Absence of photoinduced electron transfer from the excitonic electron-hole bound state in polydiacetylene conjugated polymers. *Phys. Rev. B* **1994,** *50* (16), 12044.
45. Comoretto, D.; Moggio, I.; Cuniberti, C.; Musso, G.; Dellepiane, G.; Borghesi, A.; Kajzar, F.; Lorin, A., Long-lived photoexcited states in polydiacetylenes: The photoinduced-absorption spectra of PDA-4BCMU. *Phys. Rev. B* **1998,** *57* (12), 7071.
46. Robins, L.; Orenstein, J.; Superfine, R., Observation of the triplet excited state of a conjugated-polymer crystal. *Phys. Rev. Lett.* **1986,** *56* (17), 1850-1853.
47. Pratt, F. L.; Wong, K. S.; Hayes, W.; Bloor, D., Infrared photo-induced absorption in polydiacetylene. *J. Phys. C* **1987,** *20* (3), L41.
48. Dellepiane, G.; Cuniberti, C.; Comoretto, D.; Lanzani, G.; Musso, G.; Piaggio, P.; Tubino, R.; Borghesi, A.; Dell'Erba, C.; Garbarino, G., Photoexcitations in polycarbazolyldiacetylenes. *Phys. Rev. B* **1992,** *45* (12), 6802.
49. Brabec, C.; Johansson, H.; Cravino, A.; Sariciftci, N.; Comoretto, D.; Dellepiane, G.; Moggio, I., The spin signature of charged photoexcitations in carbazolyl substituted polydiacetylene. *J. Chem. Phys.* **1999,** *111* (22), 10354-10361.
50. Dellepiane, G.; Cuniberti, C.; Comoretto, D.; Musso, G.; Figari, G.; Piaggi, A.; Borghesi, A., Long-lived photoexcited states in symmetrical polydicarbazolyldiacetylene. *Phys. Rev. B* **1993,** *48* (11), 7850.
51. (a) Song, J. H.; Kang, T. J.; Cho, Y. D.; Lee, S. H.; Kim, J. S., The fabrication and characterization of the photovoltaic cells composed of polydiacetylene and fullerene. *Fiber. Polym.* **2006,** *7* (3), 217-222; (b) Muthitamongkol, P.; Thanachayanont, C.; Sukwattanasinitt, M., Fabrication and characterization of solar cells containing polydiacetylene. *Curr. App. Phys.* **2011,** *11* (1), S163-S165; (c) Reanprayoon, C.; Gasiorowski, J.; Sukwattanasinitt, M.; Sariciftci, N. S.; Thamyongkit, P.,

Polydiacetylene-nested porphyrin as a potential light harvesting component in bulk heterojunction solar cells. *RSC Adv.* **2014,** *4* (6), 3045-3050.

52. (a) Prock, A.; Shand, M. L.; Chance, R. R., Solid-state photopolymerization of diacetylenes. *Macromolecules* **1982,** *15* (2), 238-241; (b) Mondong, R.; Bässler, H., Determination of the chain length in polydiacetylenes by scanning electron microscopy. *Chem. Phys. Lett.* **1981,** *78* (2), 371-374; (c) Siegel, D.; Sixl, H.; Enkelmann, V.; Wenz, G., Polymerization of TS-12 diacetylene crystals: Crystal structures of monomer and polymer and spectroscopy of reaction intermediates. *Chem. Phys.* **1982,** *72* (1–2), 201-212.
53. Wegner, G., Topochemical reactions of monomers with conjugated triple ‐ bonds. IV. Polymerization of bis ‐ (p ‐ toluene sulfonate) of 2.4 ‐ hexadiin ‐ 1.6 ‐ diol. *Die Makromol. Chem.* **1971,** *145* (1), 85-94.
54. Jin, H.; Plonka, A. M.; Parise, J. B.; Goroff, N. S., Pressure induced topochemical polymerization of diiodobutadiyne: a single-crystal-to-single-crystal transformation. *Cryst. Eng. Comm.* **2013,** *15* (16), 3106-3110.
55. Baughman, R. H., Solid-state synthesis of large polymer single crystals. *J. Polym. Sci. Pol. Phys.* **1974,** *12* (8), 1511-1535.
56. Wegner, G., Introductory lecture: Solid-state polymerization. *Faraday Discuss. Chem. Soc* **1979,** *68*, 494-508.
57. Enkelmann, V., The crystal structure of the low-temperature phase of poly[1,2-bis(p-tolylsulphonyloxymethylene)-1-buten-3-ynylene]. *Acta Crystallogr. Sect. B-Struct. Sci.* **1977,** *33* (9), 2842-2846.
58. Curtis, S. M.; Le, N.; Fowler, F. W.; Lauher, J. W., A Rational Approach to the Preparation of Polydipyridyldiacetylenes: An Exercise in Crystal Design. *Crystal Growth & Design* **2005,** *5* (6), 2313-2321.
59. Ikeshima, M.; Mamada, M.; Katagiri, H.; Minami, T.; Okada, S.; Tokito, S., Synthesis and solid-state polymerization of diacetylene derivatives with an *N*-carbazolylphenyl group. *B. Chem. Soc. Jpn.* **2015**.
60. Wang, S.; Li, Y.; Liu, H.; Li, J.; Li, T.; Wu, Y.; Okada, S.; Nakanishi, H., Topochemical polymerization of unsymmetrical aryldiacetylene supramolecules with nitrophenyl substituents utilizing C-H···π interactions. *Org. Biomol. Chem.* **2015,** *13* (19), 5467-5474.
61. Matsuo, H.; Okada, S.; Nakanishi, H.; Matsuda, H.; Takaragi, S., Solid-state polymerization of monomers possessing two diphenylbutadiyne moieties with amido groups to form ladder polymers. *Polym. J.* **2002,** *34* (11), 825-834.
62. Néabo, J. R.; Tohoundjona, K. I. S.; Morin, J.-F., Topochemical polymerization of a diarylbutadiyne derivative in the gel and solid states. *Org. Lett.* **2011,** *13* (6), 1358-1361.
63. Xu, R.; Gramlich, V.; Frauenrath, H., Alternating diacetylene copolymer utilizing perfluorophenyl−phenyl interactions. *J. Am. Chem. Soc.* **2006,** *128* (16), 5541-5547.
64. Okada, S.; Ohsugi, M.; Masaki, A.; Matsuda, H.; Takaragi, S.; Nakanishi, H., Preparation and nonlinear optical property of polydiacetylenes from unsymmetrical diphenylbutadiynes with trifluoromethyl substituents. *Mol. Cryst. Liq. Cryst.* **1990,** *183*, 81-90.
65. Milburn, G.; Werninck, A.; Tsibouklis, J.; Bolton, E.; Thomson, G.; Shand, A., Synthesis and properties of some novel unsymmetrically substituted diacetylenes. *Polymer* **1989,** *30* (6), 1004-1007.

66. Fowler, F. W.; Lauher, J. W., A rational design of molecular materials. *J. Phys. Org. Chem.* **2000,** *13* (12), 850-857.
67. Lauher, J. W.; Fowler, F. W.; Goroff, N. S., Single-crystal-to-single-crystal topochemical polymerizations by design. *Acc. Chem. Res.* **2008,** *41* (9), 1215-1229.
68. Li, Z.; Fowler, F. W.; Lauher, J. W., Weak Interactions Dominating the Supramolecular Self-Assembly in a Salt: A Designed Single-Crystal-to-Single-Crystal Topochemical Polymerization of a Terminal Aryldiacetylene. *J. Am. Chem. Soc.* **2009,** *131*, 634-643.
69. Sun, A.; Lauher, J. W.; Goroff, N. S., Preparation of poly(diiododiacetylene), an ordered conjugated polymer of carbon and iodine. *Science* **2006,** *312* (5776), 1030-1034.
70. Luo, L.; Wilhelm, C.; Sun, A.; Grey, C. P.; Lauher, J. W.; Goroff, N. S., Poly (diiododiacetylene): preparation, isolation, and full characterization of a very simple poly (diacetylene). *J. Am. Chem. Soc.* **2008,** *130* (24), 7702-7709.
71. Shirakawa, H.; Louis, E. J.; MacDiarmid, A. G.; Chiang, C. K.; Heeger, A. J., Synthesis of electrically conducting organic polymers: halogen derivatives of polyacetylene, $(CH)_x$. *J. Chem. Soc. Chem. Commun.* **1977,** (16), 578-580.
72. Becquerel, A., On electric effects under the influence of solar radiation. *CR Acad. Sci* **1839,** *9*, 711-714.
73. Green, M. A., Silicon solar cells: evolution, high-efficiency design and efficiency enhancements. *Semicond. Sci. Technol.* **1993,** *8*, 1.
74. Masuko, K.; Shigematsu, M.; Hashiguchi, T.; Fujishima, D.; Kai, M.; Yoshimura, N.; Yamaguchi, T.; Ichihashi, Y.; Mishima, T.; Matsubara, N.; Yamanishi, T.; Takahama, T.; Taguchi, M.; Maruyama, E.; Okamoto, S., Achievement of More Than 25% Conversion Efficiency With Crystalline Silicon Heterojunction Solar Cell. *IEEE J. Photovoltaics* **2014**, 1-3.
75. Wagner, S.; Shay, J. L.; Migliorato, P.; Kasper, H. M., CuInSe2/CdS heterojunction photovoltaic detectors. *Appl. Phys. Lett.* **1974,** *25*, 434-435.
76. Rau, U.; Schock, H.-W., Electronic properties of Cu (In, Ga) Se_2 heterojunction solar cells–recent achievements, current understanding, and future challenges. *Appl. Phys. A* **1999,** *69* (2), 131-147.
77. Singh, U. P.; Patra, S. P., Progress in Polycrystalline Thin-Film Cu(In,Ga)Se2 Solar Cells. *Int. J. Photoenerg.* **2010,** *2010*.
78. Powalla, M.; Jackson, P.; Witte, W.; Hariskos, D.; Paetel, S.; Tschamber, C.; Wischmann, W., High-efficiency Cu(In,Ga)Se2 cells and modules. *Sol. Energ. Mat. Sol. C.* **2013,** *119*, 51-58.
79. Powalla, M.; Witte, W.; Jackson, P.; Paetel, S.; Lotter, E.; Wuerz, R.; Kessler, F.; Tschamber, C.; Hempel, W.; Hariskos, D.; Menner, R.; Bauer, A.; Spiering, S.; Ahlswede, E.; Friedlmeier, T. M.; Blazquez-Sanchez, D.; Klugius, I.; Wischmann, W., CIGS Cells and Modules With High Efficiency on Glass and Flexible Substrates. *IEEE J. Photovoltaics* **2014,** *4*, 440-446.
80. Reinhard, P.; Chirila, A.; Blosch, P.; Pianezzi, F.; Nishiwaki, S.; Buechelers, S.; Tiwari, A. N., Review of progress toward 20% efficiency flexible CIGS solar cells and manufacturing issues of solar modules. *IEEE J. Photovoltaics* **2013,** *3*, 572-580.
81. Lindström, S., An all‐sputtering process and equipment for CIGS solar cells. *Vakuum in Forschung und Praxis* **2013,** *25* (5), 43-45.
82. Shah, A.; Torres, P.; Tscharner, R.; Wyrsch, N.; Keppner, H., Photovoltaic technology: The case for thin-film solar cells. *Science* **1999,** *285* (5428), 692-698.

83. Sproul, A., Understanding the *p-n* Junction.
84. Koide, N.; Islam, A.; Chiba, Y.; Han, L., Improvement of efficiency of dye-sensitized solar cells based on analysis of equivalent circuit. *J. Photochem. Photobiol., A* **2006,** *182* (3), 296-305.
85. Shockley, W.; Queisser, H. J., Detailed balance limit of efficiency of p‐n junction solar cells. *J. Appl. Phys.* **1961,** *32*, 510-519.
86. Siebentritt, S., What limits the efficiency of chalcopyrite solar cells? *Sol. Energ. Mat. & Sol. C.* **2011,** *95*, 1471-1476.
87. Orgassa, K.; Rau, U.; Nguyen, Q.; Werner Schock, H.; Werner, J. H., Role of the CdS buffer layer as an active optical element in Cu (In, Ga) Se_2 thin‐film solar cells. *Prog. Photovoltaics Res. Appl.* **2002,** *10* (7), 457-463.
88. (a) Wang, F.; Tan, Z. a.; Li, Y., Solution-processable metal oxides/chelates as electrode buffer layers for efficient and stable polymer solar cells. *Energy Environ. Sci.* **2015,** *8* (4), 1059-1091; (b) Po, R.; Carbonera, C.; Bernardi, A.; Camaioni, N., The role of buffer layers in polymer solar cells. *Energy Environ. Sci.* **2011,** *4* (2), 285-310.
89. Wang, J.-C.; Weng, W.-T.; Tsai, M.-Y.; Lee, M.-K.; Horng, S.-F.; Perng, T.-P.; Kei, C.-C.; Yu, C.-C.; Meng, H.-F., Highly efficient flexible inverted organic solar cells using atomic layer deposited ZnO as electron selective layer. *J. Mater. Chem.* **2010,** *20* (5), 862-866.
90. Kim, J. Y.; Kim, S. H.; Lee, H.-H.; Lee, K.; Ma, W.; Gong, X.; Heeger, A. J., New architecture for high-efficiency polymer photovoltaic cells using solution-based titanium oxide as an optical spacer. *Adv. Mater.* **2006,** *18* (5), 572-576.
91. Shrotriya, V.; Li, G.; Yao, Y.; Chu, C.-W.; Yang, Y., Transition metal oxides as the buffer layer for polymer photovoltaic cells. *Appl. Phys. Lett.* **2006,** *88* (7), 073508.
92. Li, G.; Chu, C.; Shrotriya, V.; Huang, J.; Yang, Y., Efficient inverted polymer solar cells. *Appl. Phys. Lett.* **2006,** *88* (25), 253503-253503.
93. Peumans, P.; Bulović, V.; Forrest, S. R., Efficient photon harvesting at high optical intensities in ultrathin organic double-heterostructure photovoltaic diodes. *Appl. Phys. Lett.* **2000,** *76*, 2650-2652.
94. (a) Gommans, H.; Verreet, B.; Rand, B. P.; Muller, R.; Poortmans, J.; Heremans, P.; Genoe, J., On the Role of Bathocuproine in Organic Photovoltaic Cells. *Adv.Funct. Mater.* **2008,** *18* (22), 3686-3691; (b) Vogel, M.; Doka, S.; Breyer, C.; Lux-Steiner, M. C.; Fostiropoulos, K., On the Function of a Bathocuproine Buffer Layer in Organic Photovoltaic Cells. *Appl. Phys. Lett.* **2006,** *89* (16), 163501-163501-3.
95. Kim, J. Y.; Kim, S. H.; Lee, H.-H.; Lee, K.; Ma, W.; Gong, X.; Heeger, A. J., New architecture for high-efficiency polymer photovoltaic cells using solution-based titanium oxide as an optical spacer. *Adv. Mater.* **2006,** *18*, 5.
96. Chan, M. Y.; Lee, C. S.; Lai, S. L.; Fung, M. K.; Wong, F. L.; Sun, H. Y.; Lau, K. M.; Lee, S. T., Efficient organic photovoltaic devices using a combination of exciton blocking layer and anodic buffer layer. *J. Appl. Phys.* **2006,** *100*.
97. Naka, S.; Okada, H.; Onnagawa, H.; Tsutsui, T., High electron mobility in bathophenanthroline. *Appl. Phys. Lett.* **2000,** *76* (2), 197-199.
98. Li, C.; Schwab, M.; Zhao, Y.; Chen, L.; Bruder, I.; Münster, I.; Erk, P.; Müllen, K., A phenanthroline derivative as exciton blocking material for organic solar cells. *Dyes Pigments* **2013,** *97*, 258-261.

99. (a) Tripathi, V.; Datta, D.; Samal, G. S.; Awasthi, A.; Kumar, S., Role of Exciton Blocking Layers in Improving Efficiency of Copper Phthalocyanine based Organic Solar Cells. *J. Non-Crys. Solids* **2008,** *354* (19–25), 2901-2904; (b) Wang, N.; Yu, J.; Zang, Y.; Huang, J.; Jiang, Y., Effect of Buffer Layers on the Performance of Organic Photovoltaic Cells based on Copper Phthalocyanine and C60. *Sol. Energ. Mat. Sol. C.* **2010,** *94* (2), 263-266; (c) Yu, J.; Wang, N.; Zang, Y.; Jiang, Y., Organic photovoltaic cells based on TPBi as a cathode buffer layer. *Sol. Energy Mater. Sol. Cells* **2011,** *95* (2), 664-668.
100. Tang, C. W.; VanSlyke, S. A., Organic electroluminescent diodes. *Appl. Phys. Lett.* **1987,** *51* (12), 913-915.
101. Kathirgamanathan, P.; Surendrakumar, S.; Vanga, R. R.; Ravichandran, S.; Antipan-Lara, J.; Ganeshamurugan, S.; Kumaraverl, M.; Paramaswara, G.; Arkley, V., Arylvinylene phenanthroline derivatives for electron transport in blue organic light emitting diodes. *Org. Electron.* **2011,** *12* (4), 666-676.

Chapter 2 Synthesis and Co-Crystal Preparation of Push-Pull Diynes

2.1 Design of Push-Pull Diynes and Electron-Poor Diynes for Synthesizing Novel PDAs

To a great extent, synthesis of PDAs has been limited by the self-organization capacity of diyne monomers. In the solid-state, push-pull diynes can arrange in many ways, such as head-to-head, or head-to-tail, or random head-to-head/head-to-tail, which makes organizing monomers more challenging. As discussed in Chapter 1, there is very limited reported work on push-pull PDAs, especially single crystals of push-pull PDAs. This project mainly focuses on a novel approach to synthesize such PDAs. The distinctive approach takes advantage of the host-guest strategy used in our group to synthesize PIDA. We proposed that push-pull diyne monomers could be organized in host-guest co-crystals with suitable geometry for polymerization as shown in Figure 2.1.

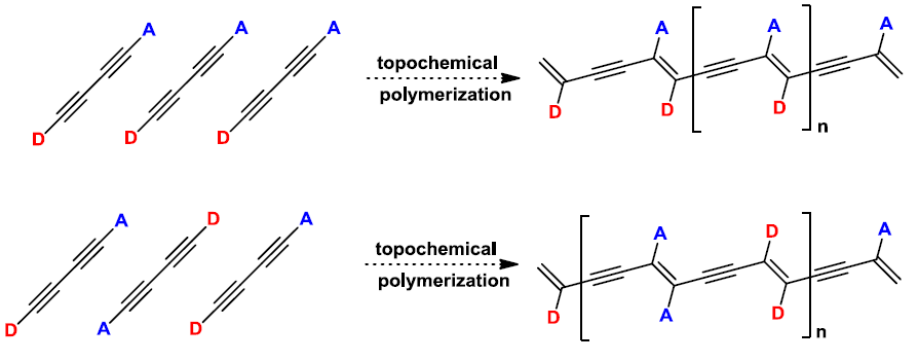

Figure 2.1 Proposed 1,4-topochemical polymerization of push-pull diynes in a head-to-head way or head-to-tail way

We initially proposed several diynes capped with electron donating and withdrawing groups as monomers. While the electron sufficient iodine was targeted as one capping group, common electron deficient carboxylic acid or nitrile group was selected as the other. Six push-pull

conjugated diynes were then targeted (Figure 2.2). In addition to electron donors and acceptors, acetylenic phenyl and alkenyl groups were introduced to extend conjugation of the polymer backbone.

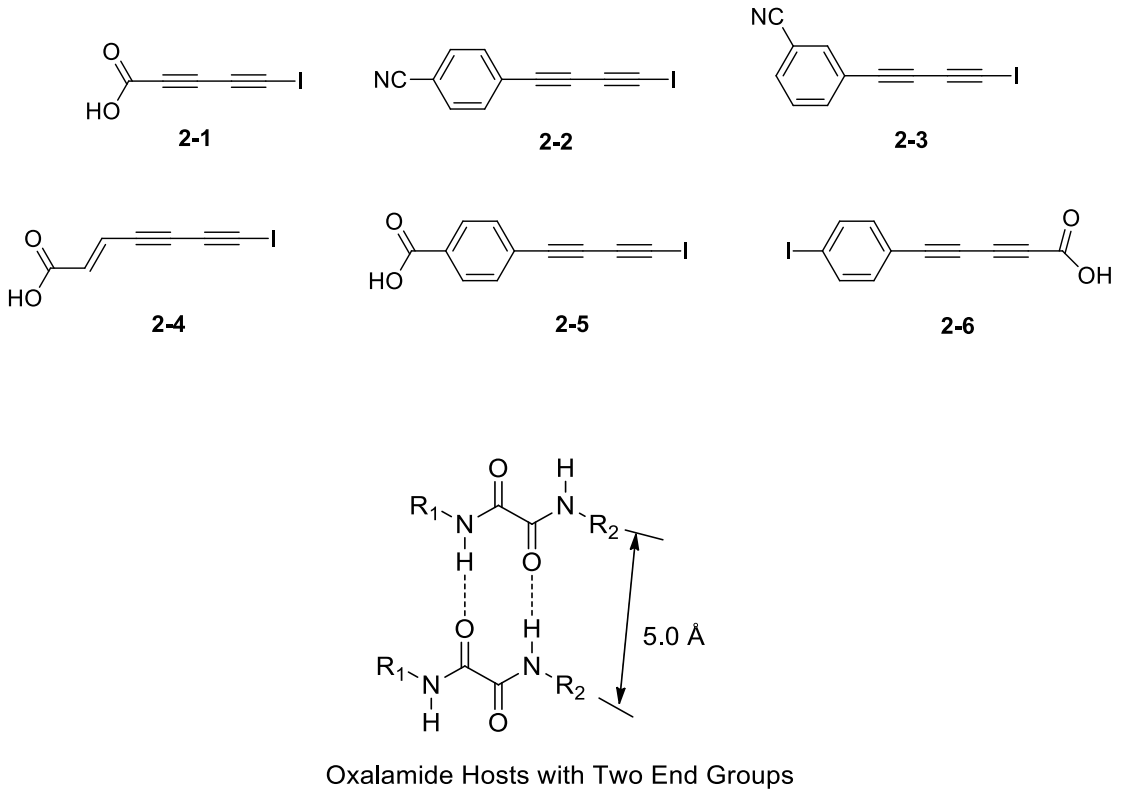

Figure 2.2 Targeted push-pull diyne monomers and host molecules

As an electron-withdrawing end-cap group, nitrile is highly conjugated, and not a bulky end that could prevent polymerization. The lone pair on the nitrogen makes nitrile a good Lewis base to participate in the Lewis acid-base interaction. However, since iodine is Lewis acidic, opposite to nitrile, challenges arose when preparing co-crystals. When forming crystals from solution through slow evaporation, iodine can interact with nitrile strongly, facilitating monomers self-aggregate instead of forming co-crystals with host molecules. To enhance the interaction between host and guest, we designed several oxalamide host molecules (Figure 2.2), including symmetric ($R_1 = R_2$,

both R_1 and R_2 Lewis basic) and nonsymmetric (R_1 Lewis acidic, R_2 Lewis basic) oxalamide hosts, and attempted various crystallization methods.

In addition to nitrile, carboxylic acid is also a well-known electron-withdrawing functionality on polymers. Diynes capped with carboxylic acid and iodine have both sides Lewis acidic. When forming co-crystals, they are likely to form co-crystals with oxalamide hosts with both R_1 and R_2 Lewis basic, which is advantageous over diynes capped with nitrile and iodine. On the other hand, the challenge lies in the limited solubility of carboxylic acid in organic solvents. Therefore, most oxalamide hosts employed bear Lewis basic pyridines, which are soluble in protic solvents, similar to carboxylic acid.

PDAs exclusively capped by strong electron deficient groups have also drawn our attention since the electron deficiency might also offer special properties. One of our targets was poly(bis(nitrile) diyne) (**2-7**) (Scheme 2.1). Since there is no bulky protecting groups in the polymer of diyne **2-7**, the polymer can potentially be used to predict properties of the linear allotrope of carbon. One of our previous group members Racquel Decicco explored synthesis of bis(nitrile) diyne **2-7** in detail. However, diyne **2-7** was reported extremely sensitive to air,[102] and according to the work done in our lab,[103] the final step produced unidentifiable black precipitates (Scheme 2.1). Therefore, diyne **2-7** was never synthesized successfully in our lab.

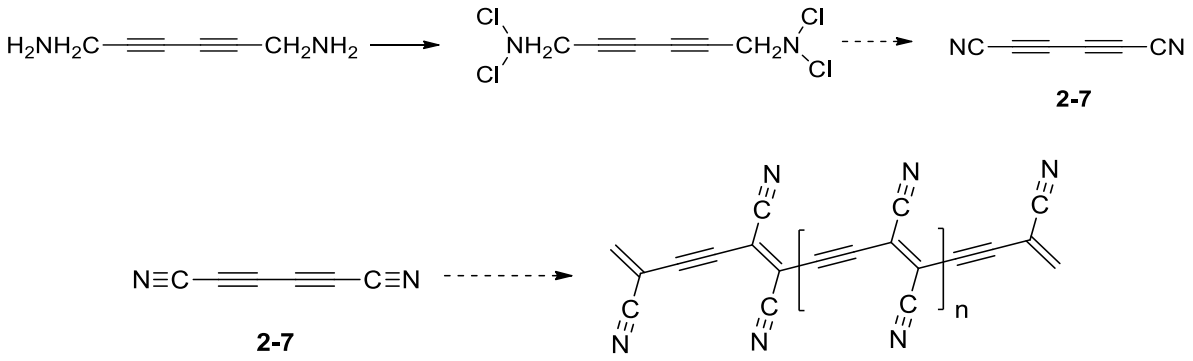

Scheme 2.1 Designed synthetic route for diyne **2-7**[103] and proposed polymerization

Bis(carboxylic acid) capped diyne **2-8** is also electron-deficient, and carbodylic acid is suitable to form hydrogen-bonds with host molecules.[67] The desired polymer, as shown in Scheme 2.2, contains an electron-deficient backbone and soluble side groups in polar solvents. One of our previous group members Allison Black attempted synthesis of diyne **2-8,** but did not accomplish it.[104] After that I synthesized diyne **2-8** successfully through a Hay-coupling reaction and attempted preparing co-crystals of diyne **2-8** and host molecules.

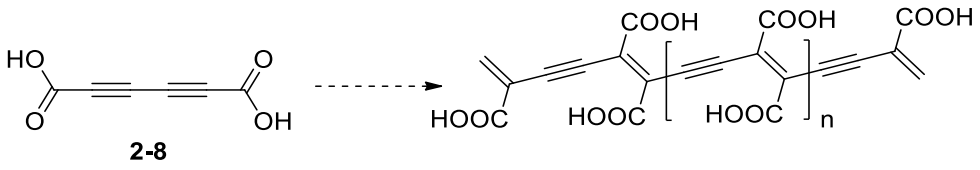

Scheme 2.2 Proposed polymerization of diyne **2-8**

2.2 Results and Discussion

2.2.1 Synthesis

Synthesis of nonsymmetric diynes has been achieved by palladium or copper catalyzed coupling reactions between terminal alkynes and haloalkynes. Two of the most employed reactions are Sonogashira coupling, and Cadiot-Chodkiewicz coupling. For instance, the Nakanishi group[105]

employed Cadiot-Chodkiewicz coupling reaction to synthesize several nonsymmetric diynes containing a urethane group as one side group and thienyl or quinolyl moiety as the other, to investigate their third-order NLO. Employing the two reactions, all targeted nonsymmetric diynes were synthesized successfully.

Synthesis of 5-iodopenta-2,4-diynenitrile (2-9)

5-Iodopenta-2,4-diynenitrile **2-9** (Scheme 2.3) was first synthesized by one of our previous group members Racquel C. DeCicco, starting with propargyl amine. The synthetic route was reproduced for this work several times. Cadiot-Chodkiewicz coupling between Boc- group protected propargyl amine **2-10** and (bromoethynyl)triisopropylsilane **2-11** produce diyne **2-12** in a high yield, following the procedures described by Hwang and co-workers.[106] The following deprotection of Boc- group gives amine **2-13**. The resulting amine is dehydrogenated to generate nitrile using trichloroisocyanuric acid (TCCA) followed by trimethylamine, according to procedures reported by De Luca and Giacomelli.[107] The final step is to convert triisopropyl (TIPS) group to iodine.[108] Diyne **2-9** decomposes and turns black at 100°C, suggesting its stability is comparable to diiodobutadiyne, which decomposed at 90 °C.

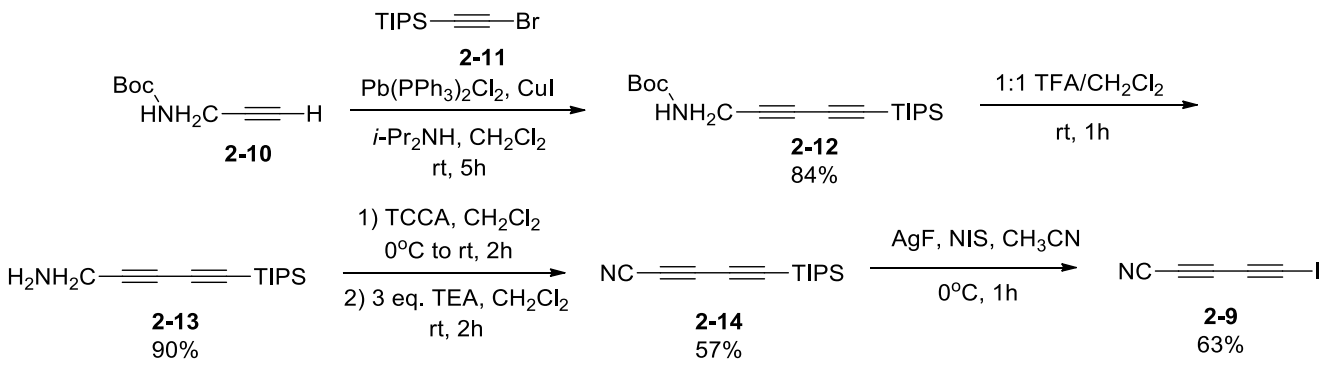

Scheme 2.3 Synthesis of 5-iodopenta-2,4-diynenitrile

Synthesis of *para*(*meta*)-(iodobuta-1,3-diyn-1-yl)benzonitrile (2-2 and 2-3)

Synthetic routes of diyne **2-2** and **2-3** are similar (Scheme 2.4), starting with Sonogashira coupling between bromobenzonitrile **2-15**/**2-16** and trimethylsilylacetylene (TMSacetylene) **2-17**, according to procedures reported by Christopher Richardson and co-workers.[109] Excess **2-17** (1.5 eq.) is required to push the reaction to completion. The following Cadiot-Chodkiewicz coupling between **2-18/2-19** and **2-11** yields diyne **2-20/2-21** employing Hwang and co-workers' condition.[106] Homo-coupling reactions can be reduced by minimizing oxygen in the reaction system and adding minimum catalytic amount of CuI. Diyne **2-2** and **2-3** are synthesized both as light yellow solids in a moderate yield.

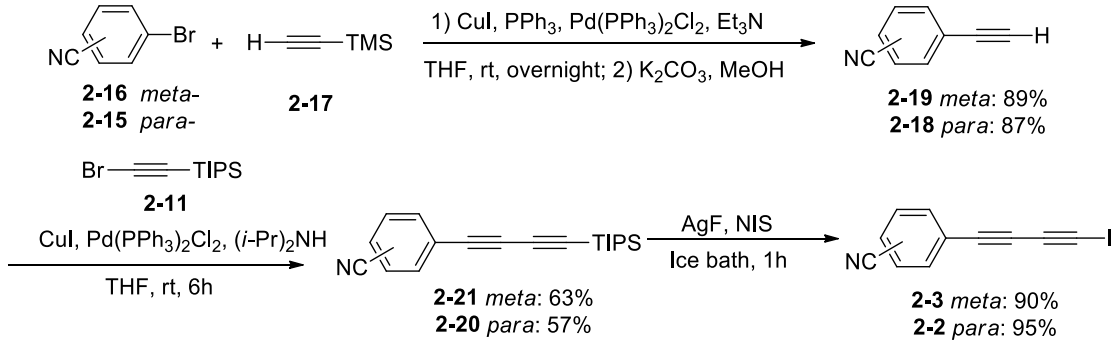

Scheme 2.4 Synthesis of *para*(*meta*)-(iodobuta-1,3-diyn-1-yl)benzonitrile

Synthesis of 4-(iodobuta-1,3-diyn-1-yl)benzoic acid (2-5)

Synthetic route of diyne **2-5** was initially designed with diyne **2-25** as the key intermediate (Scheme 2.5). Removing the methyl group and converting TIPS to iodine could then give the target molecule. Sonogashira coupling between compound **2-22** and **2-17** yields compound **2-23** in an almost quantitative yield. This Sonogashira coupling requires 50 ℃ to go to completion. Removing TMS gives terminal acetylene **2-24**. Diyne **2-25** is then synthesized in a moderate yield through Cadiot-Chodkiewicz coupling between terminal acetylene **2-24** and bromoacetylene **2-11**.

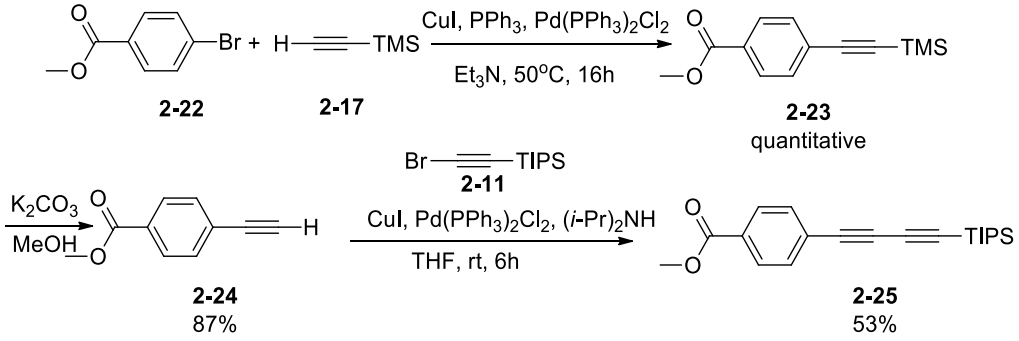

Scheme 2.5 Synthesis of intermediate **2-25**

Significant efforts were put on converting intermediate **2-25** to the target diyne **2-5**. Two possible routes were attempted. One is to convert methyl benzoate to benzoic acid before convert TIPS to iodine, and the other is in the reversed order (Scheme 2.6).

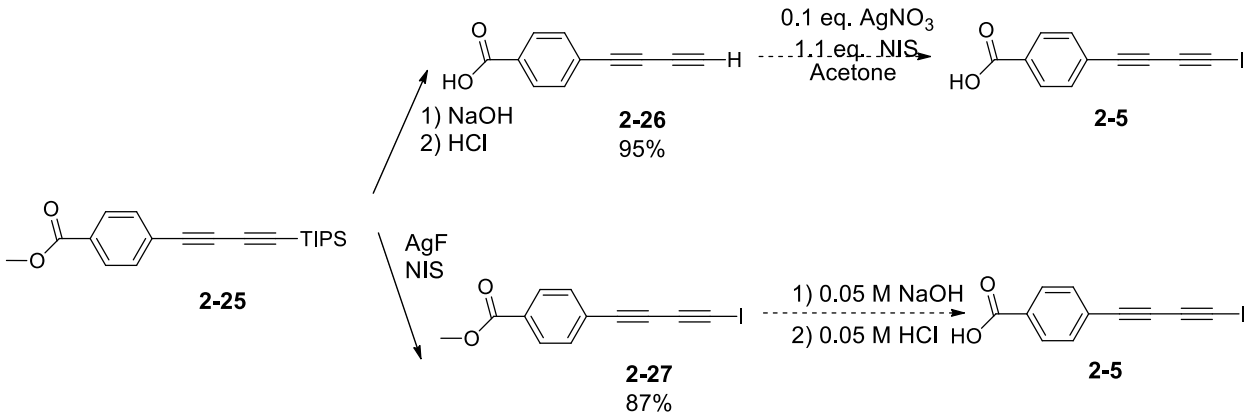

Scheme 2.6 Two possible routes to synthesize diyne **2-5**

In the first route, strong inorganic base is employed on diyne **2-25** to remove the methyl group, which is a common method to turn methyl ester to acid. However, the C-Si bond proves too weak to survive the basic condition. TIPS group is therefore removed as well as the methyl group, although the sodium hydroxide solution employed is as dilute as 0.05 M. As a result, instead of yielding the desired diyne end-capped with benzonic acid and TIPS group, the reaction generates terminal diyne **2-26** in a high yield.

In the latter synthetic route, diyne **2-27** is synthesized in a high yield by treating diyne **2-25** with AgF and NIS at 0 ℃. However, the following basic condition used to remove methyl group is observed harsh to the C-I bond. Therefore, instead of desired diyne **2-5**, some decomposed dark brown solids are generated in the reaction system.

Based on the above attempts, both C-Si and C-I bonds are fragile in basic conditions. Therefore, instead of starting with a methyl benzoate where the methyl group is base-removable, we modified

the synthetic route to employ *t*-butyl benzoate as starting material where the *t*-butyl group is acid-removable. Diyne **2-30** was targeted as the key intermediate (Scheme 2.7). We hypothesized that C-I bond could stay robust when removing *t*-butyl group using acids.

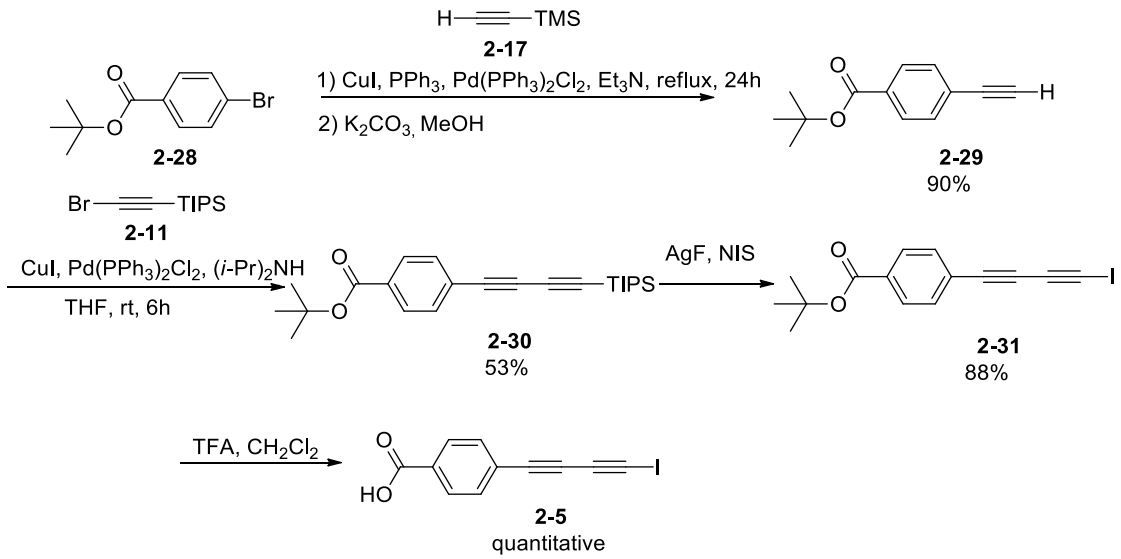

Scheme 2.7 The successful synthetic routes of diyne **2-5**

Synthetic route of diyne **2-30** is similar to that of **2-25** (Scheme 2.7). Sonogashira coupling between compound **2-28** and **2-17** under reflux gives compound **2-29** in a high yield. Higher temperature (under reflux) and double the amount of CuI and $Pd(PPh_3)_2Cl_2$, comparing to those used in synthesizing diyne **2-25**, are necessary for driving the reaction to its completion. The following Cadiot-Chodkiewicz coupling between compound **2-29** and **2-11** gives diyne **2-30** in a 53% yield. TIPS is then converted to iodine to generate diyne **2-31**. Treating diyne **2-31** with a solution of trifluoroacetic acid (TFA) in methylene chloride in one hour removes the *t*-butyl group completely. Diyne **2-5** can be isolated simply by removing all the solvents, excess TFA and by-products under vacuum, without further purification. The target diyne **2-5** is therefore obtained as

a pale yellow solid in an almost quantitative yield. Diyne **2-5** is stable in its pure form at room temperature, and it can be stored in its methanol solution in the refrigerator for weeks, according to NMR spectroscopy.

Synthesis of 5-(4-Iodophenyl)penta-2,4-diynoic acid (2-6)

Compound **2-35** is targeted as the key intermediate for synthesizing diyne **2-6** (Scheme 2.8). According to procedures reported by the Low group,[110] iodoaniline is employed as the starting material of Sonogashira coupling reactions under reflux overnight to yield compound **2-33**. The reaction to covert compound **2-33** to **2-34** is reproduced based on Li and co-workers.[111] Compound **2-33** is mixed with 6 M HCl and $NaNO_2$ solution to form a benzendiazonium chloride intermediate. The diazonium chloride is then substituted by iodide through adding an ice-cold sodium iodide (NaI) aqueous solution dropwise. After 4 h reaction time, compound **2-34** is generated in a moderate yield, easily isolated by column chromatography. The key intermediate **2-35** is then synthesized in high yield.

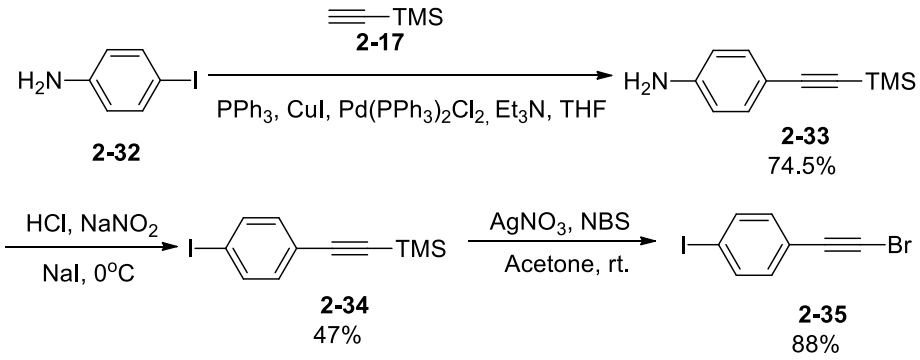

Scheme 2.8 Successful synthesis of intermediate **2-35**

A challenge arose when coupling compound **2-35** with a terminal alkyne. Since both iodine and

bromine are reactive under either Cadiot-Chodkiewicz or Sonogashira coupling conditions in the presence of $Pd(PPh_3)Cl_2$ and CuI as catalysts. Competing coupling reactions happening on both iodine and bromine would make the reaction much less effective. Iodine is even more reactive than bromine under the coupling conditions. It is essential to find a palladium-free coupling condition, so that the reaction takes place only on the bromoalkyne instead of the aryliodide (Scheme 2.9).

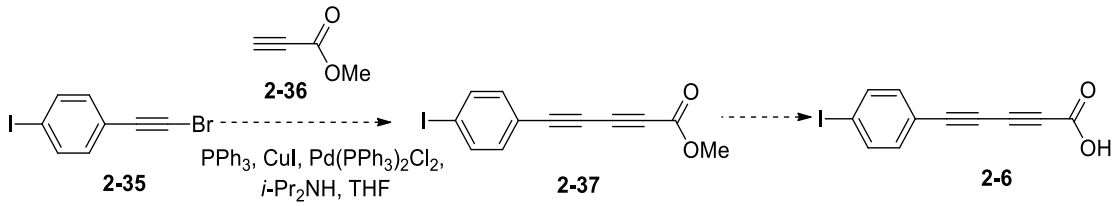

Scheme 2.9 Proposed synthetic route from intermediate **2-35** to diyne **2-6**

There has been very limited literature about palladium-free Cadiot-Chodkiewicz coupling reactions including propiolic acid as a starting material. Dikusar and co-workers[112] are able to couple alkynyl acid and haloalkyne efficiently through Cadiot-Chodkiewicz reaction employing only Cu(I) as the metal catalyst. Using the same condition on compound **2-35** and propiolic aid **2-38**, target diyne **2-6** is achieved as white crystals in a yield of 70% (Scheme 2.10). Therefore, this Cadiot-Chodkiewicz coupling condition is observed very effective and efficient. Diyne **2-6** is very stable in its pure form, and can be stored in the refrigerator for months without obvious decomposition according to NMR spectroscopy.

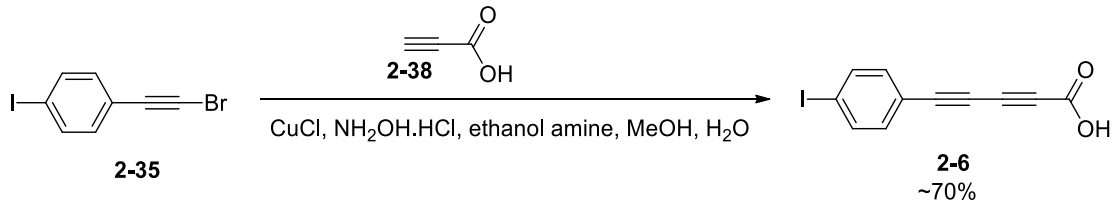

Scheme 2.10 Successful synthesis from compound **2-35** to diyne **2-6**

Synthesis of (*E*) 7-Iodohepta-2-en-4,6-diynoic acid (2-4)

According to the previous synthesis of diyne **2-5**, the bond between acetylenic carbon and iodine is fragile under basic condition, while relatively stable under acidic condition. Therefore, diyne **2-41**, bearing the *t*-butyl group that can be removed in acidic conditions, is targeted as the key intermediate to synthesize diyne **2-4** (Scheme 2.11). The C-I bond is hypothesized stable when removing *t*-butyl group using a strong acid. Diyne **2-41** is synthesized through coupling between compound **2-39** and TIPSdiyne **2-40** under Sonogashira coupling conditions.

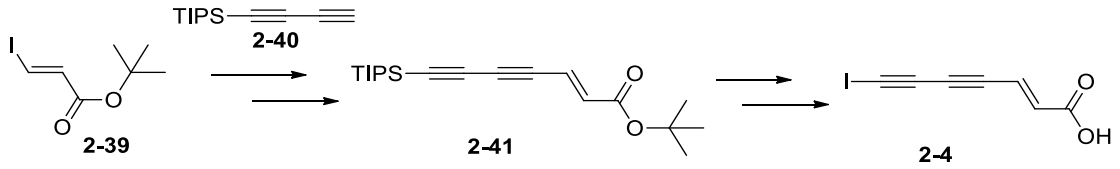

Scheme 2.11 Synthesis of diyne **2-4**

Iodoacrylic acid **2-42** is synthesized by refluxing propiolic acid and 57% aqueous hydroiodic acid together for 24 h (Scheme 2.12).[113] Both *E*- and *Z*-iodoacrylic acids are synthesized as geometrical isomers, but they have very different solubilities in water at room temperature. Therefore, the *E*-isomer **2-42** precipitates out as white needle crystals. Washing the white needles with cold water affords pure *E*-iodoacrylic acid **2-42**. The esterification reaction is performed by treating compound **2-42** with t-butyl acetate with catalytic amount of triflic acid in methylene chloride at room temperature for 2 h, according to Dixon et al.[114] Compound **2-39** is synthesized in 70% yield (Scheme 2.12).

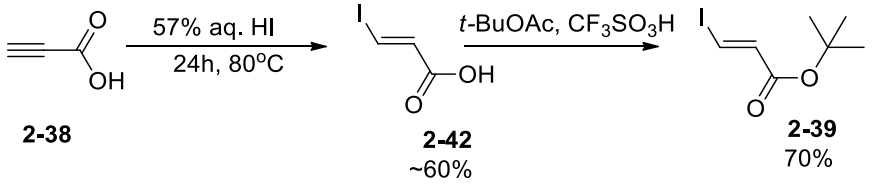

Scheme 2.12 Synthesis of **2-39**[114]

Diyne **2-40** is synthesized over three steps according to procedures reported by Doak, Scanlon, and Simpson.[115] Diyne **2-41** is then synthesized by Sonogashira coupling between compound **2-39** and terminal diyne **2-40**, in a moderate yield (Scheme 2.13). Homo-coupling of terminal diyne **2-40** competes with the cross coupling reaction, excess diyne **2-40** (1.5 to 2 eq.) is required to drive the cross coupling reaction. Converting TIPS to iodine and removing the *t*-butyl group lead to the target diyne **2-4**, as a very pale yellow, almost white solid. Diyne **2-4** is stable in solution in the refrigerator over a few weeks according to NMR spectroscopy.

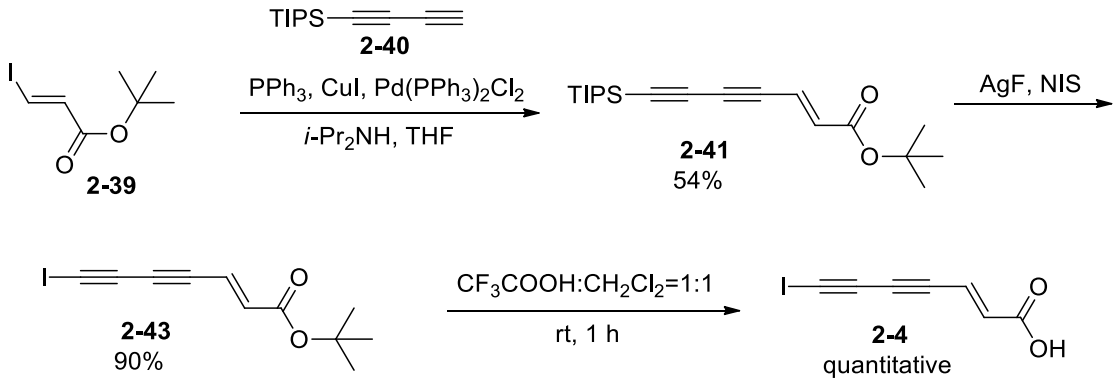

Scheme 2.13 Synthesis of diyne **2-4**

Synthesis of 5-Iodopenta-2,4-diynoic acid (2-1)

Diyne **2-1** was first synthesized by one of our previous group members Allison Black. I optimized the synthetic route to make it more efficient (Scheme 2.14). *t*-Butyl propiolate **2-44** is prepared in

the same method as described above for the synthesis of (*E*) *t*-butyl iodoacrylate (Scheme 2.12). The Cadiot-Chodkiewicz coupling is challenging. It is observed that the reaction has to be remained in ice bath and run for less than 3 hours. Either room temperature or a longer reaction time period results in black precipitates immediately. However, after isolation and purification, diyne **2-45** stays reasonably stable in neat at room temperature. The final diyne **2-1** is synthesized as a light yellow powdery solid, which gradually decomposes over time at room temperature.

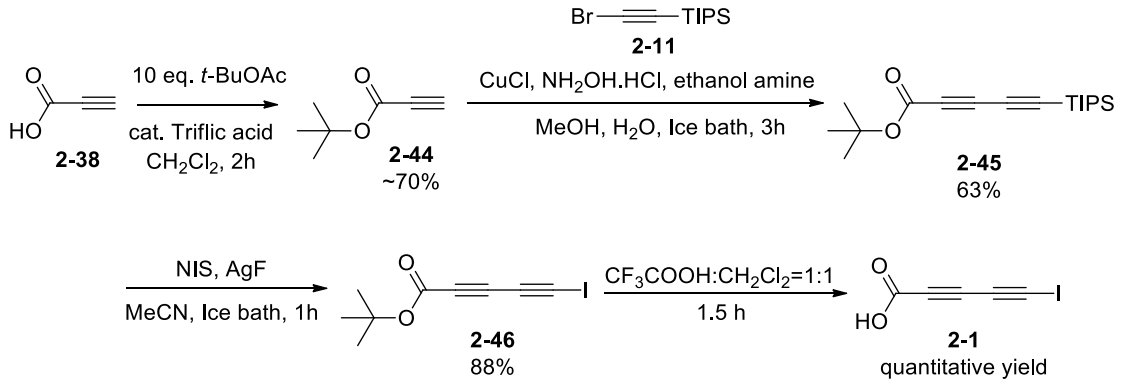

Scheme 2.14 Synthetic route of diyne **2-1**

Synthesis of Hexa-2,4-diynedioic acid (2-8)

Hexa-2,4-diynedioic acid **2-8** was first synthesized by Baeyer in 1885.[116] Synthesis of it was mainly reported in the late 19th century and early 20th century. It has been synthesized through homo-coupling of propiolic acid,[116] Cadiot- Chodkiewicz Coupling between bromo propiolic acid and propiolic acid,[117] carboxylation of diacetylene,[118] and oxidation of (2*E*,8*E*)-deca-2,8-dien-4,6-diyne.[119] In 2015, the Empire Technology Development LLC[120] published a patent about the synthesis of dicarbonyl compounds, including diyne **2-8**, from carbon dioxide and terminal alkane or alkyne. The single crystal structure of diyne **2-8** was described by Dunitz and Robertson.[121]

In this work, hexa-2,4-diynedioic acid **2-8** has been synthesized through a Cu(I) catalyzed Hay-

coupling of *t*-butyl propiolate **2-49** followed by removal of the *t*-butyl group. In the previous synthetic route proposed and performed by Allison Black, diyne **2-48** was the intermediate (Scheme 2.15). However, diyne **2-48** was not synthesized successfully. The optimized synthetic route, which successfully generates diyne **2-8**, has diyne **2-49** as the key intermediate (Scheme 2.16). In the first Hay-coupling reaction, TLC indicates diyne **2-49** forms at 0 °C within minutes, and the reaction system has to be quenched within 15 min; otherwise, decomposed black solids appear very quickly over time. Diyne **2-49** is generated as a white solid after isolation and purification, and is stable at room temperature. After removing the *t*-butyl group in TFA, target diyne **2-8** precipitates as white needles. Washing with cold hexane removes excess TFA and byproducts. Although its reported melting point is 170-180°C,[122] diyne **2-8** turns pink gradually in air at room temperature within one hour.

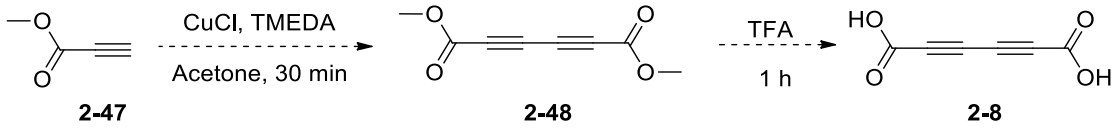

Scheme 2.15 Previous attempts for synthesizing diyne **2-8**

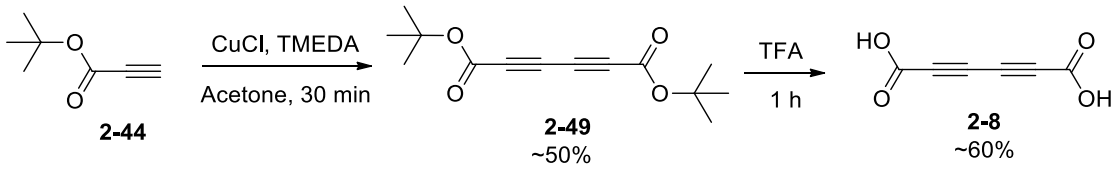

Scheme 2.16 Synthetic route of diyne

2.2.2 Preparing Co-crystals of Diynes and Hosts

The host-guest strategy developed by Fowler and Lauher[67] is proposed to organize synthesized

push-pull diynes with appropriate geometry for 1,4-polymerization.[103] Figure 2.3 shows the proposed interaction between host and guest molecules. Oxalamide-based host molecules are employed, because the alignment of oxalamide functionalities has a repeat distance of 5.0 Å and the side groups can interact with diynes through Lewis acid-base interaction. As described in Chapter 1, the ideal parameters for 1,4-polymerization of diynes include a repeat distance (*r*) of 4.9-5.0 Å between monomers, a C1-C4 distance (*d*) of 3.5 Å, and an angle θ = 45°. All co-crystal preparation attempts employ the slow evaporation method. If hosts and guests form a co-crystal during the crystallization process, the appearance, and the melting point of such a complex can be different from either those of the host or the guest. Single-crystal XRD can determined the structure of the co-crystal if its quality is sufficiently good.

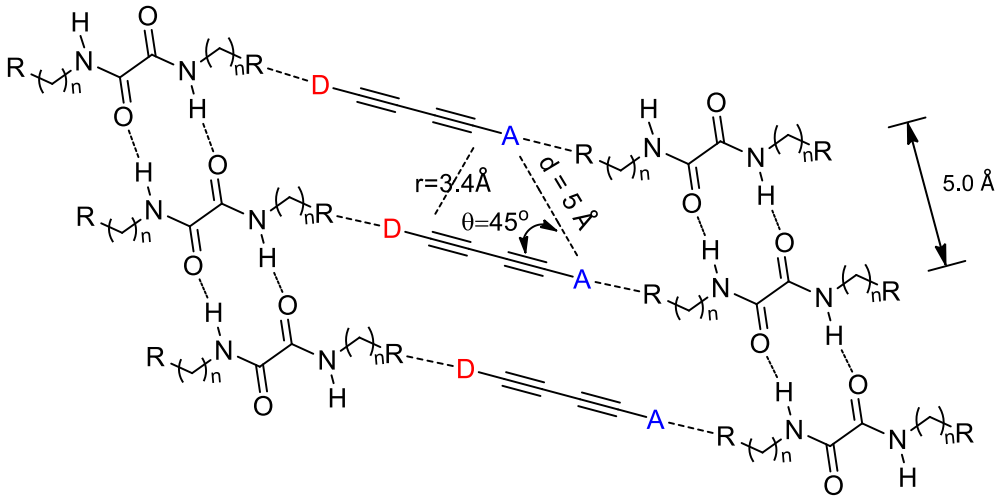

Figure 2.3 Proposed interaction between host and guest molecules

Preparing Co-Crystals of Diyne 2-2/2-3 and Hosts

When the nitrile is served as the electron acceptor group, the interaction between diynes and symmetric hosts is hypothesized to be on one side. Figure 2.4a shows the proposed co-crystal structure between diyne **2-2** and host **1-8**. Figure 2.4 b shows the proposed co-crystal structure

between diyne **2-2** and host **2-50**. The competition between monomer self-aggregation and co-crystal formation stays a challenge.

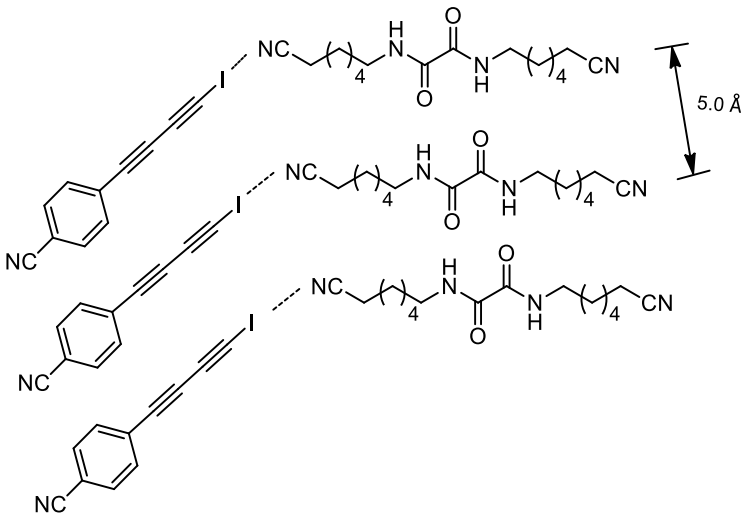

(a)

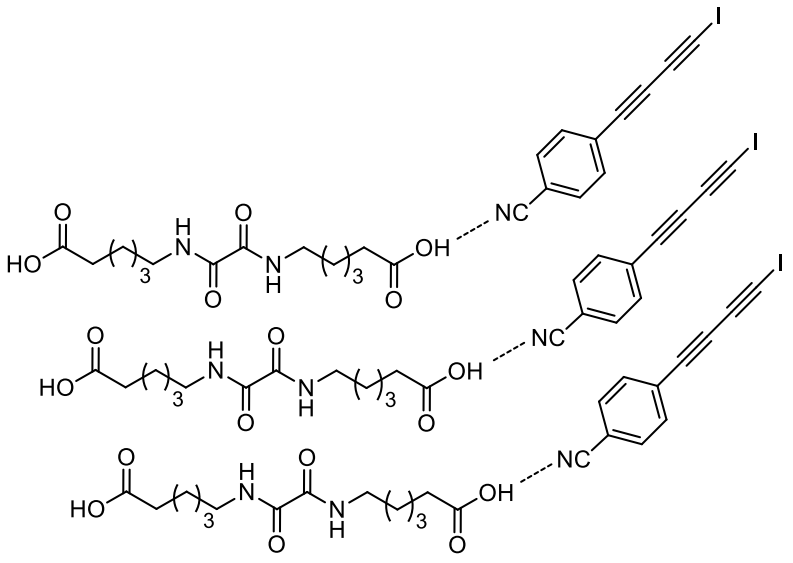

(b)

Figure 2.4 Proposed structures of co-crystals of monomers containing the nitrile

Preparing co-crystals of diyne **2-3** and Bis(nitrile) oxalamide host **1-8** is attempted in various

conditions. Results are summarized in Table 2.1. We proposed Lewis acidic iodine in the diyne would interact with the Lewis basic nitrile in host molecules to form co-crystals. However, all attempts resulted in light yellow solids.

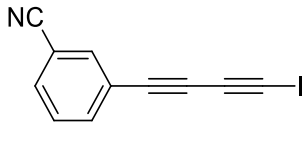

2-3

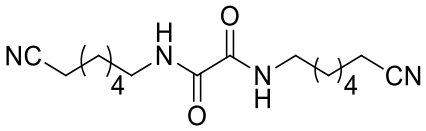

1-8

Table 2.1 Preparing co-crystals of diyne **2-3** and host **1-8**

Solvents	Ratio (H:G)	Temperature (℃)	Time (h)	Results	Melting Point (℃)
CH_2Cl_2	1: 2	25	24	Yellow crystal	100 – 101 turns black
	1: 2	0	24	Yellow crystal	
THF	1: 2	25	24	Yellow crystal	
	1: 2	0	24	Yellow crystal	
THF	1: 2	25	24	Yellow crystal	
	1: 2	0	24	Yellow crystal	
MeCN	1: 2	25	24	Yellow crystal	
	1: 2	0	24	Yellow crystal	

Similarly, preparing co-crystals of diyne **2-2** and bis(nitrile) oxalamide host **1-8** is attempted in CH_2Cl_2, THF and MeCN. Results are summarized in Table 2.2. All attempts on forming co-crystals generate light yellow crystals, which have almost the same melting point as host **1-8** (117 ℃), indicating host crystals contaminated with decomposed diyne **2-2**.

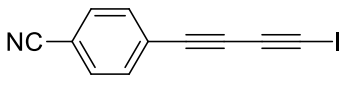

2-2

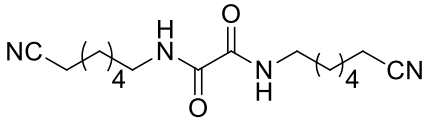

1-8

Table 2.2 Preparing co-crystals of diyne **2-2** and host **1-8**

Solvents	Ratio (H:G)	Temperature (℃)	Time (h)	Results	Melting Point (℃)
CH_2Cl_2: MeOH = 5:1	1:1	25	24	Light Yellow crystal (Hosts)	117 turn black
THF	1:1	25	24	Light Yellow crystal (Hosts)	
MeCN	1:1	25	24	Light Yellow crystal (Hosts)	

In addition, bis(carboxylic acid) oxalamide host **2-50** is employed in preparing co-crystals with diyne **2-2**. We expected interaction between nitrile and the carboxylic acid would lead to co-crystals. However, host **2-50** has limited solubility in many organic solvents, except for a few protic solvents such as methanol and ethanol, which narrows feasible conditions to form co-crystals. Attempts on preparing co-crystals are performed in methanol. As summarized in Table 2.3, all experiments result in mixed solids containing host molecules and decomposed diynes. There is no conclusive evidence that any co-crystal formed.

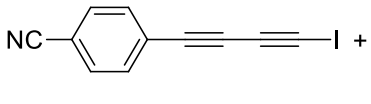

2-2

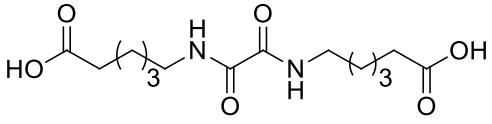

2-50

Table 2.3 Preparing co-crystals of diyne **2-2** and host **2-50**

Solvents	Ratio(H:G)	Temperature (℃)	Time (h)	Results
MeOH	1:2	25	24	Separate solids
MeOH	1:1	25	24	Light yellow solids

Preparing Co-Crystals of Diyne 2-5 and Hosts

Diyne **2-5** is proposed to have a better chance of forming co-crystals with host molecules than diyne **2-2** and **2-3**. It contains two Lewis acidic capped groups, iodine and carboxylic acid, which allows both ends to interact with host molecules through either hydrogen-bonds or Lewis acid-base interactions to form co-crystals. Figure 2.5 shows a proposed geometry the co-crystal of diyne **2-5** and bis(pyridyl) host **1-10**. Preparing co-crystals of diyne **2-5** and 3-pyridinyl host **1-9**, 4-pyridinyl host **1-10** and bis(carboxylic acid) oxalamide host **2-50** are explored and summarized in Tables 2.4, 2.5 and 2.6. Protic solvents such as methanol, ethanol and water are employed because of limited solubility of the compounds containing pyridyl/carboxylic acid groups.

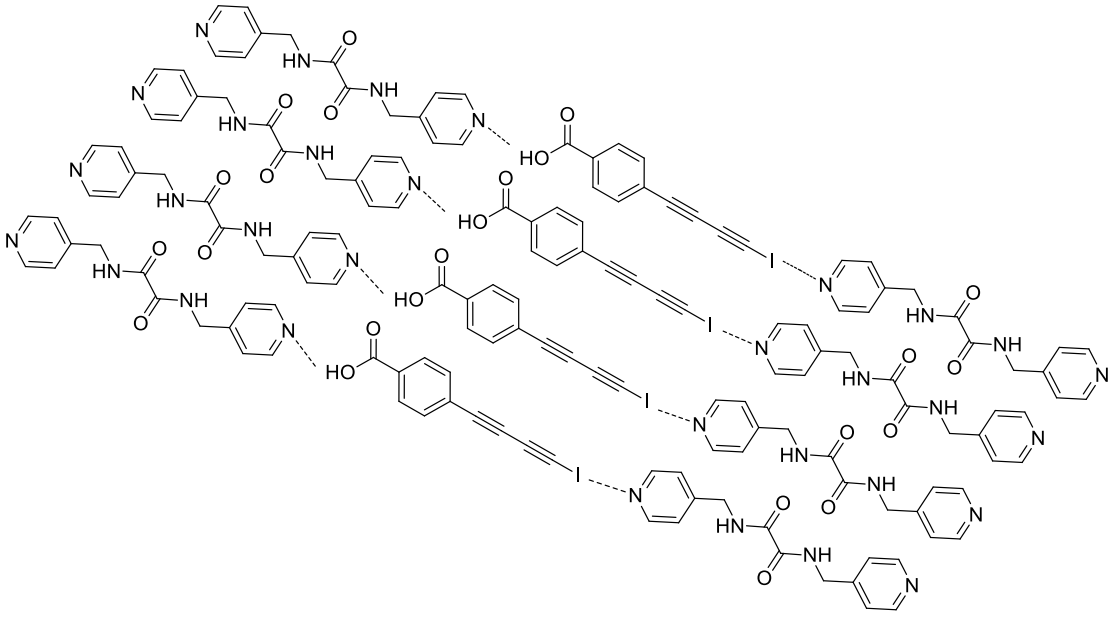

Figure 2.5 Proposed interaction between diyne **2-5** and host **1-10**

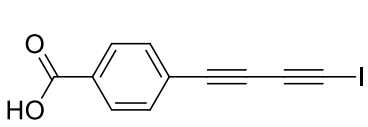

2-5

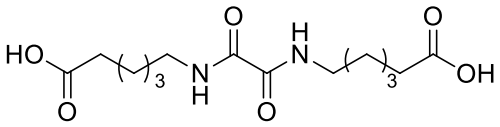

2-50

Table 2.4 Preparing co-crystals of diyne **2-5** and host **2-50**

Solvents	Host: Guest	Temperature (℃)	Time (h)	Results
MeOH	1:1	0/25	24	Separate solids
	1:2	0/25	24	Separate solids

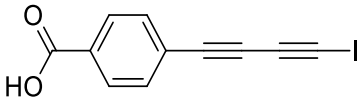

2-5

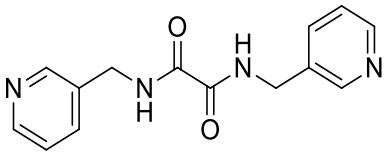

1-9

Table 2.5 Preparing co-crystals of diyne **2-5** and host **1-9**

Solvents	Host:Guest	Temperature (℃)	Time (h)	Results
MeOH	1:1	0/25	24	Separate solids
	1:2	0/25	24	Separate solids
EtOH	1:1	0/25	24	Separate solids
	1:2	0/25	24	Separate solids
MeOH: H_2O=10:1	1:1	0/25	24	Separate solids
	1:2	0/25	24	Separate solids

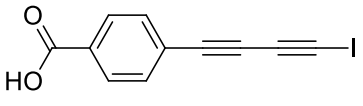

2-5

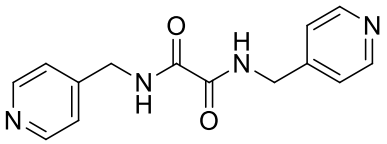

1-10

Table 2.6 Preparing co-crystals of diyne **2-5** and host **1-10**

Solvents	Host: Guest	Temperature (℃)	Time (h)	Results	Melting Point (℃)
MeOH	1:1	0/25	24	Mostly white solids	88 turns dark
	1:2	0/25	24	Red co-crystal and extra white solids	135 – 147 turns black
MeOH: H_2O=10:1	1:2	25	24	Red co-crystal	
	1:2	0	24	Red-co-crystal	

Results indicate that, diyne **2-5** does not form co-crystals with host **1-9** or **2-50** under conditions we have attempted so far. However, the red color co-crystal of diyne **2-5** and bis(pyridyl) host **1-10** has been prepared by slow evaporation, as presented in Table 2.6. After washing the co-crystal with cold water and methanol alternately until the washing layer is colorless, FTIR shows functionalities of both the host and the guest. The red co-crystals turn dark quickly at 135 ℃. The crystal structure has been determined by single-crystal XRD. The detailed analysis will be discussed in **2.2.3.**

Preparing Co-Crystals of Diyne 2-6 and Hosts

Preparing co-crystals of diyne **2-6** and hosts **1-9** and **1-10** is explored. Similar to diyne **2-5**, diyne **2-6** contains the carboxylic group, which makes it soluble in protic solvents. Therefore, bis(pyridyl) hosts **1-9** and **1-10**, which are also soluble in protic solvents, are employed. However, all attempts generate white solids after solvent evaporation. Part of the solids has the same melting point as the host, while others have the same melting point as the guest. Therefore, we can conclude that we

obtained separate solids. Results are summarized in Table 2.7, 2.8.

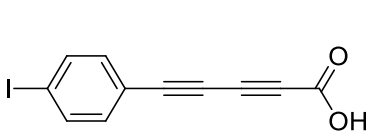

2-6

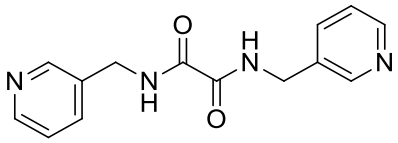

1-9

Table 2.7 Preparing co-crystals of diyne **2-6** and host **1-9**

Solvents	Host: Guest	Temperature (℃)	Time (h)	Results
MeOH	1:1	0/25	24	Separate solids
	1:2	0/25	24	
EtOH	1:1	0/25	24	
	1:2	0/25	24	
MeOH: H_2O=10:1	1:1	0/25	24	
	1:2	0/25	24	

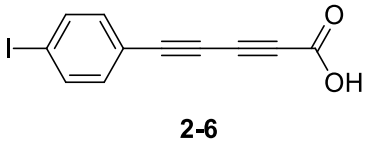

2-6

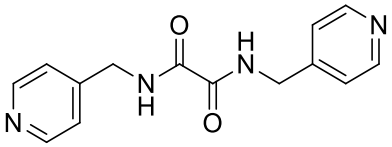

1-10

Table 2.8 Preparing co-crystals of diyne **2-6** and host **1-10**

Solvents	Host: Guest	Temperature (℃)	Time (h)	Results
MeOH	1:1	0/25	24	Separate solids
	1:2	0/25	24	
EtOH	1:1	0/25	24	
	1:2	0/25	24	
MeOH: H_2O=10:1	1:1	0/25	24	
	1:2	0/25	24	

Preparing Co-Crystals of Diyne 2-4 and Hosts

Several conditions are attempted to preparing co-crystals of diyne **2-4** and hosts **1-10**. All attempts generate a mixture of the host and the guest after solvent evaporation. Results are summarized in

Table 2.9. There is no conclusive evidence that co-crystal has formed.

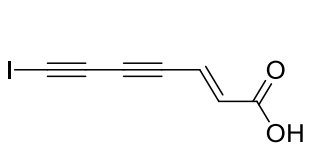

2-4

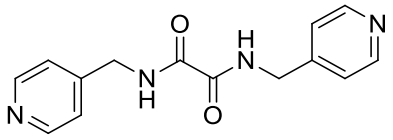

1-10

Table 2.9 Preparing co-crystals of diyne **2-4** and host **1-10**

Solvents	Host: Guest	Temperature (℃)	Time (h)	Results	Melting Point (℃)
MeOH:H_2O=5:1	1:1	0	24	White solids	145-150 turns dark
	1:2	0	24	White solids	145-150 turns dark
MeOH:MeCN=5:1	1:2	0	24	White solids	145-150 turns dark

Preparing Co-Crystals of Diyne 2-1 and Hosts

Preparing co-crystals of diyne **2-1**, and bis(pyridyl) oxalamide hosts **1-10** and **2-51** is attempted. Pyridine is a much stronger Lewis base than nitrile, which may have strong interaction with diyne **2-1** to form co-crystals. In addition, diyne **2-1** and hosts **1-10**/**2-51** have decent solubility in protic solvents such as methanol, which is likely to help forming co-crystals through solvent evaporation. Results are summarized in Table 2.10 – 2.13.

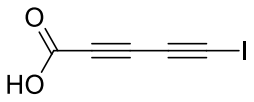

2-1

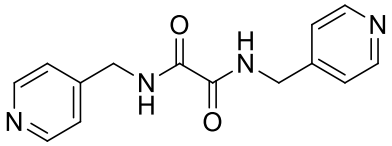

1-10

Table 2.10 Preparing co-crystals of diyne **2-1** and host **1-10**

Solvents	Host: Guest	Temperature (℃)	Time (h)	Results
MeOH	1:1	0/25	24	Pink solids
	1:2	0/25	24	Pink solids

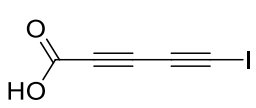

2-1

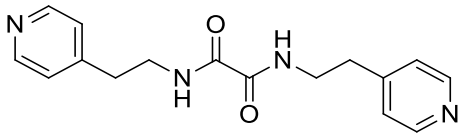

2-51

Table 2.11 Preparing co-crystals of diyne **2-1** and host **2-51**

Solvents	Host: Guest	Temperature (℃)	Time (h)	Results
MeOH:CH_2Cl_2=3:1	1:1	0/25	24	Pink solids
	1:2	0/25	24	Pink solids

Based on our observation, bis(pyridyl) hosts **1-10** and **2-51** seem to have proton-transfer reactions with diyne **2-1** in methanol. A pink solid precipitates out of the solution immediately when mixing them together, and the pink solids cannot re-dissolve. The resulted pink solid turns dark once heated, so that the melting points are difficult to determine. We therefore turn to bis(nitrile) hosts **1-7** and **1-8**, where the nitrile is not a proton acceptor. Since hosts **1-7** and **1-8** are not quite soluble in methanol, 25% CH_2Cl_2 or MeCN is added to help dissolve the hosts. However, all attempts result in pale yellow or white solids. Part of the solids has the same melting point as the host, while others have the same melting point as the guest. Therefore, we can conclude that we obtained separate solids.

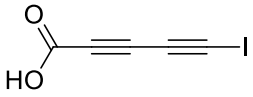

2-1

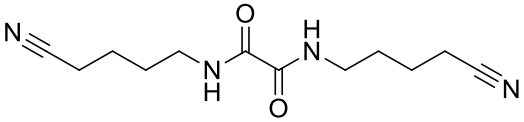

1-7

Table 2.12 Preparing co-crystals with diyne **2-1** and host **1-7**

Solvents	Host: Guest	Temperature (℃)	Time (h)	Results
MeOH:CH_2Cl_2=3:1	1:1	0	24	Separate solids
	1:2	0	24	Separate solids

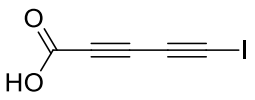

2-1

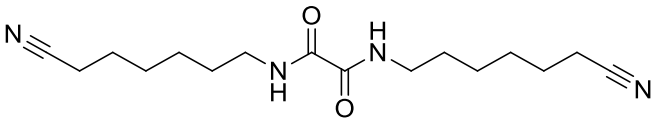

1-8

Table 2.13 Preparing co-crystals of diyne **2-1** and host **1-8**

Solvents	Host: Guest	Temperature (℃)	Time (h)	Results
MeOH:MeCN=3:1	1:1	0	24	Separate solids
	1:2	0	24	Separate solids

Preparing Co-Crystals of Diyne 2-8 and Hosts

1,4-Bis(pyridyl) oxalamide host **1-10** is considered feasible forming co-crystals with hexa-2,4-diynedioic acid **2-8**, since the carboxylic acid groups can form hydrogen bonds with the pyridyl groups. Results are summarized in Table 2.14. Attempts in methanol afford colorless crystals, which turn black at 110 ℃. The black solid did not display any polymeric en-yne peak in Raman spectrum, which indicates no appropriate alignment in the colorless crystals.

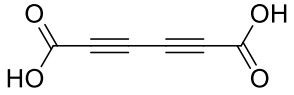

2-8

+

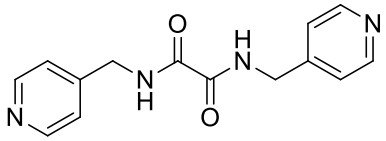

1-10

Table 2.14 Preparing co-crystals of diyne **2-8** and host **1-10**

Solvents	Host: Guest	Temperature (℃)	Time (h)	Results
MeOH	1:1	0/25	24	Colorless crystals 110 ℃ turn dark
	1:2	0/25	24	

2.2.3 Analysis of 1-10:2-5 Co-Crystal Structure

Among all co-crystal preparation attempts, we obtained one red co-crystal of diyne **2-5** and host **1-10** through slow evaporation (Table 2.15).

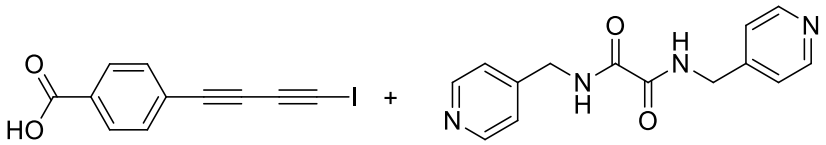

2-5 **1-10**

Table 2.15 Preparing co-crystals of diyne **2-5** and host **1-10**

Solvents	Host: Guest	Temperature (℃)	Time (h)	Results
MeOH	1:2	25	24	Red co-crystals
	1:2	0	24	135 ℃ turn dark

Single-crystal XRD determines the structure of the ruby-like co-crystal, as shown in Figure 2.6. Diyne moleules are organized by the host molecuels through the Lewis acid-base interaction between the iodine and the pyridyl group, and hydrogen bonds between the carboxylic acid groups and the pyridyl or the oxalamide group. There is water included in the crystal structure. The host molecules have two orientations (Figure 2.6c). The hydrogen-bonding networks which is proposed formed by the oxalamide groups are interrupted by the carbonyl groups on the diyne molecules. Therefore only one set of hydrogen bonds forms and aligns the host molecules.

The repeat distance of diyne monomers is 11.48 Å, which is much larger than the desired distance, 4.9 Å, for diynes to react with each other. In addition, the repeat angle between the axis and diynes is measured 97.74°, which does not agree with the desired angle, 45°. After heating in the oven at 60 ℃ for one week, although the color of co-crystals turn redish brown, Raman spectrum shows no conclusive peaks that polymers are formed.

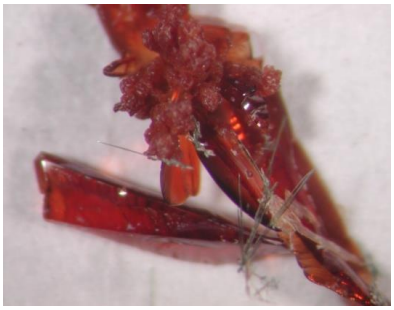

(a)

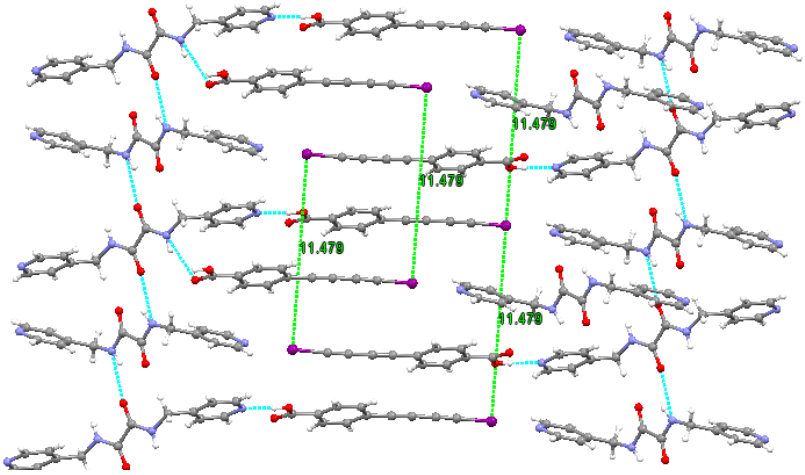

(b)

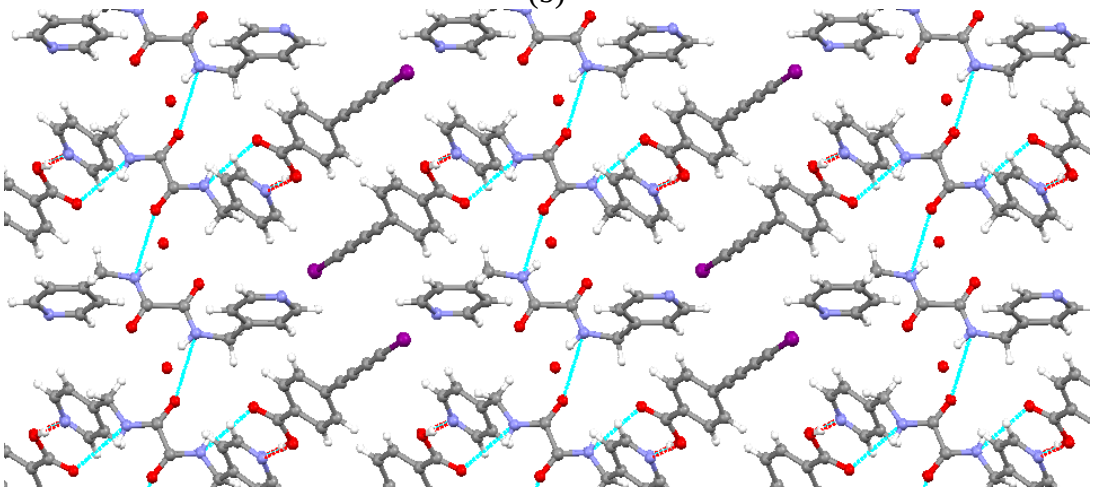

(c)

Figure 2.6 2-5:1-10 Co-crystal and its crystal structure (a) the picture of co-crystal **2-5: 1-10**; (b) crystal structure determined by single-crystal XRD, water is removed for clarity; (c) crystal structure determined by single-crystal XRD

2.2.4 Modification of Host and Guest Molecules

To preserve the favored interaction between the Lewis basic pyridine, and the Lewis acidic carboxylic acid and iodine, as well as to design the co-crystal strucuture, we develop new hosts (**2-52, 2-53, 2-54**) and guest (**2-62**), as shown in Figure 2.7 and 2.9.

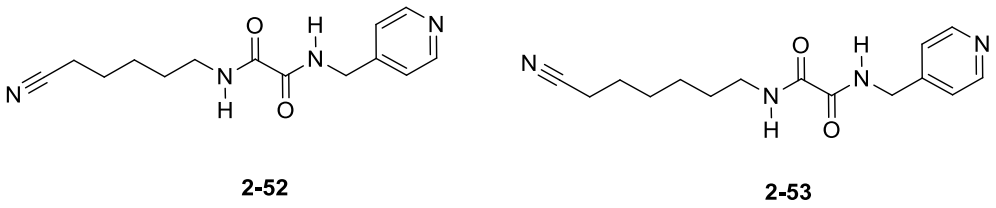

Figure 2.7 Targeted nonsymmetric hosts **2-52** and **2-53**

Two non-symmetric host molecules (**2-52** and **2-53**) are targeted. Oxalamide functionalities are preserved to form hydrogen bonding networks with desired repeat distance. The methylpyridyl group is one side group to form hydrogen bond with carboxylic acid. The pentylnitrile or hexylnitrile group is the other side group that can interact with iodine. The alkyl chain containing five or six methylenes is hypothesized to impose the diyne functionalities lining up in a nearly linear way (Figure 2.8). The proposed geometry is shown in Figure 2.8.

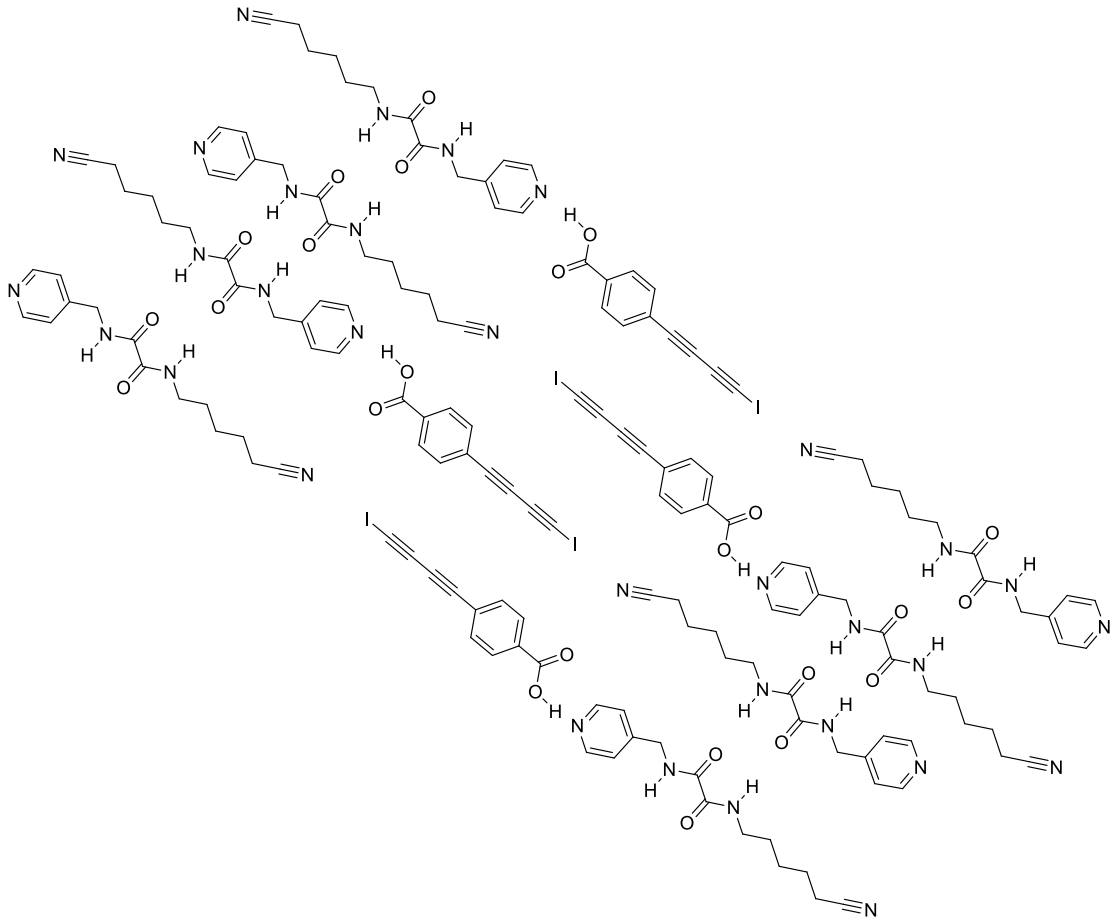

Figure 2.8 Proposed co-crystal structure of diyne **2-5** and host **2-52**

The two non-symmetric hosts **2-52** and **2-53** have been synthesized successfully. Preparing co-crystals of diyne **2-5** and host **2-52**, as well as diyne **2-5** and host **2-53** under various conditions are attempted. All attempts result in separate solids.

A symmetric bis(pyridyl) host **2-54** is also targeted. Comparing to host **1-10**, the longer methylene chain is hypothesized to keep the carbonyl groups of the diyne monomers away from forming hydrogen bonds with the oxalamide groups, and therefore protect the hydrogen-bonding networks. Host **2-54** has been synthesized successfully in a moderate yield (Scheme 2.17), and it is not as

crystalline as host **1-10** because of the longer methylene chain. Attempts on forming co-crystals do not give any positive result, either.

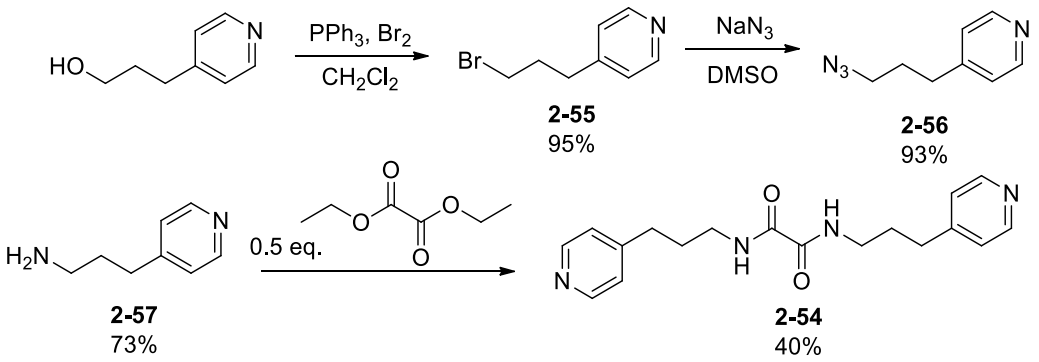

Scheme 2.17 Targeted symmetric host **2-54** and synthetic route

On the other hand, a new push-pull diyne monomer is targeted (Figure 2.9), containing *p*-iodophenyl and *p*-benzoic acid as capped groups. Because the size of one iodine is comparable to that of one carboxylic acid group, diynes are likely to align linearly in co-crystals. In addition, symmetric hosts are more crystalline than nonsymmetric ones. Figure 2.9 shows the proposed co-crystal structure.

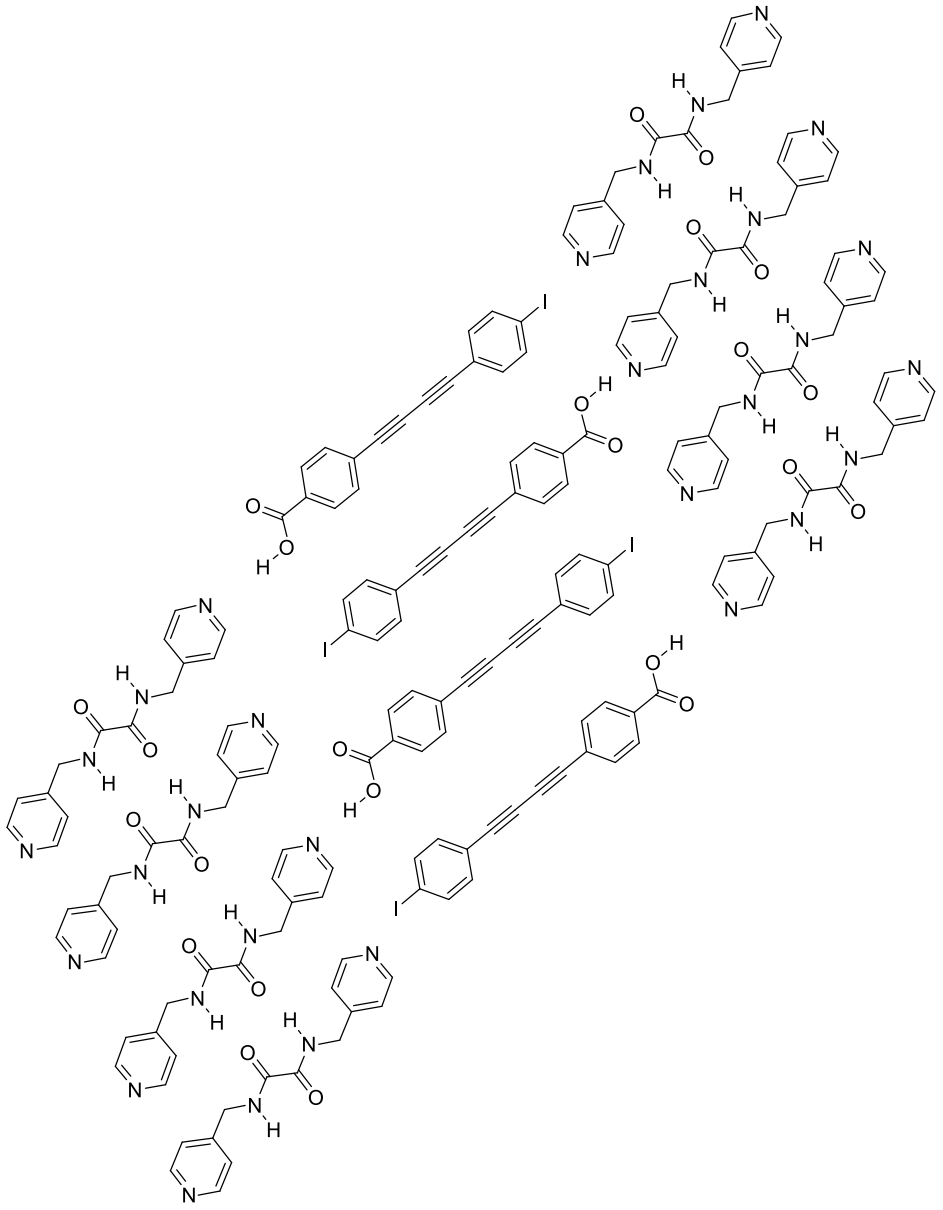

Figure 2.9 Proposed co-crystal structure of host **1-10** and diyne **2-62**

Synthetic route of diyne **2-62** is proposed with diyne **2-60** as the key intermediate (Scheme 2.18). Synthesis of **2-60** was reproduced according to the Zhou and Toone group[123] through a Glaser coupling. 5 eq. Ethynylbenzenamine was added to compel the cross-coupling reaction. The Glaser coupling produces diyne **2-60** in a mediocre yield. However, the following step from diyne **2-60** to **2-61** cannot proceed effectively, likely due to limited solubility of diyne **2-60** or **2-61** in the

reaction system. Crude products cannot be identified. The synthetic route is not pursued after several attempts.

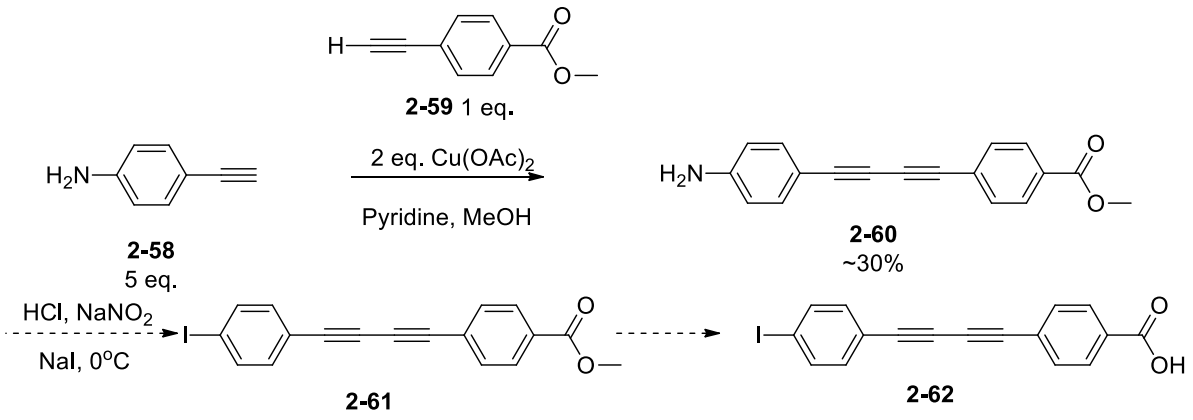

Scheme 2.18 Proposed synthetic route of diyne **2-62**

2.3 Conclusion & Future work

Push-pull conjugated PDAs have been attractive for potential applications in photovoltaic technology and nonlinear optics. Experimental results on such PDAs are lacking because diyne monomers do not usually align with the appropriate geometry for polymerization in the solid state. In this project we proposed a new approach to synthesize such PDAs, a host-guest strategy, where host compounds can help the organization of diynes (guest) in co-crystals.

We target the iodine as the electron donor group, and the nitrile and the carboxylic acid group as the electron acceptor group. In addition to diynes capped with electron donors and acceptors, we also design aryl or alkenyl group directly substituted diynes capped with electron donors and acceptors. Several novel non-symmetric diynes have therefore been designed, and they have all been synthesized.

Co-crystal preparation has been explored. A solution of host and guest is allowed to evaporate slowly to generate co-crystal. We successfully prepared one co-crystal of diyne **2-5**, capped with iodine and benzoic acid, and bis(pyridyl) host **1-10**. The structure is determined by single-crystal XRD. Host molecules are aligned by hydrogen bonds formed by their oxalamide functionalities. Both side groups of diyne **2-5** interact with host molecules so that diynes are aligned in the co-crystal. However, the geometry of diynes is not appropriate for further polymerization reactions.

Although we have not synthesized one push-pull PDA successfully thus far, the exploration of pre-organizing non-symmetric diynes through the host-guest strategy is innovative. Our results indicate that non-symmetric diynes can interact with oxalamide-based host compounds on both ends. By introducing stronger Lewis acidic (Lewis basic) groups as capped groups of diynes, and strongly Lewis basic (Lewis acidic) groups as side groups to hosts, it may enhance the interaction between diynes and hosts to form co-crystals. On the other hand, we need to attempt various conditions of preparing co-crystal, such as adding additives, or vapor diffuse.

2.4 Experimental Procedures

General Methods: Excepted stated, reagents were purchased at reagent grade from Aldrich, Fisher Scientific/Acros Organics, or VWR, and were used without further purification. Column chromatography: Silica gel-60 (230-400 mesh) from Sorbent Technologies. Thin Layer Chromatography (TLC): plastic sheets covered with silica gel purchased from Acros. Melting points were measured on a Thomas Hoover Capillary melting point apparatus. ^{1}H and ^{13}C NMR spectra were obtained using Varian Gemini-300 MHz, Inova-400 MHz, Inova-500 MHz, Bruker-400 MHz, or Bruker-500 MHz instruments, and were taken in deuterated chloroform unless noted otherwise.

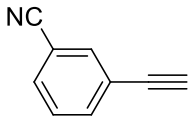

2-19

3-Ethynylbenzonitrile (2-19)[109]

Into a 50 mL round bottom flask was added with 3-bromobenzonitrile (0.497 g, 1 eq., 2.73 mmol), PPh_3 (0.018g, 0.068 mmol, 0.025 eq.), $Pd(PPh_3)_2Cl_2$ (0.096g, 0.136 mmol, 0.05 eq.) and a stir bar. The round bottom flask was evacuated-refilled three times with Ar. Then THF (6 mL), Et_3N (1.14 mL, 0.827 g, 8.19 mmol), and ethynyltrimethylsilane (0.587 mL, 1.5 eq., 4.10 mmol) were added by syringe. The mixture was stirred for 15 min under Ar, and then CuI (0.013 g, 0.068 mmol, 0.025 eq.) was added. The reaction was allowed to stir at room temperature overnight. THF was then removed, 20 mL hexane was added and the mixture was filtered over celite. The filtrate was washed with H_2O and concentrated. The residue solid was dissolved in 6 mL MeOH. K_2CO_3 (0.03 g, 0.22 mmol, to make a 0.05 M solution) was added, and the mixture was stirred at room temperature for 1.5 h. The reaction was then diluted with water (25 mL), extracted with diethyl ether (4×20 mL). The organic extract was dried over $MgSO_4$ and concentrated. Product was obtained as white needles (0.310 g, 89% yield). Lit. mp 42 – 44 °C.[124] ^{1}H-NMR (500 MHz, $CDCl_3$) δ 7.69 (s, 1H), 7.64(d, *J* = 8.0 Hz, 1H), 7.59 (d, *J* = 8.0 Hz, 1H), 7.40 (t, *J* = 7.5, 8.0 Hz, 1H); ^{13}C-NMR (125 MHz, $CDCl_3$) δ 135.9, 135.2, 131.8, 129.1, 123.5, 117.6, 112.6, 80.9, 79.8.[109]

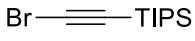

2-11

(Bromoethynyl) triisopropylsilane (2-11) [125]

Into a round-bottom flask wrapped with aluminum foil was added triisopropylsilyl acetylene (1 g, 5.55 mmol) and 50 mL acetone. $AgNO_3$ (0.076 g, 0.56 mmol) and recrystallized *N*-bromosuccinimide (1.09 g, 6.08 mmol) were added. The reaction mixture was allowd to sir in the dark at room temperature for 1.5 h. Ice water (50 mL) was added to quench the reaction. Hexanes (25 mL × 3) was used to extract the product. The combined organic layers were washed with 25 mL water and dried with $NaSO_4$. Filtration and removal of solvent generated compound 2-11 as a colorless oil (1.26 g, 19.26 mmol, 87.3% yield). ^{1}H NMR (400 MHz, $CDCl_3$): δ 1.08 (s). ^{13}C NMR (100 MHz, $CDCl_3$): δ 83.5, 62.0, 18.5, 11.3.[125]

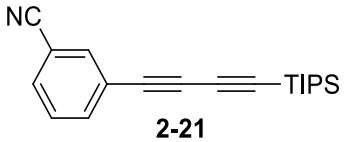

2-21

3-((Triisopropylsilyl)buta-1,3-diyn-1-yl)benzonitrile (2-21)

Compound **2-11** (0.925 g, 1.5 eq., 3.54 mmol) was dissolved in 20 mL THF, and 3-ethynylbenzonitrile **2-19** (0.300 g, 1 eq., 2.36 mmol) was added. CuI (0.02g, 0.12 mmol, 0.05 eq.), and $Pd(PPh_3)_2Cl_2$ (0.084 g, 0.12 mmol, 0.05 eq.) was added. (*i*-Pr)$_2$NH (0.98 mL, 0.71 g, 7 mmol, 2 eq.) was added to the reaction mixture dropwise. After stirring under Ar at room temperature for 5 h, 30 mL saturated NH_4Cl solution was added and the reaction was extracted with 3×30 mL Et_2O. A mixture of both homo-coupling and cross-coupling products was obtained after concentration. Column chromatography (SiO_2, Hex: Et_2O = 5:1) was used to isolate the product as very light yellow solid (0.68 g, 63% yield). mp 105-108 ºC. EIMS, *m/z* 309.80 ([M-C(CH$_3$)$_3$] = 264.10). ^{1}H-NMR (400 MHz, $CDCl_3$) δ 7.76 (s, 1H), 7.70 (d, *J* = 8.0 Hz, 1H), 7.62 (d, *J* = 8.0 Hz, 1H), 7.44 (t, *J* = 7.5, 8.0 Hz, 1H), 1.11 (s, 21H); ^{13}C-NMR (100 MHz, $CDCl_3$) δ 136.5, 135.8, 132.2, 129.4, 123.3, 117.7, 113.1, 90.1, 88.7, 76.8, 72.6, 18.5, 11.2.

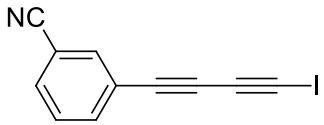

2-3

3-(Iodobuta-1,3-diyn-1-yl)benzonitrile (2-3)

Compound **2-21** (0.2 g, 0.651 mmol) was dissolved in 30 mL CH_3CN. AgF (0.289 g, 2.278 mmol) and NIS (0.512 g, 2.278 mmol) were added, and the reaction was allowed to stir at 0 ºC in the dark for 1h. The reaction was quenched with 30 mL ice water and extracted with 3×30 mL hexane. The combined organic extract was dried over $MgSO_4$. Solvent was removed, and the crude product was further purified by column chromatography (SiO_2, Hex : EA = 5:1), resulting in a light yellow solid (0.16 g, 90% yield). mp 100 – 101 °C. EIMS, *m/z* 276.95. ^{1}H-NMR (500 MHz, $CDCl_3$) δ = 7.74 (t, 1H), 7.70 (d, *J* = 8.0 Hz, 1H), 7.63 (d, *J* = 8.0 Hz, 1H), 7.45 (t, *J* = 7.5, 8.0 Hz, 1H); ^{13}C-NMR (125MHz, $CDCl_3$) δ = 136.9, 136.2, 132.5, 129.4, 122.6, 117.6, 113.1, 77.7, 77.3, 70.8, 5.4. IR 2924, 2239, 2202, 2105, 1670, 1602, 1499, 1403, 1272, 1104, 1011, 836, 736 cm^{-1}.

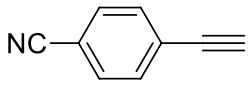

2-18

4-Ethynylbenzonitrile (2-18) [109]

Into a 50 mL round bottom flask was added 4-bromobenzonitrile (0.497 g, 1 eq., 2.73 mmol), PPh_3 (0.018g, 0.068 mmol, 0.025 eq.), $Pd(PPh_3)_2Cl_2$ (0.096g,0.136 mmol, 0.05 eq.) and a stir bar. The flask was evacuated-refilled three times with Ar. Then THF (6 mL), Et_3N (1.14 mL, 0.827 g, 8.19 mmol), and ethynyltrimethylsilane (0.587 mL, 0.41 g, 1.5 eq., 4.10 mmol) were added by syringe. The mixture was stirred for 15 min under Ar before CuI (0.013 g, 0.068 mmol, 0.025 eq.) was added ant the reaction stirred at room temperature overnight. After reaction, THF was removed under reduced pressure, hexane added and the mixture filtered over celite. The filtrate was washed with H_2O and the hexane removed. The residue solid was dissolved in 6 mL MeOH, K_2CO_3 (0.03 g, 0.22 mmol, to make a 0.05 M solution) was added, and the mixture was stirred at room temperature for 1.5 h. Methanol was removed by evaporation, and water was added to dilute the reaction system. After extraction with ether (4×20 mL), drying with $MgSO_4$, and removal of solvent, product was obtained as white needles (0.303 g, 87% yield). Lit. mp 156 – 158 °C.[126] ^{1}H-NMR (500 MHz, $CDCl_3$) δ 7.55-7.62(m, 4H), 3.30(s, 3H); ^{13}C-NMR (125 MHz, $CDCl_3$) δ 132.6, 132.0, 126.9, 118.2, 112.3, 81.8,81.5.[109]

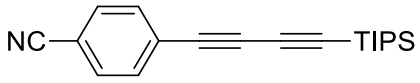

2-20

4-((Triisopropylsilyl)buta-1,3-diyn-1-yl)benzonitrile (2-20)

Compound **2-11** (0.925 g, 1.5 eq., 3.54 mmol) was dissolved in 20 mL THF, and 4-ethynylbenzonitrile (0.300 g, 1 eq., 2.36 mmol) was added. CuI (0.02g, 0.12 mmol, 0.05 eq.), and

$Pd(PPh_3)_2Cl_2$ (0.084 g, 0.12 mmol, 0.05 eq.) was added in one portion, and $(i\text{-}Pr)_2NH$ (0.98 mL, 0.708 g, 7 mmol, 2 eq.) was added to the reaction mixture dropwise. After stirring under N_2 at room temperature for 5 h, 30 mL saturated NH_4Cl solution was added and the reaction was extracted with 3×30 mL Et_2O. Solvent was removed, a mixture of both homo-coupling and cross-coupling products was obtained. Column chromatography (SiO_2/Hex: Et_2O = 5:1) was used to isolate product as a white solid (0.62 g, 57% yield). mp 99-103 ºC. EIMS, *m/z* 307.21 ([M-C(CH_3)$_3$] = 264.17). ^{1}H-NMR (500 MHz, $CDCl_3$) δ 7.56-7.61 (m, 4H), 1.11 (s, 21H); ^{13}C-NMR (125MHz, $CDCl_3$) δ 133.1, 132.0, 126.6, 118.2, 112.4, 91.2, 88.7, 78.7, 73.4, 18.5, 11.2.

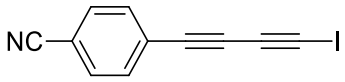

2-2

4-(Iodobuta-1,3-diyn-1-yl)benzonitrile (2-2)

4-((Triisopropylsilyl)buta-1,3-diyn-1-yl)benzonitrile (0.2 g, 0.651 mmol) was dissolved in 30 mL CH_3CN. AgF (0.289 g, 2.278 mmol) and NIS (0.512 g, 2.278 mmol) were added, and the reaction was allowed to stir at 0 ºC in the dark for 1h. The reaction was quenched with 30 mL ice water and extracted with 3×30 mL portions of hexane. The combined organic extract was dried over $MgSO_4$. Solvent was removed, and the crude product was further purified by column chromatography (SiO_2, Hex : EA = 5:1), resulting in a light yellow solid (0.17 g, 95% yield). 100 ℃ turns dark, 120 ℃ turns black. EIMS, *m/z* 276.97. ^{1}H-NMR (500 MHz, $CDCl_3$) δ = 7.56 – 7.62 (m, 4H) ppm; ^{13}C-NMR (125 MHz, $CDCl_3$) δ 133.5, 132.0, 125.9, 118.1, 112.7, 78.8, 77.8, 71.4, 6.4. IR 2924, 2239, 2202, 2105, 1670, 1602, 1499, 1403, 1272, 1104, 1011, 836, 736 cm^{-1}.

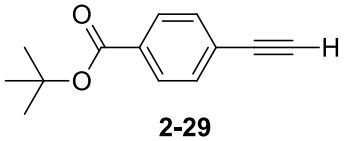

2-29

***t*-Butyl 4-ethynylbenzoate (2-29)**[127]

A mixture of *t*-butyl 4-bromobenzoate (0.151 g, 0.6mmol), ethynyltrimethylsilane (0.1 g, 1mmol), $Pd(PPh_3)_2Cl_2$ (0.084 g, 0.12 mmol, 0.2 eq.), PPh_3 (0.031 g, 0.12 mmol, 0.2 eq.) and CuI (0.011 g, 0.06 mmol) in Et_3N (0.25 mL, 0.181 g, 3 eq.) was stirred under nitrogen atmosphere under reflux for 16 h. After cooling to room temperature, the mixture was diluted with 20 mL CH_2Cl_2 and then washed with water (2×20 mL). The organic layer was dried with $MgSO_4$ and evaporated under reduced pressure to dryness. The obtained light brown solid was dissolved in 6 mL methanol, and K_2CO_3 (0.03 g, 0.22 mmol, to make a 0.05 M solution) was added. The mixture was allowed to stir at room temperature for 1.5 h. Some methanol was removed by rotary evaporation. The reaction system was diluted with water, extracted with ether (4×20 mL), dried with $MgSO_4$. Compound **2-29** was obtained as a colorless oil (0.109 g, 90% yield) after solvent evaporation. Lit. mp 128°C.[127] ^{1}H-NMR (500 MHz, $CDCl_3$) δ 7.93(d, *J* = 8.5 Hz, 2H), 7.51(d, *J* = 8.5 Hz, 2H), 3.21(s, 1H), 1.59(s, 9H). ^{13}C-NMR (125MHz, $CDCl_3$) δ 165.0, 132.0, 131.9, 129.3, 126.1, 82.9, 81.4, 79.7, 28.1.[127]

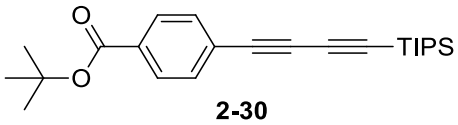

2-30

***t*-Butyl 4-((Triisopropylsilyl)buta-1,3-diyn-1-yl)benzoate (2-30)**

Compound **2-11** (0.956 g, 1.5 eq., 3.66 mmol) was dissolved in 20 mL THF, and compound **2-29** (0.493 g, 1 eq., 2.44 mmol) was added. CuI (0.023g, 0.122 mmol, 0.05 eq,), and $Pd(PPh_3)_2Cl_2$ (0.085g, 0.122 mmol, 0.05 eq.) was added in one portion, and *i*-Pr_2NH (1 mL, 0.722 g, 7.32 mmol, 3 eq.) was added to the reaction mixture dropwise. After stirring under N_2 at room temperature for 5 h, 30 mL saturated NH_4Cl solution was added and the reaction was extracted with 3×30 mL Et_2O. A mixture of both homo-coupling and cross-coupling products were obtained. Column chromatography (SiO_2, Hex : Et_2O = 5:1) was used to isolate compound **2-30** as light yellow liquid (0.495 g, 53% yield). MS (ES-API+), positive, $[M+H]^+$ = 383.1, $[M-C(CH_3)_3+2H]^+$ = 327.1. ^{1}H-NMR (400MHz, $CDCl_3$) δ 7.92(d, *J* = 8.4 Hz, 2H), 7.52(d, *J* = 8.4 Hz, 2H), 1.58(s, 9H), 1.12(s, 21H). ^{13}C-NMR (100MHz, $CDCl_3$) δ 164.9, 132.4, 132.2, 129.3, 125.6, 89.6, 89.1, 81.5, 74.7, 28.1, 18.6, 11.3.

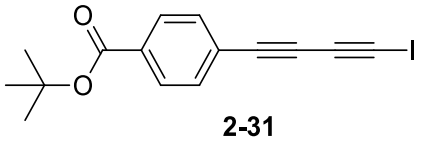

2-31

***t*-Butyl 4-(iodobuta-1,3-diyn-1-yl)benzoate (2-31)**

Compound **2-30** (0.249 g, 0.651 mmol) was dissolved in 30 mL CH_3CN. AgF (0.289 g, 2.278 mmol) and NIS (0.512 g, 2.278 mmol) were added, and the reaction was allowed to stir at 0 ℃ in the dark for 1 h. The reaction was quenched with 50 mL ice water and extracted with 3×30 mL portions of hexane. The combined organic extract was washed with 20 mL sat. aq. Na_2SO_4 and dried over $MgSO_4$. Solvent was removed, and column chromatography was utilized to purify the compound (SiO_2, Hex : EA = 10:1), which resulted in a pale yellow solid (0.202 g, 88% yield). mp 88 ℃. MS (ES-API+), positive, $[M+H]^+$ = 352.9, $[M-C(CH_3)_3+2H]^+$ = 296.9. ^{1}H-NMR (500MHz, $CDCl_3$) δ 7.92(d, *J* = 8.0 Hz, 2H), 7.51(d, *J* = 8.5 Hz, 2H), 1.58(s, 9H). ^{13}C-NMR (125MHz, $CDCl_3$) δ 164.8, 132.8, 132.5, 129.3, 124.9, 81.5, 78.0, 72.8, 28.1, 4.7.

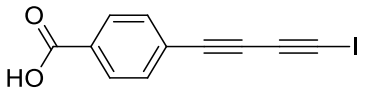

2-5

4-(Iodobuta-1,3-diyn-1-yl)benzoic acid (2-5)

Compound **2-31** (0.1 g, 0.28 mmol) was dissolved in 5 mL TFA (Trifluoroacetic acid) : CH_2Cl_2 = 1:1 solution. The reaction mixture was stirring at room temperature for 2 h. Then the excess TFA and *t*-butanol were removed under vacuum, resulting in a pale yellow solid (0.083 g, quantitative yield). 163 - 177 ℃ turned dark. MS(ES-API), negative, $[M-H]^-$ = 294.9. ^{1}H-NMR (500MHz, MeOD) δ 8.00(d, *J* = 8.0 Hz, 2H), 7.58(d, *J* = 8.5Hz, 2H); ^{13}C-NMR (125MHz, MeOD) δ 168.8, 134.0, 132.7, 130.8, 126.8, 78.1, 77.7, 72.7, 12.2. IR: 2550, 2361, 2160, 2028, 1978, 1683, 1653, 1604, 1558, 1427, 1320, 1296, 1280, 1181, 1112, 860, 770 cm^{-1}.

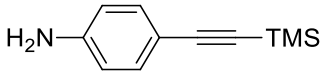

2-33

4-((Trimethylsilyl)ethynyl)aniline (2-33)[110]

Triethylamine (2.5 mL, 1.81 g, 0.018 mol), *p*-iodoaniline (1.024 g, 4.67 mmol), CuI (0.089 g, 0.467 mmol), $Pd(PPh_3)_2Cl_2$ (0.164 g, 0.234 mmol) and trimethylsilyl acetylene (1 mL, 7.00 mmol) were added in THF under argon atmosphere. The above mixture was refluxed overnight. 30 mL saturated NH_4Cl solution was added and the reaction was extracted with 3×30 mL Et_2O. The product was purified by silica gel plug (Et_2O: Hex = 1: 5). The product was obtained as a white solid (0.66 g, 74.5% yield). Lit. mp 93 – 95 °C.[128] ^{1}H NMR (500 MHz, $CDCl_3$) δ 7.30 (d, *J* = 8.5 Hz, 2H), 6.57 (d, *J* = 8.5 Hz, 2H), 3.83 (br. s, 2H), 0.28 (s, 9H). ^{13}C NMR (125MHz, $CDCl_3$) δ 146.8, 133.2, 114.4, 112.2, 106.1, 91.3, 0.08 ppm.[110]

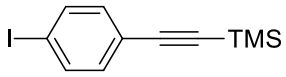

2-34

((4-Iodophenyl)ethynyl)trimethylsilane (2-34) [111]

To a solution of compound **2-33** (530 mg, 2.8 mmol) in HCl (6 M, 40 mL), cooled at 0 ℃, is added sodium nitrite, $NaNO_2$, (232 mg, 3.36 mmol) in one portion. After 1h at 0 ℃, the solution is added dropwise to an ice-cold solution of potassium iodide KI (697 mg, 4.2 mmol), and 40 mL of CH_2Cl_2 is poured in this solution. The resulting mixture is allowed to reach room temperature and is stirred for 4 h. The aqueous phase is extracted twice with CH_2Cl_2. The combined organic layers are washed with a saturated solution of sodium thiosulfate and dried over magnesium sulfate. The solvents are removed, and the crude product is purified by column chromatography (SiO_2, Hexane), to provide a white solid (395 mg, 47% yield). Lit. mp 52 – 54 °C.[129] ^{1}H-NMR (500 MHz, $CDCl_3$) δ 7.63(d, *J* = 8.5 Hz, 2H), 7.17(d, *J* = 8.5 Hz, 2H), 0.24(s, 9H). ^{13}C-NMR (125MHz, $CDCl_3$) δ 137.3, 133.4, 122.6, 103.9, 95.9, 94.4, -0.14.[111]

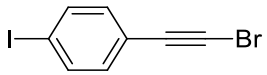

2-35

1-(Bromoethynyl)-4-iodobenzene (2-35)[130]

Compound **2-34** (0.185 g, 0.62 mmol) was dissolved in 100 mL acetone, and $AgNO_3$ (0.371 g, 2.17 mmol, 3.5 eq.) and NBS (0.386 g, 2.17 mmol, 3.5 eq.) was added into the solution. The reaction mixture was stirred at room temperature for 4 h. The reaction was quenched with 50 mL ice water and extracted with 3×30 mL portions of hexanes. The combined organic extract was washed with 20 mL sat. aq. Na_2SO_4 and dried over $MgSO_4$. Solvent was removed, resulting in white solids (0.167 g, 88% yield). Lit. mp 102 – 104 °C.[131] ^{1}H-NMR (500 MHz, $CDCl_3$) δ 7.64 (d, *J* = 8.5 Hz, 2 H), 7.16 (d, *J* = 8.5 Hz, 2 H). ^{13}C-NMR (125MHz, $CDCl_3$) δ 137.50, 133.43, 122.18, 94.69, 79.15, 51.47.[130]

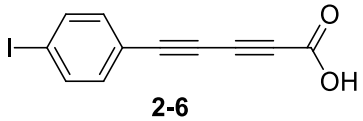

2-6

5-(4-Iodophenyl)penta-2,4-diynoic acid (2-6)

To a solution containing propiolic acid (0.14 g, 2 mmol), CuCl (0.016 g, 0.2 mmol, 0.1 eq.), hydroxylamine hydrochloride (0.16 g, 23 mmol), ethanol amine (0.8 mL, 0.808 g, 13.2 mmol) and H_2O (0.5 mL, 0.5 g, 27.8 mmol) at vigorous stirring was slowly added dropwise a solution of compound **2-35** (0.30 g, 1.67 mmol) in 5 mL methanol. The reaction was stirred at room temperature for 24 h. 20 mL 2M HCl was added to quench it. Product was extracted by diethyl ether, and solvents were removed resulting in a white solid (0.346 g, 70%). M.p. 118-123 ℃. EIMS *m/z* 295.97([M-OH]$^+$=278.9). ^{1}H-NMR (500 MHz, MeOD) δ 7.84-7.86 (d, *J* = 8.5 Hz, 2H), 7.43-7.45 (d, *J* = 8.5 Hz, 2H).^{13}C-NMR (125 MHz, MeOD) δ 153.0, 137.8, 134.5, 118.2, 98.9, 82.3, 73.9, 72.5, 68.3. IR: 3661, 2981, 1884, 2201, 2027, 1679, 1604, 1428, 1404, 1321, 1296, 1280, 1180, 1128, 860, 820, 769, 742, 720, 691 cm^{-1}.

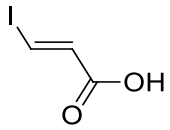

2-42

(*E*)-3-Iodoacrylic acid (2-42)[132]

A solution of propiolic acid (1 g, 0.014 mol) in 4 ml of 57% aqueous hydroiodic acid was stirred for 24 h at 80 °C (preheated bath) and then allowed to cool down in ice bath. White crystals were formed and filtered and washed with cold water (1.66g, 60% yield). Lit. mp 143 – 145 °C.[133] ^{1}H-NMR (400 MHz, $CDCl_3$) δ 8.05 (d, *J* = 14.8 Hz, 1H), 6.88-6.91(d, *J* = 14.8 Hz, 1H). ^{13}C-NMR (100 MHz, $CDCl_3$) δ 168.8, 135.8, 102.8.[132]

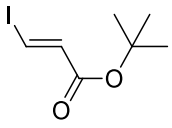

2-39

(*E*)-*t*-Butyl 3-iodoacrylate (2-39)[132]

Compound **2-42** (0.3 g, 1.52 mmol) was dissolved in 10 mL CH_2Cl_2, and a catalytic amount of triflic acid was added. The reaction mixture was stirred at room temperature for 1 h, then 2M KOH was added to quench it. Products were extracted by ethyl ether and solvents were removed in vaco. (*E*)-t-Butyl 3-iodoacrylate **2-39** was obtained as colorless oil (0.27 g, 70% yield). ^{1}H-NMR (400 MHz, $CDCl_3$) δ 7.65 -7.69 (d, *J* = 14.8 Hz, 1H), 6.72 (d, *J* = 14.8 Hz, 1H), 1.43 (s, 9H). ^{13}C-NMR (100 MHz, $CDCl_3$) δ 163.1, 138.2, 97.9, 81.2, 27.9.[132]

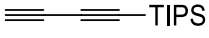

2-40

Buta-1,3-diynyltriisopropylsilane(2-40) [115]

N-Butylamine (0.9 mL, 0.67 g, 9 mmol, 3 eq.), 2-methylbut-3-yn-2-ol (0.59 mL, 0.51 g, 6 mmol, 2 eq.), CuCl (6 mg, 0.06 mmol, 0.01 eq.) and hydroxylamine hydrochloride (62 mg, 0.9 mmol, 0.3 eq.) were added in order to a solution of 15 mL methanol : water = 2:1. (Bromoethynyl)triisopropylsilane (0.8 g, 3 mmol, 1 eq.) was diluted with methanol (8 mL) and added dropwise over 30 min. The solution was left stirring at room temperature for 24 h. The solution was then diluted with water (20 mL) and extracted with diethyl ether (3 × 15 mL). The combined organic layers were washed with water (1 × 15 mL) and brine (2 × 15 mL), dried over anhydrous $MgSO_4$, filtered and evaporated. Purification by flash chromatography (SiO_2, Hex : EA = 5:1) gave 2-methyl-6-(triisopropylsilyl)hexa-3,5-diyn-2-ol as a colorless oil (0.31 g, 78%). 2-Methyl-6-(triisopropylsilyl)hexa-3,5-diyn-2-ol (504 mg, 1.86 mmol, 1 eq.) was added to a solution of crushed potassium hydroxide (210 mg, 3.73 mmol, 2 eq.) in toluene (15 mL) and the solution heated to 80 °C for 2.5 h. The solution was then cooled and diluted with water (20 mL) and extracted with hexane (3 × 15 mL). The combined organic layers were dried over anhydrous $MgSO_4$, filtered and evaporated to give orange oil. Purification by filtration through SiO_2, eluting with hexane gave the product as an orange / red oil (360 mg, 91% yield). The product needs to be stored in solution in the freezer. ^{1}H-NMR (400 MHz, $CDCl_3$) δ 2.07 (s, 1H), 1.09 (s, 21H). ^{13}C-NMR (100 MHz, $CDCl_3$) δ 89.1, 81.9, 68.6, 65.5, 18.5, 11.2.[115]

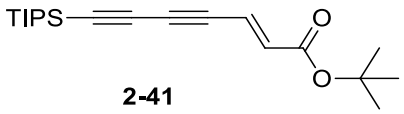

2-41

(*E*)- *tert*-Butyl 7-(triisopropylsilyl)hepta-2-en-4,6-diynoate (2-41)

A 50 mL round bottom flask was charged with (*E*)-*t*-butyl 3-iodoacrylate **2-39** (0.121 g, 1 eq., 0.476 mmol), PPh_3 (0.006 g, 0.024 mmol, 0.05 eq.), $Pd(PPh_3)_2Cl_2$ (0.017 g, 0.024 mmol, 0.05 eq.) and a stir bar. The round bottom flask was evacuated-refilled three times with Ar. Then THF (5 mL), Et_3N (0.21 mL, 0.15 g, 1.5 mmol, 3 eq.), and compound **2-40** (0.147 g, 1.5eq, 0.714 mmol) were added by syringe. The mixture was stirred for 15 mins under Ar before CuI (0.003 g, 0.012 mmol, 0.025 eq., 190.45 g / mol) was added. The reaction was stirred at room temperature overnight. THF was removed by evaporation. After adding diethyl ether and filter the mixture over celite, the filtrate was washed with water. Removing diethyl ether and purification through column chromatography (SiO_2, Hex : EA = 9 : 1) gave compound **2-41** as a pink oily solid (0.076 g, 54% yield). mp 76 -77 °C. MS (ES-API), positive, $[M\text{-}C(CH_3)_3+2H]^+$ = 277.1. ^{1}H-NMR (500 MHz, $CDCl_3$) δ 6.63 (d, *J* = 16 Hz, 1H), 6.25 (d, *J* = 16 Hz, 1H), 1.48(s, 9H), 1.09(s, 21H).^{13}C-NMR (125MHz, $CDCl_3$) δ 164.5, 135.3, 122.5, 92.1, 88.8, 82.2, 81.4, 72.3, 28.0, 18.5, 11.2. IR: 2943, 2866, 2161, 2033, 1715 cm^{-1}.

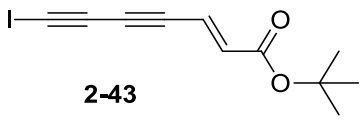

2-43

(*E*)-*tert*-Butyl 7-iodohepta-2-en-4,6-diynoate (2-43)

Compound diynoate **2-41** (0.216 g, 0.651 mmol, 332.55 g / mol) was dissolved in 30 mL CH_3CN. AgF (0.289 g, 2.278 mmol, 126.87 g / mol) and N-Iodosuccinimide (NIS) (0.512 g, 2.278 mmol, 224.98 g / mol) were added, and the reaction was allowed to stir at 0 ℃ in the dark for 1 h. The

reaction was quenched with 50 mL ice water and extracted with 3×30 mL portions of hexane. The combined organic extract was washed with 20 mL sat. aq. Na_2SO_4 and dried over $MgSO_4$. Solvent was removed, resulting in pale yellow needles (0.177 g, 90% yield). mp 74-77 ℃. MS (ES-API), positive, $[M\text{-}H\text{-}C(CH_3)_3+2H]^+$ = 246.9. ^{1}H-NMR (500MHz, $CDCl_3$) δ 6.67 (d, *J* = 15.5 Hz, 1H), 6.26 (d, *J* = 16 Hz, 1H), 1.47 (s, 9H). ^{13}C-NMR (125MHz, $CDCl_3$) δ 164.4, 136.3, 121.8, 82.3, 81.5, 77.9, 70.4, 28.0, 7.4. IR: 2973, 2928, 2198, 1685, 1608, 1456, 1368, 1393, 1322, 1258, 1215, 1147, 953, 863, 831, 763, 723 cm^{-1}.

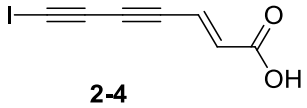

2-4

4-(Iodobuta-1,3-diyn-1-yl)benzoic acid (2-4)

Compound **2-43** (0.301 g, 1 mmol) was dissolved in 5 mL TFA : CH_2Cl_2 = 1:1 solution. The reaction mixture was stirring at room temperature in dark for 1 h. Then the excess TFA and *t*-butanol were removed by rotary-evaporation, resulting in quantitative yield of a pale yellow solid. 122 ℃ decompose. MS (ES-API), negative, $[M\text{-}H]^-$ = 244.9, $[M\text{-}COOH]^-$ = 200.9. ^{1}H-NMR (400MHz, MeOD) δ 6.79 (d, *J* = 12.8 Hz, 1H), 6.34 (d, *J* = 12.4 Hz, 1H).^{13}C-NMR (100MHz, MeOD) δ 168.1, 135.9, 124.2, 83.5, 77.5, 70.3, 15.5. IR: 2851, 2681, 2544, 2198, 1687, 1613, 1420, 1298, 1281, 1217, 1205, 959, 943, 907, 869, 842, 725, 683 cm^{-1}.

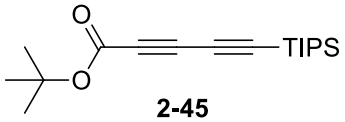

2-45

***tert*-Butyl 5-(triisopropylsilyl)penta-2,4-diynoate (2-45)**

To a solution containing *t*-butyl propiolate (2 mmol, 0.14 g), CuCl (0.016 g, 0.2 mmol, 0.1 eq.), hydroxylamine hydrochloride (0.16 g, 23 mmol), ethanol amine (0.8 mL, 0.808 g, 13.2 mmol) and H_2O (0.5 mL, 0.5 g, 27.8 mmol) at vigorous stirring was slowly added dropwise a solution of (bromoethynyl)triisopropylsilane (0.572 g, 2.2 mmol) in 5 mL methanol. The reaction was stirred at room temperature for 24 h, then 20 mL 2M HCl was added to quench it. Products were extracted by diethyl ether, and solvents were removed resulting in a white solid (0.386 g, 63% yield). 120 ℃ decompose. EIMS, *m/z* 306.51($[M\text{-}CH_3]^+$=291.37). ^{1}H NMR (500 MHz, $CDCl_3$) δ 1.48 (s, 21H), 1.07 (s, 9H). ^{13}C NMR (125 MHz, $CDCl_3$) δ 151.6, 91.4, 87.6, 84.3, 69.1, 67.1, 27.9, 18.4, 11.1.

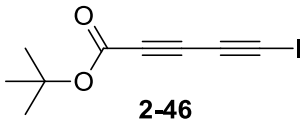

2-46

***tert*-Butyl 5-iodopenta-2,4-diynoate (2-46)**

Compound **2-45** (0.199 g, 0.651 mmol) was dissolved in 30 mL CH3CN and cooled down in ice bath to 0 ℃. AgF (0.289 g, 2.278 mmol) and NIS (0.512 g, 2.278 mmol) were added, and the reaction was allowed to stir at 0 ℃ in the dark for 1 h. The reaction was quenched with 30 mL ice water and extracted with 3×30 mL portions of hexane. The combined organic extract was washed with 20 mL sat. aq. Na_2SO_4 and dried over $MgSO_4$. Solvent was removed, resulting in a pale

yellow solid (0.158 g, 88% yield). 105 ℃ decompose. EIMS, *m/z* 276.01, $[M\text{-}OC(CH_3)_3]^+$ = 202.87. ^{1}H-NMR (400 MHz, $CDCl_3$) δ 1.48 (s, 21H). ^{13}C-NMR (100 MHz, $CDCl_3$) δ 151.1, 84.6, 69.0, 65.0, 30.9, 27.9, 7.7.

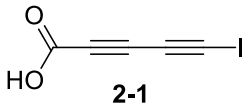

2-1

5-Iodopenta-2,4-diynoic acid (2-1)

Compound **2-46** (0.1 g, 0.36 mmol) was dissolved in 5 mL TFA (Trifluoroacetic acid) : CH_2Cl_2 = 1:1 solution. The reaction mixture was stirring at room temperature for 2 h. Then the excess TFA and t-butanol were removed under vacuum, resulting in a pale yellow solid (0.08 g, quantitative yield). 105 °C turn dark. EIMS, *m/z* 220.0, $[M\text{-}OH]^+$ = 203.0. ^{1}H-NMR (500 MHz, MeOD) δ 5.11(s, 1H).^{13}C-NMR (125 MHz, MeOD) δ 154.7, 76.3, 71.4, 64.6, 16.6. IR: 3660, 2981, 2971, 2889, 2275, 2193, 1661, 1599, 1473, 1382, 1252, 1136, 1073, 953, 824, 801, 738 cm^{-1}.

2-49

Di-*tert*-butyl hexa-2,4-diynedioate (2-49)[134]

CuCl (0.118 g, 1.19 mmol) was dissolved in 4 mL acetone and Tetramethylethylenediamine (TMEDA) (0.06 mL, 46.6 mg, 0.39 mmol) was added. Oxygen was bubbled through the solution for 2 h, and the solution was cooled to 0 ℃. A solution of t-butyl propiolate (1.63 mL, 1.498 g, 11.9 mmol) in 7 mL acetone was added, and oxygen was bubbled through the solution for 30 min at 0 ℃. The reaction mixture was directly run through a plug (SiO_2, Hex : EA = 5:1), resulting in white needles (0.75 g, 50% yield). 80 ℃ turn dark. Mass spectrum indicates that the t-butyl group is easily removed. EIMS, $[M\text{-}C(CH_3)_3+H]$ = 194.11, $[M\text{-}OC(CH_3)_3]^+$ = 177.11, $[M\text{-}C(CH_3)_3\text{-}OC(CH_3)_3+H]$ = 121.01. ^{1}H-NMR (400MHz, $CDCl_3$) δ 1.48 (s, 18H); ^{13}C-NMR (100MHz, $CDCl_3$) δ 150.6, 85.3, 73.3, 66.1, 27.9. IR: 2988, 2154, 1701, 1478, 1460, 1391, 1370, 1238, 1136, 1035, 931, 912, 834, 747 cm^{-1}. [134]

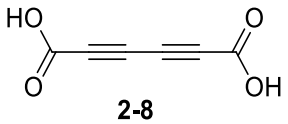

2-8

Hexa-2,4-diynedioic acid (2-8)

Compound **2-49**(0.1 g, 0.4 mmol) was dissolved in 5 mL TFA : CH_2Cl_2 = 1:1 solution. The reaction mixture was stirring at room temperature for 1 h. White needle crystal precipitated out. After filtration, the white crystal was washed by a small amount of hexane and air dried (33 mg, 60% yield). The crystals turned pink immediately and dark gradually after laying out at room temperature. mp 170 – 180 °C (Lit. mp 170-180 °C).[122] EIMS, *m/z* 137.93, $[M\text{-}COOH+H]^+$ = 93.95. ^{1}H-NMR (500MHz, MeOD) δ 5.03 (s, 2H); ^{13}C-NMR (125MHz, MeOD) δ 153.9, 74.2, 67.4. IR: 2853, 2513, 2154, 1668, 1393, 1372, 1240, 1144, 837, 742 cm^{-1}.

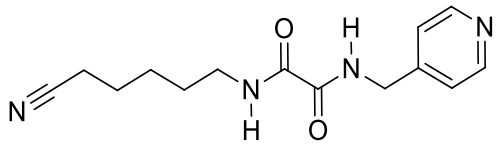

2-52

N^1-(5-Cyanopentyl)-N^2-(pyridin-4-ylmethyl)oxalamide (2-52)

Ethyl chloro(oxo)acetate (1.14 mL, 10.2 mmol) was added to a solution of 1 -pyridin-4-ylmethanamine (1 g, 9.25 mmol) in anhydrous THF (30 mL) at 0 °C followed by triethylamine (2 mL, 13.9 mmol). The reaction mixture was slowly warmed to ambient temperature and stirring overnight. The mixture was dilute with saturated aqueous $NaHCO_3$ and extracted with EA. The combined organic extracts were washed with saturated brine, dried over $MgSO_4$, and concentrated to give ethyl 2-oxo-2-((pyridin-4-ylmethyl)amino)acetate (15.7 g, 81% yield).[135] Ethyl 2-oxo-2-((pyridin-4-ylmethyl)amino)acetate (0.416 g, 2 mmol) was dissolved in methanol, and 6-aminohexanenitrile (0.224 g, 2 mmol) was added. The reaction mixture was stirred for 24 hours, and concentrated by vacuum evaporation. Crude product was almost white solid and recrystallized in methanol to be white solid (0.387 g, 70% yield after recrystallization). mp 103-105 ℃. MS(+ESI-MS), $[M+H]^+$ = 275.22, $[M+Na]^+$ = 297.21. ^{1}H-NMR (500 MHz, DMSO): δ 9.42 (br. s, 1H), 8.86 (1H), 8.51 (d, *J* = 5.5 Hz, 2H), 7.26 (d, *J* = 5.5 Hz, 2H), 4.37 (d, *J* = 5.5 Hz, 2H), 3.16 (m, 2H), 2.48-2.53(m, 3H), 1.35-1.60 (m, 8H); ^{13}C-NMR (125 MHz, DMSO): δ 160.5, 159.6, 149.5, 147.5, 122.1, 120.6, 41.4, 38.4, 27.8, 25.3, 24.3, 16.0. IR: 3291, 2954, 2245, 1650, 1599, 1561, 1515, 1436, 1415, 1372, 1279, 1258, 1235, 1219, 1093, 993, 924, 896, 796, 773, 757, 704 cm^{-1}.

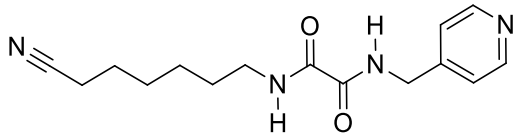

2-53

N^1-(6-Cyanohexyl)-N^2-(pyridin-4-ylmethyl)oxalamide (2-53)

Ethyl chloro(oxo)acetate (1.14 mL, 10.2 mmol) was added to a solution of 1 -pyridin-4-ylmethanamine (1 g, 9.25 mmol) in anhydrous THF (30 mL) at 0 °C followed by triethylamine (2 mL, 13.9 mmol). The reaction mixture was slowly warmed to ambient temperature and stirring overnight. The mixture was dilute with saturated aqueous $NaHCO_3$ and extracted with EA. The combined organic extracts were washed with saturated brine, dried over $MgSO_4$, and concentrated to give ethyl 2-oxo-2-((pyridin-4-ylmethyl)amino)acetate (15.7 g, 81% yield).[135] Ethyl 2-oxo-2-((pyridin-4-ylmethyl)amino)acetate (0.416 g, 2 mmol) was dissolved in methanol, and 7-aminohexanenitrile (0.252 g, 2 mmol) was added. The reaction mixture was stirred for 24 hours, and concentrated by vacuum evaporation. Crude product was almost white solid and recrystallized in methanol to be white solid (0.374 g, 65% after recrystallization). mp 103-106 ℃. MS(+ESI-MS), $[M+H]^+$ = 289.24, $[M+Na]^+$ = 311.22. ^{1}H-NMR (500 MHz, DMSO): δ 9.42 (br. s, 1H), 8.83 (br. s, 1H), 8.52 (d, *J* = 5.5 Hz, 2H), 7.26 (d, *J* = 5.5 Hz, 2H), 4.37 (d, *J* = 5.5 Hz, 2H), 3.34 (s, 1H), 3.15 (m, 2H), 2.48-2.53 (m, 2H), 1.29-1.58 (m, 8H). ^{13}C-NMR (125 MHz, DMSO): δ 160.5,

159.6, 149.4, 147.5, 122.1, 120.6, 41.4, 28.3, 27.6, 25.4, 24.6, 16.0. IR: 3287, 2923, 2856, 1651, 1597, 1562, 1464, 1436, 1415, 1361, 1256, 1228, 1209, 1168, 767 cm^{-1}.

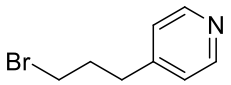

2-55

4-(3-Bromopropyl)pyridine (2-55)[136]

To a 0 ℃ solution of PPh_3 (0.826 g, 3.1 mmol) in 10 mL CH_2C1_2 was added bromine (0.50 g, 3.1 mmol, 0.16 mL) over 1 min. PPh_3 was added (< 0.05 g) until the yellow color disappeared, and then a solution of 3-(4-pyridyl)-l-propanol (0.288 g, 2.1 mmol) in 5 mL CH_2C1_2 was added dropwise for 5 min. After 15 min more at 0 ℃ and 1 h at room temperature, 10 mL of diethyl ether was added and the mixture extracted with 15 mL×2 water and 5 mL×2 1M HC1 (aqueous). The combined aqueous washes were extracted once with 20 mL of ether and then made basic (pH >13) with 2M NaOH solution. The basic aqueous layer was extracted with 50 mL×3 diehtyl ether. The combined extracts were dried over $MgSO_4$, filtered, and concentrated to afford **2-55** as a colorless oil (0.589 g, 95% yield). ^{1}H-NMR (500 MHz, $CDCl_3$): δ 8.42 (d, *J* = 7.5 Hz, 2H), 7.05 (d, *J* = 7.0 Hz, 2H), 3.29 (t, *J* = 8.0 Hz, 2H), 2.68 (t, *J* = 9.0, 10.0 Hz, 2H), 2.06-2.13 (m, 2H).^{13}C-NMR (125 MHz, $CDCl_3$): δ 149.6, 123.7, 33.0, 32.6, 32.3.[136]

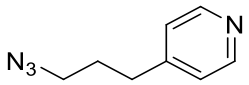

2-56

3-(4-Pyridyl)-1-propylazide (2-56)[137]

A solution of **2-55** (0.824 g, 4.12 mmol) in DMSO (15 mL) was treated with sodium azide (0.3 g, 4.53 mmol) and stir at 25° C. for 24 h. The solution was diluted with EtOAc, washed with H_2O and saturated $NaHCO_3$. The H_2O washing was basified to pH =11 and extracted with EtOAc. The organic layers were combined, dried with $MgSO_4$, filtered and evaporated to give **2-56** as a yellow oil (0.62 g, 93% yield). ^{1}H-NMR (500 MHz, $CDCl_3$) δ 8.40 (br.s, 2H), 6.99 (d, *J* = 6.0 Hz, 2H), 3.15 (t, *J* = 8.5 Hz, 2H), 2.54 (t, *J* = 9.0, 10.0 Hz, 2H), 1.74 (m, 2H); ^{13}C-NMR ($CDCl_3$, 125 MHz): δ 149.43, 123.49, 50.05, 31.65, 28.95.[137]

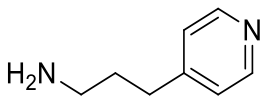

2-57

3-(4-Pyridyl)-1-propylamine (2-57)[137]

A solution of **2-56** (0.73 g, 4.12 mmol) in H_2O (10 mL) and THF (20 mL) was treated with PPh_3 (4.33 g, 16.5 mmol) and the reaction mixture was stirred vigorously for 24 h. The solution was diluted with EtOAc and washed with 1M HCl. The aqueous layers were combined and basified to pH=13 with 1M NaOH and extracted repeatedly with CH_2Cl_2. The CH_2Cl_2 layers were combined, dried with brine and concentrated to give compound **2-57** as an almost colorless oil (0.409 g, 73% yield). ^{1}H-NMR (400 MHz, MeOD) δ 7.90 (d, *J* = 6.0 Hz, 2H), 6.54 (d, *J* = 6.0 Hz, 2H), 2.04 (m,

4H), 1.13-1.21 (m, 2H), 0.92(br.s, 2H). ^{13}C-NMR (100 MHz, MeOD): δ 150.0, 148.4, 122.6, 52.7, 40.3, 32.9, 31.2.[137]

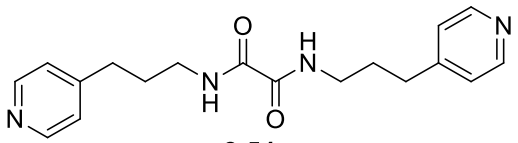

2-54

N^1,N^2-Bis(3-(pyridin-4-yl)propyl)oxalamide (2-54)

To a rapidly stirring solution of compound **2-57** (0.136 g, 1 mmol) in 5 mL THF was added diethyl oxalate (0.073 g, 0.5 mmol) drop-wisely. After stirring at room temperature for 12 h, the mixture was condensed under vacuum and a yellow oil was recovered. 20 mL ethyl acetate was added to dissolve the crude product and 10 mL×2 1M HCl was used to acidify and extract the product into the water layer. 2M NaOH was then used to basify the water layer to have a pH > 13, after which CH_2Cl_2 20 mL × 3 was used to extract the product into organic layer. After drying the organic layer over $MgSO_4$ and condense it under vacuum, white solid was recovered (0.163 g, 40% yield). mp 126-130 ℃. MS(+ESI-MS), $[M+H]^+$ = 327.26. ^{1}H-NMR (500 MHz, $CDCl_3$): δ 8.47 (d, *J* = 6.0 Hz, 2H), 7.65 (br. s, 2H), 7.12 (d, *J* = 6.0 Hz, 4H), 3.32-3.36 (t, 4H), 2.62 (t, *J* = 7.5, 8.0 Hz, 4H), 1.87-1.95 (m, 4H).^{13}C-NMR (125 MHz, $CDCl_3$): δ 159.8, 149.9, 149.8, 123.7, 39.0, 32.3, 29.6. IR: 3292, 2933, 1650, 1603, 1557, 1519, 1440, 1415, 1363, 1312, 1254, 1223, 1177, 1119, 1071, 992, 888, 802, 767, 740, 698 cm^{-1}.

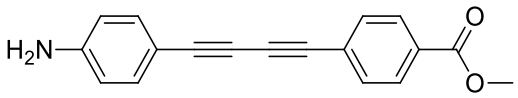

2-60

Methyl 4-((4-aminophenyl)buta-1,3-diyn-1-yl)benzoate(2-60)[123]

Copper (II) acetate (0.23 g, 1.24 mmol, 2 eq.) was added at room temperature and under Ar to a solution of methyl ethynylbenzoate (0.10 g, 0.62 mmol) and 4-ethynylbenzenamine (0.53 g, 3.1 mmol, 5 equiv) in pyridine (5 mL), and MeOH (5 mL). The reaction was stirred at room temperature for 24h. The resulting blue solution was quenched with water (20 mL) and extracted with ethyl acetate (20 mL×3). The organic layer was dried over anhydrous $MgSO_4$, and the condensed crude product was purified by column chromatography (SiO_2, Hex : EA = 4:1) to afford **2-60** as a yellow solid (58 mg, 30% yield). ^{1}H-NMR (500 MHz, DMSO): δ 7.97 (d, *J* = 8.0 Hz, 2H), 7.69(d, *J* = 8.5 Hz, 2H), 7.26(d, *J* = 8.5 Hz, 2H), 6.54(d, *J* = 8.5 Hz, 2H), 3.86(s, 3H). ^{13}C-NMR (125 MHz, DMSO): δ 165.4, 150.9, 134.0, 132.3, 129.6, 129.3, 125.9, 113.5, 104.9, 86.2, 79.7, 77.5, 71.0, 52.3.[123]

CuCl Purification[104]

Copper chloride (5.35 g, 54.0 mmol) was dissolved in 60 mL 0.1M HCl and stirred for 10 min. Deionized water was added to the blue/green suspension, causing a white precipitate to form which was isolated using vacuum filtration. The solid was washed with 20 mL portions of methanol, ethanol, acetone, and diethyl ether, and dried in the vacuum oven. The purified compound was stored in a desiccator in the dark.

CuI Purification[104]

Potassium iodide (18.2 g, 109 mmol) was dissolved in 32 mL H_2O and 1.25 g CuI (6.54 mmol) was added. After stirring under argon for 1 h, 1.27g (106 mmol) charcoal was added and the mixture was stirred with moderate heat for 30 min. The mixture was cooled to room temperature and filtered under argon. 30 mL H_2O was added and the white precipitate that formed was isolated after 45 min using vacuum filtration (under Ar). The solid was washed with water, ethanol, and ether (10 mL portions) and dried over-night in the vacuum oven (~100°C). The purified compound was stored in a Schlenk flask that had been degassed and filled with Ar, and was placed in a desiccator.

General Method of Preparing Co-crystals

All the diyne monomers were synthesized according to the procedures described above and used within one day after synthesized. To a 0.01 M solution of diynes in 5 mL corresponded solvent, 1 eq. of host (host:guest = 1:1) in 5 mL solvent was added. The solution was sonicated for 1 min to dissolve and mix host and guest completely. Centrifugation for 10 min was used if there is any undissolved particles. The solution was then decanted into four 50 mL crystallization dishes. The dishes were then covered with aluminum foil, which was punctured 10 times using a needle. The dishes were then placed either at room temperature or in the cooling bath at necessary temperature. Solvent was allowed to evaporate slowly to afford crystals.

Single crystal X-ray diffraction (XRD).

Crystals were selected and mounted on glass fibers using epoxy adhesive. Each crystal was centered, and the X-ray intensity data were measured on an Oxford Gemini A Enhance diffractometer by using graphite-monochromated Mo radiation.The experiments were conducted at low temperature, using a CryojetHT. The data was collected using the Crysalis Pro 171.34.44 software.23 WinGX 1.80.0511, SIR97 and SHLEX 97 were used to process the data.

Microscopy

Optical microscope images were taken under polarized light with a Nikon SMZ800 optical microscope (Nikon Instruments, Incorporated, Melville, New York).

References:

67. Lauher, J. W.; Fowler, F. W.; Goroff, N. S., Single-crystal-to-single-crystal topochemical polymerizations by design. *Acc. Chem. Res.* **2008,** *41* (9), 1215-1229.
102. Schermann, G.; Grösser, T.; Hampel, F.; Hirsch, A., Dicyanopolyynes: A homologuous series of end-capped linear sp carbon. *Chem. Eur. J.* **1997,** *3*, 8.
103. DeCicco, R. C. The synthesis and polymerization behavior of polyynes. Stony Brook University, Stonybrook, 2012.
104. Black, A. An Exploration of alkyne-alkyne cross-coupling reactions and attempts towards controlled polymerization of diiodooctatetrayne. State University of New York at Stony Brook, 2013.
105. Sarkar, A.; Okada, S.; Nakanishi, H.; Matsuda, H., Polydiacetylenes from asymmetrically substituted diacetylenes containing heteroaryl side groups for third-order nonlinear optical properties. *Macromolecules* **1998,** *31* (26), 9174-9180.
106. Hwang, S.; Kang, H. R.; Kim, S., Synthesis of polyynes by in situ desilylative bromination and palladium-catalyzed coupling: (7-benzyloxy)hepta-1,3,5-triynyltriisopropylsilane. *Org. Syn.* **2009,** *86*, 225-235.
107. De Luca, L.; Giacomelli, G., An insight of the reactions of amines with trichloroisocyanuric acid. *Syn. Lett.* **2004,** *2004*, 5.
108. Lee, T.; Kang, H. R.; Kim, S.; Kim, S., Facile one-pot syntheses of bromoacetylenes from bulky trialkylsilyl acetylenes. *Tetrahedron* **2006,** *62*, 5.
109. Richardson, C.; Reed, C. A., Synthesis of meso-Extended Tetraarylporphyrins. *J. Org. Chem.* **2007,** *72*, 4750-4755.
110. Marqués-González, S.; Yufit, D. S.; Howard, J. A. K.; Martín, S.; Osorio, H. M.; Garcia-Suarez, V. M.; Nichols, R. J.; Higgins, S. J.; Ceac, P.; Low, P. J., Simplifying the conductance profiles of molecular junctions: the use of the trimethylsilylethynyl moiety as a molecule–gold contact. *Dalton Trans* **2013,** *42*, 338-341.
111. Li, Q.; Jin, C.; Petukhov, P. A.; Rukavishnikov, A. V.; Zaikova, T. O.; Phadke, A.; LaMunyon, D. H.; Lee, M. D.; Keana, J. F. W., Synthesis of well-defined tower-shaped 1,3,5-trisubstituted adamantanes incorporating a macrocyclic trilactam ring system. *J. Org. Chem.* **2004,** *69*, 10.
112. Dikusar, E. A.; Yuvchenko, A. P.; Zvereva, T. D.; Zhukovskaya, N. A.; Moiseichuk, K. L., Synthesis and characterization of functionally substituted diacetylene peroxide. *Russ. J. Org. Chem.* **1998,** *36*, 5.
113. Suh, Y.-G.; Jung, J.-K.; Seo, S.-Y.; Min, K.-H.; Shin, D.-Y.; Lee, Y.-S.; Kim, S.-H.; Park, H.-J., Total synthesis of (+)-Brefeldin A. *J. Org. Chem.* **2002,** *67* (12), 4127-4137.
114. Dixon, D. J.; Ley, S. V.; Longbottom, D. A., Total synthesis of the plasmoidal pigment physarorubinic acid, a polyenoyl tetramic acid. *J. Chem. Soc., Perkin Trans. 1* **1999,** (16), 2231-2232.
115. Doak, B. C.; Scanlon, M. J.; Simpson, J. S., Synthesis of unsymmetrical 1,1'-disubstituted bis(1,2,3-triazole)s using monosilylbutadiynes *Org. Lett.* **2011,** *23* (3), 537-539.
116. Baeyer, *Chem. Ber.* **1885,** *18* (676).
117. Bohlmann, F., *Chem. Ber.* **1964,** *97*, 12.
118. Straus; Kollek; Hauptmann, *Chem. Ber.* **1930,** *63*, 1897.
119. Bohlmann; Sinn, *Chem. Ber.* **1955,** *88*, 21.

120. Klein, J. P. Methods of producing dicarbonyl compounds. WO 2015060862 A1. April 30, 2015.
121. Dunitz, J. D.; Robertson, J. M., The crystal and molecular structure of certain dicarboxylic acids. Part III. Diacetylenedicarboxylic acid dihydrate. *J. Chem. Soc.* **1947**, 12.
122. Bohlmann; Sinn, *Chem. Ber.* **1955,** *88*, 1876-1896.
123. Liang, X.; Lee, C.-J.; Chen, X.; Chung, H. S.; Zeng, D.; Raetz, C. R. H.; Li, Y.; Zhou, P.; Toone, E. J., Syntheses, structures and antibiotic activities of LpxC inhibitors based on the diacetylene scaffold. *Bioorg. Med. Chem.* **2011,** *19* (2), 852-860.
124. Berger, O.; Kaniti, A.; van Ba, C. T.; Vial, H.; Ward, S. A.; Biagini, G. A.; Bray, P. G.; O'Neill, P. M., Synthesis and antimalarial activities of a diverse set of triazole-containing furamidine analogues. *ChemMedChem.* **2011,** *6* (11), 2094-2108.
125. Jiang, M. X.-W.; Rawat, M.; Wulff, W. D., Contingency and serendipity in the reactions of fischer carbene complexes with conjugated triynes. *J. Am. Chem. Soc.* **2004,** *126* (19), 5970-5971.
126. Valášek, M.; Edelmann, K.; Gerhard, L.; Fuhr, O.; Lukas, M.; Mayor, M., Synthesis of molecular tripods based on a rigid 9,9′ -spirobifluorene scaffold. *J. Org. Chem.* **2014,** *79* (16), 7342-7357.
127. Molt, O.; Rübeling, D.; Schrader, T., A selective biomimetic tweezer for noradrenaline. *J. Am. Chem. Soc.* **2003,** *125* (40), 12086-12087.
128. Kelly, S. M.; Lipshutz, B. H., Chemoselective reductions of nitroaromatics in water at room temperature. *Org. Lett.* **2014,** *16* (1), 98-101.
129. Flatt, A. K.; Yao, Y.; Maya, F.; Tour, J. M., Orthogonally functionalized oligomers for controlled self-assembly. *J. Org. Chem* **2004,** *69* (5), 1752-1755.
130. Thaler, T.; Guo, D. L.-N.; Mayer, D. P.; Knochel, P. D. P., Highly Diastereoselective C(sp3)C(sp) Cross-Coupling Reactions between 1,3- and 1,4-Substituted Cyclohexylzinc Reagents and Bromoalkynes through Remote Stereocontrol. *Angewandte Chemie* **2011,** *50* (9), 2174-2177.
131. Aakeröy, C. B.; Baldrighi, M.; Desper, J.; Metrangolo, P.; Resnati, G., Supramolecular hierarchy among halogen-bond donors. *Chem. Eur. J.* **2013,** *19* (48), 16240-16247.
132. Dixon, D. J.; Ley, S. V.; Longbottom, D. A., Total synthesis of the plasmoidal pigment physarorubinic acid, a polyenoyl tetramic acid. *J. Chem. Soc., Perkin Trans.* **1999,** *1*, 2231-2232.
133. Takeuchi, R.; Tanabe, K.; Tanaka, S., Stereodivergent synthesis of (*E*)- and (*Z*)-2-alken-4-yn-1-ols from 2-propynoic acid: a practical route via 2-alken-4-ynoates. *J. Org. Chem.* **2000,** *65* (5), 1558-1561.
134. Dr., J. A. V.; Prof., L. C.; Prof., M. M.; Dr., J. M.; Prof., C. S., Regiocontrolled One-Step Synthesis of 3,3′ -Disubstituted 2,2′ -Bipyridine Ligands by Cobalt(I)-Catalyzed Cyclotrimerization. *Chem. Eur. J.* **2001,** *7*, 5203-5213.
135. Pelletier, G.; Charette, A. B., Triflic anhydride mediated synthesis of imidazo[1,5-a]azines. *Org. Lett.* **2013,** *15* (9), 2290-2293.
136. Forner, D. F.; Quiñones, M. P.; Albero, M. A. B. Quinuclidine derivatives and their use as muscarinic M3 receptor ligands. US 6750226 B2. June 15, 2004.
137. Askew, B. C.; Hartman, G. D.; Duggan, M. E.; Young, S. D.; Hutchinson, J. H.; Wai, J. S.; Egbertson, M. S.; Vassallo, L. M.; Libby, L. A.; Krause, A. E.; Halczenko, W.; Ihle, N. C. Fibrinogen receptor antagonists. US 5852045 A1. December 22, 1998.

Chapter 3 Exploration of Controlled Topochemical Polymerization of Diiodooctatetrayne

3.1 Introduction

3.1.1 Synthesis and Polymerization of Tetraynes

As mentioned in Chapter 1, polydiacetylenes (PDAs) from tetraynes and longer polyynes have been of great interest because extended π-conjugation can lead to higher non-linear polarizability. Synthesis of such PDAs has been challenging not only because of instability of either monomers or polymers, but also the increased possible structures of polymers. The arrangements of tetraynes in the solid state influence the repeat distance and angle in between, and therefore can result in 1,4-, 1,6-, 1,8-, 3,6-polymerizaton reactions or combinations of two or more. The study on octatetrayne compounds started in the 1970s by Baughman and Yee.[138]

In 1991, the Okada group[33] reported structures of polymers obtained by the solid-state polymerization of a diyne, a triynes and two tetraynes with long-alkyl side chains. Polymerizations were by ^{60}Co γ-ray irradiation. All monomers went through 1,4-polymerization. As to the alkyl substituted tetrayne (such as **14-4A-14** in Figure 3.1), the increasing absorption around 635 nm indicates formation of polymers. The IR spectrum shows acetylene stretching band remains, even though weak and broad. If there were only acetylene units in the polymer backbone, the stretching bands should disappear because of the symmetric structure around acetylene units. Therefore, one or more acetylene bonds must be in the side chains. The solid-state ^{13}C-NMR confirms 1,4-polymerization of the tetrayne with a diyne side chain. They explained the exclusively 1,4-polymerization by the solid-state self-arrangement of monomers. Taking the **14-4A-14** (Figure 3.1) as an example, its solid-state packing results in a repeat distance of 4.5 Å between alkyl side chains

as well as 3.4 Å between tetraacetylenic moieties, which then lead to a repeat distance d ≈5 Å, and θ≈45°. These structural parameters make 1,4-polymerization predominate.

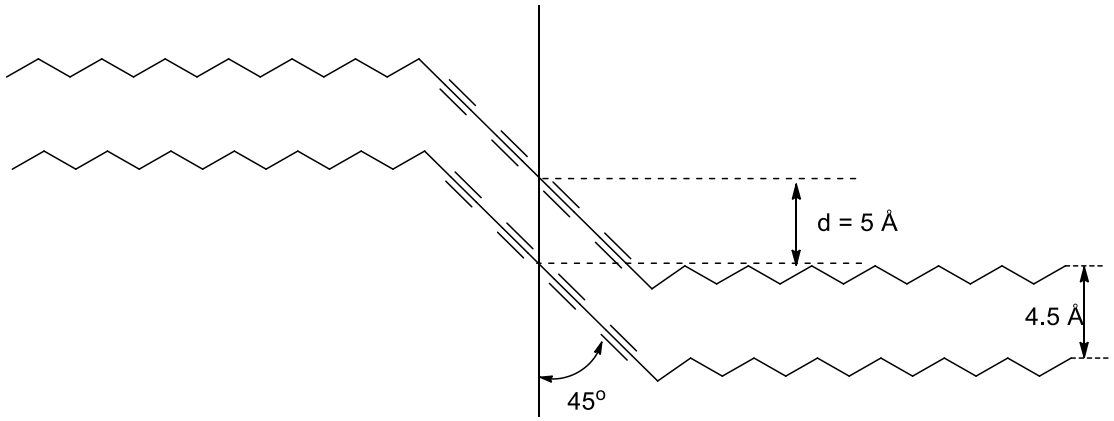

Figure 3.1 Solid-state packing of **14-A-14**[33]

In 1994, the Okada group[139] reported a solid-state polymerization of 15,17,19,21-hexatriacontatetrayne (Figure 3.2), where the R substituent is the tetradecyl group. By monitoring the chemical shifts changes in the ^{13}C MAS-NMR spectrum during polymerization, they proposed that tetradecyl end-capped tetraynes polymerize through 1,4- and 5,8-addition subsequently to form a laddered structure polymer (Figure 3.2). According to Myers and Finney,[140] the annulene cannot be stable, and it immediately cycloaromatizes to form a diradical structure. Therefore, according to characterizations by ^{13}C MAS-NMR, ESR Spectra, and powder XRD, they concluded that the polymerization of 15,17,19,21-hexatriacontatetrayne eventually results in either a graphene-like polymer or a three-dimensional highly conjugated polymer.

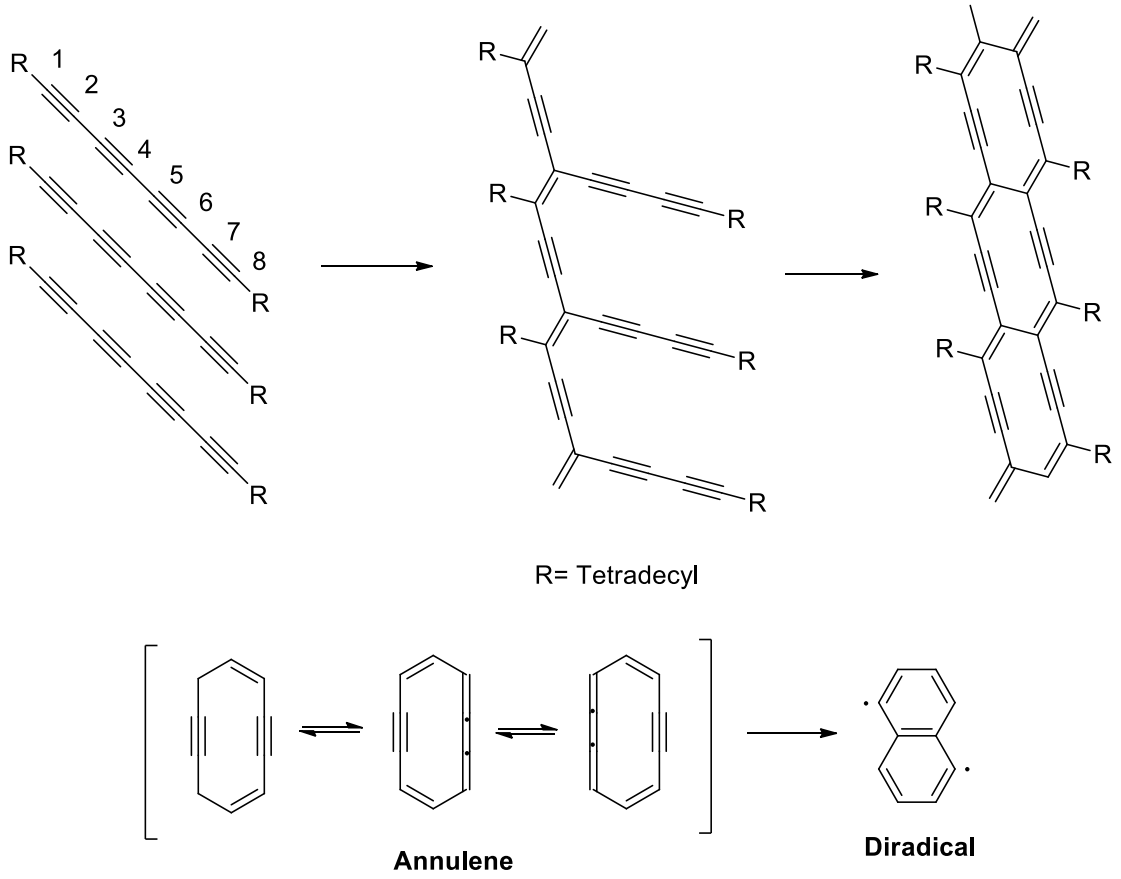

Figure 3.2 Subsequent 1,4- and 5,8-polymerization of tetrayne[141]

In 1998, Nakanishi group[142] reported the preparation and polymerization of octatetrayne capped with aromatic 2-thienyl and 3-quinolyl groups (Figure 3.3). These two monomers polymerize within minutes at 150 °C (2-thienyl) and 198 °C (3-quinolyl), and the polymerization rates are directly related to heating rate. The FTIR spectrum shows intensity of acetylene peaks diminishing gradually over polymerization process. Correspondingly, the solid-state ^{13}C-NMR shows absence of polymeric acetylenic carbons. Powder XRD displays new peaks formation during polymerization. All these measurements indicate that the final polymer product do not have a PDA structure. The single crystal of 2-thienyl octatetrayne displays the angle between molecules and stacking axis 71°, which is not suitable for 1,4-polymerization. The repeat distance between

monomers (3.9 Å) excludes the 1,6- (6.25 Å) or 1,8- (8.48 Å) polymerizations. Therefore, Okada and co-workers concluded that the monomer went through subsequent 1,2-additions to give totally aromatized products (Figure 3.3).

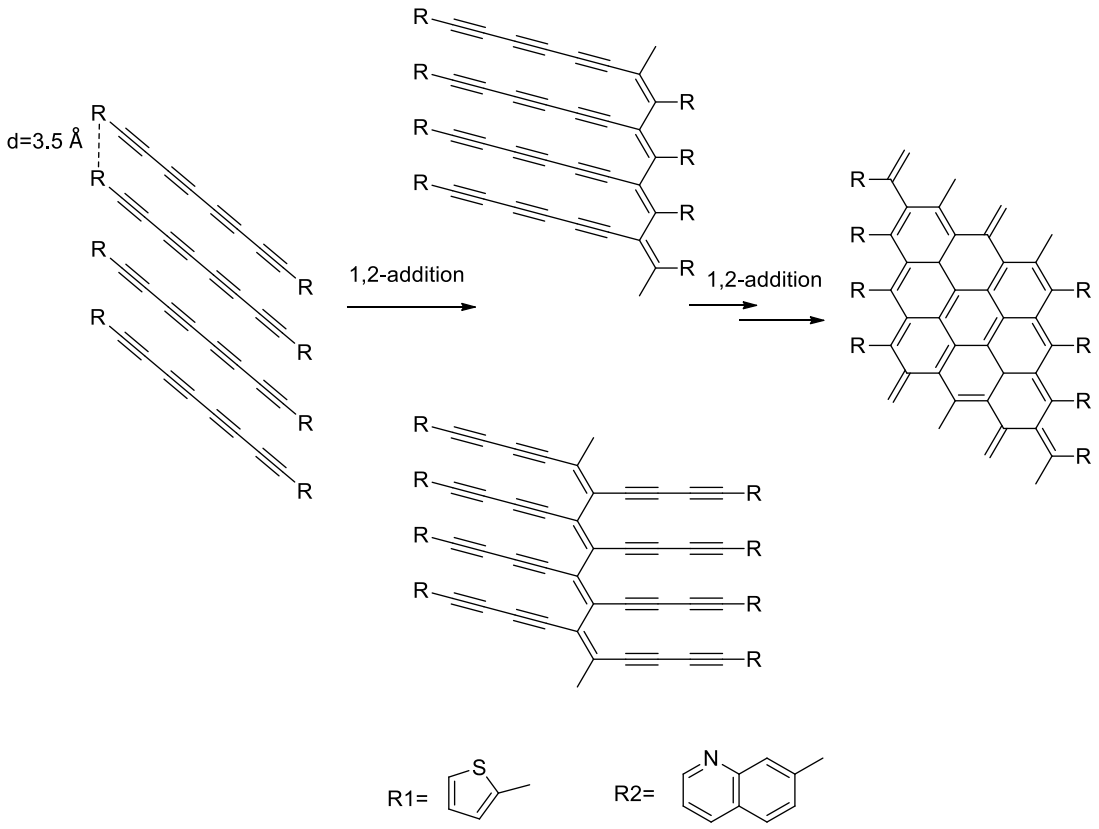

Figure 3.3 Cycloaromatization of tetrayne[142]

In 2006, Szafert and Gladysz[143] summarized the crystal packing parameters for various tetraynes. None of the tetraynes aligns with a required large repeat distance for 1,8-polymerization, probably because such an alignment is not energetically favored. In fact, most later reported tetraynes[144] go through 1,4-polymerization preferentially, or have the desired structural parameters. The obtained polymers are usually amorphous and take several characterization methods to clarify the structures.

3.1.2 Possible Polymerization Fashions of Diiodooctatetrayne

The topochemical polymerization possibilities of diiodooctatetrayne (C_8I_2, **3-2**) based on a host-guest strategy (mentioned in Chapter 1) are attractive for two reasons. 1) The polymers resulted from C_8I_2 **3-2** with acetylenic side-chains are expected to have very interesting optical and electronic properties. 2) It is possible to control the arrangement of monomers by employing different host molecules and lead to 1,4-, 1,6-, or 1,8-polymerization selectively. According to the host-guest strategy, the repeat distance of monomers in the co-crystal is inherited from repeat distance of host molecules, which is determined by functionalities in the host molecules that form hydrogen-bonding networks. Therefore, by modifying the structure of the host molecule, tetrayne monomers may align with different structural parameters that can result in different polymers (Figure 3.4).

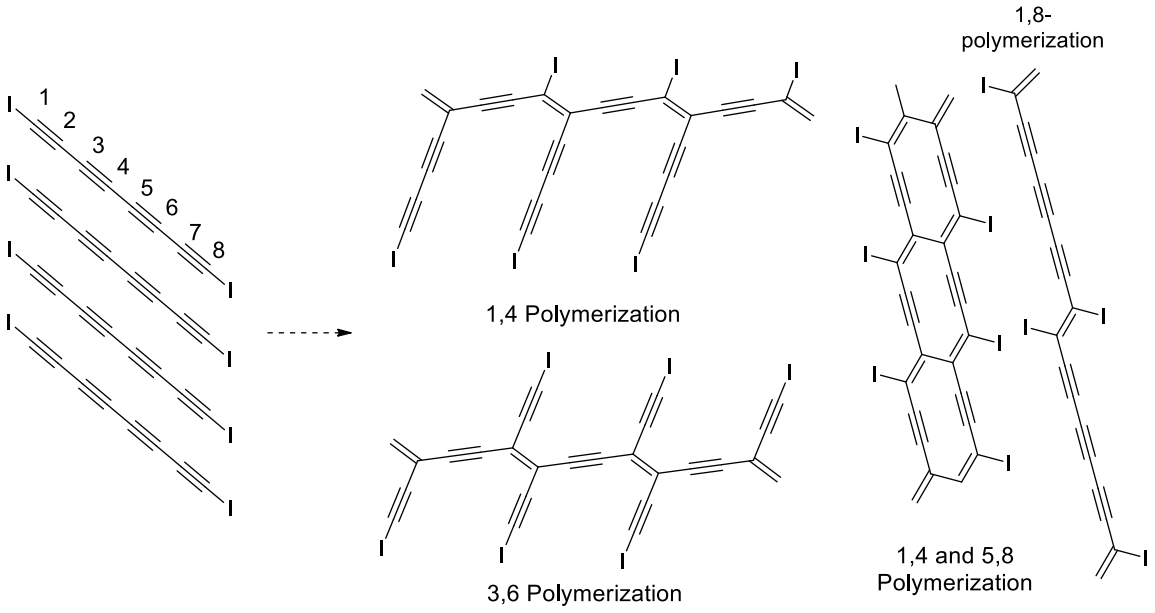

Figure 3.4 Possible polymerization fashions of C_8I_2 **3-2**

3.1.3 Synthesis and Co-Crystal Preparation of of Diiodooctatetrayne

The synthetic route of tetrayne **3-2** was developed by Allison Black (Scheme 3.1).[104] Tetrayne **3-2** has been synthesized efficiently with a moderate total yield. It appears a pale yellow powdery solid that explodes at 90 ℃. Dark brown decomposed solids appears within minutes when C_8I_2 stays at room temperature in its pure form.

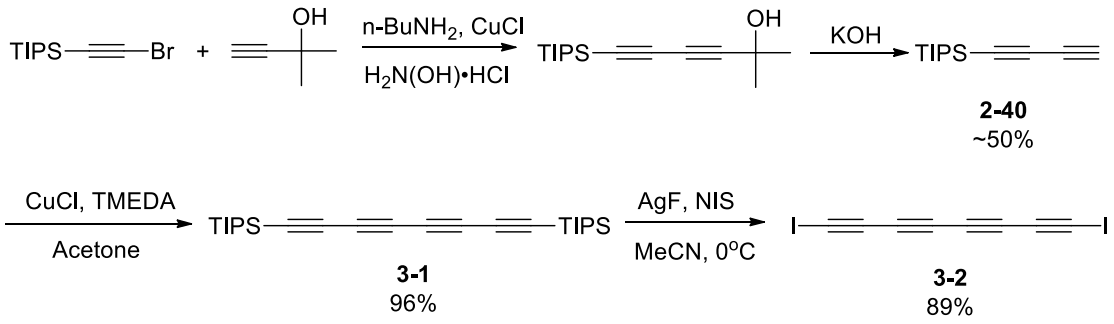

Scheme 3.1 Synthetic route towards C_8I_2 **3-2**

Both Liang Luo and Allison Black have prepared **3-2:1-9** and **3-2:1-10** co-crystal from a 1:1 ratio of host to guest solution in methanol at 0 °C or below. Both co-crystals are green initially. Liang Luo solved crystal structure of both **3-2:1-9** and **3-2:1-10** co-crystal. The **3-2:1-10** co-crystal has an ideal repeat distance *d* = 5.1 Å for potential 1,4-polymerization. However, the tile angle is very large (θ=60°) for making it feasible. The **3-2:1-9** co-crystal has appropriate geometry (d = 5.02 Å, θ = 47°, C1-C4 contact distance = 3.71 Å) for 1,4-polymerization. However, host **1-9** is highly disordered with two different orientations within the co-crystal. Polymerization attempts by Luo lead to gradually disordered crystal structure monitored by XRD, which indicates several partial polymerization fashions simultaneously.[145]

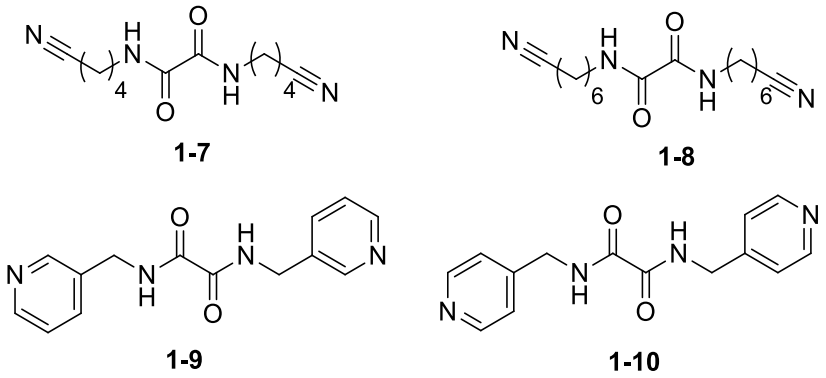

Figure 3.5 Bis(pyridyl) hosts **1-9** and **1-10**, bis(nitrile) host **1-7** and **1-8**

Allison Black then introduces bis(nitrile) oxalamide hosts **1-8** and **1-7** (Figure 3.5) to prepare C_8I_2 monomer co-crystals, and solves the crystal structure.[104] The structure of co-crystal **3-2:1-7** cannot be determined by single-crystal XRD, while the structure of co-crystal **3-2:1-8** can. My research in this project mainly focuses on reproducing preparing co-crystals, trying to achieve controlled polymerization by attempting various polymerization conditions, and using ^{13}C MAS-NMR to characterize materials obtained.

3.2 Results and Discussion

3.2.1 Reproduce Co-Crystal Preparation and Characterization

The co-crystal **3-2:1-8:MeCN** is prepared as described in Table 3.1. It is light green needles whose color turns darker gradually and becomes dark brown within days at room temperature. Single-crystal XRD shows the solvent acetonitrile participates in the crystallization. One of the iodines in C_8I_2 **3-2** halogen bonds to the nitrile of host **1-8**, while the other halogen bonds to the nitrile of acetonitrile (Figure 3.6). The structural parameters include a repeat distance *d* =5.144 Å, tilt angle θ = 48.0°, C1-C4 distance of 3.606 Å, C3-C6 distance of 3.528 Å, and C5-C8 distance of 3.647

Å(C1 is close to acetonitrile, C8 is close to host nitrile). The alignment is likely to favor 1,4- and 3,6-polymerization. The top view also shows host **1-8** arranges in two different orientations. A Raman spectrum was taken immediately after the solvent evaporation (Figure 3.7). The two distinct peaks around 1400 cm^{-1} and 2100 cm^{-1}, which are comparable to the Raman spectrum of C_4I_2 polymer co-crystals, indicates a small amount of oligomers forming spontaneously.

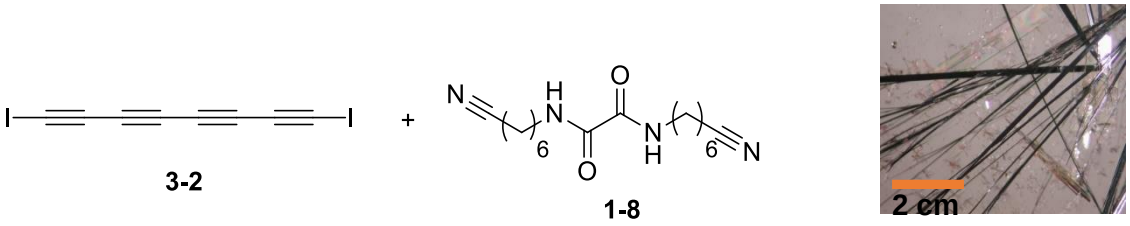

Table 3.1 Preparing co-crystal **3-2:1-8:MeCN**

Solvents	Host: Guest	Temperature (℃)	Time (h)	Results
MeCN	1:2	0	24	Light green co-crystal

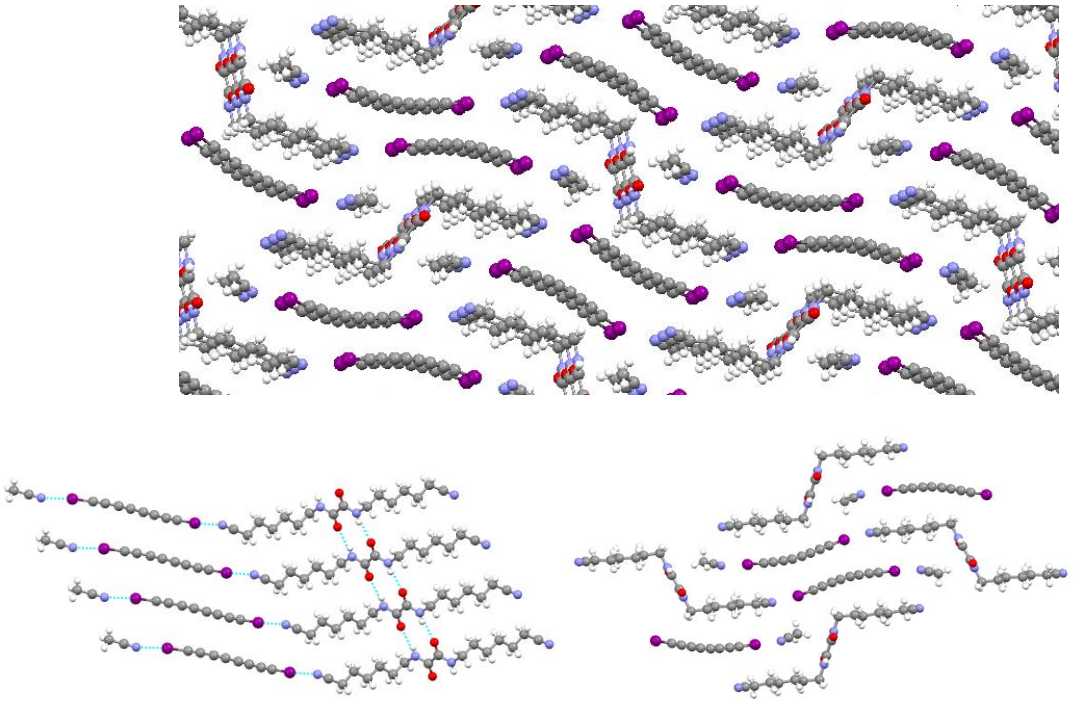

Figure 3.6 Crystal structure of tetrayne **3-2** and bis(nitrile) oxalamide host **1-8**

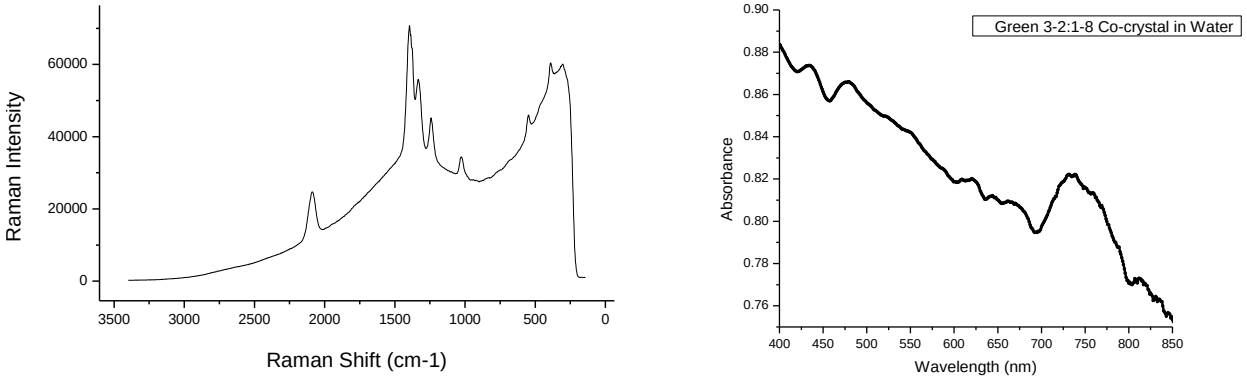

(b) (c)

Figure 3.7 (a) Green **3-2:1-8** co-crystals (b) Raman and (c) UV spectrum taken immediately after solvent evaporation

3.2.2 Attempts towards Ordered Polymerization and Material Characterization

The included acetonitrile causes additional difficulty to ordered topochemical polymerization. The acetonitrile molecules are small and they evaporate easily. The co-crystal would break without them holding the C_8I_2 **3-2**. The other challenge is the instability of C_8I_2 **3-2**. It decomposes much easier than diiodobutadiyne or diiodohexatriyne.

We attempted several polymerization conditions. 1) To slowly warm the monomer co-crystals at 35 ℃ overnight. However, the Raman spectrum displays only a broad background with no distinct peaks, indicating decomposition or random polymerizations. 2) To keep the co-crystals at 15 ℃ in the cooling bath, which would slow down both the acetonitrile evaporation and the polymerization. The single-crystal XRD still gives a monomer co-crystal structure with a slightly higher R_1 value.

The Raman spectrum does not display an enhanced peak corresponding to the polymer backbone (Figure 3.8). 3) To leave the co-crystals at room temperature. The Raman spectrum does not display an enhanced peak corresponding to the polymer backbone (Figure 3.9). 4) UV-irradiation at 0 ℃, which would provide intensive energy for a quick polymerization while preserving the acetonitrile at a low temperature. However, the Raman spectrum shows peaks with low intensity, indicating decomposition (Figure 3.10).

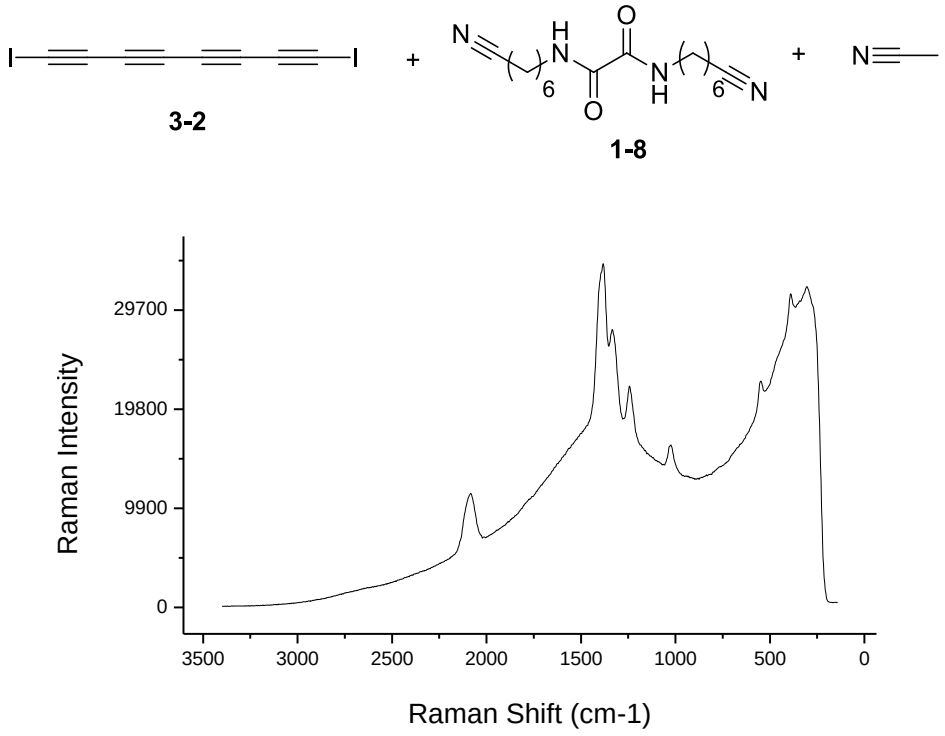

Figure 3.8 Raman spectrum of **3-2:1-8:MeCN** co-crystals after staying at 15℃ for one week

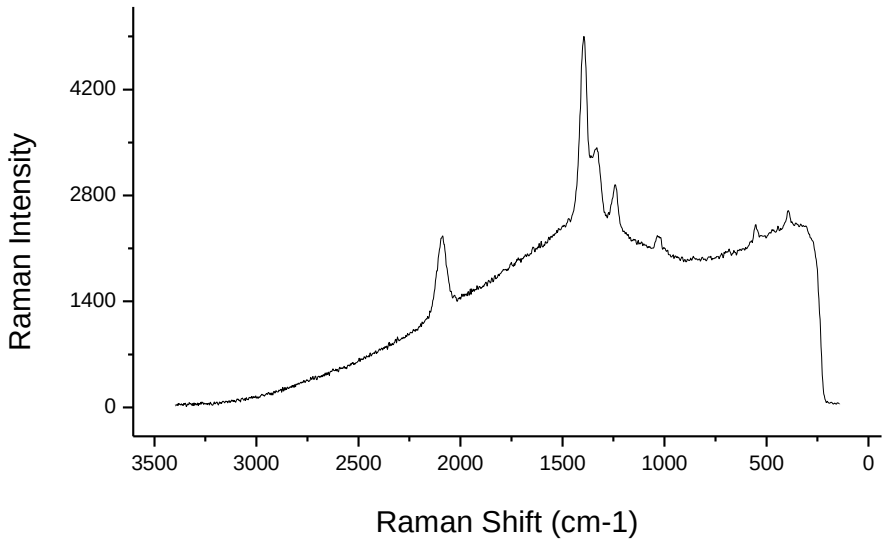

Figure 3.9 Raman spectrum of **3-2:1-8:MeCN** co-crystals after staying at room temp. for two weeks

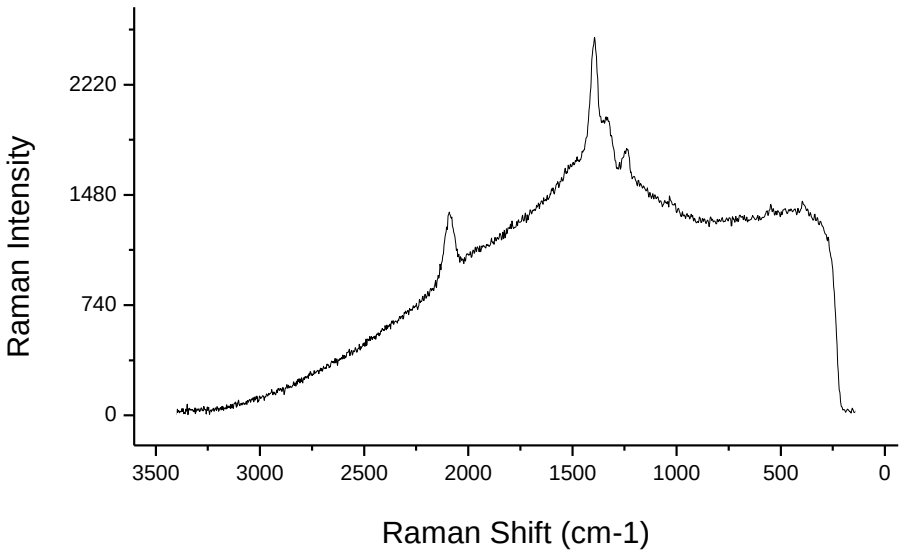

Figure 3.10 Raman spectrum of **3-2:1-8:MeCN** co-crystals after 350 nm UV irradiation for 1 h

^{13}C MAS-NMR is also employed to investigate structural information of co-crystals. Monomers and polymers have different chemical shifts, so do polymers from 1,4-polymerization and 3,6-polymerization. As shown in Figure 3.11, the 1,4-polymerization generates a non-symmetric backbone structure, while 3,6-polymerization generates a symmetric backbone structure.

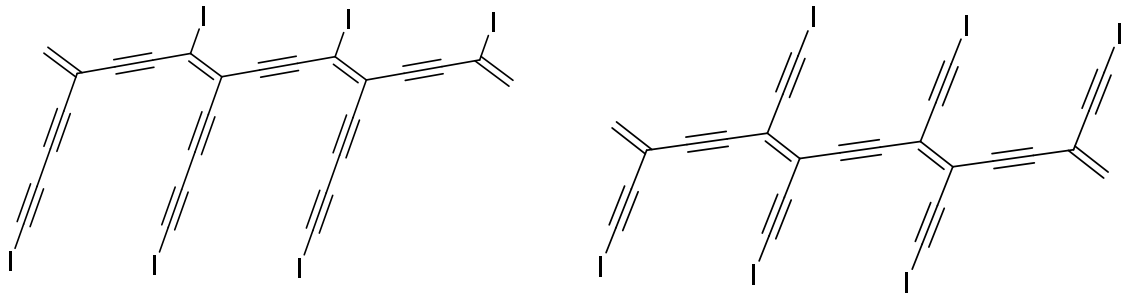

1,4 Polymerization of C_8I_2 **3-2**

3,6 Polymerization of C_8I_2 **3-2**

Figure 3.11 Polymer structures generated by 1,4-polymerization and 3,6-polymerization

According to previous work done by Matthew Freitag in our group, ^{13}C MAS-NMR spectrum shows a full and explicit 1,4-polymerization of diiodohexatriyne in the co-crystal. In Figure 3.12b, the blue arrow on 0.6 ppm indicates C1 and C6 in the monomer, while on 60 and 80 ppm indicates C2, C3, C4 and C5. After polymerization, in Figure 3.12a, the red arrows indicate 0.6 (C1), 90 (C2), 95(C6), 105(C5), 108(C4), 125(C3) ppm.

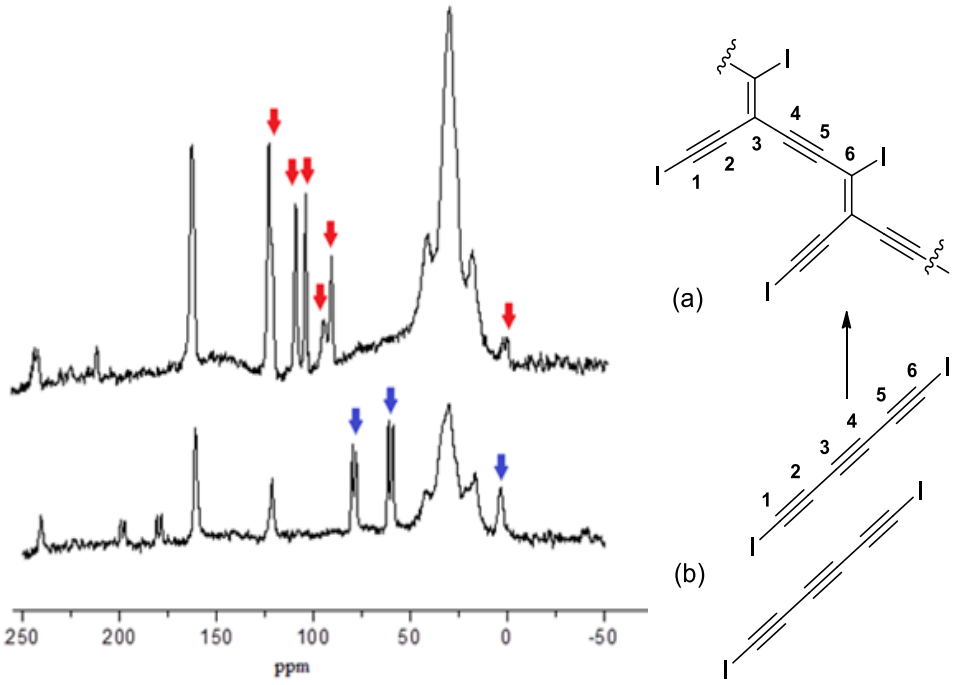

Figure 3.12 ^{13}C MAS-NMR spectra for (b) diiodohexatriyne monomer co-crystal and (a) polymer (These are the results of Matthew Freitag in our group)

(Blue arrows correspond to carbons of the monomer, red arrows correspond to carbons of the polymer)

In the ^{13}C MAS-NMR spectrum of **3-2:1-8:MeCN** monomer co-crystal (Figure 3.13a), the peak around 1.8 ppm suggests the C1 overlapped by the methyl carbon in the acetonitrile, and peaks around 60 and 80 ppm are corresponding to the other C2, C3 and C4. After the monomer co-crystals stay at room temperature for two weeks, almost all acetylenic carbon peaks diminish. However, no distinct peaks corresponding to vinyl carbons emerge. Short oligomer species are likely formed, by random polymerization, whose peaks hide in the background.

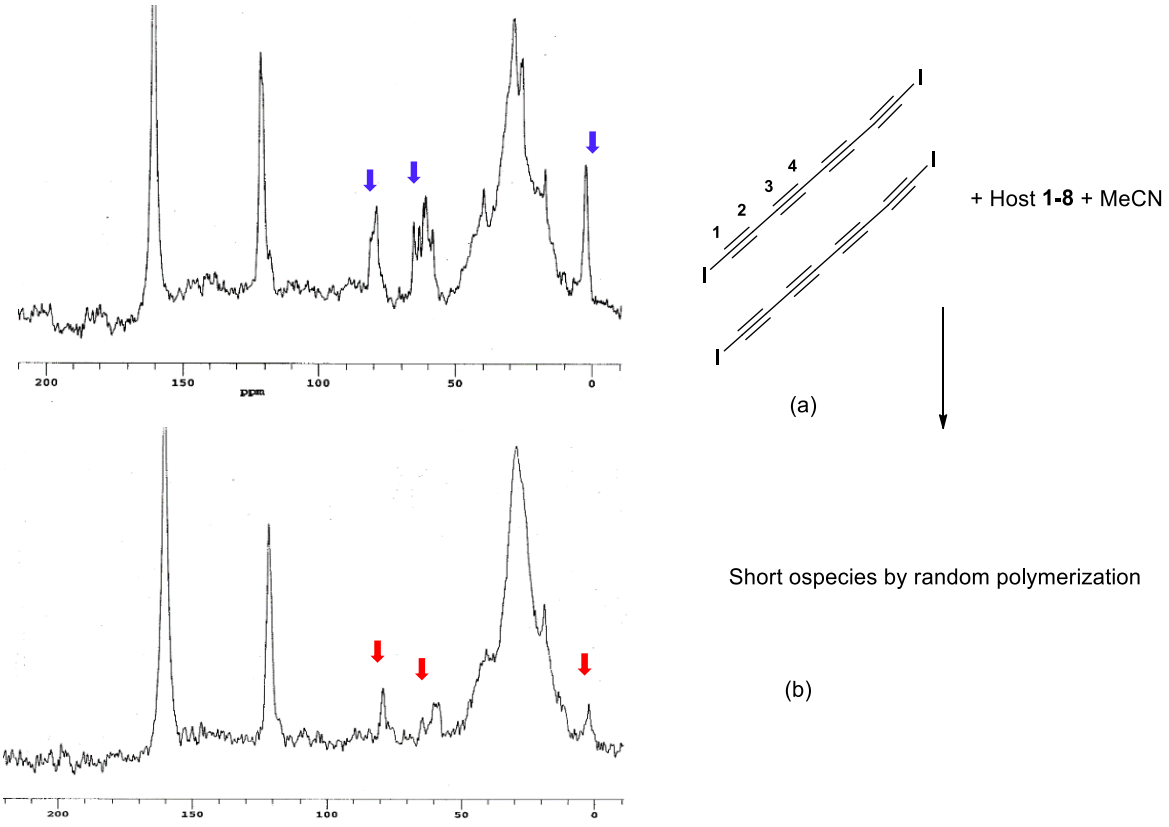

Figure 3.13 ^{13}C MAS-NMR spectrum of (a) **3-2:1-8** monomer co-crystal; (b) **3-2:1-8** monomer co-crystal laid out at room temperature for two weeks

3.3 Conclusion & Future work

Ordered polymerization of tetrayne has been studied for decades because the proposed polymer that potentially can be generated have extensive conjugation and therefore attractive optical and electronic properties. However, it is challenging because tetraynes are much more reactive than diynes and triynes, and the generated polymeric materials may contain multiple fashions of polymerization that are difficult to characterize. Based on the previous successful co-crystal preparation and polymerization of diiodobutadiyne (C_4I_2) and diiodohexatriyne (C_6I_2), we attempted organizing tetrayne C_8I_2 **3-2** in co-crystals and generating ordered polymers. Our

previous group members have synthesized C_8I_2 **3-2**, prepared the co-crystal of C_8I_2 **3-2** and bis(nitrile) oxalamide host **1-8**, and determined its structure by single-crystal XRD.

My work in this project includes attempting several sets of conditions to induce C_8I_2 **3-2 to** polymerize, and employing ^{13}C MAS-NMR to characterize materials before and after polymerization attempts. Although C_8I_2 **3-2** molecules are aligned in co-crystal with parameters close to the desired parameters for 1,4-polymerization, all attempted polymerizations lead to short oligomer species from random polymerization, or decomposed solids. ^{13}C MAS-NMR spectroscopy does not give any conclusive evidence of forming ordered polymers.

3.4 Experimental Procedures

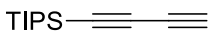

2-40

Buta-1,3-diynyltriisopropylsilane (2-40)[146]

N-Butylamine (0.9 mL, 9 mmol, 3 eq.), 2-methylbut-3-yn-2-ol (0.59 mL, 0.6 mmol, 2 eq.), copper (I) chloride (6 mg, cat.) and hydroxylamine hydrochloride (62 mg, 0.9 mmol, 0.3 eq.) were added in order to a solution of methanol : water (2:1, 15 mL). (Bromoethynyl)triisopropylsilane (0.8 g, 3 mmol, 1 eq.) was diluted with methanol (8 mL) and added dropwise over 30 mins. The solution was left stirring at room temperature for 24 h. The solution was then diluted with water (20 mL) and extracted with diethylether (3 × 15 mL). The combined organic layers were washed with water (1 × 15 mL) and brine (2 × 15 mL), dried over anhydrous magnesium sulfate, filtered and evaporated. Purification by flash chromatography (SiO_2, Hex to Hex : EA = 5:1) gave 2-methyl-6-(triisopropylsilyl)hexa-3,5-diyn-2-ol as a colorless oil (0.31 g, 78% yield). 2-Methyl-6-(triisopropylsilyl)hexa-3,5-diyn-2-ol (504 mg, 1.86 mmol, 1 eq.) was added to a solution of crushed potassium hydroxide (210 mg, 3.73 mmol, 2 eq.) in benzene (15 mL) and the solution heated to 80 °C for 2.5 hours. The solution was then cooled and diluted with water (20 mL) and extracted with hexane (3 × 15 mL). The combined organic layers were dried over anhydrous magnesium sulfate, filtered and evaporated to give an orange oil. Purification by filtration through silica, eluting with hexane gave the product as an orange / red oil (360 mg, 91% yield). The product was stored in solution in the freezer. ^1H-NMR (400 MHz, $CDCl_3$) δ 2.07 (s, 1H), 1.09 (s, 21H). ^{13}C-NMR (100 MHz, $CDCl_3$) δ 89.1, 81.9, 68.6, 65.5, 18.5, 11.2.[146]

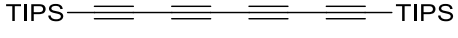

3-1

1,8-Bis(triisopropylsilyl)octa-1,3,5,7-tetrayne (3-1) [147]

CuCl (0.118 g, 1.19 mmol) was dissolved in 4 mL acetone and TEMDA (0.06 mL, 0.39 mmol) was added. Oxygen was bubbled through the solution for 2 h. 2.45 g Buta-1,3-diynyltriisopropylsilane was then dissolved in 7 mL aetone, and the solution was added dropwise into the previous catalyst's solution. Reaction was stirred at room temperature overnight, and solvent was evaporated by vaco. 20 mL ethyl acetate was added to re-dissolve the products, and the organic layer was washed by 20 mL sat. NH_4Cl for three times, followed by 20 mL brine once. Crude products was purified by flushing a plug (SiO_2, Hex). The product was obtained as white crystals (2.35g, 96% yield). ^1H NMR (500 MHz, $CDCl_3$, 25 °C): δ 1.09 (s, 42H). ^{13}C NMR (125 MHz, $CDCl_3$, 25 °C): δ 89.6, 85.6, 62.2, 61.4, 18.5, 11.3..[147]

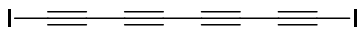

3-2

1,8-Diiodoocta-1,3,5,7-tetrayne (3-2)[148]

Compound **3-1** (0.065 g, 0.165 mmol) was dissolved in 30 mL CH_3CN. AgF (0.143 g, 1.125 mmol) and NIS (0.253 g, 1.125 mmol) were added, and the reaction was allowed to stir at 0ºC in the dark for 1h. The reaction was quenched with 30 mL ice water and extracted with 3 × 20 mL portions of hexane. The combined organic extract was washed with 20 mL sat. aq. Na_2SO_4 and dried over $MgSO_4$. Solvent was removed, resulting in light yellow solid (0.08 g, 90% yield). ^{13}C NMR (125 MHz, $CDCl_3$, 25 °C): δ 78.9, 62.1, 59.0, 1.40.[148]

Raman Spectroscopy.

Raman spectroscopy was performed by Christopher Young of the Halada group in the Material Sciences Department at Stony Brook University. A Thermo Nicolet Almega dispersive Raman spectrometer coupled with an infinity-corrected, confocal design microscope was used. A 785-nm class I laser was used, and the data were collected in the reflection mode of the microscope at a slit width of 25 μm. The data were analyzed using the Origin Pro 8.5 Software (OriginLab Corporation, USA).

Single crystal X-ray diffraction (XRD).

Crystals were selected and mounted on glass fibers using epoxy adhesive. Each crystal was centered, and the X-ray intensity data were measured on an Oxford Gemini A Enhance diffractometer by using graphite-monochromated Mo radiation. Wavelength (ANG): A1: 0.70930 A2: 0.71359 B1: 0.63229. The experiments were conducted at low temperature, using a CryojetHT. The data was collected using the Crysalis Pro 171.34.44 software.23 WinGX 1.80.0511, SIR97 and SHLEX 97 were used to process the data.

Solid-state ^{13}C NMR

Solid-state ^{13}C NMR data were acquired with a 500 MHz Varian Infinity-plus spectrometer, operating at 125.68 and 499.79 MHz for ^{13}C and ^1H respectively, and a Varian double-resonance T3-type MAS probe assembly configured for 4 mm (outside diameter) rotors. The sample spinning rate was 15 kHz. The $^{13}C(^1H)$ CP/MAS experiments employed a 50 kHz transverse ^1H field and a linear ramp of the ^{13}C field of ±7 kHz about the first sideband match condition. The $^1H \rightarrow ^{13}C$ contact time was 10 ms and the relaxation delay 2 s. The ^{13}C chemical shifts were measured relative to the methylene carbon of adamantane, taken to be +38.5 ppm. A ^{13}C single-pulse MAS spectrum was taken by direct excitation with a 5 μs pulse (90°) and 200 s relaxation delay. A 50-70 kHz ^1H decoupling field was applied during acquisition.

Microscopy

Optical microscope images were taken under polarized light with a Nikon SMZ800 optical microscope (Nikon Instruments, Incorporated, Melville, New York).

References:

33. Okada, S.; Hayamizu, K.; Matsuda, H.; Masaki, A.; Nakanishi, H., Structures of the polymers obtained by the solid-state polymerization of diyne, triyne, and tetrayne with long-alkyl substituents. *Bull. Chem. Soc. Jpn.* **1991,** *64* (3), 857-863.
104. Black, A. An Exploration of alkyne-alkyne cross-coupling reactions and attempts towards controlled polymerization of diiodooctatetrayne. State University of New York at Stony Brook, 2013.
138. Baughman, R.; Yee, K., Solid-state polymerization of linear and cyclic acetylenes. *J. Polym. Sci. Macromol. Rev.* **1978,** *13* (1), 219-239.
139. Okada, S.; Hayamizu, K.; Matsuda, H.; Masaki, A.; Minami, N.; Nakanishi, H., Solid-state Polymerization of 15,17,19,21,23,25-Tetracontahexay. *Macromolecules* **1994,** *27*, 6259-6266.
140. Myers, A. G.; Finney, N. S., Synthesis of 1,6-didehydro[10]annulene. Observation of its exceptionally facile rearrangement to form the biradical 1,5-dehydronaphthalene. *J. Am. Chem. Soc.* **1992,** *114* (27), 10986-10987.
141. Okada, S.; Hayamizu, K.; Matsuda, H.; Masaki, A.; Minami, N.; Nakanishi, H., Solid-state polymerization of 15,17,19,21,23,25-tetracontahexayne. *Macromolecules* **1994,** *27* (22), 6259-6266.
142. Sarkar, A.; Okada, S.; Komatsu, K.; Nakanishi, H.; Matsuda, H., Octatetraynes with directly linked aromatic sidegroups: Preparation and polymerization. *Macromolecules* **1998,** *31* (17), 5624-5630.
143. Szafert, S.; Gladysz, J., Update 1 of: Carbon in one dimension: structural analysis of the higher conjugated polyynes. *Chem. Rev.* **2006,** *106* (11), PR1-PR33.
144. (a) Lee, L.-H.; Lynch, V.; Lagow, R. J., The synthesis and structural characterization of the first bis (benzocrown ethers) with polyyne linkages. *J. Chem. Soc., Perkin Trans. 1* **2000,** (16), 2805-2809; (b) Gulia, N.; Ejfler, J.; Szafert, S., Macromolecular polyyne-containing benzoxazines for cross-linked polymerization. *Tetrahedron Lett.* **2012,** *53* (41), 5471-5474; (c) Kendall, J.; McDonald, R.; Ferguson, M. J.; Tykwinski, R. R., Synthesis and solid-state structure of perfluorophenyl end-capped polyynes. *Org. Lett.* **2008,** *10* (11), 2163-2166.
145. Luo, L., *Preparation and comprehensive characterization of poly (diiododiacetylene) and spectroscopic studies of its reactions with Lewis bases*. State University of New York at Stony Brook: 2009.
146. Doak, B. C.; Scanlon, M. J.; Simpson, J. S., Synthesis of unsymmetrical 1, 1′ -disubstituted bis(1, 2, 3-triazole)s using monosilylbutadiynes. *Org. Lett.* **2011,** *13* (3), 537-539.
147. DeCicco, R. C.; Black, A.; Li, L.; Goroff, N. S., An Iterative Method for the Synthesis of Symmetric Polyynes. *Eur. J. Org. Chem.* **2012,** *2012* (25), 4699-4704.
148. Gao, K.; Goroff, N. S., Two new iodine-capped carbon rods. *J. Am. Chem. Soc.* **2000,** *122* (38), 9320-9321.

Chapter 4 Tunable Hole-Blocking Layer in CIGS Thin-Film Solar Cells

4.1 Introduction

4.1.1 Architecture of CIGS Cells

To overcome disadvantages of the typical CIGS architecture and to optimize the power conversion efficiency, the Eisaman group in the Sustainable Energy Department in Brookhaven National Lab proposed a novel architecture for CIGS-based thin-film photovoltaic cell (Figure 4.1). The essential modification is to introduce graphene as both an *n*-doping layer and an electrode to transport charges, taking the place of both CdS and ZnO layers. In addition, the electronic properties of graphene can be tuned by doping, and the transparency of graphene across the visible spectrum minimizes optical loss. In between CIGS and graphene, a "hole-blocking layer" (HBL) is also introduced to reduce charge recombination by assisting electron transport as well as blocking carriers. Furthermore, a HBL can also stabilize CIGS surface. This proposed architecture provides great advantages over previous designs, to reach near SQ-limit efficiencies (33% as described in Chapter 1).

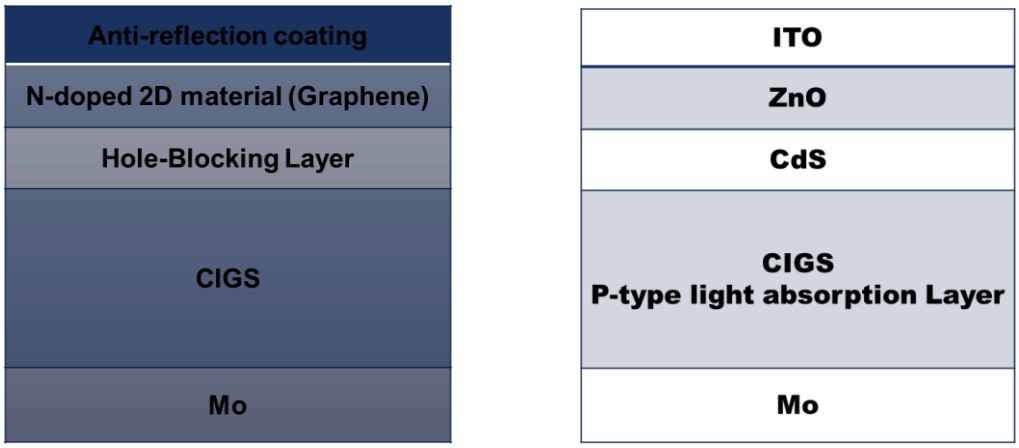

(a) (b)

Figure 4.1 (a) Novel architecture developed by the Eisaman group; (b) Typical architecture

4.1.2 1,7-Phenanthroline Derivatives as HBL Material

The popular HBL materials described in Chapter 1 (**1.2.4**) are mostly 1,10-phenanthroline derivatives. However, 1,10-phenanthroline derivatives are not suitable in CIGS cells for they are known to bind strongly to copper[149], which is one of the active components in CIGS, and therefore are likely to interfere with the functions of CIGS. Therefore, 1,7-phenanthroline derivatives were targeted, whose structures are very similar to that of 1,10-phenanthroline but have two nitrogens far apart. We can expect similar electronic properties and much less chelating possibilities.

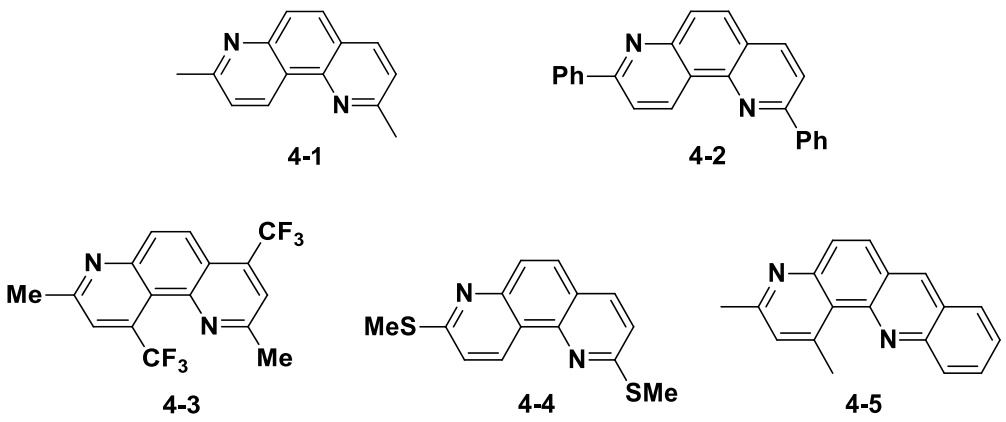

Figure 4.2 Structures of targeted molecules

Five 1,7-phenanthroline derivatives were targeted initially. The alkyl- and aryl-substituted 1,7-phenanthrolines, **4-1, 4-2** and **4-5**, are the most likely to have similar electronic properties to BCP for having similar functional groups. The methylthio phenanthroline **4-4** was targeted because sulfur compounds have been found to help passivate CIGS and enhance the efficiency.[150] The trifluoromethyl phenanthroline was targeted because the strong electron-withdrawing ability of trifluoromethyl group can be used to increase the electron affinity if necessary.

4.1.3 Synthesis of 1,7-Phenanthroline Derivatives

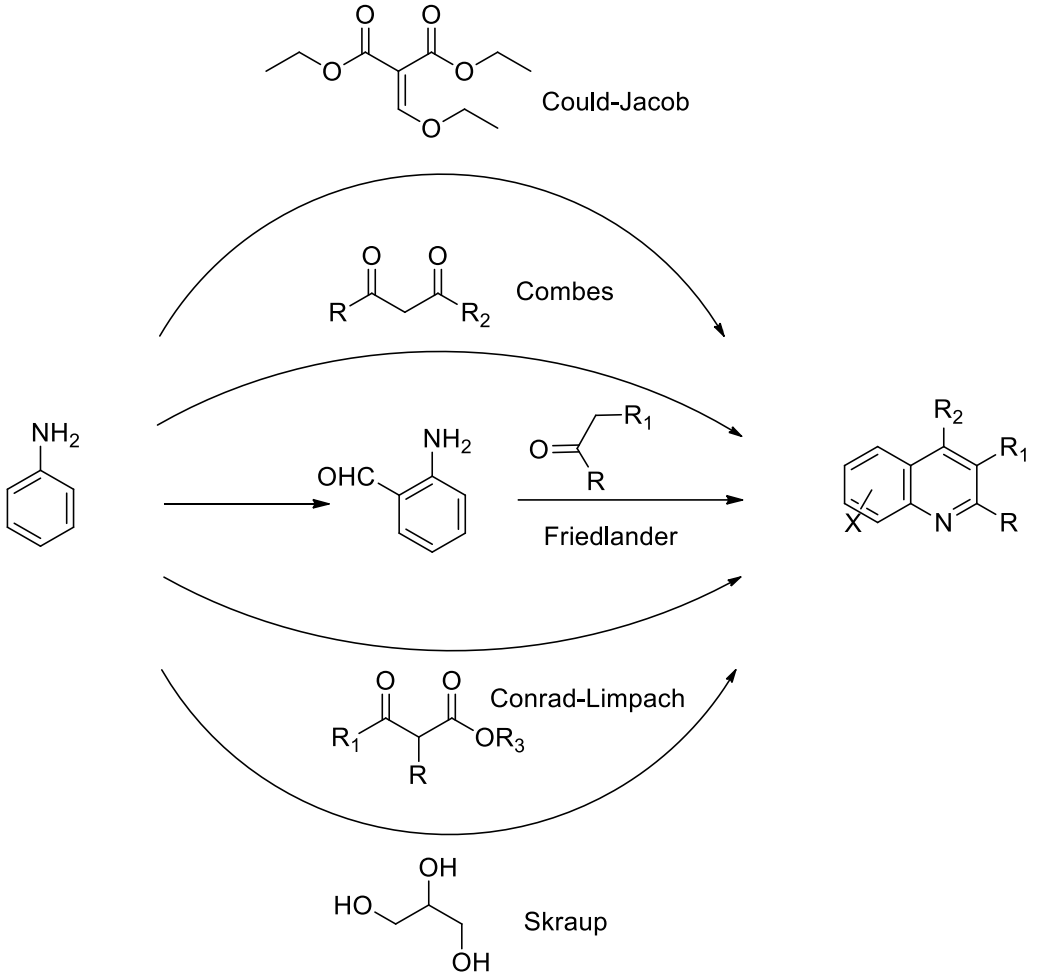

Figure 4.3 Classic synthetic methods towards quinoline derivatives[151]

Synthesis of phenanthrolines is based on synthesis of quinoline derivatives, which has been studied extensively over the past century. Traditional routes are mostly based on ring-closure between anilines and ketones, followed by dehydrogenation. The most prevalent strategies initially developed in 1880s included Skraup,[152] Doebner-Miller, Combes[153], Friedlander[154], Conrad-Limpach[155], and Gould-Jacobs[156] synthesis. Figure 4.3 describes some of the synthetic routes. Whereas these classic synthetic routes are one-pot synthesis using simple starting materials, they

usually demand harsh reaction conditions, including high temperature, strong acid or base, and tedious isolation from a fairly large number of side-products (Figure 4.4).[151] The earliest synthesis of 1,7-phenanthroline was reported in 1882.[157]

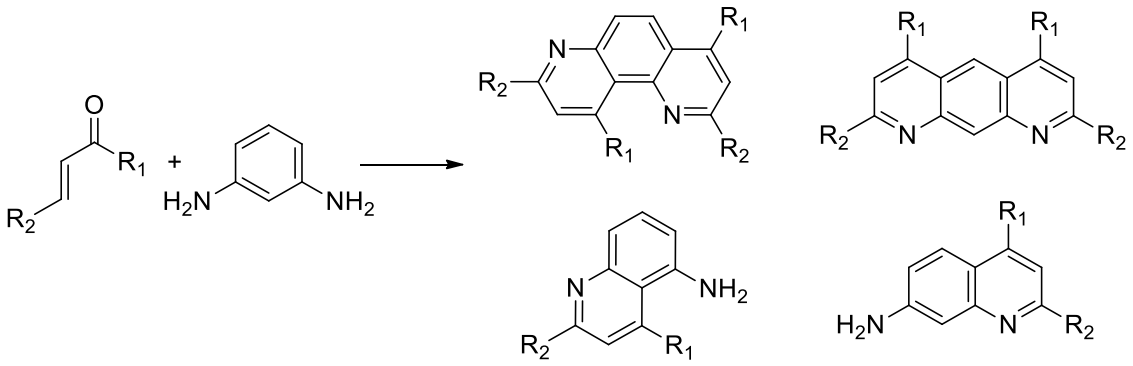

Figure 4.4 Possible products through traditional synthesis

To enable mild reaction conditions and to expand substrate scope, more recent approaches were developed by using *ortho*-functionalized anilines to promote cyclization. These reactions are catalyzed by metals or organocatalysts.[158] Even though they are more efficient than traditional methods, some starting materials and catalysts remain challenging to prepare. Therefore, only several substituted 1,7-phenanthrolines have been synthesized[159] for the past fifty years, without full characterization.

To bypass the challenge of synthesizing 1,7-phenahtroline derivatives by establishing quinoline rings asymmetrically, emphasis was put on attaching functional groups on carbon next to nitrogen. Many synthetic routes have been reported halogenating the 2-position and employing coupling conditions to attach further functional groups.[160] A simpler way to achieve 2-position functionalized phenanthrolines was investigated through two steps by the Fan group (Scheme 4.1).

[161]Alkyl/aryllithium was observed initiating a 1,2-nucleophilic addition, and resulting in a tetrahydroquinoline as the intermediate. Further oxidation generated the 2,9-alkyl/aryl phenanthrolines

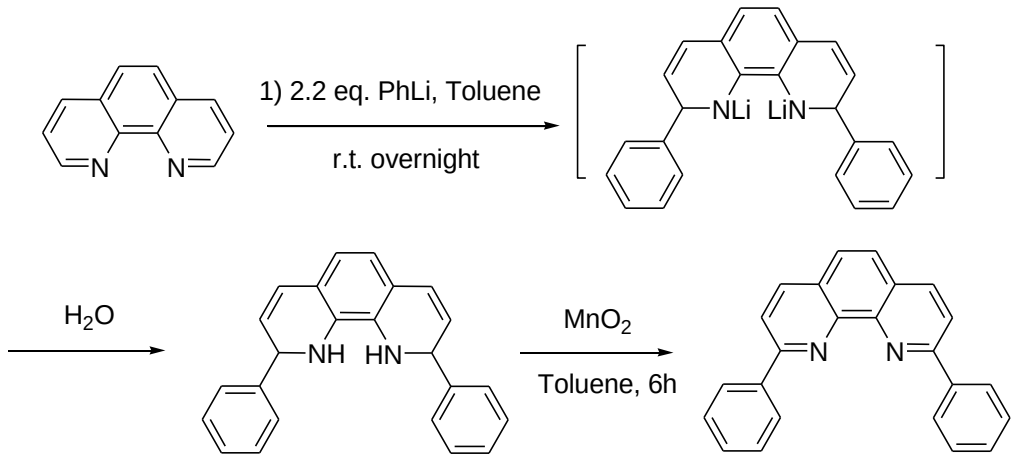

Scheme 4.1 Synthesis of 2,9-diphenyl-1,10-phenanthroline[161]

4.2 Results and Discussion on 1,7-Phenanthroline Derivatives

4.2.1 Synthesis of Targeted 1,7-Phenanthroline Derivatives

The simple functionalization method employing alkyl/aryl lithium and MnO_2 was utilized to make substituted 1,7-phenanthrolines(Scheme 4.2). In initial attempts, 2.2 eq. of phenyllithium was added, and di-substitution on both 2 and 8 positions was expected. However, GC-MS indicated crude products were a mixture of two mono-substituted and one di-substituted intermediates. After oxidation, the three products shared similar R_f values. The di-substituted intermediate was difficult to be isolated. Further exploration clarified that excess (5 eq.) of PhLi was required for complete di-substitution. After chromatography, recrystallization of phenanthroline **4-2** in a minimum amount of methylene chloride in ice bath was utilized to obtain pure compounds, which appeared as yellow crystals. Although the overall yield of phenanthroline **4-2** after purification was mediocre (15%), this synthetic route provided sufficient material for study effectively.

Dimethylation of 1,7-phenanthroline was then achieved employing an excess of methyllithum (5 eq.), and the yield of phenanthroline **4-1** was moderate (30%).

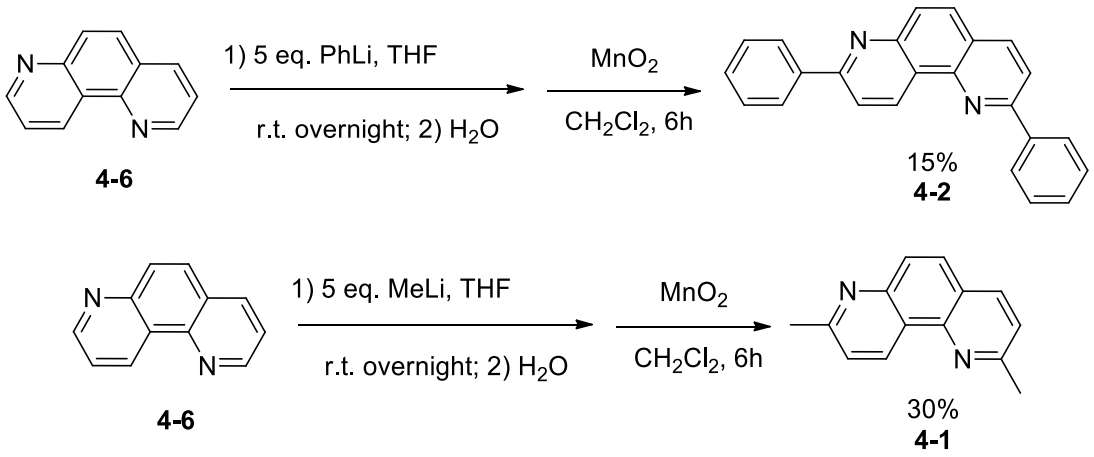

Scheme 4.2 Synthesis of 2,8-diphenyl-1,7-phenanthroline (**4-2**) and 2,8-dimethyl-1,7-phenanthroline (**4-1**)

The Ila group[162] reported a modified Skraup annulation between anilines and 3-bis(methylthio)acrolein (Scheme 4.3). They investigated cyclization of compound **4-7** with anilines bearing a strong activating group *ortho* or *para* to the amine group, and figured that *m*-methoxyaniline and compound **4-7** proceeded cyclization in refluxing acetic acid smoothly to give 7-methoxy-2-(methylthio)quinoline.[163] Further investigation by the Ila group indicated treating *m*-phenylenediamine with compound **4-7** in refluxing acetic acid could afford 2,8-bis(methylthio)-1,7-phenanthroline **4-8** in 67% yield. This synthetic procedure was attempted several times. Compound **4-7** was synthesized successfully, but the cyclization yielded a mixture of compounds. Only a trace amount of desired molecule **4-4** was observed in ^{1}H-NMR after purification through chromatography, and the side products were difficult to characterize and remove. Because here

was no related reported work found supported this synthetic route, it was not pursued after several trials.

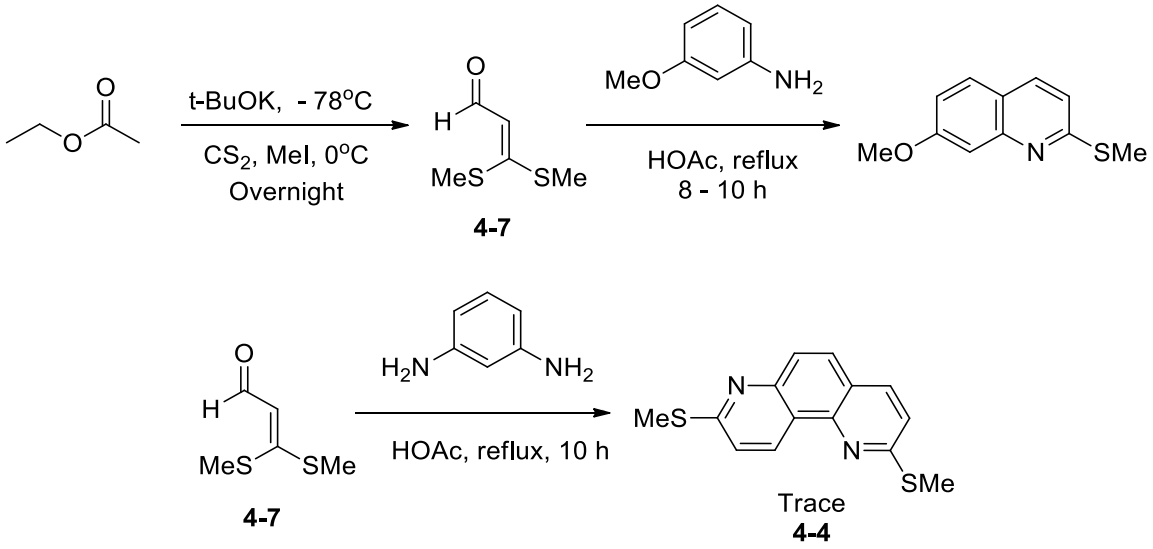

Scheme 4.3 Reported synthesis of 2,8-bis(methylthio)-1,7-phenanthroline[162]

Su and co-workers[164] recently reported a synthesis of acridine derivatives by $ZnCl_2$-promoted intramolecular cyclization of an *o*-arylaminophenyl Schiff base. Plausible mechanism is shown in Scheme 4.4, where $ZnCl_2$ acts as a Lewis acid to activate the imine and promote the annulation. Related polycyclic aza-aromatic compounds, including some 1,7-phenanthroline derivatives, were reported[164] synthesized through this route. 2,4-Dimethylbenzo[j][1,7]phenanthroline (**4-5**), especially, was reported a high yield (95-96%) from the Schiff base precursor. The synthetic route was reproduced successfully (Scheme 4.4). Compound **4-8** was synthesized by treating 2 eq. benzene-1,3-diamine with 1 eq. pentane-2,4-dione to cyclize on one side. One eq. compound **4-8** was then treated with 2 eq. n-butyllithium at -78°C in THF. The reaction was warmed up to room temperature and stirred overnight to ensure all amine converted to its lithium salt. The THF solution was added to a THF solution of compound **4-9** through cannula at room temperature. After 48 h reaction at room temperature, Schiff base **4-10** was isolated with an average 10% yield.

Reaction conditions including temperature and stoichiometry of reagents were modified, but the yield stayed mediocre. It was observed that dryness of all chemicals was the key of success, so that further optimization reached the best yield of 51% of Schiff base **4-10**. The $ZnCl_2$ promoted cyclization of Schiff base **4-10** went smoothly and gave phenanthroline **4-5** almost quantitative yield. Overall, this synthetic route is efficient.

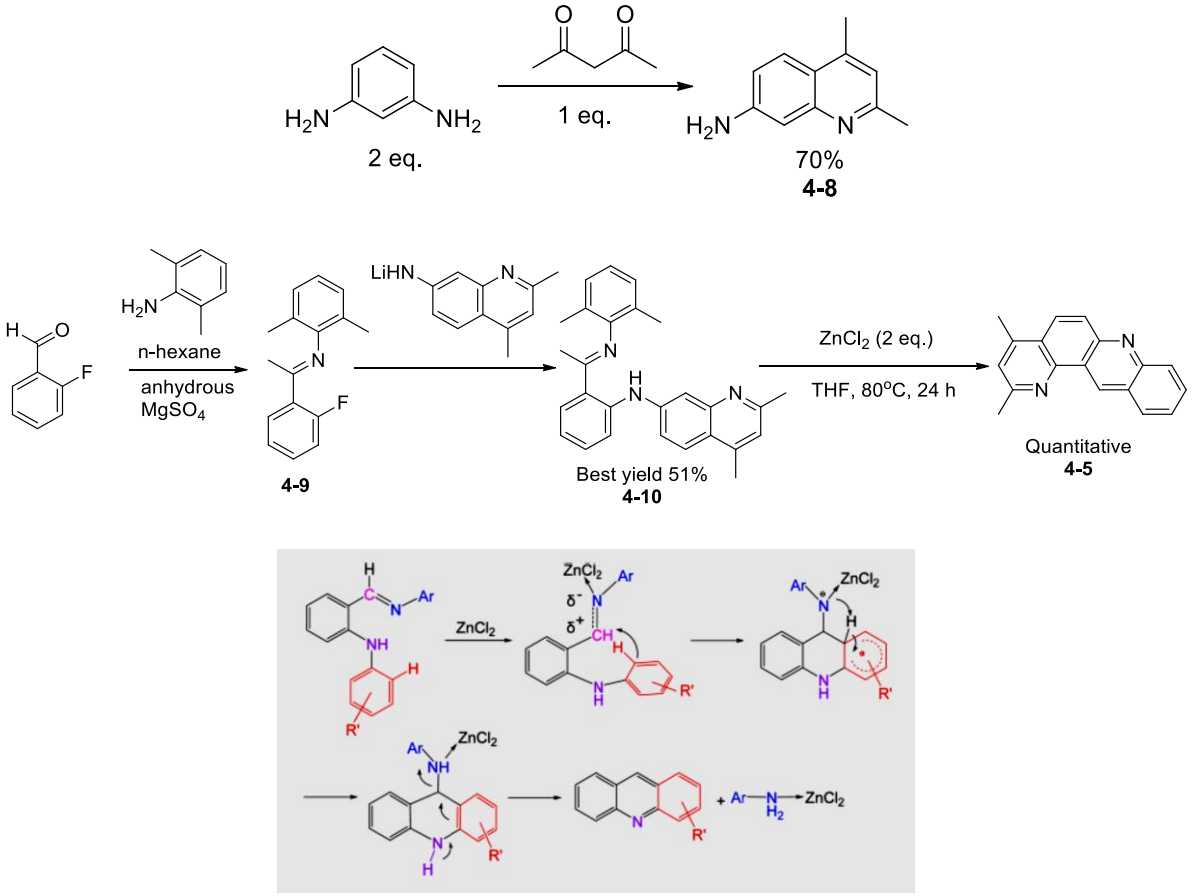

Scheme 4.4 $ZnCl_2$-promoted cyclization and plausible mechanism[164]

(Reprinted with permission from Ref. 164, Copyright 2014, American Chemical Society)

Both phenanthrolines **4-2** and **4-5** appeared very crystalline. However, forming crystals over time in the solid state would change morphology, cause defects, and affect electronic properties in the long-term, so it is not an advantageous property for a HBL material. On the other hand, di-aryl

substituted 1,7-phenanthrolines are promising candidates for being HBL materials since their similar structures, and likely similar electronic properties, to BCP. Therefore, we proposed new 1,7-phenanthrolines attaching phenyl rings bearing alkyl groups. We proposed that alkyl chains of appropriate length would interfere with molecular packing in the solid-state to make them less crystalline than phenanthroline **4-2**. We started with the simplest 3-methylphenyl group substituted 1,7-phenanthroline **4-11** (Scheme 4.5), according to a related reported synthesis of 2,9-dimethylphenyl-1,10-phenanthroline.[165] To employ the alkyl/aryl lithium addition strategy, 3-bromotoluene and *t*-BuLi were mixed to generate lithium reagent **4-12**, after which lithium reagent **4-12** was added dropwisely into 1,7-phenanthroline solution in THF. The addition reaction took two days, followed by MnO_2 oxidation to result in phenanthroline **4-11**. Unexpectedly, phenanthroline **4-11** appeared as yellow oily solid forming a thin film on the bottom of flask. Re-crystallization attempts in various solvents did not solidify the compound. Since the yellow and oily compound did not meet the requirements to be HBL material, we stopped pursuing its properties.

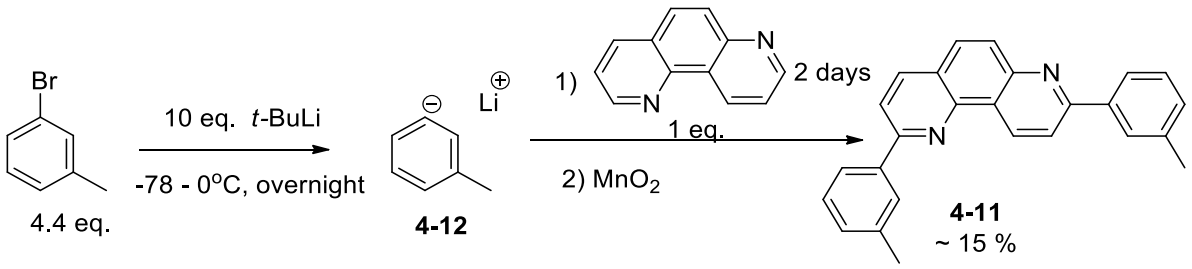

Scheme 4.5 Synthesis of 2,8-ditolyl-1,7-phenanthroline[165]

To further extend the scope of 1,7-phenathroline derivatives, one traditional synthesis reported by Eifert and Hamilton[159] was reproduced to make phenanthroline **4-13** (Scheme 4.6). Ferric chloride ($FeCl_3$) and catalytic amount of zinc chloride ($ZnCl_2$) were added to catalyze cyclization and

oxidation. This overnight reaction gave about 70% yield and the target molecule **4-13** was the major product. Taking advantage of this reaction we may be able to attach groups on positions other than the 2-position, as well as attach different groups on the two nitrogen-fused rings separately. Therefore, it would open a new gate for synthesis of diverse asymmetrically substituted 1,7-phenanthrolines, if necessary.

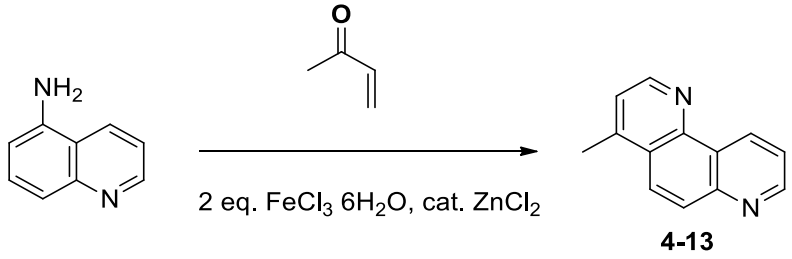

4-13

Scheme 4.6 Synthesis of 4-methyl-1,7-phenanthroline[159]

4.2.3 Optical and Electronic Properties of Synthetic 1,7-Phenanthroline Derivatives

The optical band gaps of synthesized 1,7-phenanthroline derivatives in dichloromethane were determined by UV-Vis spectroscopy. They are mostly somewhat higher than 3.5 eV, which can make them transparent across the visible spectrum. Figure 4.5 demonstrates that addition of methyl groups to 1,7-phenanthroline does not change the absorption significantly while addition of phenyl groups causes a red shift.

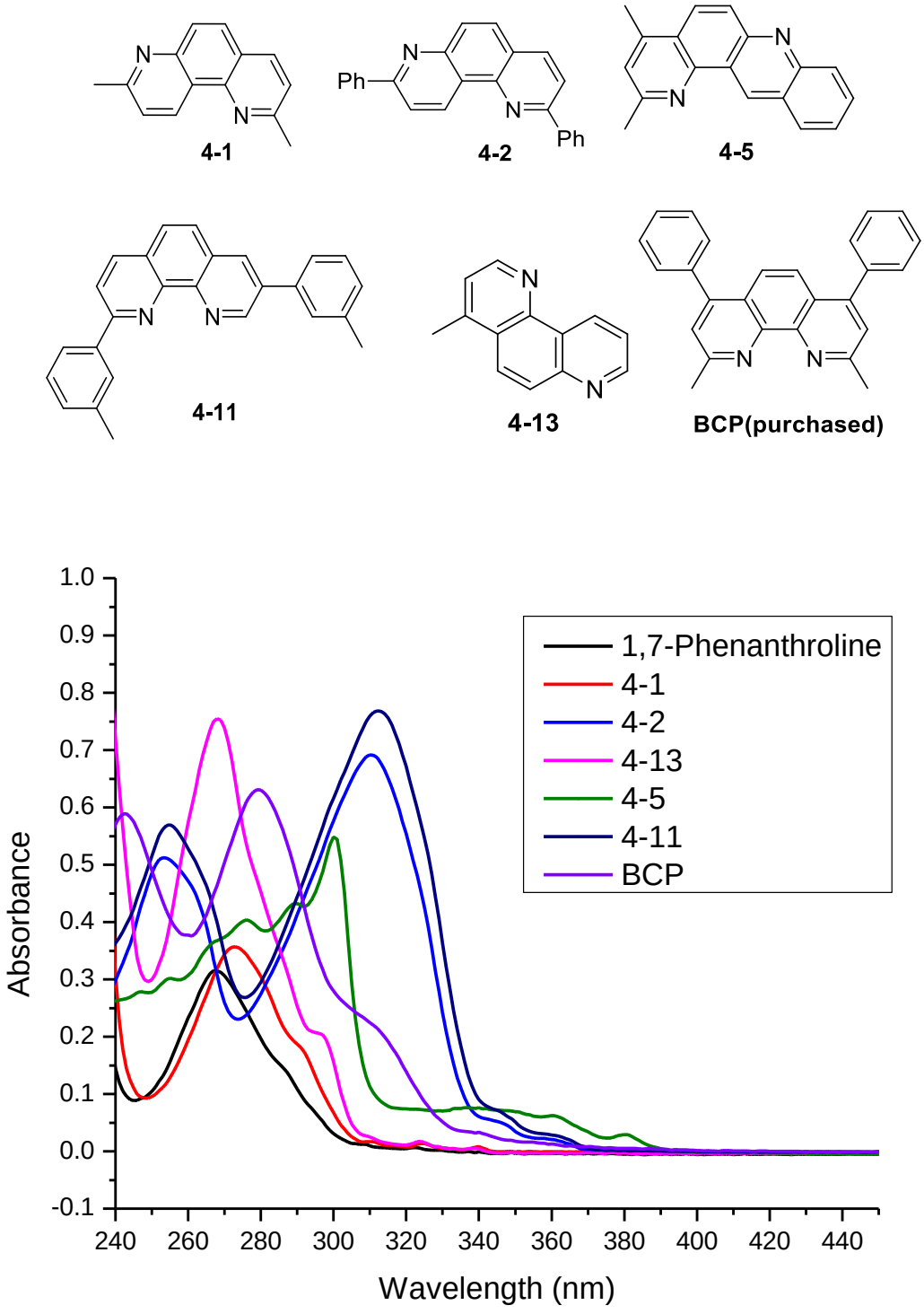

Figure 4.5 UV absorption of phenanthroline derivatives

Table 4.1 Measurement of optical energy band gap based on UV absorption in solution

Compound	1,7-phenanthroline	**4-1**	**4-2**	**4-11**	**4-5**	**4-13**	BCP
Maximum absorption λ (nm)	268	273 236	310 254	312	300	268	279
Cut-off Wavelength λ (nm)	312	315	340	345	370	310	335
E_{gap} (eV) = hc/λ	3.97	3.94	3.65	3.59	3.35	4.00	3.70

Maximum UV-absorption and cut-off wavelength were measured in dichloromethane solution

The cyclic voltammetry (CV) in the solution phase measures the HOMO and LUMO levels for one organic molecule by measuring the least energy required to extract an electron from one organic molecule (oxidative process) (HOMO), and the least energy needed to inject an electron to one organic molecule (reductive process) (LUMO). The redox potentials E_{red} and E_{ox} generated from CV can be used to calculate the HOMO and LUMO energy levels (reference electrode $AgNO_3$ is 5.0V vs. vacuum). Results are shown in Figure 4.6 and Table 4.2. Comparing to 1,7-phenanthroline, addition of the methyl group increases both the HOMO and LUMO but does not change the band gap, while addition of the aryl groups narrows the band gap.

$$E_{HOMO} = -e(E_{ox} + 5.0\ V)$$

$$E_{LUMO} = -e(E_{red} + 5.0\ V)$$

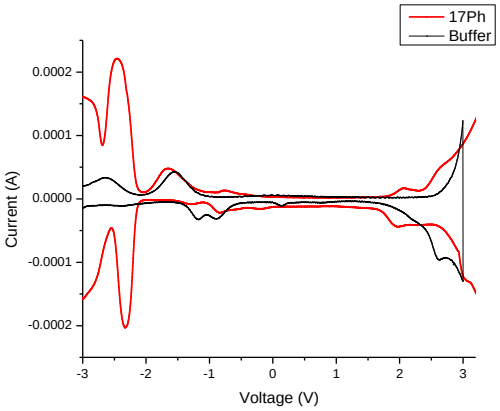
17Ph
Buffer
Current (A)
Voltage (V)

(a)

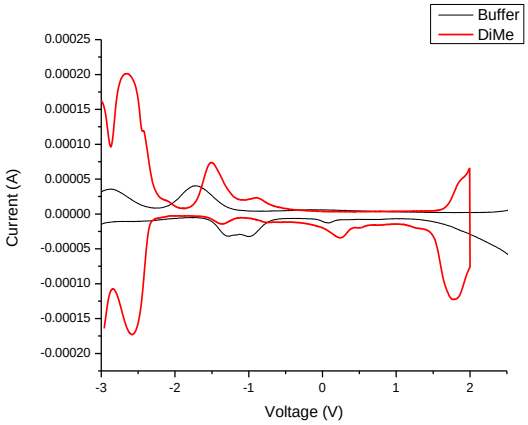
Buffer
DiMe
Current (A)
Voltage (V)

(b)

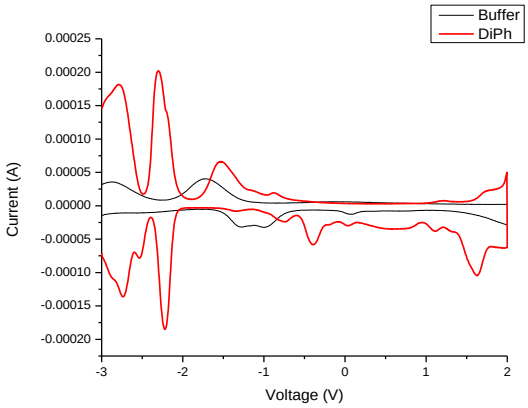
Buffer
DiPh
Current (A)
Voltage (V)

(c)

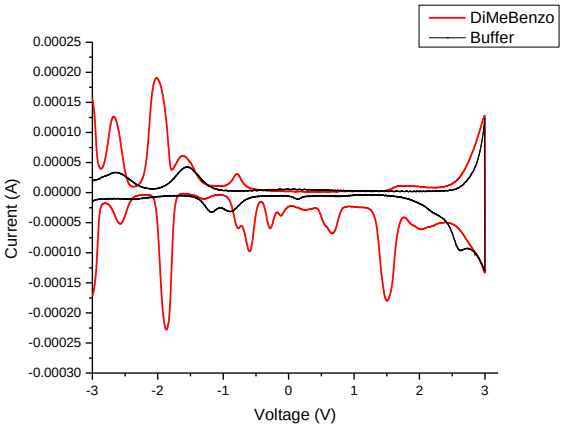
DiMeBenzo
Buffer
Current (A)
Voltage (V)

(d)

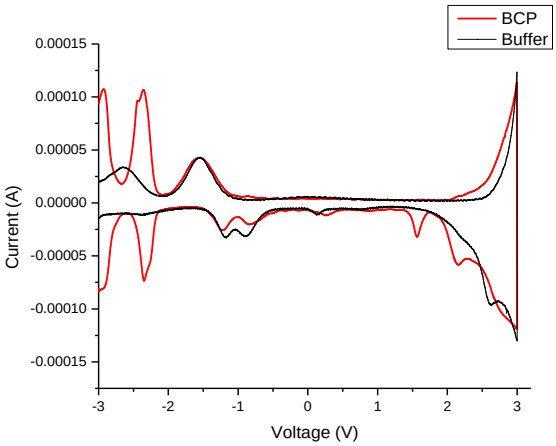
BCP
Buffer
Current (A)
Voltage (V)

(e)

Figure 4.6 (a) Cyclic voltammetry results of 1,7-phenanthroline; (b) Cyclic voltammetry results of **4-1**; (c) Cyclic voltammetry results of **4-2**; (d) Cyclic voltammetry results of **4-5**; (e) Cyclic voltammetry results of BCP

Table 4.2 Measurement of HOMO and LUMO based on Cyclic Voltammetry

Compound	HOMO (eV)	LUMO (eV)	LUMO-HOMO (eV)
1,7-Ph	-6.97	-2.53	4.44
4-1	-6.78	-2.34	4.44
4-2	-6.63	-2.70	3.93
4-5	-6.52	-2.99	3.53
BCP	-6.56	-2.65	3.91

Working methods: Squarewave voltammetry; Buffer: 0.1 M Tetrabutylamonium hexafluoro phosphate ($TBATF_6$) in MeCN; Reference electrode: 1 mM $Ag/AgNO_3$ in MeCN; Working electrode: Glassy carbon; Counter electrode: Platinum wire; Scan rate 100 mV/s, -3 V~2V

From the measurements on the optical energy band gap and the energy level of HOMO and LUMO, we can conclude that compound **4-1** has the largest HOMO/LUMO gap among all synthesized 1,7-phennathroline derivatives.

4.2.3 Thin-Film Fabrication and Characterization

4.2.3.1 Thin-Film Fabrication

10 nm Thin-films of 2,8-dimethyl-1,7-phenanthroline (**4-1**) (Figure 4.7 a, b) and 2,8-diphenyl-1,7-phenanthroline (**4-2**) (Figure 4.7 c, d) on Si wafer were fabricated by vacuum thermal evaporation, in collaboration with Kostas Alexandrou in the Kymissis group in the Columbia University. Phenanthroline **4-2** forms crystals easily on Si substrate within ten days since it was deposited. Therefore, AFM exhibited scattered particles (40 – 60 nm diameter) instead of homogeneous thin-

film. Phenanthroline **4-1** displayed better stability, as indicated by AFM. Since forming crystals easily would result in unstable electronic properties of thin films, molecular structure of phenanthroline **4-2** needs to be modified to achieve a less crystalline morphology. As a result, we targeted phenanthroline **4-1** as the hole-blocking material in further measurements.

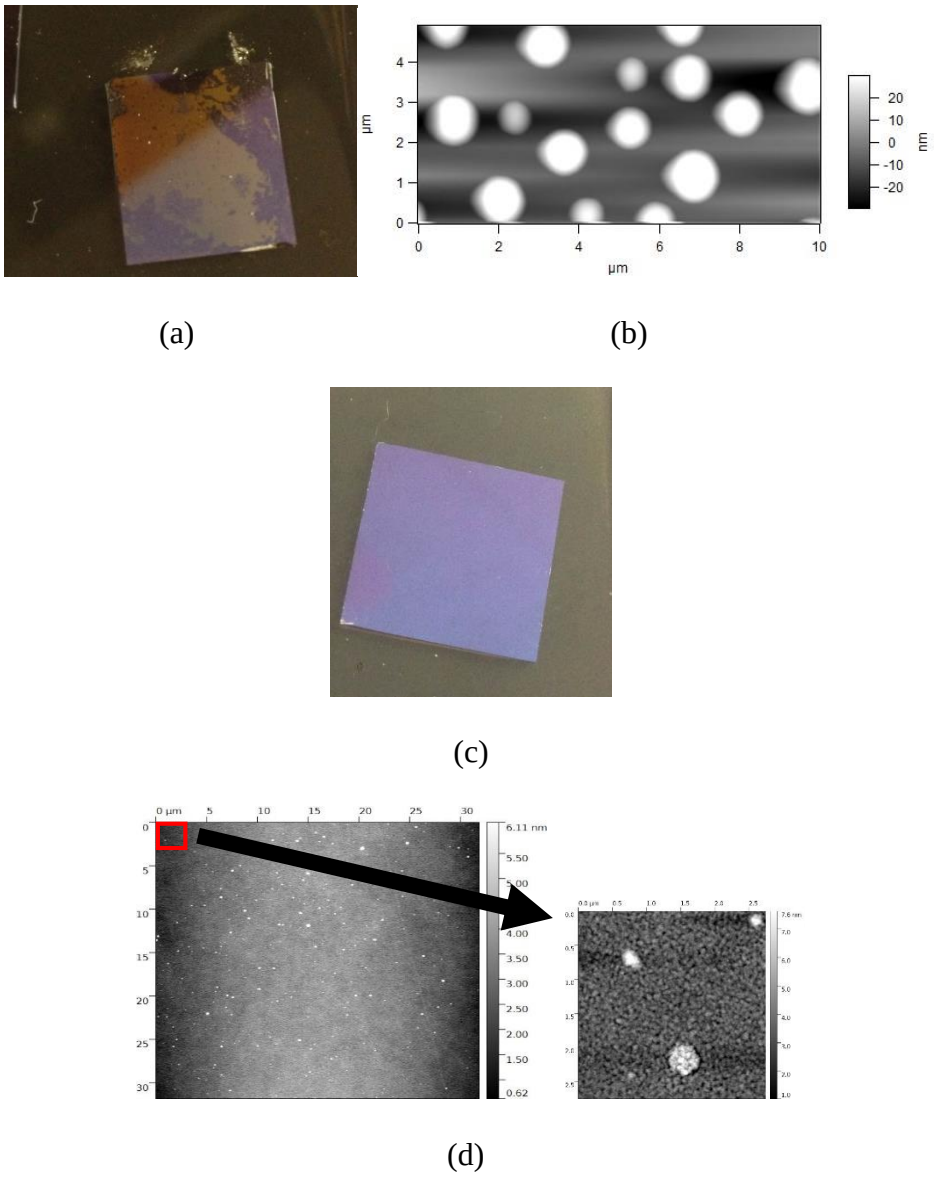

Figure 4.7 (a) Thin-film of 2,8-diphenyl-1,7-phenanthroline on Si; (b) AFM of thin-film a; (c) Thin-film of 2,8-dimethyl-1,7-phenanthroline on Si; (d) AFM of thin-film c.

4.2.3.2 Optical Properties of Thin Film of Phenanthroline 4-1

Solid-state optical absorption was measure by UV spectroscopy on **4-1** thin-film on a glass slide. When a light beam (I_0) goes through an absorbing film supported by a substrate, part of the beam is reflected (I_R), another part is transmitted (I_T), and the rest is absorbed (I_A) within the film. Figure 4.8b shows the onset absorption is 450.9 nm, from which we calculated the solid-state optical band gap of phenanthroline **4-1** is 2.75 eV, which is much lower than that measured in the solution.

$$(I_T + I_R + I_A) / I_0 = 1$$

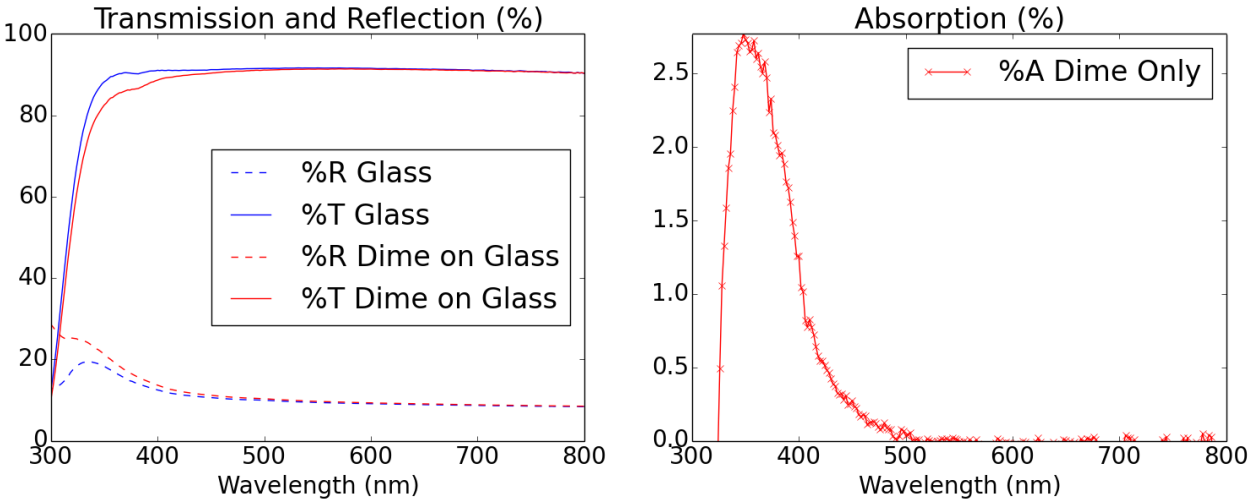

(a) (b)

Figure 4.8 (a) Solid-state UV measurements on phenanthroline **4-1** thin film; (b)Solid UV-absorption of compound **4-1**

We also utilized Variable Angle Spectroscopic Ellipsometry (VASE) to determine the properties of thin film of phenanthroline **4-1** on glass. Both VASE measurement and date analysis were completed by Ahsan Ashraf. VASE is known to offer precise thickness and refractive index after data analysis, based on the change in polarization state of light reflected from the surface of a thin-

film non-destructively (Figure 4.9).[166] The incident beam is a linear polarized light consisting of *p*-direction and *s*-direction components (*p*-direction is parallel to *E*-field polarization, *s*-direction is perpendicular to *E*-field polarization). The *s*- and *p*- polarized light are reflected differently from the surface to become an elliptically polarized light. Therefore, the measured ellipsometric parameters can be expressed by the relative amplitude change ($\Psi(\lambda)$), and the relative phase change ($\Delta(\lambda)$). These parameters are related to the complex ratio ρ of Fresnel reflection coefficients in *p*- and *s*- directions, r_p and r_s.[166a] Ψ and Δ are dependent on the photon energy and the sample structure, the material dielectric function ε, and the angle of incidence θ.[167]

$$\rho = r_p / r_s = \tan \Psi(\lambda) \exp (i \Delta(\lambda)) \qquad \text{Eq. 4-1}$$

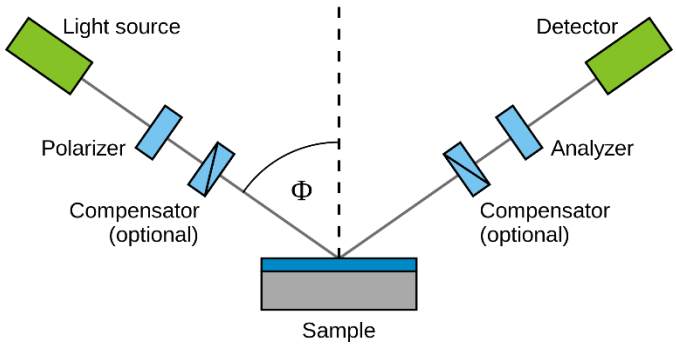

Figure 4.9 Geometry of an ellipsometry experiment[166a]

(Buntgarn, at the English Wikipedia project [GFDL (http://www.gnu.org/copyleft/fdl.html) or CC-BY-SA-3.0 (http://creativecommons.org/licenses/by-sa/3.0/)], via Wikimedia Commons)

Data fitting yields a complex index of refraction N (Eq. 4.2), where the real n is the refractive index and the imaginary k is the extinction coefficient (or the absorption index). Absorption index k indicates the amount of absorption loss when light passes through the sample, from which we can in fact learn the onset absorption wavelength of our phenanthroline **4-1** thin-film. Figure 4.10 shows the actual results we obtained on the phenanthroline **4-1** thin-film. By converting the onset

absorption wavelength (330.1 nm) to energy (eV), we learned the optical energy band gap of phenanthroline **4-1** is approximately 3.75 eV, higher than 3.5 eV. The high energy band gap could make it possible to block the carriers, and do not absorb visible light.

$$N = n + ik \qquad \text{Eq. 4-2}$$

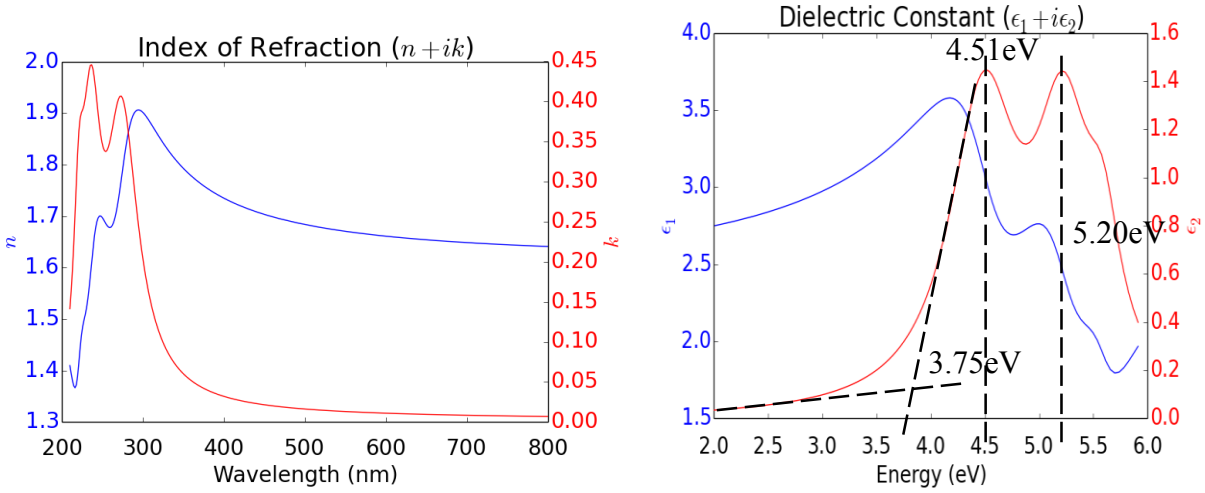

(a) (b)

Figure 4.10 (a) Index of refraction; (b) Dielectric constant converted by index of refraction

4.2.4 MIM Device

In MIM (metal-insulator-metal) diodes tunneling is the predominant electron transport mechanism. MIM devices are composed of two metals and one insulator in between. The energy band diagram can be determined by the work function of M1, M2, electron affinity of the insulator, and energy band gap of the insulator. In our system, we regarded compound **4-1** as the insulator. Applying voltage on M1 can increases energy of electrons in M1 until they start to tunnel through insulator into the empty states in M2 (holes tunnel through in the opposite direction simultaneously). Similarly, applying voltage on M2 increases energy of electrons in M2 until they start to tunnel through into the empty states in M1 (holes tunnel through in the opposite direction simultaneously).

We expected to see electrons tunneling along one direction could be much easier than the other, which would indicate that in this direction electron transport is allowed where carrier transport is forbidden. Architecture of MIM devices is shown in Figure 4.11. By employing different metals as cathodes and injecting electrons through the organic layer to learn the turn-on voltages, we can learn the injection barrier of the organic compound with respect to the metals. The reverse breakdown voltage can also provide hole-barrier-potential of the organic film.

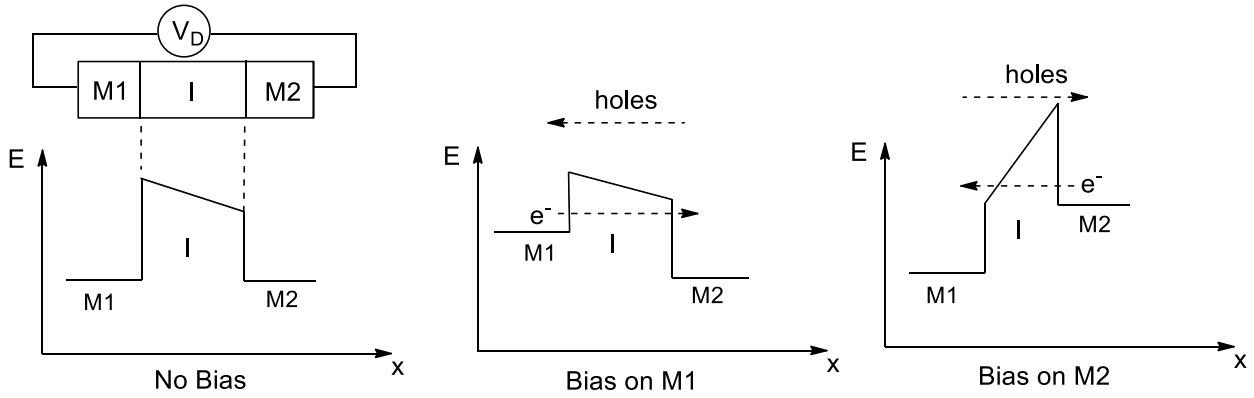

Al (50 nm) anode
Phenanthroline (10 nm)
Al/Au/Ag (30 nm) cathode
Subatrate (Glass)

Figure 4.11 Energy diagram and architectures of MIM devices[168]

Kostas Alexandrou in Columbia University made two MIM devices, Al–(**4-1**)–Al and Al–(**4-1**)–Au, through thermal evaporation. AFM was employed to determine the topography of both devices. By applying a voltage bias across the electrodes of a device, current change following voltage change can be measured and generated in an I-V curve. All the measurements were completed by

Ahsan Ashraf in Brookhaven National Lab, and results are shown in Figure 4.12. The Al–(**4-1**)–Al device shows a slight capacitive switching between -0.5 and 0.5 V (between -1.0 and 0.8 nA) (Figure 4.12a) potentially due to metal migration through the 10 nm phenanthroline **4-1** layer. By varying voltage ramps rates, Ashraf was able to extract non-capacitive components, which displays nice diode behavior (Figure 4.12b). The forward and backward bias were almost symmetric, and the turn-on voltage was around 0.5 V. However, the I-V curve of Au–(**4-1**)–Al device displays resistive switching behavior (Figure 4.12c), where resistivity changed while switching voltage between forward and backward bias. Possible metal diffusion into phenanthroline **4-1** film when applying voltage in one direction could make the film a conductor with one conductivity, while reversed metal diffusion when applying voltage in the reversed direction could result in a different conductivity.

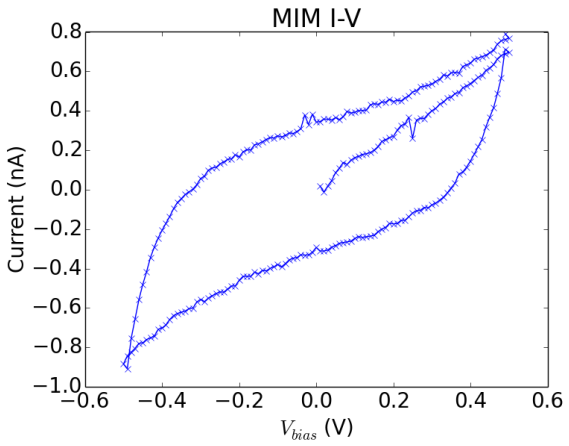

(a)

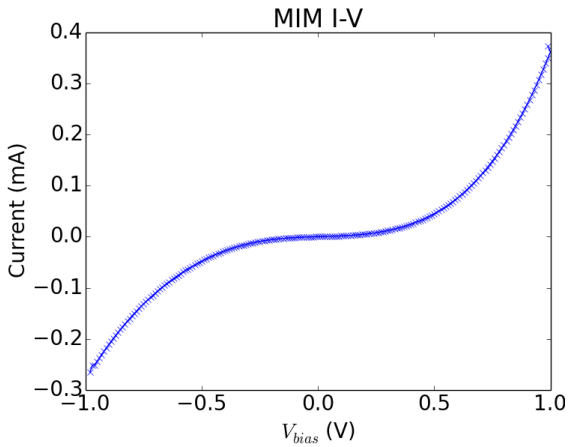

(b)

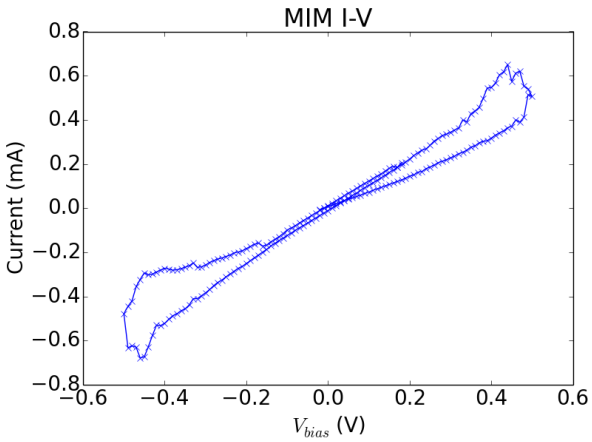

(c)

Figure 4.12 (a) Capacitive switching behavior of Al– (**4-1**) –Al device; (b) Diode behavior of Al–(**4-1**)–Al device; (c) Resistive switching behavior of Au–(**4-1**)–Al device

As an improvement of the MIM measurement, we fabricated an MIM junction with a spacing of 10 nm. The device was fabricated by Ahsan Ashraf on a thermal oxide substrate patterned using electron-beam lithography. Gold contacts were deposited using electron-beam evaporation with 10 nm spacings (Figure 4.13a). Phenanthroline **4-1** was deposited onto the substrate to form the junction, which was done in the Kymissis group. At the metal/insulator interface, we expect to get a Schottky contact depending on the electronic barrier height. By measuring dark current-voltage curves from this device at varying temperature (150K – 300K) and fitting to a diode model, Ashraf was able to extract the reverse saturation current densities (J_0) as a function of temperature (Figure 4.13b), and get a Schottky barrier height (0.906 eV). Based on the work function of gold (-5.0 eV) and the extracted barrier height, the LUMO level of phenanthroline **4-1** was calculated to be −4.09 eV. According to the optical band gap of 3.75 eV measured by VASE, we can therefore calculate the HOMO level to be −7.84 eV. Comparing to the results generated from cyclic voltammetry

measurements, the optical band gap of phenanthroline **4-1** is lower in the solid state than in the solution, but both values are higher than the required 3.5 eV for HBL.

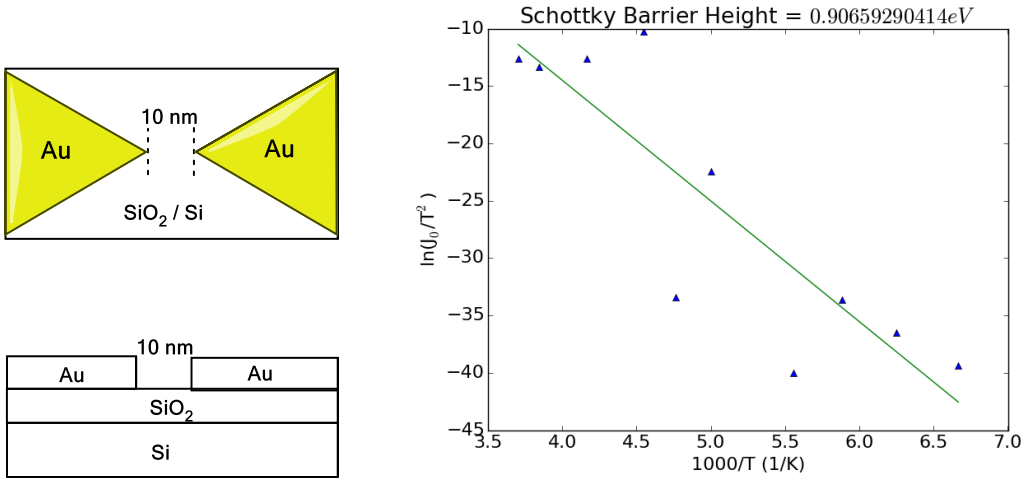

Figure 4.13 (a) Architecture of the MIM device; (b) The Schottky barrier height for the junction extracted using low temperature current voltage curves on a 10nm device. The barrier height is calculated to be 0.91eV

4.2.5 Phenanthroline 4-1 as HBL in Organic and CIGS Photovoltaice Devices

We incorporated phenanthroline **4-1** as HBL material in both organic and CIGS photovoltaic devices. All the devices were fabricated by Ahsan Ashraf in the Eisaman group in Brookhaven National Lab. Thermal evaporation of phenanthroline **4-1** was performed by Kostas Alexandrou in the Kymissis group in Columbia University. Architectures of the devices are shown in Figure 4.14(a) and Figure 4.15(a). The architecture of the organic photovoltaic device is standard. The P3HT:PCBM heterojunction is the active *p-n* heterojunction. The poly(3-hexylthiophene-2,5-diyl) (P3HT) absorbs sunlight and transfers electrons to the phenyl-C_{61}-butyric acid methyl ester (PCBM). The PEDOT:PSS is a standard electron-blocking (hole-transporting) layer. In the CIGS thin-film photovoltaic device, we employed the novel architecture including graphene as the *n*-layer. Two organic devices and two CIGS devices were prepared. 10 nm phenanthroline **4-1** was

deposited on one of the two devices as HBL, while the other was the control. Ashraf measured performance of all devices on a solar simulator (AM 1.5 G) in the Eisaman group and analyzed the IV curves generated. Our best results among all attempts are summarized in Table 4.3 and Table 4.4. Including phenanthroline **4-1** as HBL enhances the PCE of the organic device from 0.9 to 5.0%, and the CIGS device from 3.2×10^{-4} to 0.11%. The efficiencies measured are not as high as reported, because the devices are fabricated at Brookhaven National Lab., except for the HBL of each device is deposited at Columbia University. During the transportation, devices were exposed to air and moisture for at least 24 h during the fabrication process. However, the improvement of efficiencies indicates the synthesized phenanthroline **4-1** is a promising HBL. In the future, fabricating the whole device under nitrogen or argon is necessary to confirm the improvement of PEC and to improve the reproducibility. Looking for an optimum thickness of the HBL is also necessary for optimize the performance of the devices.

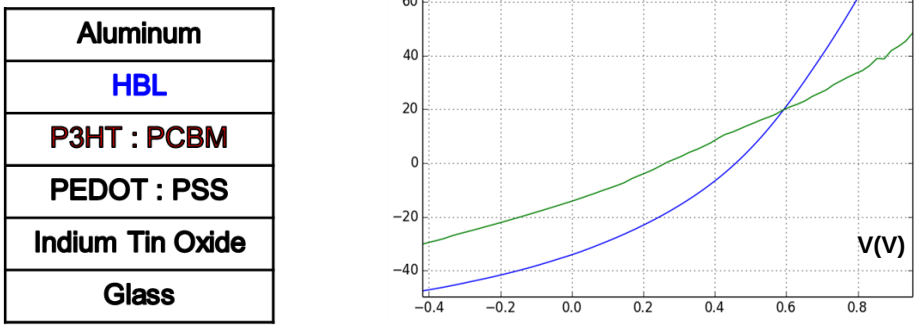

(a) (b)

Figure 4.14 (a) Architecture of the organic photovoltaic device; (b) IV characteristics of organic photovoltaic devices with and without a HBL (1mm by 1mm device)

Table 4.3 Performance of organic photovoltaic devices with and without a HBL (1mm by 1mm device)

	V_{oc} (V)	J_{sc} (mA/cm^2)	*FF* (%)	PCE (%)
No HBL	0.288	-11.833	27.109	0.926
With HBL	0.463	-33.037	32.845	5.019

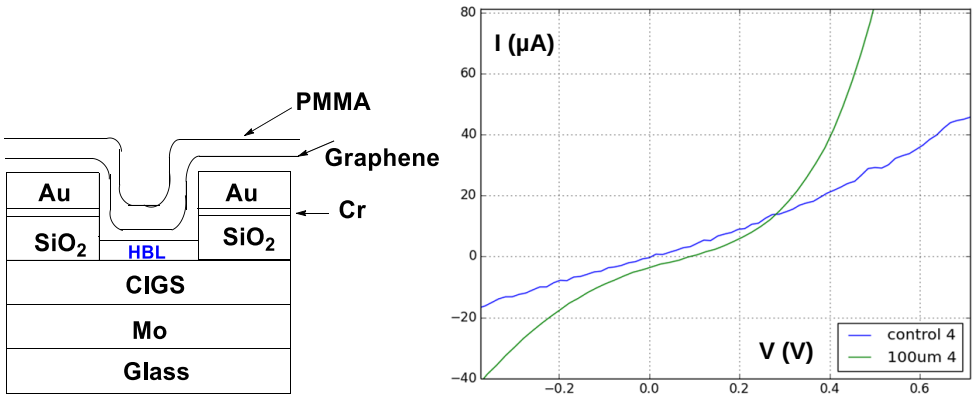

(a) (b)

Figure 4.15 (a) Architecture of CIGS/Graphene photovoltaic device (b) IV characteristics of CIGS/Graphene photovoltaic devices with and without a HBL (10μm by 10μm device)

Table 4.4 Performance of CIGS/Graphene photovoltaic devices with and without a HBL (10μm by 10μm device)

	V_{oc} (V)	J_{sc} (mA/cm^2)	*FF* (%)	PCE (%)
No HBL	0.0052	-0.199	31.249	3.250e-4
With HBL	0.0872	-4.934	25.350	0.109

4.3 Results and Discussion on 2,4-Diphenyl Quinoline Derivatives

4.3.1 Synthesis of 2,4-Diphenyl Quinoline derivatives

According to the desired properties of HBL materials, target organic small molecules need to: 1) appear as a white solid, indicating wide optical band gap, > 3.5 eV; 2) have appropriate HOMO and LUMO energy levels; 3) have a melting point of about 200°C, making it stay reasonably stable while device fabrication; 4) be stable as homogeneous thin films. The aryl groups functionalized 1,7-phenanthrolines, such as **4-2** and **4-11**, are likely to have smaller optical band gap than 3.5 eV because of high conjugation. 2,4-Diphenyl-quinoline derivatives (Figure 4.16) were targeted to expand the scope of organic small molecules as HBL materials. Many 2,4-diphenyl-quinoline derivatives are reported as white solids with high melting points. Synthesis of quinilines has been well established. These quinoline derivatives have been known for their bioactivity,[169] but no one has reported using them as HBL materials.

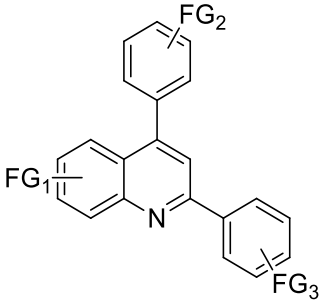

Figure 4.16 2,4-Diphenyl qunoline derivatives

Synthesis of target quinoline derivatives was reported very recently by the Ghorai group[170] through a "transition-metal-free cycloisomerization of *o*-cinnamylanilines" [170] (Scheme 4.7). Rhenium(VII) oxide (Re_2O_7) was used as Lewis acid catalyst to activate the alcohol and then facilitate *ortho*-

functionalization of an aniline through Friedel-Crafts (FC) alkylation. Both N-alkylated and C-alkylated products can be generated in the metal-catalyzed FC reaction. Rhenium(VII) oxide, Re_2O_7, is one of the few catalysts that results in almost all desired C-alkylated (C-alkylated: N-alkylated = 95:5) product. The following oxidative cyclization contains *t*-BuOK and DMSO at room temperature. Even strong electron-withdrawing substituted are compatible with the reaction conditions and can result in good yield.

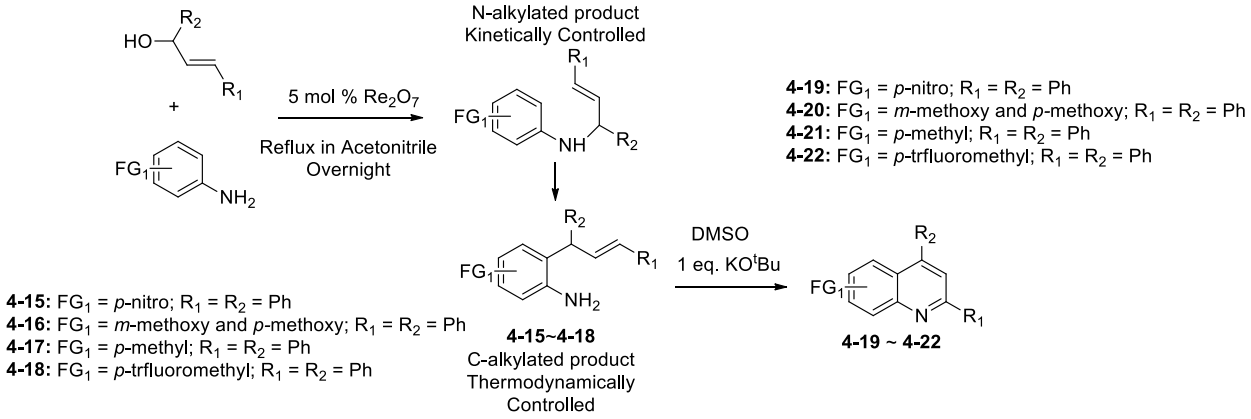

Scheme 4.7 Synthesis of quinoline derivatives[170]

Four quinoline derivatives were synthesized following the reported synthetic route in decent yields (Figure 4.17). Quinolines **4-19**, **4-20** and **4-22** are all white solids, as reported,[170] and having melting points around or higher than 150°C. The nitro and trifluoromethyl groups were electron withdrawing, while methoxy group was electron donating. Methyl substituted quinoline **4-21** was synthesized as a reference compound to learn how electron withdrawing/donating groups could affect their optical band gaps.

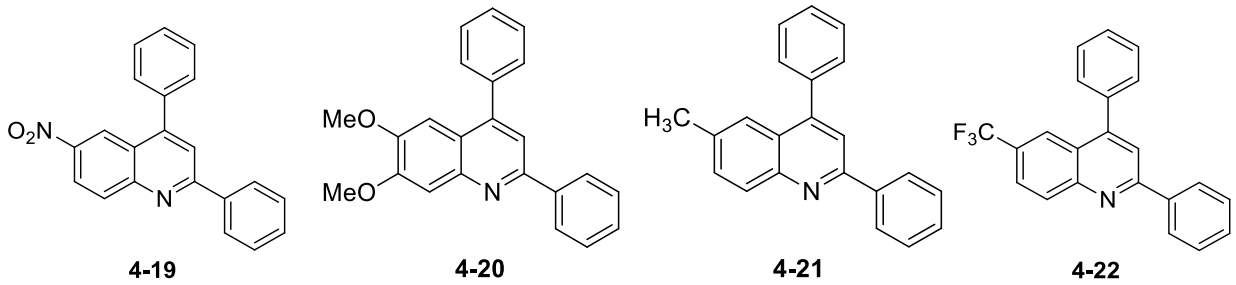

4-19 4-20 4-21 4-22

Figure 4.17 Synthesized 2,4-diphenyl-quinoline derivatives

4.3.2 Optical Properties of Synthesized Quinolines

Optical band gaps of synthesized quinoline derivatives were measured based on UV/Vis spectroscopy (Figure 4.18, Table 4.5). Comparing to quinoline **4-21**, electron withdrawing groups were expected to lower both HOMO/LUMO energy levels but not change the band gap very much. Among the four quinoline derivatives, trifluomethyl substituted quinoline **4-22** has an onset absorption at approximately 350 nm, which corresponds to the optical energy band gap of 3.54 eV. The 3.54 eV is higher than required minimum 3.5 eV for HBL materials. Furthermore, the melting point of quinoline **4-22** is 148 – 150 °C, making it potentially stable during device fabrication. Further investigation on the optical and electronic properties in the solid state is required to determine whether it is a promising HBL material. In addition, synthesis of diphenyl quinoline with other substituents, or with more than one substituents, e.g. two trifluoromethyl groups, can be attempted to reach optimized properties.

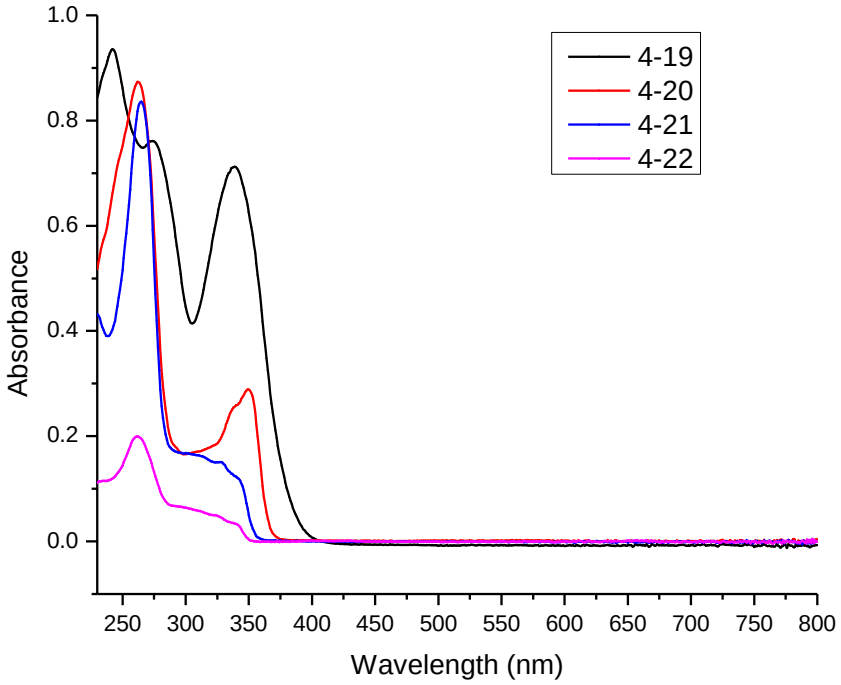

Figure 4.18 UV absorption of synthesized quinoline derivatives

Table 4.5 Measurement of optical energy band gap based on UV absorption in solution

Compound	BCP	**4-19**	**4-20**	**4-21**	**4-22**
Maximum absorption λ (nm)	279	339	350	265	262
Onset Wavelength λ (nm)	335	400	375	360	360
E_g (eV) = hc/λ	3.70	3.10	3.31	3.44	3.44

Maximum UV-absorption and onset wavelength were measured in dichloromethane solution. E_g is calculated from onset wavelength.

4.4 Conclusion & Future Work

In this project, we targeted conjugated organic small molecules as HBL materials in a novel architecture of CIGS-based thin film photovoltaic cells. A HBL is placed in between CIGS layer

and *n*-type graphene layer to minimize charge recombination, as well as passivate CIGS layer. The new CIGS-based thin-film photovoltaic cell has a great potential to approach a theoretical maximum PCE of 33%. There are not many organic HBL materials reported. The widely used ones have their own disadvantages. Therefore, we introduce organic compounds that could meet all the required properties. They can be feasibly synthesized. Their properties can be tuned by modifying substituents to meet the requirements.

Several 1,7-phenanthroline derivatives are targeted that have similar structures to the popular BCP and BPhen HBL, which may lead to similar desired electronic properties. Five compounds, **4-1**, **4-2**, **4-5**, **4-11**, and **4-13** have been synthesized successfully. According to their optical and electronic properties, as well as morphologies in the solid state, we considered phenanthroline **4-1** the most promising candidate. We deposited phenanthroline **4-1** as the HBL in both the organic and the CIGS photovoltaic devices, and measured the performance of fabricated devices. The best results indicate that comparing to the reference devices without HBL, including phenanthroline **4-1** as the HBL enhanced PCE of an organic device from 0.9 to 5.0%, and the CIGS device from 3.2×10^{-4} to 0.11%. In the future, we need to 1) determine the reproducibility of the PCE improvement; 2) make comparison between the hole-blocking performance of synthesized 1,7-phenanthroline derivatives and BCP in both the organic and CIGS/Graphene devices; 3) investigate the optimum thickness of HBL in the devices; and 4) modify the structures of targeted molecules so that the compound can have high energy band gap, high melting point, and powdery morphology.

In addition to 1,7-phenanthroline derivatives, we targeted a series of 2,4-diphenyl quinoline derivatives **4-19** – **4-22** as HBL materials. We synthesized target compounds, and measured their optical band gaps by UV spectroscopy. Trifluoromethyl functionalized diphenyl quinoline is promising since its optical band gap is close to 3.5 eV and it appears as a white powdery solid with a melting point of 148-150 °C (Lit.[170] 148-150°C). Further characterizations are required to measure further properties.

4.5 Experimental Procesures

General Methods: Excepted stated, reagents were purchased at reagent grade from Aldrich, Fisher Scientific/Acros Organics, or VWR, and were used without further purification. Column chromatography: Silica gel-60 (230-400 mesh) from Sorbent Technologies. Thin Layer Chromatography (TLC): plastic sheets covered with silica gel purchased from Acros. Melting points were measured on a Thomas Hoover Capillary melting point apparatus. ^{1}H and ^{13}C NMR spectra were obtained using Varian Gemini-300 MHz, Inova-400 MHz, Inova-500 MHz, Bruker-400 MHz, or Bruker-500 MHz instruments, and were taken in deuterated chloroform unless noted otherwise.

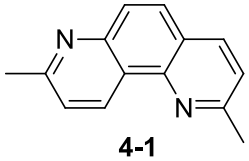

4-1

2,8-Dimethyl-1,7-phenanthroline (4-1)[171]

1,7-phenanthroline (0.2 g, 1.1 mmol, 1 eq.) in dry THF (15 mL) was cooled to 0 °C. 1.5 M methyllithium in hexane (3.7 mL, 5.5 mmol, 5 eq.) was added slowly into the solution. The resulting deep red-brown solution was stirred for 10 mins at 0 °C, and then warmed to room temperature and stirred overnight. The reaction was quenched by aqueous sat. NH_4Cl (5 mL) and 20 mL water. After extracting the aqueous layer three times with CH_2Cl_2 (3×15 mL), the solvent was evaporated in vacuum, and the crude product was purified roughly through a short plug (SiO_2, Hex : EA = 1:1). The intense yellow oil obtained was then dissolved into 15 mL CH_2Cl_2, and activated MnO_2 (1.5 g, 17.3 mmol) was added. The mixture was allowed to stir for 6 h and filtered over celite, and evaporated. Column chromatography (SiO_2, Hex : EA = 5:1) was then utilized to isolate the desired compound as a pale yellow solid (68 mg, 30% yield). mp 95-98 ℃ (Lit. 96.5 - 97.5 °C).[171a] HRMS (TOF MS ES+), $[M+H]^+$ = 209.1. ^{1}H-NMR (400 MHz, $CDCl_3$) δ 9.44 (d, *J* = 8.4 Hz, 1H), 8.06 (d, *J* = 8.0 Hz, 1H), 7.94 (d, *J* = 8.8 Hz, 1H), 7.85 (d, *J* = 9.2 Hz, 1H), 7.48 (d, *J* = 8.4 Hz, 1H), 7.38 (d, *J* = 8.0 Hz, 1H), 2.82 (s, 3H), 2.81 (s, 3H);[171b] ^{13}C-NMR (100 MHz, $CDCl_3$) δ 159.8, 158.3, 149.1, 145.3, 135.9, 132.9, 128.7, 127.5, 124.5, 123.6, 122.3, 122.2, 25.3, 25.2. IR 2917, 1965, 1618, 1604, 1584, 1561, 1512, 1487, 1410, 1394, 1369, 1351, 1319, 1279, 1238, 1226, 1238, 1226, 1186, 1142, 1134, 1087, 1032, 987, 890, 849, 844, 815, 791, 742, 729, 693, 672 cm^{-1}.

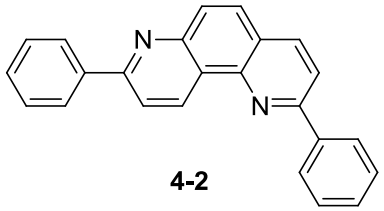

4-2

2,8-Diphenyl-1,7-phenanthroline (4-2)[172]

1,7-phenanthroline (0.2 g, 1.1 mmol, 1 eq.) in dry THF (15 mL) was cooled to 0 °C. 1.9 M phenyllithium in hexane (3 mL, 5.5 mmol, 5 eq.) was added slowly into the solution. The resulting deep red-brown solution was stirred for 10 mins at 0°C, and then warmed to room temperature and stirred overnight. The reaction was quenched by aqueous sat. NH_4Cl (5 mL) and 20 mL water. After extracting the aqueous layer three times with CH_2Cl_2 (3×15 mL), the solvent was evaporated in vacuum, and the crude product was purified roughly through a short plug (SiO_2, Hex: EA = 1:1). The intense yellow oil obtained was then dissolved into 15 mL CH_2Cl_2, and activated MnO_2 (1.5 g, 17.3 mmol) was added. The mixture was allowed to stir for 6 h and filtered over celite, and evaporated. Column chromatography (SiO_2, Hex:EA = 5:1) was then utilized to isolate the desired compound. Recrystallization in CH_2Cl_2 at 0 °C resulted in light yellow crystals (50 mg, 15% overall yield). mp 153-155 °C (Lit. 164 °C).[172] HRMS (TOF MS ES+), $[M+H]^+$ = 333.1. ^{1}H-NMR (500 MHz, $CDCl_3$) δ 9.73 (d, *J* = 8.5 Hz, 1H), 8.34 (d, 2H), 8.26-8.23 (m, 3H), 8.13-8.11 (m, 2H), 8.10 (d, *J* = 8.5 Hz, 1H), 7.93 (d, *J* = 8.5 Hz, 1H), 7.60-7.36 (m, 7H); ^{13}C-NMR (125 MHz, $CDCl_3$) δ 158.3, 156.1, 149.8, 145.6, 139.5, 139.4, 136.6, 133.7, 129.4, 129.4, 129.1, 128.8, 127.6, 127.4, 125.9, 124.8, 119.2. IR: 3053, 1966, 1613, 1587, 1554, 1518, 1480, 1449, 1431, 1388, 1353, 1296, 1275, 1181, 1142, 1107, 1077, 1061, 1032, 973, 879, 849, 826, 760, 689, 677 cm^{-1}.

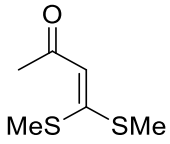

4-7

3,3-Bis(methylthio)acrylaldehyde (4-7)[163]

t-BuOK (1.61 g, 16 mmol) in 20 mL dry THF was added slowly to a solution of vinyl acetate (1.38 mL, 15 mmol) in dry THF 15 mL under Ar at -78 °C. Carbon disulfide (0.90 mL, 15 mmol) in dry THF (6 mL) was then added dropwise and the reaction mixture was stirred for another 1 h at 0 °C. The enolate generated was then methylated with methyl iodide (1.9 mL, 30 mmol) and stirred for 12 h at 0 °C. The reaction mixture was quenched by 50 mL ice water, extracted with CH_2Cl_2 (3 × 20 mL), dried with $MgSO_4$, concentrated and purified by column chromatography (SiO_2, Hex : EA = 5:1, R_f = 0.2). The product appeared an orange oil (1.09 g, 45% yield). ^{1}H-NMR (500 MHz, $CDCl_3$) δ 9.69 (d, *J* = 6.5 Hz, 1H), 5.78(d, *J* = 6.5 Hz, 1H), 2.37 (s, 3H), 2.27 (s, 3H); ^{13}C-NMR (100 MHz, $CDCl_3$) δ 16.3, 16.6, 120.4, 166.6, 185.7.[163]

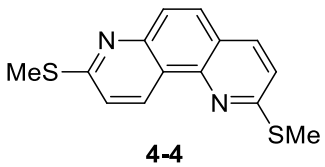

4-4

2,8-Bis(methylthio)-1,7-phenanthroline (4-4)[163]

3,3-Bis(methylthio)acrylaldehyde (**10**) (0.5 g, 3.37 mmol, 2.2 eq.) and *m*-phenylenediamine (0.16 g, 1.54 mmol) was added into 20 mL acetic acid. The mixture was allowed to reflux for 10 h, and cooled down to room temperature. It was basified by 2M NaOH until pH = 14, extracted by CH_2Cl_2 (3×20 mL), dried over $MgSO_4$. After removal of solvent, a trace amount of product was isolated from a mixture of compounds through column chromatography (SiO_2, Hex: EA = 5:1, R_f = 0.7). ^{1}H-NMR (500 MHz, $CDCl_3$) spectrum contains the peaks matching the product, but shows a large percentage of impurities.[163] The amount of the material was too small to take a ^{13}C-NMR.

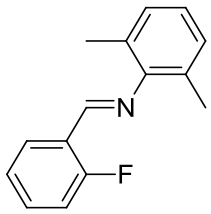

4-9

(*E*)-*N*-(2-Fluorobenzylidene)-2,6-dimethylbenzenamine (4-9)[173]

A mixture of *o*-fluoro-benzaldehyde (1 mL, 1.19 g, 9.43 mmol), 2,6-dimethylamine (1.55 mL, 1.53 g, 9.43 mmol), and anhydrous $MgSO_4$ 0.5 g in hexanes (20 mL) was stirred at room temperature for 4 h. The mixture was filtered and the solvent evaporated to dryness to give bright yellow oil. The crude product was purified by flushing it through a plug by hexane to generate a colorless oil (2.10 g, 98% yield). ^{1}H-NMR (500 MHz, $CDCl_3$) δ 8.75 (s, 1H), 8.48 (m, 1H), 7.60 (m, 1H), 7.40 (m, 1H), 7.27 (m, 3H), 7.17 (m, 3H). 2.37 (s, 6H). ^{13}C-NMR (100 MHz, $CDCl_3$) δ 163.7, 161.7, 156.1, 156.1, 151.1, 132.9, 132.8, 128.0, 127.5, 126.9, 124.4, 124.4, 123.8, 123.7, 123.6, 115.9, 115.7, 18.2.[173]

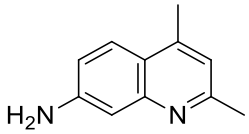

4-8

2,4-Dimethylquinolin-7-amine (4-8)[174]

To a solution of *m*-phenylenediamine (2.12 g, 19.6 mmol) in 10 mL of ethanol was added a mixture of concentrated HCl (0.8 mL, 9.8 mmol) and acetyl acetone (1 mL, 9.8 mmol) at room temperature. The mixture was stirred until a large amount of yellow solid precipitated. The solid was collected by filtration, washed with ethanol and dried. The solid was dissolved in 20 mL 1M NaOH, and extracted by CH_2Cl_2 20 mL ×3. The combined organic layer was dried and condensed. Compound **4-8** was obtained as a white crystal (1.17 g, 70% yield). Mp 94 – 96°C (Lit. 94 – 100 °C).[175] ^{1}H-NMR (500 MHz, $CDCl_3$) δ 7.68(d, *J* = 8.5 Hz, 1H), 7.12 (s, 1H), 6.82-6.89 (dd, 2H), 4.09 (s, 2H), 2.58 (s, 2H), 2.51 (s, 2H). ^{13}C-NMR (125 MHz, $CDCl_3$) δ 158.74, 149.34, 147.33, 143.77, 124.62, 120.08, 119.52, 116.96, 109.40, 25.02, 18.27.[174]

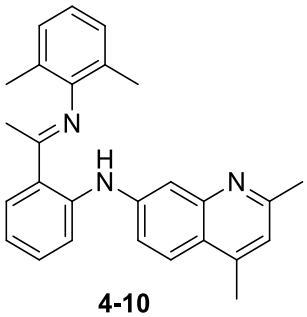

4-10

(*E*)-*N*-(2-(1-(2,6-Dimethylphenylimino)ethyl)phenyl)-2,4-dimethylquinolin-7-amine (4-10)[164]
A solution of n-BuLi (2.5 M, 6 mmol) in hexane was added to **4-8** (0.516 g, 3 mmol) in THF 4.5 mL at –78 °C. The mixture was warmed to room temperature and stirred overnight. The resulting solution was transferred through cannula into a solution of **4-9** (0.681 g, 3 mmol) in 4.5 mL THF at 25 °C. After stirring for 48 h, the reaction was quenched by water 20 mL, and organic phase was extracted by CH_2Cl_2 (15 mL ×3). Dry and condense the combined organic layer gave brown oil. Column chromatography (SiO_2, Hex : EA = 5:1, 1% trimethylamine, R_f = 0.1) was employed to isolate the desired compound (0.06 g, 51% yield) as a yellow oil. ^{1}H-NMR (500 MHz, $CDCl_3$) δ 11.64 (s, 1H), 8.37 (s, 1H), 8.02 (s, 1H), 7.86 (d, *J* = 8.5 Hz, 1H), 7.81 (d, *J* = 8.5 Hz, 1H), 7.35-7.41 (m, 3H), 6.94-7.14 (m, 5H), 2.68 (s, 3H), 2.62 (s, 3H), 2.24 (s, 6H). ^{13}C-NMR (125 MHz, $CDCl_3$) δ 165.8, 159.1, 150.1, 149.0, 144.9, 143.8, 134.8, 132.1, 128.2, 127.8, 124.6, 124.1, 122.4, 121.1, 121.0, 118.9, 118.2, 115.4, 114.1, 25.1, 18.6, 18.4.[164]

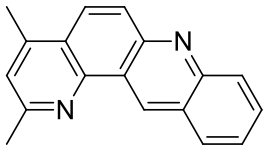

4-5

2,4-Dimethylbenzo[*j*][1,7]phenanthroline (4-5)[164]
A mixture of $ZnCl_2$ (0.054 g, 0.4 mmol) and compound **4-10** (0.08 g, 0.2 mmol) in THF 2 mL was stirred at 80 °C for 24 h. Water was added to quench the reaction. CH_2Cl_2 (15 mL × 3) was used to extract organic phase. The combined organic layer was dried over $MgSO_4$ and evaporated to dryness to give crude product. The crude product was purified by column chromatography (Hex : EA = 10:1, R_f = 0.4). Product **4-5** was obtained as a white solid (51 mg, quantitative yield). mp 143 – 145 °C. ^{1}H-NMR (500 MHz, $CDCl_3$) δ 9.90 (s, 1H), 8.21(d, *J* = 8.5 Hz, 1H), 8.06(d, *J* = 8.0 Hz, 1H), 7.89(s, 2H), 7.78-7.75(m, 1H), 7.54-7.50(m, 1H), 7.02(s, 1H), 2.66(s, 3H), 2.49(s, 3H). ^{13}C-NMR (125 MHz, $CDCl_3$) δ 157.4, 149.7, 148.7, 145.7, 143.9, 133.3, 130.2, 128.8, 127.4, 126.6, 126.2, 125.6, 125.2, 123.8, 122.5, 24.9, 18.5.[164]

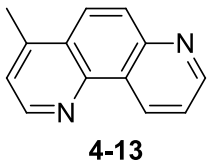

4-13

4-Methyl-1,7-phenanthroline (4-13)[159]

Ferric chloride hexahydrate (1.97 g, 7.28 mmol), 5-aminoquinoline (0.5 g, 3.47 mmol) and 0.05 g anhydrous zinc chloride were mixed in 4.5 mL ethanol. The mixture was warmed up to 60 °C, and methyl vinyl ketone (0.31 g, 3.82 mmol) was added dropwisely by syringe. After addition, the reaction was allowed to reflux for two hours and cooled to room temperature overnight. 20 mL water was added to quench the reaction, and crude product was extracted by CH_2Cl_2 (20 mL × 3). The crude product was purified by column chromatography (Hex : EA = 5:1, R_f = 0.4), and white needles were obtained (0.34 g, 50% yield). Mp 104 – 105 °C (Lit. 104-104.5 °C).[159] ^{1}H-NMR (400 MHz, $CDCl_3$) δ 9.55(dd, *J* = 8.4 Hz, 1H), 9.03(dd, *J* = 8.4 Hz, 1H), 8.86(d, *J* = 8.4 Hz, 1H), 8.15 – 8.06 (m, 2H), 7.64-7.60(dd, *J* = 8.4 Hz, 1H), 7.38(d, *J* = 4.4, 1H), 2.76(s, 3H). ^{13}C-NMR (100 MHz, $CDCl_3$) δ 151.1, 149.1, 149.1, 145.6, 144.4, 133.0, 128.5, 127.2, 125.7, 125.1, 123.5, 121.9, 18.9.

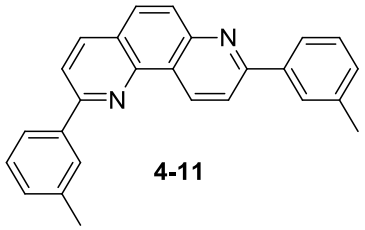

4-11

2,8-Di-*m*-tolyl-1,7-phenanthroline (4-11)

2.7 mL 1.5 M solution of t-butyllithium in pentane was added into a solution of 3-bromotoluene (0.2 mL, 1.6 mmol) in THF at -78 °C. The mixture was allowed to warm up to room temperature overnight. The resulting solution was added dropwise into a solution of 1,7-phenahthroline (0.065 g, 0.37 mmol) in THF in ice bath. The reaction was in dark redish brown and stirred for 48 h. The reaction was quenched by 20 mL sat. NH_4Cl, and crude intermediate was extracted by CH_2Cl_2 (20 mL× 3). The solution of crude intermediate was then oxidized by activated MnO_2 (0.5 g, 5.75 mmol) for 6 h, filtered through celite and concentrated. Column chromatography will give bright yellow oily solids forming a thin film on the bottom of round bottom flask (0.019 g, 15% yield). +ESI-MS, $[M+H]^+$ = 361.16. ^{1}H-NMR (500 MHz, $CDCl_3$) δ 9.75 (d, *J* = 8.5 Hz, 1H), 8.28 (d, *J* = 8.5 Hz, 1H), 8.16-8.09 (m, 5H), 8.05-8.00 (m, 2H), 7.98-7.96(d, *J* = 9.5 Hz, 1H), 7.49-7.44 (m, 2H), 7.33-7.30 (t, 2H), 2.54(s, 3H), 2.52(s, 3H). ^{13}C-NMR (125 MHz, $CDCl_3$) δ 158.4, 156.4, 149.6, 145.5, 139.4, 138.6, 138.5, 136.6, 133.9, 130.3, 130.2, 129.0, 128.8, 128.3, 128.1, 125.9, 124.8, 124.8, 124.6, 119.4, 119.4, 21.7, 21.6 .

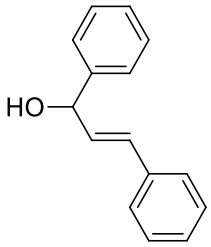

4-14

(*E*)-1,3-Diphenylprop-2-en-1-ol (4-14)[176]

A 50 mL round bottom flask was filled with Ar, and 10 mL distilled THF was added into it. Cinnamyl aldehyde (0.18 mL, 0.189 g, 1.47 mmol) was added. The solution was then cooled to 0 °C and 0.54 mL (1.1 eq.) 3M phenyl magnesium bromide solution was added by syringe slowly. The reaction system was then allowed to warm to room temperature and stir overnight. Reaction

was quenched by adding 5mL saturated NH_4Cl slowly. Filter the mixture through celite to remove magnesium salts. The water layer was then extracted by diethyl ether (20 mL × 3). The combined organic layer was concentrated. Purification through column chromatography (SiO_2, Hex) resulted in white solids (0.31 g, quantitative yield). Lit. mp 57 – 58 °C.[177] ^{1}H-NMR (400 MHz, $CDCl_3$) δ 7.51-7.28 (m, 10H), 6.71 (d, *J* = 20 Hz, 1H), 6.39 (dd, *J* = 8 Hz, 1H), 5.41-5.39 (dd, *J* = 8Hz, 1H), 2.85 (s, 1H). ^{13}C-NMR (100 MHz, $CDCl_3$) δ 142.7, 136.4, 131.5, 130.3, 128.5, 128.4, 127.6, 127.6, 126.5, 126.3, 74.9.[176]

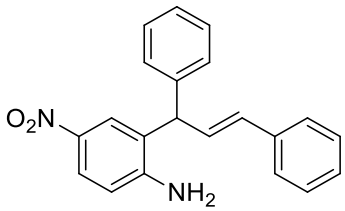

4-15

(*E*)-2-(1,3-Diphenylallyl)-4-nitroaniline (4-15)[178]

Compound **4-14** (0.1 g, 0.48 mmol, 1 eq.), nitroaniline (0.072 g, 0.52 mmol, 1.1 eq.), and Re_2O_7 (0.012 g, 5 mol%) were added in acetonitrile (5 mL). The reaction mixture was refluxed overnight. 10 mL water was added to quench the reaction and ethyl acetate (20 mL × 3) was used in extraction. Crude product purified by column chromatography (neutral Al_2O_3, Hex : EA = 9:1, R_f = 0.2) resulted in yellow oil (0.11 g, 70% yield). ^{1}H-NMR (500 MHz, $CDCl_3$) δ 8.07-8.09(m, 2H), 7.27-7.43(m, 10H), 6.68(d, *J* = 6, 1H), 6.65(d, *J* = 8.5, 1H), 6.36(d, *J* = 15, 1H), 4.85(d, *J* = 7, 1H), 4.32(br, 2H). ^{13}C-NMR (125 MHz, $CDCl_3$) δ 150.5, 140.0, 139.4, 136.5, 132.8, 129.2, 128.6, 128.5, 127.8, 127.5, 126.7, 126.5, 125.8, 124.6, 114.9, 49.6.[178]

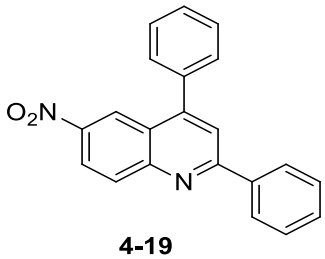

4-19

6-Nitro-2,4-diphenylquinoline (4-19)[170]

Compound **4-15** (0.05 g, 0.15 mmol) and 17 mg K^{t}OBu (1 eq.) in DMSO (0.5 mL) was mixed in a round bottom flask. The flask was purged with Ar for 15 min and allowed to stir at room temperature for 4 h. The reaction was quenched by water and extracted by ethyl acetate (10 mL × 3). NMR indicated 50% conversion probably due to insufficient reaction time. Crude product was purified by chromatography (SiO_2, Hex : EA = 5:1, R_f = 0.6). 0.022 g white solid was obtained with a moderate yield (0.022 g, 45 % yield). mp 195-197°C (Lit. 197-200°C).[170] ^{1}H-NMR (500 MHz, $CDCl_3$) δ 8.86 (d, *J* = 2.5, 1H), 8.50 (dd, *J* = 2.5, 4.5, 1H), 8.35-8.32 (d, *J* = 9.5, 1H), 8.26-8.24 (dd, 2H), 7.99 (s, 1H), 7.56 – 7.51 (m, 8H). ^{13}C-NMR (125 MHz, $CDCl_3$) δ 160.1, 151.3, 151.1, 145.4, 138.5, 136.9, 131.8, 130.5, 129.5, 129.3, 129.1, 129.1, 127.8, 124.8, 123.1, 122.9, 120.7.[170]

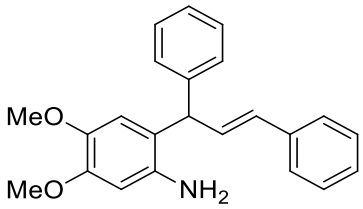

4-16

(*E*)-2-(1,3-Diphenylallyl)-4,5-dimethoxyaniline (4-16)[178]

Compound **4-14** (0.1 g, 0.48 mmol, 1 eq.), nitroaniline (0.080 g, 0.52 mmol, 153 g / mol 1.1 eq.), and Re_2O_7 (0.012 g, 5 mol%) were added in acetonitrile (5 mL). The reaction mixture was refluxed overnight. 10 mL water was added to quench the reaction and ethyl acetate (20 mL × 3) was used in extraction. Crude product purified by column chromatography (neutral Al_2O_3, Hex : EA = 9:1, R_f = 0.7) resulted in a yellow oil (0.11 g, 65% yield). ^{1}H-NMR (500 MHz, $CDCl_3$) δ 7.44 – 7.26(m, 10H), 6.75 - 6.70(m, 2H), 6.37 – 6.34(m, 2H), 4.92(d, *J* = 6.5, 1H), 3.87(s, 3H), 3.79(s, 3H). ^{13}C-NMR (125 MHz, $CDCl_3$) δ 148.5, 141.9, 141.8, 138.1, 137.0, 131.3, 131.2, 128.6, 128.5, 128.4, 127.2, 126.6, 126.2, 119.4, 114.1, 101.6, 56.7, 55.7, 48.9.[178]

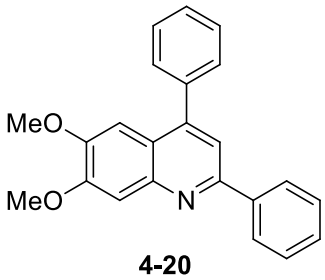

4-20

6,7-Dimethoxy-2,4-diphenylquinoline (4-20)[170]

Compound **4-16** (0.104 g, 0.3 mmol) and K^{t}OBu (34 mg, 0.3 mmol, 1 eq.) in DMSO (1 mL) was mixed in a round bottom flask. The flask was purged with Ar for 15 min and allowed to stir at room temperature for 4 h. The reaction was quenched by water and extracted by ethyl acetate (10 mL × 3). NMR indicated 50% conversion probably due to insufficient reaction time. Crude product was purified by column chromatography (SiO_2, Hex : EA = 5:1, R_f = 0.6). White solid was obtained with a moderate yield (0.056 g, 55 %). mp 160-162°C (Lit. 160-162°C).[170] ^{1}H-NMR (500 MHz, $CDCl_3$) δ 8.15 – 8.13(m, 2H), 7.68(s, 1H), 7.59 – 7.50(m, 8H), 7.50(t, *J* = 7.5, 1H), 7.17(s, 1H), 4.08(s, 3H), 3.86(s, 3H). ^{13}C-NMR (125 MHz, $CDCl_3$) δ 155.2, 152.5, 149.8, 147.6, 146.0, 140.0, 139.0, 129.4, 129.0, 128.9, 128.8, 128.5, 127.4, 121.2, 118.0, 108.8, 103.4, 56.3, 56.0.[170]

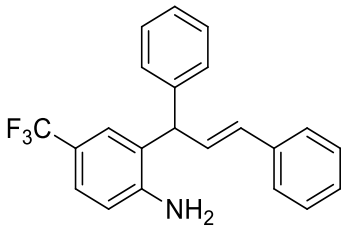

4-18

(*E*)-2-(1,3-Diphenylallyl)-4-(trifluoromethyl)aniline (4-18) [178]

Compound **4-14** (0.1 g, 0.48 mmol, 1 eq.), 72 mg nitroaniline (72 mg, 0.52 mmol, 138 g / mol 1.1 eq.), and Re_2O_7 (0.012 g, 5 mol%) was added in acetonitrile (5 mL). The reaction mixture was

refluxed overnight. 10 mL water was added to quench the reaction and ethyl acetate (20 mL × 3) was used in extraction. Crude product purified by column chromatography (neutral Al_2O_3, Hex : EA = 9:1, R_f = 0.7) resulted in a yellow oil (0.136 g, 80% crude yield). NMR indicates a mixture of product and trifluoro aniline.[178]

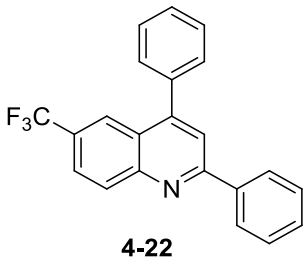

4-22

2,4-Diphenyl-6-(trifluoromethyl)quinoline (4-22)[170]

Compound **4-18** (0.106 g, 0.3 mmol) and K^{t}OBu (34 mg, 0.3 mmol, 1 eq.) in DMSO (1 mL) was mixed in a round bottom flask. The flask was purged with Ar for 15 min and allowed to stir at room temperature for 4 h. The reaction was quenched by water and extracted by ethyl acetate (10 mL×3). NMR indicated 50% conversion probably due to insufficient reaction time. Crude product was purified by chromatography (SiO_2, Hex : EA = 9:1, R_f = 0.5). White solid was obtained with a moderate yield (0.055 g, 53 %). mp 148-150 °C (Lit. 148-150 °C).[170] ^{1}H-NMR (500 MHz, $CDCl_3$) δ 8.35 (d, *J* = 9, 1H), 8.25 – 8.23(m, 3H), 7.93 – 7.91(m, 2H), 7.62 – 7.50(m, 8H). ^{13}C-NMR (125 MHz, $CDCl_3$) δ 158.8, 150.1, 149.8, 138.9, 137.4, 131.2, 129.9, 129.4, 128.9, 128.9, 127.7, 125.2, 125.2, 124.8, 123.7, 123.6, 123.0, 120.3.[170]

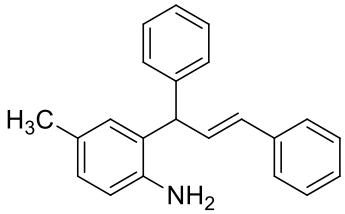

4-17

(*E*)-2-(1,3-Diphenylallyl)-4-methylaniline(4-17)[178]

Compound **4-14** (0.1 g, 0.48 mmol, 1 eq.), 56 mg nitroaniline (56 mg, 0.52 mmol, 108 g / mol 1.1 eq.), and Re_2O_7 (0.012 g, 5 mol%) was added in acetonitrile (5 mL). The reaction mixture was refluxed overnight. 10 mL water was added to quench the reaction and ethyl acetate (20 mL × 3) was used in extraction. Crude product purified by chromatography (neutral Al_2O_3, Hex : EA = 9:1, R_f = 0.7) resulted in a yellow oil (0.079 g, 56% yield). ^{1}H-NMR (500 MHz, $CDCl_3$) δ 7.48 – 7.29 (m, 10H), 7.06 – 7.00(m, 2H), 6.75(dd, *J* = 7Hz, 1H), 6.36(d, *J* = 16Hz, 1H), 4.96(d, *J* = 7Hz, 1H), 2.33(s, 3H). ^{13}C-NMR (125 MHz, $CDCl_3$) δ 141.8, 141.7, 137.1, 131.5, 131.3, 129.7, 128.8, 128.6, 128.5, 128.1, 128.0, 126.7, 126.3, 116.6, 49.6, 20.7.[178]

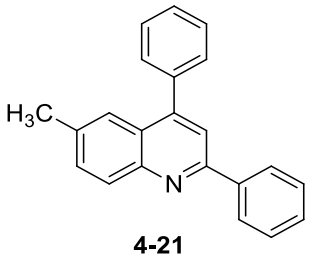

4-21

6-Methyl-2,4-diphenylquinoline(4-21)[170]

Compound **4-17** (0.09 g, 299 g / mol, 0.3 mmol) and K^{t}OBu (34 mg, 0.3 mmol, 1 eq.) in DMSO (1 mL) was mixed in a round bottom flask. The flask was purged with Ar for 15 min and allowed to stir at room temperature for 4 h. The reaction was quenched by water and extracted by ethyl acetate (10 mL × 3). NMR indicated 50% conversion probably due to insufficient reaction time. Crude product was purified by chromatography (SiO_2, Hex : EA = 5:1, R_f = 0.7). Yellow oily solid was obtained with a moderate yield (0.053 g, 60 %). mp 118-120 °C (Lit. 120-123 °C).[170] ^{1}H-NMR (500 MHz, $CDCl_3$) δ 8.19 – 8.14(m, 3H), 7.78(s, 1H), 7.65(s, 1H), 7.58 – 7.51(m, 8H), 7.47(m, 1H), 2.48(s, 3H). ^{13}C-NMR (125 MHz, $CDCl_3$) δ 156.0, 148.4, 147.4, 139.8, 138.6, 136.3, 131.7, 129.8, 129.5, 129.1, 128.8, 128.6, 128.3, 127.5, 125.7, 124.4, 119.4, 21.8.[170]

UV-Vis Spectroscopy. The absorption spectra of organic small molecules in methylene chloride were collected using an Evolution 201 spectrophotometer using a 1-cm quartz cuvette, scanning from 800 nm to 200 nm with a resolution of 1 nm.

Atomic Force Microscopy

Thickness of thin-films were confirmed using atomic force microscopy in tapping mode using the film scratch method (AFM, Asylum Research Model MFP-3D).

Variable Angle Spectroscopic Ellipsometry (VASE)

Measurements were made using a J. A. Woollam V.A.S.E. M-2000 based on the diode array rotating compensator ellipsometer technology. Ellipsometric measurements were first made on the cleaned bare substrate. All data were taken in the wavelength range of 210 to 1700 nm at angles of 45 to 75 degrees in divisions of 7.5 degrees. The built-in auto-alignment function of the M-2000 was used to align the sample before the measurement. Data was then collected from the thin film on glass and analyzed based on a general oscillator model to yield solutions for the complex refractive index and the film thickness. The ellipsometric data was analyzed by fitting a model for the active layer on the substrate using the WVASE32 software (version 3.770, J. A. Woollam Co.). The best fit for the optical constants was found by minimizing the mean square error (MSE) between the measured and the modeled curves using the Levenberg–Marquardt multivariate regressions algorithm. Thickness results from ellipsometry were confirmed using atomic force microscopy in tapping mode using the film scratch method (AFM, Asylum Research Model MFP-3D). (This part is written by Ahsan Ashraf)

Cyclic Voltammetry

Working method is Square wave voltammetry. Buffer is 0.1 M Tetrabutylamonium hexafluoro phosphate ($TBATF_6$) in MeCN. Reference electrode: 0.01 M Ag/AgNO3 in buffer; working

electrode: Glassy carbon; Counter electrode: Platinum wire (or gold wire). Synthetic compounds were dissolved in buffer to make 10 mL 0.1M solution in a 50 mL beaker. Working electrode, reference electrode and counter electrode were put into the solution without touching the wall or the bottom of the beaker. Scan rate could be adjusted between 50 and 100 mV/s, and scans were taken between -3 to 3 V. Data was then analyzed by OriginPro 8.5.

Vacuum Thermal Evaporation

The evaporation was all done by Kostas Alexandrou in the John Kymissis group in the Columbia University. Angstrom thermal evaporator inside a N_2 filled glovebox was employed. Deposition was conducted with base pressure of $< 5\times10^{-6}$ torr. Deposition rate of 0.5 Å/s, using the Alq3 profile with deposition power: 12%-15%. Organic small molecules were deposited onto silicon or glass substrate, and the thickness was further confirmed using atomic force microscopy in tapping mode using the film scratch method (AFM, Asylum Research Model MFP-3D).

References:

149. Sammes, P. G.; Yahioglu, G., 1, 10-Phenanthroline: a versatile ligand. *Chem. Soc. Rev.* **1994,** *23*, 327-334.
150. (a) Ohashi, D.; Nakada, T.; Kunioka, A., Improved CIGS thin-film solar cells by surface sulfurization using In_2S_3 and sulfur vapor. *Sol. Energ. Mat. Sol. C* **2001,** *67* (1–4), 261-265; (b) Nagoya, Y.; Kushiya, K.; Tachiyuki, M.; Yamase, O., Role of incorporated sulfur into the surface of Cu(In, Ga)Se_2 thin-film absorber. *Sol. Energ. Mat. Sol. C* **2001,** *67* (1–4), 247-253; (c) Kobayashi, T.; Sugimoto, H.; Kato, T.; Yamaguchi, H.; Nakada, T., Impacts of surface sulfurization on high-efficiency CIGS thin film solar cells. *Proc. 23rd PVSEC Taipei Taiwan* **2013**.
151. Prajapati, S. M.; Patel, K. D.; Vekariya, R. H.; Panchal, S. N.; Patel, H. D., Recent advances in the synthesis of quinolines: a review. *RSC Advances* **2014,** *4* (47), 24463-24476.
152. Yamashkin, S.; Oreshkina, E., Traditional and modern approaches to the synthesis of quinoline systems by the Skraup and Doebner-Miller methods.(Review). *Chem. Heterocyclic Comp.* **2006,** *42*, 701-718.
153. Born, J. L., Mechanism of formation of benzo[g]quinolones via the Combes reaction. *J. Org. Chem.* **1972,** *37* (24), 3952-3953.
154. Friedlaender, P., Ueber o-Amidobenzaldehyd. *Ber. Dtsh. Chem. Ges.* **1882,** *15* (2), 2572-2575.
155. Conrad, M.; Limpach, L., Synthesen von chinolinderivaten mittelst acetessigester. *Ber. Dtsh. Chem. Ges.* **1887,** *20* (1), 944-948.
156. Gould, R. G.; Jacobs, W. A., The synthesis of certain substituted quinolines and 5,6-benzoquinolines. *J. Am. Chem. Soc.* **1939,** *61* (10), 2890-2895.
157. Surrey, A. R.; Cutler, R. A., The Synthesis of Some 4,10-Disubstituted-1,7-phenanthroline Derivatives. *J. Am. Chem. Soc.* **1954,** *76*, 1109-1113.
158. (a) Khong, S.; Kwon, O., One-pot phosphine-catalyzed syntheses of quinolines. *J. Org. Chem.* **2012,** *77* (18), 8257-8267; (b) Korivi, R. P.; Cheng, C.-H., Nickel-catalyzed cyclization of 2-iodoanilines with aroylalkynes: an efficient route for quinoline derivatives. *J. Org. Chem.* **2006,** *71* (18), 7079-7082; (c) Toh, K. K.; Sanjaya, S.; Sahnoun, S.; Chong, S. Y.; Chiba, S., Copper-catalyzed aerobic intramolecular carbo- and amino-oxygenation of alkynes for synthesis of azaheterocycles. *Org. Lett.* **2012,** *14* (9), 2290-2292; (d) Kong, L.; Zhou, Y.; Huang, H.; Yang, Y.; Liu, Y.; Li, Y., Copper-catalyzed synthesis of substituted quinolines via C–N coupling/condensation from *ortho*-acylanilines and alkenyl iodides. *J. Org. Chem.* **2014,** *80* (2), 1275-1278.
159. Eifert, R. L.; Hamilton, C. S., Some Methylphenanthrolines and Corresponding Aldehydes. *J. Am. Chem. Soc.* **1955,** *77*, 1818-1819.
160. (a) Kuzmina, O. M.; Steib, A. K.; Flubacher, D.; Knochel, P., Iron-catalyzed cross-coupling of *N*-heterocyclic chlorides and bromides with arylmagnesium reagents. *Org. Lett.* **2012,** *14* (18), 4818-4821; (b) Iglesias, M. J.; Prieto, A.; Nicasio, M. C., Kumada–Tamao–Corriu coupling of heteroaromatic chlorides and aryl ethers catalyzed by (IPr)Ni(allyl)Cl. *Org. Lett.* **2012,** *14* (17), 4318-4321; (c) Fürstner, A.; Leitner, A.; Méndez, M.; Krause, H., Iron-catalyzed cross-coupling reactions. *J. Am. Chem. Soc.* **2002,** *124* (46), 13856-13863; (d) Ohmiya, H.; Yorimitsu, H.; Oshima, K., Cobalt-

catalyzed cross-coupling reaction of chloropyridines with Grignard reagents. *Chem. Lett.* **2004,** *33* (10), 1240-1241.
161. Wang, T.; Chen, F.; Qin, J.; He, Y.-M.; Fan, Q.-H., Asymmetric Ruthenium-Catalyzed Hydrogenation of 2- and 2,9-Substituted 1,10-Phenanthrolines. *Angewandte Chemie* **2013,** *125*, 7313-7317.
162. Panda, K.; Siddiqui, I.; Mahata, P. K.; Ila, H.; Junjappa, H., Heteroannulation of 3-Bis(methylthio)acrolein with Aromatic Amines - A Convenient Highly Regioselective Synthesis of 2-(Methylthio)quinolines and their Benzo/Hetero Fused Analogs - A Modified Skraup Quinoline Synthesis. *Synlett* **2004,** *2004*, 449-452.
163. Mahata, P. K.; Barun, O.; Ila, H.; Junjappa, H., Formation of acetaldehyde enolate from vinyl acetate and its reaction with aromatic and heteroaromatic aldehydes: an efficient synthesis of enals and polyenals. *Synlett.* **2000,** *9*, 1345-1347.
164. Su, Q.; Li, P.; He, M.; Wu, Q.; Ye, L.; Mu, Y., Facile Synthesis of Acridine Derivatives by ZnCl2-Promoted Intramolecular Cyclization of o-Arylaminophenyl Schiff Bases. *Org. Lett.* **2013,** *16*, 18-21.
165. Annunziata, R.; Benaglia, M.; Cinquini, M.; Raimondi, L.; Cozzi, F., A molecular gate: control of free intramolecular rotation by application of an external signal. *J. Phys. Org. Chem.* **2004,** *17* (9), 749-751.
166. (a) Khoshman, J. M. Spectroscopic ellipsometry characterization of single and multilayer aluminum nitride/indium nitride thin film systems. Ohio University, 2005; (b) Woollam, J. A.; Johs, B. D.; Herzinger, C. M.; Hilfiker, J. N.; Synowicki, R. A.; Bungay, C. L. In *Overview of variable-angle spectroscopic ellipsometry (VASE): I. Basic theory and typical applications*, Optical Metrology, 1999; pp 3-28.
167. (a) Jellison, J. G. E., Spectroscopic ellipsometry data analysis: measured versus calculated quantities. *Thin Solid Films* **1998,** *313–314* (0), 33-39; (b) Synowicki, R., Spectroscopic ellipsometry characterization of indium tin oxide film microstructure and optical constants. *Thin Solid Films* **1998,** *313*, 394-397.
168. (a) Eliasson, B. J. Metal-insulator-metal diodes for solar energy conversion. University of Colorado, 2001; (b) Grover, S.; Moddel, G., Applicability of metal/insulator/metal (MIM) diodes to solar rectennas. *IEEE J. Photovoltaics* **2011,** *1* (1), 78-83.
169. (a) Afzal, O.; Kumar, S.; Haider, M. R.; Ali, M. R.; Kumar, R.; Jaggi, M.; Bawa, S., A review on anticancer potential of bioactive heterocycle quinoline. *Euro. J. Med. Chem* **2015,** *97* (0), 871-910; (b) R Solomon, V.; Lee, H., Quinoline as a privileged scaffold in cancer drug discovery. *Curr. Med. Chem.* **2011,** *18* (10), 1488-1508.
170. Rehan, M.; Hazra, G.; Ghorai, P., Synthesis of polysubstituted quinolines via transition-metal-free oxidative cycloisomerization of *o*-cinnamylanilines. *Org. Lett.* **2015,** *17* (7), 1668-1671.
171. (a) El'tsov, *Zh. Org. Khim+* **1972,** *8*, 1309, 1324, 1329, 1332; (b) Jordis, U.; Sauter, F.; Rudolf, M.; Cai, G., Syntheses of novel quinolone-chemotherapeutics, I: Pyridoquinolines and pyridophenanthrolines as derivatives of "lin-benzo-nalidixic acid". *Monatsh. Chem.* **1988,** *119*, 20.
172. Borsche; Wagner-Roemmich, *Justus Liebigs Ann. Chem.* **1940,** *544*, 5.
173. Long, J.; Gao, H.; Song, K.; Liu, F.; Hu, H.; Zhang, L.; Zhu, F.; Wu, Q., Synthesis and Characterization of NiII and PdII Complexes Bearing N,N,S Tridentate Ligands and Their Catalytic Properties for Norbornene Polymerization. *Eur. J. Inorg. Chem.* **2008,** *2008*, 4296-4305.

174. Su, Q.; He, M.; Wu, Q.; Gao, W.; Xu, H.; Ye, L.; Mu, Y., The supramolecular assemblies of 7-amino-2,4-dimethylquinolinium salts and the effect of a variety of anions on their luminescent properties. *Cryst. Eng. Comm.* **2012,** *14* (21), 12.
175. Marckwald, *Justus Liebigs Ann. Chem.* **1893,** *274*.
176. Watson, I. D. G.; Styler, S. A.; Yudin, A. K., Unusual selectivity of unprotected aziridines in Palladium-catalyzed allylic amination enables facile preparation of branched aziridines. *J. Am. Chem. Soc.* **2004,** *126* (16), 5086-5087.
177. Mamillapalli, N. C.; Sekar, G., Metal free chemoselective reduction of α-keto amides using TBAF as catalyst. *RSC Advances* **2014,** *4* (105), 61077-61085.
178. Nallagonda, R.; Rehan, M.; Ghorai, P., Chemoselective C-benzylation of unprotected anilines with benzyl alcohols using Re_2O_7 catalyst. *J. Org. Chem.* **2014,** *79* (7), 2934-2943.

References:

1. Chernick, E. T.; Tykwinski, R. R., Carbon-rich nanostructures: the conversion of acetylenes into materials. *J. Phys. Org. Chem.* **2013,** *26* (9), 742-749.
2. Kroto, H. W.; Heath, J. R.; O'Brien, S. C.; Curl, R. F.; Smalley, R. E., C_{60}: buckminsterfullerene. *Nature* **1985,** *318* (6042), 162-163.
3. De Volder, M. F. L.; Tawfick, S. H.; Baughman, R. H.; Hart, A. J., Carbon nanotubes: present and future commercial applications. *Science* **2013,** *339* (6119), 535-539.
4. Gao, P.; Li, A. R.; Tai, M. H.; Liu, Z. Y.; Sun, D. D., A Hierarchical Nanostructured Carbon Nanofiber–In2S3 Photocatalyst with High Photodegradation and Disinfection Abilities Under Visible Light. *Chem. Asian. J.* **2014,** *9* (6), 1663-1670.
5. Novoselov, K., Nobel lecture: Graphene: Materials in the flatland. *Rev. Mod. Phys.* **2011,** *83* (3), 837.
6. McNeill, R.; Siudak, R.; Wardlaw, J.; Weiss, D., Electronic conduction in polymers. I. The chemical structure of polypyrrole. *Aust. J. Chem.* **1963,** *16* (6), 1056-1075.
7. (a) Bolto, B. A.; McNeill, R.; Weiss, D., Electronic conduction in polymers. III. Electronic properties of polypyrrole. *Aust. J. Chem.* **1963,** *16* (6), 1090-1103; (b) Bolto, B. A.; Weiss, D., Electronic conduction in polymers. II. electrochemical reduction of polypyrrole at controlled potential. *Aust. J. Chem.* **1963,** *16* (6), 1076-&.
8. Shirakawa, H.; Louis, E. J.; MacDiarmid, A. G.; Chiang, C. K.; Heeger, A. J., Synthesis of electrically conducting organic polymers: halogen derivatives of polyacetylene,$(CH)_x$. *J. Chem. Soc., Chem. Commun.* **1977,** (16), 578-580.
9. Nobelprize.org. Nobel Media AB. The Nobel Prize in Chemistry 2000. http://www.nobelprize.org/nobel_prizes/chemistry/laureates/2000/ (accessed Dec. 9, 2015).
10. (a) Günes, S.; Neugebauer, H.; Sariciftci, N. S., Conjugated polymer-based organic solar cells. *Chem. Rev.* **2007,** *107* (4), 1324-1338; (b) Hauch, J. A.; Schilinsky, P.; Choulis, S. A.; Childers, R.; Biele, M.; Brabec, C. J., Flexible organic P3HT:PCBM bulk-heterojunction modules with more than 1 year outdoor lifetime. *Sol. Energ. Mat. Sol. C.* **2008,** *92* (7), 727-731.
11. Ajayaghosh, A., Donor–acceptor type low band gap polymers: polysquaraines and related systems. *Chem. Soc. Rev.* **2003,** *32* (4), 181-191.
12. (a) Chen, Z.; Cai, P.; Chen, J.; Liu, X.; Zhang, L.; Lan, L.; Peng, J.; Ma, Y.; Cao, Y., Low band-Gap conjugated polymers with strong interchain aggregation and very high hole mobility towards highly efficient thick-film polymer solar cells. *Adv. Mater.* **2014,** *26* (16), 2586-2591; (b) Steckler, T. T.; Henriksson, P.; Mollinger, S.; Lundin, A.; Salleo, A.; Andersson, M. R., Very low band gap thiadiazoloquinoxaline donor–acceptor polymers as multi-tool conjugated polymers. *J. Am. Chem. Soc.* **2014,** *136* (4), 1190-1193; (c) Lei, T.; Dou, J.-H.; Ma, Z.-J.; Yao, C.-H.; Liu, C.-J.; Wang, J.-Y.; Pei, J., Ambipolar polymer field-effect transistors based on fluorinated isoindigo: high performance and improved ambient stability. *J. Am. Chem. Soc.* **2012,** *134* (49), 20025-20028.
13. You, J.; Dou, L.; Yoshimura, K.; Kato, T.; Ohya, K.; Moriarty, T.; Emery, K.; Chen, C.-C.; Gao, J.; Li, G., A polymer tandem solar cell with 10.6% power conversion efficiency. *Nature Commun.* **2013,** *4*, 1446.

14. Ryu, T. I.; Yoon, Y.; Kim, J.-H.; Hwang, D.-H.; Ko, M. J.; Lee, D.-K.; Kim, J. Y.; Kim, H.; Park, N.-G.; Kim, B.; Son, H. J., Simultaneous enhancement of solar cell efficiency and photostability via chemical tuning of electron donating units in diketopyrrolopyrrole-based push–pull type polymers. *Macromolecules* **2014,** *47* (18), 6270-6280.
15. Wegner, G., Topochemical reactions of monomers with conjugated triple bonds. I. Polymerization of 2.4-hexadiyn-1.6-diols deivatives in crystalline state. *Z. Naturforsch. B.* **1969,** (7), 824-&.
16. Jelinek, R.; Ritenberg, M., Polydiacetylenes–recent molecular advances and applications. *RSC Adv.* **2013,** *3* (44), 21192-21201.
17. Lee, D.-C.; Sahoo, S. K.; Cholli, A. L.; Sandman, D. J., Structural aspects of the thermochromic transition in urethane-substituted polydiacetylenes. *Macromolecules* **2002,** *35* (11), 4347-4355.
18. Schott, M., The colors of polydiacetylenes: a commentary. *J. Phys. Chem. B* **2006,** *110* (32), 15864-15868.
19. Lee, J. S. Molecular design and self-assembly of polydiacetylene for biosensors and sensor arrays. The University of Michigan, 2011.
20. (a) Ngampeungpis, W.; Tumcharern, G.; Pienpinijtham, P.; Sukwattanasinitt, M., Colorimetric UV sensors with tunable sensitivity from diacetylenes. *Dyes. Pigments.* **2014,** *101* (0), 103-108; (b) Ramakers, B. E. I.; Bode, S. A.; Killaars, A. R.; Hest, J. C. M. v.; Löwik, D. W. P. M., Sensing cell adhesion using polydiacetylene-containing peptide amphiphile fibres. *J. Mater. Chem. B* **2015**; (c) Samyn, P.; Shroff, K.; Prucker, O.; Rühe, J.; Biesalski, M., Fluorescent sensibility of microarrays through functionalized adhesive polydiacetylene vesicles. *Sensor. Actuat. A: Phys.* **2014,** *214* (0), 45-57.
21. (a) Yoon, J.; Chae, S. K.; Kim, J.-M., Colorimetric sensors for volatile organic compounds (VOCs) based on conjugated polymer-embedded electrospun fibers. *J. Am. Chem. Soc.* **2007,** *129* (11), 3038-3039; (b) Yoon, J.; Jung, Y.-S.; Kim, J.-M., A combinatorial approach for colorimetric differentiation of organic solvents based on conjugated polymer-embedded electrospun fibers. *Adv. Funct. Mater.* **2009,** *19* (2), 209-214.
22. Yoon, B.; Ham, D. Y.; Yarimaga, O.; An, H.; Lee, C. W.; Kim, J. M., Inkjet printing of conjugated polymer precursors on paper substrates for colorimetric sensing and flexible electrothermochromic display. *Adv. Mater.* **2011,** *23* (46), 5492-5497.
23. (a) Kolusheva, S.; Zadmard, R.; Schrader, T.; Jelinek, R., Color fingerprinting of proteins by calixarenes embedded in lipid/polydiacetylene vesicles. *J. Am. Chem. Soc.* **2006,** *128* (41), 13592-13598; (b) Kim, J.-M.; Lee, Y. B.; Yang, D. H.; Lee, J.-S.; Lee, G. S.; Ahn, D. J., A polydiacetylene-based fluorescent sensor chip. *J. Am. Chem. Soc.* **2005,** *127* (50), 17580-17581.
24. Kwon, I. K.; Kim, J. P.; Sim, S. J., Enhancement of sensitivity using hybrid stimulus for the diagnosis of prostate cancer based on polydiacetylene (PDA) supramolecules. *Biosens. Bioelectron.* **2010,** *26* (4), 1548-1553.
25. *Nonlinear optical materials*. American Chemical Society: 1991; Vol. 455, p 128.
26. Bredas, J. L.; Adant, C.; Tackx, P.; Persoons, A.; Pierce, B. M., Third-order nonlinear optical response in organic materials: theoretical and experimental aspects. *Chem. Rev.* **1994,** *94* (1), 243-278.
27. Rentzepis, P.; Pao, Y. H., Laser-induced optical second-harmonic generation in organic crystals. *Appl. Phys. Lett.* **1964,** *5* (8), 156-158.

28. Ray, P. C., Size and shape dependent second order nonlinear optical properties of nanomaterials and their application in biological and chemical sensing. *Chem. Rev.* **2010,** *110* (9), 5332-5365.
29. (a) Hermann, J. P.; Ricard, D.; Ducuing, J., Optical nonlinearities in conjugated systems: β - carotene. *App.Phys. Lett.* **1973,** *23* (4), 178-180; (b) Bramley, R.; Le Fevre, R., 11. Molecular polarisability: phenylpolyenals and diphenylpolyene ketones. *J. Chem. Soc. (Resumed)* **1962**, 56-63.
30. Sauteret, C.; Hermann, J. P.; Frey, R.; Pradère, F.; Ducuing, J.; Baughman, R. H.; Chance, R. R., Optical nonlinearities in one-dimensional-conjugated polymer crystals. *Phys. Rev. Lett.* **1976,** *36* (16), 956-959.
31. Sarkar, A.; Okada, S.; Matsuzawa, H.; Matsuda, H.; Nakanishi, H., Novel polydiacetylenes for optical materials: beyond the conventional polydiacetylenes. *J. Mater. Chem.* **2000,** *10* (4), 819-828.
32. Kolinsky, P., New materials and their characterization for photonic device applications. *Opt. Eng.* **1992,** *31* (8), 1676-1684.
33. Okada, S.; Hayamizu, K.; Matsuda, H.; Masaki, A.; Nakanishi, H., Structures of the polymers obtained by the solid-state polymerization of diyne, triyne, and tetrayne with long-alkyl substituents. *Bull. Chem. Soc. Jpn.* **1991,** *64* (3), 857-863.
34. (a) Matsuzawa, H.; Okada, S.; Sarkar, A.; Matsuda, H.; Nakanishi, H., Synthesis of polydiacetylenes from novel monomers having two diacetylene units linked by an arylene group. *Polym. J.* **2001,** *33* (2), 182-189; (b) Inayama, S.; Tatewaki, Y.; Okada, S., Solid-state polymerization of conjugated hexayne derivatives with different end groups. *Polym. J.* **2010,** *42* (3), 201-207; (c) Okada, S.; Hayamizu, K.; Matsuda, H.; Masaki, A.; Minami, N.; Nakanishi, H., A new conjugated ladder polymer synthesized by solid-state polymerization of a hexayne compound. *Chem. Lett.* **1992,** *21* (2), 301-304.
35. Davydov, B.; Derkacheva, L.; Dunina, V.; Zhabotinskii, M.; Zolin, V.; Koreneva, L.; Samokhina, M., Connection between charge transfer and laser second harmonic generation. *ZhETF Pisma Redaktsiiu* **1970,** *12*, 24.
36. Di Bella, S., Second-order nonlinear optical properties of transition metal complexes. *Chem. Soc. Rev.* **2001,** *30* (6), 355-366.
37. (a) Karna, S. P.; Prasad, P. N.; Dupuis, M., Nonlinear optical properties of *p* - nitroaniline: An abinitio time - dependent coupled perturbed Hartree–Fock study. *J. Chem. Phys.* **1991,** *94* (2), 1171-1181; (b) Teng, C.; Garito, A., Dispersion of the nonlinear second-order optical susceptibility of an organic system: p-nitroaniline. *Phys. Rev. Lett.* **1983,** *50* (5), 350.
38. Marder, S. R.; Kippelen, B.; Jen, A. K. Y.; Peyghambarian, N., Design and synthesis of chromophores and polymers for electro-optic and photorefractive applications. *Nature* **1997,** *388* (6645), 845-851.
39. (a) Nakano, M.; Yamaguchi, K.; Fueno, T., Coupled-Hartree-Fock calculations of the third-order hyperpolarizabilities of substituted polydiacetylenes. *Chem. Phys. Lett.* **1991,** *185* (5–6), 550-554; (b) Ohnishi, S.-i.; Orimoto, Y.; Gu, F. L.; Aoki, Y., Nonlinear optical properties of polydiacetylene with donor-acceptor substitution block. *J. Chem. Phys.* **2007,** *127* (8), 084702-084702; (c) Yoshimura, T., Theoretically predicted influence of donors and acceptors on quadratic hyperpolarizabilities in conjugated long - chain molecules. *App. Phys. Lett.* **1989,** *55* (6), 534-536; (d) Chen, W.; Yu, G.-t.; Gu, F. L.; Aoki, Y., Investigation on nonlinear optical properties of ladder-structure

polydiacetylenes derivatives by using the elongation finite-field method. *Chem. Phys. Lett.* **2009,** *474* (1–3), 175-179; (e) Kim, W. H.; Bihari, B.; Moody, R.; Kodali, N. B.; Kumar, J.; Tripathy, S. K., Self-Assembled Spin-Coated and Bulk Films of a Novel Poly(diacetylene) as Second-Order Nonlinear Optical Polymers. *Macromolecules* **1995,** *28* (2), 642-647.

40. Lochner, K.; Bässler, H.; Tieke, B.; Wegner, G., Photoconduction in polydiacetylene multilayer structures and single crystals. Evidence for band-to-band excitation. *Phys. Status Solidi B* **1978,** *88* (2), 653-661.
41. Hoofman, R. J. O. M., *Charge transport in polydiacetylenes*. TU Delft, Delft University of Technology: 2000.
42. (a) Sakamoto, M.; Wasserman, B.; Dresselhaus, M. S.; Wnek, G. E.; Elman, B. S.; Sandman, D. J., Enhanced electrical conductivity of polydiacetylene crystals by chemical doping and ion implantation. *J. Appl. Phys.* **1986,** *60* (8), 2788-2796; (b) Takami, K.; Kuwahara, Y.; Ishii, T.; Akai-Kasaya, M.; Saito, A.; Aono, M., Significant increase in conductivity of polydiacetylene thin film induced by iodine doping. *Surf. Sci.* **2005,** *591* (1), L273-L279; (c) Koichi, B.; Hitoshi, K.; Yoshikazu, S.; Shuji, O.; Hidetoshi, O.; Hiro, M.; Hachiro, N., Chemical doping into nanocrystals of poly(diacetylene). *Jpn. J. Appl. Phys.* **2008,** *47* (5R), 3769.
43. Yaron, D.; Moore, E. E.; Shuai, Z.; Brédas, J. L., Comparison of density matrix renormalization group calculations with electron-hole models of exciton binding in conjugated polymers. *J. Chem. Phys.* **1998,** *108* (17), 7451-7458.
44. Sariciftci, N.; Kraabel, B.; Lee, C.; Pakbaz, K.; Heeger, A.; Sandman, D., Absence of photoinduced electron transfer from the excitonic electron-hole bound state in polydiacetylene conjugated polymers. *Phys. Rev. B* **1994,** *50* (16), 12044.
45. Comoretto, D.; Moggio, I.; Cuniberti, C.; Musso, G.; Dellepiane, G.; Borghesi, A.; Kajzar, F.; Lorin, A., Long-lived photoexcited states in polydiacetylenes: The photoinduced-absorption spectra of PDA-4BCMU. *Phys. Rev. B* **1998,** *57* (12), 7071.
46. Robins, L.; Orenstein, J.; Superfine, R., Observation of the triplet excited state of a conjugated-polymer crystal. *Phys. Rev. Lett.* **1986,** *56* (17), 1850-1853.
47. Pratt, F. L.; Wong, K. S.; Hayes, W.; Bloor, D., Infrared photo-induced absorption in polydiacetylene. *J. Phys. C* **1987,** *20* (3), L41.
48. Dellepiane, G.; Cuniberti, C.; Comoretto, D.; Lanzani, G.; Musso, G.; Piaggio, P.; Tubino, R.; Borghesi, A.; Dell'Erba, C.; Garbarino, G., Photoexcitations in polycarbazolyldiacetylenes. *Phys. Rev. B* **1992,** *45* (12), 6802.
49. Brabec, C.; Johansson, H.; Cravino, A.; Sariciftci, N.; Comoretto, D.; Dellepiane, G.; Moggio, I., The spin signature of charged photoexcitations in carbazolyl substituted polydiacetylene. *J. Chem. Phys.* **1999,** *111* (22), 10354-10361.
50. Dellepiane, G.; Cuniberti, C.; Comoretto, D.; Musso, G.; Figari, G.; Piaggi, A.; Borghesi, A., Long-lived photoexcited states in symmetrical polydicarbazolyldiacetylene. *Phys. Rev. B* **1993,** *48* (11), 7850.
51. (a) Song, J. H.; Kang, T. J.; Cho, Y. D.; Lee, S. H.; Kim, J. S., The fabrication and characterization of the photovoltaic cells composed of polydiacetylene and fullerene. *Fiber. Polym.* **2006,** *7* (3), 217-222; (b) Muthitamongkol, P.; Thanachayanont, C.; Sukwattanasinitt, M., Fabrication and characterization of solar cells containing polydiacetylene. *Curr. App. Phys.* **2011,** *11* (1), S163-S165; (c) Reanprayoon, C.; Gasiorowski, J.; Sukwattanasinitt, M.; Sariciftci, N. S.; Thamyongkit, P.,

Polydiacetylene-nested porphyrin as a potential light harvesting component in bulk heterojunction solar cells. *RSC Adv.* **2014,** *4* (6), 3045-3050.

52. (a) Prock, A.; Shand, M. L.; Chance, R. R., Solid-state photopolymerization of diacetylenes. *Macromolecules* **1982,** *15* (2), 238-241; (b) Mondong, R.; Bässler, H., Determination of the chain length in polydiacetylenes by scanning electron microscopy. *Chem. Phys. Lett.* **1981,** *78* (2), 371-374; (c) Siegel, D.; Sixl, H.; Enkelmann, V.; Wenz, G., Polymerization of TS-12 diacetylene crystals: Crystal structures of monomer and polymer and spectroscopy of reaction intermediates. *Chem. Phys.* **1982,** *72* (1–2), 201-212.
53. Wegner, G., Topochemical reactions of monomers with conjugated triple ‐ bonds. IV. Polymerization of bis ‐ (p ‐ toluene sulfonate) of 2.4 ‐ hexadiin ‐ 1.6 ‐ diol. *Die Makromol. Chem.* **1971,** *145* (1), 85-94.
54. Jin, H.; Plonka, A. M.; Parise, J. B.; Goroff, N. S., Pressure induced topochemical polymerization of diiodobutadiyne: a single-crystal-to-single-crystal transformation. *Cryst. Eng. Comm.* **2013,** *15* (16), 3106-3110.
55. Baughman, R. H., Solid-state synthesis of large polymer single crystals. *J. Polym. Sci. Pol. Phys.* **1974,** *12* (8), 1511-1535.
56. Wegner, G., Introductory lecture: Solid-state polymerization. *Faraday Discuss. Chem. Soc* **1979,** *68*, 494-508.
57. Enkelmann, V., The crystal structure of the low-temperature phase of poly[1,2-bis(p-tolylsulphonyloxymethylene)-1-buten-3-ynylene]. *Acta Crystallogr. Sect. B-Struct. Sci.* **1977,** *33* (9), 2842-2846.
58. Curtis, S. M.; Le, N.; Fowler, F. W.; Lauher, J. W., A Rational Approach to the Preparation of Polydipyridyldiacetylenes: An Exercise in Crystal Design. *Crystal Growth & Design* **2005,** *5* (6), 2313-2321.
59. Ikeshima, M.; Mamada, M.; Katagiri, H.; Minami, T.; Okada, S.; Tokito, S., Synthesis and solid-state polymerization of diacetylene derivatives with an *N*-carbazolylphenyl group. *B. Chem. Soc. Jpn.* **2015**.
60. Wang, S.; Li, Y.; Liu, H.; Li, J.; Li, T.; Wu, Y.; Okada, S.; Nakanishi, H., Topochemical polymerization of unsymmetrical aryldiacetylene supramolecules with nitrophenyl substituents utilizing C-H···π interactions. *Org. Biomol. Chem.* **2015,** *13* (19), 5467-5474.
61. Matsuo, H.; Okada, S.; Nakanishi, H.; Matsuda, H.; Takaragi, S., Solid-state polymerization of monomers possessing two diphenylbutadiyne moieties with amido groups to form ladder polymers. *Polym. J.* **2002,** *34* (11), 825-834.
62. Néabo, J. R.; Tohoundjona, K. I. S.; Morin, J.-F., Topochemical polymerization of a diarylbutadiyne derivative in the gel and solid states. *Org. Lett.* **2011,** *13* (6), 1358-1361.
63. Xu, R.; Gramlich, V.; Frauenrath, H., Alternating diacetylene copolymer utilizing perfluorophenyl−phenyl interactions. *J. Am. Chem. Soc.* **2006,** *128* (16), 5541-5547.
64. Okada, S.; Ohsugi, M.; Masaki, A.; Matsuda, H.; Takaragi, S.; Nakanishi, H., Preparation and nonlinear optical property of polydiacetylenes from unsymmetrical diphenylbutadiynes with trifluoromethyl substituents. *Mol. Cryst. Liq. Cryst.* **1990,** *183*, 81-90.
65. Milburn, G.; Werninck, A.; Tsibouklis, J.; Bolton, E.; Thomson, G.; Shand, A., Synthesis and properties of some novel unsymmetrically substituted diacetylenes. *Polymer* **1989,** *30* (6), 1004-1007.

66. Fowler, F. W.; Lauher, J. W., A rational design of molecular materials. *J. Phys. Org. Chem.* **2000,** *13* (12), 850-857.
67. Lauher, J. W.; Fowler, F. W.; Goroff, N. S., Single-crystal-to-single-crystal topochemical polymerizations by design. *Acc. Chem. Res.* **2008,** *41* (9), 1215-1229.
68. Li, Z.; Fowler, F. W.; Lauher, J. W., Weak Interactions Dominating the Supramolecular Self-Assembly in a Salt: A Designed Single-Crystal-to-Single-Crystal Topochemical Polymerization of a Terminal Aryldiacetylene. *J. Am. Chem. Soc.* **2009,** *131*, 634-643.
69. Sun, A.; Lauher, J. W.; Goroff, N. S., Preparation of poly(diiododiacetylene), an ordered conjugated polymer of carbon and iodine. *Science* **2006,** *312* (5776), 1030-1034.
70. Luo, L.; Wilhelm, C.; Sun, A.; Grey, C. P.; Lauher, J. W.; Goroff, N. S., Poly (diiododiacetylene): preparation, isolation, and full characterization of a very simple poly (diacetylene). *J. Am. Chem. Soc.* **2008,** *130* (24), 7702-7709.
71. Shirakawa, H.; Louis, E. J.; MacDiarmid, A. G.; Chiang, C. K.; Heeger, A. J., Synthesis of electrically conducting organic polymers: halogen derivatives of polyacetylene, $(CH)_x$. *J. Chem. Soc. Chem. Commun.* **1977,** (16), 578-580.
72. Becquerel, A., On electric effects under the influence of solar radiation. *CR Acad. Sci* **1839,** *9*, 711-714.
73. Green, M. A., Silicon solar cells: evolution, high-efficiency design and efficiency enhancements. *Semicond. Sci. Technol.* **1993,** *8*, 1.
74. Masuko, K.; Shigematsu, M.; Hashiguchi, T.; Fujishima, D.; Kai, M.; Yoshimura, N.; Yamaguchi, T.; Ichihashi, Y.; Mishima, T.; Matsubara, N.; Yamanishi, T.; Takahama, T.; Taguchi, M.; Maruyama, E.; Okamoto, S., Achievement of More Than 25% Conversion Efficiency With Crystalline Silicon Heterojunction Solar Cell. *IEEE J. Photovoltaics* **2014**, 1-3.
75. Wagner, S.; Shay, J. L.; Migliorato, P.; Kasper, H. M., CuInSe2/CdS heterojunction photovoltaic detectors. *Appl. Phys. Lett.* **1974,** *25*, 434-435.
76. Rau, U.; Schock, H.-W., Electronic properties of Cu (In, Ga) Se_2 heterojunction solar cells–recent achievements, current understanding, and future challenges. *Appl. Phys. A* **1999,** *69* (2), 131-147.
77. Singh, U. P.; Patra, S. P., Progress in Polycrystalline Thin-Film Cu(In,Ga)Se2 Solar Cells. *Int. J. Photoenerg.* **2010,** *2010*.
78. Powalla, M.; Jackson, P.; Witte, W.; Hariskos, D.; Paetel, S.; Tschamber, C.; Wischmann, W., High-efficiency Cu(In,Ga)Se2 cells and modules. *Sol. Energ. Mat. Sol. C.* **2013,** *119*, 51-58.
79. Powalla, M.; Witte, W.; Jackson, P.; Paetel, S.; Lotter, E.; Wuerz, R.; Kessler, F.; Tschamber, C.; Hempel, W.; Hariskos, D.; Menner, R.; Bauer, A.; Spiering, S.; Ahlswede, E.; Friedlmeier, T. M.; Blazquez-Sanchez, D.; Klugius, I.; Wischmann, W., CIGS Cells and Modules With High Efficiency on Glass and Flexible Substrates. *IEEE J. Photovoltaics* **2014,** *4*, 440-446.
80. Reinhard, P.; Chirila, A.; Blosch, P.; Pianezzi, F.; Nishiwaki, S.; Buechelers, S.; Tiwari, A. N., Review of progress toward 20% efficiency flexible CIGS solar cells and manufacturing issues of solar modules. *IEEE J. Photovoltaics* **2013,** *3*, 572-580.
81. Lindström, S., An all‐sputtering process and equipment for CIGS solar cells. *Vakuum in Forschung und Praxis* **2013,** *25* (5), 43-45.
82. Shah, A.; Torres, P.; Tscharner, R.; Wyrsch, N.; Keppner, H., Photovoltaic technology: The case for thin-film solar cells. *Science* **1999,** *285* (5428), 692-698.

83. Sproul, A., Understanding the *p-n* Junction.
84. Koide, N.; Islam, A.; Chiba, Y.; Han, L., Improvement of efficiency of dye-sensitized solar cells based on analysis of equivalent circuit. *J. Photochem. Photobiol., A* **2006,** *182* (3), 296-305.
85. Shockley, W.; Queisser, H. J., Detailed balance limit of efficiency of p‐n junction solar cells. *J. Appl. Phys.* **1961,** *32*, 510-519.
86. Siebentritt, S., What limits the efficiency of chalcopyrite solar cells? *Sol. Energ. Mat. & Sol. C.* **2011,** *95*, 1471-1476.
87. Orgassa, K.; Rau, U.; Nguyen, Q.; Werner Schock, H.; Werner, J. H., Role of the CdS buffer layer as an active optical element in Cu (In, Ga) Se_2 thin‐film solar cells. *Prog. Photovoltaics Res. Appl.* **2002,** *10* (7), 457-463.
88. (a) Wang, F.; Tan, Z. a.; Li, Y., Solution-processable metal oxides/chelates as electrode buffer layers for efficient and stable polymer solar cells. *Energy Environ. Sci.* **2015,** *8* (4), 1059-1091; (b) Po, R.; Carbonera, C.; Bernardi, A.; Camaioni, N., The role of buffer layers in polymer solar cells. *Energy Environ. Sci.* **2011,** *4* (2), 285-310.
89. Wang, J.-C.; Weng, W.-T.; Tsai, M.-Y.; Lee, M.-K.; Horng, S.-F.; Perng, T.-P.; Kei, C.-C.; Yu, C.-C.; Meng, H.-F., Highly efficient flexible inverted organic solar cells using atomic layer deposited ZnO as electron selective layer. *J. Mater. Chem.* **2010,** *20* (5), 862-866.
90. Kim, J. Y.; Kim, S. H.; Lee, H.-H.; Lee, K.; Ma, W.; Gong, X.; Heeger, A. J., New architecture for high-efficiency polymer photovoltaic cells using solution-based titanium oxide as an optical spacer. *Adv. Mater.* **2006,** *18* (5), 572-576.
91. Shrotriya, V.; Li, G.; Yao, Y.; Chu, C.-W.; Yang, Y., Transition metal oxides as the buffer layer for polymer photovoltaic cells. *Appl. Phys. Lett.* **2006,** *88* (7), 073508.
92. Li, G.; Chu, C.; Shrotriya, V.; Huang, J.; Yang, Y., Efficient inverted polymer solar cells. *Appl. Phys. Lett.* **2006,** *88* (25), 253503-253503.
93. Peumans, P.; Bulović, V.; Forrest, S. R., Efficient photon harvesting at high optical intensities in ultrathin organic double-heterostructure photovoltaic diodes. *Appl. Phys. Lett.* **2000,** *76*, 2650-2652.
94. (a) Gommans, H.; Verreet, B.; Rand, B. P.; Muller, R.; Poortmans, J.; Heremans, P.; Genoe, J., On the Role of Bathocuproine in Organic Photovoltaic Cells. *Adv.Funct. Mater.* **2008,** *18* (22), 3686-3691; (b) Vogel, M.; Doka, S.; Breyer, C.; Lux-Steiner, M. C.; Fostiropoulos, K., On the Function of a Bathocuproine Buffer Layer in Organic Photovoltaic Cells. *Appl. Phys. Lett.* **2006,** *89* (16), 163501-163501-3.
95. Kim, J. Y.; Kim, S. H.; Lee, H.-H.; Lee, K.; Ma, W.; Gong, X.; Heeger, A. J., New architecture for high-efficiency polymer photovoltaic cells using solution-based titanium oxide as an optical spacer. *Adv. Mater.* **2006,** *18*, 5.
96. Chan, M. Y.; Lee, C. S.; Lai, S. L.; Fung, M. K.; Wong, F. L.; Sun, H. Y.; Lau, K. M.; Lee, S. T., Efficient organic photovoltaic devices using a combination of exciton blocking layer and anodic buffer layer. *J. Appl. Phys.* **2006,** *100*.
97. Naka, S.; Okada, H.; Onnagawa, H.; Tsutsui, T., High electron mobility in bathophenanthroline. *Appl. Phys. Lett.* **2000,** *76* (2), 197-199.
98. Li, C.; Schwab, M.; Zhao, Y.; Chen, L.; Bruder, I.; Münster, I.; Erk, P.; Müllen, K., A phenanthroline derivative as exciton blocking material for organic solar cells. *Dyes Pigments* **2013,** *97*, 258-261.

99. (a) Tripathi, V.; Datta, D.; Samal, G. S.; Awasthi, A.; Kumar, S., Role of Exciton Blocking Layers in Improving Efficiency of Copper Phthalocyanine based Organic Solar Cells. *J. Non-Crys. Solids* **2008,** *354* (19–25), 2901-2904; (b) Wang, N.; Yu, J.; Zang, Y.; Huang, J.; Jiang, Y., Effect of Buffer Layers on the Performance of Organic Photovoltaic Cells based on Copper Phthalocyanine and C60. *Sol. Energ. Mat. Sol. C.* **2010,** *94* (2), 263-266; (c) Yu, J.; Wang, N.; Zang, Y.; Jiang, Y., Organic photovoltaic cells based on TPBi as a cathode buffer layer. *Sol. Energy Mater. Sol. Cells* **2011,** *95* (2), 664-668.
100. Tang, C. W.; VanSlyke, S. A., Organic electroluminescent diodes. *Appl. Phys. Lett.* **1987,** *51* (12), 913-915.
101. Kathirgamanathan, P.; Surendrakumar, S.; Vanga, R. R.; Ravichandran, S.; Antipan-Lara, J.; Ganeshamurugan, S.; Kumaraverl, M.; Paramaswara, G.; Arkley, V., Arylvinylene phenanthroline derivatives for electron transport in blue organic light emitting diodes. *Org. Electron.* **2011,** *12* (4), 666-676.
102. Schermann, G.; Grösser, T.; Hampel, F.; Hirsch, A., Dicyanopolyynes: A homologuous series of end-capped linear sp carbon. *Chem. Eur. J.* **1997,** *3*, 8.
103. DeCicco, R. C. The synthesis and polymerization behavior of polyynes. Stony Brook University, Stonybrook, 2012.
104. Black, A. An Exploration of alkyne-alkyne cross-coupling reactions and attempts towards controlled polymerization of diiodooctatetrayne. State University of New York at Stony Brook, 2013.
105. Sarkar, A.; Okada, S.; Nakanishi, H.; Matsuda, H., Polydiacetylenes from asymmetrically substituted diacetylenes containing heteroaryl side groups for third-order nonlinear optical properties. *Macromolecules* **1998,** *31* (26), 9174-9180.
106. Hwang, S.; Kang, H. R.; Kim, S., Synthesis of polyynes by in situ desilylative bromination and palladium-catalyzed coupling: (7-benzyloxy)hepta-1,3,5-triynyltriisopropylsilane. *Org. Syn.* **2009,** *86*, 225-235.
107. De Luca, L.; Giacomelli, G., An insight of the reactions of amines with trichloroisocyanuric acid. *Syn. Lett.* **2004,** *2004*, 5.
108. Lee, T.; Kang, H. R.; Kim, S.; Kim, S., Facile one-pot syntheses of bromoacetylenes from bulky trialkylsilyl acetylenes. *Tetrahedron* **2006,** *62*, 5.
109. Richardson, C.; Reed, C. A., Synthesis of meso-Extended Tetraarylporphyrins. *J. Org. Chem.* **2007,** *72*, 4750-4755.
110. Marqués-González, S.; Yufit, D. S.; Howard, J. A. K.; Martín, S.; Osorio, H. M.; Garcia-Suarez, V. M.; Nichols, R. J.; Higgins, S. J.; Ceac, P.; Low, P. J., Simplifying the conductance profiles of molecular junctions: the use of the trimethylsilylethynyl moiety as a molecule–gold contact. *Dalton Trans* **2013,** *42*, 338-341.
111. Li, Q.; Jin, C.; Petukhov, P. A.; Rukavishnikov, A. V.; Zaikova, T. O.; Phadke, A.; LaMunyon, D. H.; Lee, M. D.; Keana, J. F. W., Synthesis of well-defined tower-shaped 1,3,5-trisubstituted adamantanes incorporating a macrocyclic trilactam ring system. *J. Org. Chem.* **2004,** *69*, 10.
112. Dikusar, E. A.; Yuvchenko, A. P.; Zvereva, T. D.; Zhukovskaya, N. A.; Moiseichuk, K. L., Synthesis and characterization of functionally substituted diacetylene peroxide. *Russ. J. Org. Chem.* **1998,** *36*, 5.
113. Suh, Y.-G.; Jung, J.-K.; Seo, S.-Y.; Min, K.-H.; Shin, D.-Y.; Lee, Y.-S.; Kim, S.-H.; Park, H.-J., Total synthesis of (+)-Brefeldin A. *J. Org. Chem.* **2002,** *67* (12), 4127-4137.

114. Dixon, D. J.; Ley, S. V.; Longbottom, D. A., Total synthesis of the plasmoidal pigment physarorubinic acid, a polyenoyl tetramic acid. *J. Chem. Soc., Perkin Trans. 1* **1999,** (16), 2231-2232.
115. Doak, B. C.; Scanlon, M. J.; Simpson, J. S., Synthesis of unsymmetrical 1,1'-disubstituted bis(1,2,3-triazole)s using monosilylbutadiynes *Org. Lett.* **2011,** *23* (3), 537-539.
116. Baeyer, *Chem. Ber.* **1885,** *18* (676).
117. Bohlmann, F., *Chem. Ber.* **1964,** *97*, 12.
118. Straus; Kollek; Hauptmann, *Chem. Ber.* **1930,** *63*, 1897.
119. Bohlmann; Sinn, *Chem. Ber.* **1955,** *88*, 21.
120. Klein, J. P. Methods of producing dicarbonyl compounds. WO 2015060862 A1. April 30, 2015.
121. Dunitz, J. D.; Robertson, J. M., The crystal and molecular structure of certain dicarboxylic acids. Part III. Diacetylenedicarboxylic acid dihydrate. *J. Chem. Soc.* **1947**, 12.
122. Bohlmann; Sinn, *Chem. Ber.* **1955,** *88*, 1876-1896.
123. Liang, X.; Lee, C.-J.; Chen, X.; Chung, H. S.; Zeng, D.; Raetz, C. R. H.; Li, Y.; Zhou, P.; Toone, E. J., Syntheses, structures and antibiotic activities of LpxC inhibitors based on the diacetylene scaffold. *Bioorg. Med. Chem.* **2011,** *19* (2), 852-860.
124. Berger, O.; Kaniti, A.; van Ba, C. T.; Vial, H.; Ward, S. A.; Biagini, G. A.; Bray, P. G.; O'Neill, P. M., Synthesis and antimalarial activities of a diverse set of triazole-containing furamidine analogues. *ChemMedChem.* **2011,** *6* (11), 2094-2108.
125. Jiang, M. X.-W.; Rawat, M.; Wulff, W. D., Contingency and serendipity in the reactions of fischer carbene complexes with conjugated triynes. *J. Am. Chem. Soc.* **2004,** *126* (19), 5970-5971.
126. Valášek, M.; Edelmann, K.; Gerhard, L.; Fuhr, O.; Lukas, M.; Mayor, M., Synthesis of molecular tripods based on a rigid 9,9′ -spirobifluorene scaffold. *J. Org. Chem.* **2014,** *79* (16), 7342-7357.
127. Molt, O.; Rübeling, D.; Schrader, T., A selective biomimetic tweezer for noradrenaline. *J. Am. Chem. Soc.* **2003,** *125* (40), 12086-12087.
128. Kelly, S. M.; Lipshutz, B. H., Chemoselective reductions of nitroaromatics in water at room temperature. *Org. Lett.* **2014,** *16* (1), 98-101.
129. Flatt, A. K.; Yao, Y.; Maya, F.; Tour, J. M., Orthogonally functionalized oligomers for controlled self-assembly. *J. Org. Chem* **2004,** *69* (5), 1752-1755.
130. Thaler, T.; Guo, D. L.-N.; Mayer, D. P.; Knochel, P. D. P., Highly Diastereoselective C(sp3)C(sp) Cross-Coupling Reactions between 1,3- and 1,4-Substituted Cyclohexylzinc Reagents and Bromoalkynes through Remote Stereocontrol. *Angewandte Chemie* **2011,** *50* (9), 2174-2177.
131. Aakeröy, C. B.; Baldrighi, M.; Desper, J.; Metrangolo, P.; Resnati, G., Supramolecular hierarchy among halogen-bond donors. *Chem. Eur. J.* **2013,** *19* (48), 16240-16247.
132. Dixon, D. J.; Ley, S. V.; Longbottom, D. A., Total synthesis of the plasmoidal pigment physarorubinic acid, a polyenoyl tetramic acid. *J. Chem. Soc., Perkin Trans.* **1999,** *1*, 2231-2232.
133. Takeuchi, R.; Tanabe, K.; Tanaka, S., Stereodivergent synthesis of (*E*)- and (*Z*)-2-alken-4-yn-1-ols from 2-propynoic acid: a practical route via 2-alken-4-ynoates. *J. Org. Chem.* **2000,** *65* (5), 1558-1561.

134. Dr., J. A. V.; Prof., L. C.; Prof., M. M.; Dr., J. M.; Prof., C. S., Regiocontrolled One-Step Synthesis of 3,3′ -Disubstituted 2,2′ -Bipyridine Ligands by Cobalt(I)-Catalyzed Cyclotrimerization. *Chem. Eur. J.* **2001,** *7*, 5203-5213.
135. Pelletier, G.; Charette, A. B., Triflic anhydride mediated synthesis of imidazo[1,5-a]azines. *Org. Lett.* **2013,** *15* (9), 2290-2293.
136. Forner, D. F.; Quiñones, M. P.; Albero, M. A. B. Quinuclidine derivatives and their use as muscarinic M3 receptor ligands. US 6750226 B2. June 15, 2004.
137. Askew, B. C.; Hartman, G. D.; Duggan, M. E.; Young, S. D.; Hutchinson, J. H.; Wai, J. S.; Egbertson, M. S.; Vassallo, L. M.; Libby, L. A.; Krause, A. E.; Halczenko, W.; Ihle, N. C. Fibrinogen receptor antagonists. US 5852045 A1. December 22, 1998.
138. Baughman, R.; Yee, K., Solid-state polymerization of linear and cyclic acetylenes. *J. Polym. Sci. Macromol. Rev.* **1978,** *13* (1), 219-239.
139. Okada, S.; Hayamizu, K.; Matsuda, H.; Masaki, A.; Minami, N.; Nakanishi, H., Solid-state Polymerization of 15,17,19,21,23,25-Tetracontahexay. *Macromolecules* **1994,** *27*, 6259-6266.
140. Myers, A. G.; Finney, N. S., Synthesis of 1,6-didehydro[10]annulene. Observation of its exceptionally facile rearrangement to form the biradical 1,5-dehydronaphthalene. *J. Am. Chem. Soc.* **1992,** *114* (27), 10986-10987.
141. Okada, S.; Hayamizu, K.; Matsuda, H.; Masaki, A.; Minami, N.; Nakanishi, H., Solid-state polymerization of 15,17,19,21,23,25-tetracontahexayne. *Macromolecules* **1994,** *27* (22), 6259-6266.
142. Sarkar, A.; Okada, S.; Komatsu, K.; Nakanishi, H.; Matsuda, H., Octatetraynes with directly linked aromatic sidegroups: Preparation and polymerization. *Macromolecules* **1998,** *31* (17), 5624-5630.
143. Szafert, S.; Gladysz, J., Update 1 of: Carbon in one dimension: structural analysis of the higher conjugated polyynes. *Chem. Rev.* **2006,** *106* (11), PR1-PR33.
144. (a) Lee, L.-H.; Lynch, V.; Lagow, R. J., The synthesis and structural characterization of the first bis (benzocrown ethers) with polyyne linkages. *J. Chem. Soc., Perkin Trans. 1* **2000,** (16), 2805-2809; (b) Gulia, N.; Ejfler, J.; Szafert, S., Macromolecular polyyne-containing benzoxazines for cross-linked polymerization. *Tetrahedron Lett.* **2012,** *53* (41), 5471-5474; (c) Kendall, J.; McDonald, R.; Ferguson, M. J.; Tykwinski, R. R., Synthesis and solid-state structure of perfluorophenyl end-capped polyynes. *Org. Lett.* **2008,** *10* (11), 2163-2166.
145. Luo, L., *Preparation and comprehensive characterization of poly (diiododiacetylene) and spectroscopic studies of its reactions with Lewis bases*. State University of New York at Stony Brook: 2009.
146. Doak, B. C.; Scanlon, M. J.; Simpson, J. S., Synthesis of unsymmetrical 1, 1′ -disubstituted bis(1, 2, 3-triazole)s using monosilylbutadiynes. *Org. Lett.* **2011,** *13* (3), 537-539.
147. DeCicco, R. C.; Black, A.; Li, L.; Goroff, N. S., An Iterative Method for the Synthesis of Symmetric Polyynes. *Eur. J. Org. Chem.* **2012,** *2012* (25), 4699-4704.
148. Gao, K.; Goroff, N. S., Two new iodine-capped carbon rods. *J. Am. Chem. Soc.* **2000,** *122* (38), 9320-9321.
149. Sammes, P. G.; Yahioglu, G., 1, 10-Phenanthroline: a versatile ligand. *Chem. Soc. Rev.* **1994,** *23*, 327-334.

150. (a) Ohashi, D.; Nakada, T.; Kunioka, A., Improved CIGS thin-film solar cells by surface sulfurization using In_2S_3 and sulfur vapor. *Sol. Energ. Mat. Sol. C* **2001,** *67* (1–4), 261-265; (b) Nagoya, Y.; Kushiya, K.; Tachiyuki, M.; Yamase, O., Role of incorporated sulfur into the surface of Cu(In, Ga)Se_2 thin-film absorber. *Sol. Energ. Mat. Sol. C* **2001,** *67* (1–4), 247-253; (c) Kobayashi, T.; Sugimoto, H.; Kato, T.; Yamaguchi, H.; Nakada, T., Impacts of surface sulfurization on high-efficiency CIGS thin film solar cells. *Proc. 23rd PVSEC Taipei Taiwan* **2013**.
151. Prajapati, S. M.; Patel, K. D.; Vekariya, R. H.; Panchal, S. N.; Patel, H. D., Recent advances in the synthesis of quinolines: a review. *RSC Advances* **2014,** *4* (47), 24463-24476.
152. Yamashkin, S.; Oreshkina, E., Traditional and modern approaches to the synthesis of quinoline systems by the Skraup and Doebner-Miller methods.(Review). *Chem. Heterocyclic Comp.* **2006,** *42*, 701-718.
153. Born, J. L., Mechanism of formation of benzo[g]quinolones via the Combes reaction. *J. Org. Chem.* **1972,** *37* (24), 3952-3953.
154. Friedlaender, P., Ueber o-Amidobenzaldehyd. *Ber. Dtsh. Chem. Ges.* **1882,** *15* (2), 2572-2575.
155. Conrad, M.; Limpach, L., Synthesen von chinolinderivaten mittelst acetessigester. *Ber. Dtsh. Chem. Ges.* **1887,** *20* (1), 944-948.
156. Gould, R. G.; Jacobs, W. A., The synthesis of certain substituted quinolines and 5,6-benzoquinolines. *J. Am. Chem. Soc.* **1939,** *61* (10), 2890-2895.
157. Surrey, A. R.; Cutler, R. A., The Synthesis of Some 4,10-Disubstituted-1,7-phenanthroline Derivatives. *J. Am. Chem. Soc.* **1954,** *76*, 1109-1113.
158. (a) Khong, S.; Kwon, O., One-pot phosphine-catalyzed syntheses of quinolines. *J. Org. Chem.* **2012,** *77* (18), 8257-8267; (b) Korivi, R. P.; Cheng, C.-H., Nickel-catalyzed cyclization of 2-iodoanilines with aroylalkynes: an efficient route for quinoline derivatives. *J. Org. Chem.* **2006,** *71* (18), 7079-7082; (c) Toh, K. K.; Sanjaya, S.; Sahnoun, S.; Chong, S. Y.; Chiba, S., Copper-catalyzed aerobic intramolecular carbo- and amino-oxygenation of alkynes for synthesis of azaheterocycles. *Org. Lett.* **2012,** *14* (9), 2290-2292; (d) Kong, L.; Zhou, Y.; Huang, H.; Yang, Y.; Liu, Y.; Li, Y., Copper-catalyzed synthesis of substituted quinolines via C–N coupling/condensation from *ortho*-acylanilines and alkenyl iodides. *J. Org. Chem.* **2014,** *80* (2), 1275-1278.
159. Eifert, R. L.; Hamilton, C. S., Some Methylphenanthrolines and Corresponding Aldehydes. *J. Am. Chem. Soc.* **1955,** *77*, 1818-1819.
160. (a) Kuzmina, O. M.; Steib, A. K.; Flubacher, D.; Knochel, P., Iron-catalyzed cross-coupling of *N*-heterocyclic chlorides and bromides with arylmagnesium reagents. *Org. Lett.* **2012,** *14* (18), 4818-4821; (b) Iglesias, M. J.; Prieto, A.; Nicasio, M. C., Kumada–Tamao–Corriu coupling of heteroaromatic chlorides and aryl ethers catalyzed by (IPr)Ni(allyl)Cl. *Org. Lett.* **2012,** *14* (17), 4318-4321; (c) Fürstner, A.; Leitner, A.; Méndez, M.; Krause, H., Iron-catalyzed cross-coupling reactions. *J. Am. Chem. Soc.* **2002,** *124* (46), 13856-13863; (d) Ohmiya, H.; Yorimitsu, H.; Oshima, K., Cobalt-catalyzed cross-coupling reaction of chloropyridines with Grignard reagents. *Chem. Lett.* **2004,** *33* (10), 1240-1241.
161. Wang, T.; Chen, F.; Qin, J.; He, Y.-M.; Fan, Q.-H., Asymmetric Ruthenium-Catalyzed Hydrogenation of 2- and 2,9-Substituted 1,10-Phenanthrolines. *Angewandte Chemie* **2013,** *125*, 7313-7317.

162. Panda, K.; Siddiqui, I.; Mahata, P. K.; Ila, H.; Junjappa, H., Heteroannulation of 3-Bis(methylthio)acrolein with Aromatic Amines - A Convenient Highly Regioselective Synthesis of 2-(Methylthio)quinolines and their Benzo/Hetero Fused Analogs - A Modified Skraup Quinoline Synthesis. *Synlett* **2004,** *2004*, 449-452.
163. Mahata, P. K.; Barun, O.; Ila, H.; Junjappa, H., Formation of acetaldehyde enolate from vinyl acetate and its reaction with aromatic and heteroaromatic aldehydes: an efficient synthesis of enals and polyenals. *Synlett.* **2000,** *9*, 1345-1347.
164. Su, Q.; Li, P.; He, M.; Wu, Q.; Ye, L.; Mu, Y., Facile Synthesis of Acridine Derivatives by ZnCl2-Promoted Intramolecular Cyclization of o-Arylaminophenyl Schiff Bases. *Org. Lett.* **2013,** *16*, 18-21.
165. Annunziata, R.; Benaglia, M.; Cinquini, M.; Raimondi, L.; Cozzi, F., A molecular gate: control of free intramolecular rotation by application of an external signal. *J. Phys. Org. Chem.* **2004,** *17* (9), 749-751.
166. (a) Khoshman, J. M. Spectroscopic ellipsometry characterization of single and multilayer aluminum nitride/indium nitride thin film systems. Ohio University, 2005; (b) Woollam, J. A.; Johs, B. D.; Herzinger, C. M.; Hilfiker, J. N.; Synowicki, R. A.; Bungay, C. L. In *Overview of variable-angle spectroscopic ellipsometry (VASE): I. Basic theory and typical applications*, Optical Metrology, 1999; pp 3-28.
167. (a) Jellison, J. G. E., Spectroscopic ellipsometry data analysis: measured versus calculated quantities. *Thin Solid Films* **1998,** *313–314* (0), 33-39; (b) Synowicki, R., Spectroscopic ellipsometry characterization of indium tin oxide film microstructure and optical constants. *Thin Solid Films* **1998,** *313*, 394-397.
168. (a) Eliasson, B. J. Metal-insulator-metal diodes for solar energy conversion. University of Colorado, 2001; (b) Grover, S.; Moddel, G., Applicability of metal/insulator/metal (MIM) diodes to solar rectennas. *IEEE J. Photovoltaics* **2011,** *1* (1), 78-83.
169. (a) Afzal, O.; Kumar, S.; Haider, M. R.; Ali, M. R.; Kumar, R.; Jaggi, M.; Bawa, S., A review on anticancer potential of bioactive heterocycle quinoline. *Euro. J. Med. Chem* **2015,** *97* (0), 871-910; (b) R Solomon, V.; Lee, H., Quinoline as a privileged scaffold in cancer drug discovery. *Curr. Med. Chem.* **2011,** *18* (10), 1488-1508.
170. Rehan, M.; Hazra, G.; Ghorai, P., Synthesis of polysubstituted quinolines via transition-metal-free oxidative cycloisomerization of *o*-cinnamylanilines. *Org. Lett.* **2015,** *17* (7), 1668-1671.
171. (a) El'tsov, *Zh. Org. Khim+* **1972,** *8*, 1309, 1324, 1329, 1332; (b) Jordis, U.; Sauter, F.; Rudolf, M.; Cai, G., Syntheses of novel quinolone-chemotherapeutics, I: Pyridoquinolines and pyridophenanthrolines as derivatives of "lin-benzo-nalidixic acid". *Monatsh. Chem.* **1988,** *119*, 20.
172. Borsche; Wagner-Roemmich, *Justus Liebigs Ann. Chem.* **1940,** *544*, 5.
173. Long, J.; Gao, H.; Song, K.; Liu, F.; Hu, H.; Zhang, L.; Zhu, F.; Wu, Q., Synthesis and Characterization of NiII and PdII Complexes Bearing N,N,S Tridentate Ligands and Their Catalytic Properties for Norbornene Polymerization. *Eur. J. Inorg. Chem.* **2008,** *2008*, 4296-4305.
174. Su, Q.; He, M.; Wu, Q.; Gao, W.; Xu, H.; Ye, L.; Mu, Y., The supramolecular assemblies of 7-amino-2,4-dimethylquinolinium salts and the effect of a variety of anions on their luminescent properties. *Cryst. Eng. Comm.* **2012,** *14* (21), 12.
175. Marckwald, *Justus Liebigs Ann. Chem.* **1893,** *274*.

176. Watson, I. D. G.; Styler, S. A.; Yudin, A. K., Unusual selectivity of unprotected aziridines in Palladium-catalyzed allylic amination enables facile preparation of branched aziridines. *J. Am. Chem. Soc.* **2004,** *126* (16), 5086-5087.
177. Mamillapalli, N. C.; Sekar, G., Metal free chemoselective reduction of α-keto amides using TBAF as catalyst. *RSC Advances* **2014,** *4* (105), 61077-61085.
178. Nallagonda, R.; Rehan, M.; Ghorai, P., Chemoselective C-benzylation of unprotected anilines with benzyl alcohols using Re_2O_7 catalyst. *J. Org. Chem.* **2014,** *79* (7), 2934-2943.

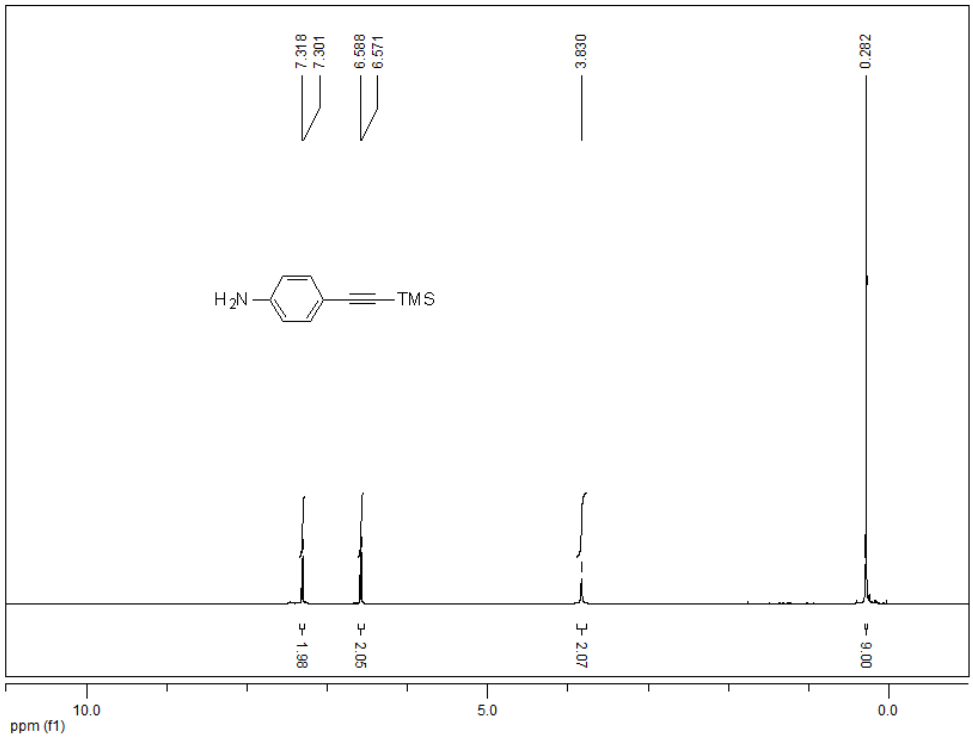

^{1}H-NMR (500 MHz, $CDCl_3$) spectrum of compound **2-33**

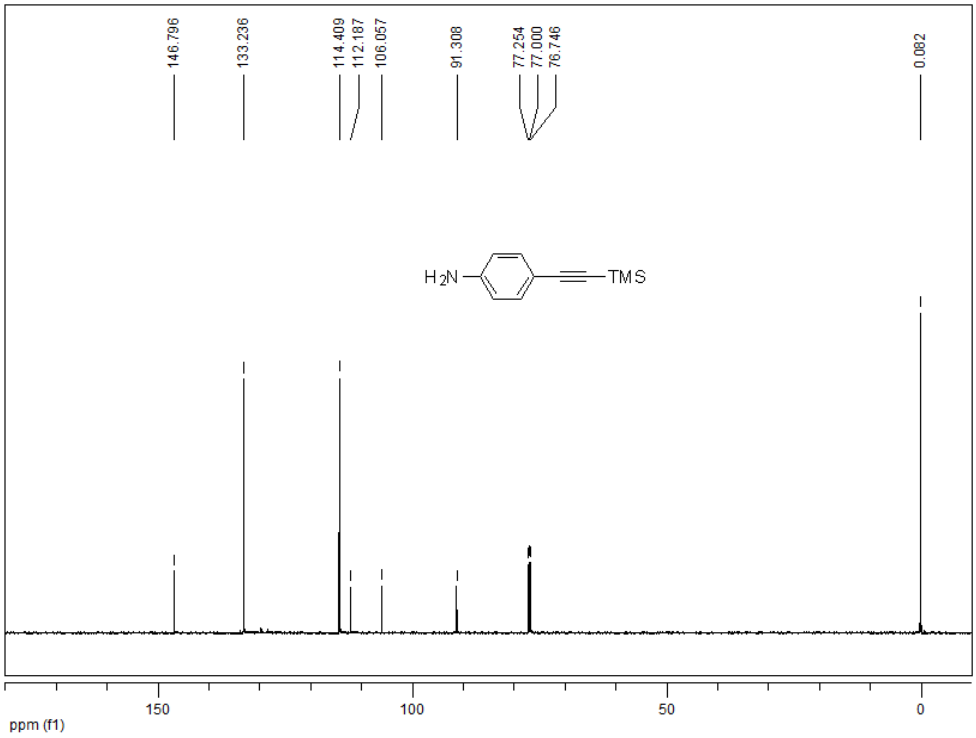

^{13}C-NMR (125 MHz, $CDCl_3$) spectrum of compound **2-33**

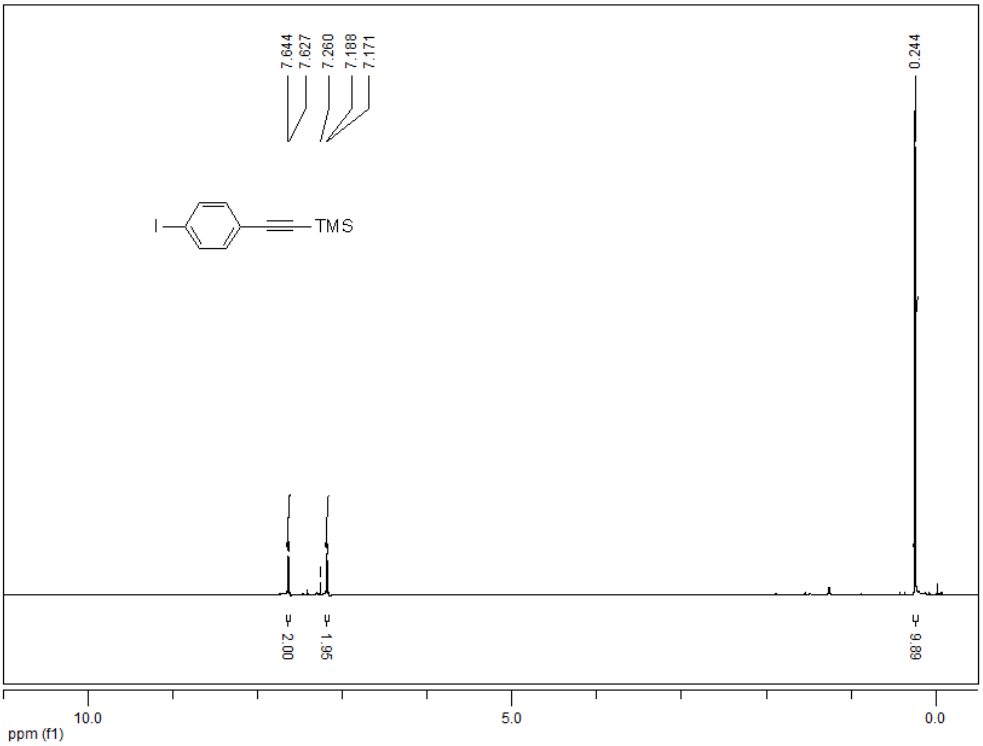

^{1}H-NMR (500 MHz, $CDCl_3$) spectrum of compound **2-34**

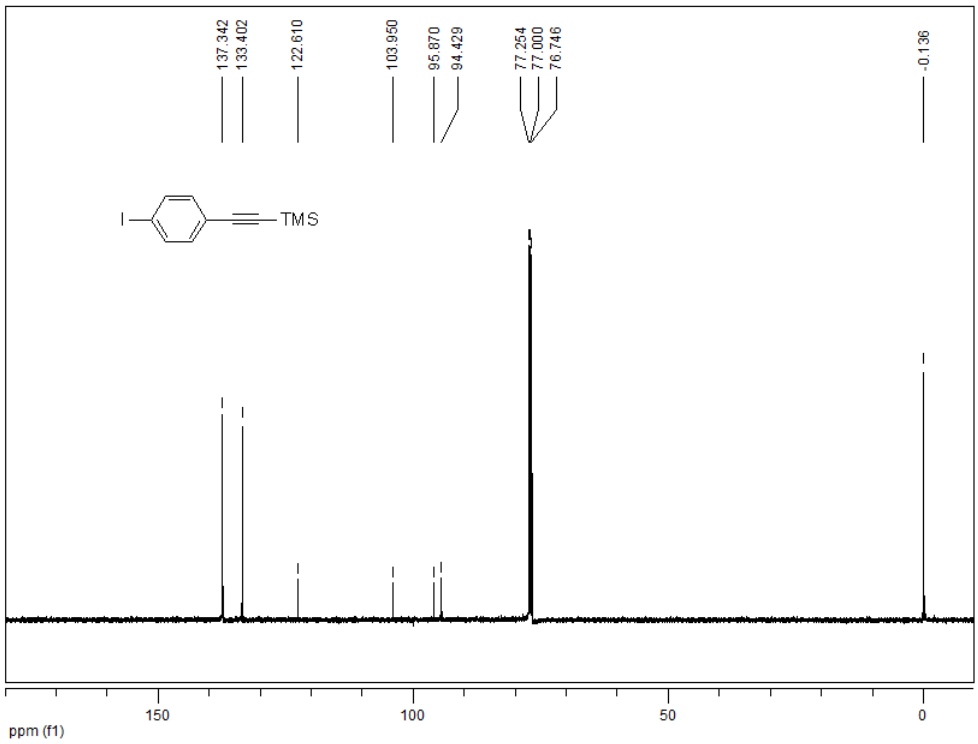

^{13}C-NMR (125 MHz, $CDCl_3$) spectrum of compound **2-34**

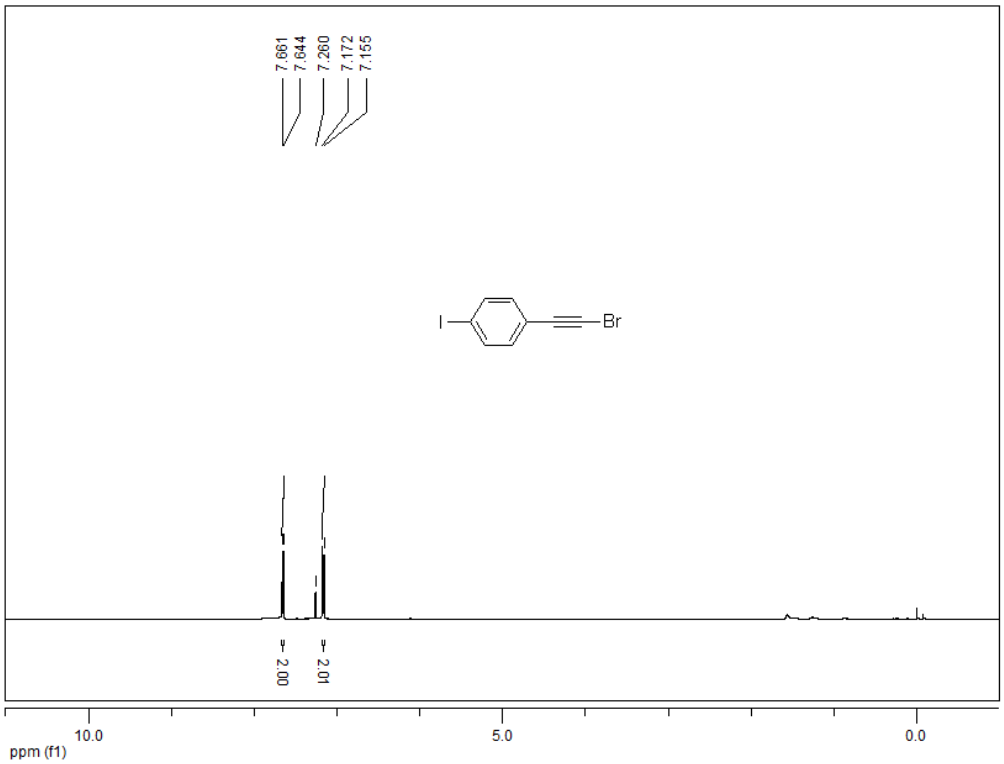

^{1}H-NMR (500 MHz, $CDCl_3$) spectrum of compound **2-35**

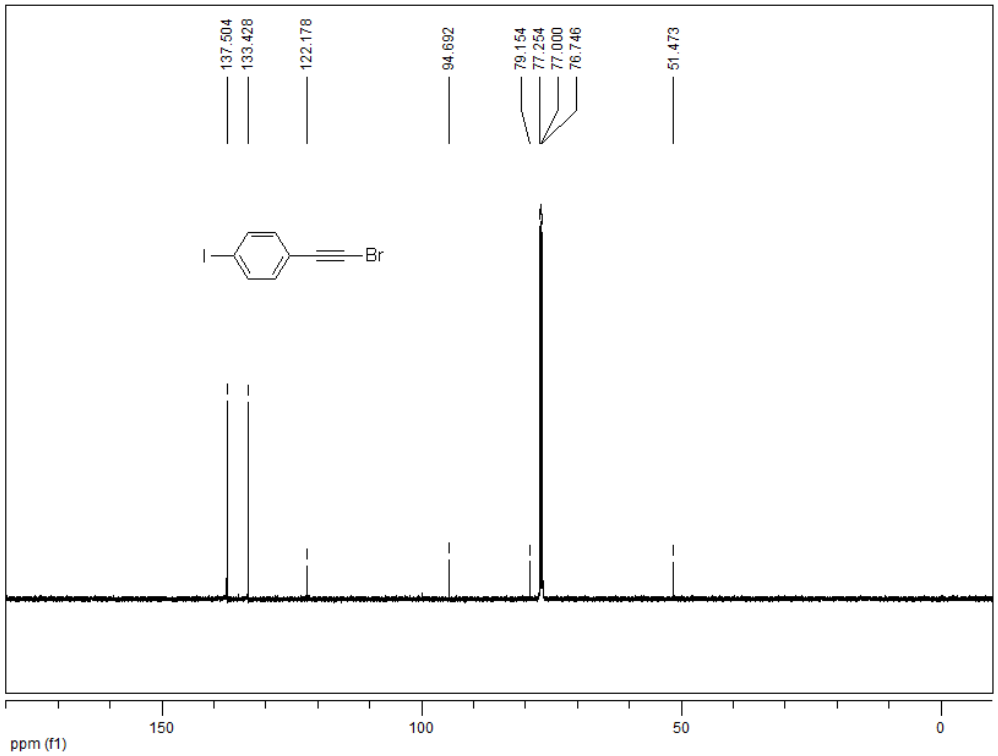

^{13}C-NMR (125 MHz, $CDCl_3$) spectrum of compound **2-35**

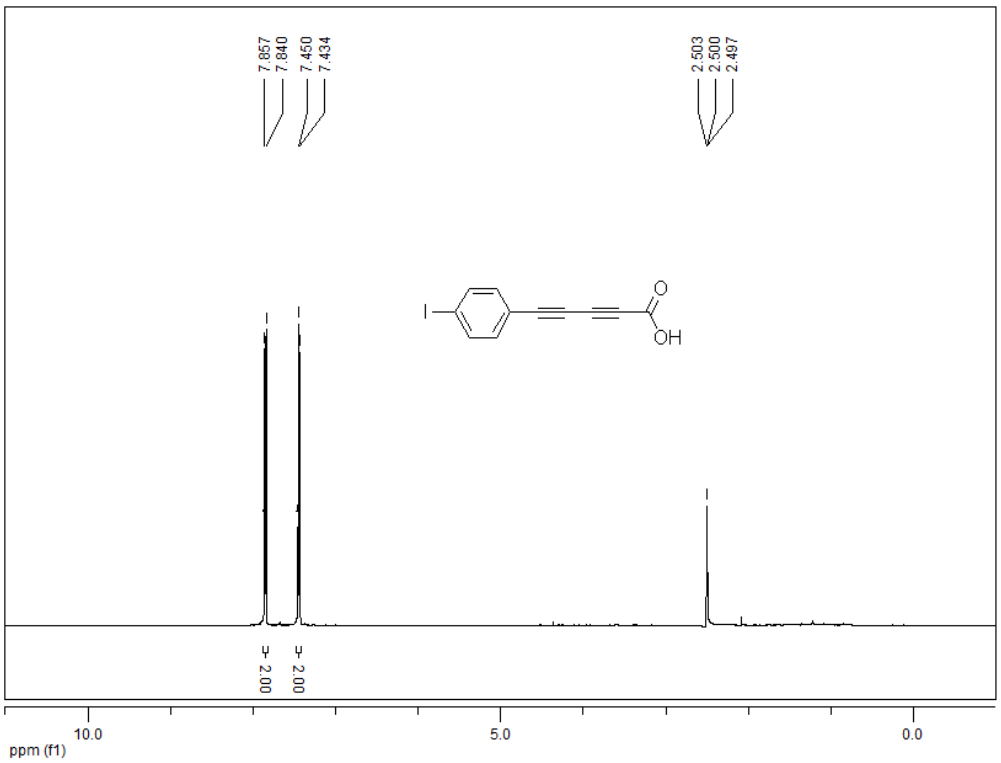

^{1}H-NMR (500 MHz, $CDCl_3$) spectrum of compound **2-6**

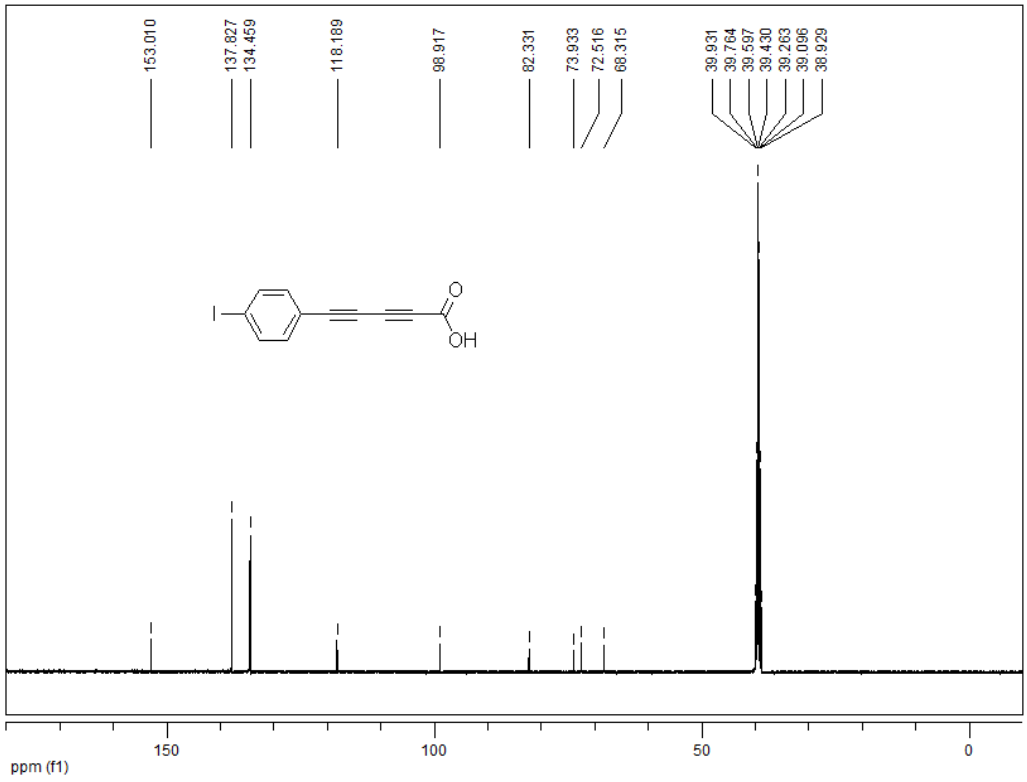

^{13}C-NMR (125 MHz, $CDCl_3$) spectrum of compound **2-6**

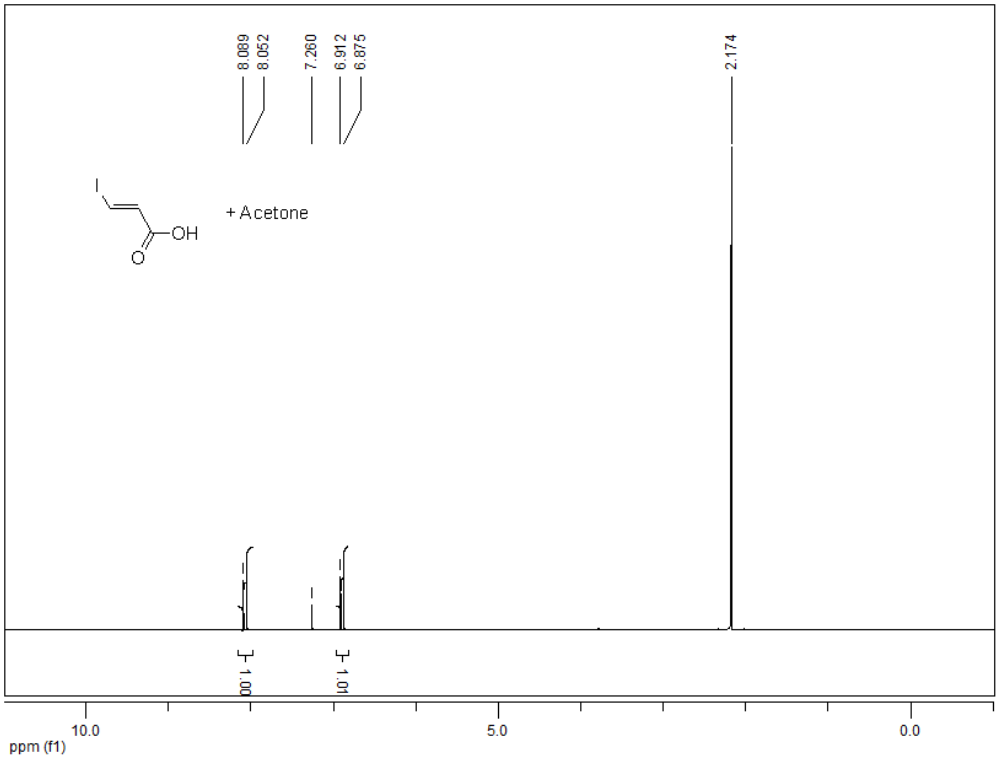

^{1}H-NMR (400 MHz, $CDCl_3$) spectrum of compound **2-42**(2.17 indicates acetone)

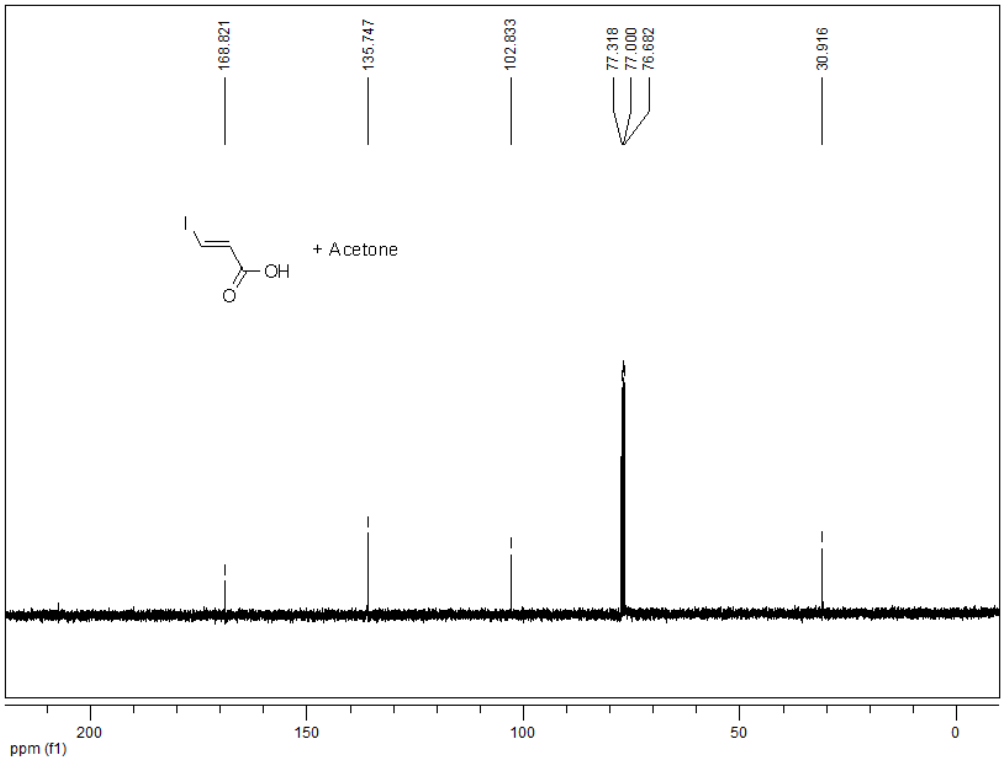

^{13}C-NMR (100 MHz, $CDCl_3$) spectrum of compound **2-42**(30.92 indicates acetone)

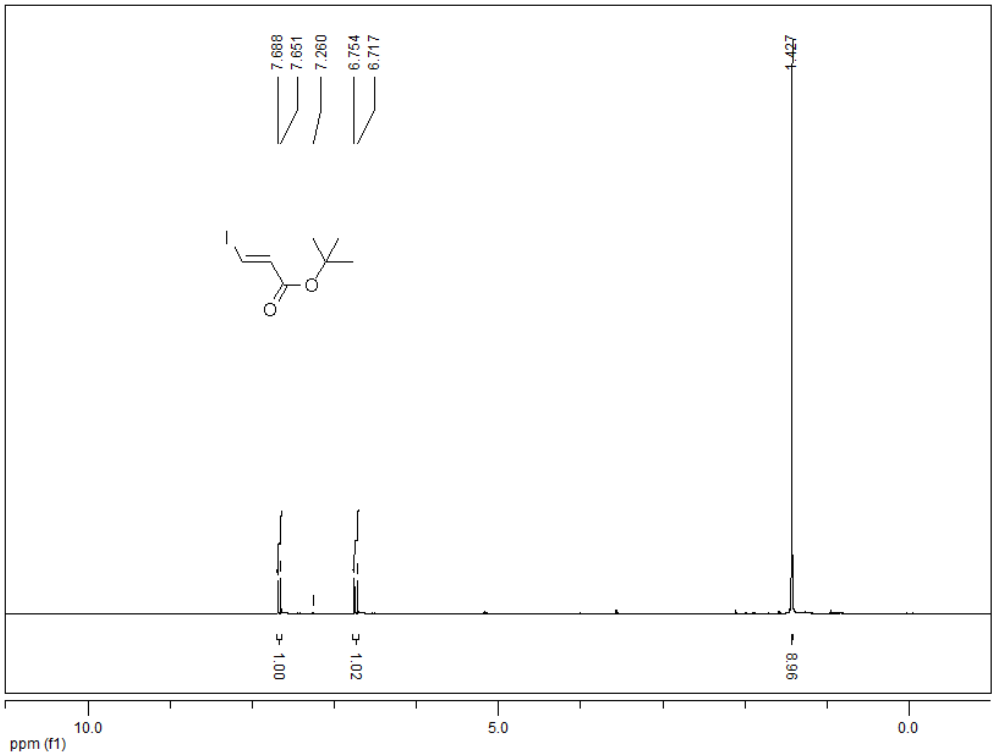

^{1}H-NMR (400 MHz, $CDCl_3$) spectrum of compound **2-39**

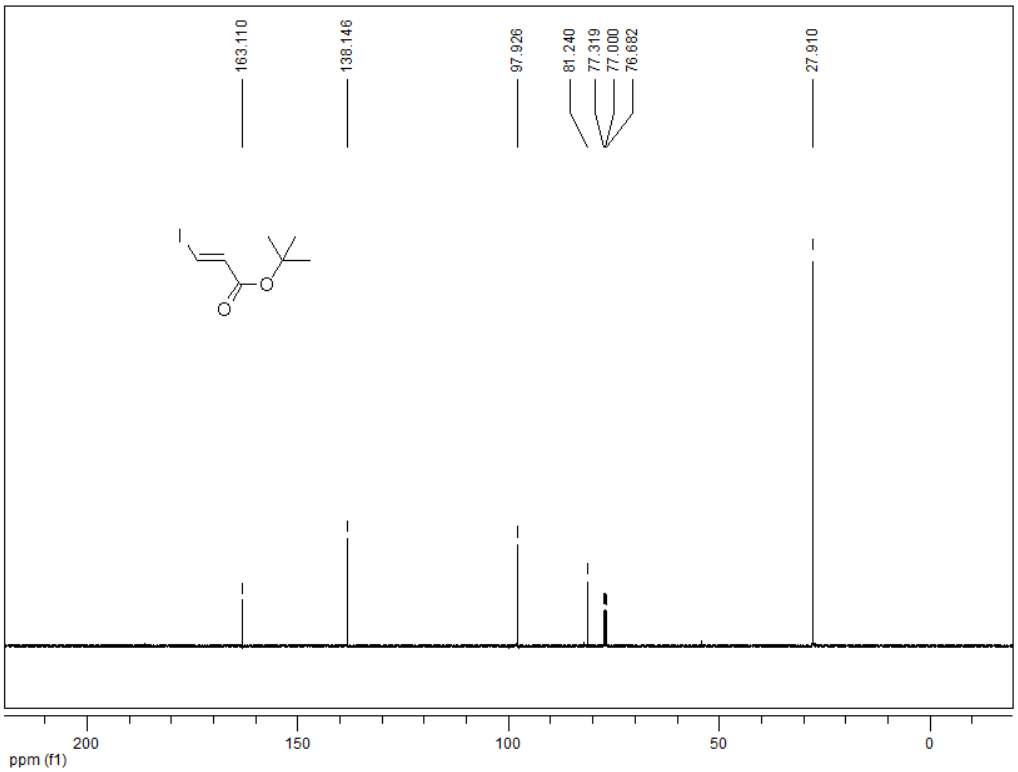

^{13}C-NMR (100 MHz, $CDCl_3$) spectrum of compound **2-39**

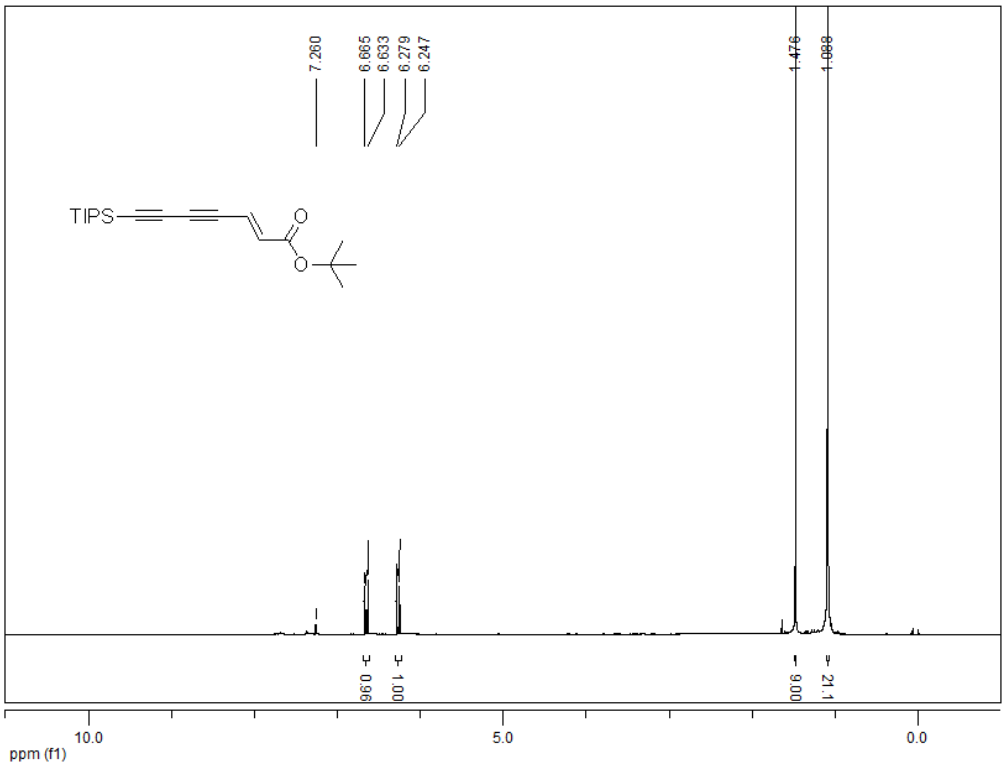

^{1}H-NMR (500 MHz, $CDCl_3$) spectrum of compound **2-41**

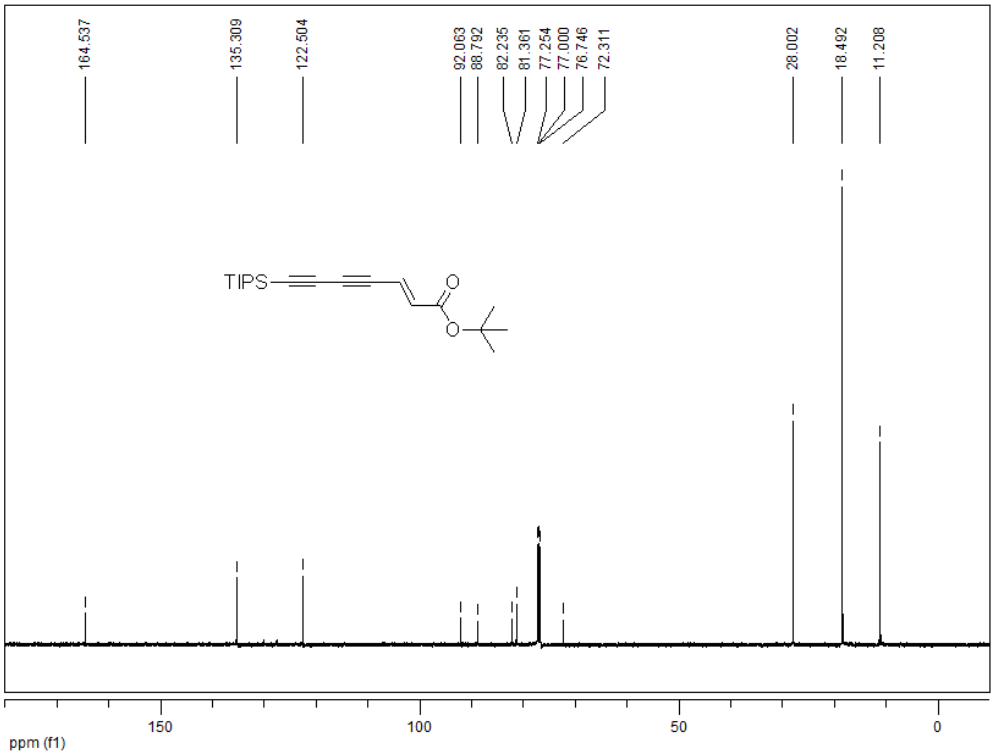

^{13}C-NMR (125 MHz, $CDCl_3$) spectrum of compound **2-41**

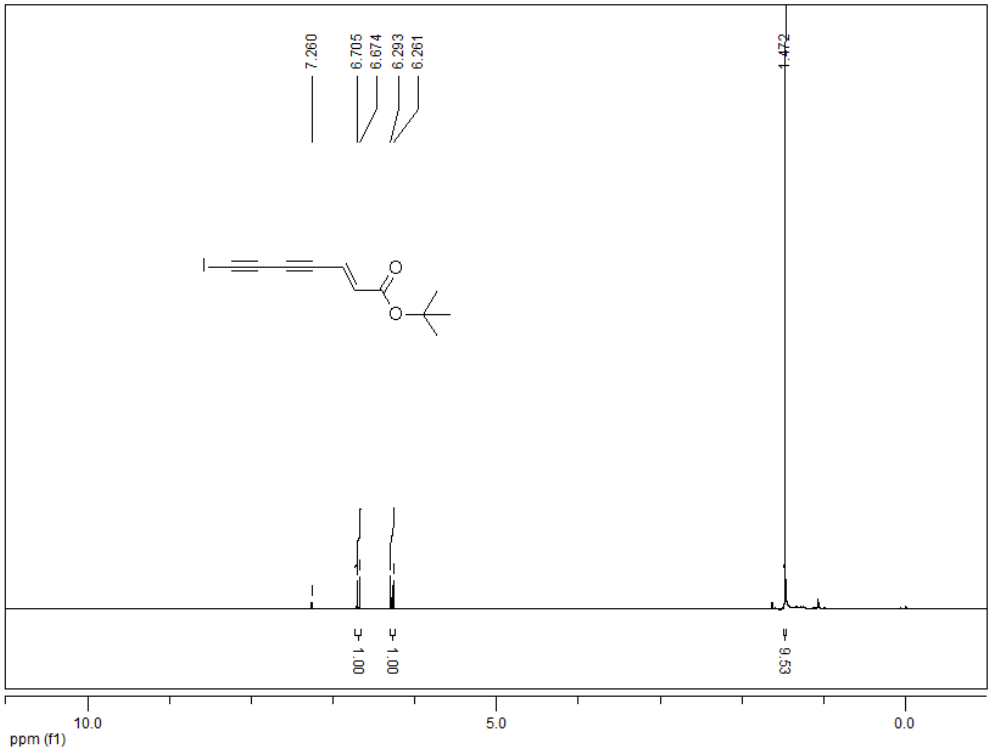

^{1}H-NMR (500 MHz, $CDCl_3$) spectrum of compound **2-43**

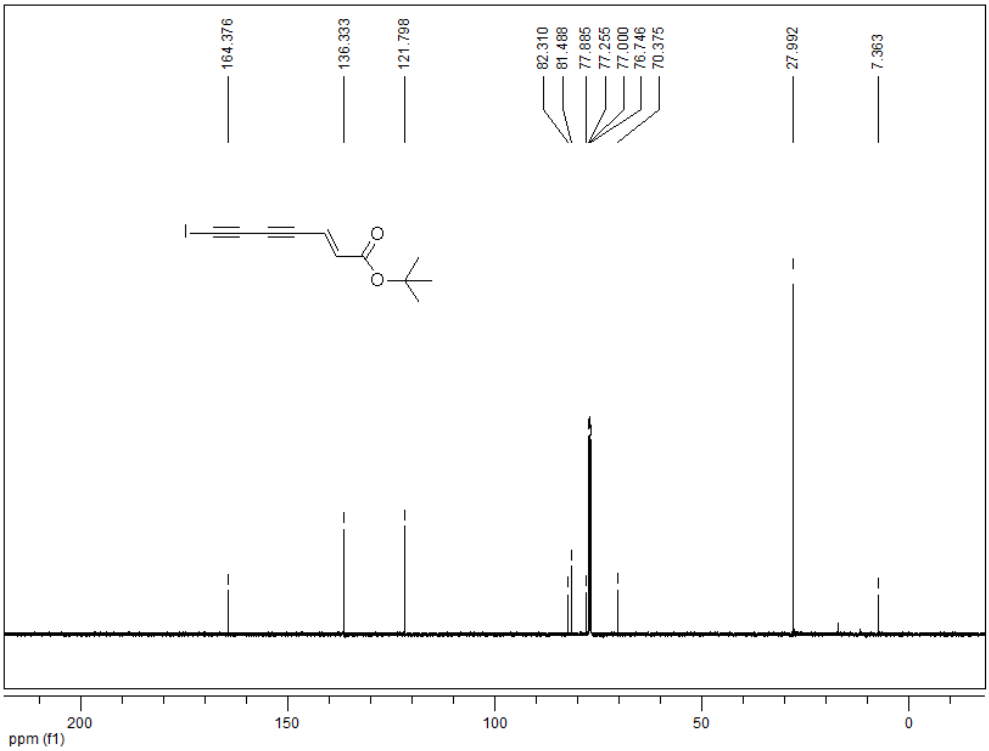

^{13}C-NMR (125 MHz, $CDCl_3$) spectrum of compound **2-43**

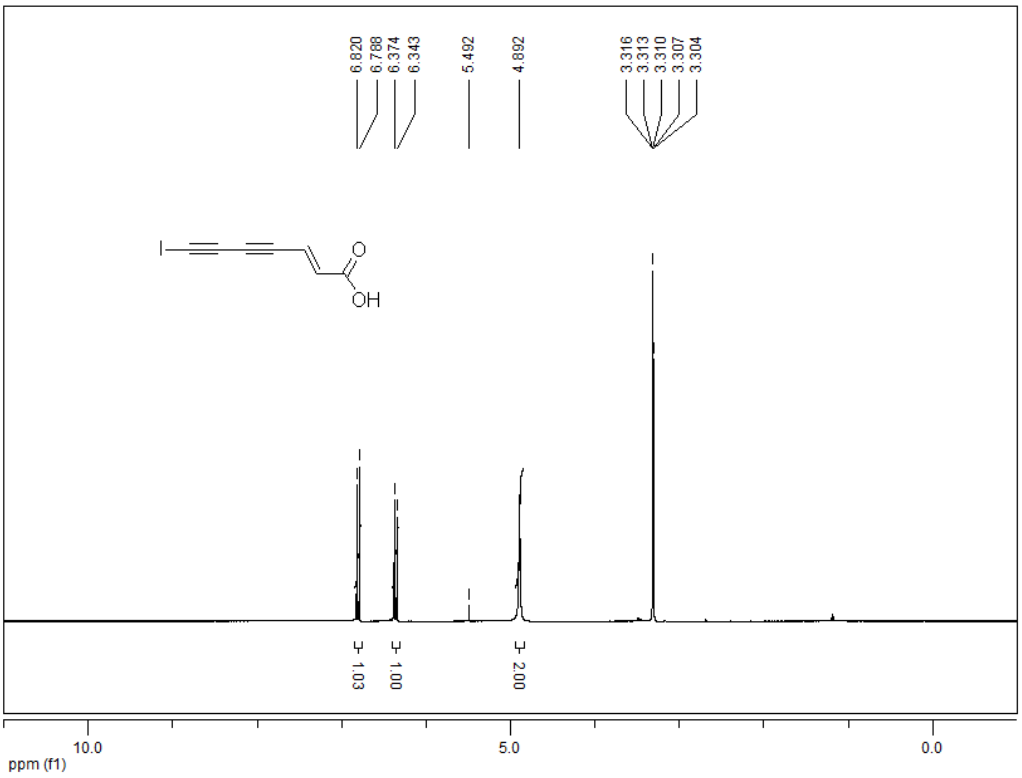

^{1}H-NMR (400 MHz, MeOD) spectrum of compound **2-4**

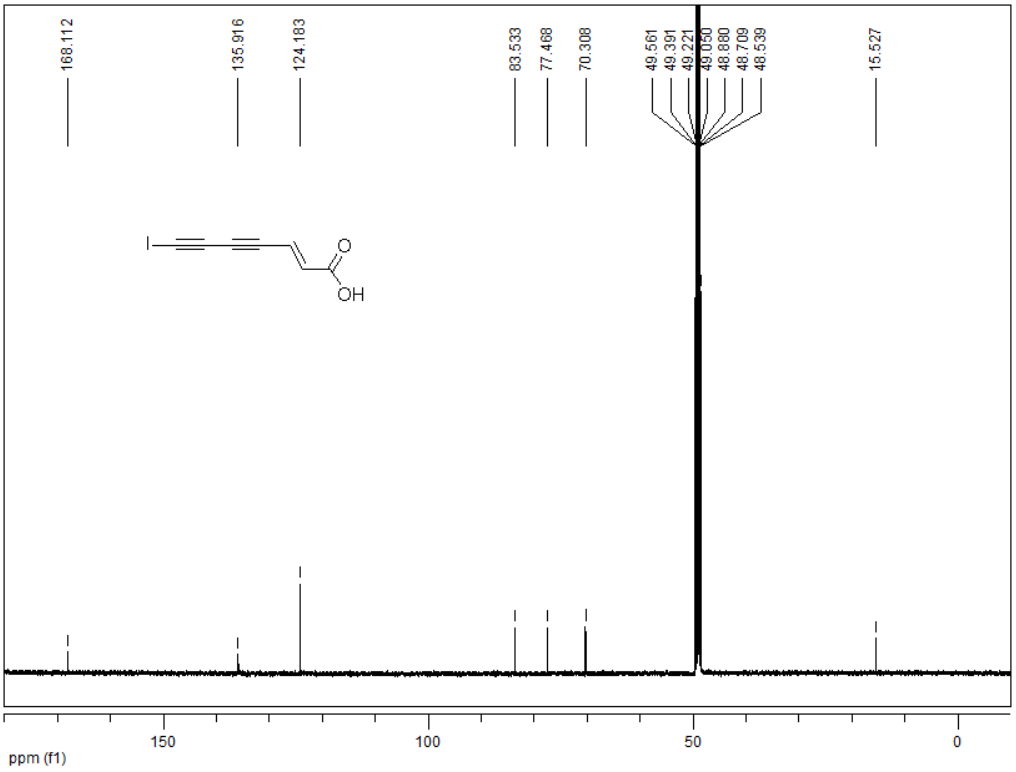

^{13}C-NMR (100 MHz, MeOD) spectrum of compound **2-4**

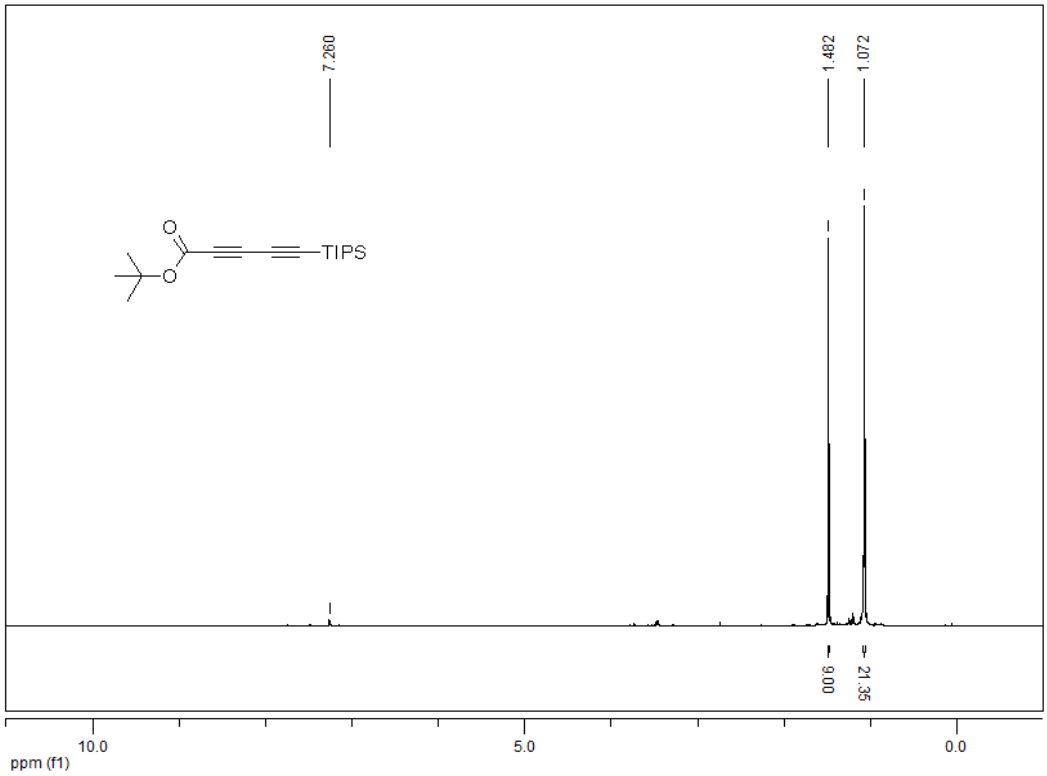

^{1}H-NMR (500 MHz, $CDCl_3$) spectrum of compound **2-45**

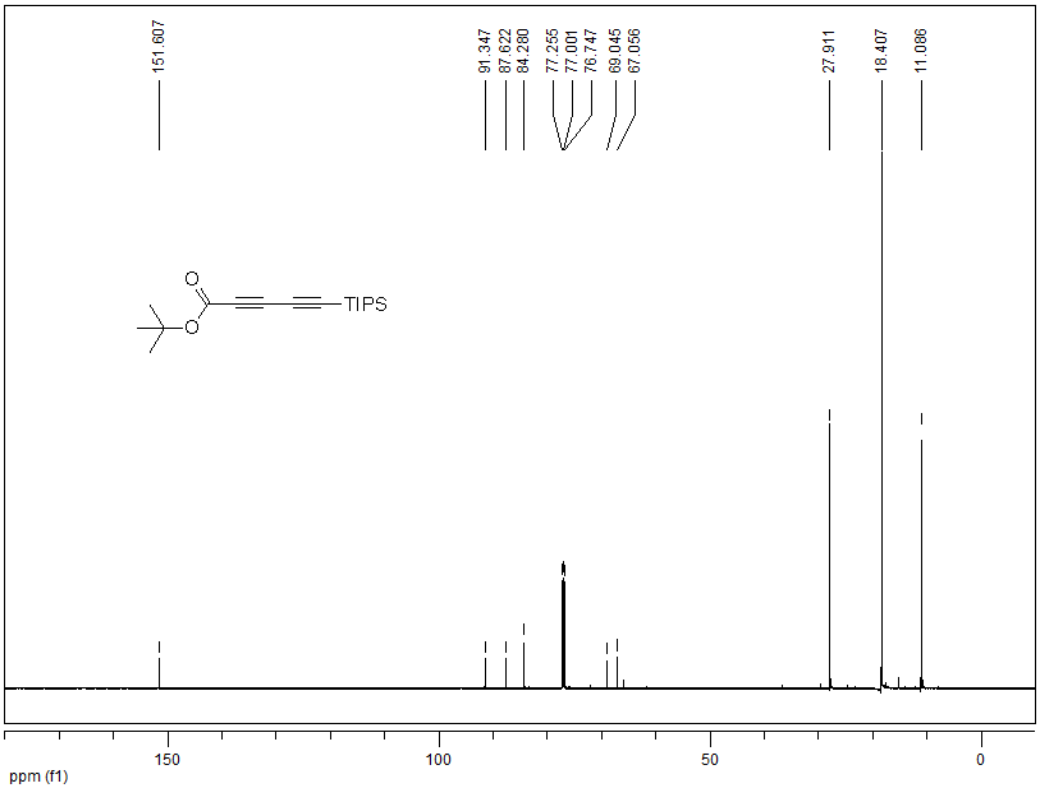

^{13}C-NMR (125 MHz, $CDCl_3$) spectrum of compound **2-4**

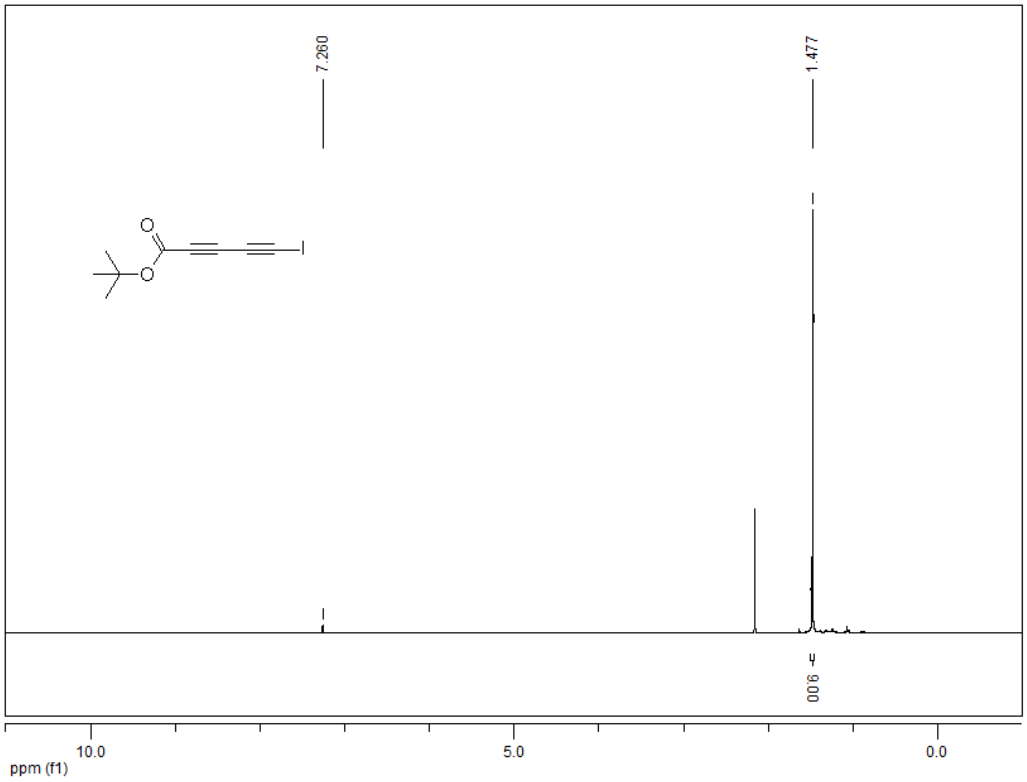

^{1}H-NMR (400 MHz, $CDCl_3$) spectrum of compound **2-46**

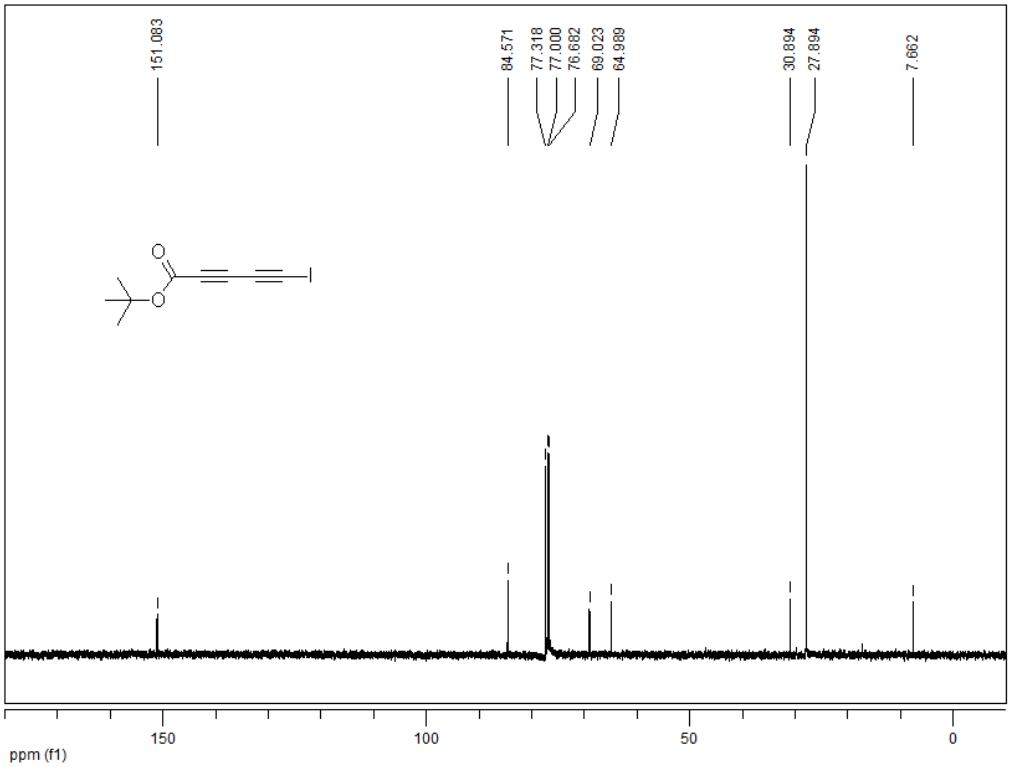

^{13}C-NMR (100 MHz, $CDCl_3$) spectrum of compound **2-46**

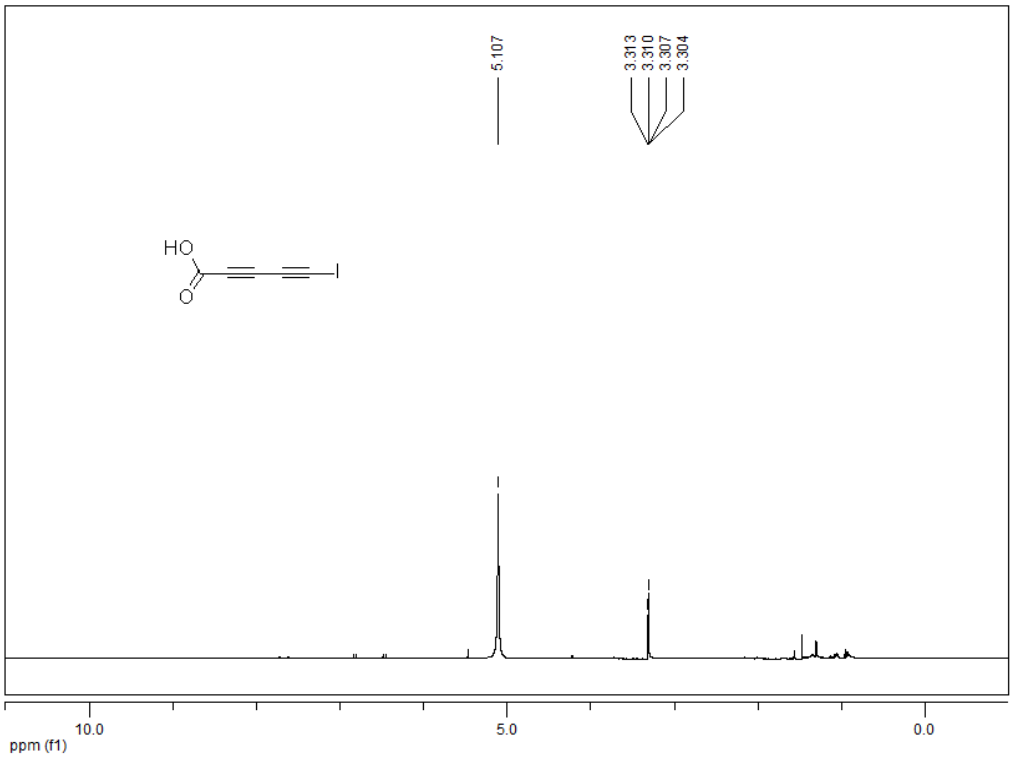

^{1}H-NMR (500 MHz, MeOD) spectrum of compound **2-1**

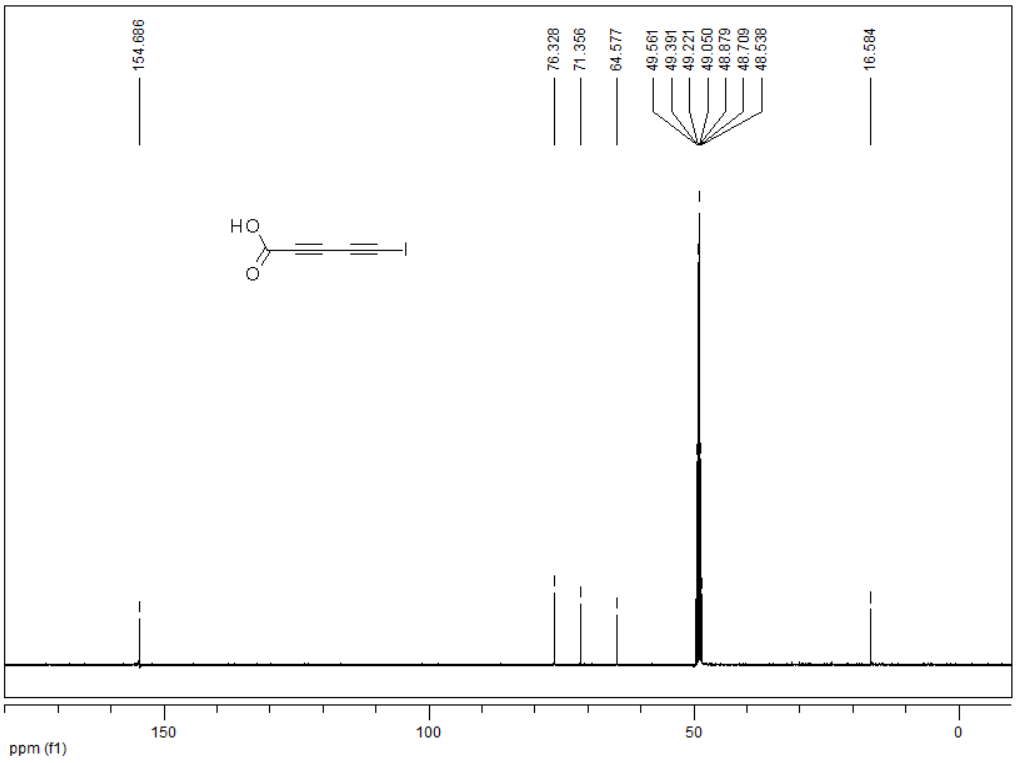

^{13}C-NMR (125 MHz, MeOD) spectrum of compound **2-1**

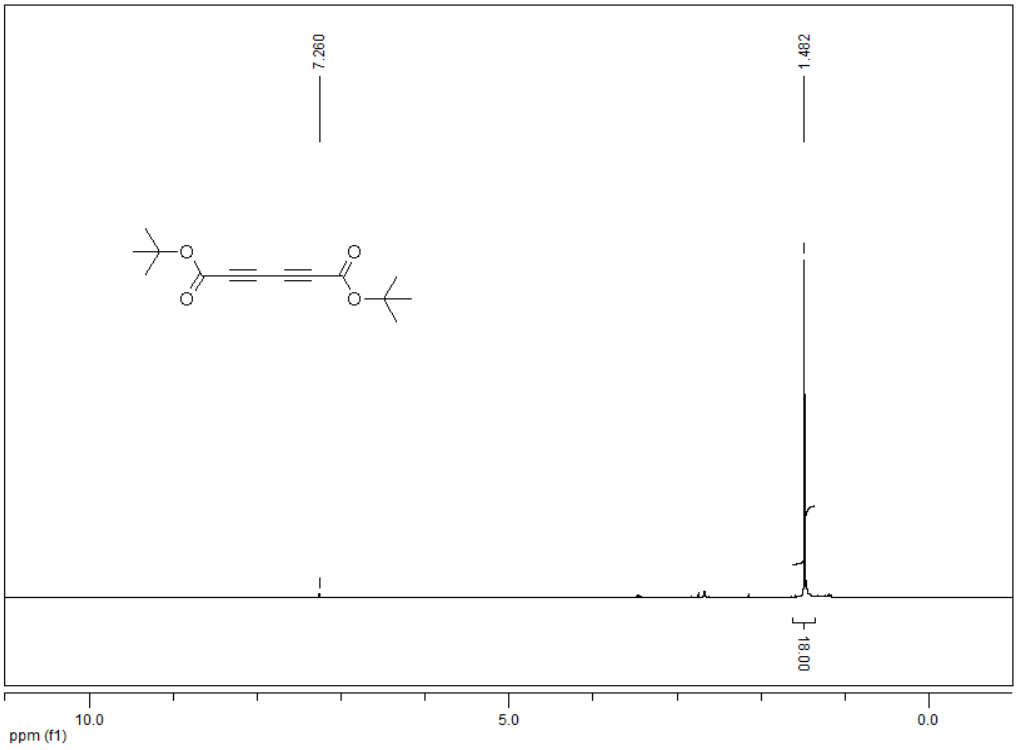

^{1}H-NMR (400 MHz, $CDCl_3$) spectrum of compound **2-49**

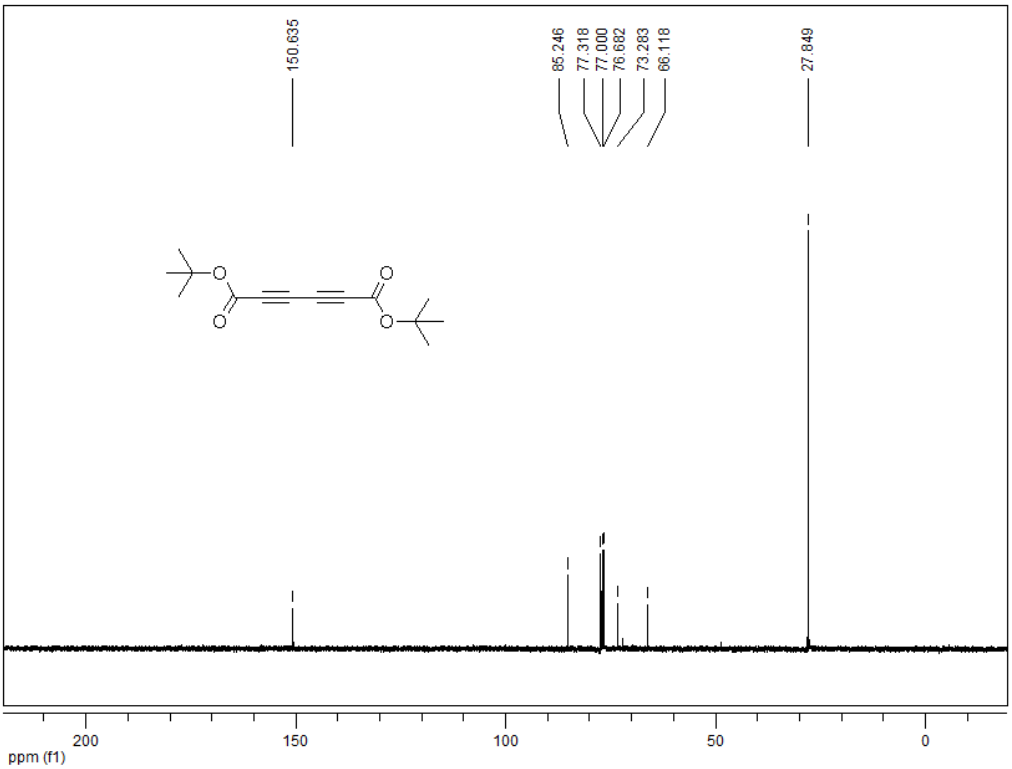

^{13}C-NMR (100 MHz, $CDCl_3$) spectrum of compound **2-49**

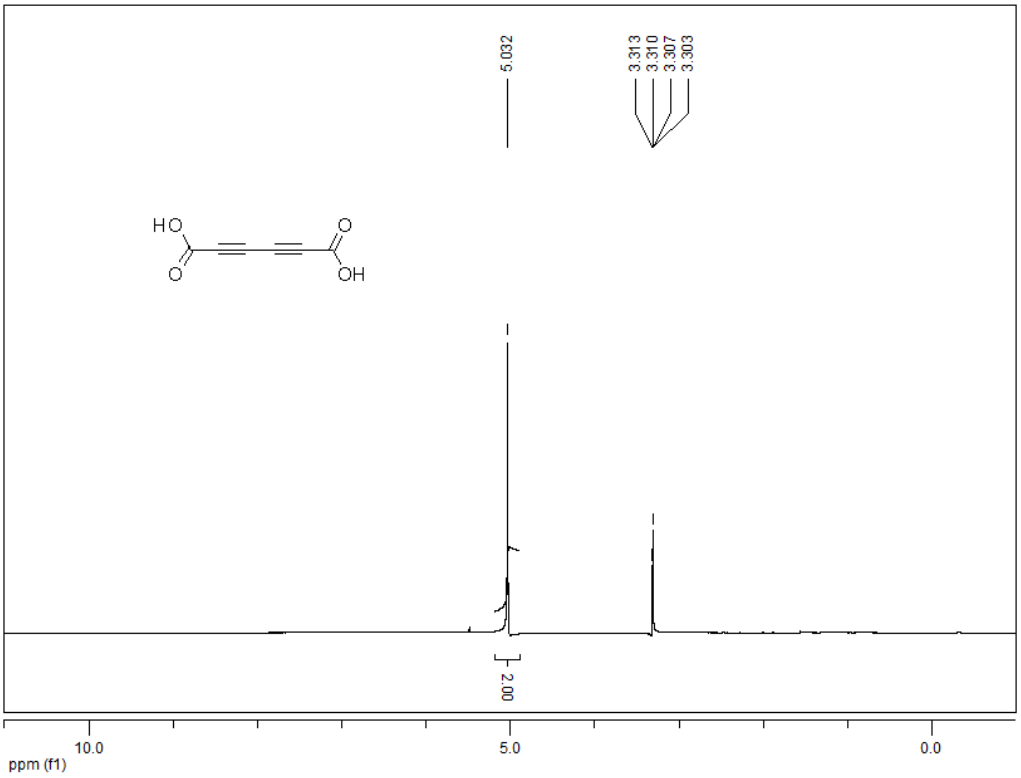

^{1}H-NMR (500 MHz, MeOD) spectrum of compound **2-8**

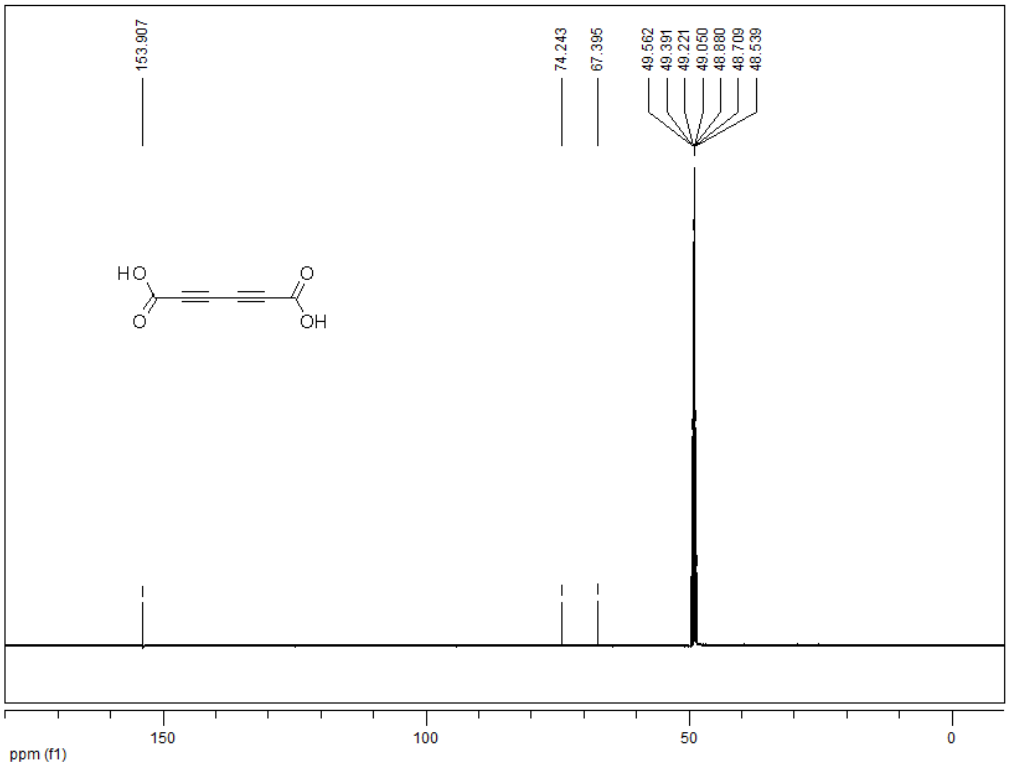

^{13}C-NMR (125 MHz, MeOD) spectrum of compound **2-8**

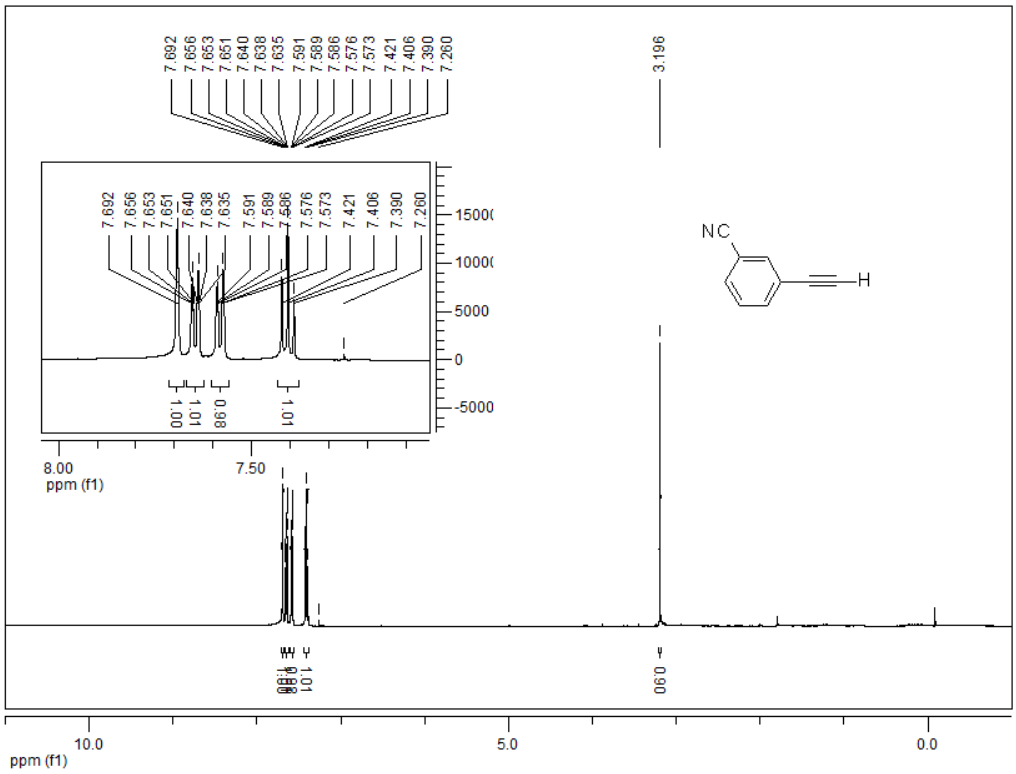

^{1}H-NMR (500 MHz, $CDCl_3$) spectrum of compound **2-19**

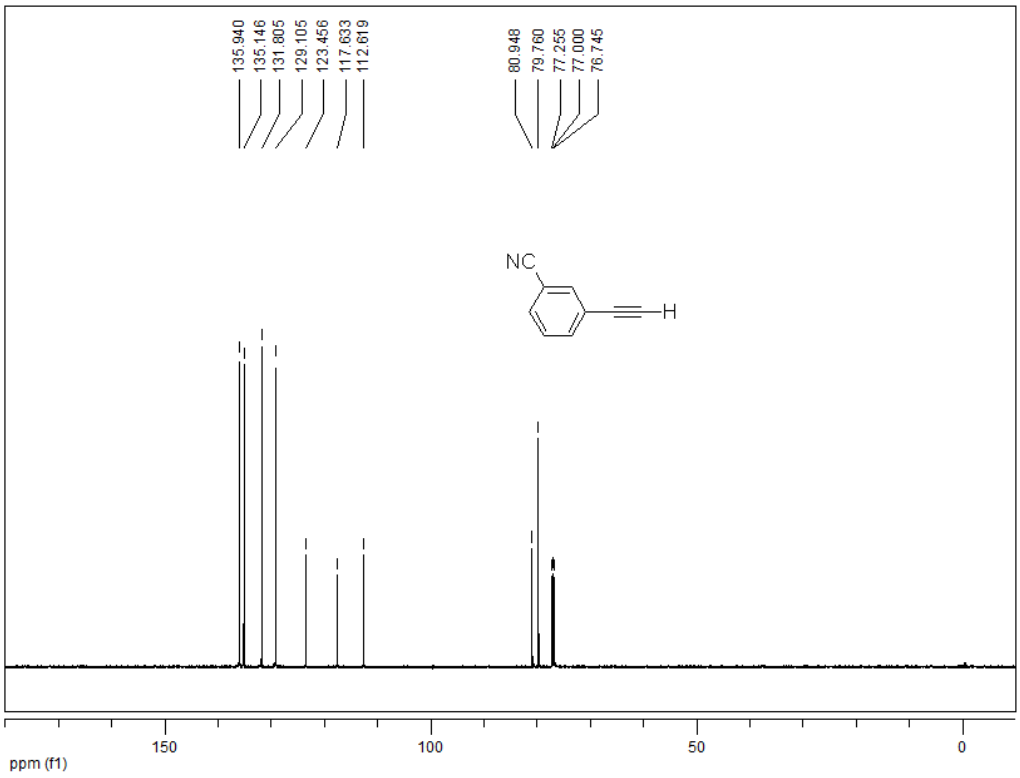

^{13}C-NMR (125 MHz, $CDCl_3$) spectrum of compound **2-19**

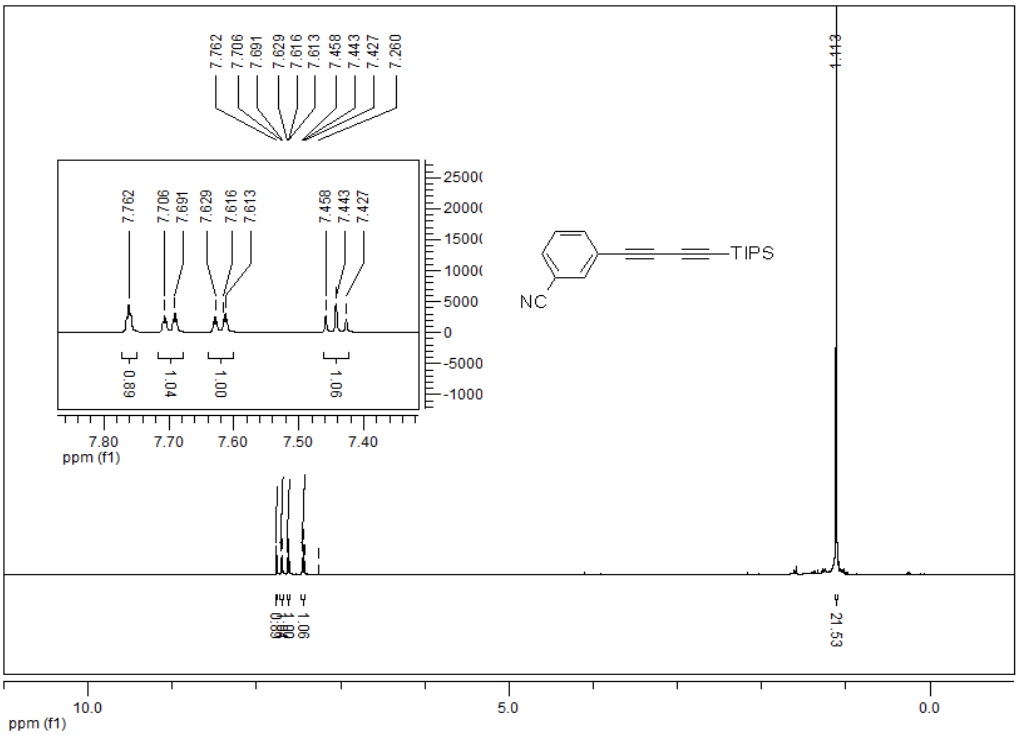

^{1}H-NMR (400 MHz, $CDCl_3$) spectrum of compound **2-21**

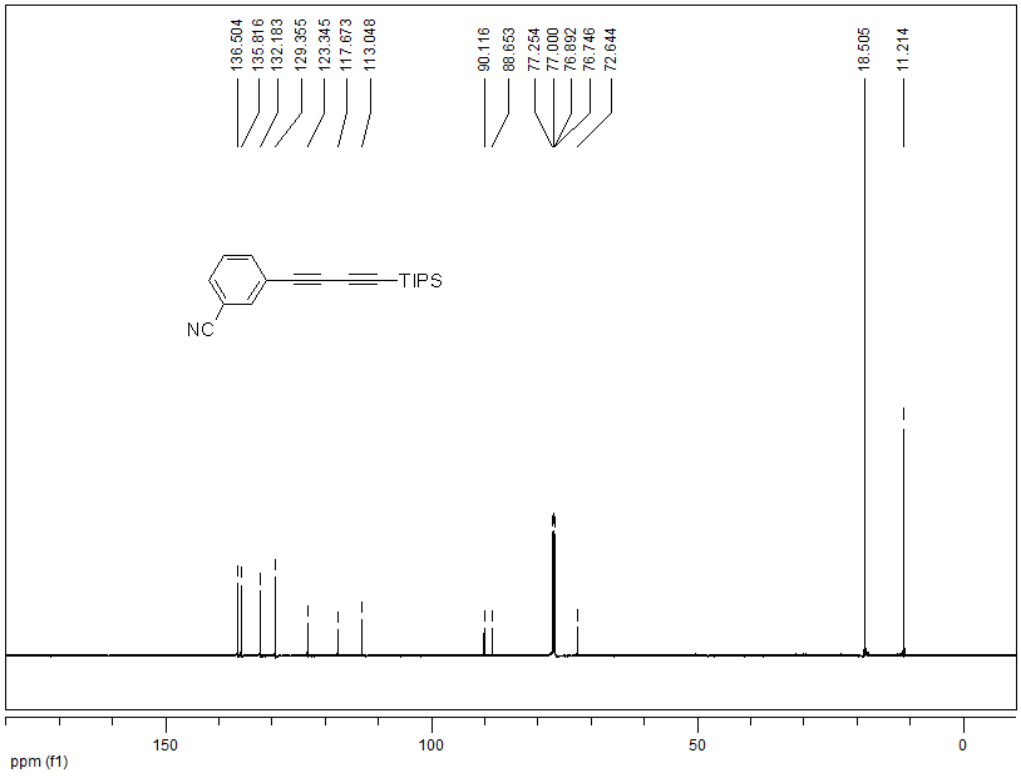

^{13}C-NMR (100 MHz, $CDCl_3$) spectrum of compound **2-21**

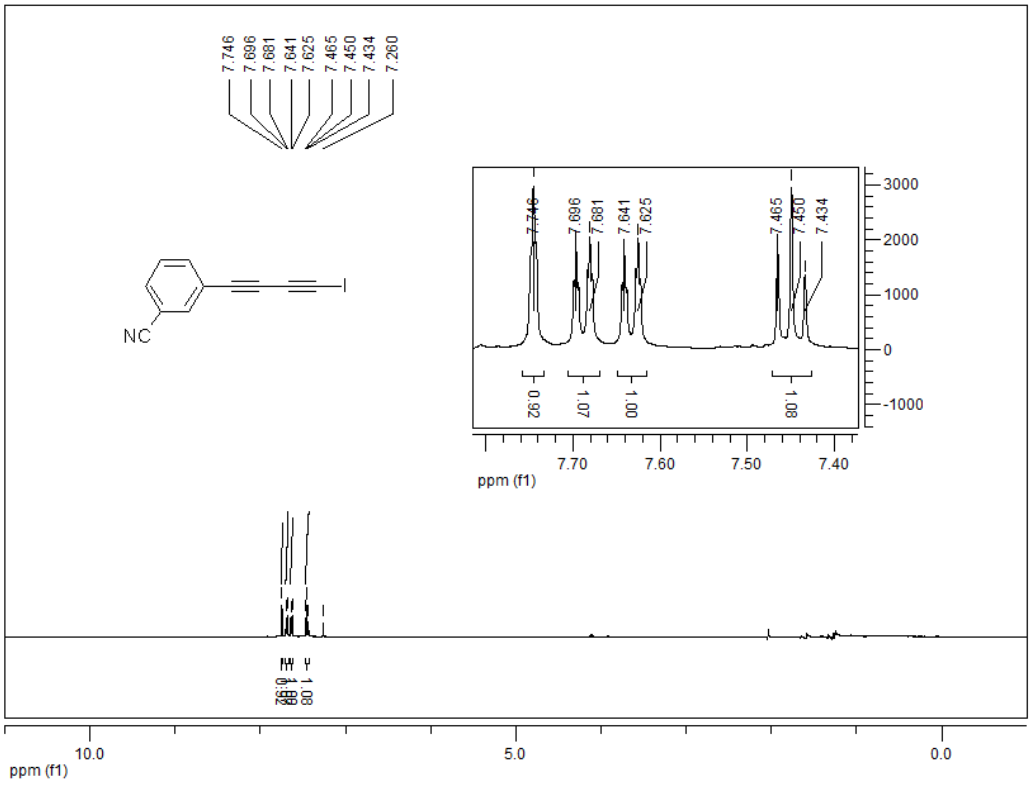

^{1}H-NMR (500 MHz, $CDCl_3$) spectrum of compound **2-3**

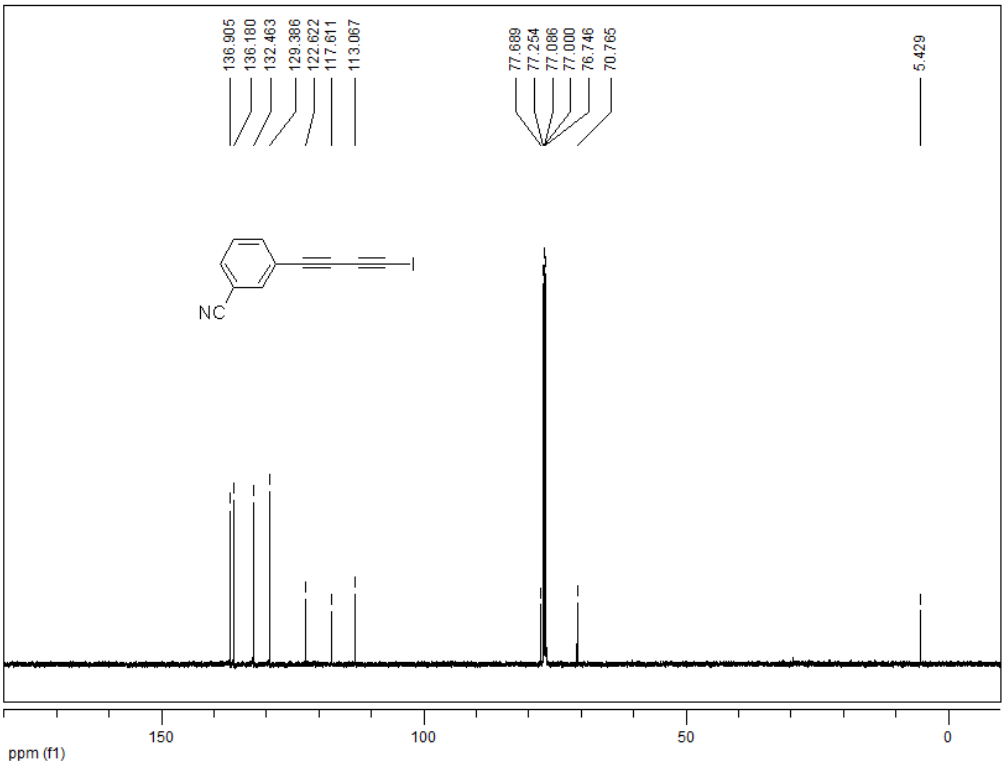

^{13}C-NMR (125 MHz, $CDCl_3$) spectrum of compound **2-3**

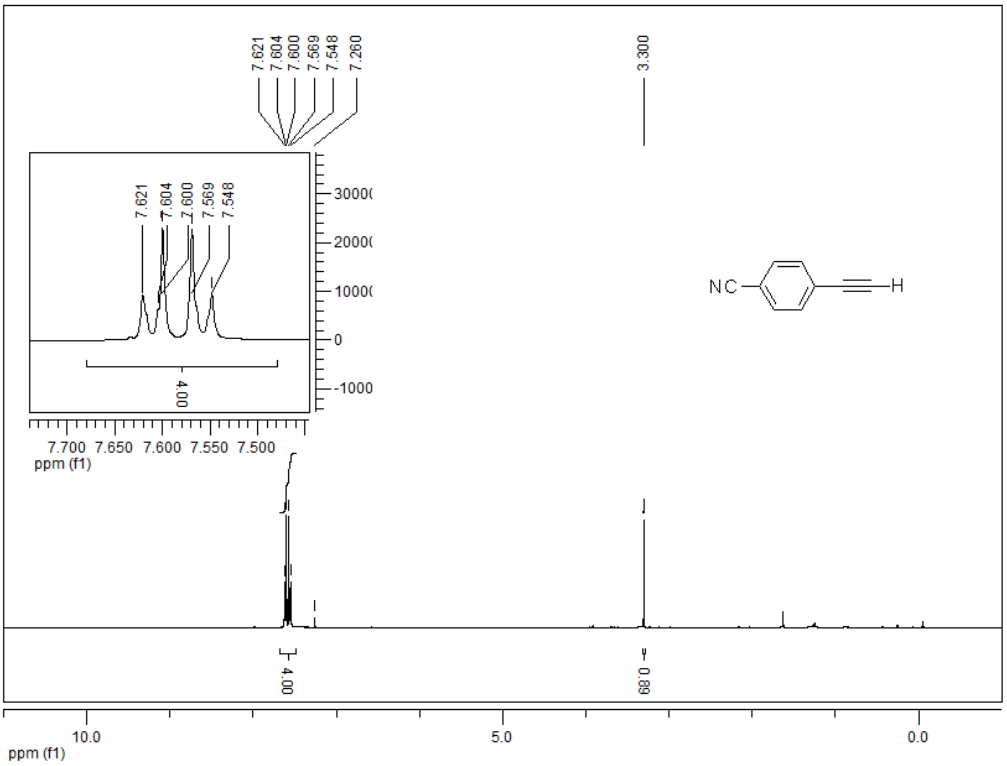

^{1}H-NMR (500 MHz, $CDCl_3$) spectrum of compound **2-18**

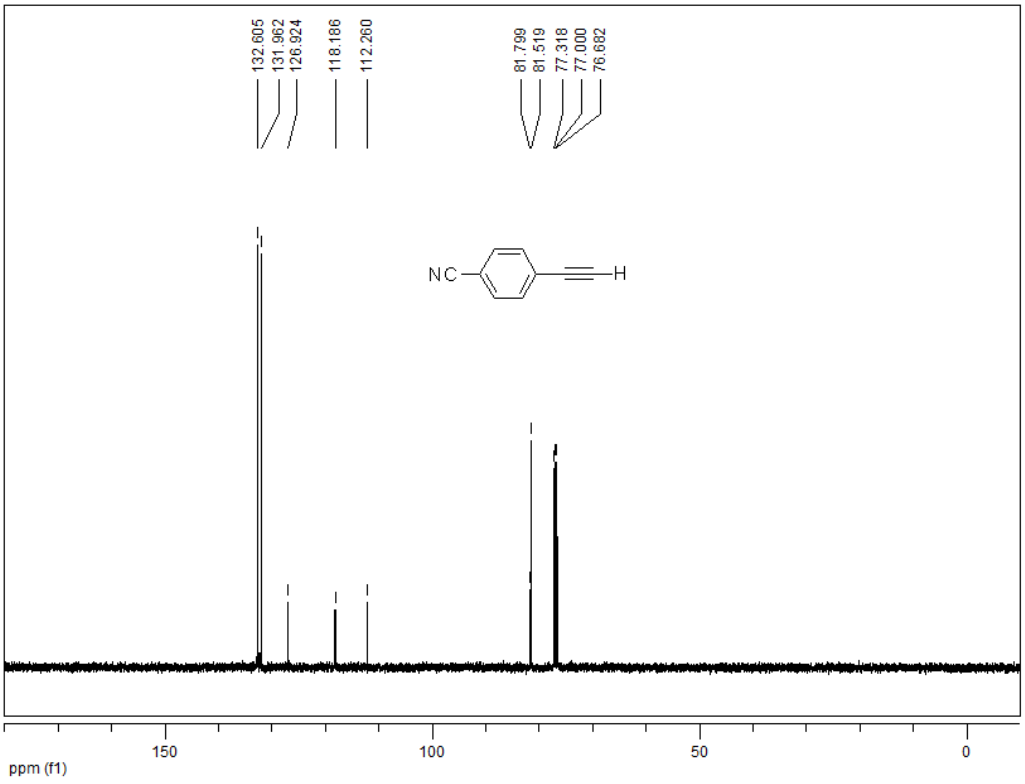

^{13}C-NMR (125 MHz, $CDCl_3$) spectrum of compound **2-18**

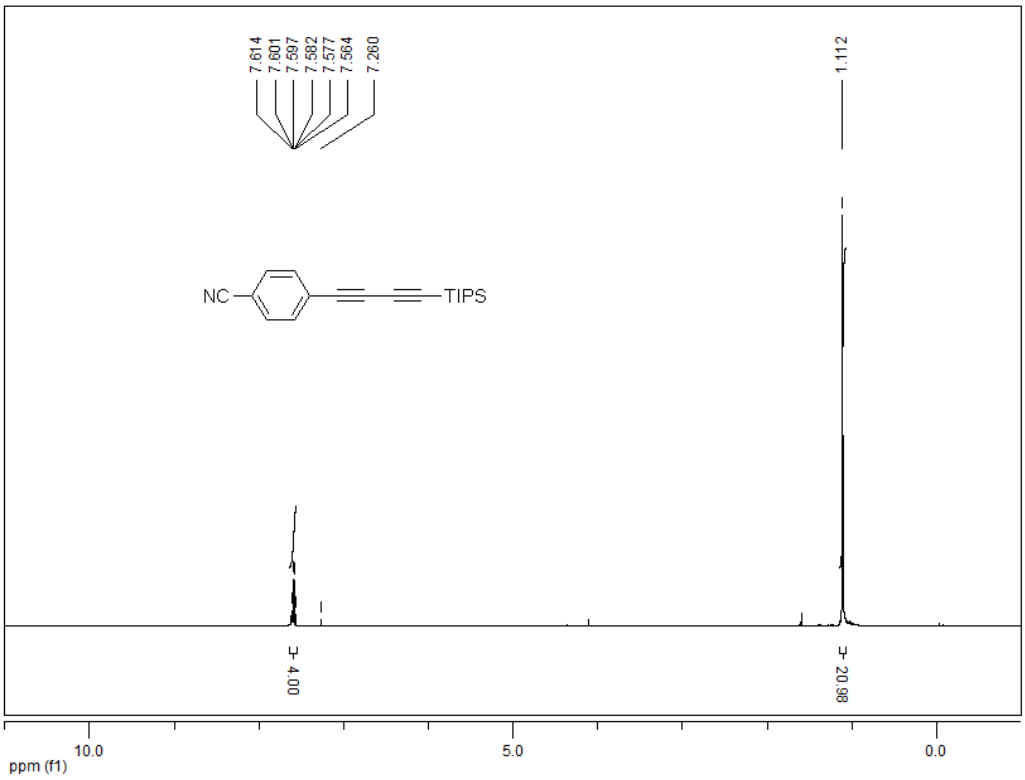

^{1}H-NMR (500 MHz, $CDCl_3$) spectrum of compound **2-20**

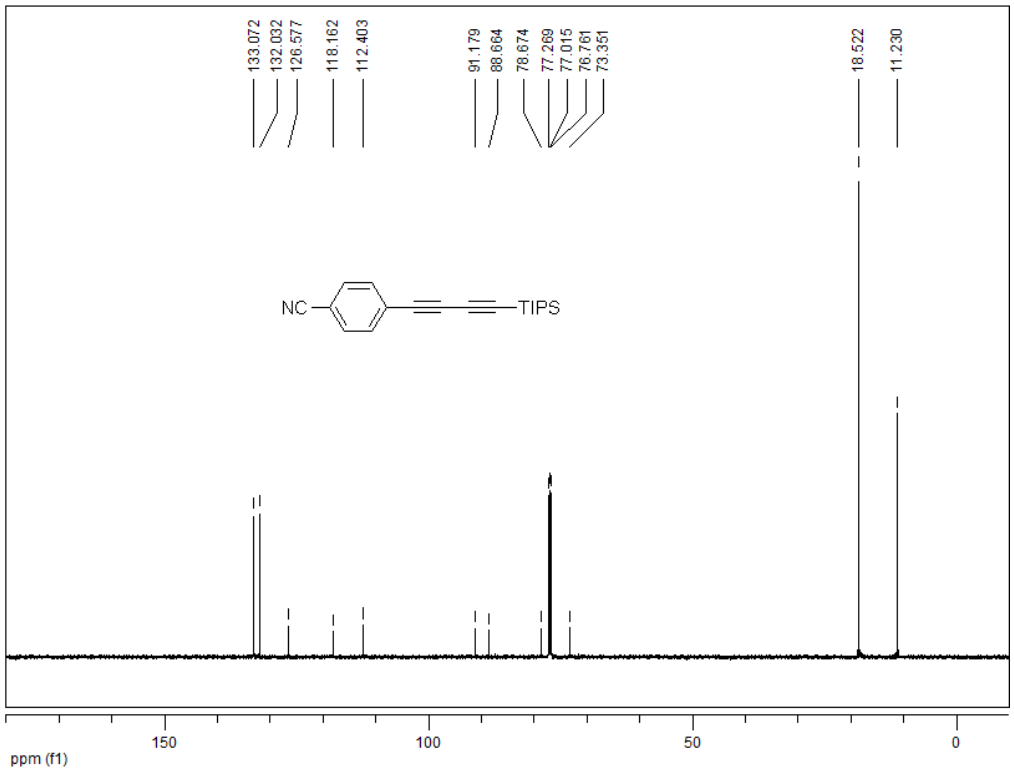

^{13}C-NMR (125 MHz, $CDCl_3$) spectrum of compound **2-20**

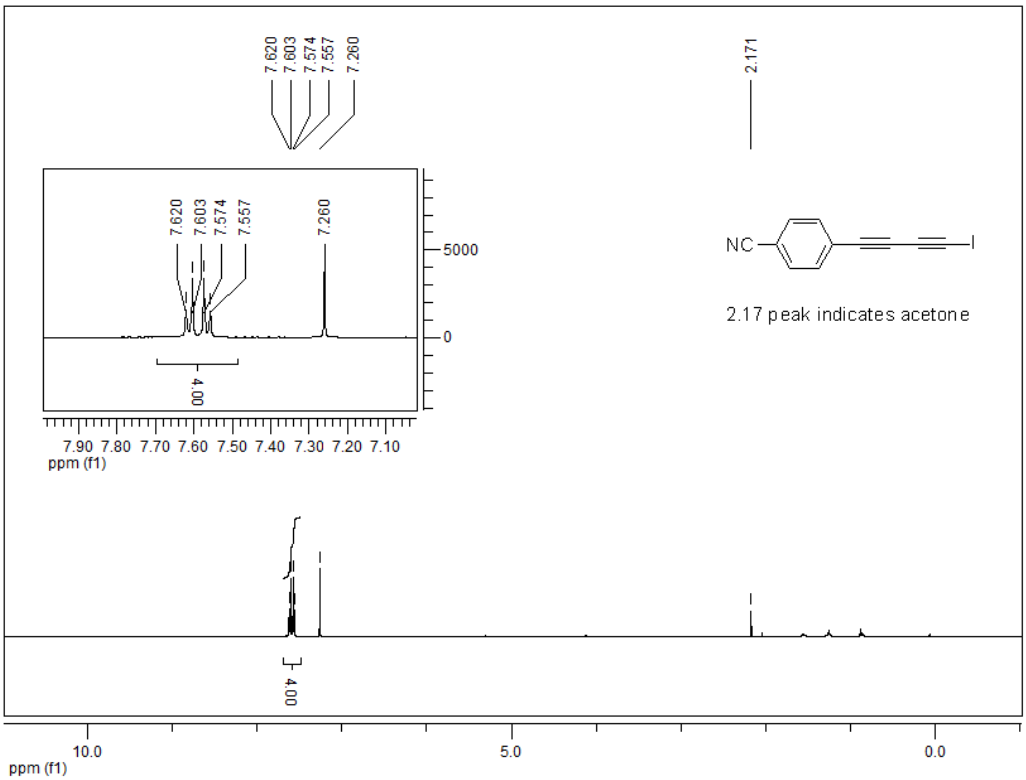

^{1}H-NMR (500 MHz, $CDCl_3$) spectrum of compound **2-2**

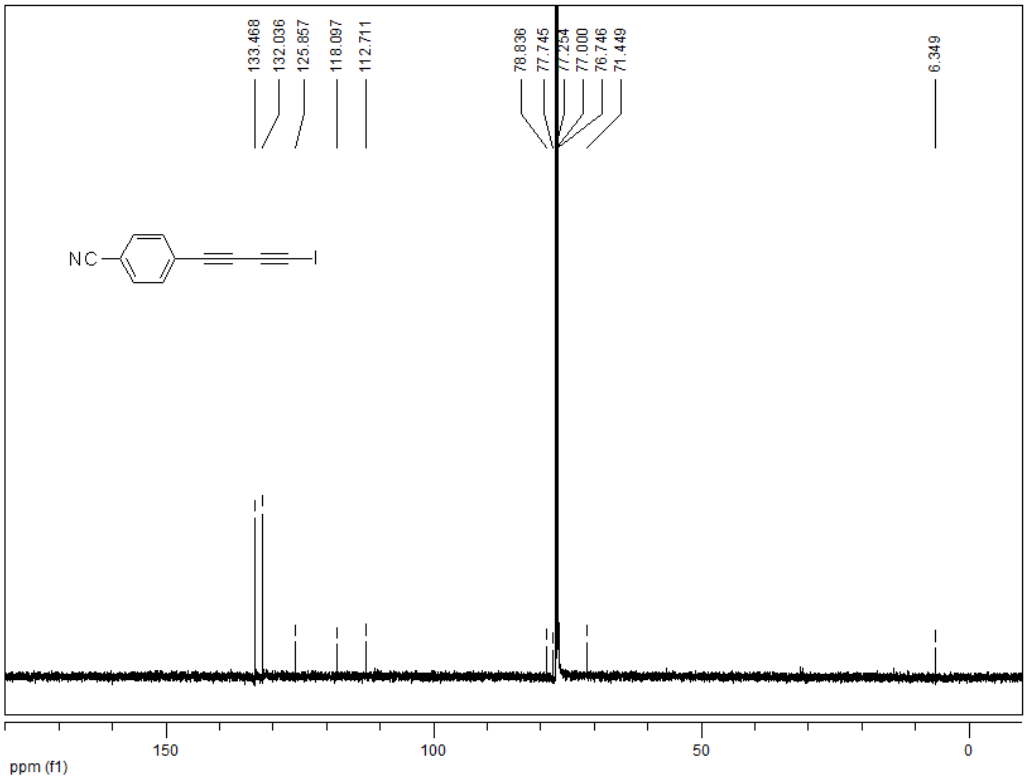

^{13}C-NMR (125 MHz, $CDCl_3$) spectrum of compound **2-2**

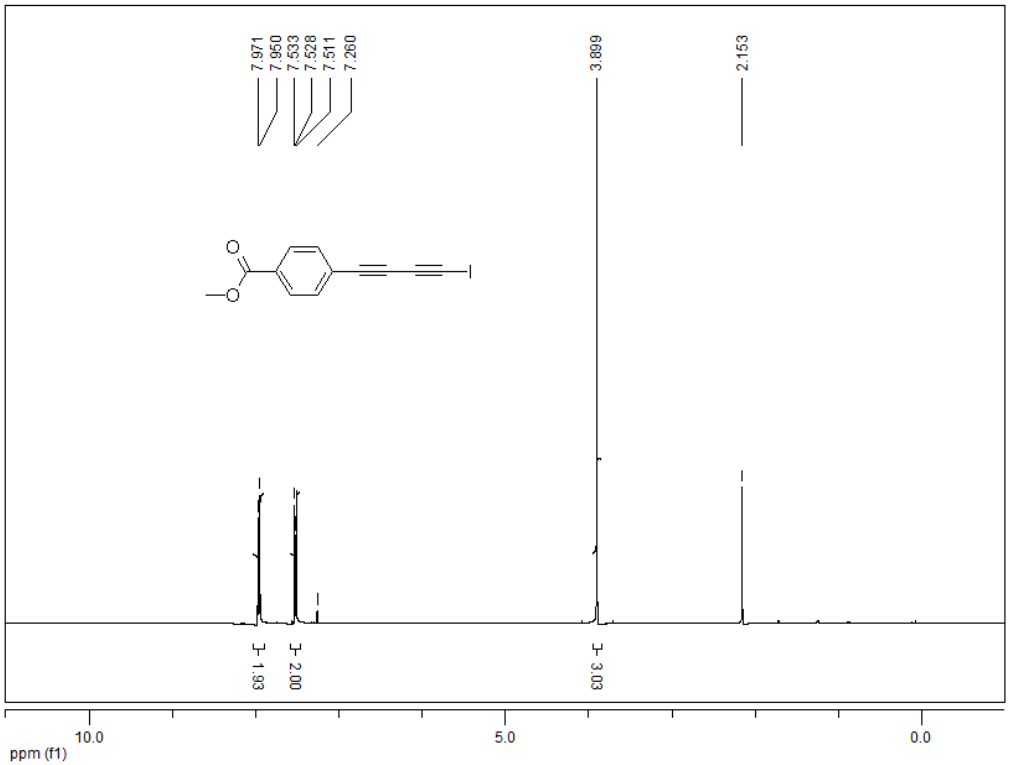

^{1}H-NMR (400 MHz, $CDCl_3$) spectrum (2.153 is acetone)

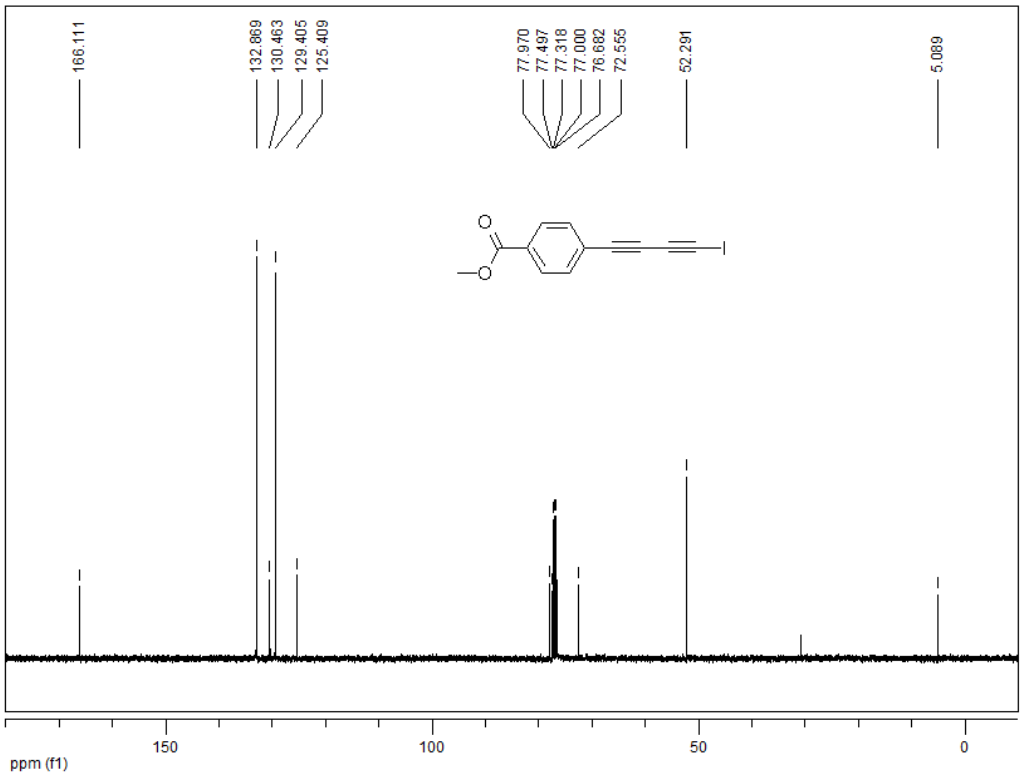

^{13}C-NMR (100 MHz, $CDCl_3$) spectrum

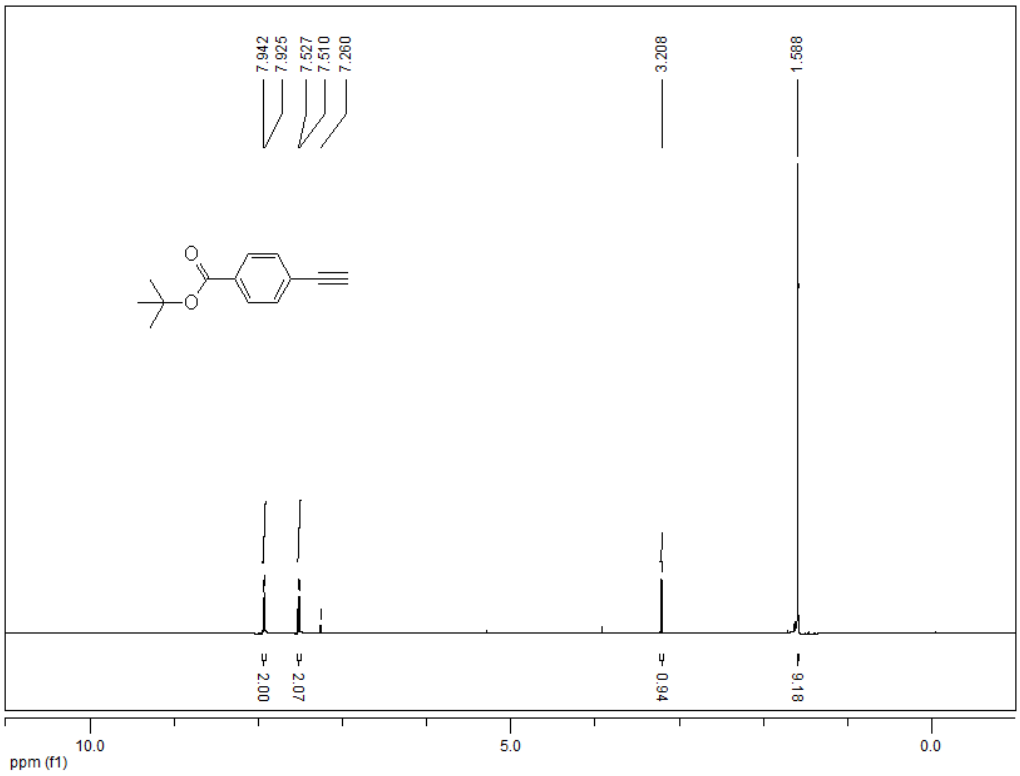

^{1}H-NMR (500 MHz, $CDCl_3$) spectrum of compound **2-29**

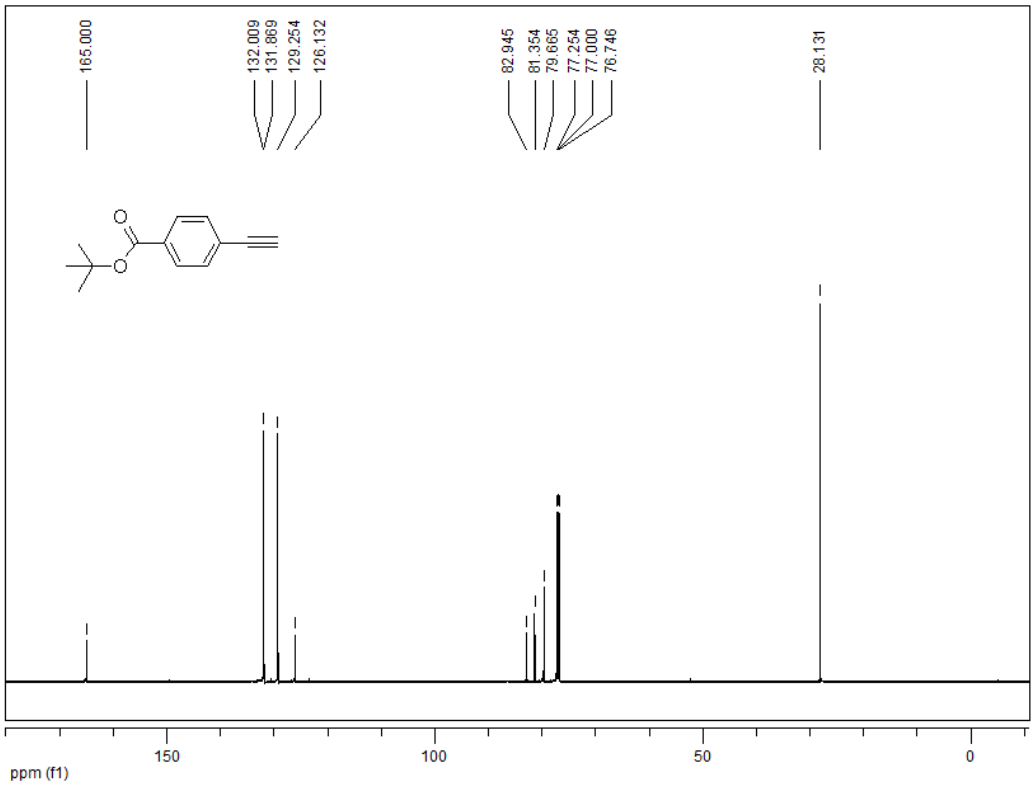

^{13}C-NMR (125 MHz, $CDCl_3$) spectrum of compound **2-29**

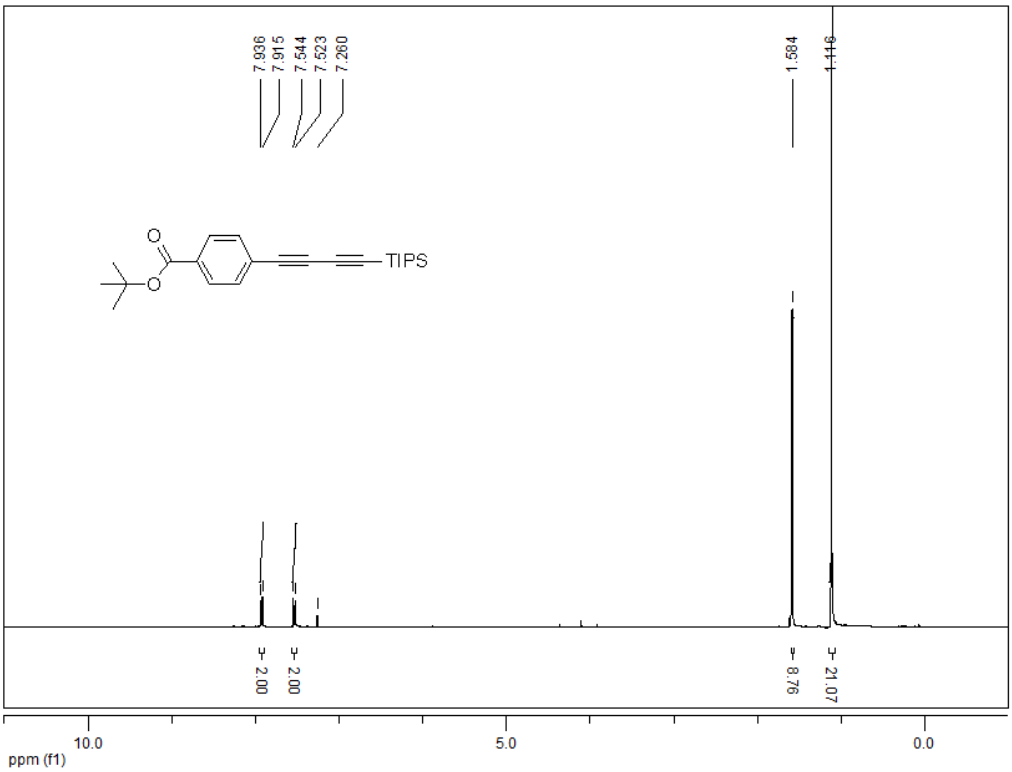

^{1}H-NMR (400 MHz, $CDCl_3$) spectrum of compound **2-30**

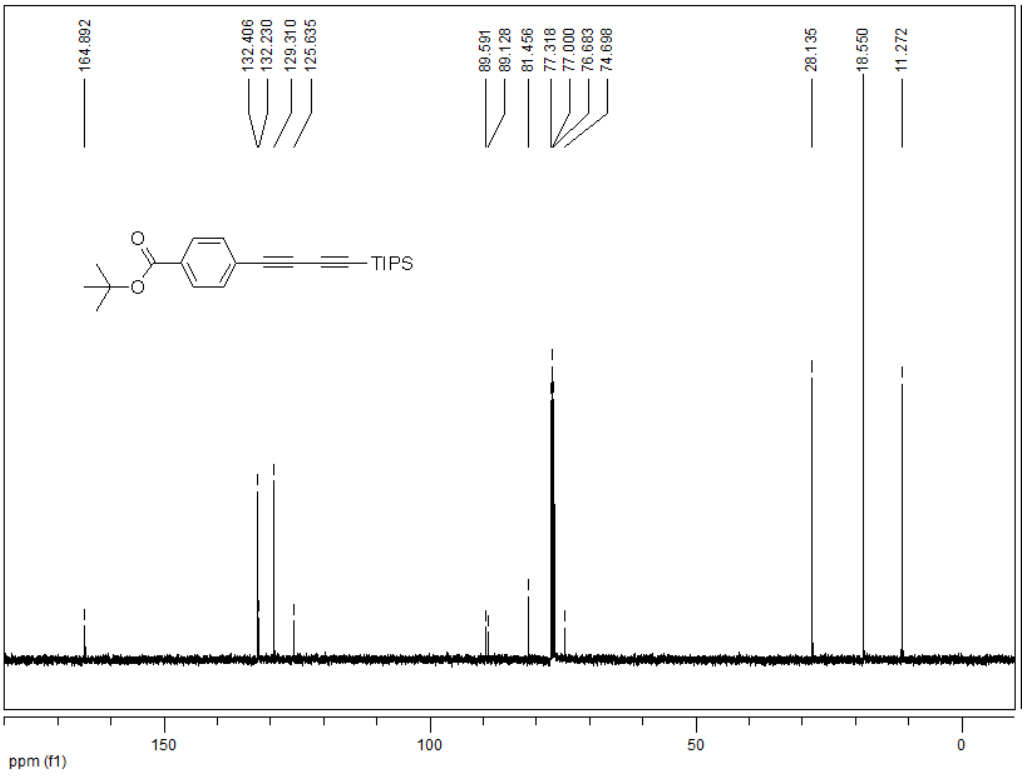

^{1}H-NMR (100 MHz, $CDCl_3$) spectrum of compound **2-30**

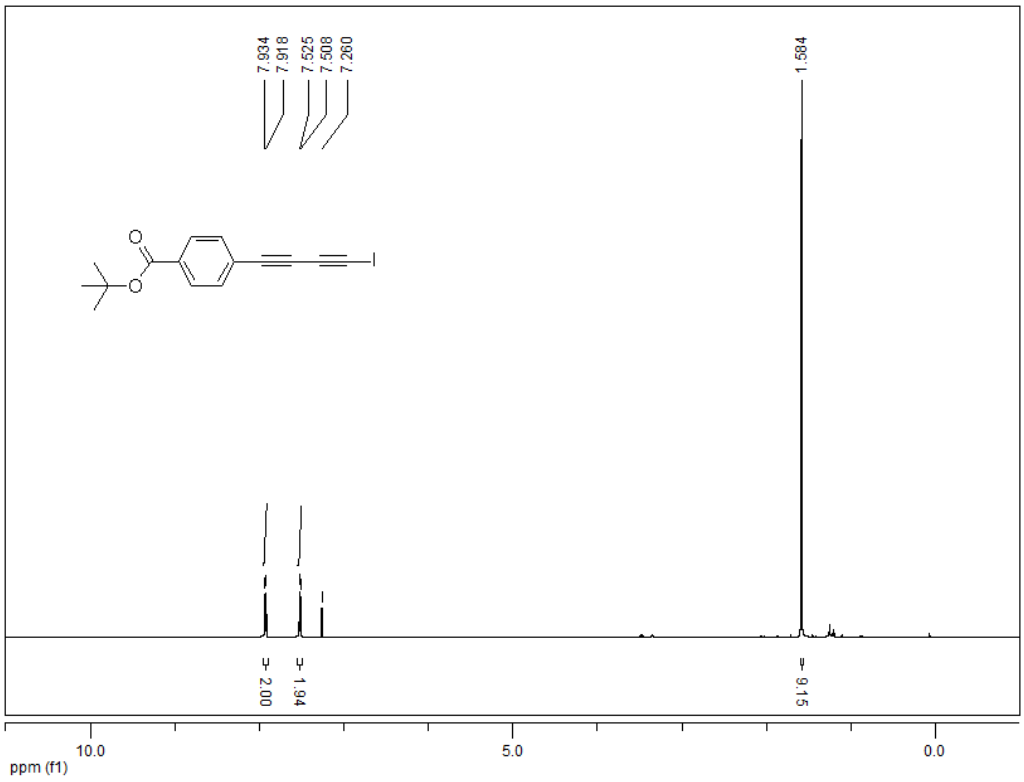

^{1}H-NMR (500 MHz, $CDCl_3$) spectrum of compound **2-5**

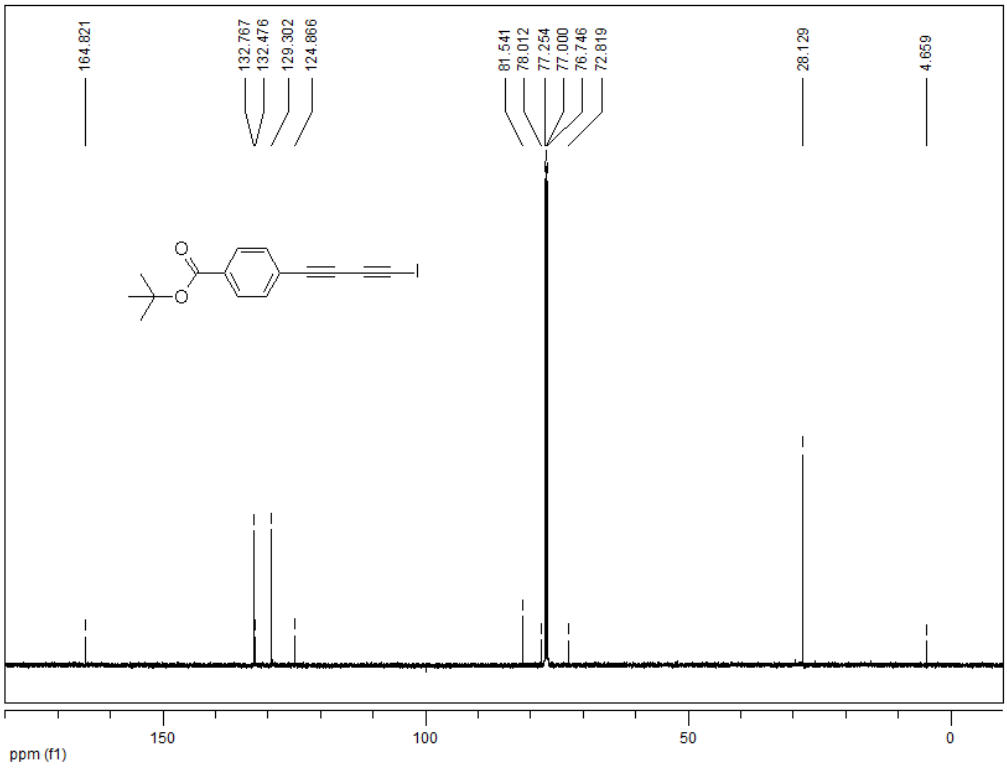

^{13}C-NMR (125 MHz, $CDCl_3$) spectrum of compound **2-5**

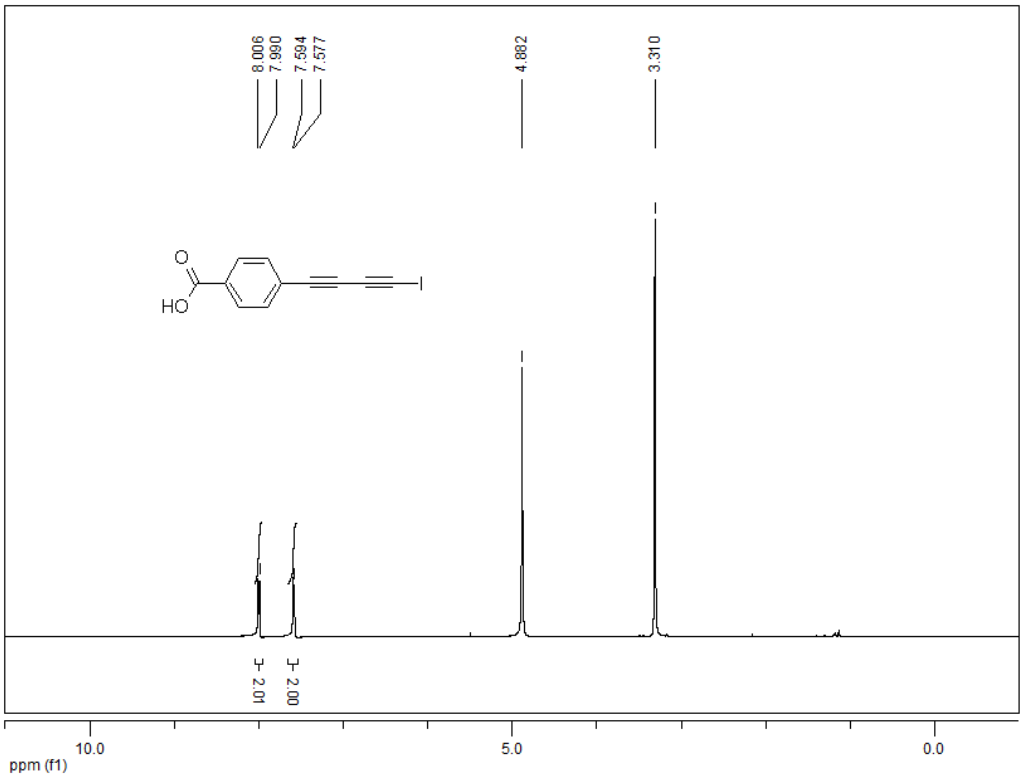

^{1}H-NMR (500 MHz, MeOD) spectrum of compound **2-5**

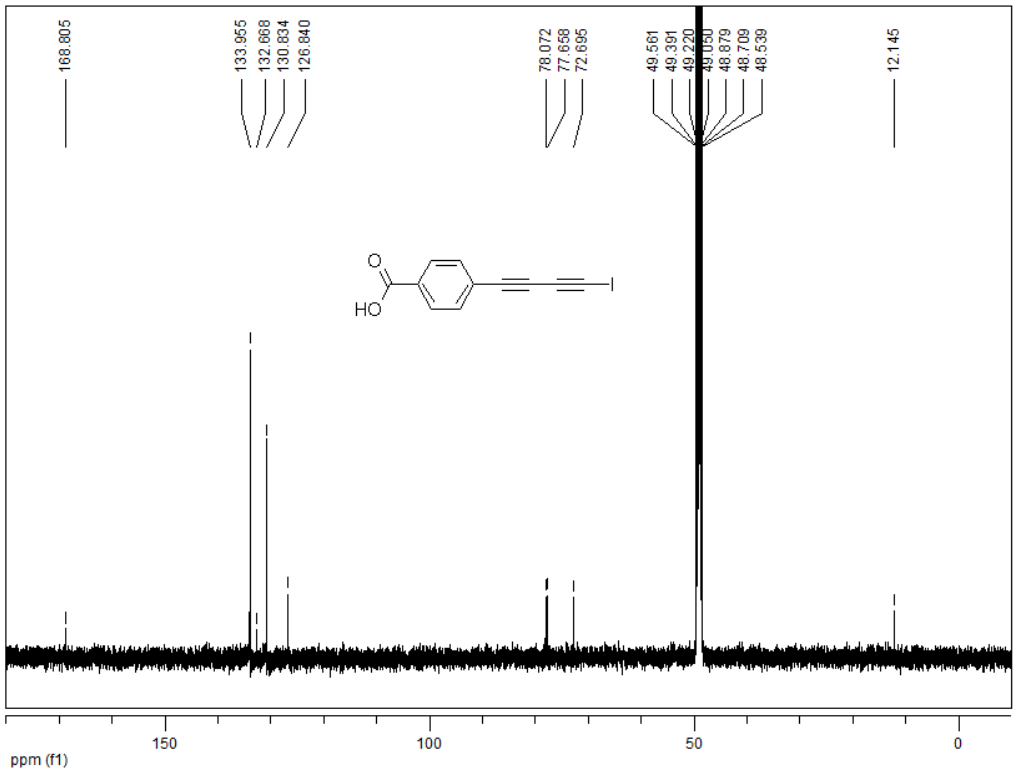

^{13}C-NMR (125 MHz, MeOD) spectrum of compound **2-5**

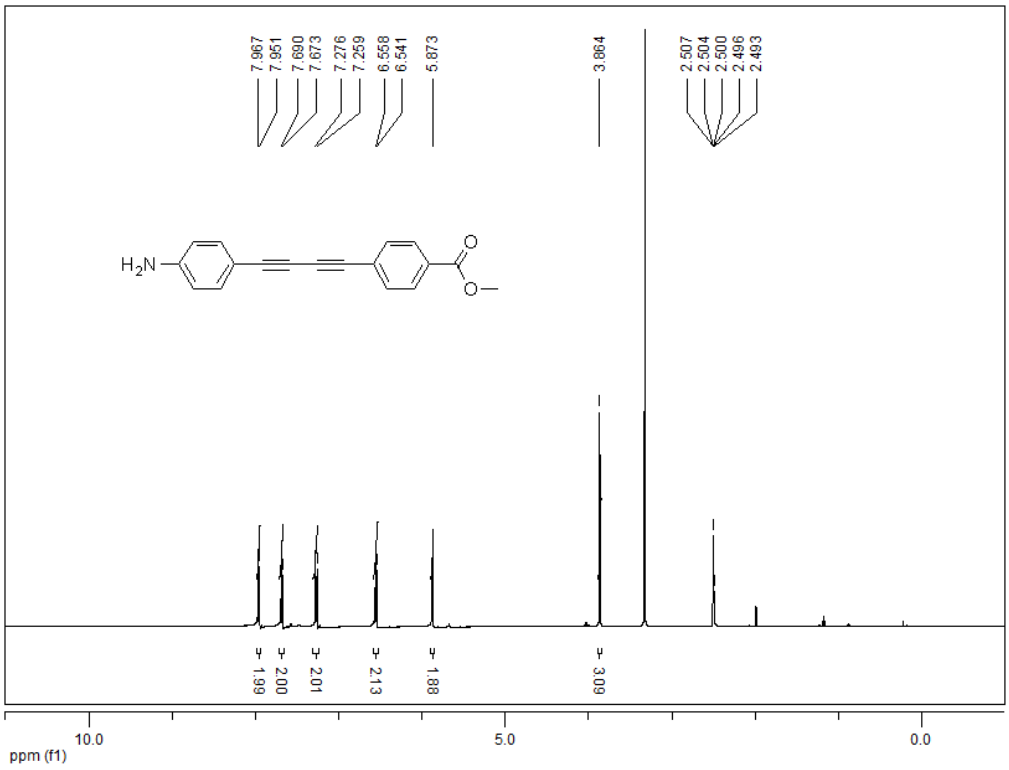

^{1}H-NMR (500 MHz, DMSO) spectrum of compound **2-60**

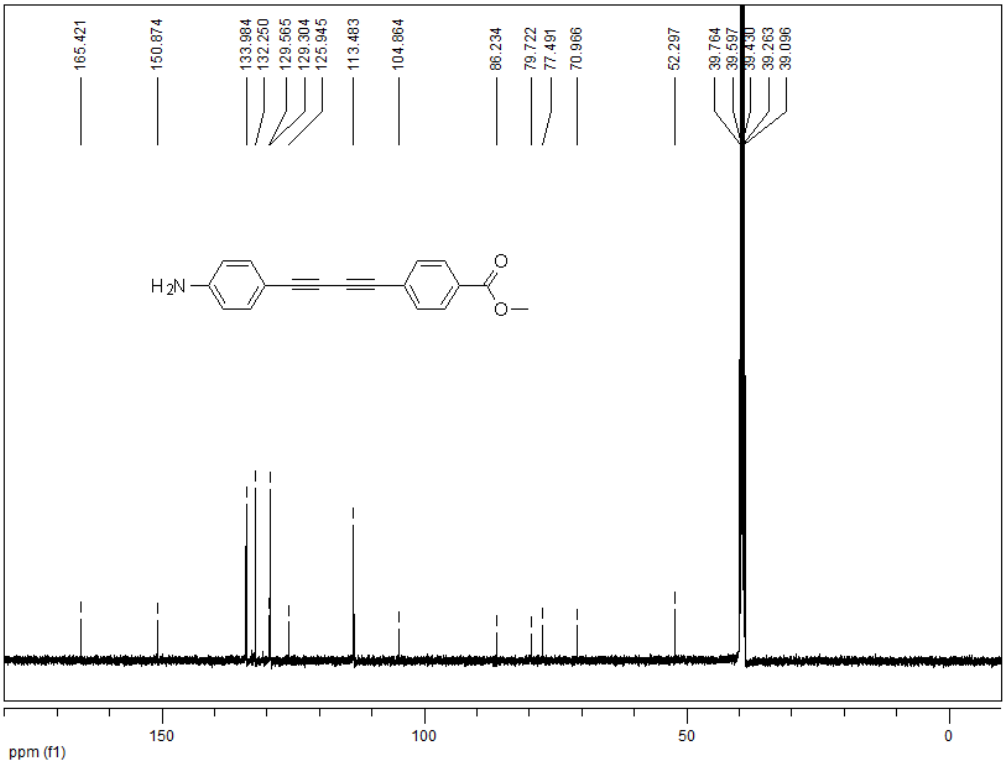

^{13}C-NMR (125 MHz, DMSO) spectrum of compound **2-60**

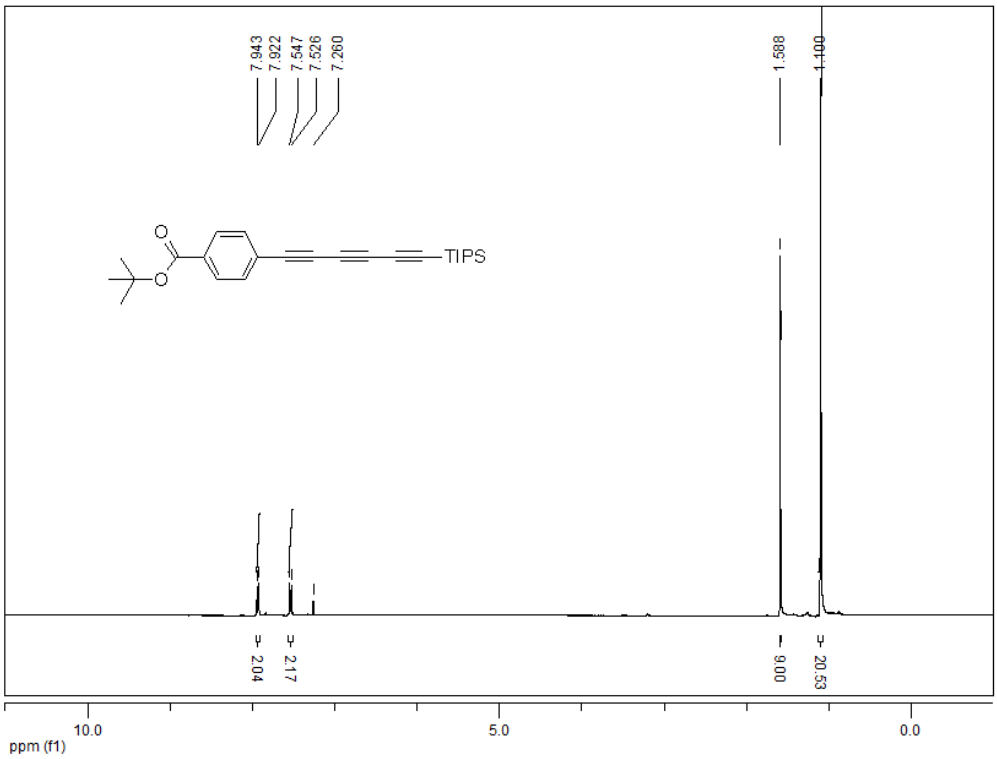

^{1}H-NMR (400 MHz, $CDCl_3$) spectrum

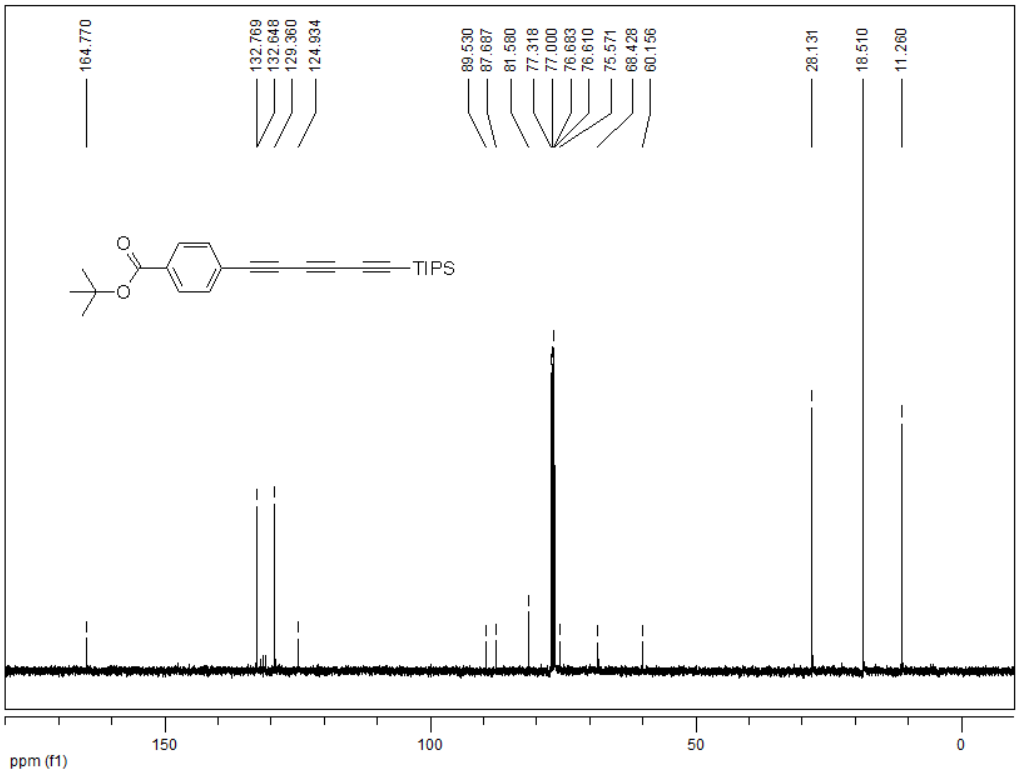

^{13}C-NMR (100 MHz, $CDCl_3$) spectrum

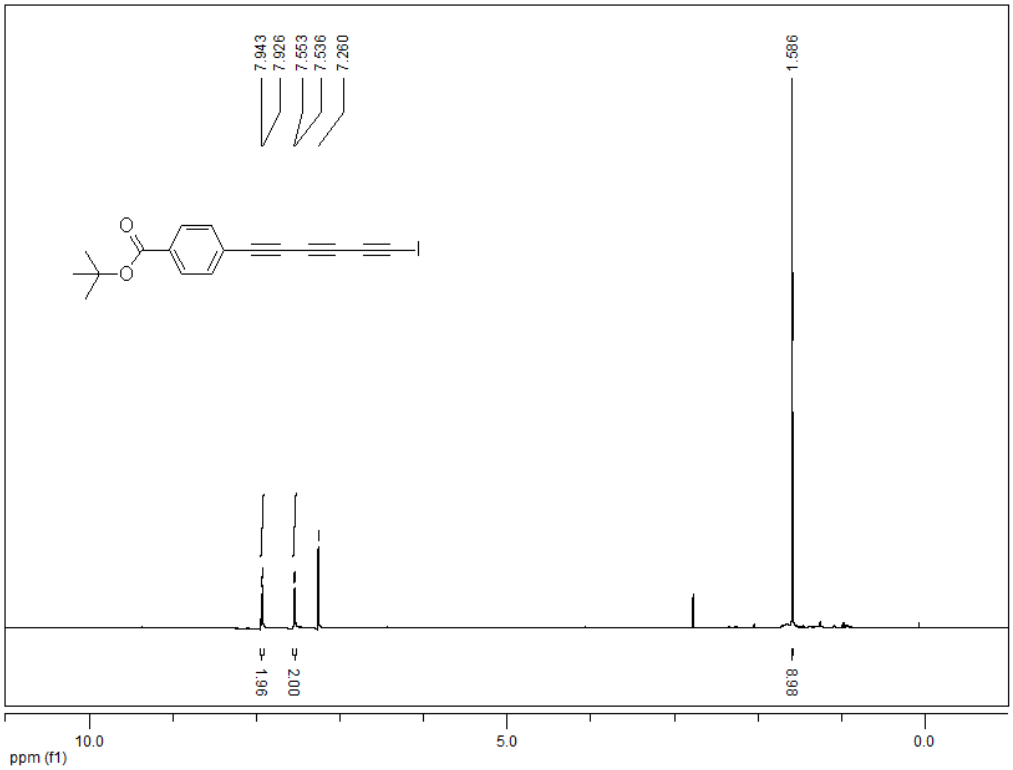

^{1}H-NMR (500 MHz, $CDCl_3$) spectrum

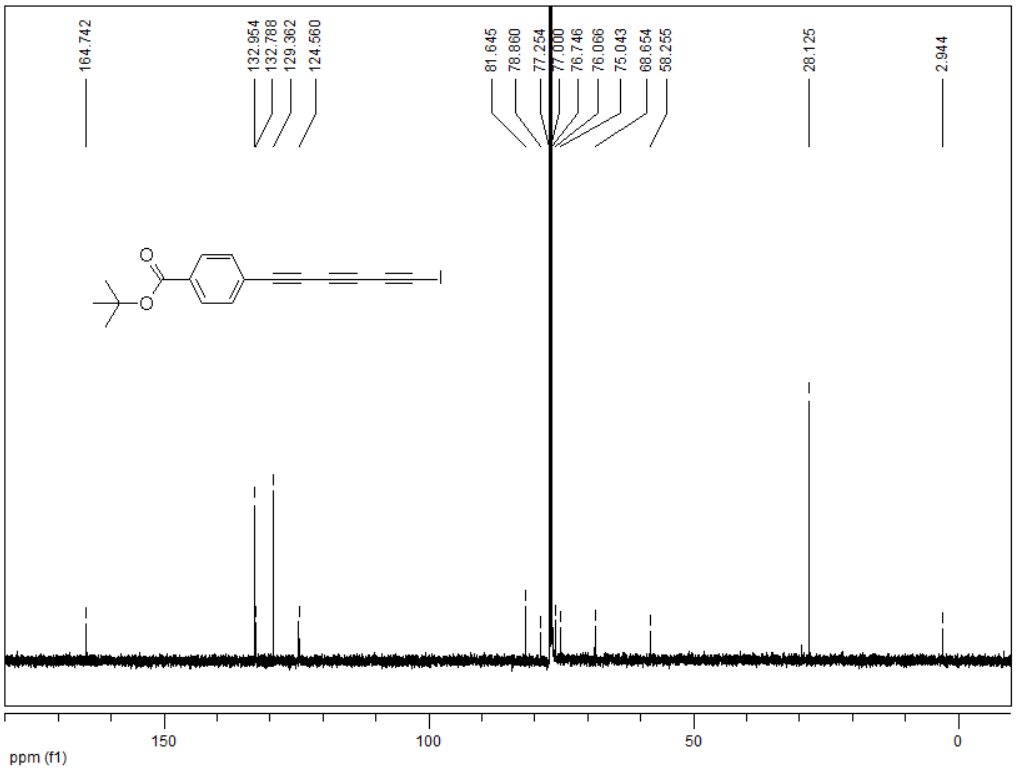

^{13}C-NMR (125 MHz, $CDCl_3$) spectrum

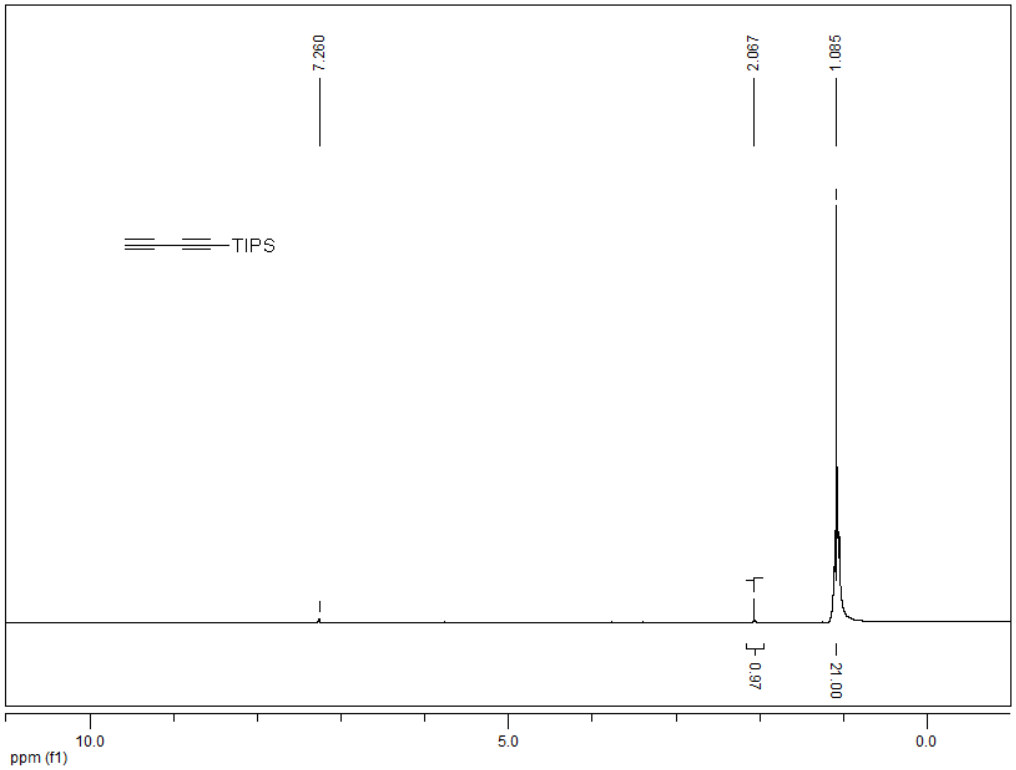

^{1}H-NMR (400 MHz, $CDCl_3$) spectrum of compound **2-40**

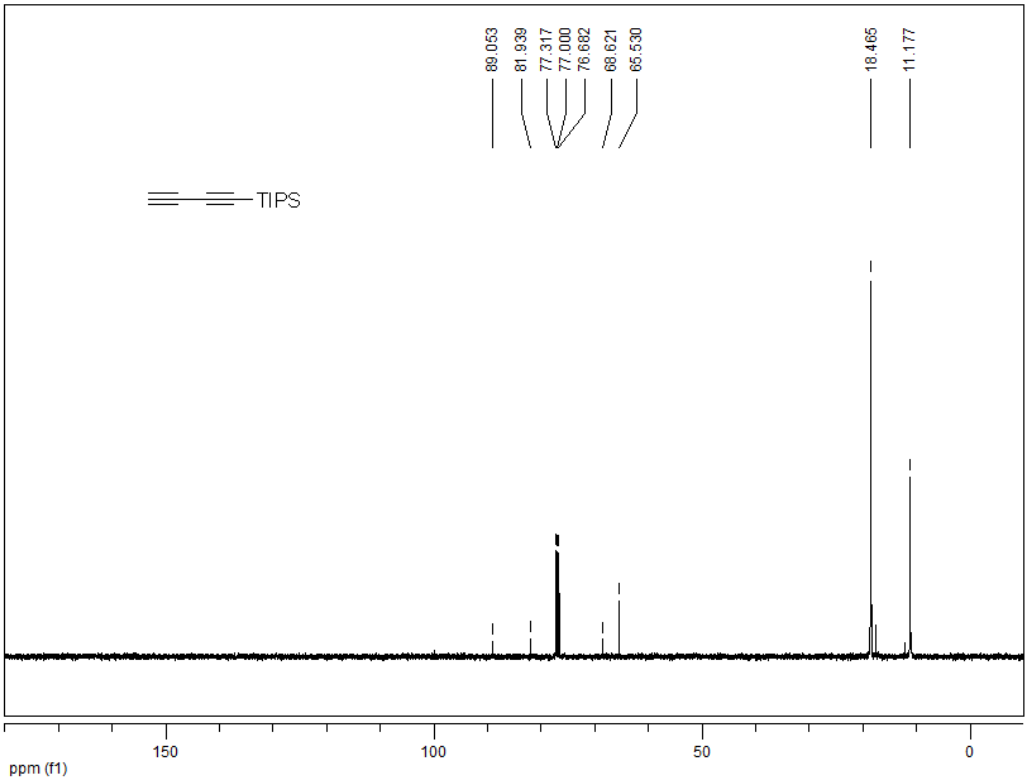

^{13}C-NMR (100 MHz, $CDCl_3$) spectrum of compound **2-40**

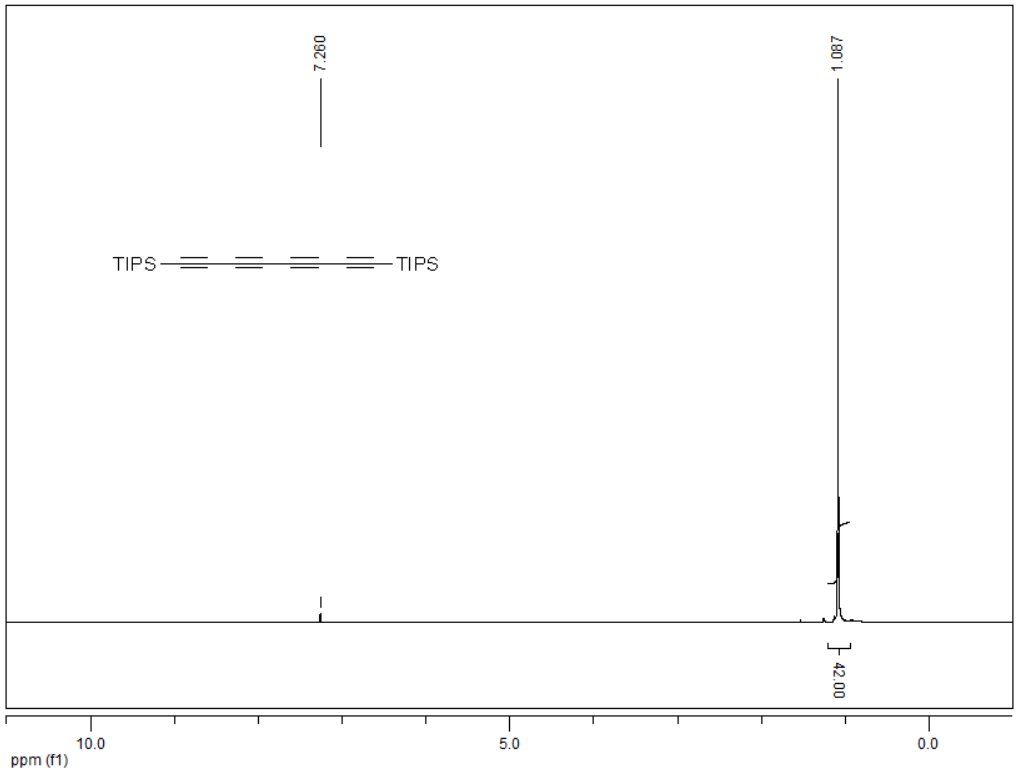

^{1}H-NMR (500 MHz, $CDCl_3$) spectrum of compound **3-1**

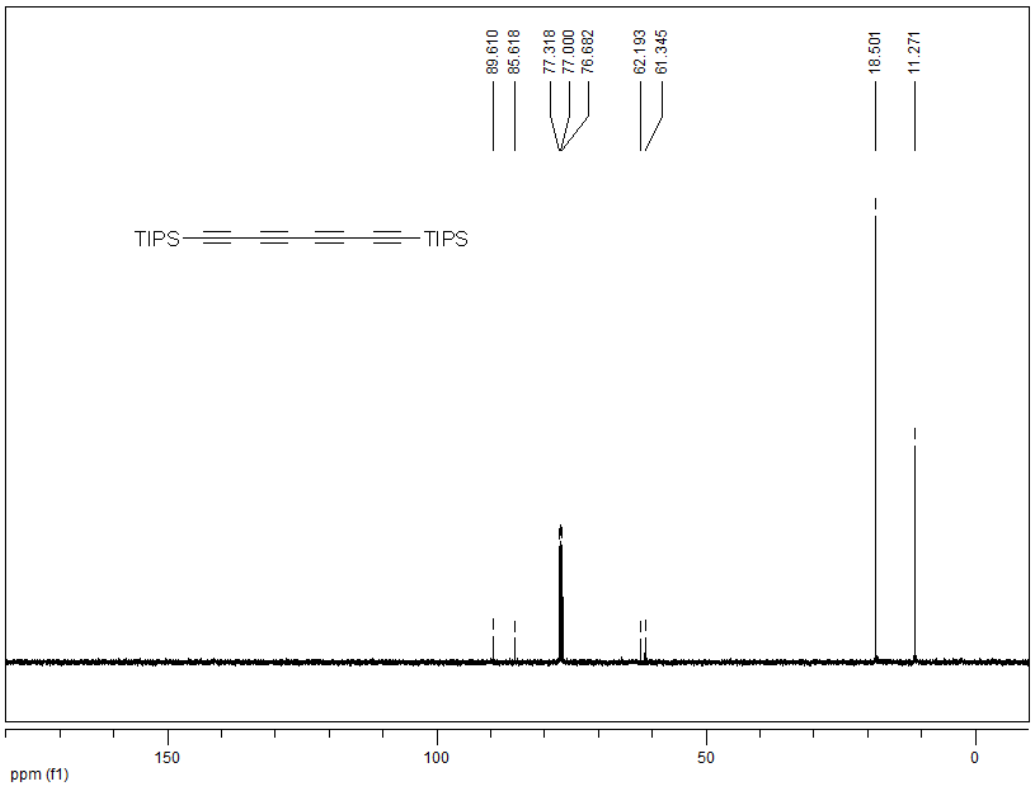

^{13}C-NMR (125 MHz, $CDCl_3$) spectrum of compound **3-1**

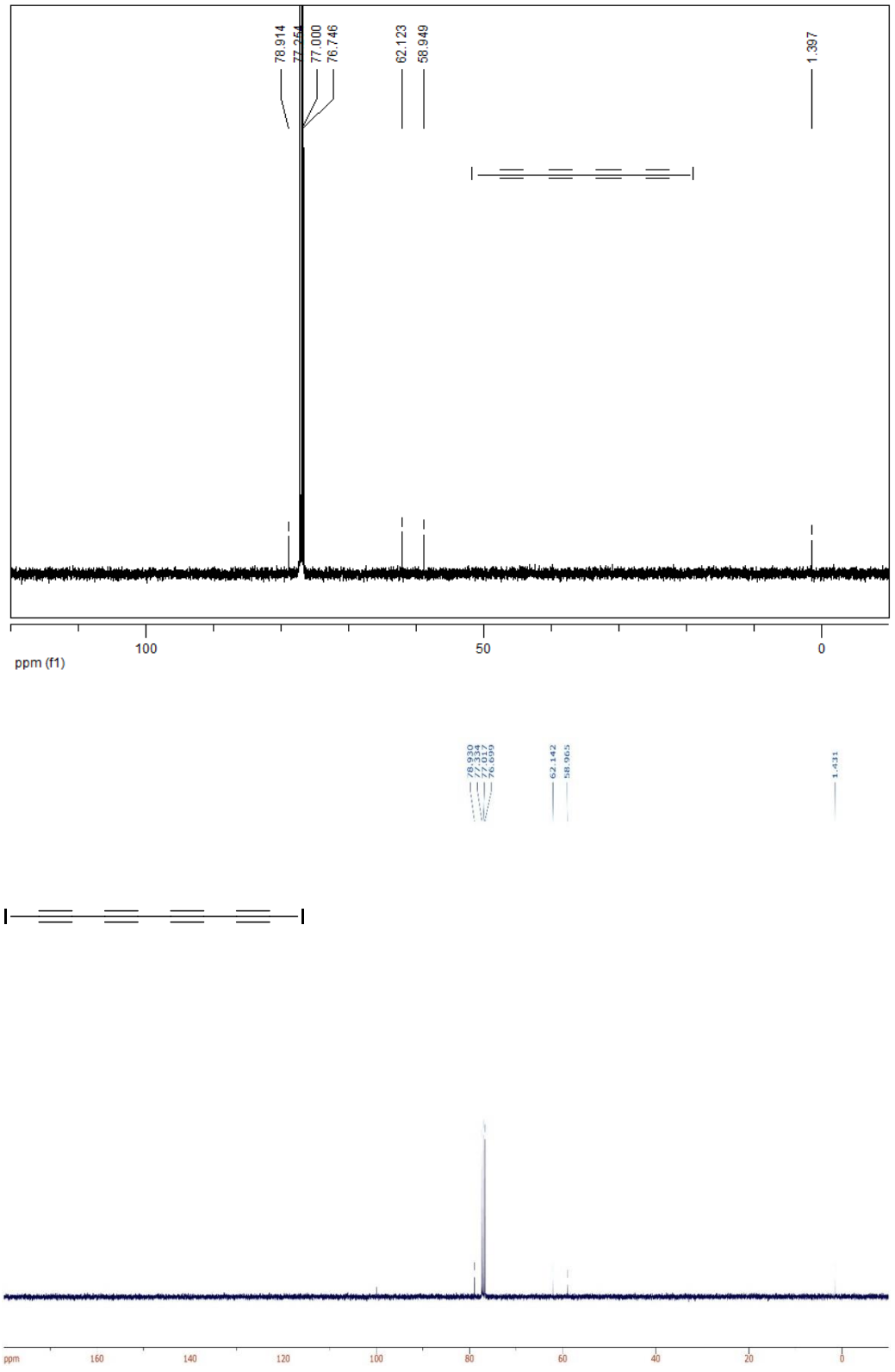

^{13}C-NMR (125 MHz, $CDCl_3$) spectrum of compound **3-2**

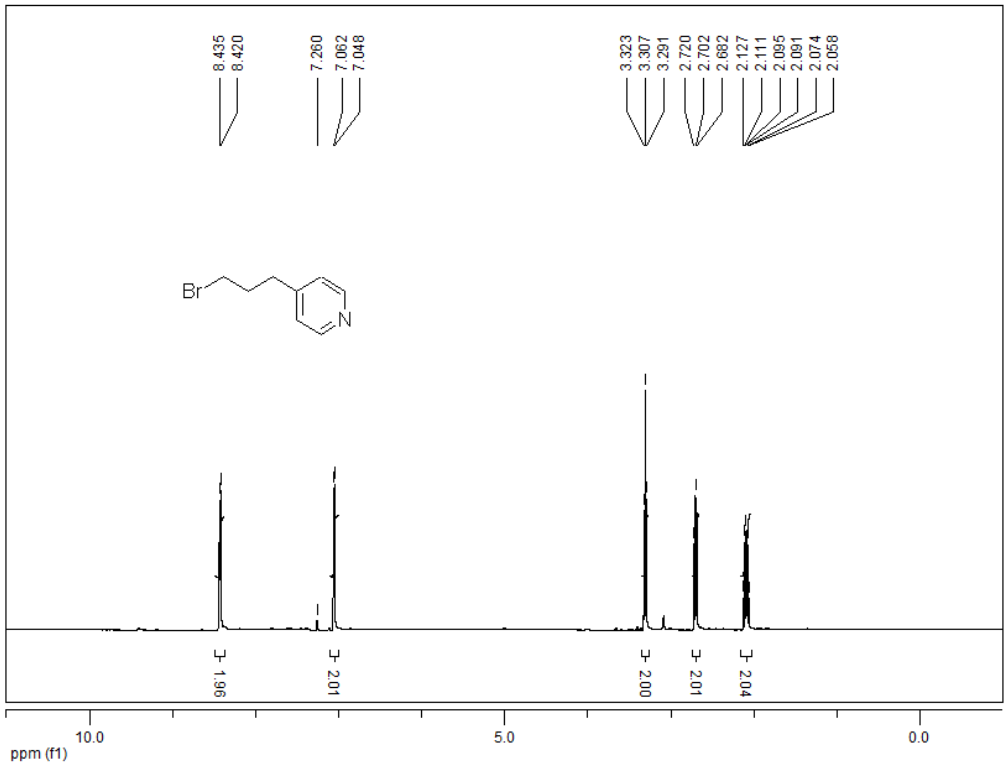

^{1}H-NMR (500 MHz, $CDCl_3$) spectrum of compound **2-55**

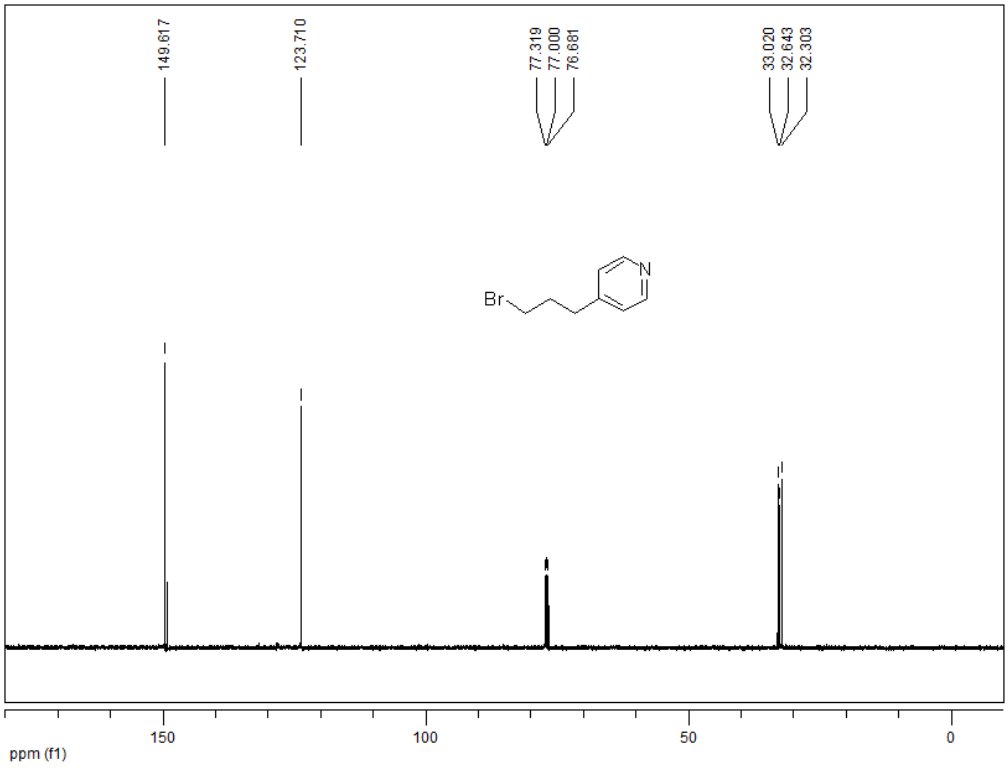

^{13}C-NMR (125 MHz, $CDCl_3$) spectrum of compound **2-55**

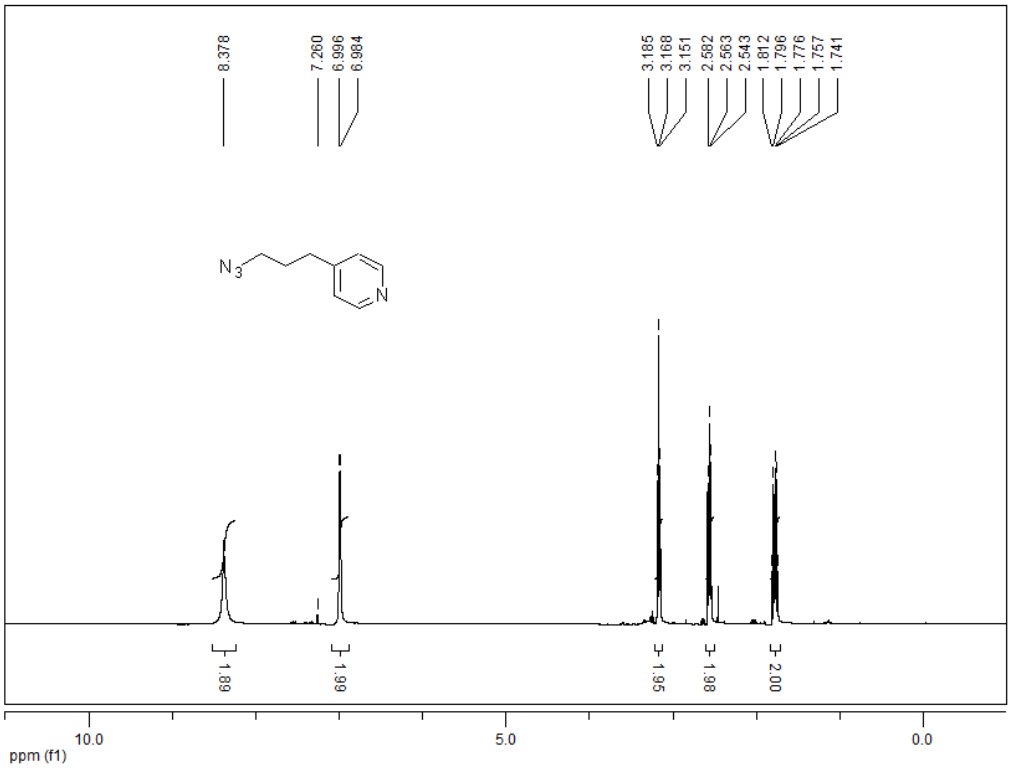

^{1}H-NMR (500 MHz, $CDCl_3$) spectrum of compound **2-56**

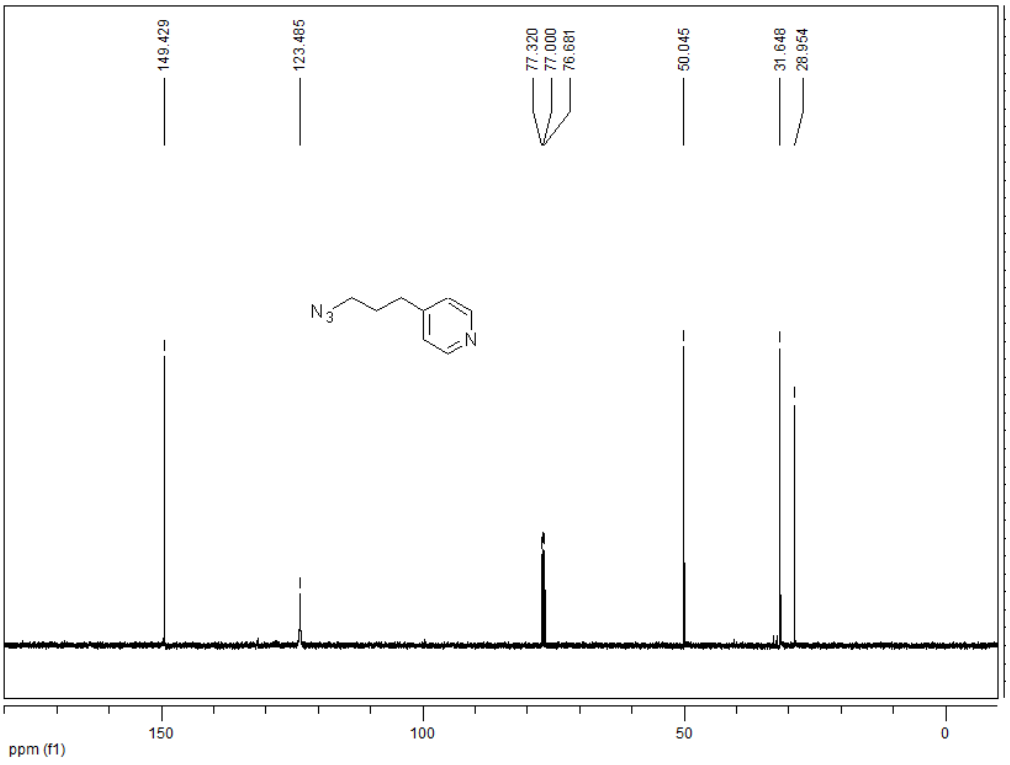

^{13}C-NMR (125 MHz, $CDCl_3$) spectrum of compound **2-56**

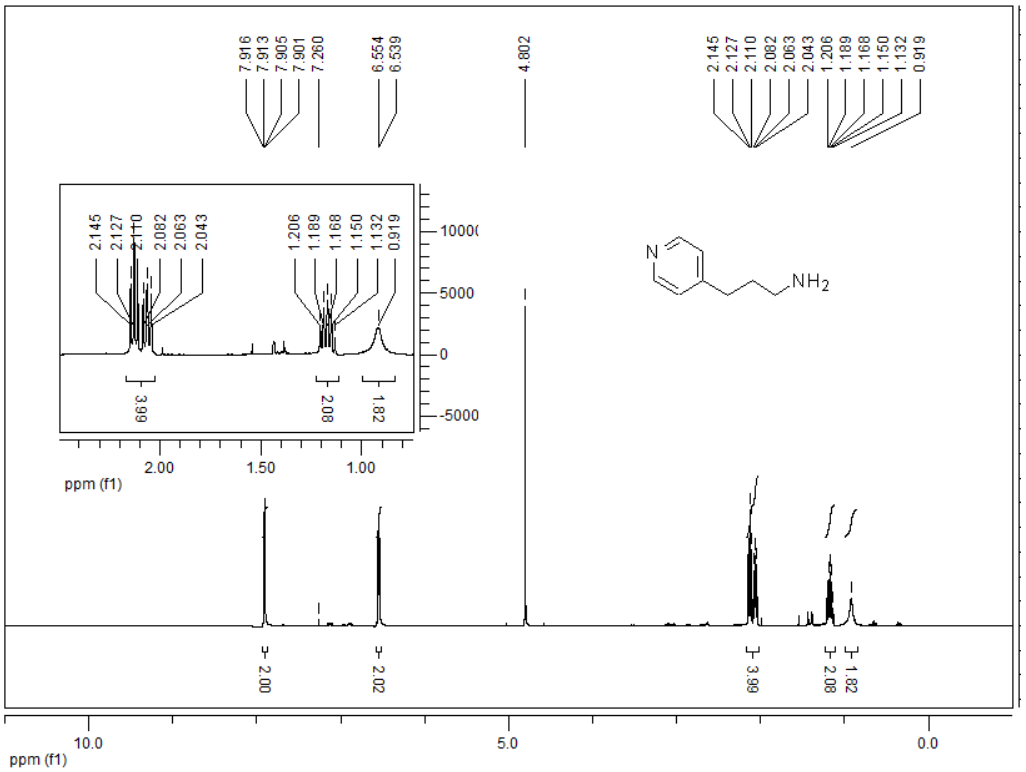

^{1}H-NMR (500 MHz, $CDCl_3$) spectrum of compound **2-57**

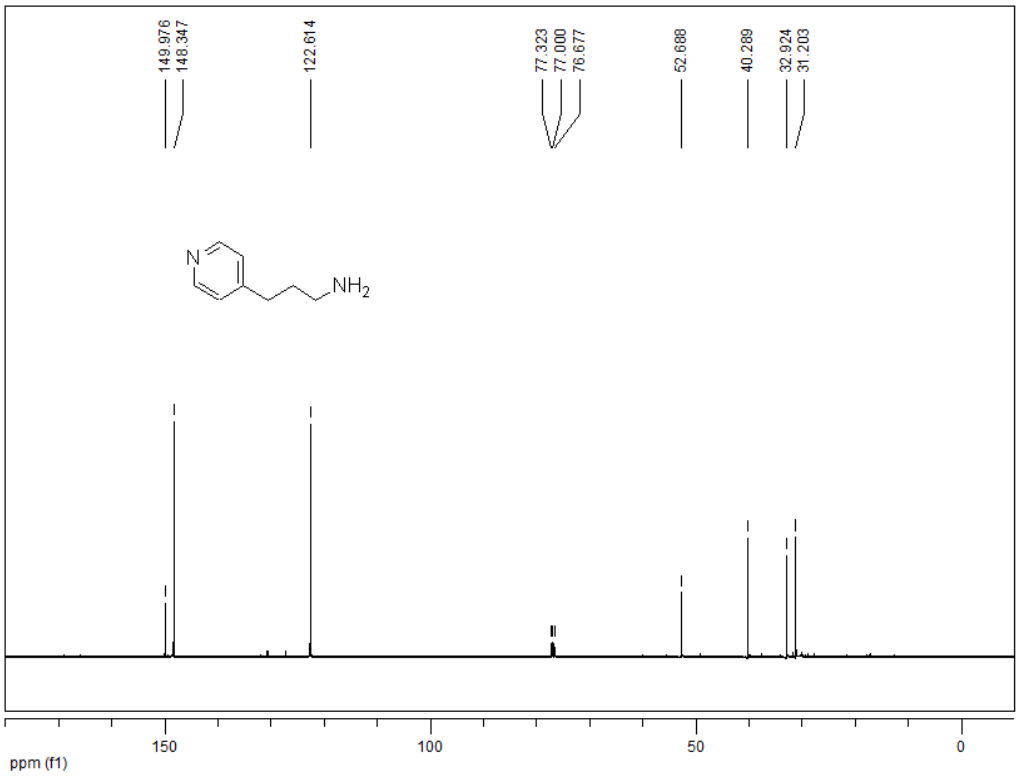

^{1}H-NMR (125 MHz, $CDCl_3$) spectrum of compound **2-57**

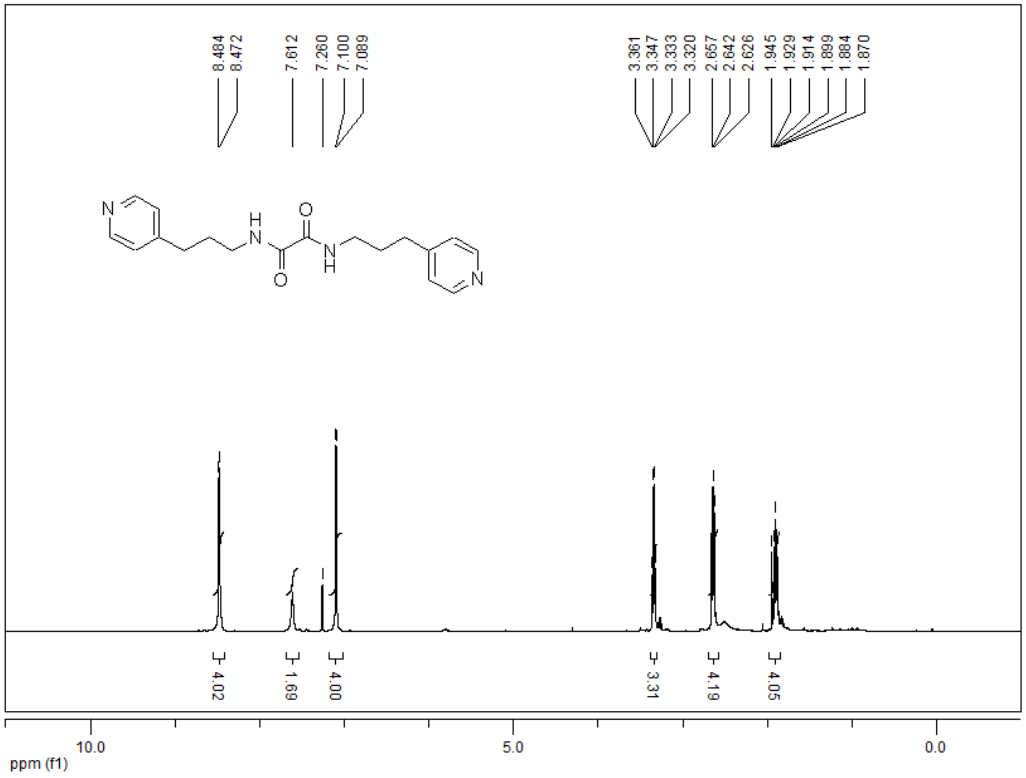

^{1}H-NMR (500 MHz, $CDCl_3$) spectrum of compound **2-54**

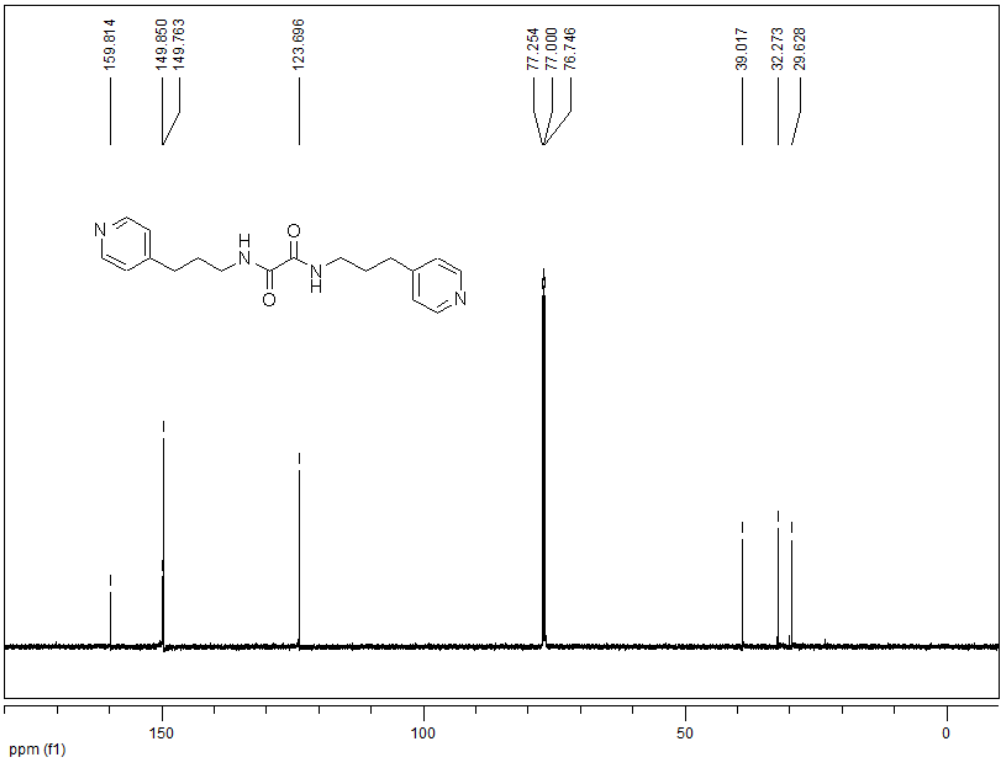

^{13}C-NMR (125 MHz, $CDCl_3$) spectrum of compound **2-54**

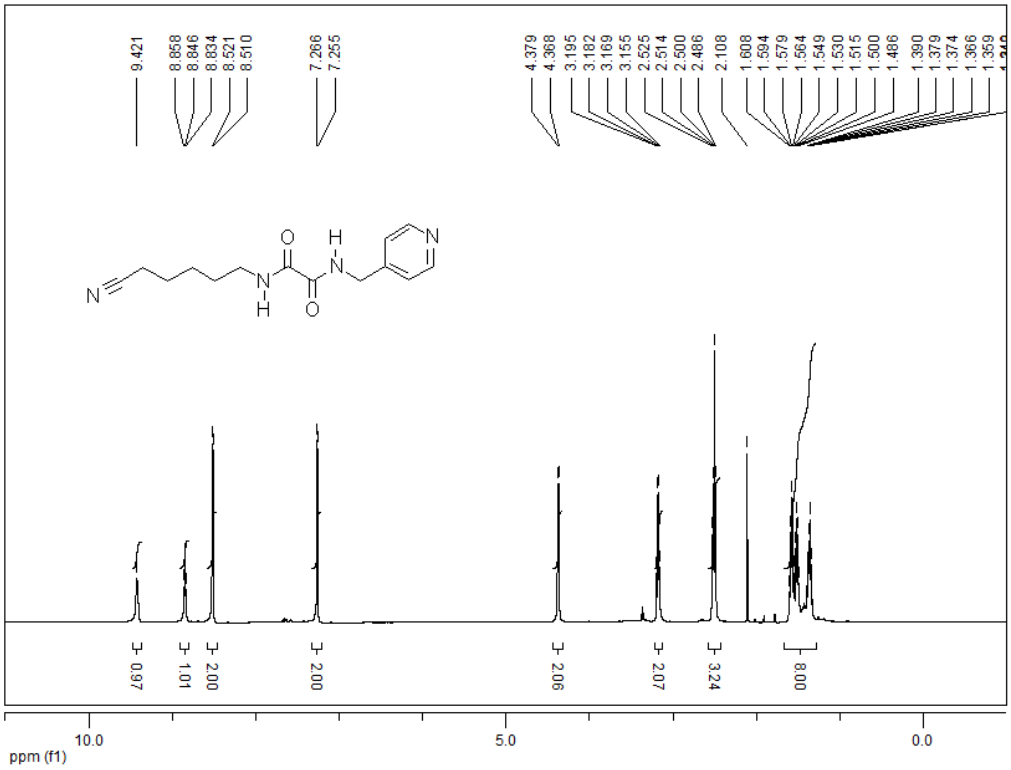

^{1}H-NMR (500 MHz, DMSO) spectrum of compound **2-52**

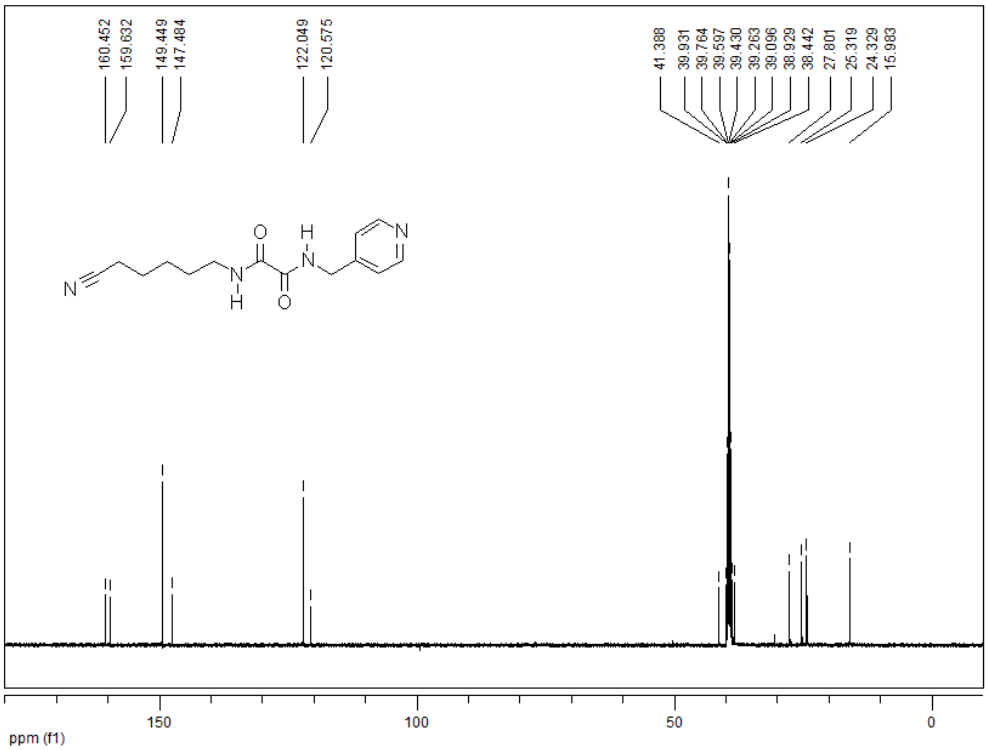

^{13}C-NMR (125 MHz, DMSO) spectrum of compound **2-52**

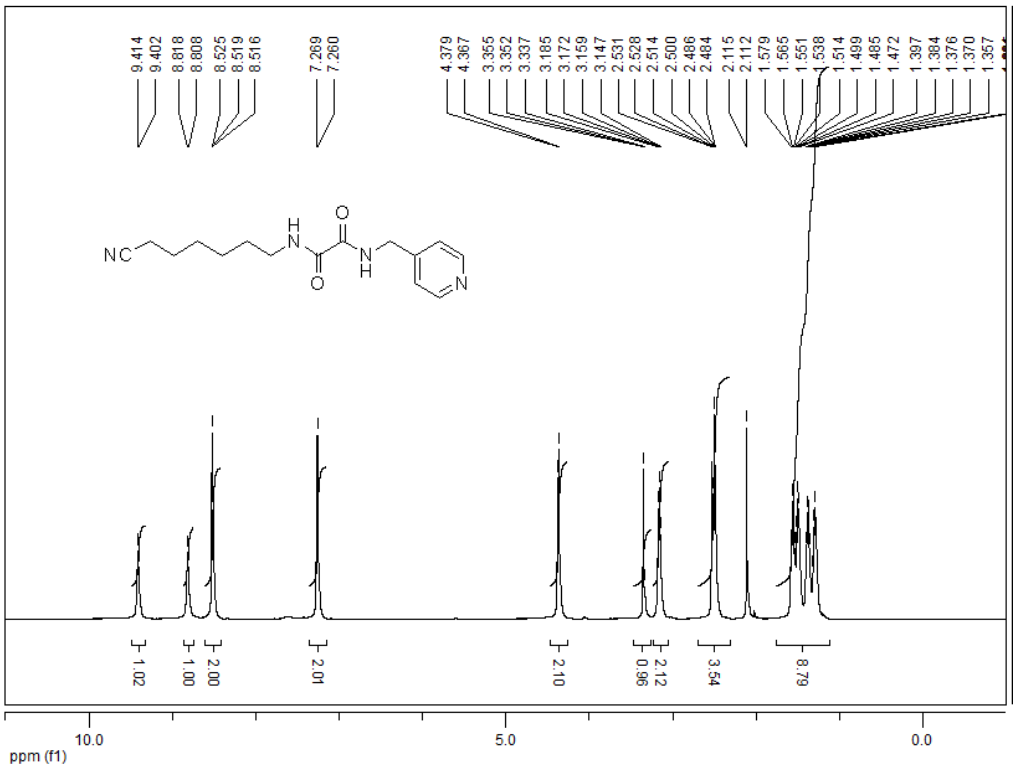

^{1}H-NMR (500 MHz, DMSO) spectrum of compound **2-53**

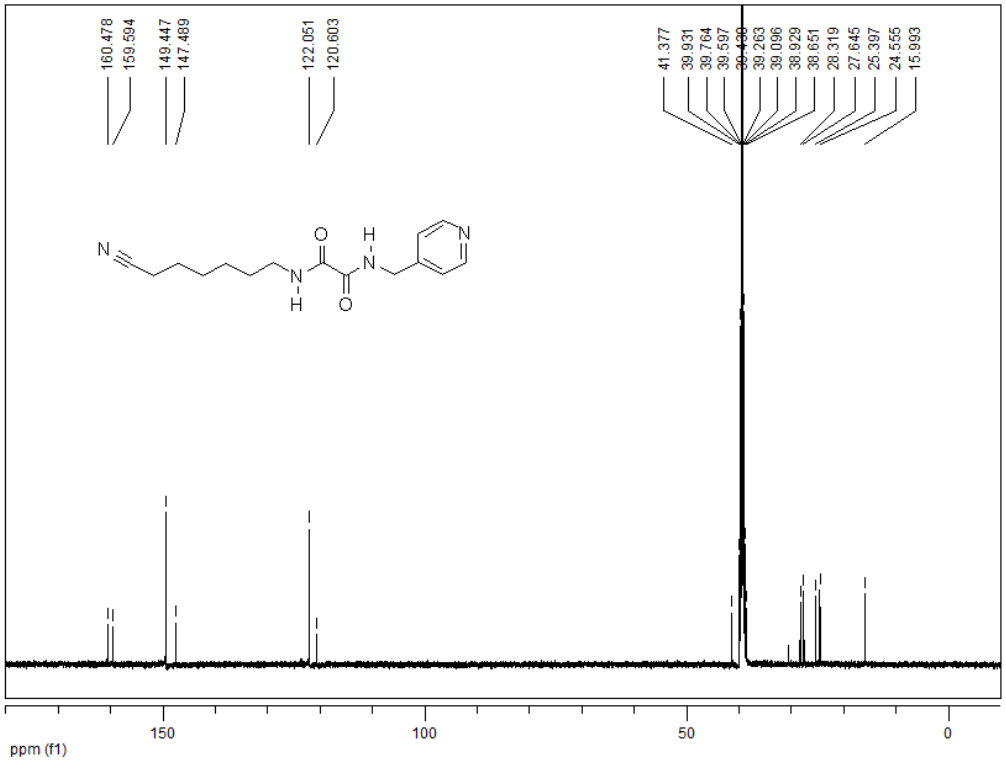

^{13}C-NMR (125 MHz, DMSO) spectrum of compound **2-53**

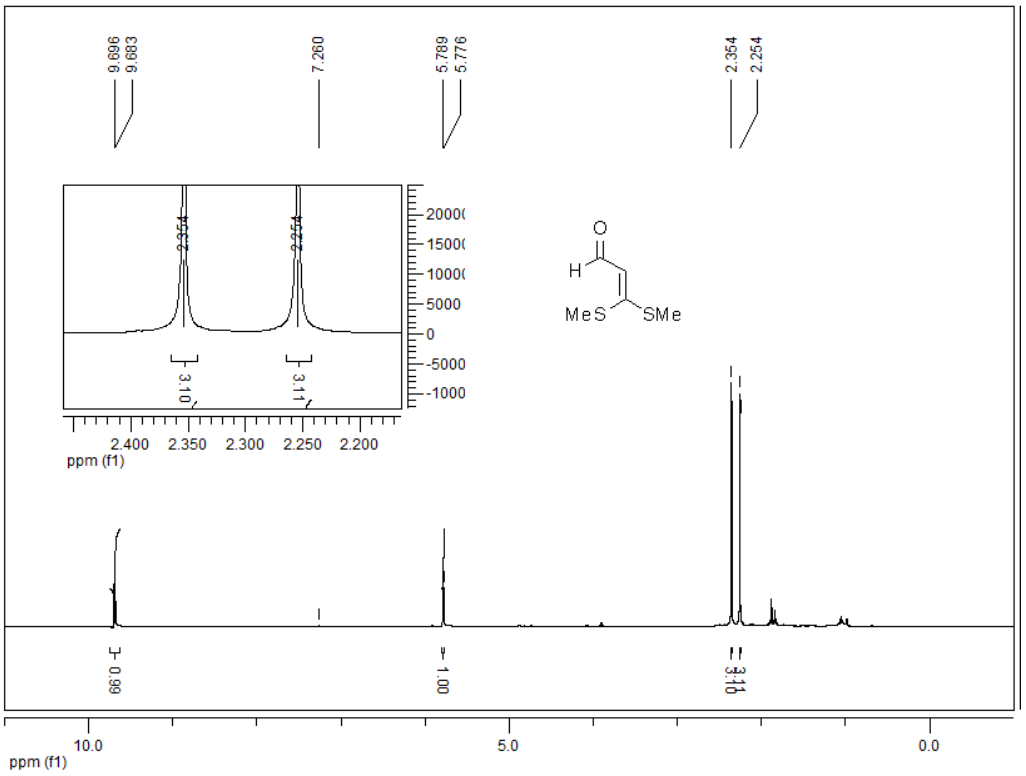

^{1}H-NMR (500 MHz, $CDCl_3$) spectrum of compound **4-7**

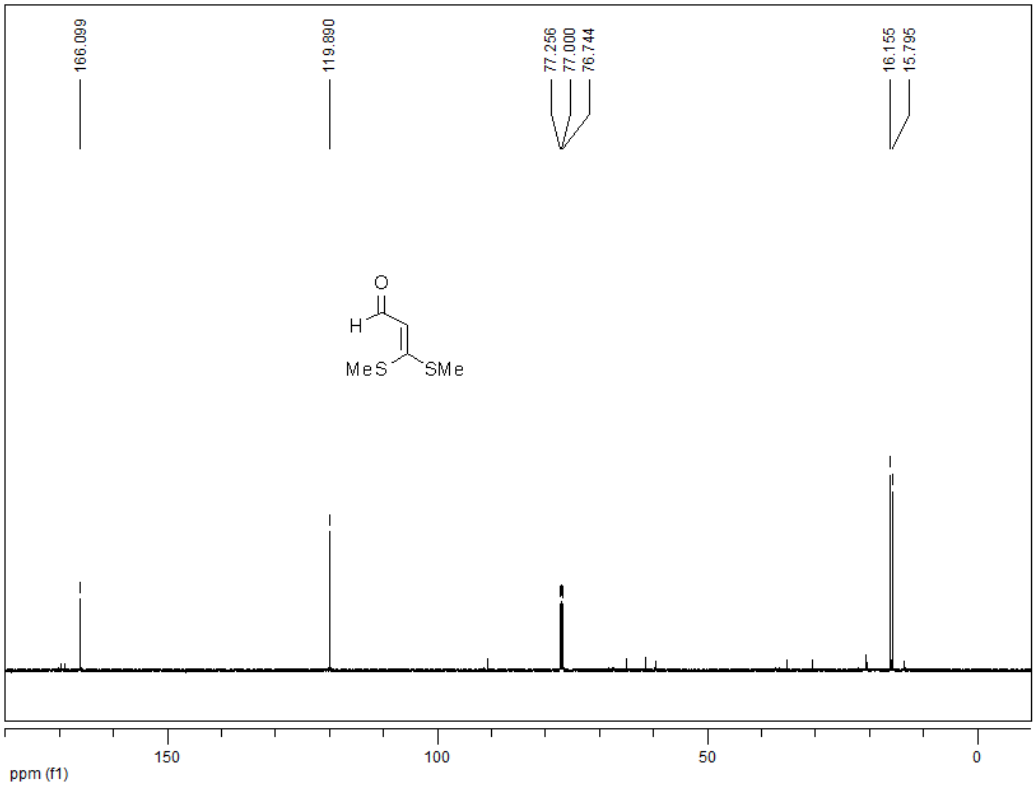

^{13}C-NMR (125 MHz, $CDCl_3$) spectrum of compound **4-7**

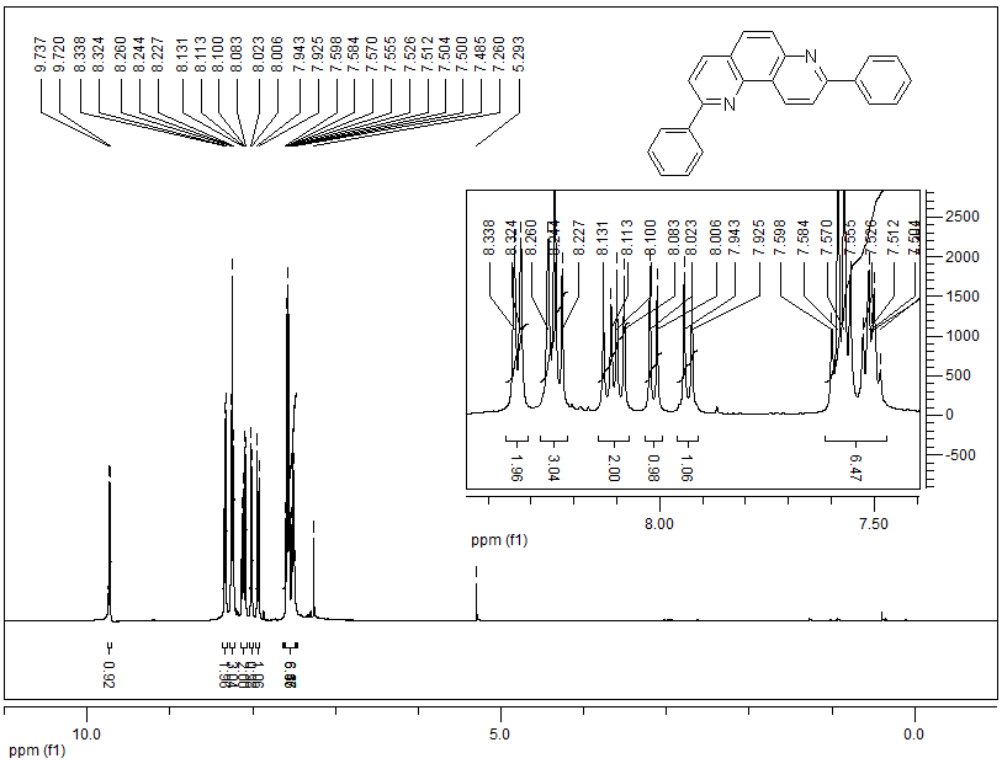

^{1}H-NMR (500 MHz, $CDCl_3$) spectrum of compound **4-2,** 5.293 indicates CH_2Cl_2

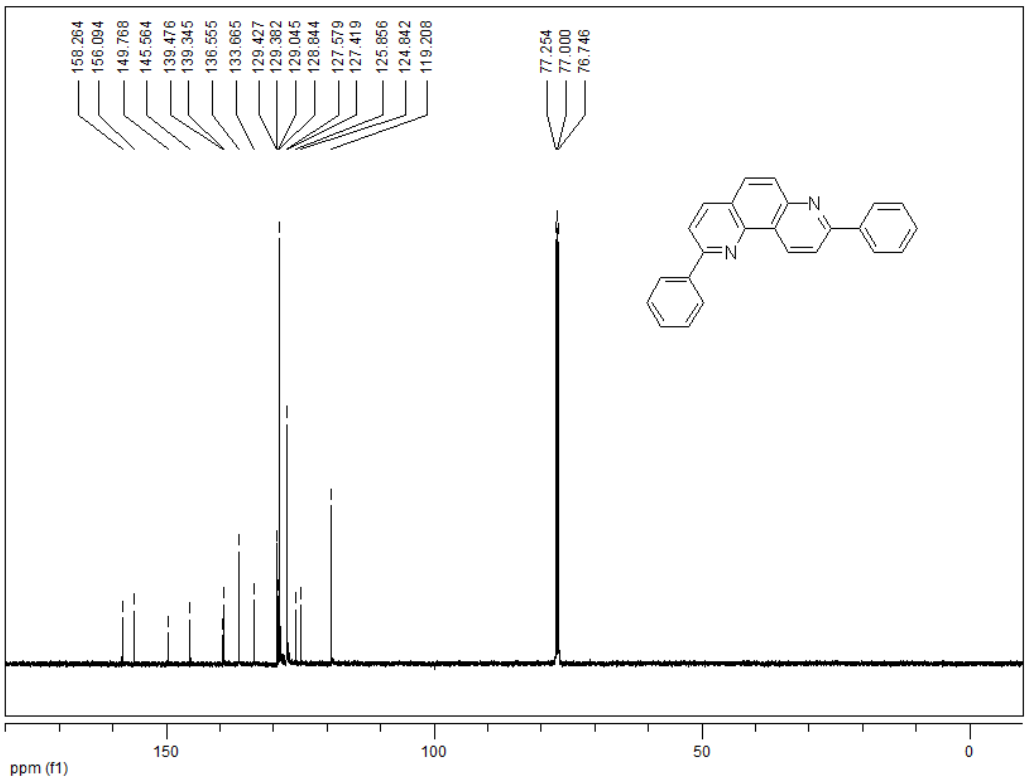

^{13}C-NMR (125 MHz, $CDCl_3$) spectrum of compound **4-2**

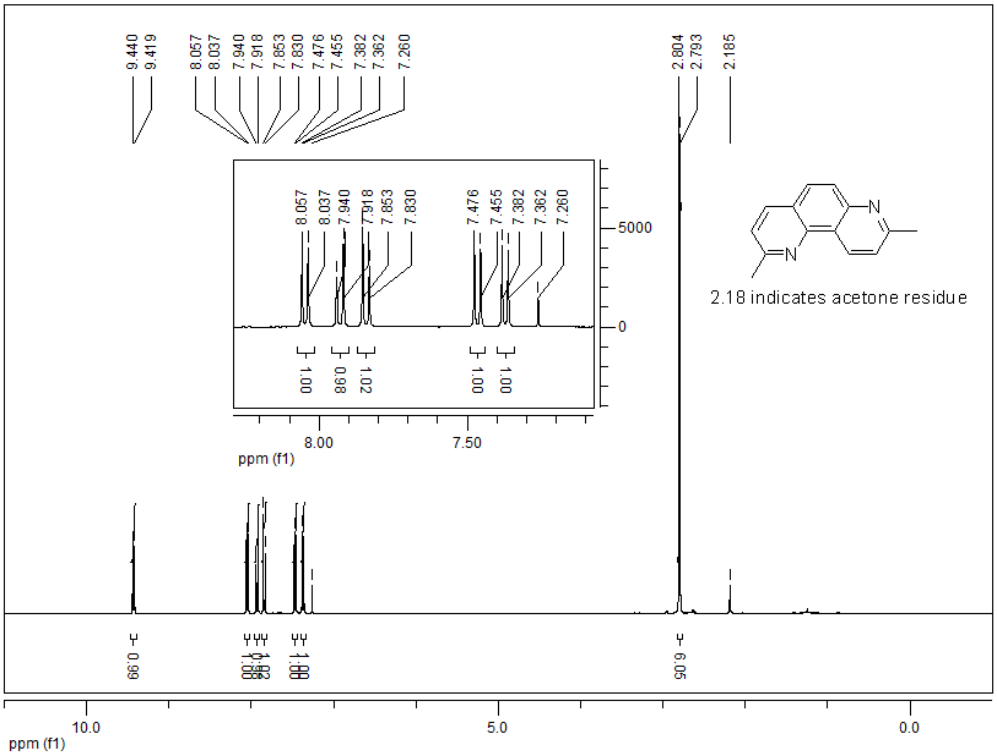

^{1}H-NMR (400 MHz, $CDCl_3$) spectrum of compound **4-1**

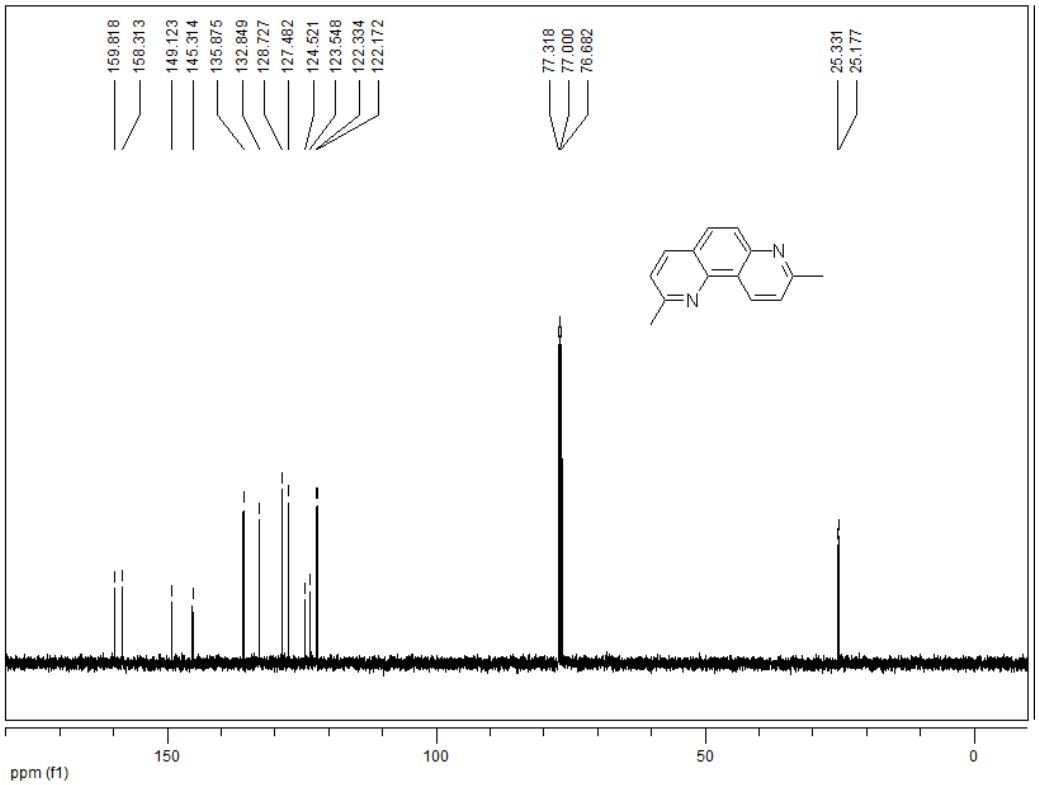

^{13}C-NMR (100 MHz, $CDCl_3$) spectrum of compound **4-1**

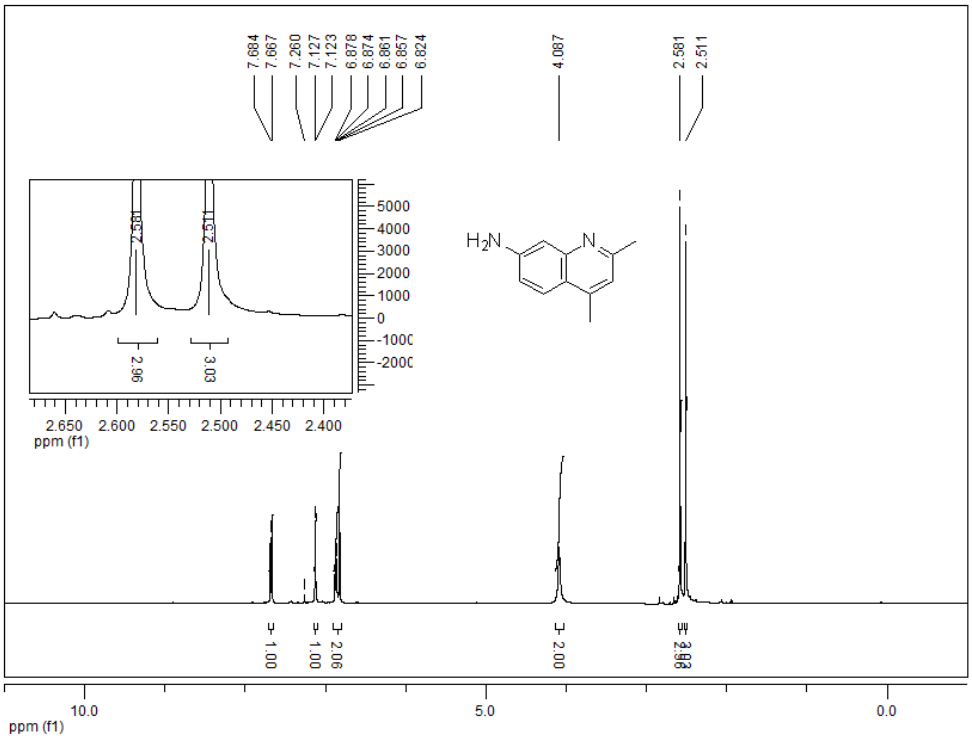

^{1}H-NMR (500 MHz, $CDCl_3$) spectrum of compound **4-8**

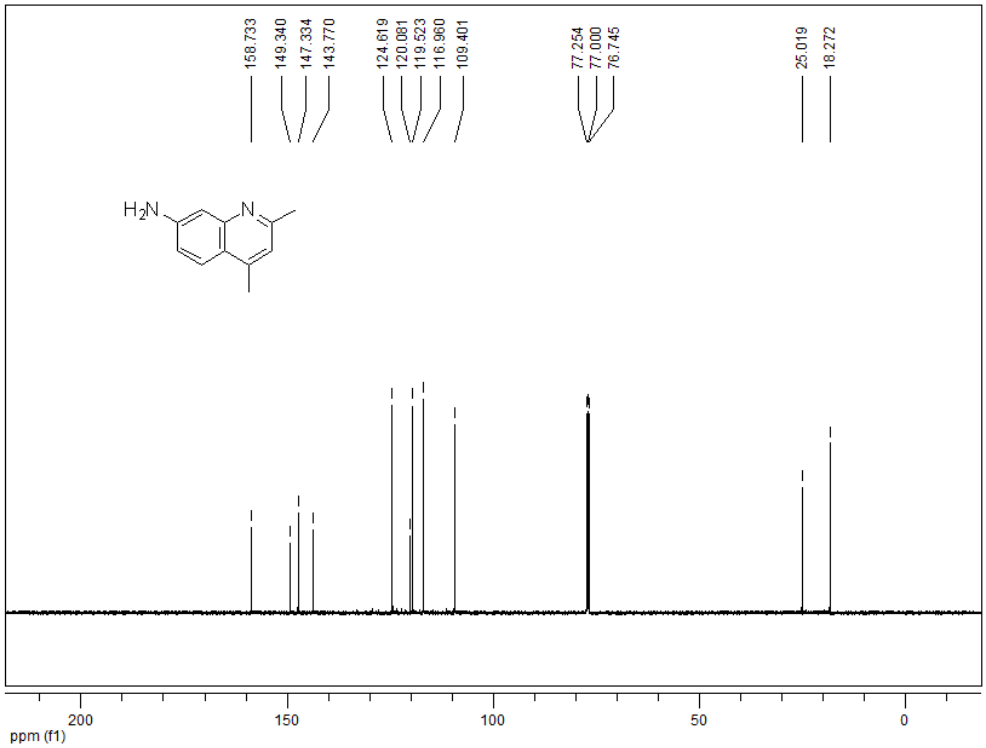

^{13}C-NMR (125 MHz, $CDCl_3$) spectrum of compound **4-8**

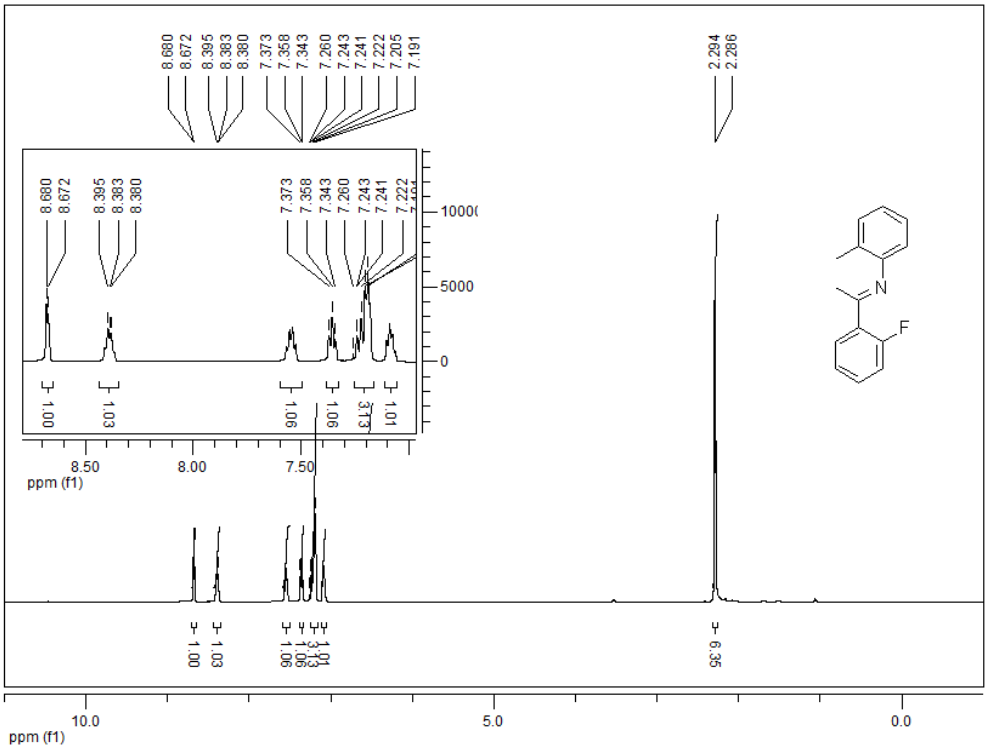

^{1}H-NMR (500 MHz, $CDCl_3$) spectrum of compound **4-9**

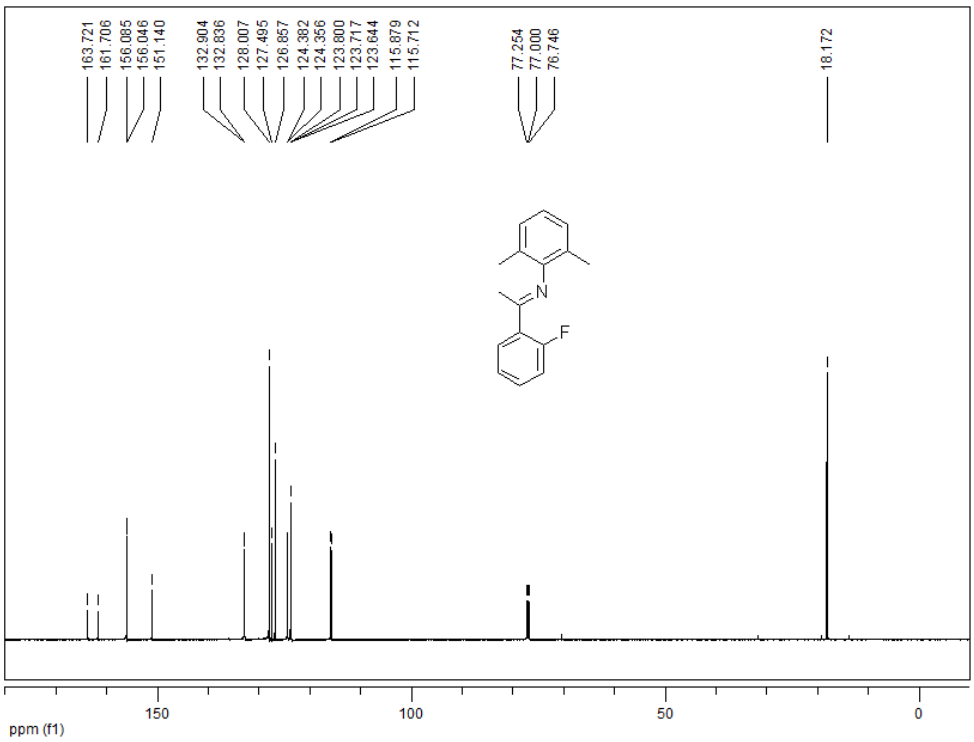

^{13}C-NMR (125 MHz, $CDCl_3$) spectrum of compound **4-9**

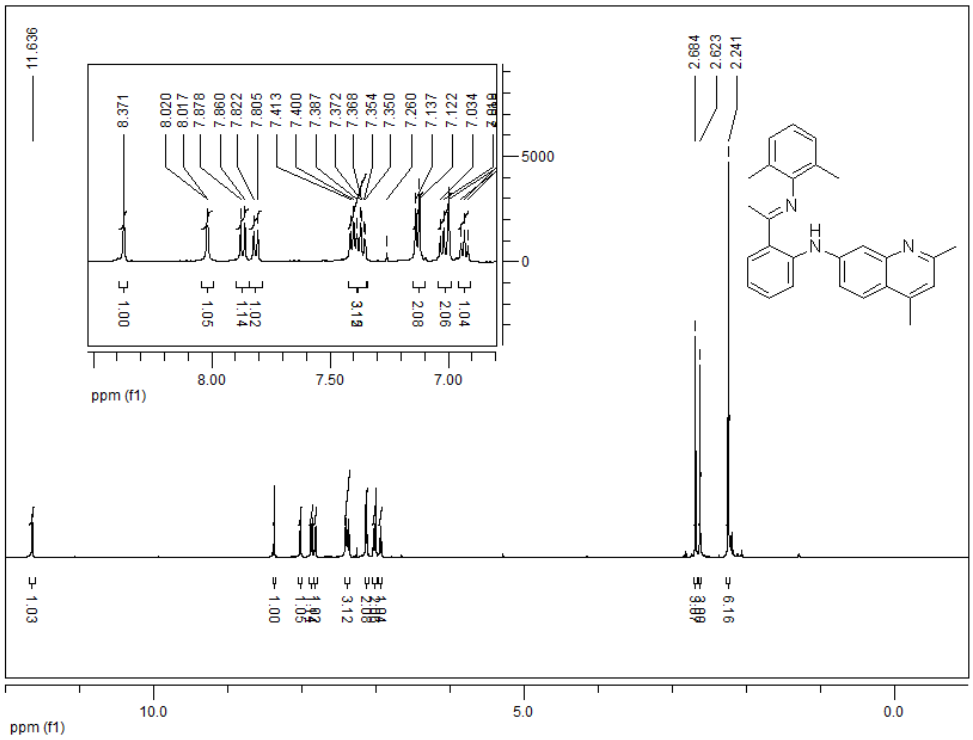

^{1}H-NMR (500 MHz, $CDCl_3$) spectrum of compound **4-10**

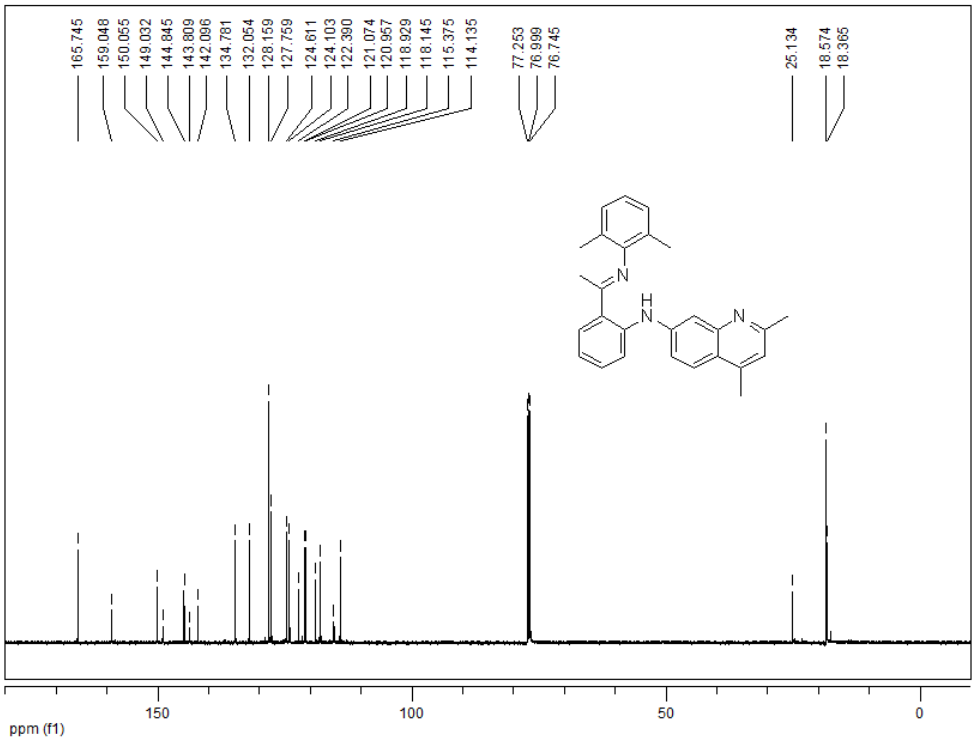

^{13}C-NMR (125 MHz, $CDCl_3$) spectrum of compound **4-10**

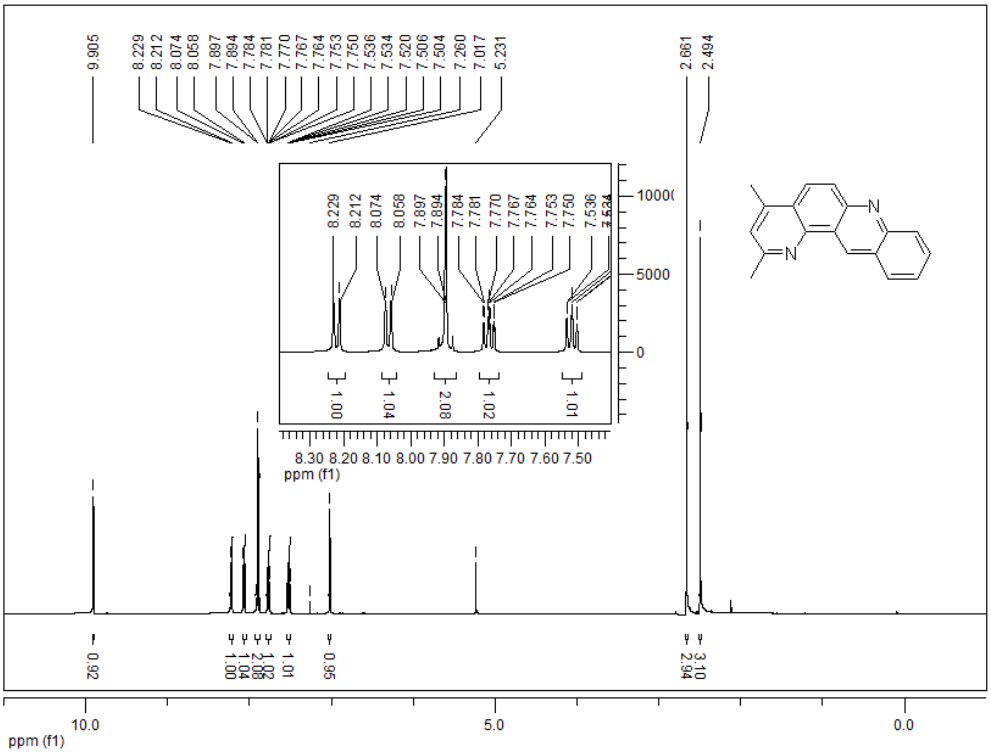

^{1}H-NMR (500 MHz, $CDCl_3$) spectrum of compound **4-5**, 5.231 is CH_2Cl_2

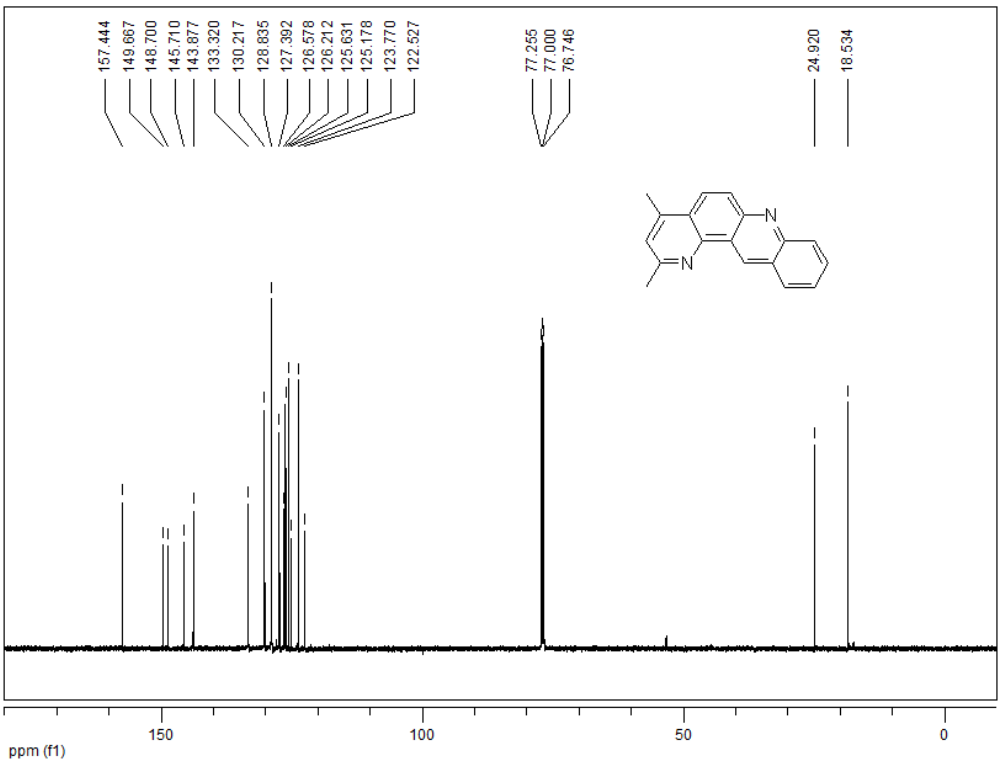

^{13}C-NMR (125 MHz, $CDCl_3$) spectrum of compound **4-5**

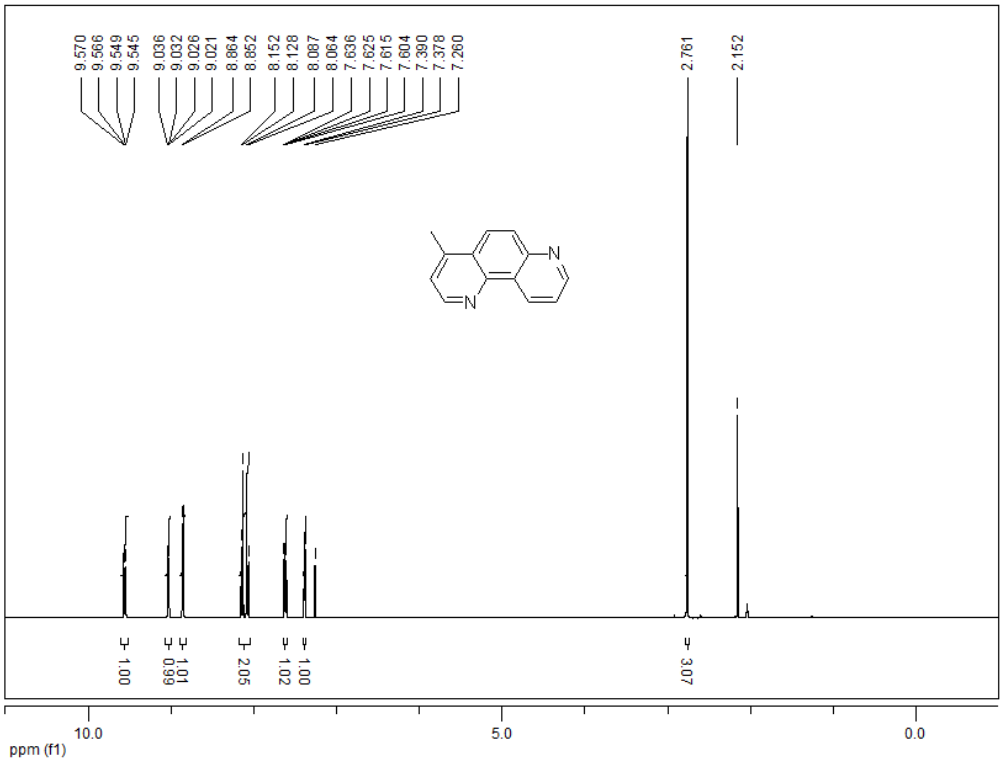

^{1}H-NMR (500 MHz, $CDCl_3$) spectrum of compound **4-13**, 2.152 indicates acetone

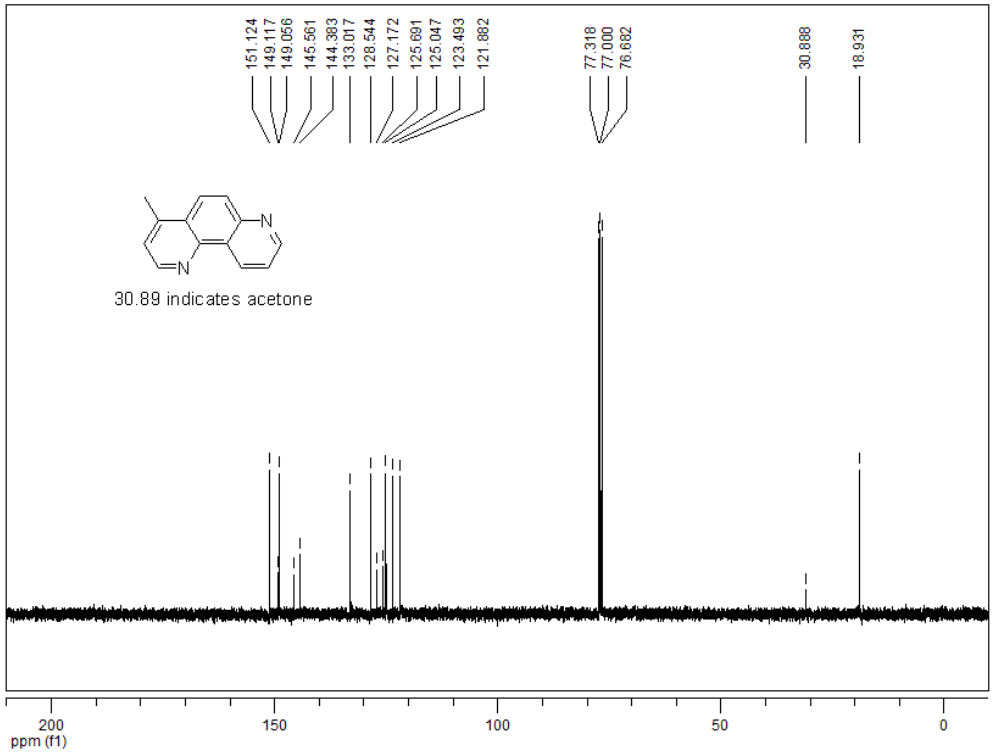

^{13}C-NMR (125 MHz, $CDCl_3$) spectrum of compound **4-13**

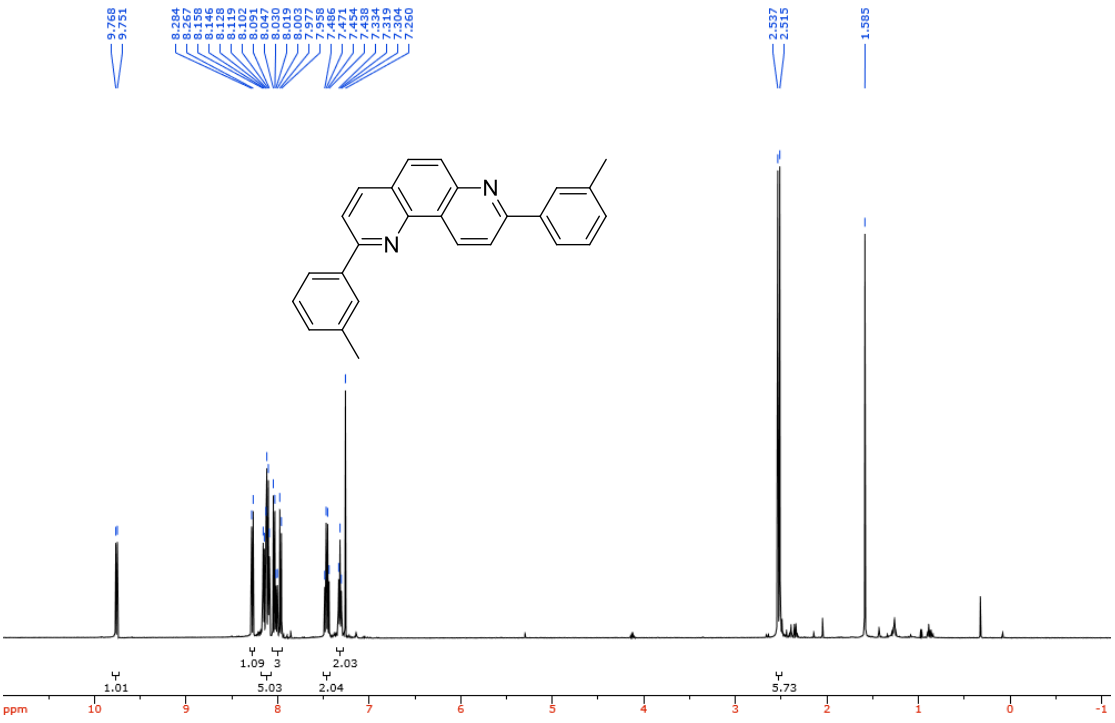

^{1}H-NMR (500 MHz, $CDCl_3$) spectrum of compound **4-11**

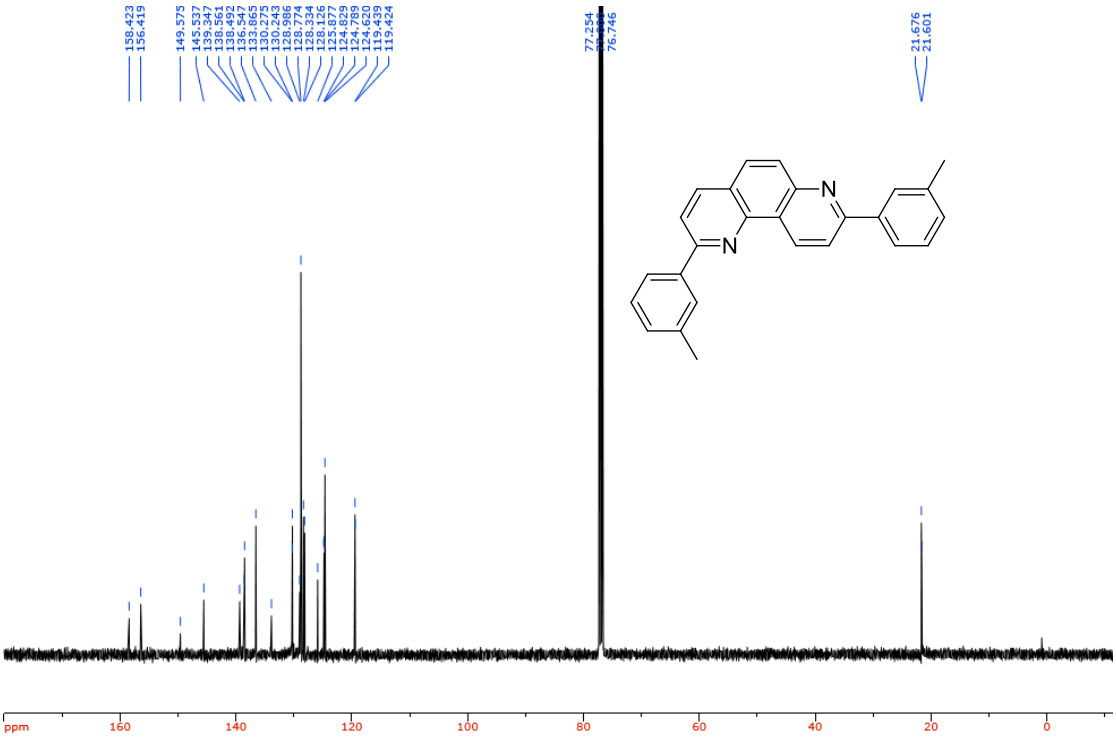

^{13}C-NMR (125 MHz, $CDCl_3$) spectrum of compound **4-11**

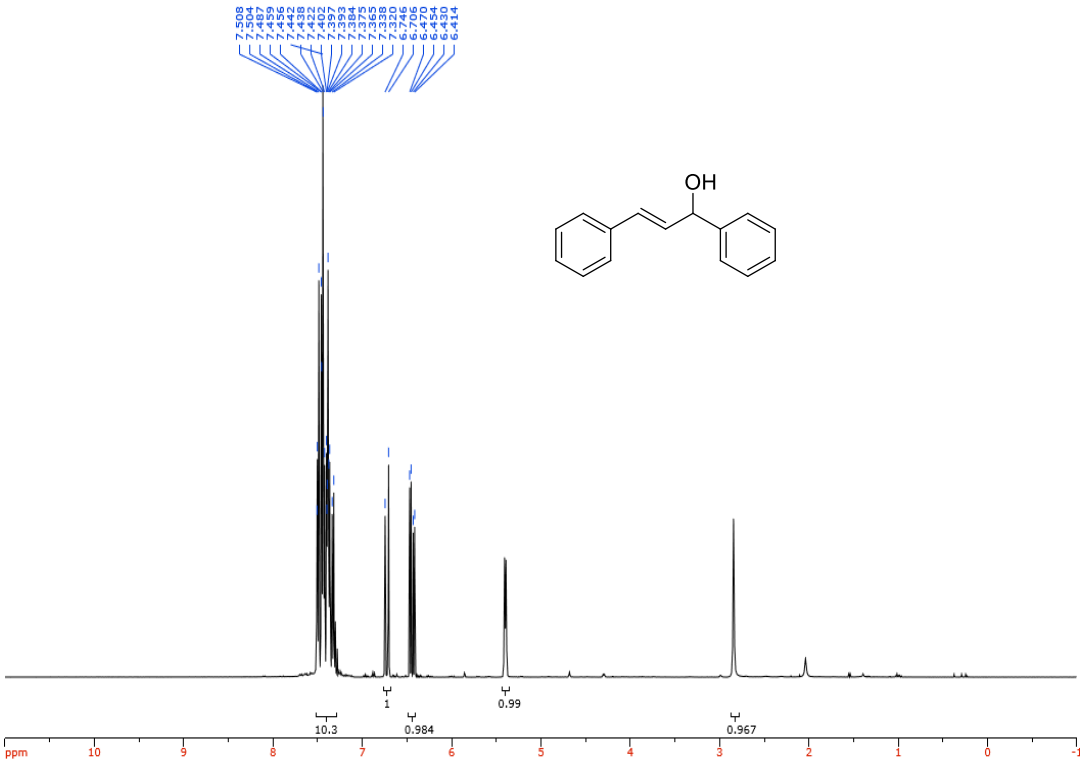

^{1}H-NMR (500 MHz, $CDCl_3$) spectrum of compound **4-14**

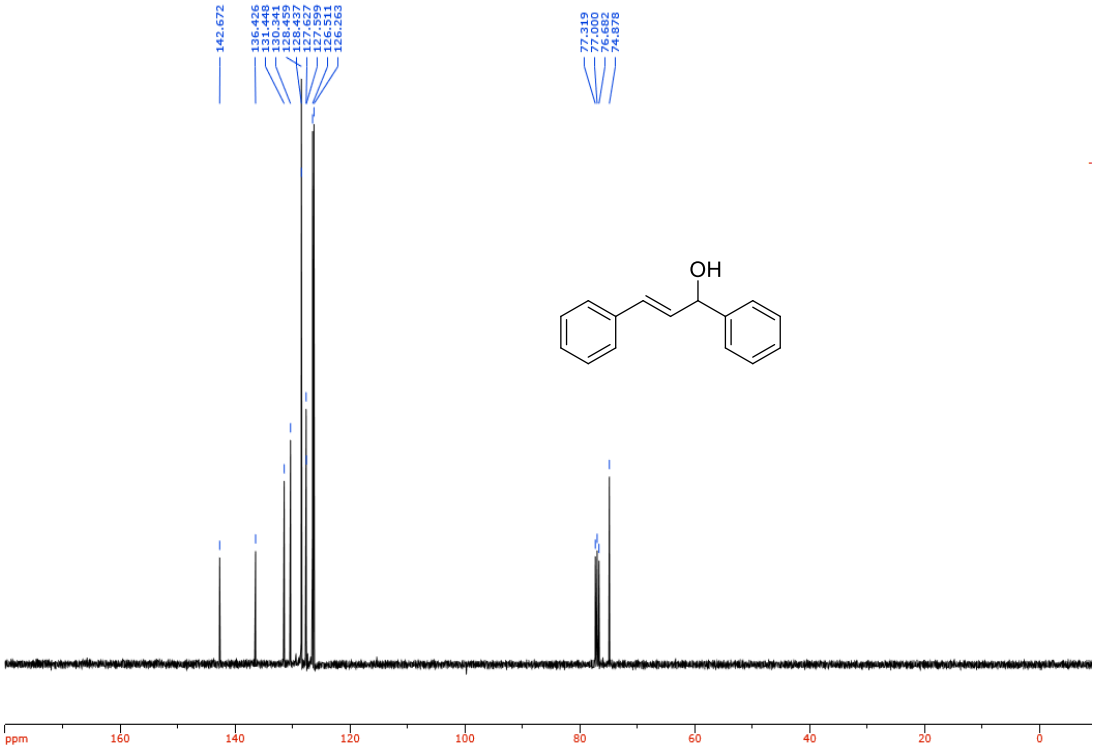

^{13}C-NMR (125 MHz, $CDCl_3$) spectrum of compound **4-14**

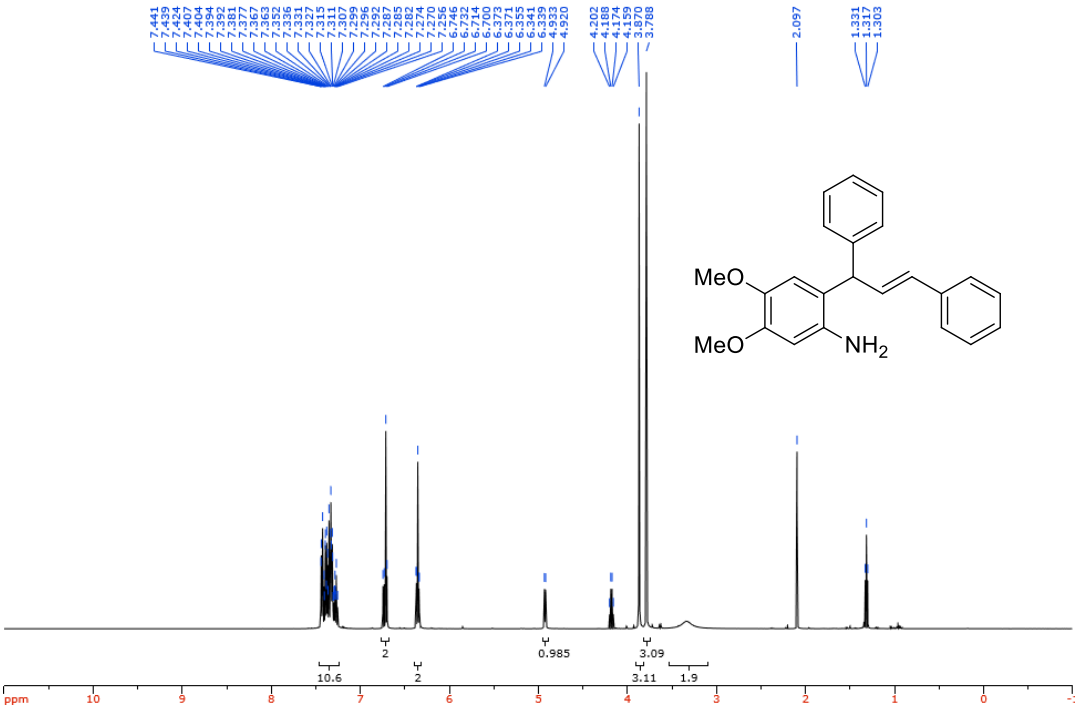

^{1}H-NMR (500 MHz, $CDCl_3$) of compound **4-16**, with ethyl acetate

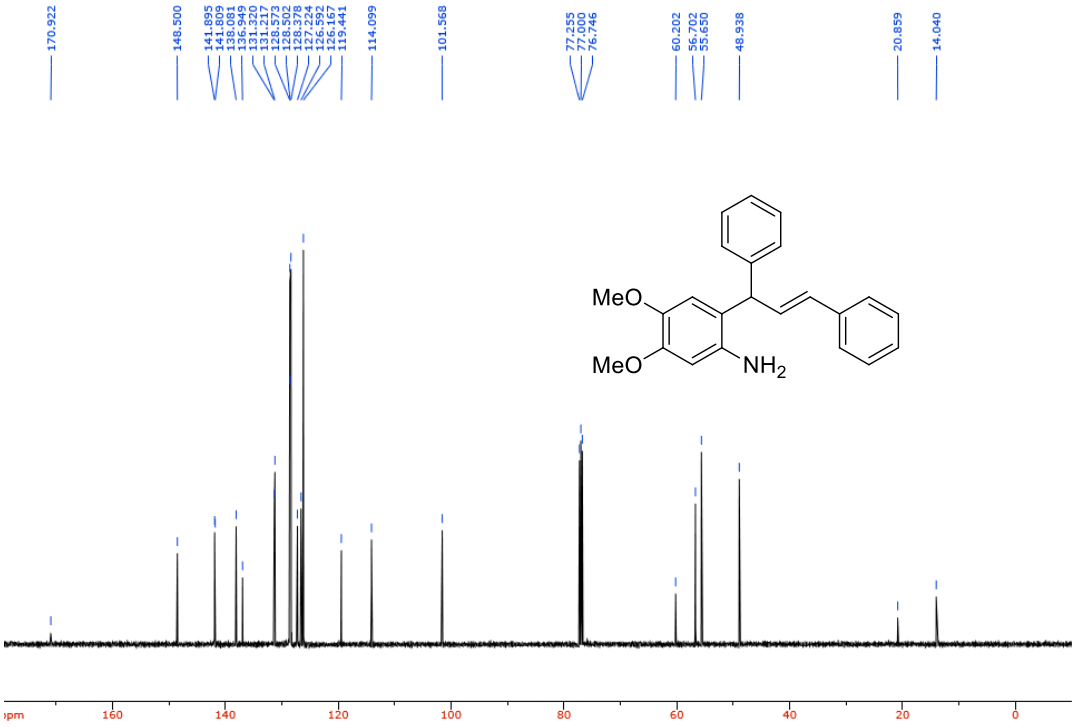

^{13}C-NMR (125 MHz, $CDCl_3$) spectrum of **4-16**, with ethyl acetate

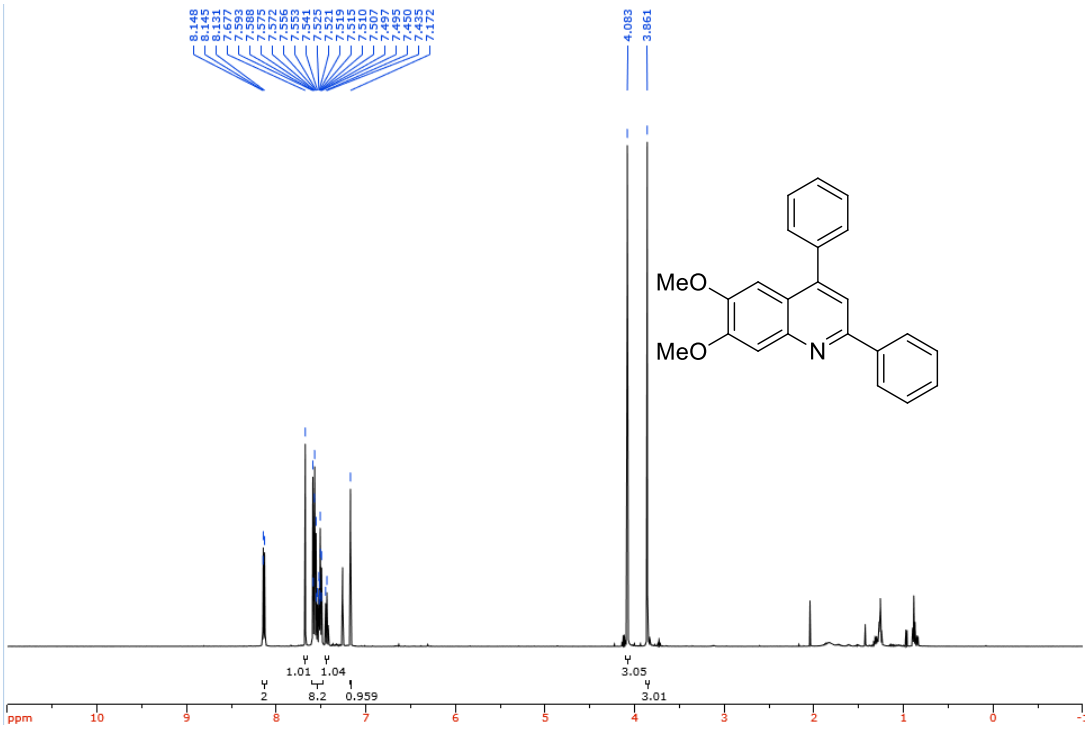

^{1}H-NMR (500 MHz, $CDCl_3$) spectrum of compound **4-20**

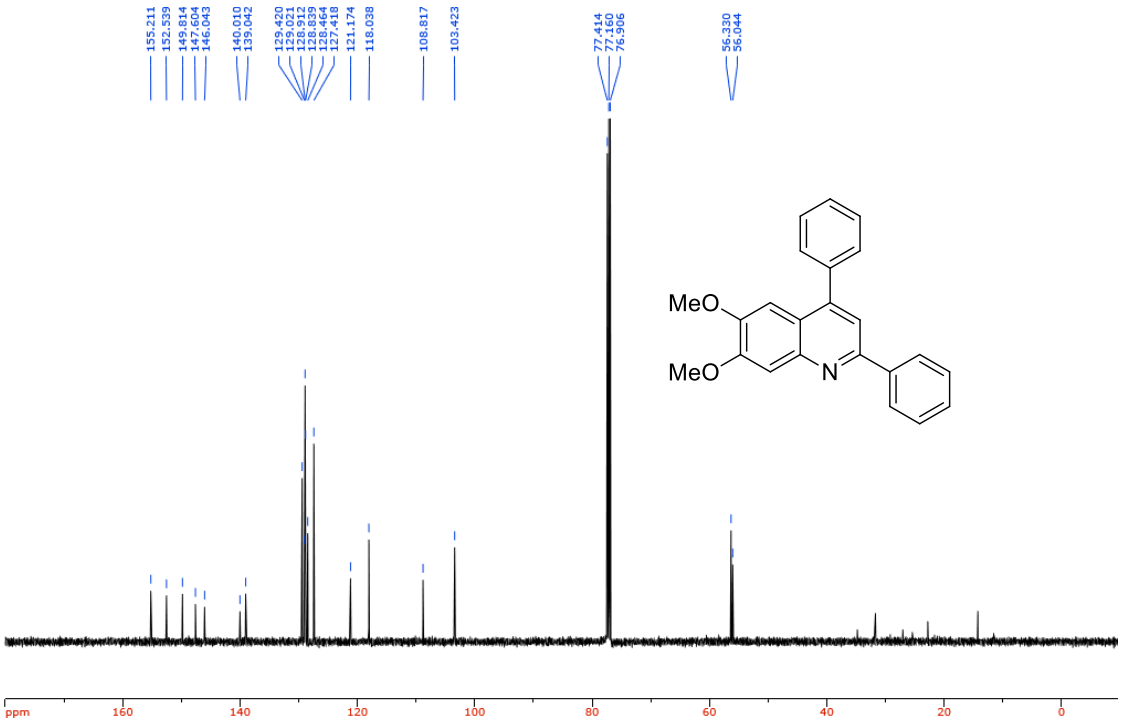

^{13}C-NMR (125 MHz, $CDCl_3$) spectrum of compound **4-20**

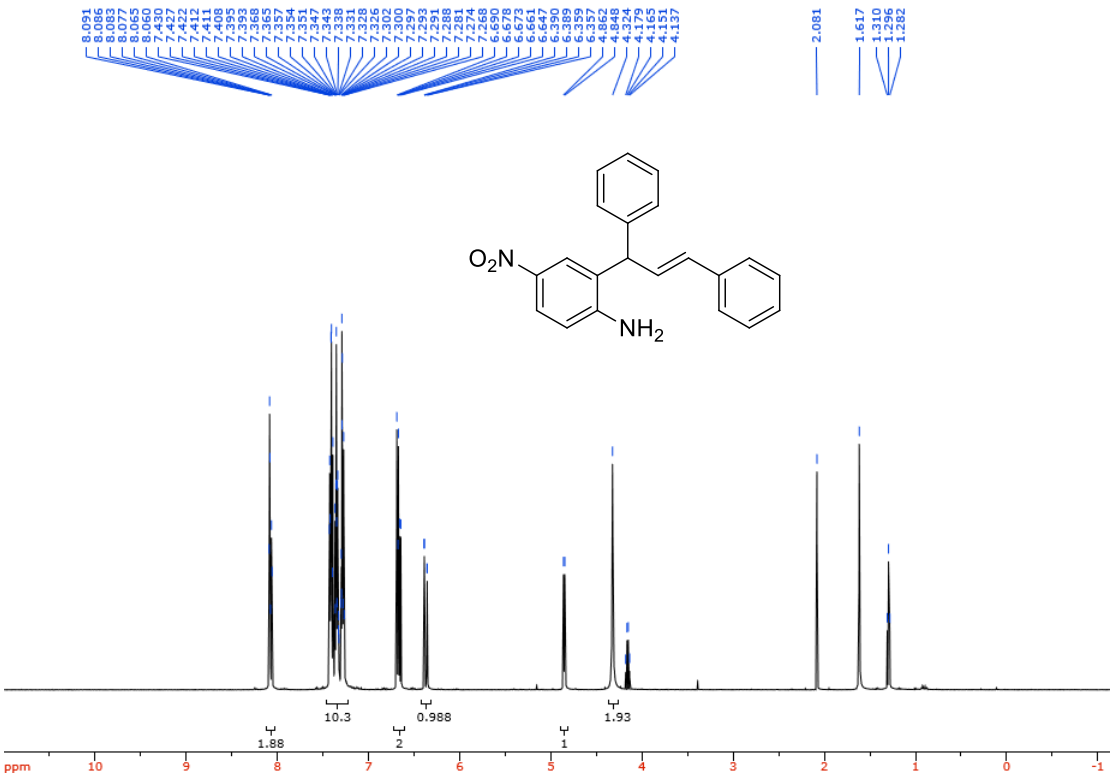

^{1}H-NMR (500 MHz, $CDCl_3$) spectrum of compound **4-15**

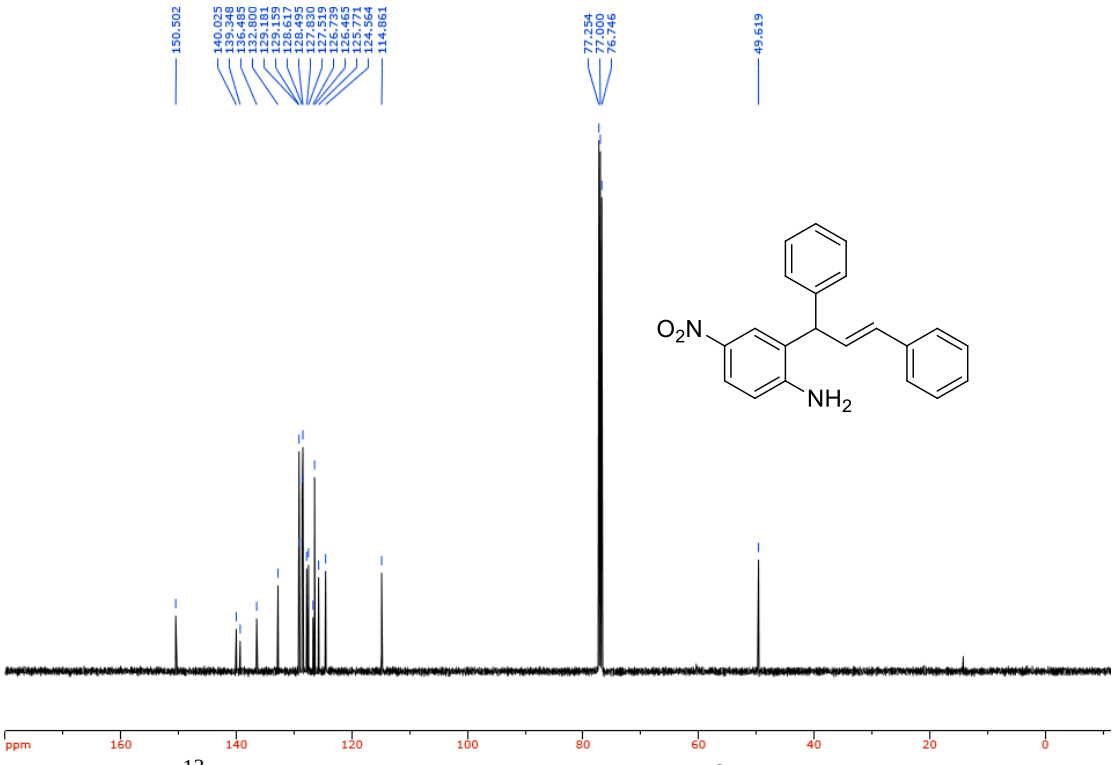

^{13}C-NMR (125 MHz, $CDCl_3$) spectrum of compound **4-15**

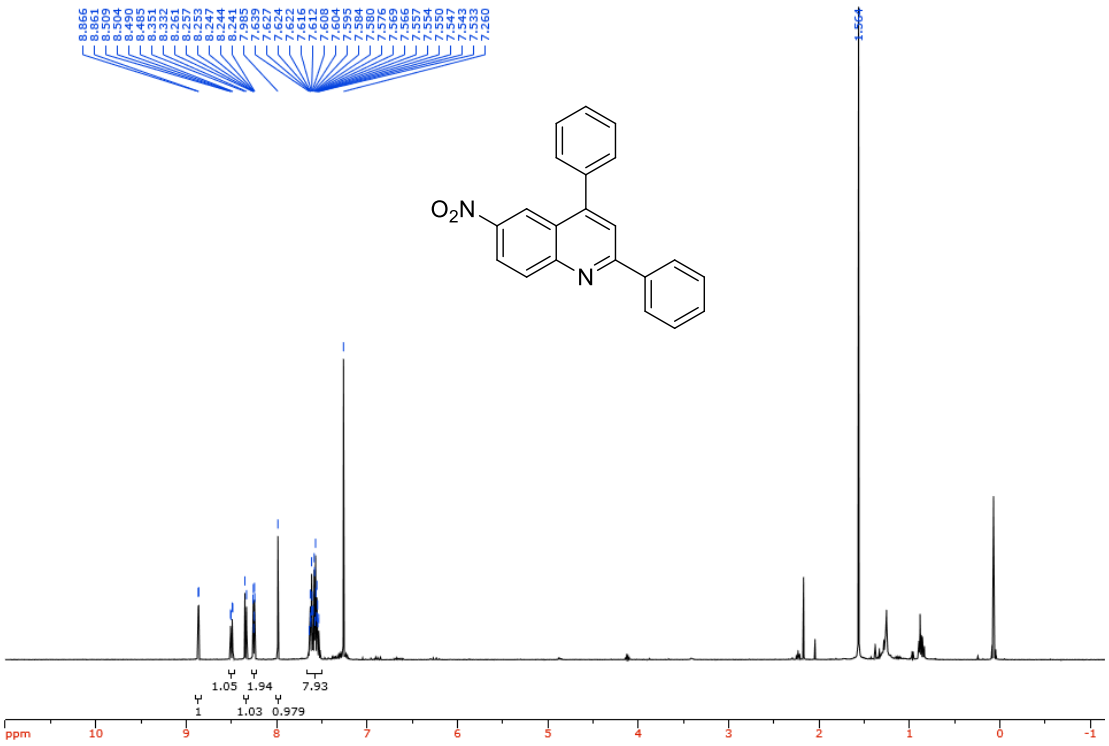

^{1}H-NMR (500 MHz, $CDCl_3$) spectrum of compound **4-19** with hexane residues

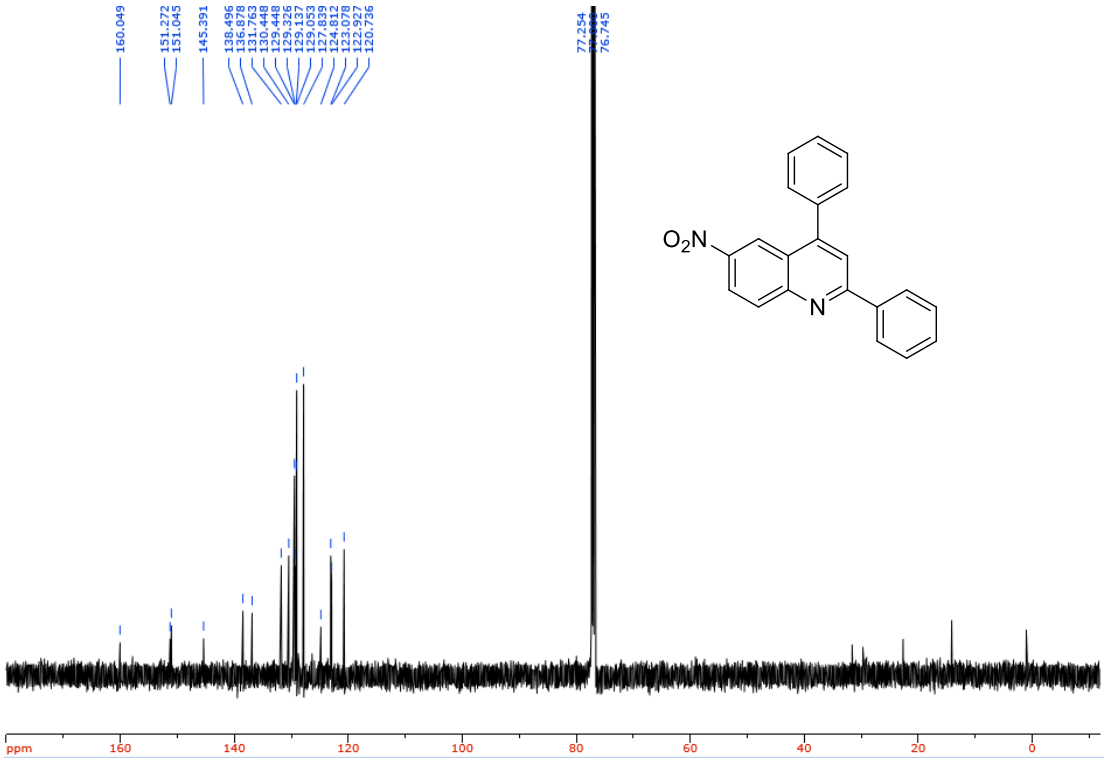

^{13}C-NMR (125 MHz, $CDCl_3$) spectrum of compound **4-19** with hexane residues

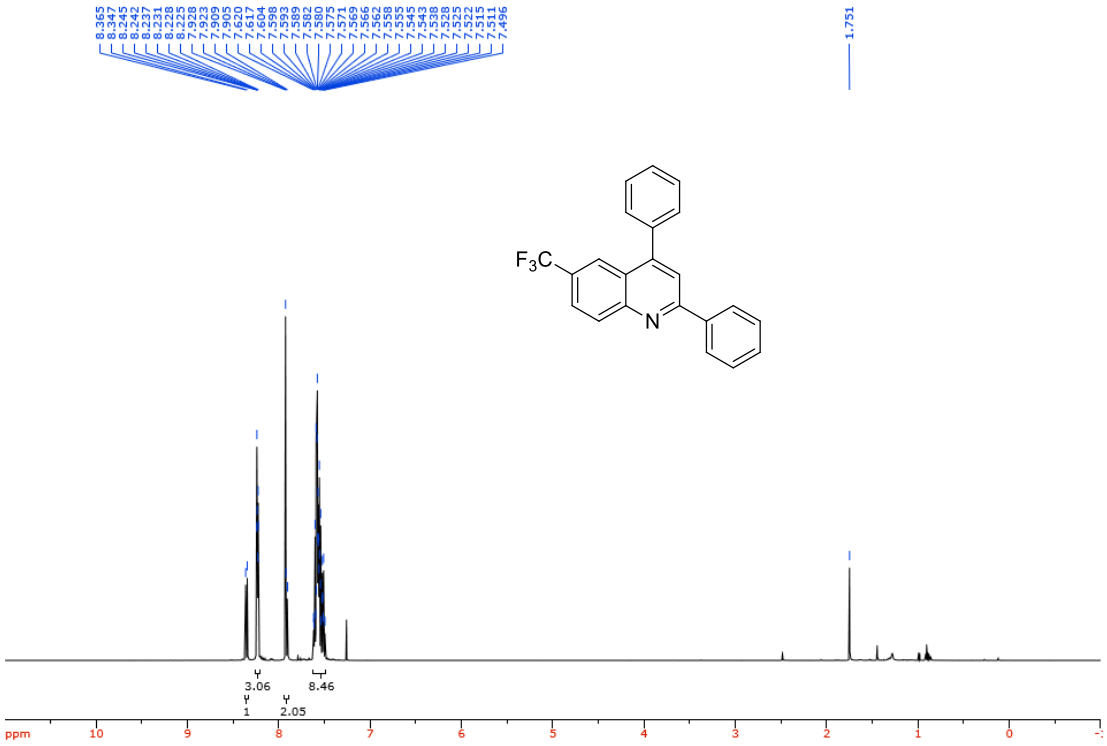

^{1}H-NMR (500 MHz, $CDCl_3$) spectrum of compound **4-22**

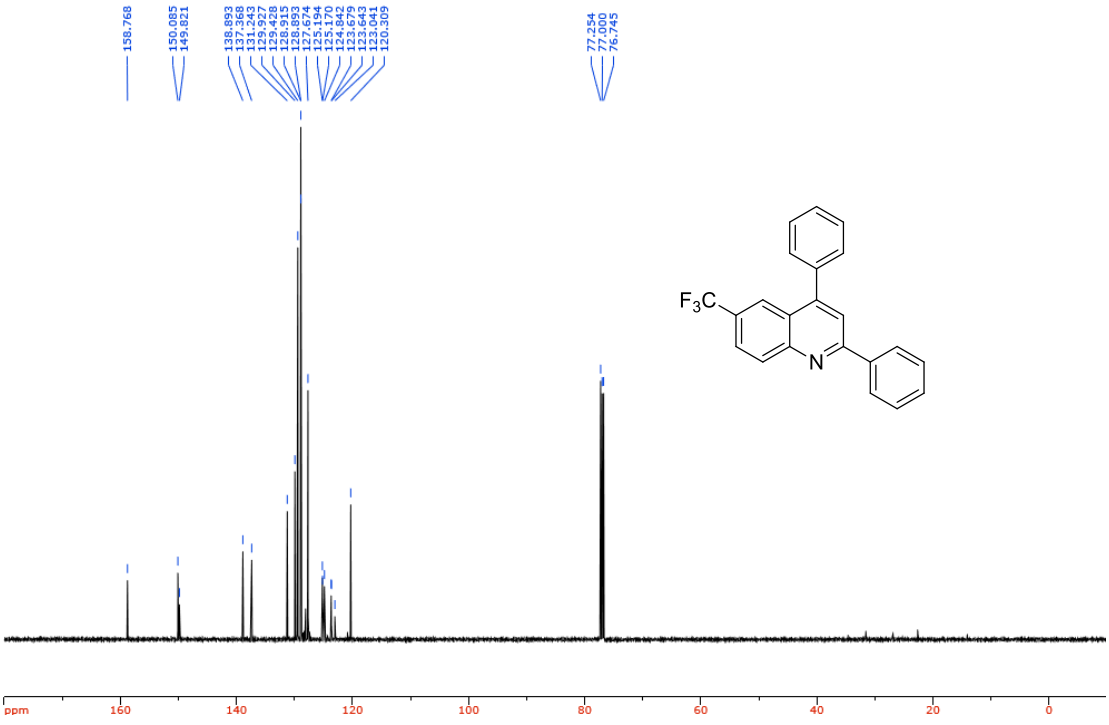

^{13}C-NMR (125 MHz, $CDCl_3$) spectrum of compound **4-22**

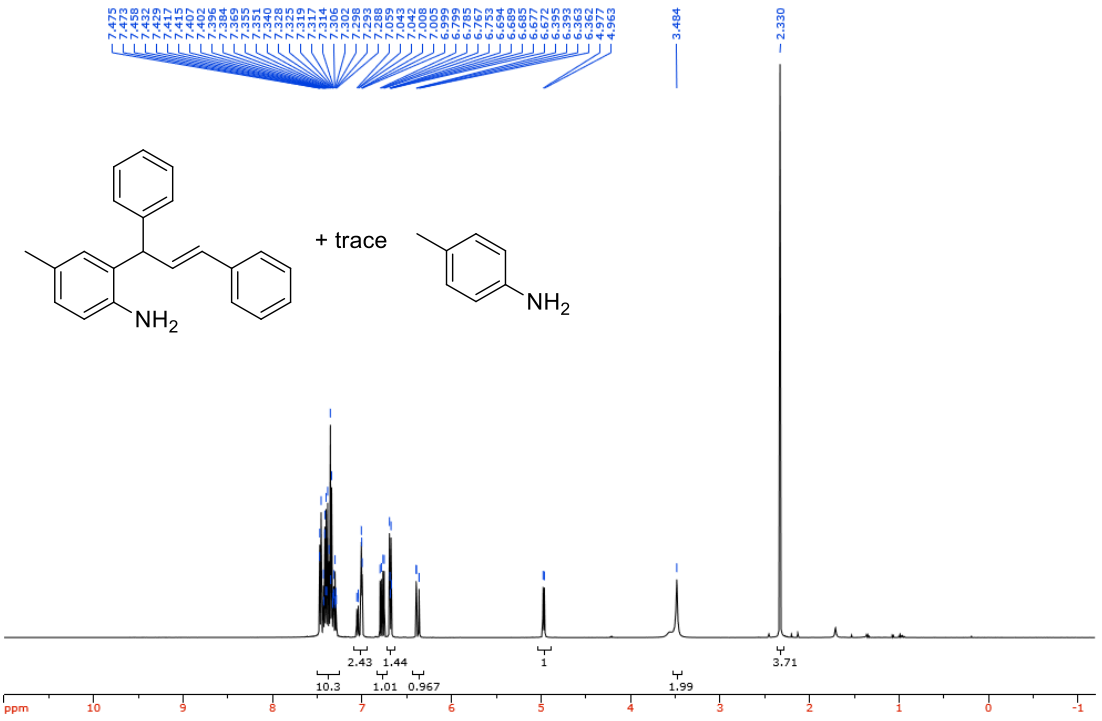

^{1}H-NMR (500 MHz, $CDCl_3$) spectrum of compound **4-17**

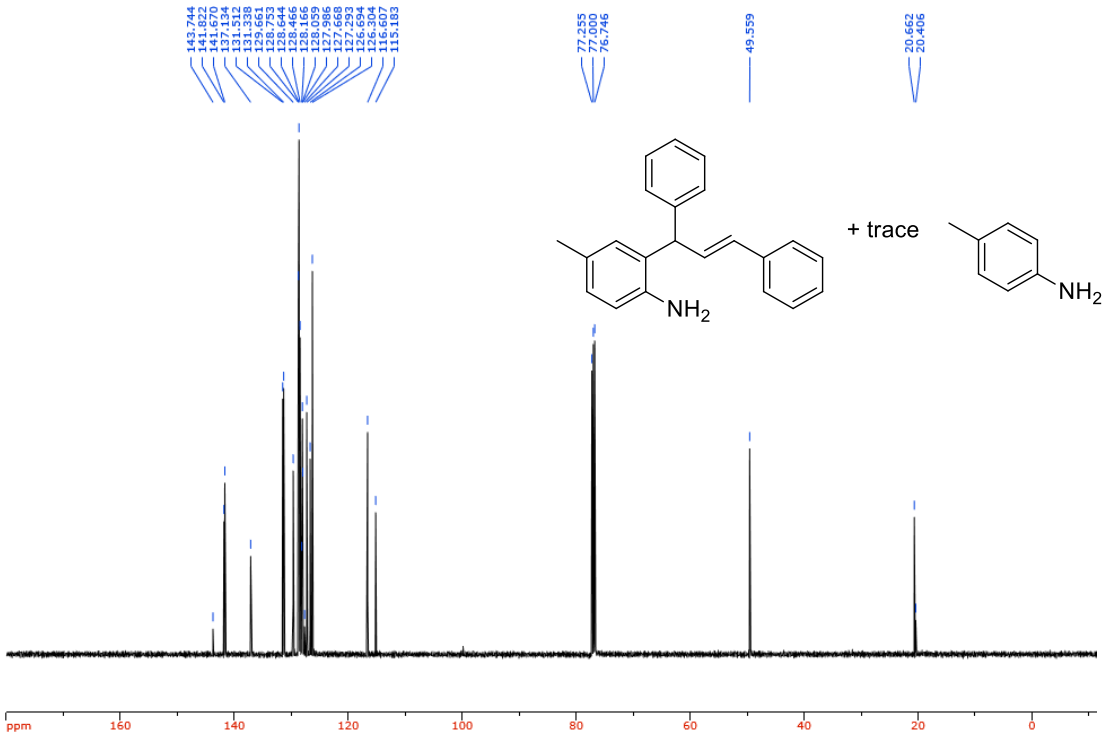

^{13}C-NMR (125 MHz, $CDCl_3$) spectrum of compound **4-17**

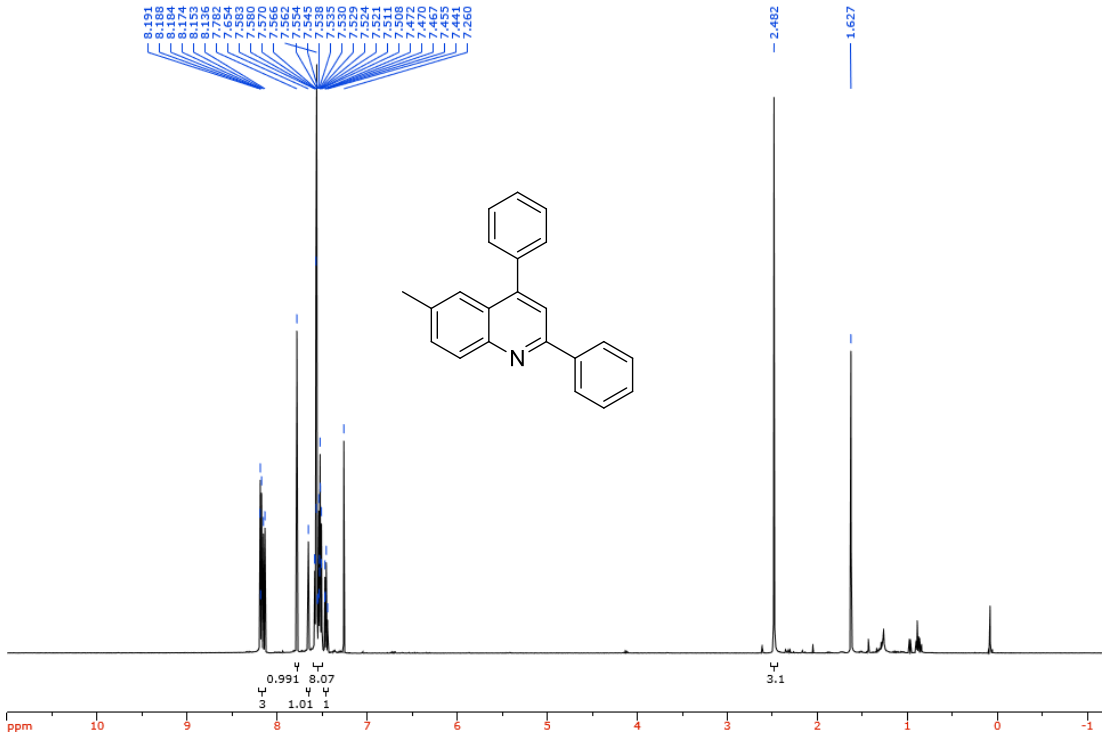

^{1}H-NMR (500 MHz, $CDCl_3$) spectrum of compound **4-21**

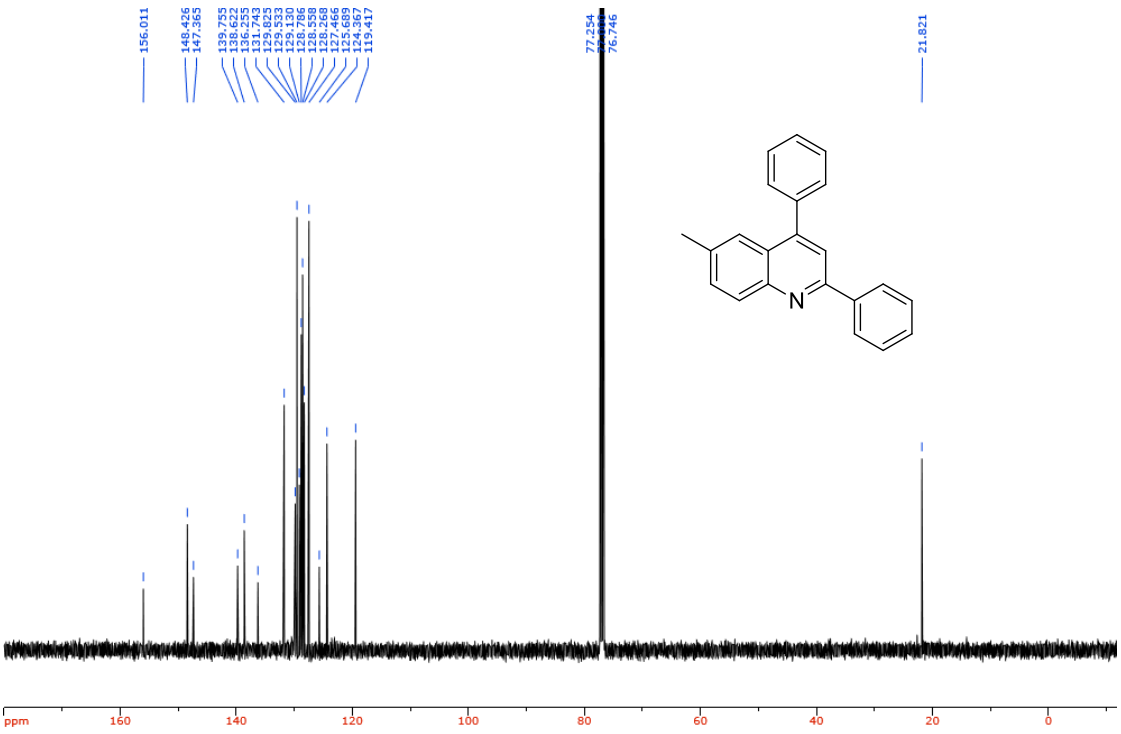

^{13}C-NMR (125 MHz, $CDCl_3$) spectrum of compound **4-21**

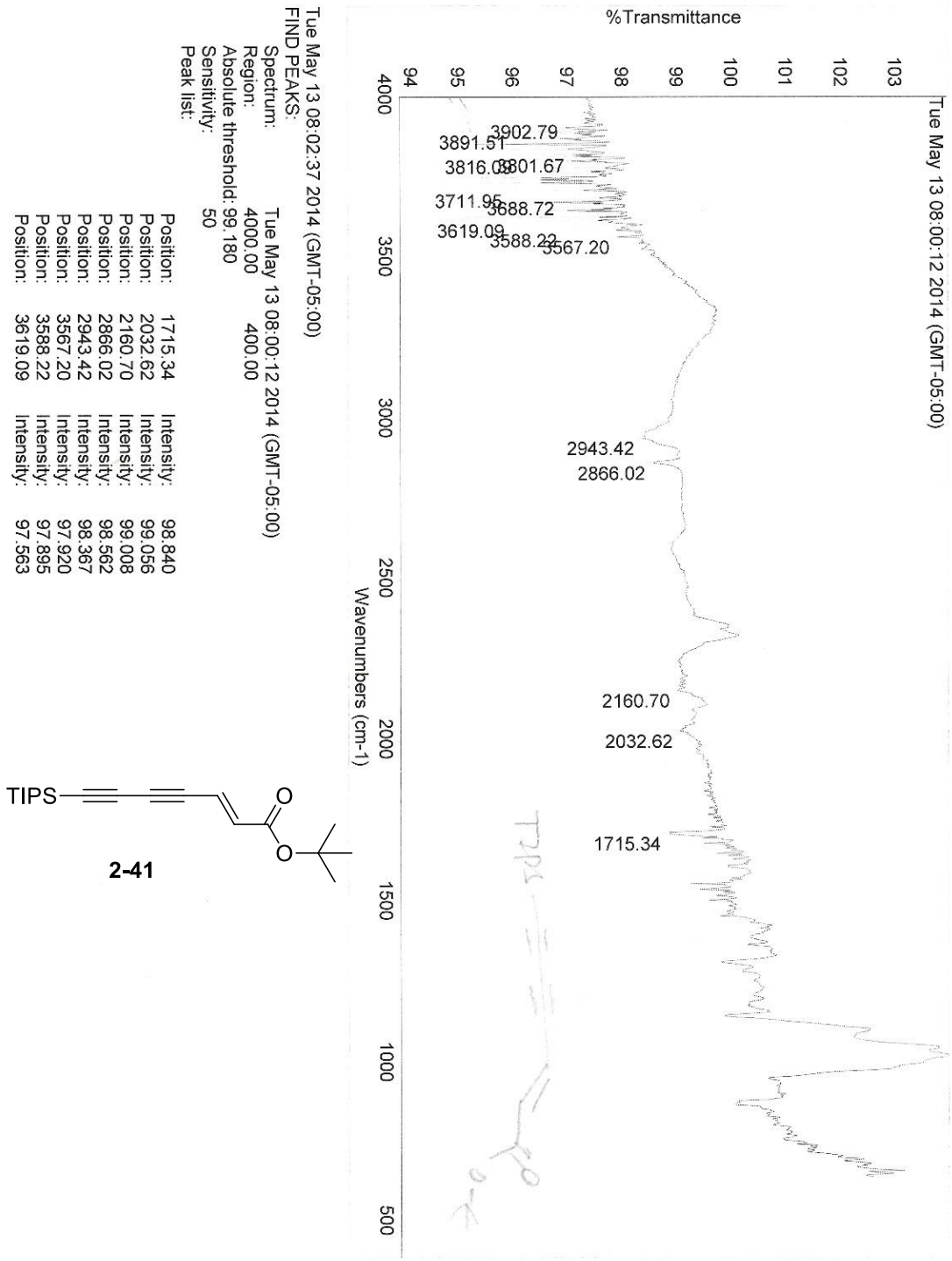

Tue May 13 08:02:37 2014 (GMT-05:00)
FIND PEAKS:
Spectrum: Tue May 13 08:00:12 2014 (GMT-05:00)
Region: 4000.00 400.00
Absolute threshold: 99.180
Sensitivity: 50
Peak list:

Position:	1715.34	Intensity:	98.840
Position:	2032.62	Intensity:	99.056
Position:	2160.70	Intensity:	99.008
Position:	2866.02	Intensity:	98.562
Position:	2943.42	Intensity:	98.367
Position:	3567.20	Intensity:	97.920
Position:	3588.22	Intensity:	97.895
Position:	3619.09	Intensity:	97.563

IR spectrum of compound **2-41**

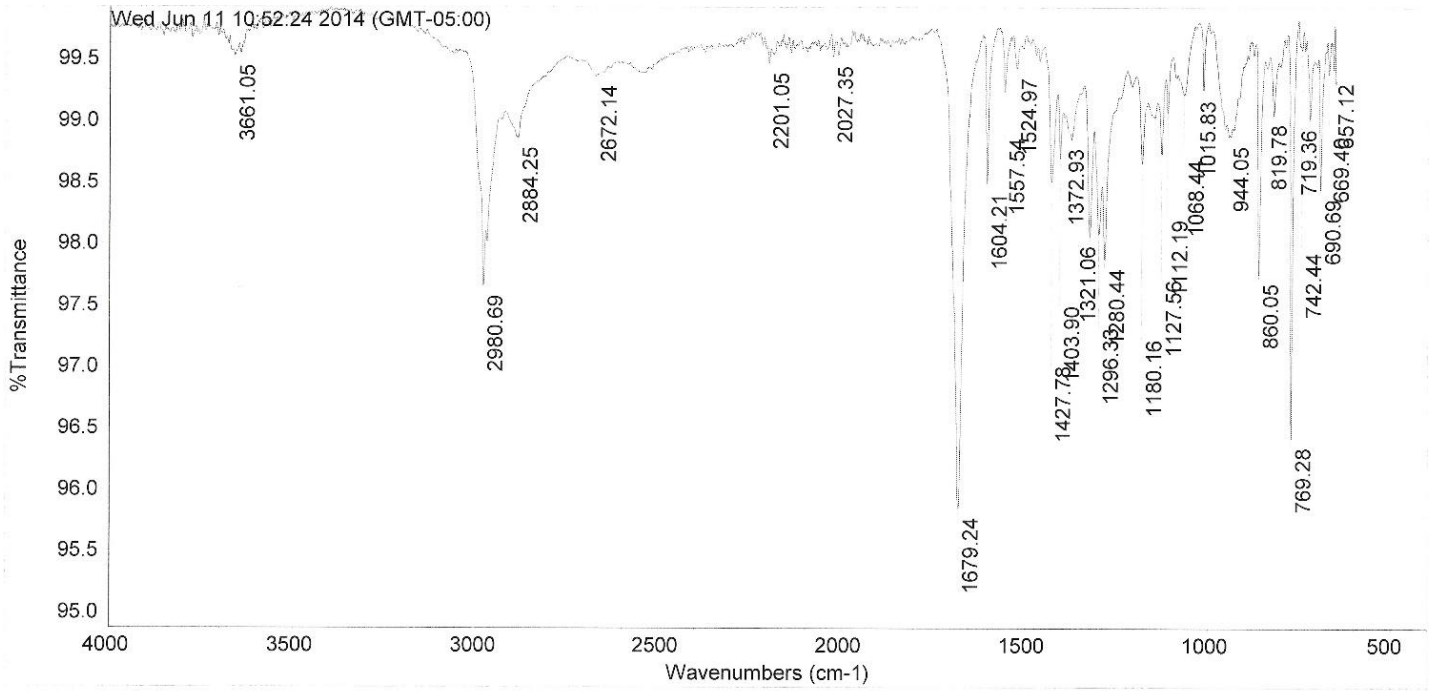

Wed Jun 11 10:54:36 2014 (GMT-05:00)
FIND PEAKS:

Spectrum:	Wed Jun 11 10:52:24 2014 (GMT-05:00)		
Region:	4000.00	400.00	
Absolute threshold:	99.672		
Sensitivity:	50		
Peak list:			
Position:	657.12	Intensity:	99.414
Position:	669.40	Intensity:	99.383
Position:	690.69	Intensity:	98.437
Position:	719.36	Intensity:	99.012
Position:	742.44	Intensity:	99.574
Position:	769.28	Intensity:	96.399
Position:	819.78	Intensity:	99.046
Position:	860.05	Intensity:	97.750

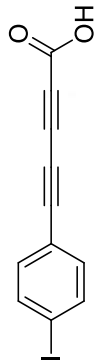

2-6

IR spectrum of compound **2-6**

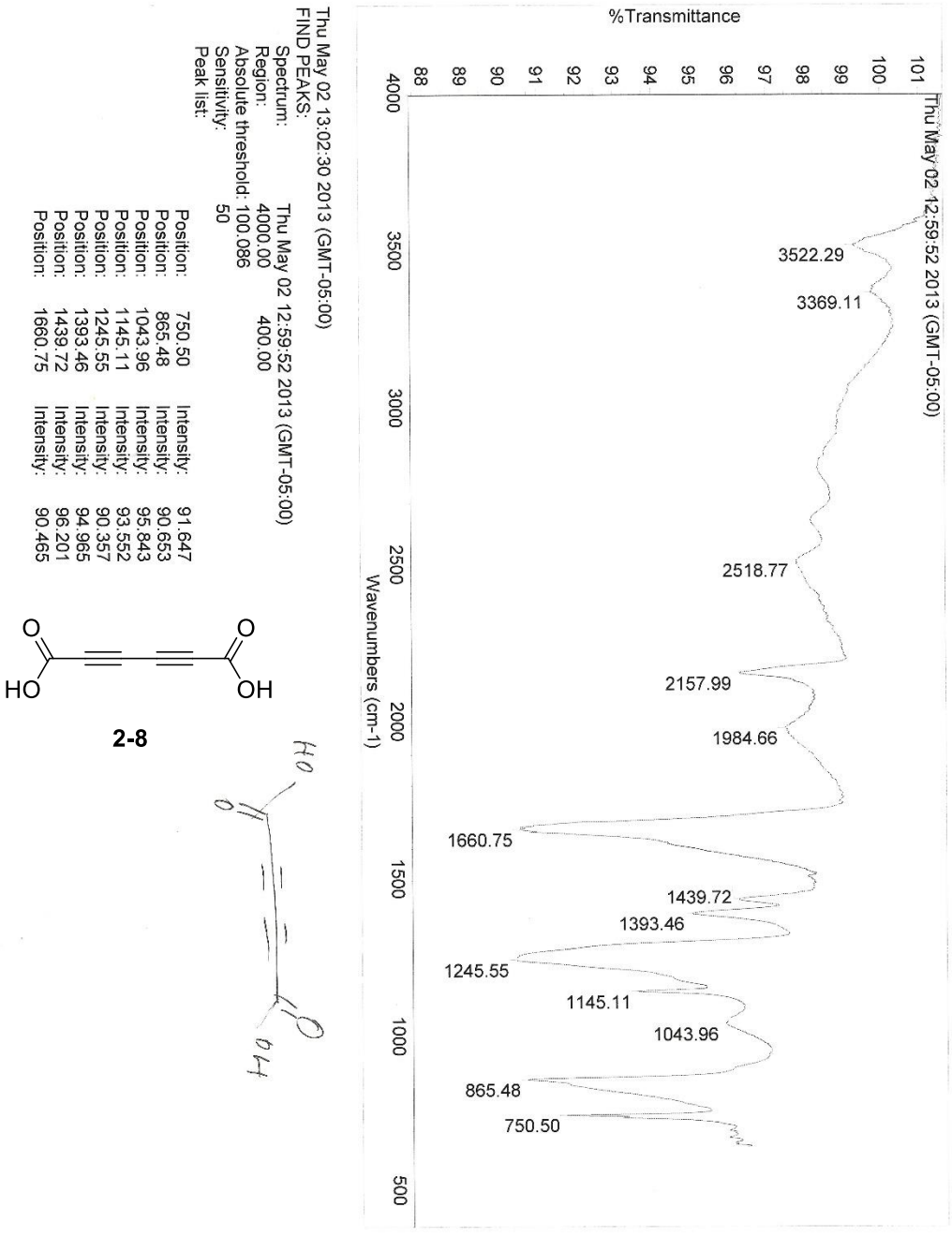

2-8

IR spectrum of compound **2-8**

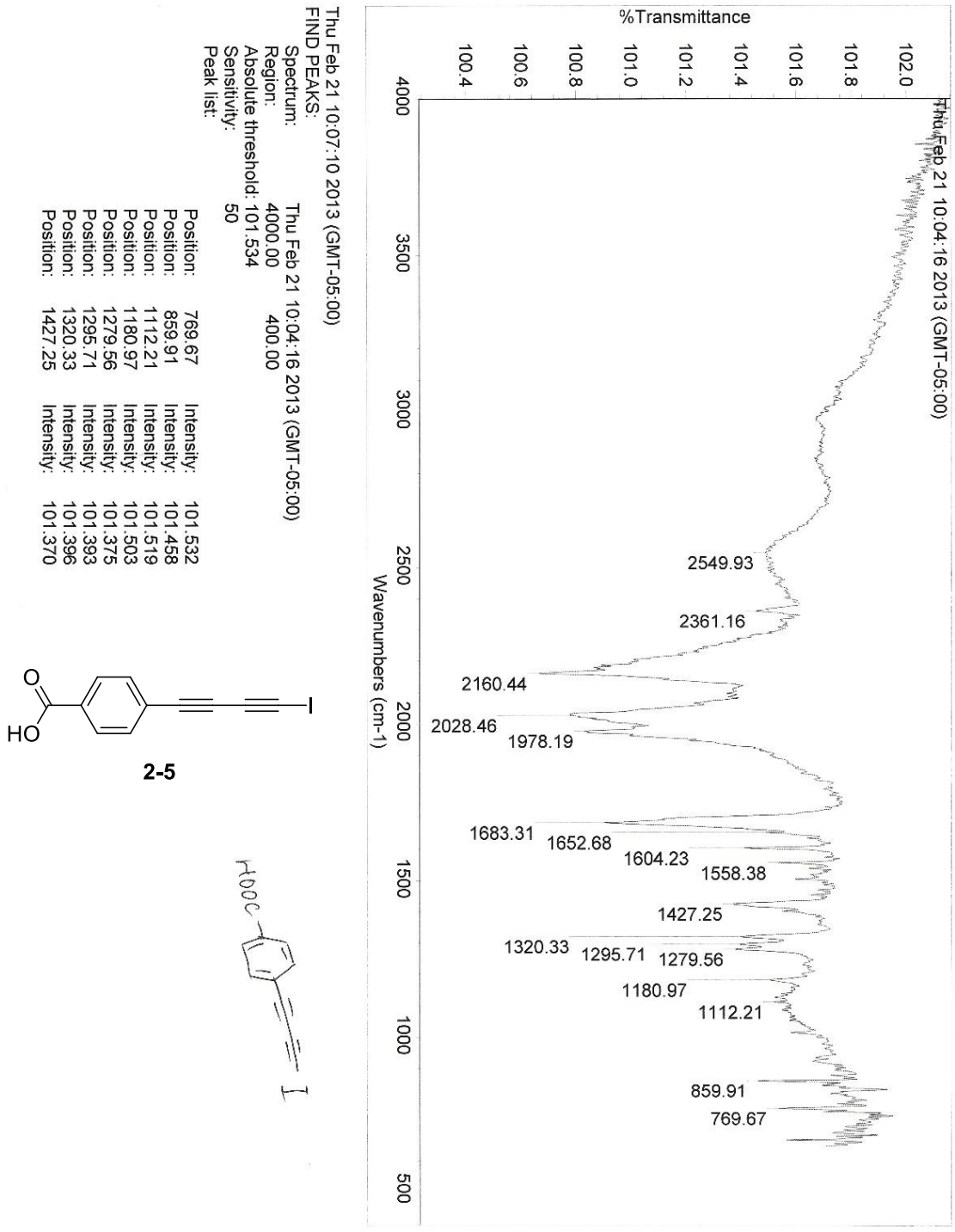

IR spectrum of compound **2-5**

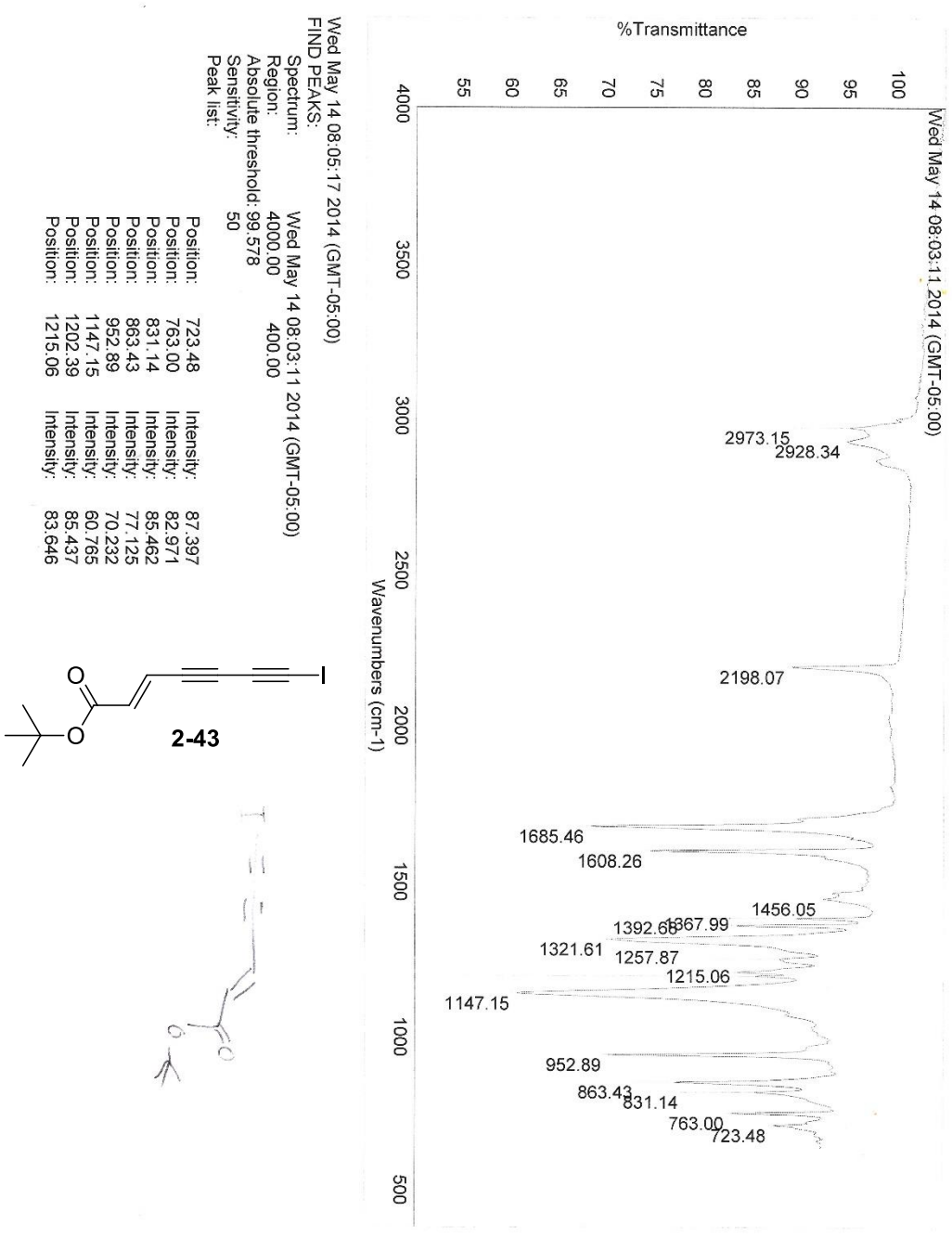

IR spectrum of compound **2-43**

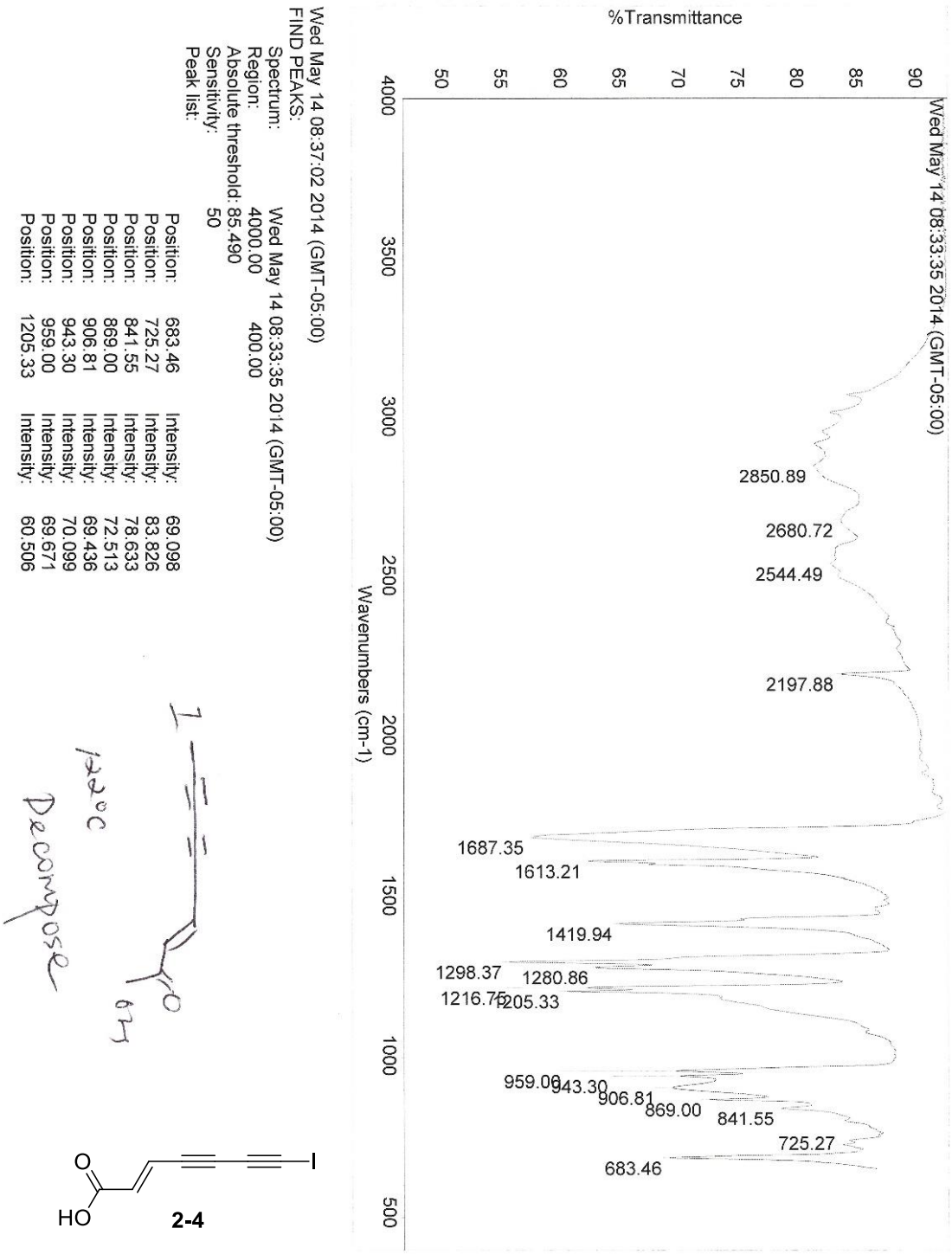

IR spectrum of compound **2-4**

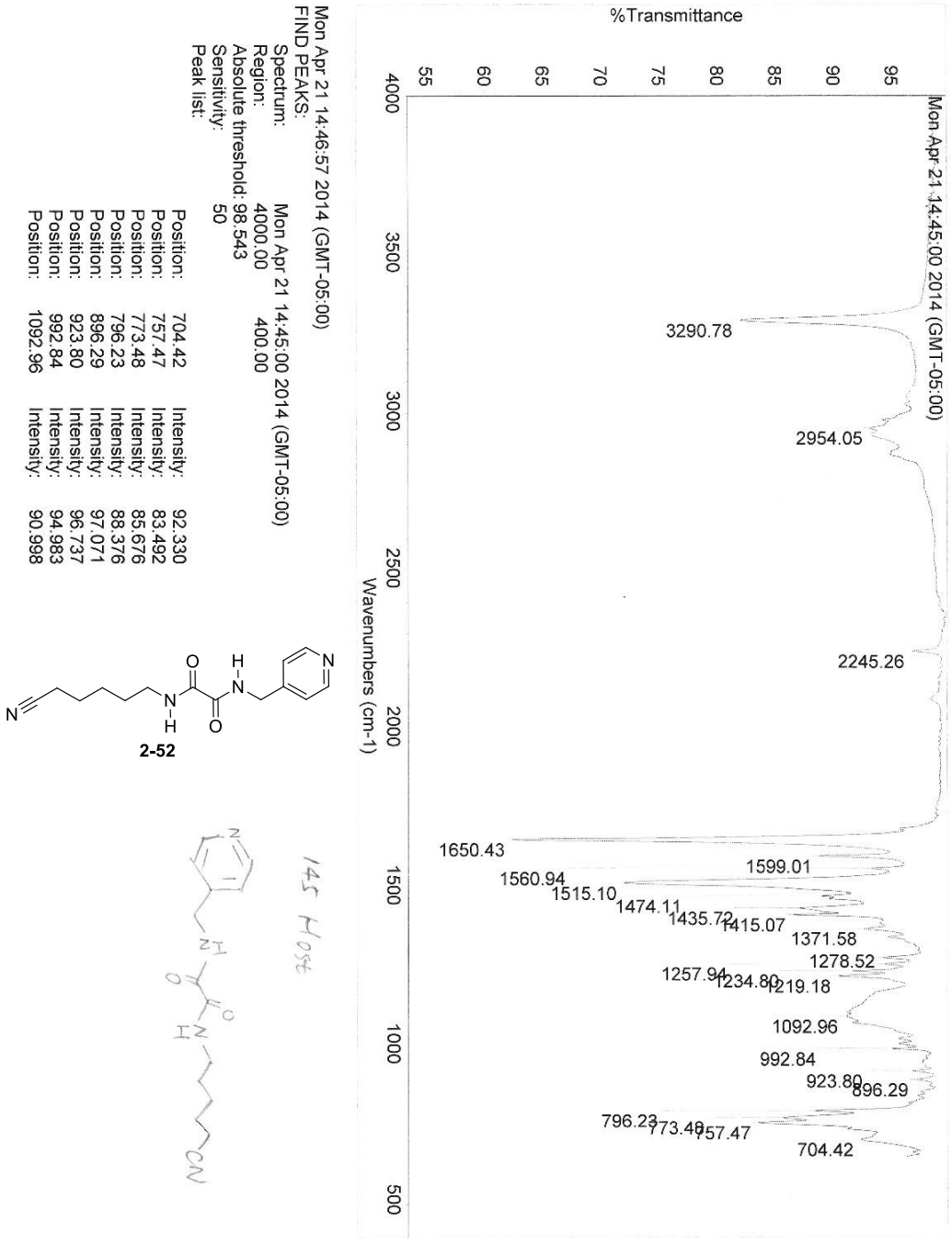

IR spectrum of compound **2-52**

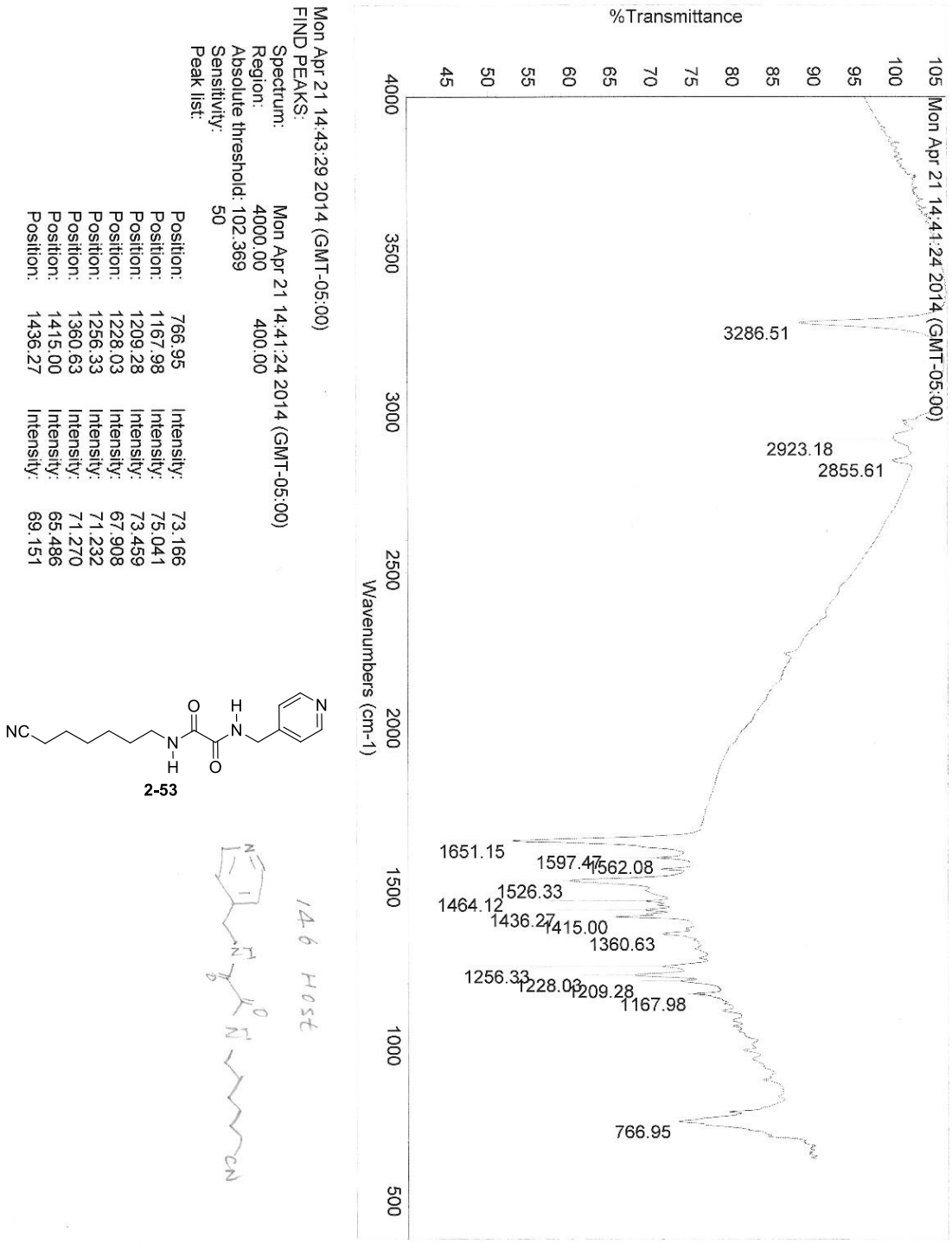

IR spectrum of compound **2-53**

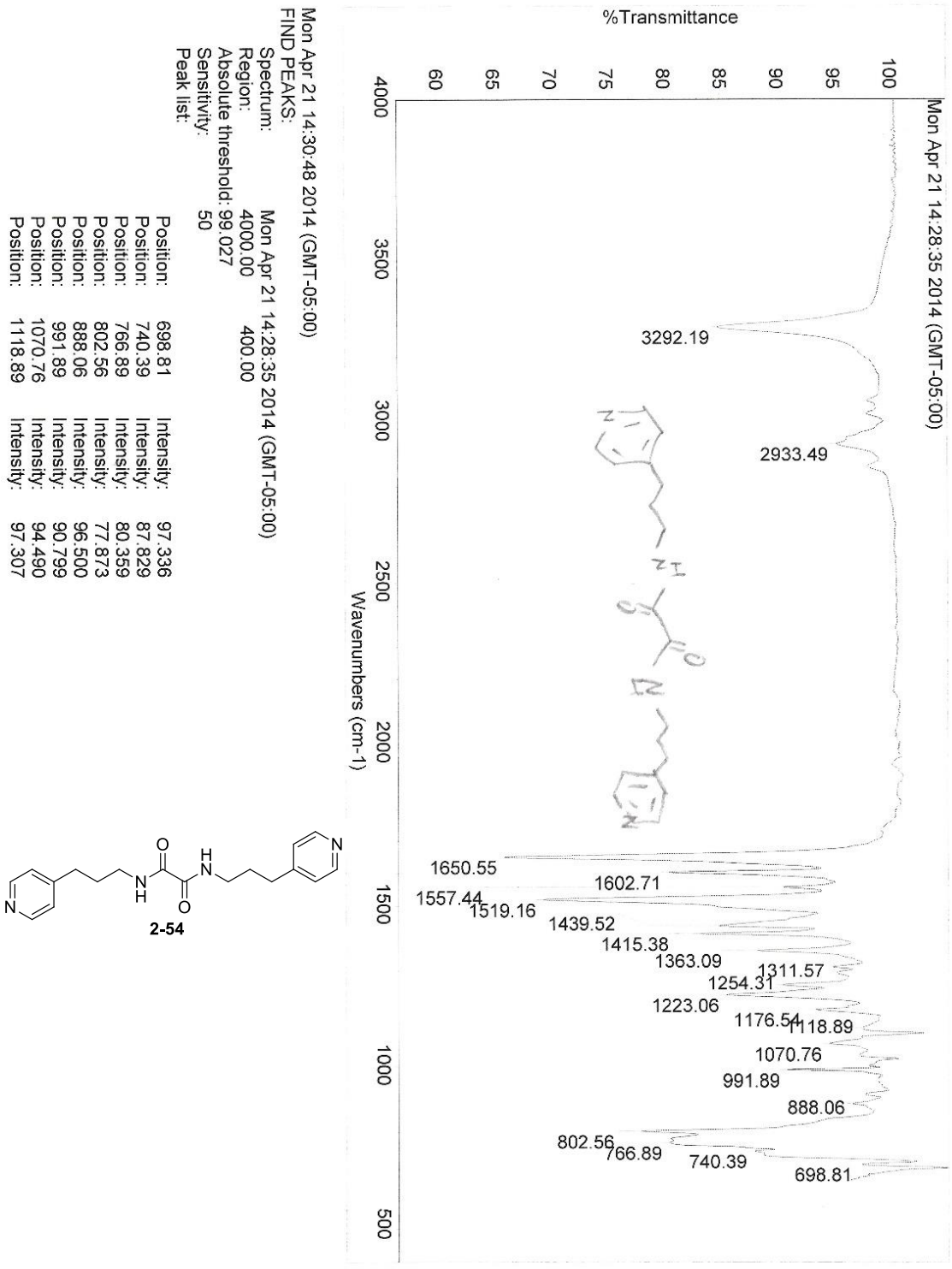

IR spectrum of compound **2-54**

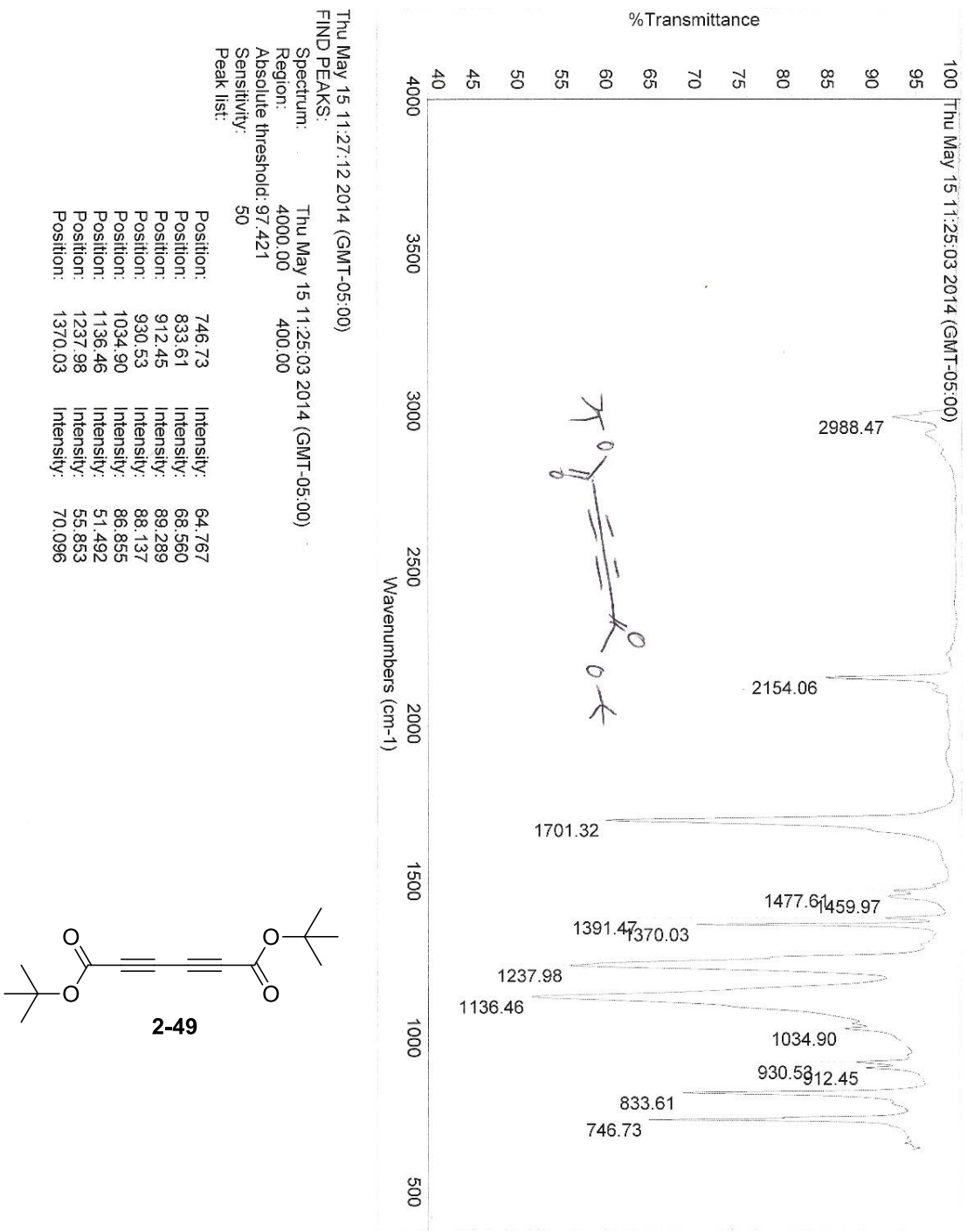

2-49

IR spectrum of compound **2-49**

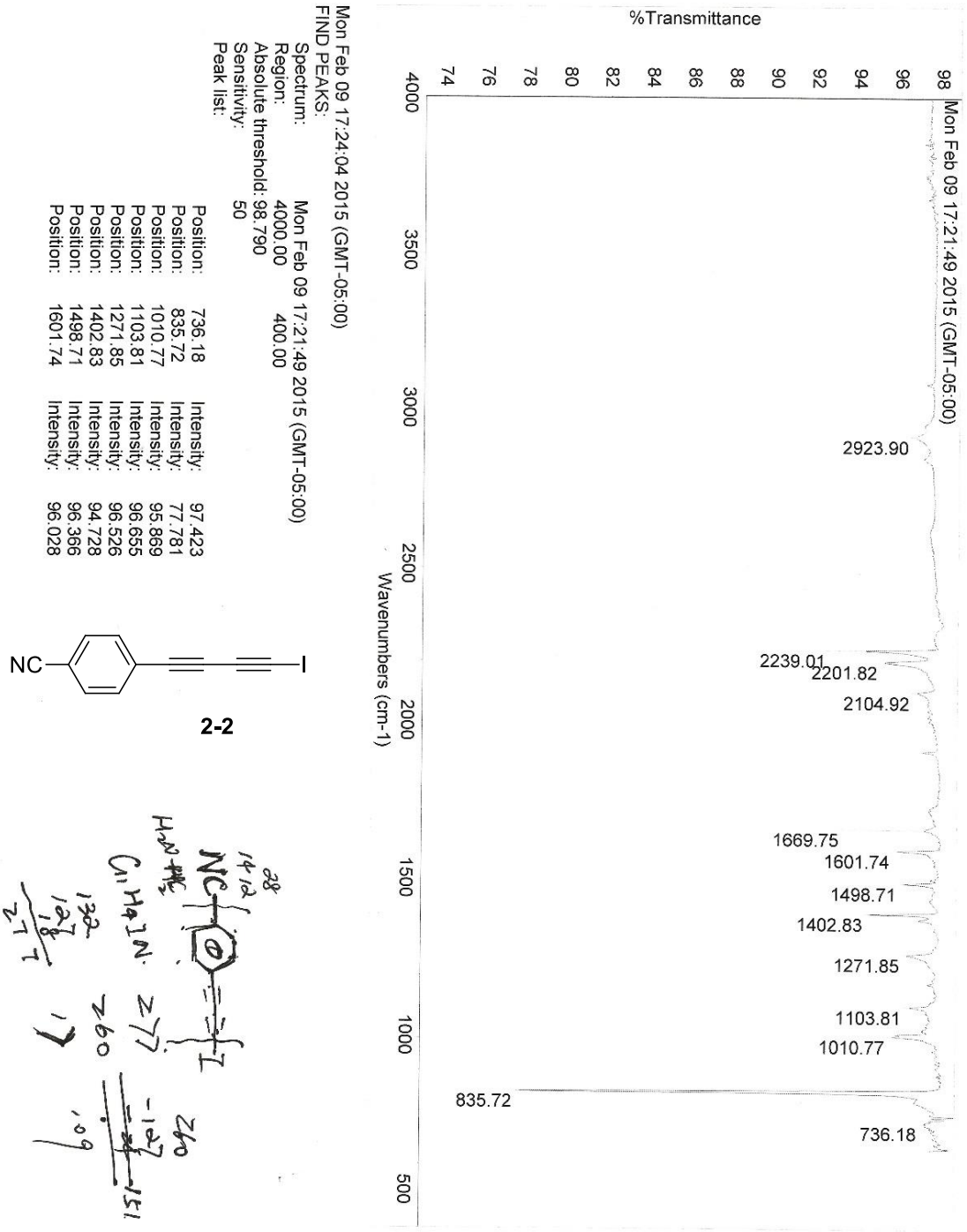

IR spectrum of compound **2-2**

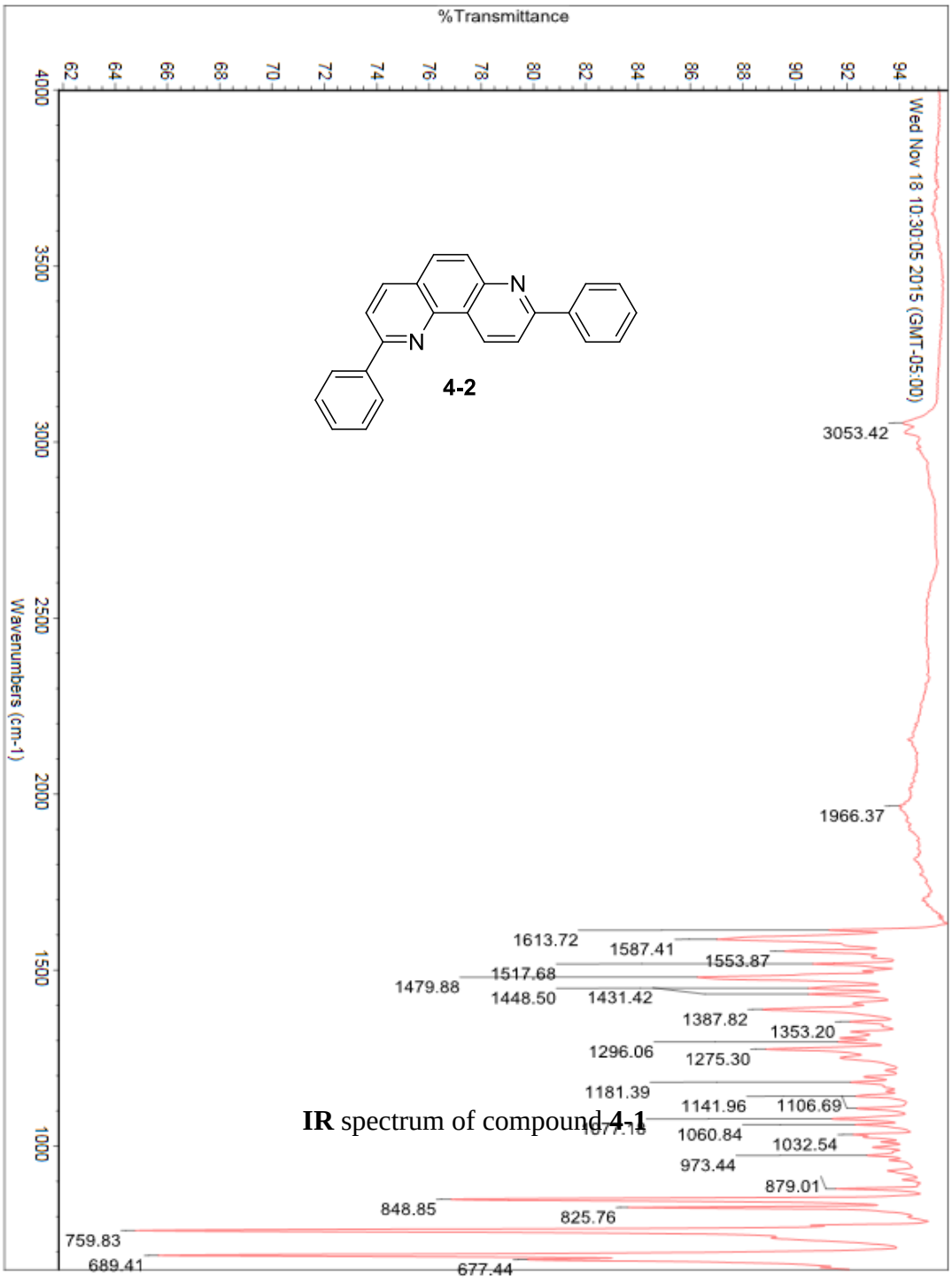

IR spectrum of compound **4-1**

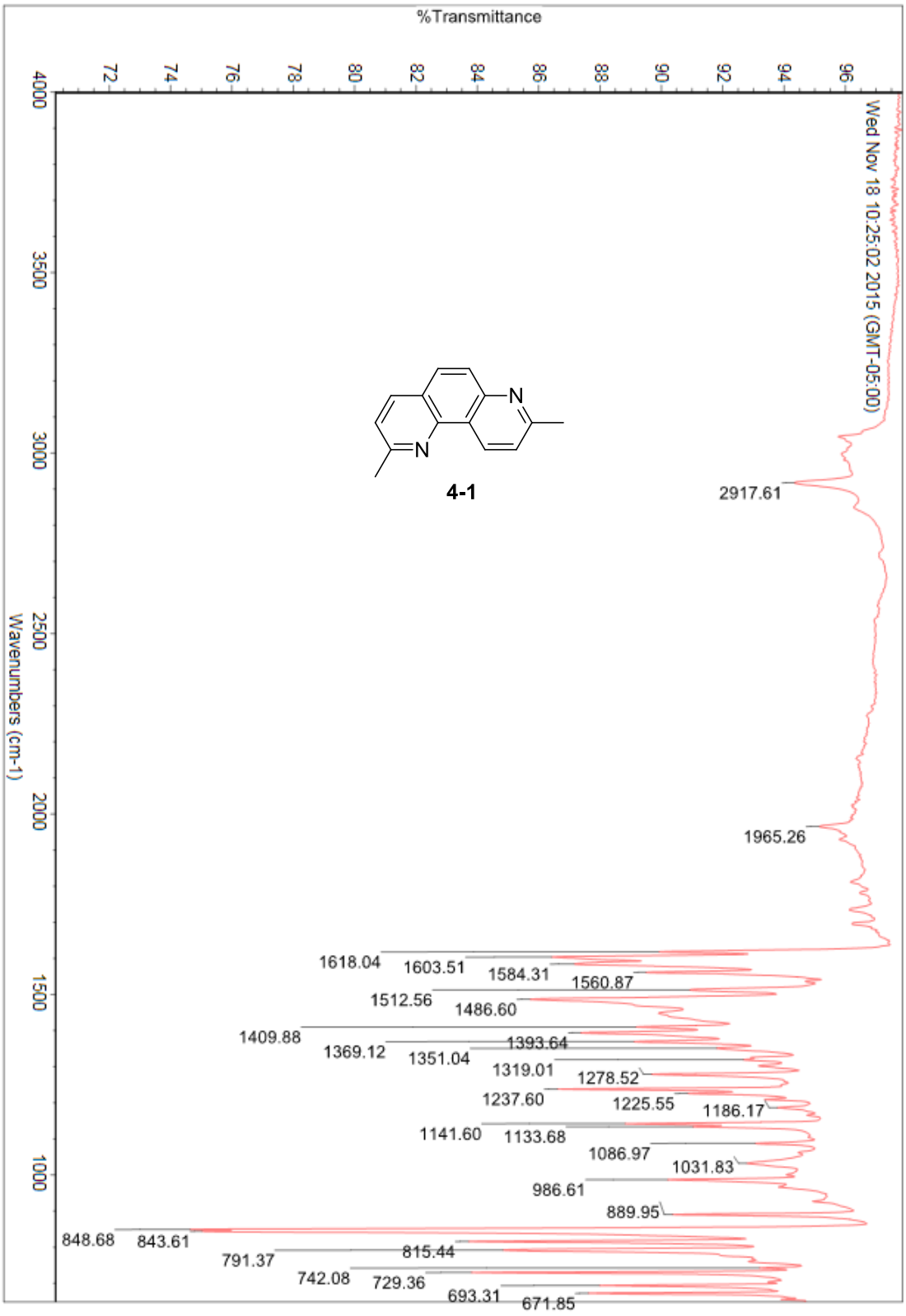
%Transmittance
72
74
76
78
80
82
84
86
88
90
92
94
96
4000
3500
3000
2500
2000
1500
1000
Wavenumbers (cm-1)
Wed Nov 18 10:25:02 2015 (GMT-05:00)
N
N
4-1
2917.61
1965.26
1618.04
1603.51
1584.31
1560.87
1512.56
1486.60
1409.88
1393.64
1369.12
1351.04
1319.01
1278.52
1237.60
1225.55
1186.17
1141.60
1133.68
1086.97
1031.83
986.61
889.95
848.68
843.61
815.44
791.37
742.08
729.36
693.31
671.85

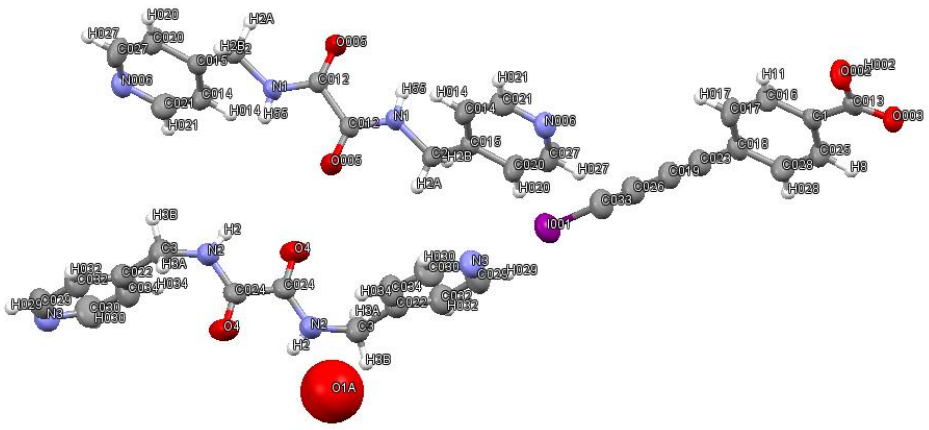

Figure Crystal structure for **2-5:1-10** co-crystal

Table 1 Crystal data and structure refinement for the **2-5:1-10** co-crystal

Identification code	iodobenzoicaciddiyne_cocrystal
Empirical formula	C25 H19 I N4 O5
Formula weight	582.34
Temperature/K	293(2)
Crystal system	Triclinic
Space group	P -1
a/Å	7.1475(3)
b/Å	11.4791(5)
c/Å	16.5782(8)
α/°	88.237(4)
β/°	78.605(4)
γ/°	76.309(4)
Volume/Å^3	1295.31(10)
Z	2
ρ_{calcmg}/mm^3	1.493
m/mm^{-1}	1.272
F(000)	564.0
Crystal size/mm^3	N/A × N/A × N/A
2θ range for data collection	7.52° to 52.74°
Index ranges	$-8 \le h \le 8$, $-14 \le h \le 14$, $-20 \le l \le 20$
Reflections collected	11203
Independent reflections	5274[R(int) =0.0262]
Data/restraints/parameters	5274/0/316
Goodness-of-fit on F^2	1.136
Final R indexes [I >= 2σ (I)]	R_1 = 0.0498, wR_2 = 0.1393

Final R indexes [all data]	R_1 = 0.0659, wR_2 = 0.1520
Largest diff. peak/hole / e Å^{-3}	0.932/-0.503

Table 2 Fractional Atomic Coordinates (×10^4) and Equivalent Isotropic Displacement Parameters (Å^2×10^3) for the **2-5:1-10** co-crystal**.** U_{eq} is defined as 1/3 of the trace of the orthogonalised U_{IJ} tensor

Atom	***x***	***y***	***z***	U_{eq}
C1	1.3381(6)	0.6075(4)	1.1612(2)	0.0395(9)
C2	0.4540(6)	0.3509(4)	0.3551(3)	0.0447(9)
C3	-0.5613(8)	1.1252(4)	0.6677(3)	0.0611(13)
C012	0.4824(6)	0.4427(3)	0.4832(3)	0.0410(9)
C013	1.5073(6)	0.5723(4)	1.2047(3)	0.0436(9)
C014	0.1129(7)	0.4728(4)	0.3472(3)	0.0539(11)
C015	0.2725(6)	0.3805(3)	0.3198(2)	0.0389(8)
C016	1.3273(7)	0.5455(5)	1.0927(3)	0.0527(11)
C017	1.1694(7)	0.5801(5)	1.0546(3)	0.0568(12)
C018	1.0163(6)	0.6785(4)	1.0845(3)	0.0465(10)
C019	0.7094(7)	0.7475(4)	1.0151(3)	0.0541(11)
C020	0.2609(7)	0.3127(4)	0.2536(3)	0.0550(11)
C021	-0.0463(7)	0.4948(4)	0.3092(3)	0.0576(12)
C022	-0.3964(7)	1.0664(4)	0.7115(3)	0.0527(11)
C023	0.8520(7)	0.7157(4)	1.0450(3)	0.0533(11)
C024	-0.5295(8)	1.0026(4)	0.5480(3)	0.0555(12)
C025	1.1878(7)	0.7044(4)	1.1917(3)	0.0546(11)
C026	0.5497(8)	0.7853(5)	0.9779(3)	0.0579(12)
C027	0.0967(7)	0.3413(5)	0.2190(3)	0.0615(13)
C028	1.0288(7)	0.7404(4)	1.1530(3)	0.0568(12)
C029	-0.2830(9)	1.0134(5)	0.8372(4)	0.0705(14)
C030	-0.0695(8)	0.9670(6)	0.7180(4)	0.0755(16)
C032	-0.4338(8)	1.0651(5)	0.7972(3)	0.0642(13)
C033	0.4127(7)	0.8194(5)	0.9446(3)	0.0622(13)
C034	-0.2093(8)	1.0156(5)	0.6723(4)	0.0695(14)
N1	0.4782(5)	0.4485(3)	0.4037(2)	0.0435(8)
N2	-0.5158(7)	1.1040(4)	0.5800(3)	0.0582(11)
N3	-0.1018(7)	0.9654(4)	0.7990(3)	0.0670(12)
N006	-0.0555(6)	0.4307(4)	0.2456(2)	0.0521(9)
O002	1.6511(5)	0.4858(3)	1.1668(2)	0.0603(9)
O003	1.5101(5)	0.6184(3)	1.2684(2)	0.0583(8)
O4	-0.5781(7)	0.9200(3)	0.5860(2)	0.0766(11)
O005	0.4615(6)	0.3583(3)	0.5281(2)	0.0645(10)
I001	0.18998(5)	0.87839(3)	0.88540(2)	0.06766(17)
O1A	-0.012(3)	1.2312(16)	0.5065(11)	0.334(8)

Table 3 Anisotropic Displacement Parameters ($Å^2 \times 10^3$) for the **2-5:1-10** co-crystal
The Anisotropic displacement factor exponent takes the form: $-2\pi^2[h^2a^{*2}U_{11}+...+2hka \times b \times U_{12}]$

Atom	U_{11}	U_{22}	U_{33}	U_{23}	U_{13}	U_{12}
C1	44(2)	42(2)	38(2)	-12.6(17)	-19.6(18)	8.7(16)
C2	52(2)	37(2)	50(2)	-4.5(17)	-26(2)	-5(17)
C3	67(3)	52(3)	68(3)	-3(2)	-32(3)	-5(2)
C012	45(2)	39(2)	44(2)	-8(16)	-23.3(18)	3.6(17)
C013	50(2)	42(2)	46(2)	-15.2(19)	-24(2)	10.8(18)
C014	58(3)	50(3)	56(3)	-5(2)	-25(2)	-13(2)
C015	43(2)	37(2)	42(2)	-9.7(16)	-19.9(17)	4.7(16)
C016	44(2)	57(3)	54(3)	4(2)	-20(2)	-8(2)
C017	54(3)	68(3)	50(3)	-3(2)	-26(2)	-14(2)
C018	42(2)	55(3)	46(2)	-10.7(19)	-20(19)	6.5(19)
C019	48(2)	62(3)	53(3)	-7(2)	-19(2)	-2(2)
C020	53(3)	57(3)	57(3)	-1(2)	-27(2)	-14(2)
C021	45(2)	54(3)	74(3)	-3(2)	-22(2)	-6(2)
C022	55(3)	47(2)	60(3)	-8(2)	-25(2)	0(2)
C023	51(3)	58(3)	53(3)	-7(2)	-21(2)	2(2)
C024	70(3)	37(2)	61(3)	-1(2)	-31(2)	3(2)
C025	58(3)	57(3)	52(3)	-5(2)	-26(2)	-9(2)
C026	56(3)	63(3)	55(3)	-8(2)	-20(2)	0(2)
C027	58(3)	73(3)	61(3)	-13(2)	-29(2)	-17(2)
C028	52(3)	53(3)	64(3)	4(2)	-25(2)	-11(2)
C029	77(4)	81(4)	58(3)	-18(3)	-24(3)	10(3)
C030	50(3)	85(4)	84(4)	6(3)	-19(3)	-5(3)
C032	53(3)	75(3)	63(3)	-8(2)	-16(2)	-3(3)
C033	53(3)	75(3)	61(3)	-8(2)	-23(2)	-2(3)
C034	65(3)	85(4)	57(3)	-6(3)	-20(3)	-4(3)
N1	59(2)	39.6(18)	43(19)	-17.3(16)	-29.4(17)	9.5(15)
N2	80(3)	44(2)	60(3)	-15(2)	-35(2)	6(19)
N3	66(3)	64(3)	74(3)	-4(2)	-34(2)	2(2)
N006	47(2)	59(2)	58(2)	-14.1(18)	-27.8(18)	3.9(18)
O002	48.8(17)	75(2)	60(2)	-1.5(16)	-31.8(16)	-5.2(17)
O003	69(2)	57.9(19)	55.2(19)	-9.2(16)	-36.8(17)	-1.2(15)
O4	120(3)	42.6(19)	67(2)	-23(2)	-15(2)	5.5(17)
O005	115(3)	43.1(17)	47.8(18)	-29.6(18)	-33.2(19)	8.5(14)
I001	55.8(2)	76.2(3)	76.7(3)	-9.48(17)	-35.34(19)	10.66(18)

Table 4 Bond lengths for the **2-5:1-10** co-crystal

Atoms 1,2	d 1,2 [Å]	Atoms 1,2	d 1,2 [Å]
C1—C025	1.378(6)	C020—C027	1.374(6)
C1—C016	1.384(6)	C020—H020	0.9300
C1—C013	1.497(5)	C021—N006	1.324(6)
C2—N1	1.462(5)	C021—H021	0.9300
C2—C015	1.489(5)	C022—C034	1.364(7)
C2—H2A	0.9700	C022—C032	1.393(7)
C2—H2B	0.9700	C024—O4	1.204(6)
C3—N2	1.439(7)	C024—N2	1.327(6)
C3—C022	1.518(7)	C024—C024^{ii}	1.562(10)
C3—H3A	0.9700	C025—C028	1.387(6)
C3—H3B	0.9700	C025—H8	0.99(6)
C012—O005	1.223(5)	C026—C033	1.197(7)
C012—N1	1.324(5)	C027—N006	1.320(6)
C012—C012^{i}	1.537(8)	C027—H027	0.9300
C013—O003	1.201(5)	C028—H028	0.9300
C013—O002	1.318(6)	C029—N3	1.319(7)
C014—C015	1.372(6)	C029—C032	1.382(8)
C014—C021	1.376(7)	C029—H029	0.9300
C014—H014	0.9300	C030—N3	1.318(8)
C015—C020	1.391(6)	C030—C034	1.375(8)
C016—C017	1.372(6)	C030—H030	0.9300
C016—H11	0.77(5)	C032—H032	0.9300
C017—C018	1.398(6)	C033—I001	2.006(5)
C017—H017	0.9300	C034—H034	0.9300
C018—C028	1.387(6)	N1—H55	0.819(3)
C018—C023	1.427(6)	N2—H2	0.79(6)
C019—C023	1.197(6)	O002—H002	0.8200
C019—C026	1.378(7)		

(i) 1-x, 1-y, 1-z; (ii) -1-x, 2-y, 1-z.

Table 5 Bond angles for the **2-5:1-10** co-crystal

Atoms 1,2,3	Angle 1,2,3 [°]	Atoms 1,2,3	Angle 1,2,3 [°]
C025—C1—C016	119.5(4)	C034—C022—C032	116.7(5)
C025—C1—C013	118.2(4)	C034—C022—C3	124.1(5)
C016—C1—C013	122.2(4)	C032—C022—C3	119.1(5)
N1—C2—C015	113.9(3)	C019—C023—C018	177.4(5)
N2—C3—C022	114.2(4)	O4—C024—N2	125.9(5)
O005—C012—N1	126.5(4)	O4—C024—C024^{ii}	121.3(5)
O005—C012—C012^{i}	120.9(4)	N2—C024—C024^{ii}	112.8(5)
N1—C012—C012^{i}	112.6(4)	C1—C025—C028	120.1(4)
O003—C013—O002	123.5(4)	C033—C026—C019	178.8(6)

O003—C013—C1	122.9(4)	N006—C027—C020	123.4(4)
O002—C013—C1	113.6(3)	C018—C028—C025	120.8(4)
C015—C014—C021	120.2(4)	N3—C029—C032	123.8(5)
C014—C015—C020	116.3(4)	N3—C030—C034	124.6(5)
C014—C015—C2	124.6(4)	C029—C032—C022	119.2(5)
C020—C015—C2	119.1(4)	C026—C033—I001	177.9(5)
C017—C016—C1	120.6(4)	C022—C034—C030	119.5(5)
C016—C017—C018	120.6(4)	C012—N1—C2	124.3(3)
C028—C018—C017	118.3(4)	C024—N2—C3	121.2(5)
C028—C018—C023	120.6(4)	C3—N2—H2	130.(5)
C017—C018—C023	121.1(4)	C030—N3—C029	116.1(5)
C023—C019—C026	177.8(6)	C027—N006—C021	117.2(4)
C027—C020—C015	119.8(4)		
N006—C021—C014	123.2(4)		

(i) 1-x, 1-y, 1-z; (ii) -1-x, 2-y, 1-z.

Table 6 Hydrogen Atom Coordinates (Å $\times 10^4$) and Equivalent Isotropic Displacement Parameters (Å$^2 \times 10^3$) for the **2-5:1-10** co-crystal

Atom	***x***	***y***	***z***	U_{eq}
H2A	4516	2814	3896	54
H2B	5669	3295	3104	54
H3A	-6767	10957	6908	73
H3B	-5938	12110	6782	73
H014	1123	5206	3915	65
H017	11642	5376	10086	68
H020	3639	2483	2329	66
H021	-1527	5577	3291	69
H027	926	2952	1745	74
H028	9294	8068	11732	68
H029	-3108	10123	8944	85
H030	568	9329	6897	91
H032	-5587	10985	8271	77
H034	-1765	10138	6151	83
H002	17394	4703	11932	90
H8	1195(8)	753(5)	1239(3)	68(15)
H11	1410(7)	490(4)	1076(3)	39(12)
H55	4883	5119	3811	39(12)
H2	-514(9)	1150(6)	544(4)	80(2)

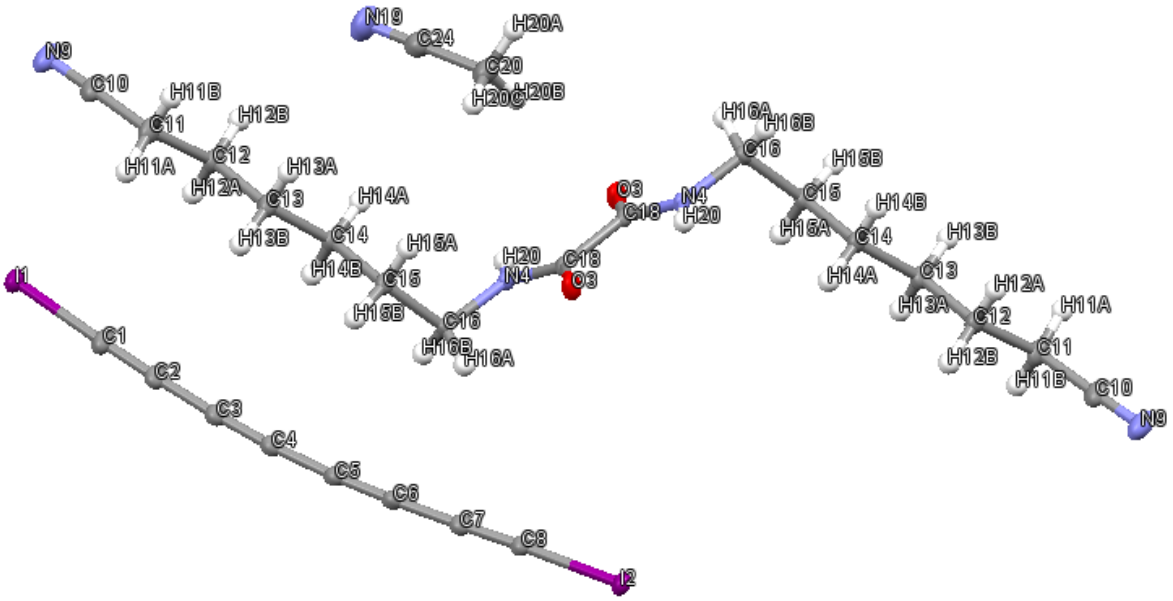

Figure Crystal structure for the **3-2:1-8:MeCN** co-crystal

Table 1 Crystal data and structure refinement for the **3-2:1-8:MeCN** co-crystal

Identification code	C8I2nitrilecocrystal
Empirical formula	C36 H32 I4 N6 O2
Formula weight	1088.27
Temperature/K	100
Crystal system	Monoclinic
Space group	P $2_1/c$
a/Å	5.144(5)
b/Å	14.442(5)
c/Å	26.480(5)
α/°	90.000(5)
β/°	92.445(5)
γ/°	90.000(5)
Volume/$Å^3$	1965(2)
Z	2
ρ_{calc}mg/mm^3	1.839
m/mm^{-1}	3.209
F(000)	1036
Crystal size/mm^3	0.5×0.2×0.1
2θ range for data collection	6.428° to 55.996°
Index ranges	$-6 \le h \le 6$, $-18 \le h \le 19$, $-24 \le l \le 24$
Reflections collected	11249
Independent reflections	4725[R(int) = 0.0252]

Data/restraints/parameters	4725/0/237
Goodness-of-fit on F^2	1.124
Final R indexes [I >= 2σ (I)]	R_1 = 0.0275, wR_2 = 0.0529
Final R indexes [all data]	R_1 = 0.0323, wR_2 = 0.0547
Largest diff. peak/hole / e $Å^{-3}$	0.781/-0.916

Table 2 Fractional Atomic Coordinates ($\times 10^4$) and Equivalent Isotropic Displacement Parameters ($Å^2 \times 10^3$) for the **3-2:1-8:MeCN** co-crystal. U_{eq} is defined as 1/3 of the trace of the orthogonalised U_{IJ} tensor

Atom	***x***	***y***	***z***	**U_{eq}**
C1	3315(5)	565(2)	6964.4(11)	19.6(6)
C2	4876(5)	568(2)	6639.1(11)	18.4(6)
C3	6704(5)	593.5(19)	6278(11)	18.2(6)
C4	8339(5)	650.7(19)	5964.2(11)	17.1(6)
C5	10190(5)	771.3(19)	5620.4(11)	16(6)
C6	11838(5)	924.2(19)	5315.4(11)	16.3(6)
C7	13631(5)	1127.5(19)	4967.4(11)	15.8(6)
C8	15165(5)	1327.2(19)	4654.7(11)	15.5(5)
C10	2775(5)	3061(2)	8023(11)	19.7(6)
C11	5056(5)	3020(2)	7707.2(11)	21.2(6)
C12	4458(5)	3171(2)	7143.5(11)	16.9(6)
C13	6940(5)	3075(2)	6853(11)	16.5(6)
C14	6553(5)	3180.6(19)	6283.8(11)	15.4(5)
C15	9129(5)	3082.9(19)	6019.3(10)	14.3(5)
C16	8872(5)	3076.4(18)	5449(11)	14.2(5)
C18	10410(5)	4535.3(17)	5120.9(10)	12.7(5)
C20	6361(6)	6001(2)	6027.9(13)	27.7(7)
C24	4230(6)	5824(2)	6355.9(12)	24.8(7)
N4	8436(4)	3994.8(16)	5229(9)	12.2(5)
N9	1037(5)	3080(2)	8268.7(10)	27.3(6)
N19	2575(5)	5678(2)	6617.2(12)	36.9(7)
O3	12728(3)	4339(13)	5195.4(8)	17.7(4)
I1	838.8(3)	596.2(2)	7525.4(2)	18.23(6)
I2	17623.1(3)	1620.8(2)	4110.7(2)	15.78(5)

Table 3 Anisotropic Displacement Parameters ($Å^2×10^3$) for the **3-2:1-8:MeCN** co-crystal. The Anisotropic displacement factor exponent takes the form: $-2\pi^2[h^2a^{*2}U_{11}+...+2hka×b×U_{12}]$

Atom	U_{11}	U_{22}	U_{33}	U_{23}	U_{13}	U_{12}
C1	19.7(13)	24.4(15)	14.7(15)	-0.8(12)	0.9(11)	-2.4(12)
C2	18(13)	20.2(14)	16.6(15)	-0.9(12)	-1.7(11)	-3.4(12)
C3	18.7(13)	17.7(13)	18(15)	-1.5(12)	-1.4(11)	-0.4(11)
C4	19.1(13)	14.6(13)	17.3(15)	-0.8(11)	-1.8(11)	-0.3(11)
C5	18(12)	15.1(13)	14.6(14)	-1.5(11)	-0.9(10)	1.2(11)
C6	17.5(12)	14.6(13)	16.7(15)	-2(11)	-1.5(10)	3.8(11)
C7	16.1(12)	16.1(13)	14.7(15)	-1.5(11)	-3.5(10)	1.2(11)
C8	16.8(12)	16.8(13)	12.6(14)	-0.7(11)	-1.2(10)	1.2(11)
C10	19.7(13)	26.5(15)	12.5(15)	-0.1(12)	-2.5(11)	-0.7(12)
C11	14.4(12)	32.9(16)	16.5(15)	1.2(13)	2.4(10)	-0.7(13)
C12	15.1(12)	20.7(14)	15(15)	1.6(11)	2.1(10)	1.3(11)
C13	15(12)	20.8(13)	13.7(14)	1.3(11)	0.4(10)	-0.9(11)
C14	13.7(12)	17.6(13)	15.1(14)	1.6(11)	2.4(10)	1.2(11)
C15	12.5(11)	16.5(13)	13.9(14)	1.5(11)	1(10)	-0.5(11)
C16	16(12)	10.9(12)	15.9(14)	2(11)	4.2(10)	-0.3(10)
C18	12.6(11)	15.5(13)	10(13)	0.4(11)	1.2(9)	-1.6(11)
C20	29(16)	33.4(18)	21.1(18)	-2.1(14)	6.2(13)	1.6(15)
C24	26.3(15)	26.7(16)	21.2(17)	-1.8(13)	-1.1(12)	4.6(13)
N4	10.1(10)	14.1(11)	12.6(12)	1.8(9)	1.7(8)	2.4(9)
N9	22.8(12)	42.3(16)	17.1(14)	-2.9(12)	2.3(10)	0.4(12)
N19	29.5(14)	51.1(19)	30.8(18)	4.4(15)	9.7(12)	7.4(14)
O3	11.3(8)	21.2(10)	20.8(11)	7.5(9)	1.4(7)	2.7(8)
I1	16.4(9)	23.06(10)	15.47(10)	-0.22(7)	3.37(6)	-1.04(7)
I2	15.15(8)	20.13(9)	12.14(9)	1.81(7)	1.45(6)	0.99(7)

Table 4 Bond lengths for the **3-2:1-8:MeCN** co-crystal

Atoms 1,2	d 1,2 [Å]	Atoms 1,2	d 1,2 [Å]
C1—C2	1.203(4)	C13—H13B	0.9700
C1—I1	1.998(3)	C14—C15	1.532(4)
C2—C3	1.370(4)	C14—H14A	0.9700
C3—C4	1.210(4)	C14—H14B	0.9700
C4—C5	1.356(4)	C15—C16	1.510(4)
C5—C6	1.216(4)	C15—H15A	0.9700
C6—C7	1.363(4)	C15—H15B	0.9700
C7—C8	1.203(4)	C16—N4	1.462(3)
C8—I2	2.002(3)	C16—H16A	0.9700

C10—N9	1.128(4)	C16—H16B	0.9700
C10—C11	1.471(4)	C18—O3	1.233(3)
C11—C12	1.527(4)	C18—N4	1.322(3)
C11—H11A	0.9700	C18—C18^{i}	1.538(5)
C11—H11B	0.9700	C20—C24	1.450(4)
C12—C13	1.524(4)	C20—H20A	0.9600
C12—H12A	0.9700	C20—H20B	0.9600
C12—H12B	0.9700	C20—H20C	0.9600
C13—C14	1.520(4)	C24—N19	1.139(4)
C13—H13A	0.9700	N4—H20	0.77(3)

(i) 2-x, 1-y, 1-z.

Table 5 Bond angles for the **3-2:1-8:MeCN** co-crystal

Atoms 1,2,3	**Angle 1,2,3 [°]**	**Atoms 1,2,3**	**Angle 1,2,3 [°]**
C2—C1—I1	177.3(3)	C15—C14—H14A	109.300
C1—C2—C3	178.0(3)	C13—C14—H14B	109.300
C4—C3—C2	177.5(3)	C15—C14—H14B	109.300
C3—C4—C5	176.4(3)	H14A—C14—H14B	108.000
C6—C5—C4	176.9(3)	C16—C15—C14	114.7(2)
C5—C6—C7	177.6(3)	C16—C15—H15A	108.600
C8—C7—C6	178.1(3)	C14—C15—H15A	108.600
C7—C8—I2	177.3(3)	C16—C15—H15B	108.600
N9—C10—C11	179.0(4)	C14—C15—H15B	108.600
C10—C11—C12	114.7(2)	H15A—C15—H15B	107.600
C10—C11—H11A	108.600	N4—C16—C15	113.5(2)
C12—C11—H11A	108.600	N4—C16—H16A	108.900
C10—C11—H11B	108.600	C15—C16—H16A	108.900
C12—C11—H11B	108.600	N4—C16—H16B	108.900
H11A—C11—H11B	107.600	C15—C16—H16B	108.900
C13—C12—C11	110.0(2)	H16A—C16—H16B	107.700
C13—C12—H12A	109.700	O3—C18—N4	125.2(2)
C11—C12—H12A	109.700	O3—C18—C18^{i}	120.9(3)
C13—C12—H12B	109.700	N4—C18—C18^{i}	113.9(3)
C11—C12—H12B	109.700	C24—C20—H20A	109.500
H12A—C12—H12B	108.200	C24—C20—H20B	109.500
C14—C13—C12	114.5(2)	H20A—C20—H20B	109.500
C14—C13—H13A	108.600	C24—C20—H20C	109.500
C12—C13—H13A	108.600	H20A—C20—H20C	109.500
C14—C13—H13B	108.600	H20B—C20—H20C	109.500
C12—C13—H13B	108.600	N19—C24—C20	179.2(4)
H13A—C13—H13B	107.600	C18—N4—C16	121.1(2)
C13—C14—C15	111.4(2)	C18—N4—H20	118.(2)
C13—C14—H14A	109.300	C16—N4—H20	121.(2)

Table 6 Hydrogen Atom Coordinates (Å $\times 10^4$) and Equivalent Isotropic Displacement Parameters (Å$^2 \times 10^3$) for the **3-2:1-8:MeCN** co-crystal

Atom	***x***	***y***	***z***	$\mathbf{U_{eq}}$
H11A	5879	2420	7753	36(10)
H11B	6297	3486	7825	41(11)
H12A	3188	2719	7021	22(8)
H12B	3725	3784	7089	23(8)
H13A	8177	3539	6976	13(7)
H13B	7696	2472	6925	17(8)
H14A	5803	3783	6207	21(8)
H14B	5343	2713	6156	13(7)
H15A	10261	3591	6125	29(9)
H15B	9964	2512	6131	21(8)
H16A	10444	2817	5317	9(7)
H16B	7433	2677	5344	16(8)
H20A	7030	6613	6091	66(15)
H20B	5748	5952	5681	51(12)
H20C	7717	5555	6095	74(16)
H20	7060(6)	4200(2)	5198(12)	9(8)